Canadian Nuclear Safety Commission | Commission canadienne de sûreté nucléaire

CMD 26-H105.1-REF5
Part 10 of 14

Date: 2026-06-29

Written Submission from Orano Canada Inc.

Mémoire d' Orano Canada Inc.

In the matter of

À l'égard d'

Orano Canada Inc.

Orano Canada Inc.

Application to renew the McClean Lake Operating Licence for 2-year term

Demande pour le renouvellement du permis d'exploitation de McClean Lake pour une période de deux ans

Hearing in writing based on written submissions

Audience par écrit fondée sur des mémoires

September 2026

Septembre 2026

Document ID: QQQVZZNDK725-166150894-13335 (PDF)

Canada

Appendix D

Section D

Subsection D: Demopoulos Group CRD Final Report

Final Report

Identification

Program Name: Collaborative Research and Development Grant
Due Date: 2015-04-15
George GP. Demopoulos
Dept of Mining & Materials Engineering.
McGill University
WONG BLDG RM 2140
3610 RUE UNIVERSITY
MONTREAL QC H3A0C5
Telephone: 514-398-2046
Extension:
E-mail Address: george.demopoulos@mcgill.ca
Project Title: Process and mineralogical controls of arsenic in coprecipitated tailings solids

File Number: CRDPJ 417861 - 2011
Co-Applicant: De-Tong DT. Jiang, Physics, Guelph
Collaborator: Jeffrey JN. Cutler, Chemistry, Saskatchewan
Supporting Organization: AREVA Resources Canada Inc.
Cameco Endowment Trust Fund

Public Summary of Outcomes and Benefits to Canada

In this project researchers from McGill University, Guelph University and Canadian Light Source collaborated in partnership with two uranium mining companies, Areva Resources Canada and Cameco Corporation, to study and control the deportment of arsenic in the waste solids generated during ore processing. The work undertaken as part of this project has brought new insight into the complex processing and mineralogical factors that influence the long term stability of the tailings hence ensuring the prevention of arsenic release to the environment. The findings of this work go beyond the operations of the two sponsoring companies as they can benefit the non-ferrous metals industry at large in adopting environmentally robust solutions in dealing with a host of other toxic waste materials. The present study focused in particular on the production of calcium-iron(II, III)-aluminum (II)- arsenic(V) phases via low temperature neutralization, their comprehensive characterization, and evaluation of their environmental stability via accelerated ageing under oxidizing or non-oxidizing conditions. We have found that co-ions like Ca(II), Fe(II), Ni(II) and Al(III) all contribute to production of higher stability Fe(III)-As(V) coprecipitated solids. The stabilizing role of Ni(II) and Al(III) is primarily through the generation of supplementary sorption sites to immobilize residual As(V) species via surface adsorption with the bulk of arsenic fixed as ferric arsenate/As-adsorbed ferrihydrite. The latter through powerful analysis performed at Canadian Light Source we demonstrated that at around neutral pH transform with progressive ageing to scorodite-like phases. In the meantime we found ferrous iron and calcium to help immobilize arsenate species via the formation of phases like the minerals symplesite and yukonite. Symplesite is thermodynamically very stable in sub-oxic (partly reducing) environment but it converts to arsenate-adsorbed ferrihydrite upon oxidation hence the design of tailings disposal facilities should take this behaviour into consideration. Air sparging during tailings generation by neutralization was found not to be effective. Yukonite in the presence of gypsum provides an effective arsenic sink in oxidizing environment but its exposure to atmospheric carbon dioxide should be limited as it may lead to its destabilization. Overall this project has generated a wealth of data that can help in meaningful way Canada's mining industry adopt sustainable industrial tailings generation and disposal practices. The success of the project is attributed to the excellent interdisciplinary (science and engineering) and dynamic (two-way) academic-industrial collaboration made possible by the NSERC CRD program.

Progress Towards Objectives/Milestones

To what extent were the objectives of the grant achieved? Rate your answer on a scale from 1 to 7.

Not at all			Somewhat			To a great extent
○ 1	○ 2	○ 3	○ 4	○ 5	○ 6	● 7

1.1 Brief Description of the Overall Objectives

The object of this project was to study *the retention of arsenic in co-precipitated solids generated in ferrous/ferric sulphate effluent treatment neutralization circuits. This work focused equally on (1) the process of tailings production involving oxidation, coprecipitation, and lime neutralization; (2) the characterization/identification of the mode of arsenic retention (with emphasis on the role of co-ions such as Fe(II), Ca, Ni, and Al) in the produced co-precipitated solids including the synthesis of a number of model compounds (such as ferrous arsenate-symplesite and ferric arsenite-tooeleite); and (3) the evaluation of solubility-stability of the co-precipitates and model compounds under oxic and anoxic conditions.* In this way a body of knowledge has been developed that can help the operating companies in the analysis of the more complex industrial tailings systems and thus contribute to long-term safe waste management practices.

1.2 Description of the Progress Made

The progress that was been made with reference to the various project components is described below.

1.2.1 Study the stability of Yukonite

The present project component builds on previous work completed in our laboratory and reported by Gomez et al. [1]. That work elucidated the general formula for synthetic yukonite to be: $Ca_2Fe_{3-5}(AsO_4)_3(OH)_{4-10}{\cdot}xH_2O$ where x = 2-11. We have now revised the formula based to extensive experimentation undertaken by MEng student Matthew Bohan to the following one: $Ca_3Fe_5(AsO_4)_4(OH)_9{\cdot}4H_2O$. This formula now is used in thermodynamic modeling studies finalized by our collaborator Dr. John Mahoney. In addition our previous work had generated oxic stability data showing that synthetic yukonite is stable in the presence of gypsum, i.e. when excess calcium ions are available in the surrounding water [2]. Over the course of the present project we were able to improve the synthesis method of yukonite and arrive to more reliable solubility data. Details are given in M. Bohan's Master's thesis [3]. M. Bohan by careful analysis of the synthesized yukonite samples and comparison to natural samples was able to show that in addition to Ca-Fe-AsO_4 various minor elements/species like Na,Mg, SO_4 are incorporated in the yukonite structure that need to be taken into account. Another important finding was that the synthetic yukonites tend to have less structural water than the natural counterparts (14-15% vs. 18-20%)-a characteristic that can have have an impact on yukonite's stability. The new improved synthesis method makes use of higher arsenic concentration (9 g/L vs. 1.4 g/L As) and involves first neutralization at room temperature (as opposed to the previous work [2] that involved neutralization at 95°C) and then raising the temperature to 95°C to induce conversion of precursor precipitate (looking like pc-ferric arsenate) to yukonite. In this way we found the synthetic yukonite prepared within 24 h to be closer to natural counterparts. The up-to-date solubility data for the cases of absence or presence of gypsum are graphically summarized below (FIG 1):

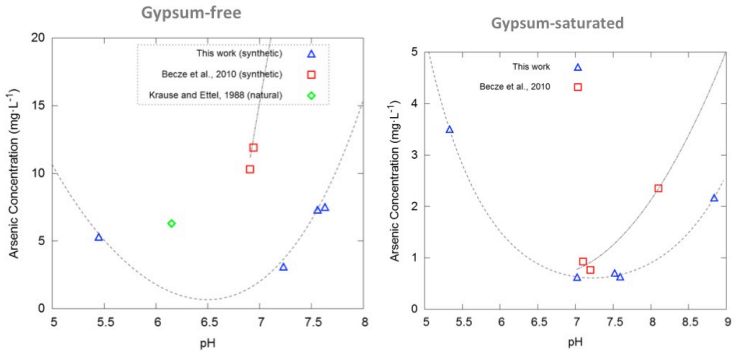

FIG 1: Solubility of yukonite as a f(pH) and gypsum presence

However, tests performed in the presence of carbonate species, either as sparged CO_2 or added $NaHCO_3$ revealed yukonite to be vulnerable to reaction and release of arsenic-see data in FIG 2- with concomitant formation of $CaCO_3$. Further we investigated the resistance of yukonite

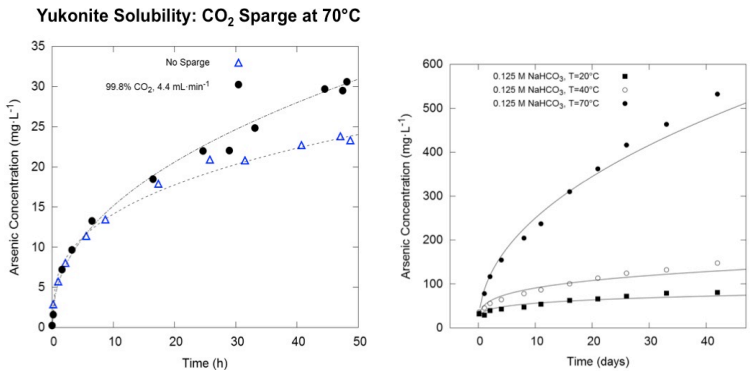

FIG 2: The reaction of yukonoite with CO_2 and $NaHCO_3$

to reducing agents under sub-oxic (sulphites; 200 mV) and anoxic conditions (sulphides; -200mV)-see reslts in FIG 3. As it can be see yukonite is stable in the former environment but not the latter. Hence these factors need to be taken into account in the design and operation of tailings management facilities.

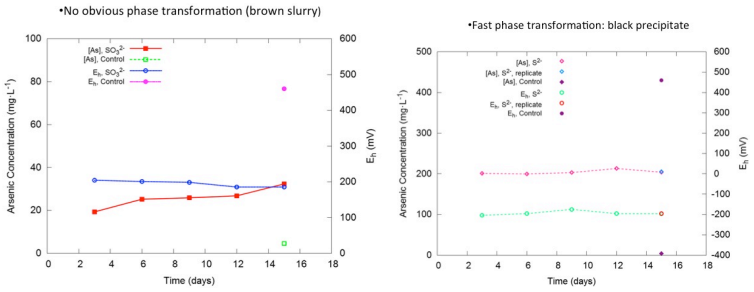

FIG 3: Sub-oxic (left) and anoxic (right) stability test data

1.2.2 Evaluate the impact of Fe(II) and Al(III) on coprecipitate stability under oxic and anoxic conditions

Industrial solutions may contain part of iron as ferrous. In this work we have examined in systematic way how ferrous iron behaves vis-à-vis arsenate during co-precipitation with or without oxidation by air sparging. Similarly ferrous may form due to partial reduction of ferric under mild reducing conditions within the mass of buried tailings and thus we have examined the response to reductive chemicals like sulphites or sulphides of Fe(III)-As(V) continuously produced coprecipitates but also Fe(III)-Al(III)-As(V) coprecipitates in an effort to probe the possible stabilizing role of Al)III) on arsenic retention.

Fe(II)-Fe(III)-As(V)-SERIES WITH AIR SPARGING-stability behavior under oxic conditions

In this series that was carried out by MEng research assistant Renaud Daenzer, the effect of air sparging on arsenic removal in a two-stage continuous coprecipitation circuit and the stability of the resultant coprecipitates was considered. In this series either mixed ferrous/ferric sulphate/arsenate solution (Fe(II)/Fe(III)=1, Test RD 9) or only ferrous/arsenate solution (Test RD 10) (with Fe/As=4 in both cases) was used and air sparging was done in reactor 2. For the case of mixed Fe(II)/Fe(III) system (RD 9) it was observed all arsenic (~0.2 ppm soluble As) and Fe(III) to precipitate in Reactor 1 but not Fe(II). Upon raise of pH to 8 (Reactor 2) and air sparging more than 90% of Fe(II) was oxidized and precipitated while soluble As conc dropped down to 50ppb. Long term stability testing of the produced coprecipitated solids under oxic conditions, however showed air sparging to result in less stability than the test withour air sparging (RD 7)-compare the results in FIG 4(left). In the second CCPTN test involving air sparging in Reactor 2 (RD 10) all iron was introduced as ferrous sulphate+ arsenate. The results collected are very interesting; thus it was found all arsenic (down to <0.2 ppm) to have precipitated with ferrous at a ratio corresponding near the stoichiometry of symplesite-ferrous arsenate-in Reactor 1 that was operated at pH 6. Upon raise of pH in Reactor 2 and air sparging

we observed only free Fe(II) to oxidize to Fe(III) but not that associated with arsenate (as presumed symplesite). Over long-term ageing however (oxic conditions) arsenic release was the same independent of applied air sparging or not (see data in FIG 4(right)). It was concluded that ferrous arsenate gradually oxidized to ferric arsenate and/or ferrihydrite on which arsenate was fixed via adsorption. Thus there is no justification for using air sparging.

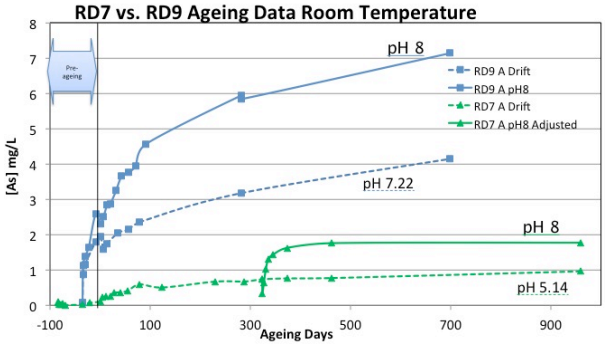

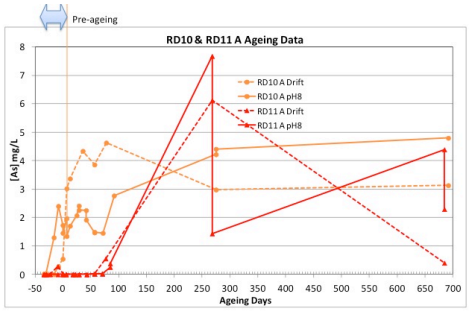

FIG 4: The effect of air sparging (RD 9 & 10) compared to no air sparging (RD7&11) on As release

Fe(II)-Fe(III)-As(V) SERIES (NO AIR SPARGING)-stability under intermittent Eh adjustment

In this series three continuous co-precipitation tests (involving two stages-one at pH 4 and the other at pH 8) with mixed Fe(II)/As(V)=4 (CD2), Fe(II)/Fe(III)/As(V)=2/2/1 (CD3), and Fe(III)/As(V)=4 (CD4) solutions were run (without air sparging) to produce coprecipitated solids for subsequent stability testing under oxic and non-oxic (periodic exposure to reducing agents). This part of the work was conducted by MEng student Christoph Dörfelt and details can be found in his thesis [4]. Under oxic conditions (Eh~580mV) the coprecipitates containing Fe(II) initially released slightly higher As(V) concentrations than Fe(III) alone namely: 1 ppm for Fe(III)/As vs. 2 ppm for Fe(III)/Fe(II)/As-2/2/1 vs. 3 ppm for Fe(II)/As. These results are truly encouraging further confirming the earlier observation that the presence of ferrous essentially provides equivalent stability to As(V) like Fe(III) does only marginally affecting arsenic release (1-3ppm range). The sub-oxic and anoxic stability data also indicated relatively marginal differentiation among the three iron (II,III)/As(V) cases.

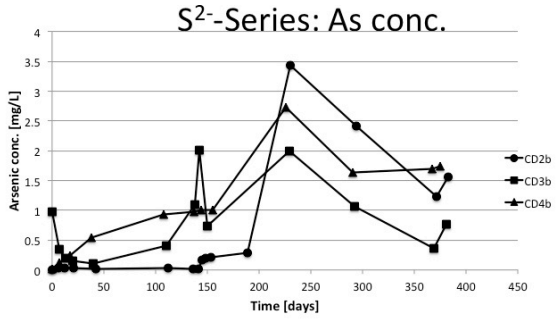

FIG 5: As release over time under periodic exposure to Na_2S

A sample of the data (Anoxic-S^2 condition) is shown in Figure 5. As it can be seen there was limited arsenic release despite the frequent exposure to strong dosing with Na_2S. Analysis of the solids showed, despite the frequent adjustment down to 0 mV of Eh with S^{2-}, ferrous to have almost fully oxidized. Hence the observed arsenic reversal towards the end of the test may be due to "recapturing" of soluble arsenate by the generated ferric either as ferric arsenate or via adsorption on ferrihydrite or a combination of the two.

Fe(III)-(Al)-As(V)-SERIES-stability under severe continuous reducing conditions

As was shown in the previous series the maintenance of low Eh (anoxic conditions) was not effective over the long run hence a new procedure was developed relying on sample preparation/handling in a glovebox and fully sealed sample containers (sceptic bottles) for total exclusion of air. Again the same reducing agents were used as above, namely SO_3^{2-} and S^{2-}. No pH or Eh adjustment was further applied as each sceptic bottle represented a single sample. For

this series of tests two types of coprecipitates (again produced in the 2-stage continuous circuit) were tested: Fe(III)/As(V)=4 (CD4) and Fe(III)/Al(III)/As(V)=2/2/1 (CD5). The intent with this series was to evaluate the "worst case scenario" in terms of reductive decomposition of ferric arsenate coprecipitates and the possible stabilizing effect the presence of aluminum can bring in this case knowing that unlike iron, Al is not susceptible to redox reactions and as such could provide an "insurance" sink (via adsorption) for any mobilized arsenate/arsenite. FIG 6 summarizes the most important set of data from this series.

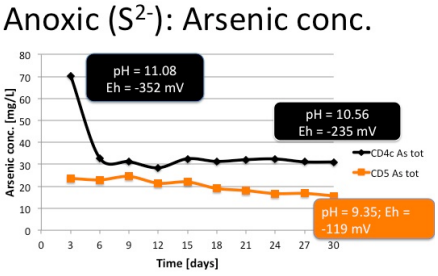

FIG 6: Release of As under strong Reducing potential

As it can be seen in this case the E_h was successfully maintained at very low level (-100 to -200 mV) while the pH ranged from 9.3 (in the presence to Al) to 11 (Fe(III) only). Despite these aggressive conditions less than 30 mg/L As was released with the system containg Al to be the most stable of the two. It is interesting that analysis of the reacted precipitates found only half of iron(III) to have been reduced to Fe(II), which may explain the relatively minor fraction of mobilized arsenic due to apparent formation of ferrous arsenate. Analysis found rather insignificant reduction of As(V) to As(III) and this issue remains to be studied in future work.

1.2.3 Elucidate the role of Ni and Al on arsenic retention via Synchrotron characterization

Here the analysis of synthetic multi-ion coprecipitated solids was undertaken with the objective of identifying how Ni and Al contribute to lower As solubility. Thus all the solids (Ni and Al containing) that they had been already produced and aged in our laboratory for nearly 3 years were subjected to XAFS characterization at CLS by Guelph MSc student Zachary Arthur and undergraduate research assistants Edward Kim and Stephen Glazier, under the supervision of co-applicant Jiang and in collaboration with Drs. Chen, Reid and Cutler of CLS. The progress is summarized in the following four aspects: 1) Development in XANES analysis of poorly-crystalline materials aided with *ab initio* FDMNES modeling (characterization of annabergite (nickel arsenate); 2) Characterization of Ni co-ion effect in ferric arsenate retention; 3) XANES Detection of phase evolution in aged As-Fe-Ni coprecipitation systems – emergence of scorodite-like species; 4) EXAFS Debye-Waller (DW) characterization for arsenate.

1) Two facts related to the systems encountered in this project motivated our effort in developing the XANES analysis approach involving *ab initio* calculations: first, by virtue of the low kinetic energy of the photoelectrons involved and the strong resonance effects, XANES has a significantly longer probing distance than that of EXAFS; second, the arsenate systems here all have their basic As-O tetrahedron structures intact in forming various species therefore we need to work beyond the most common spectral features which are dictated by the basic tetrahedral structure. We have made usage of large scale computational user facilities such as Sharcnet and Westgrid and 32-core/128Gb cluster constructed at Guelph, dedicated for this development. The As and Ni K-edge XANES of both crystalline and poorly-crystalline annabergites synthesized at McGill have been measured at the CLS and analyzed via FDMNES simulations by the Guelph/CLS group [5]. The nanoscale structure of the poorly-crystalline annabergite is characterized to be ~1 nm size sheets in the (010) planes of the crystalline annabergite.

2) The FDMNES calculation aided XANES analysis described in (1) has been applied to the analysis of the arsenical nickel hydroxide model compounds (amorphous and crystalline). There have been some XANES signatures identified for the arsenic loading to the nickel hydroxide [5]. Meanwhile, an extensive analysis of the RP7 (Ni-containing coprecipitated) series of samples

prepared at McGill have been carried out including transmission mode full XAFS (XANES and EXAFS) at As, Ni and Fe K-edges. This series includes samples aged (for 1449 days) at fixed pH=8 as well as at drifting pH at different temperatures (RT (22°C, 40°C and 70°C). Data analysis is still on-going but some preliminary trends have emerged:

- Local structure of As in RP7 (Fe(III)/As(V)=4, Ni/As=1 co-precipitation system) has its 2nd shell ordering dependent on having the pH fixed or drifting (pH~6.5) during ageing; with the latter having a noticeably better ordered 2nd shell region;
- The impact of aging temperatures (RT, 40 °C, 70 °C) on the As local structure is subtle but consistently detectable in XANES; however within the probing distance range of EXAFS the As local structure appears to be insensitive to the aging temperature. The aging temperature appears to have significant influence on Fe and Ni local structures reflected by EXAFS; however, with apparently opposite effects to Fe and Ni: rising aging temperature improves the 2nd shell ordering of Fe but not clearly so for Ni and sometimes even degrades the 2nd shell ordering for Ni;
- Ni does not alter the XANES of As in the RP7's in any significant manner, leaving the As XANES to be (expectedly) that of poorly-crystalline ferric arsenate;
- The presence of arsenic in the vicinity of Ni is detected in the Ni XANES for the fixed pH 8 samples, but not for the drifting pH (~6.5) samples; in all these cases the Ni K-edge XANES indicates that the Ni local structure bears resemblance of that of nickel hydroxide.
- Forcing pH to remain fixed at around 8 during ageing seems to lead to a deteriorating As 2nd shell structure; while letting pH to drift and stabilize at ~6.33-6.57 is seen to lead to improved As 2nd shell ordering.

3) As mentioned in (2), subtle but consistent XANES features are identified to relate to the aging of the coprecipitates. When compared with the XANES of the reference compounds, arsenate adsorbed on ferrihydrite and poorly-crystalline ferric arsenate (also referred to as amorphous scorodite), it is concluded that the XANES feature of the poorly-crystalline ferric arsenate increases in intensity during aging and the higher the aging temperature the faster the rate of increase. This observation is suggestive to the eventual fate of the coprecipitates that it appears to be evolving towards a scorodite-like phase under the tested pH condition which mimicks that at the McClean mine site operation. Based on the discussion in (1), the XANES features of interest here appear to be related to the nanoscale morphology of the coprecipitates, which appears to suggest a subtle nanoscale structure evolution that escapes the detection of EXAFS but not XANES.

4) Our preliminary results on the EXAFS Debye-Waller (DW) factors for the multiple scattering (MS) paths within two different arsenate tetrahedra have been reported [6] and a more detailed paper is in preparation. Spectroscopically the EXAFS signal of these MS paths could interfere with that of the second nearest neighbouring atomic shells from the arsenic absorbing atom, therefore the lack of well-established values of these intensity parameters could lead to various ambiguities and even controversies for the final chemical speciation. With this in mind the Guelph/CLS team has investigated the DW factors for three most significant MS paths within the arsenate in $Na_2HAsO_4{\cdot}7H_2O$, namely the collinear nearest neighbour triangular double-scattering path, collinear nearest neighbour triple-scattering path and non-collinear nearest neighbour triple-scattering path. The EXAFS data were measured from polycrystalline $Na_2HAsO_4{\cdot}7H_2O$ in transmission mode and isolated arsenate tetrahedra in high pH (pH=14) aqueous solution of $Na_2HAsO_4{\cdot}7H_2O$ in fluorescence mode, respectively. The physical correlations between MS DWs and averaged DW of the single scattering (SS) nearest neighbour are considered in the analysis and the final MS DWs are reported as the ratios to the SS DW for applying the results to the analysis of other arsenate-bearing systems. Arsenate tetraheda under mutual and the high pH have significantly different levels of distortions from an ideal tetrahedron, therefore different static DW values. Indeed, the DWs in the powder sample is about 1.5 times of that in the high

pH solution sample. However, the results from the two different arsenates show that the DW ratio between the triangular MS to that of SS path is invariant to the level of tetrahedron distortion and the ratio is found to be 2.0 ± 0.1. The implications of these results are twofold: first, the conservation of the ratio suggests that the value that could be applied to the arsenates falls in between the two rather extreme sampling cases; second, the value of the ratio itself is twice as much as some of the previous assumed values in the literature, highlighting the level of uncertainty where this value was required in the previous curve-fitting analysis.

1.2.4 Synthesis, characterization and solubility of model compounds

As it becomes clear from the above, arsenic is expected to precipitate/be retained in different forms under the different coprecipitation conditions. At the same time development of reducing (anaerobic) conditions in the tailings site could produce reduced iron (II) and arsenic(III) compounds. In order to facilitate the analysis of complex tailings systems better knowledge of individual compounds is required. In this context during the course of this project we have spent considerable time to achieve the synthesis of good quality symplesite [$Fe(II)_3(As(V)O_4)_2 \cdot 8H_20$] (triclinic) for characterization (performed at CLS) and stability testing/solubility measurement. The work was conducted by Dr. Liying Xu. (The initial samples prepared were found after Rietveldt refinement by CLS' Joel Reid not to be pure). Several challenges had to be overcome including prevention of oxidation and avoidance of formation of compounds like parasymplesite and ferrisymplesite that are monoclinic variants of symplesite. Different synthesis methods tried including pH raising at different target values and temperatures and precipitation at fixed pH. The best symplesite material was found to form by adding slowly Fe(II) solution (90 mM) into an As(V) solution (Fe(II)/As(V)=1.5) while pH was kept constant at pH 8 at 70°C followed by ageing at that temperature and pH for 8 days. The XRD pattern of the symplesite compound is shown in Figure 7(left).

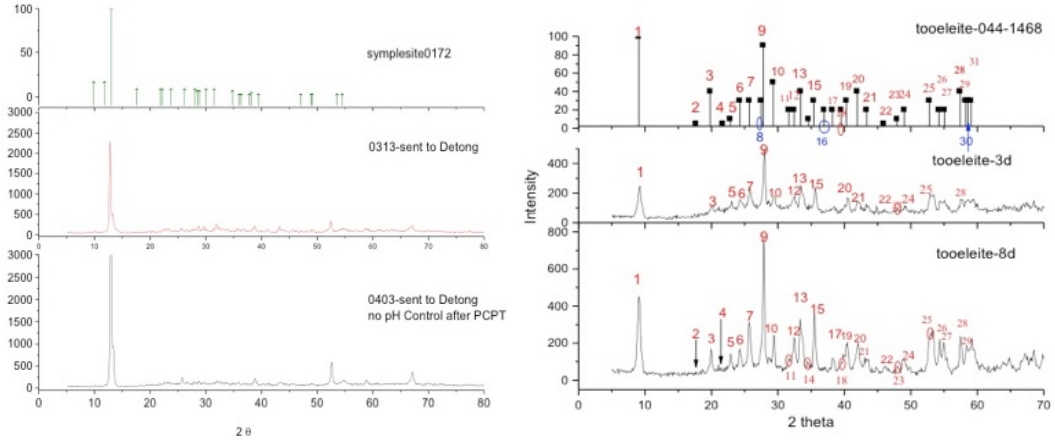

FIG 7: XTD patterns of synthetic symplesite and tooleite

By employing a similar synthesis method, that is slow addition of iron solution (in this case 0.5M Fe(III)) into an As(III) solution (Fe(III)/As(III)=1.37) at fixed pH (this time ~1.7) at 70°C and ageing for several days we also synthesized tooeleite-a ferric arsenite mineral: $Fe^{3+}{}_6(As^{3+}O_3)_4(SO_4)(OH)_4 \cdot 4H_2O$). Figure 7(right) shows that after 8 days ageing the XRD pattern of synthesized tooeleite is essentially the same with that of a standard natural specimen. The solubility study of symplesite revealed that independent of the starting pH all samples converged with time to pH ~7. At that pH the naturally attained E_h is ~250mV (tests run in a glovebox). The pseudo-equilibrium arsenic concentration under those conditions was found to be 4 mg/L. By contrast tooleite was confirmed not to play a role in arsenic retention at the pH range of the coprecipitation process as its solubility is very high >pH 3 (>80 mg/L As).

SUMMARY OF MAJOR FINDINGS

- Yukonite was shown to be very stable in slightly acidic, neutral, and slightly alkaline conditions (pH 5-8) in oxic (oxygen-rich) conditions. The stability of yukonite in oxic conditions increases by gypsum-saturation. Yukonite becomes unstable if exposed to CO_2 sparging or strong reducing potential (~-200 mV).

- Fe(III)/As(V) (and even better (Fe(III)/Al(III)/As(V)) co-precipitates under "worst-case scenario" (E_h<0mV and pH as high as 9.5) appear to be quite resistant to chemical reduction. Ferric to ferrous reduction occurs but this does not introduce destabilization. Arsenate reduction to arsenite is very limited by sulphides; unless its generation is promoted by bio-catalyzed reduction the coprecipitates should remain largely stable. The presence or in-situ generation of ferrous and aluminum provide stabilizing effects via ferrous arsenate and adsorption/surface precipitation on aluminum hydroxides.
- According to our synchrotron characterization of Ni-containing aged for 1500 days Fe(III)/As(V) coprecipitates the role of Ni appears to be limited to the formation of nickel hydroxide and the adsorption of arsenate on it at pH>7. We suspect the role of Al to be similar via formation of aluminum hydroxide and secondary arsenate adsorption on it.
- Finally the detailed nanoscale analysis of the same aged coprecipiates revealed that the XANES feature of the poorly-crystalline ferric arsenate increases in intensity during ageing and the higher the ageing temperature the faster the rate of increase. This observation is suggestive to the eventual fate of the coprecipitates that it appears to be evolving towards a scorodite-like phase under the tested pH drift condition which mimicks that at the McClean mine site operation.

1.3 Justification for any deviations from the original objectives

There were no significant deviations from the original objectives as such. The research achieved its main mission that was to elucidate key process and mineralogical factors affecting the stability of iron-arsenic coprecipitated solids.

References

1. M. A. Gomez, L. Becze, R. I. R. Blyth, J. N. Cutler, and G. P. Demopoulos, 2010, "Molecular and structural investigation of yukonite (synthetic and natural) and its relation to arseniosiderite", *Geochim. Cosmochim. Acta.* 74, 5835–5851
2. L. Becze, M.A. Gomez, V. Petkov, J.N. Cutler and G.P. Demopoulos, 2010, "The potential arsenic retention role of Ca-Fe(III)-AsO4 compounds in lime neutralized co-precipitation tailings", in *Proceedings of Uranium 2010,* Eds. E.K. Lam, J.W. Rowson, E.Özberk, CIM, Saskatoon, August 2010, Vol. 2, p.327-336.
3. Matthew Bohan, Synthesis and stability of Ca(II)-Fe(III)-AsO_4 compounds, *MEng Thesis*, McGill University (2014)
4. Christoph Doerfelt, Coprecipitation and stability of ferrous-ferric arsenates, *MEng Thesis* (2013).
5. N. Chen, E. Kim, Z. Arthur, R. Daenzer, J. Warner, G.P. Demopoulos, Y. Joly and D.T. Jiang, 2013, XAFS Study of Arsenical Nickel Hydroxide, *J. Phys. Conf. Series* 430 (012092).
6. E. Kim, N. Chen, Z. Arthur, J. Warner, G.P. Demopoulos, J.W. Rowson and D.T. Jiang, 2013, Multiple Scattering Debye-Waller Factors for Arsenate, *J. Phys. Conf. Ser.* 430 (012086).

Problems Encountered

Identify the problems encountered during the research project. (Select all that apply.)

- [ ] Technical or scientific problems
- [ ] Problems with direction of research or findings
- [ ] Equipment and facilities
- [ ] Staffing issues (e.g., availability of students, staff leaving project)
- [ ] Funding problems
- [ ] Partners withdrew from project
- [ ] Partners interaction issues
- [x] No problems were encountered
- [ ] Other (specify)

Research Team

Entry 1 of 21

Consent obtained: ● Yes ○ No

Name: George Demopoulos

Role: Applicant

If role is "Other", specify:

Contribution

Initiated and directed the whole project.

Entry 2 of 21

Consent obtained: ● Yes ○ No

Name: De-Tong Jiang

Role: Co-Applicant

If role is "Other", specify:

Contribution

Directed the synchrotron-based characterization work.

Entry 3 of 21

Consent obtained: ● Yes ○ No

Name: Ed Kim

Role: Undergraduate Student

If role is "Other", specify:

Contribution

UofGuelph student; assisted with XAFS characterization work.

Research Team

Entry 4 of 21

Consent obtained: ● Yes ○ No

Name: Stephen Glazier

Role: Undergraduate Student

If role is "Other", specify:

Contribution

UofGuelph student; assisted with XAFS characterization work.

Entry 5 of 21

Consent obtained: ● Yes ○ No

Name: Matthew Bohan

Role: Graduate Student

If role is "Other", specify:

Contribution

Worked on the synthesis and stability of Ca(II)-Fe(III)-AsO4 compounds under CO2-rich, oxic and reducing conditions.

Entry 6 of 21

Consent obtained: ● Yes ○ No

Name: Zachary Arthur

Role: Graduate Student

If role is "Other", specify:

Contribution

Zachary worked under the supervision of Professor Jiang on XAFS characterization of aged coprecipitates.

Research Team

Entry 7 of 21

Consent obtained: ● Yes ○ No
Name: Christoph Dörfelt
Role: Graduate Student
If role is "Other", specify:

Contribution

Worked on continuous and batch coprecipitation of ferrous/ferric/aluminium arsenates, their characterization and their resistance to reductive dissolution.

Entry 8 of 21

Consent obtained: ● Yes ○ No
Name: Ravi Multani
Role: Graduate Student
If role is "Other", specify:

Contribution

Performed exploratory tests on antimony behaviour during neutralization-precipitation.

Entry 9 of 21

Consent obtained: ● Yes ○ No
Name: Nima Parsi
Role: Postdoctoral Fellow
If role is "Other", specify:

Contribution

Assisted with spectroscopic characterization of precipitates.

Research Team

Entry 10 of 21

Consent obtained: ● Yes ○ No

Name: Fuqiang Guo

Role: Postdoctoral Fellow

If role is "Other", specify:

Contribution

Assisted on part time basis with the running of the experiments.

Entry 11 of 21

Consent obtained: ● Yes ○ No

Name: Thomas Feldmann

Role: Postdoctoral Fellow

If role is "Other", specify:

Contribution

Involved with the continuous coprecipitation work and long term stability tests.

Entry 12 of 21

Consent obtained: ● Yes ○ No

Name: Hassane Assaaoudi

Role: Research Associate

If role is "Other", specify:

Contribution

Advised/assisted the McGill students with spectroscopic analysis of coprecipitates.

Research Team

Entry 13 of 21

Consent obtained: ○ Yes ● No

Name:

Role: Industry Research Partner

If role is "Other", specify:

Contribution

Actively participated and facilitated McGill-Guelph-CLS project team members' participation in Cameco's Engineered Tailings Technical Meeting

Entry 14 of 21

Consent obtained: ○ Yes ● No

Name:

Role: Industry Research Partner

If role is "Other", specify:

Contribution

Entry 15 of 21

Consent obtained: ● Yes ○ No

Name: Jeff Cutler

Role: Collaborator

If role is "Other", specify:

Contribution

Canadian Light Source (CLS) scientist; have contributed with the synchrotron characterization part of the project.

Research Team

Entry 16 of 21

Consent obtained: ● Yes ○ No

Name: Yongfeng Jia

Role: Collaborator

If role is "Other", specify:

Contribution

Professor of applied ecology, Chinese Academy of Sciences; collaborated on design and analysis/characterization of gypsum-containg iron(III)-As(V) co-precipitates.

Entry 17 of 21

Consent obtained: ● Yes ○ No

Name: John Mahoney

Role: Collaborator

If role is "Other", specify:

Contribution

Geochemical Consultant; assisted with PHREEQC modeling of yukonite solubility.

Entry 18 of 21

Consent obtained: ● Yes ○ No

Name: Ning Chen

Role: Collaborator

If role is "Other", specify:

Contribution

Canadian Light Source (CLS) scientist; have contributed with the synchrotron characterization part of the project.

Research Team

Entry 19 of 21

Consent obtained: ● Yes ○ No
Name: Joel Reid
Role: Collaborator
If role is "Other", specify:

Contribution

Canadian Light Source (CLS) scientist; have contributed with the synchrotron characterization part of the project.

Entry 20 of 21

Consent obtained: ● Yes ○ No
Name: Liying Xu
Role: Other
If role is "Other", specify: Visiting Research Fellow

Contribution

She carried out synthesis, characterization and solubility measurement of model compounds like symplesite and tooleite.

Entry 21 of 21

Consent obtained: ● Yes ○ No
Name: Renaud Daenzer
Role: Other
If role is "Other", specify: MEng research assistant

Contribution

Carried out both Fe(II)-Fe(III)-As(V) coprecipitation and stability (under oxic environment) tests including the effect of air sparging during co-precipitation.

Training of Highly Qualified Personnel (HQP)

What types of interactions did the HQP have with the partners during the project? (Select all that apply.)

- [x] HQP presented research results to the partners
- [x] HQP discussed the project directly with partners to obtain input
- [ ] Partners jointly supervised thesis projects of HQP
- [ ] HQP worked regularly in the partner's facilities
- [ ] HQP did not interact with the partners
- [ ] Other (specify)

Entry 1 of 12

Name:	Edward Kim
Type:	Undergraduate Student
If type is "Other", specify:	
Start Date yyyy/mm:	2012/04
End Date yyyy/mm:	2013/04
Percentage (%) of time this individual spent on this project:	100
Percentage (%) of salary from this grant (NSERC and industry contribution):	50
Total person-months:	12
To the best of your knowledge trainee is:	Continuing Academic Training
If "Employed by Other", specify:	

Entry 2 of 12

Name:	Stephen Glazier
Type:	Undergraduate Student
If type is "Other", specify:	
Start Date yyyy/mm:	2012/04
End Date yyyy/mm:	2012/08
Percentage (%) of time this individual spent on this project:	100
Percentage (%) of salary from this grant (NSERC and industry contribution):	50
Total person-months:	4
To the best of your knowledge trainee is:	Continuing Academic Training
If "Employed by Other", specify:	

Training of Highly Qualified Personnel (HQP)

Entry 3 of 12

Name:	Christoph Doerfelt
Type:	Master's Student
If type is "Other", specify:	
Start Date yyyy/mm:	2011/09
End Date yyyy/mm:	2013/10
Percentage (%) of time this individual spent on this project:	100
Percentage (%) of salary from this grant (NSERC and industry contribution):	100
Total person-months:	25
To the best of your knowledge trainee is:	Continuing Academic Training
If "Employed by Other", specify:	

Entry 4 of 12

Name:	Matthew Bohan
Type:	Master's Student
If type is "Other", specify:	
Start Date yyyy/mm:	2012/01
End Date yyyy/mm:	2014/09
Percentage (%) of time this individual spent on this project:	100
Percentage (%) of salary from this grant (NSERC and industry contribution):	100
Total person-months:	32
To the best of your knowledge trainee is:	Employed in Industry
If "Employed by Other", specify:	

Entry 5 of 12

Name:	Zachary Arthur
Type:	Master's Student
If type is "Other", specify:	
Start Date yyyy/mm:	2012/01
End Date yyyy/mm:	2014/08
Percentage (%) of time this individual spent on this project:	70
Percentage (%) of salary from this grant (NSERC and industry contribution):	70
Total person-months:	22
To the best of your knowledge trainee is:	Continuing Academic Training
If "Employed by Other", specify:	

Training of Highly Qualified Personnel (HQP)

Entry 6 of 12

Name:	Ravi Multani
Type:	Master's Student
If type is "Other", specify:	
Start Date yyyy/mm:	2014/04
End Date yyyy/mm:	2014/12
Percentage (%) of time this individual spent on this project:	50
Percentage (%) of salary from this grant (NSERC and industry contribution):	50
Total person-months:	4
To the best of your knowledge trainee is:	Continuing Academic Training
If "Employed by Other", specify:	

Entry 7 of 12

Name:	Thomas Feldmann
Type:	Postdoctoral Fellows
If type is "Other", specify:	
Start Date yyyy/mm:	2013/10
End Date yyyy/mm:	2015/01
Percentage (%) of time this individual spent on this project:	40
Percentage (%) of salary from this grant (NSERC and industry contribution):	40
Total person-months:	6
To the best of your knowledge trainee is:	Continuing Academic Training
If "Employed by Other", specify:	

Entry 8 of 12

Name:	Fuqiang Guo
Type:	Postdoctoral Fellows
If type is "Other", specify:	
Start Date yyyy/mm:	2014/01
End Date yyyy/mm:	2014/06
Percentage (%) of time this individual spent on this project:	30
Percentage (%) of salary from this grant (NSERC and industry contribution):	30
Total person-months:	2
To the best of your knowledge trainee is:	Do not know
If "Employed by Other", specify:	

Training of Highly Qualified Personnel (HQP)

Entry 9 of 12

Name:	Nima Parsi
Type:	Postdoctoral Fellows
If type is "Other", specify:	
Start Date yyyy/mm:	2014/06
End Date yyyy/mm:	2014/12
Percentage (%) of time this individual spent on this project:	30
Percentage (%) of salary from this grant (NSERC and industry contribution):	30
Total person-months:	2
To the best of your knowledge trainee is:	Employed in Industry
If "Employed by Other", specify:	

Entry 10 of 12

Name:	Hassane Assaaoudi
Type:	Research Associate
If type is "Other", specify:	
Start Date yyyy/mm:	2011/03
End Date yyyy/mm:	2012/03
Percentage (%) of time this individual spent on this project:	25
Percentage (%) of salary from this grant (NSERC and industry contribution):	10
Total person-months:	3
To the best of your knowledge trainee is:	Employed in Industry
If "Employed by Other", specify:	

Entry 11 of 12

Name:	Renaud Daenzer
Type:	Other
If type is "Other", specify:	MEng research assistant
Start Date yyyy/mm:	2011/03
End Date yyyy/mm:	2012/08
Percentage (%) of time this individual spent on this project:	50
Percentage (%) of salary from this grant (NSERC and industry contribution):	50
Total person-months:	9
To the best of your knowledge trainee is:	Continuing Academic Training
If "Employed by Other", specify:	

Training of Highly Qualified Personnel (HQP)

Entry 12 of 12

Name:	Liying Xu
Type:	Other
If type is "Other", specify:	Visiting Research Fellow
Start Date yyyy/mm:	2012/04
End Date yyyy/mm:	2014/06
Percentage (%) of time this individual spent on this project:	100
Percentage (%) of salary from this grant (NSERC and industry contribution):	100
Total person-months:	26
To the best of your knowledge trainee is:	Employed in Academia / Faculty
If "Employed by Other", specify:	

Dissemination of Research Results

Refereed Journal Articles Submitted :	5
Refereed Journal Articles Accepted or Published:	5
Conference Presentations/ Posters:	7
Other (Technical Reports, Non-Refereed Articles, etc.):	5
How many of the publications, conference presentations, etc. identified above were co-authored with a non-academic partner?	4

Dissemination of Research Results

Refereed Journal Articles, Submitted

1. Christoph Doerfelt, T. Feldmann, R. Daenzer and G.P. Demopoulos**,** 2015, Stability of Continuously Produced Fe(II)/Fe(III)/As(V) Co-Precipitates under Periodic Exposure to Reducing Agents, *Chemosphere*.
2. Danni Zhang, Shaofeng Wang, Xiaoling Li, Kuanling Wang, Yongfeng Jia,and G.P. Demopoulos, 2015, The Role of Gypsum in the Removal and Fixation of Arsenic: Relevant to Hydrometallurgical Iron-Arsenic Coprecipitation and Scorodite Precipitation, *J. Haz. Mat.*
3. Peter E. R. Blanchard, Lisa Van Loon, Joel Reid, Jeffrey Cutler, John Rowson, Kebbi Hughes, Caitlin Brown, Liying Xu, Matthew Bohan, George P. Demopoulos, Investigating the arsenic speciation in the JEB Tailings Management Facility at McClean Lake, Saskatchewan via X-ray absorption spectroscopy, 2015, *Geochimica et Cosmochimica Acta*.
4. Christoph Doerfelt, T. Feldmann and G.P. Demopoulos, 2015, Stability of Arsenate-Bearing Fe(III)/Al(III) Co-Precipitates in the Presence of Sulfide as Reducing Agent under Anoxic Conditions, *Hydrometallurgy* (to be submitted).
5. N. Chen, E. Kim, Z. Arthur, R. Daenzer, J. Warner, J. Reid, G.P. Demopoulos, Y. Joly, D.T. Jiang, 2013, X-ray Absorption Fine Structure Studies of Crystalline and XRD-amorphous Annabergites, *Nanoscale* (to be submitted)

Refereed Journal Articles, Accepted or Published

6. R. Daenzer, T. Feldmann and G.P. Demopoulos, 2015, Oxidation of ferrous sulfate hydrolyzed slurry - kinetic aspects and impact on As(V) removal, *Ind. Eng. Chem. Res*., 2015, *54* (6), pp 1738–1747.
7. Richard J. De Klerk, Thomas Feldmann, Renaud Daenzer; George P. Demopoulos, 2015, Continuous circuit coprecipitation of arsenic(V) with ferric iron by lime neutralization: The effect of circuit staging, co-ions and equilibration pH on long-term arsenic retention, *Hydrometallurgy,* 151 (2015) 42–50.
8. R. Daenzer, L. Xu, C. Doerfelt, Y. Jia, G.P Demopoulos, 2014, Precipitation behaviour of As(V) during neutralization of acidic Fe(II)–As(V) solutions in batch and continuous modes, *Hydrometallurgy*, 146 (2014) 40–47.
9. R.J. De Klerk, Y. Jia, R. Daenzer, M.A Gomez, G.P Demopoulos, 2012, Continuous Circuit Coprecipitation of Arsenic(V) with Ferric Iron by Lime Neutralization, *Hydrometallurgy* , 111-112 (2012) 65–72.4
10. Yongfeng Jia, Danni Zhang, Rongrong Pan, Liying Xu, George P. Demopoulos, 2012, A novel two-step coprecipitation process using Fe(III) and Al(III) for the removal and immobilization of arsenate from acidic aqueous solution, *Water Research* 46, 500-508.

Papers in Conference Proceedings with oral presentation

11. George P. Demopoulos, 2014, Arsenic Immobilization Research Advances: Past, Present and Future, in *Proceedings of Arsenic Metallurgy & the Environment* symposium, A. Barnes et al, Editors, COM2014 (paper no 8560, 13p) MetSoc of CIM, Vancouver, B.C., Sept. 2014 (*invited keynote paper*).
12. Matthew T. Bohan, John J. Mahoney, George P. Demopoulos, The synthesis and stability of yukonite, *Rare Metals Extraction and Processing Symposium*, TMS Annual Meeting, San Diego, CA, February 2014.
13. N. Chen, E. Kim, Z. Arthur, R. Daenzer, J. Warner, G.P. Demopoulos, Y. Joly and D.T. Jiang, 2013, XAFS Study of Arsenical Nickel Hydroxide, *J. Phys. Conf. Series* 430 (012092); oral presentation at: *XAFS-XV: 15th International Conference on X-Ray Absorption Fine Structure*, July 22-28, 2012, Beijing, China.
14. E. Kim, N. Chen, Z. Arthur, J. Warner, G.P. Demopoulos, J.W. Rowson and D.T. Jiang, 2013, Multiple Scattering Debye-Waller Factors for Arsenate, *J. Phys. Conf. Ser.* 430 (012086); oral presentation at: *XAFS-XV: 15th International Conference on X-Ray Absorption Fine Structure*, July 22-28, 2012, Beijing, China.
15. Christoph Doerfelt, George P. Demopoulos, 2013, Continuous co-precipitation behavior and stability of arsenic(V) from Fe(II,III)-Al(III)-Ni(II) sulphate effluent solutions, in *Ni-Co 2013 Proceedings*, T. Battle et al. (Eds.) John Wiley & Sons, Inc. and TMS, 369-378 (oral presentation).

Conference Presentations without paper

16. D.T. Jiang, N. Chen, E. Kim, Z. Arthur, J. Warner, J. Reid, R. Daenzer, G.P. Demopoulos, Y. Joly, "Nanoscale Morphology of Poorly-Crystalline Annabergite", Oral presentation, *Surface Canada 2013*, London ON, May 9th, 2013.
17. Liying Xu, Yongfeng Jia, Detong Jiang, Ning Chen, Joel Reid, George P. Demopoulos. Synthesis of Symplesite ($Fe_3(AsO_4)_2 \cdot 8H_2O$), *Goldschmidt Conference*, 2013. August 25- 30, Florence, Italy (poster paper).

Other (Technical Reports, Non-Refereed Articles, Invited Lectures, Theses)

Theses

18. Matthew Bohan, Synthesis and stability of Ca(II)-Fe(III)-AsO_4 compounds, *MEng Thesis*, McGill University (2014).
19. Christoph Doerfelt, Coprecipitation and stability of ferrous-ferric arsenates, *MEng Thesis* (2013).

Invited Lectures

20. G.P. Demopoulos, "Arsenic Fixation in Non-ferrous Industry", *Int'l Workshop on Control of the Environmental Load Elements in Non-ferrous Industry*, *JOGMEC, Tokyo, Japan*, November 7-10, 2012.
21. G.P. Demopoulos, "Advanced environmental and energy material technologies via innovative aqueous solution processing", *Institute of*

Process Engineering (Beijing) and Institute of Applied Ecology (Shenyang) of Chinese Academy of Sciences and Central South University (Changsha), China, November 2013.

Other presentations

22. Joel Reid, Liying Xu, Yansun Yao, Zachary Arthur, George Demopoulos, De-Tong Jiang and Ning Chen, "A Powder Diffraction and Density Functional Theory Study of Symplesite, $Fe_3(AsO_4)_2(OH)_x(H_2O)_{8-x}$, poster presentation at the *Theory @ CLS workshop*, Saskatoon, April 2014.

Intellectual Property Protection

Filing of patent applications:	Not applicable
Registration of copyright for computer software or databases:	Not applicable
Registration of copyright for educational materials:	Not applicable
Registration of industrial designs:	Not applicable
Filing for protection of trademarks:	Not applicable
Registration of integrated circuit topographies:	Not applicable
Filing of applications for plant breeders' rights:	Not applicable
Execution of non-disclosure or confidentiality agreements:	Not applicable

Other (specify):

Collaboration with the Partners

How was this research project initiated?

- [x] The university researcher approached the partners
- [ ] The partners approached the university researcher
- [ ] The government partner approached the university
- [x] There was a previous collaboration with the partners
- [ ] This is a new collaboration
- [ ] Other (specify)

Did this project arise from a grant funded by the NSERC Strategic Workshops Program? ○ Yes ● No

Did this project arise from a grant funded by the Interaction and/or Engage Program? ○ Yes ● No

Collaboration with the Partners

Briefly describe the process.

This project was born out of a NSERC Strategic Project grant (2005-2008). The PI approached the industrial sponsors that were initially among the sponsors of the strategic project. A brief proposal was submitted to the companies and following discussion and budget planning the companies agreed to support this CRD project.

Collaboration with the Partners

To what extent were the partners involved in the project? Rate your answer on a scale from 1 to 7.

Not at all			Somewhat			To a great extent
○ 1	○ 2	○ 3	○ 4	○ 5	○ 6	● 7

In what way were the partners directly involved in the project? (Select all that apply.)

- [x] Partners were available for consultation
- [ ] Partners provided facilities
- [ ] Partners provided training
- [ ] Partners co-supervised students' theses
- [ ] Partners received training from university personnel
- [ ] Personnel from the partner organization received training from the university
- [x] Partners discussed the project regularly with the university team

  Average number of meetings per year: 2
- [x] Partners were involved in the research
- [ ] Other (specify)

Collaboration with the Partners

Describe the partners' involvement and comment on the collaboration.

Attendance of bi-annual progress review meetings; consultations and exchange of data on generation and mineralogy of arsenical tailings. Hosted review meetings in their corporate offices in Saskatoon and organized one on-site visit for the whole research team in Northern Saskatchewan where the arsenic tailings are generated and disposed of.

Future Plans

What links are you maintaining with the partners? (Select all that apply.)

- [x] Collaborating with the partners on the same research
- [ ] Collaborating with the partners on other research
- [ ] Collaborating with other partners on the same research
- [ ] Continuing the research without partners
- [ ] No contact with the partners currently and none planned
- [ ] No contact with the partners currently but future collaboration planned

Future Plans

Describe any follow-up or related work that will be undertaken as a result of this project, who will be involved in this work (including partners) and how it will be funded.

The PI and co-PI have collaborated with the sponsors for some 15 years. This has been an exceptionally fruitful collaboration on all counts. At present the PI/co-PI and sponsors have not discussed formal extension of this research via a new contract/grant but given the significant volume of data generated we expect to remain in contact as we prepare drafts of publications and discuss the significance/implications these have on their operations.

Knowledge and Technology Transfer

Research results transferred to the partners

- [x] Through informal discussions
- [x] Through reports provided to the partners
- [x] As a result of the partners participating in the research
- [x] Through formal publications
- [ ] Through patents
- [ ] Through licencing arrangements
- [ ] The research results have not been transferred to the partner
- [ ] Other (specify)

Research results being used and/or will be used by the partners

As a stimulus for future R&D:	
To enhance the skills and knowledge of personnel in the partner's organization:	Have been used
To improve an existing product:	
To improve an existing process:	Potential to be used
To improve an existing service:	
To develop a new product:	
To develop a new process:	
To develop a new service:	
To contribute to a policy, regulation or standard:	

Other (specify):

Knowledge and Technology Transfer

Briefly describe these outcomes

One of the findings of this work was the potential stabilization role the formation of phases like yukonite can have on the arsenical tailings that are saturated in gypsum. Cameco, one of our sponsors, that operates their tailings neutralization circuits at pH>8-9 conducts mineralogical studies on their historical tailings management sites in validating the role of yukonite and other arsenic-sink phases. Similarly Cameco has set up a laboratory scale mini continuous neutralization circuit as first done at McGill to investigate the arsenic precipitation chemistry in direct analogy to the industrial process. In the meantime Areva is using reference arsenical phase materials first synthesized and investigated in our laboratory in characterizing their JEB tailings accumulated over the past 15 years. In both cases synchrotron techniques used in the context of the present study involving synthetic phases are used by the sponsors in collaboration with Canadian Light Source experts in a mutually beneficial arrangement.

Knowledge and Technology Transfer

Describe any environmental or social benefit that resulted or could result in the future from this research

The knowledge generated in this research contributes to the understanding and optimization of generation and disposal of arsenical tailings thus ensuring safe environmental and sustainable practises by the mineral processing industry.

Impact on Researcher

Impact the project had on your teaching

- [ ] Creation of new courses
- [ ] New content for existing courses
- [x] Use of real world examples in courses
- [ ] Guest lectures from partners
- [ ] New equipment/material
- [ ] Project has had no impact on my teaching
- [ ] Other (specify)

Impact the project had on your research

- [ ] Influenced the direction to more industrially relevant topics
- [x] Opened up new opportunities for research beyond the original objectives
- [ ] The project has had no impact on my research
- [ ] Other (specify)

Contributions from Other Sources

Partners	Total Cash		Total In-Kind	
Company Name	**Committed**	**Received**	**Committed**	**Received**
Areva Resources Canada	150,000	150,000	40,200	50,000
Have you had previous research collaborations with this partner? Yes - In the same research area				
Cameco Endowment Trust Fund	150,000	150,000	40,200	40,000
Have you had previous research collaborations with this partner? No				
	0	0	0	0
Have you had previous research collaborations with this partner?				
	0	0	0	0
Have you had previous research collaborations with this partner?				
	0	0	0	0
Have you had previous research collaborations with this partner?				
	0	0	0	0
Have you had previous research collaborations with this partner?				
	0	0	0	0
Have you had previous research collaborations with this partner?				

Contributions from Other Sources

Other Sources	Total Cash		Total In-Kind	
		Received		Received
N/A		0		0
		0		0
		0		0
		0		0
		0		0
		0		0
		0		0
Total (partners and other sources)	**$300,000**	**$300,000**	**$80,400**	**$90,000**

Contributions from Other Sources

Variation described between commitment and actual cash and in-kind contributions

The in-kind contributions exceed the projected ones as in 2012 one of our sponsors' (Areva) organized a special one day visit to the mine site (500 km north of Saskatoon) with one of their leased planes. The other in-kind contributions were in the form of (a) salary-equivalent time devoted to the project for attendance of meetings and availability for discussions by the following company representatives and technical staff: Dr Rowson (Senior Science Advisor), Ryan Frey (Geo-environmental engineer), Dr. Kebbi Hughes (Geo-Environmental Scientist) and Glen Remple (McClean Mill Superintendent) from the side of Areva; and Drs. Kotzer (Senior Environmental Geochemist) and Warren (Senior Environmental Geochemist); data shared by the companies as pertain to their tailings in-house R&D activities; and travel expenses to attend the Montreal meeting.

Financial Information

Consolidated balance remaining at the end of the project:

Budget Items	Total Budget	Total Actual Expenditure	Percent Variation
1) Salaries and benefits			
PhD students	0	0	0
Master's students	198,000	173,000	-13
Undergraduate students	30,000	27,000	-10
Postdoctoral fellows	94,000	45,000	-52
Technical/professional assistants	76,000	57,800	-24
	0	0	0
2) Equipment or facility			
Purchase or rental	42,000	98,000	133
Operation and maintenance costs	12,000	23,500	96
User fees	60,000	49,200	-18
	0	0	0
3) Materials and supplies			
	46,000	66,800	45
	0	0	0
	0	0	0
4) Travel			
Conferences	15,000	17,000	13
Field work	6,000	7,700	28
Project related travel	18,000	24,000	33
	0	0	0
5) Dissemination			
Publication costs	0	0	0
Review Meetings	0	5,600	999
6) Technology transfer activities			
Field trials	0	0	0
Prototypes	0	0	0
	0	0	0
7) Others (specify)			
Laptop	0	1,300	999
Courier, brokerage etc	0	1,100	999
Total	597,000	597,000	0

Financial Information

Explanation for the variation of each budget item

In general the various expenditures are on line with the original budget. Here is the reasons for observed discrepancies with items such as PDF and Technical salaries and equipment/ mat&supplies. The lower amount spent on PDFs is due to the fact that we relied in the early part of the project on supplementary technical assistance from other graduate students within our group. The other reason is that the PDFs worked on part time basis hence taxing less the budget of this grant. In terms of technical personnel we spent less as the salary of Dr Liying Xu as Visiting Scientist was partly covered by her home institution. These savings in salaries were counterbalanced by increased expenditure in equipment purchases as well as higher than initially forecast material and supply expenditures. This happened in part because of the unfavourable trend with currency exchange as well significant larger costs with parts replacement and accessories. The user fees on the other hand were maintained at -20% of the original forecast value. The project involved two annual review meetings one in Montreal and one in Saskatoon and as consequence the travel related to project and the holding of the meetings cost an extra $10000.

Appendix D

Section D

Subsection E: Geochemical Results

Retention Time Test Data

Retention Time Test No.	1								
Objective :	Assess impact of incomplete As oxidation and short pH 4 RT								
Conditions	Start			1 st stage			2 nd stage		Aging
	Fe+3/Fe tot	[Fe+3]/[As]	As+5/As tot	pH	° C	mn	pH	mn	method
	0.899	3.6	0.615	4	35	15	8	60	TVOP
Physical tailings:	density :	1.112							
	% H2O :	81.09							

		Reference solutions								
		First stage	T0	T1	T7	T14	T21	T28	T35	T63
	Day		0	1	7	14	21	28	35	63
	Ref. Analysis	9079	9105	9216	9355	9555	9887	10050	10435	11043
Analysis										
pH		4.3	7.87	7.67	7.5	7.22	7.19	7.28	7.27	7.23
Eh	mV	263	127	222	268	333	308	398	344	276
Conductivity	mS/cm	9.64	4.3	4.5	4.69	4.72	4.8	4.94	5.28	5.64
Carbonate	mg/l		< 2						6.8	
Bicarbonate	mg/l		< 2						90.4	
Total alkalinity	mM/l	< 0.4	< 0.4		1.11		< 0,4		1.67	< 0,4
Al	mg/l	223	0.22		0.04		0.05		< 0,02	0.02
As total	mg/l	49.5	0.87	1.73	0.83	0.8	0.74	0.78	0.81	0.6
As (III)	mg/l	34.2	0.45		< 0.02		< 0,015		< 0,016	< 0,012
Ba	mg/l	-	0.165						0.09	
Ca	mg/l	555	520		526		515.8		571	543
Cl	mg/l	93.4	70		82.6		85.2		82.5	83.8
Co	mg/l		0.01						0.31	
Cu	mg/l		0.08						0.11	
Fe total	mg/l	197	< 0.01	< 0.02	< 0.01	< 0.02	< 0,01	< 0,02	0.022	< 0,01
Fe (II)	mg/l	168	< 0.01		< 0.01		< 0,01		0.022	< 0,01
K	mg/l	482	365		305		320.2		282.5	255
Mg	mg/l	682	98.7		245		324.8		351	395
Mn	mg/l		0.28						2.72	
Mo	mg/l		0.19						0.83	
Na	mg/l	333	298		315		277.9		335	307.8
Ni	mg/l	505	0.03	0.15	0.16	0.37	0.32	0.55	0.42	0.56
[Ni]/[As]		13.0	0.0	0.1	0.2	0.6	0.6	0.9	0.7	1.2
NH4+	mg/l		72						53.5	
NO3	mg/l	23.7	11.6		< 10		12.3		15.3	11.8
P	mg/l	0.35	0.07		0.12		0.1		0.25	0.2
Pb	mg/l		< 0.03						0.05	
Ra 226	Bg/l		1564						353.8	
S 2-	mg/l	< 100	< 100		< 100		< 100		< 100	< 100
SO4 2-	mg/l	10100	2650		3260		3490		3450	3710
S total	mg/l	3250	876.2		1126		1110		1118	1250
Si	mg/l	8.94	0.83		7.51		12.7		15.5	17.4
U	mg/l	157	0.08		0.14		0.13		0.07	0.1
Zn	mg/l		< 0.01						0.04	

Retention Time Test Data

Retention Time Test No.	2

Objective :	Short pH 4 RT represents – 15 % of tailings in current circuit								
	Start			1 st stage			2 nd stage		Aging
Conditions	Fe+3/Fe tot	[Fe+3]/[As]	As+5/As tot	pH	° C	mn	pH	mn	method
	0.907	2.88	0.999	4	35	15	8	60	TVOP

Physical tailings:	density :	1.11
	% H2O :	82.34

		Reference solutions								
		First stage	T0	T1	T7	T14	T21	T28	T35	T63
	Day		0	1	7	14	21	28	35	63
	Ref. Analysis	9080	9106	9217	9356	9556	9888	10051	10436	11044
Analysis										
pH		4.3	7.78	7.75	7.6	7.5	7.38	7.46	7.35	7.3
Eh	mV	259	139	213	252	319	250	384	334	265
Conductivity	mS/cm	9.9	4.54	4.8	4.9	4.93	4.99	5.1	5.66	5.78
Carbonate	mg/l		< 2						8.5	
Bicarbonate	mg/l		< 2						127	
Total alkalinity	mM/l	< 0.4	< 0.4		1.64		< 0,4		2.03	1
Al	mg/l	249	0.18		0.04		0.05		< 0,02	0.02
As total	mg/l	1.94	0.57	0.52	0.52	0.64	0.61	0.58	0.71	0.56
As (III)	mg/l	0.19	0.06		< 0.01		< 0,012		<0,014	< 0,011
Ba	mg/l		0.176						0.092	
Ca	mg/l	553	514		503		514.4		513	545
Cl	mg/l	94.4	72.4		82.6		81.4		81.9	81.7
Co	mg/l		0.03						0.02	
Cu	mg/l		0.08						0.05	
Fe total	mg/l	267	< 0.01	< 0.02	< 0.01	< 0.02	< 0,01	< 0,02	0.023	< 0,01
Fe (II)	mg/l	193	< 0.01		< 0.01		< 0,01		0.022	< 0,01
K	mg/l	496	355		307		315.5		290	260
Mg	mg/l	663	105		245		299.1		319	372
Mn	mg/l		0.4						0.24	
Mo	mg/l		0.26						0.98	
Na	mg/l	423	389		388		356.7		375	385.7
Ni	mg/l	452	0.6	0.13	0.16	0.23	0.34	0.37	0.42	0.47
[Ni]/[As]		297.7	1.3	0.3	0.4	0.5	0.7	0.8	0.8	1.1
NH4+	mg/l		73						53.8	
NO3	mg/l	24.7	13.6		13		13.8		18.9	17.5
P	mg/l	0.26	0.1		0.13		0.09		0.25	0.21
Pb	mg/l		< 0.03						0.05	
Ra 226	Bg/l		1483						447	
S 2-	mg/l	< 100	< 100		< 100		< 100		< 100	< 100
SO4 2-	mg/l	10700	2820		3250		3510		3640	3770
S total	mg/l	3410	959		1155		1230		1230	1230
Si	mg/l	8.66	1.48		7.64		13.2		15.4	17
U	mg/l	172.7	0.16		0.47		0.31		0.29	0.26
Zn	mg/l		< 0.01						0.03	

Retention Time Test Data

Retention Time Test No.	3

Objective :	Assess impact of lower first stage pH (reduced HFO ppt.)								
Conditions	Start			1 st stage			2 nd stage		Aging
	Fe+3/Fe tot	[Fe+3]/[As]	As+5/As tot	pH	° C	mn	pH	mn	method
	0.907	2.88	0.999	3	35	15	8	60	TVOP
Physical tailings:	density :	1.103							
	% H2O :	81.63							

		Reference solutions								
		First stage	T0	T1	T7	T14	T21	T28	T35	T63
	Day		0	1	7	14	21	28	35	63
	Ref. Analysis	9218	9261	9293	9388	9664	9991	10206	10471	11211
Analysis										
pH		3.34	7.79	7.7	7.65	7.64	7.51	7.52	7.43	7.54
Eh	mV	370	177	152	166	125	198	174	150	201
Conductivity	mS/cm	16.36	4.57	4.66	4.88	4.88	4.98	4.99	5.4	5.75
Carbonate	mg/l		< 2						< 2	
Bicarbonate	mg/l		< 2						< 2	
Total alkalinity	mM/l	< 0.4	< 0.4		2		1.91		2.24	2.1
Al	mg/l	3380	0.27		0.17		0.06		< 0,02	0.03
As total	mg/l	5.29	0.5	0.51	0.59	0.64	0.55	0.61	0.69	0.61
As (III)	mg/l	< 0.1	0.01		< 0,01		< 0,011		<0,014	< 0,012
Ba	mg/l		0.174						0.111	
Ca	mg/l	643	523		516		514.6		505	593
Cl	mg/l	119	79.1		85.4		81.7		96.5	80.5
Co	mg/l		0.03						0.02	
Cu	mg/l		0.1						0.06	
Fe total	mg/l	417	< 0.01	< 0.02	< 0.01	< 0.02	0.016	< 0.02	0.015	0.018
Fe (II)	mg/l	371	< 0.01		< 0.01		0.016		0.015	0.018
K	mg/l	535	375		317		237.2		287.5	260
Mg	mg/l	708	93.6		228		289.8		277	359
Mn	mg/l		0.27						0.07	
Mo	mg/l		0.2						0.58	
Na	mg/l	463	397		394		368.9		381	389.9
Ni	mg/l	613	0.07	0.11	0.21	0.25	0.31	0.39	0.53	0.44
[Ni]/[As]		148.1	0.2	0.3	0.5	0.5	0.7	0.8	1.0	0.9
NH4+	mg/l		71						54.6	
NO3	mg/l	25.9	14.4		14.8		15.8		16.7	14.9
P	mg/l	15	0.1		0.18		0.08		0.2	0.11
Pb	mg/l		< 0.03						0.04	
Ra 226	Bg/l		1762						644	
S 2-	mg/l	829	< 100		< 100		< 100		< 100	< 100
SO4 2-	mg/l	25500	2870		3310		3380		3400	3620
S total	mg/l	9350	982		1140		1140		1099	1230
Si	mg/l	11.6	1.72		9.24		12.6		15.9	17.5
U	mg/l	153.7	0.14		0.5		0.58		0.38	0.62
Zn	mg/l		< 0.01						0.03	

Retention Time Test Data

Retention Time Test No.	4

Objective :	Control test 1. Provide continuity with 1997 SEPA work								
	Start			1 st stage			2 nd stage		Aging
Conditions	Fe+3/Fe tot	[Fe+3]/[As]	As+5/As tot	pH	° C	mn	pH	mn	method
	0.907	2.88	0.999	4	35	90	8	60	SEPA

Physical tailings:	density :	1.11
	% H2O :	82.34

		Reference solutions								
		First stage	T0	T1	T7	T14	T21	T28	T35	T63
	Day		0	1	7	14	21	28	35	63
	Ref. Analysis	9557	9638	9665	9921	10118	10456	10644	10752	11691
Analysis										
pH		4.2	7.75	7.66	7.4	7.43	7.33	7.43	7.4	7.32
Eh	mV	292	201	120	123	207	217	219	180	170
Conductivity	mS/cm	10.05	4.65	4.87	4.88	5.01	5.59	5.72	5.59	6.01
Carbonate	mg/l		< 2						9.3	
Bicarbonate	mg/l		< 2						46.2	
Total alkalinity	mM/l	2.17	< 0,4		< 0,4		1.08		0.92	< 0,4
Al	mg/l	398	0.21		0.07		< 0,02		0.03	
As total	mg/l	0.23	0.44	0.49	0.52	0.5	0.53	0.49	0.54	0.47
As (III)	mg/l	< 0,01	< 0,01		< 0,01		< 0,011		<0,011	< 0,009
Ba	mg/l		0.166						0.077	
Ca	mg/l	536.7	499.5		508		509		503	518
Cl	mg/l	92.5	82.4		80.7		81.7		82.1	86.3
Co	mg/l		0.05						0.44	
Cu	mg/l		0.08						0.25	
Fe total	mg/l	140	0.023	< 0.02	< 0,01	< 0,02	0.014	< 0,02	< 0,01	0.17
Fe (II)	mg/l	140	0.022		< 0,01		0.014		< 0,01	< 0,01
K	mg/l	548.2	393.1		288.1		293		310	272
Mg	mg/l	650	120.6		258.2		302		297	392
Mn	mg/l		0.37						2.64	
Mo	mg/l		0.15						0.36	
Na	mg/l	403.5	384		372.3		362		381	390
Ni	mg/l	507.2	0.08	0.11	0.19	0.24	0.17	0.36	0.28	0.52
[Ni]/[As]		2817.6	0.2	0.3	0.5	0.6	0.4	0.9	0.7	1.4
NH4+	mg/l		55.6						44	
NO3	mg/l	27.1	15.6		15		15.2		15.3	15.6
P	mg/l	0.36	0.06		0.15		0.26		0.2	0.1
Pb	mg/l		< 0,03						0.06	
Ra 226	Bg/l		1263						302	
S 2-	mg/l	< 100	< 100		< 100		< 100		< 100	< 100
SO4 2-	mg/l	12000	3000		3280		3550		3430	3810
S total	mg/l	3740	1040		1170		1263		1183	1310
Si	mg/l	10.4	1.1		9.09		14.2		15.4	18.1
U	mg/l	55.4	< 0,05		0.11		0.09		< 0,05	< 0,05
Zn	mg/l		0.01						0.04	

Retention Time Test Data

Retention Time Test No.	5

Objective :	Control test 2. Assess influence of aging method on results								
Conditions	Start			1 st stage			2 nd stage		Aging
	Fe+3/Fe tot	[Fe+3]/[As]	As+5/As tot	pH	° C	mn	pH	mn	method
	0.907	2.88	0.999	4	35	90	8	60	TVOP

Physical tailings:	density :	1.103
	% H2O :	82.1

		Reference solutions								
		First stage	T0	T1	T7	T14	T21	T28	T35	T63
	Day		0	1	7	14	21	28	35	63
	Ref. Analysis	9219	9262	9294	9389	9666	9992	10207	10472	11212
Analysis										
pH		4.38	7.9	7.7	7.6	7.57	7.31	7.43	7.38	7.44
Eh	mV	277	154	162	163	130	180	172	159	202
Conductivity	mS/cm	9.5	4.59	4.69	4.88	5.01	5.01	5.06	5.5	5.9
Carbonate	mg/l		< 2						< 2	
Bicarbonate	mg/l		< 2						< 2	
Total alkalinity	mM/l	< 0.4	< 0.4		2.14		< 0,4		1.78	1
Al	mg/l	214	0.28		0.06		0.05		0.02	0.03
As total	mg/l	0.16	0.41	0.48	0.59	0.58	0.54	0.53	0.49	0.55
As (III)	mg/l	< 0.01	< 0.01		< 0,01		< 0,011		< 0,016	< 0,011
Ba	mg/l		0.144						0.092	
Ca	mg/l	541	571		515		511.1		505	535
Cl	mg/l	92.5	76.7		80.2		80.8		84.8	85.6
Co	mg/l		0.02						0.02	
Cu	mg/l		0.06						0.04	
Fe total	mg/l	124	< 0.01	< 0.02	< 0.01	< 0.02	0.016	< 0,02	0.021	< 0,01
Fe (II)	mg/l	124	< 0.01		< 0.01		0.016		0.019	< 0,01
K	mg/l	491	381		317		284.5		267.5	267.5
Mg	mg/l	646	108		232		294.2		284	370
Mn	mg/l		0.24						0.04	
Mo	mg/l		0.13						0.43	
Na	mg/l	433	401		388		364.9		378	401.3
Ni	mg/l	464	0.01	0.1	0.17	0.17	0.31	0.36	0.03	0.44
[Ni]/[As]		3705.3	0.0	0.3	0.4	0.4	0.7	0.9	0.1	1.0
NH4+	mg/l		71						54.6	
NO3	mg/l	26.4	15.1		15.1		14.8		18.1	15.5
P	mg/l	< 0,05	0.11		0.13		0.12		0.19	0.1
Pb	mg/l		< 0.03						0.04	
Ra 226	Bg/l		1968						420	
S 2-	mg/l	<100	< 100		< 100		< 100		< 100	< 100
SO4 2-	mg/l	9550	3040		3230		3410		3440	3810
S total	mg/l	3160	1029		1158		1210		1135	1260
Si	mg/l	80.8	0.94		9.46		13.9		16	18.5
U	mg/l	54.7	0.08		0.16		0.09		0.1	0.15
Zn	mg/l		< 0.01						0.04	

Retention Time Test Data

Retention Time Test No.	6

Objective :	Determine if significant increase in low pH RT changes results								
	Start			1 st stage			2 nd stage		Aging
Conditions	Fe+3/Fe tot	[Fe+3]/[As]	As+5/As tot	pH	° C	mn	pH	mn	method
	0.907	2.88	0.999	4	35	360	8	60	TVOP

Physical tailings:	density :	1.085
	% H2O :	81.86

		Reference solutions								
		First stage	T0	T1	T7	T14	T21	T28	T35	T63
	Day		0	1	7	14	21	28	35	63
	Ref. Analysis	9357	9368	9390	9639	9922	10119	10457	10645	11454
Analysis										
pH		4.24	7.7	7.57	7.5	7.3	7.2	7.24	7.27	7.18
Eh	mV	279	177	159	216	130	206	236	216	205
Conductivity	mS/cm	10.1	4.93	4.9	5.25	5.28	5.29	5.98	5.96	6.19
Carbonate	mg/l		< 2						< 2	
Bicarbonate	mg/l		< 2						116	
Total alkalinity	mM/l	< 0.4	< 0.4		< 0,4		< 0,4		1.9	0.72
Al	mg/l	396	0.11		0.07		< 0,02		< 0,02	0.02
As total	mg/l	0.4	0.26	0.37	0.58	0.46	0.45	0.5	0.51	0.41
As (III)	mg/l	< 0.01	< 0.01		< 0,01		< 0,009		< 0,011	< 0,008
Ba	mg/l		0.17						0.085	
Ca	mg/l	528	503		493.1		492		489	511
Cl	mg/l	91.6	84.3		83.6		81.6		81.5	87.4
Co	mg/l		0.04						0.03	
Cu	mg/l		0.05						0.04	
Fe total	mg/l	108	< 0.01	< 0.02	0.034	< 0,02	0.013	< 0,02	< 0,01	0.022
Fe (II)	mg/l	108	< 0.01		0.025		0.013		< 0,01	0.02
K	mg/l	503	404		317.4		301		290	281
Mg	mg/l	674	170		328		363		372	441
Mn	mg/l		0.51						0.07	
Mo	mg/l		0.08						0.22	
Na	mg/l	444	401		408.9		396		402	399
Ni	mg/l	530	0.03	0.21	0.31	0.34	0.44	0.59	0.76	1
[Ni]/[As]		1692.9	0.1	0.7	0.7	0.9	1.2	1.5	1.9	3.1
NH4+	mg/l		75						55.2	
NO3	mg/l	41.8	< 10		14.6		14.1		14.3	15.1
P	mg/l	0.06	0.05		0.14		0.22		0.28	
Pb	mg/l		< 0.03						0.05	
Ra 226	Bg/l		1193						367	
S 2-	mg/l	< 100	< 100		< 100		< 100		< 100	< 100
SO4 2-	mg/l	10900	3630		3740		3770		3840	4190
S total	mg/l	3708	1178		1200		1339		1309	1390
Si	mg/l	6.16	0.74		13.7		14.4		19.5	21.6
U	mg/l	52.78	0.07		< 0,05		< 0,05		< 0,05	0.06
Zn	mg/l		< 0.01						0.04	

Retention Time Test Data

Retention Time Test No.	7								
Objective :	Determine if significant increase in pH 3 RT improve Fe-As ppt.								
Conditions	Start			1 st stage			2 nd stage		Aging
	Fe+3/Fe tot	[Fe+3]/[As]	As+5/As tot	pH	° C	mn	pH	mn	method
	0.907	2.88	0.999	3	35	360	8	60	TVOP
Physical tailings:	density :	1.105							
	% H2O :	80.7							

		Reference solutions								
		First stage	T0	T1	T7	T14	T21	T28	T35	T63
	Day		0	1	7	14	21	28	35	63
	Ref. Analysis	9369	9391	9401	9667	9993	10208	10471	10646	11504
Analysis										
pH		3.43	7.77	7.64	7.71	7.5	7.53	7.41	7.52	7.48
Eh	mV	353	184	156	148	176	170	164	217	176
Conductivity	mS/cm	16.71	4.59	4.83	5.1	5.14	5.25	5.85	5.98	6.01
Carbonate	mg/l		< 2						8	
Bicarbonate	mg/l		< 2						153	
Total alkalinity	mM/l	< 0.4	< 0.4		2.41		1.52		2.75	1.57
Al	mg/l	3320	0.17		0.04		< 0,02		< 0,02	0.02
As total	mg/l	24.2	0.46	0.64	0.58	0.48	0.47	0.47	0.54	0.47
As (III)	mg/l		< 0,01		< 0,01		< 0,009		< 0,011	< 0,09
Ba	mg/l		0.231						0.098	
Ca	mg/l	589	525.8		518.8		501		511	526
Cl	mg/l	65.2	83.2		85.7		85.9		88.1	86.3
Co	mg/l		0.04						0.04	
Cu	mg/l		0.08						0.04	
Fe total	mg/l	578	< 0.01	< 0.02	< 0.01	< 0,02	< 0,01	< 0,02	< 0,042	< 0,01
Fe (II)	mg/l	576	< 0.01		< 0.01		< 0,01		< 0,042	< 0,01
K	mg/l	555	362.5		324.1		300		290	274
Mg	mg/l	706	102.5		290.9		343		351	403
Mn	mg/l		0.34						0.07	
Mo	mg/l		0.21						0.6	
Na	mg/l	469	391.6		395.1		394		385	401
Ni	mg/l	657	0.08	0.21	0.29	0.43	0.47	0.62	0.86	0.8
[Ni]/[As]		34.7	0.2	0.4	0.6	1.1	1.3	1.7	2.0	2.2
NH4+	mg/l		73	73					55.9	
NO3	mg/l	25.3	13.8		14.5		17		15.3	14.3
P	mg/l	8.63	0.05		0.08		0.17		0.31	
Pb	mg/l		< 0,03						0.05	
Ra 226	Bg/l		1494						506	
S 2-	mg/l	1480	< 100		< 100		< 100		< 100	< 100
SO4 2-	mg/l	26900	2890		3430		3700		3750	3820
S total	mg/l	10460	1002		1210		1186		1290	1310
Si	mg/l	76.2	1.53		9.55		13.9		18	19.9
U	mg/l	232.4	0.14		0.71		0.64		0.4	0.37
Zn	mg/l		< 0,01						0.04	

Retention Time Test Data

Retention Time Test No.	8
Objective :	Assess impact of incomplete As oxidation and long pH 4 RT

Conditions	Start			1 st stage			2 nd stage		Aging
	Fe+3/Fe tot	[Fe+3]/[As]	As+5/As tot	pH	° C	mn	pH	mn	method
	0.899	3.6	0.615	4	35	360	8	60	TVOP

Physical tailings:	density :	1.085
	% H2O :	81.92

		Reference solutions								
		First stage	T0	T1	T7	T14	T21	T28	T35	T63
	Day		0	1	7	14	21	28	35	63
	Ref. Analysis	9409	9558	9640	9889	10052	10437	10618	10692	11584
Analysis										
pH		4.18	7.72	7.65	7.4	7.47	7.29	7.28	7.28	7.21
Eh	mV	257	293	197	230	377	318	298	300	201
Conductivity	mS/cm	10.38	4.5	4.77	4.84	4.95	5.57	5.64	5.76	5.82
Carbonate	mg/l		< 2						< 2	
Bicarbonate	mg/l		< 2						136	
Total alkalinity	mM/l	5.04	< 0,4		< 0,4		1.09		2.02	
Al	mg/l	567	0.22		0.06		0.02		< 0,02	< 0,4
As total	mg/l	36.2	0.83	1.54	0.82	0.61	0.55	0.52	0.6	0.56
As (III)	mg/l	< 0,7	< 0,02		< 0,016		< 0,011		< 0,012	< 0,011
Ba	mg/l		0.153						0.077	
Ca	mg/l	539.3	512.3		513.5		511		511	521
Cl	mg/l	91.8	82.7		82.5		82.3		85.4	78.9
Co	mg/l		0.05						0.62	
Cu	mg/l		0.07						0.18	
Fe total	mg/l	136	0.028	< 0.02	< 0,01	< 0,02	0.015	< 0,02	< 0,01	0.156
Fe (II)	mg/l	136	0.026		< 0,01		0.015		< 0,01	0.014
K	mg/l	476.1	403.3		310.2		290		305	280
Mg	mg/l	688.8	137.4		302		357		378	412
Mn	mg/l		0.47						4.36	
Mo	mg/l		0.1						0.23	
Na	mg/l	319.7	319.8		291.4		333		305	316
Ni	mg/l	583.2	0.06	0.18	0.31	0.37	0.32	0.56	0.55	0.89
[Ni]/[As]		20.6	0.1	0.1	0.5	0.8	0.7	1.4	1.2	2.0
NH4+	mg/l		58.4						56.2	
NO3	mg/l	25.6	14.9		14.5		18.5		14.6	14.2
P	mg/l	< 0,5	0.04		0.12		0.21		0.32	0.08
Pb	mg/l		< 0,03						0.06	
Ra 226	Bg/l		1033						274	
S 2-	mg/l	< 100	< 100		< 100		< 100		< 110	< 100
SO4 2-	mg/l	12000	3340		3350		3600		3630	3770
S total	mg/l	3880	960		1150		1224		1325	1270
Si	mg/l	10.14	0.71		10.5		13.2		17.2	20.3
U	mg/l	56.4	0.05		0.06		0.25		0.05	< 0,05
Zn	mg/l		0.01						0.04	

FIGURES AND TABLES

Table A1 summarizes the verification calculations for lead adsorption on hydrous ferric oxide (HFO) at concentrations of 1, 10, 20, 100 and 300 mg/L (ppm) total lead. The solution composition was defined at 400 mg/L calcium, 230 mg/L sodium, 243 mg/L magnesium and 2400 mg/L sulfate. The pH was adjusted with $Ca(OH)_2$. To further simplify the calculations, only one type of adsorption site was used. Adsorption site concentrations were set at $1x10^{-3}$ moles/L of weak sites (Hfo-wOH) sites. Strong sites[1] were not included. For each calculation, the pH was fixed at 5.0, 6.0 or 7.0. The calculations were performed at a series of different solution/sorbent ratios. The initial volume of water was 1.0 liter, additional solution, without lead, was added to produce final volumes of 1.2, 1.4, 1.6, 1.8, 2.0, 3.0, 4.0 and 5.0 liters. In the PHREEQC models, the solution is added using the MIX keyword, this keyword mixes two or more solutions.

TABLE A1: Verification of EPICS Procedure-Lead Sorption Models

Initial Lead Concentration (mg/L)	pH	Kd_h^{exc}	Fs	EPICS Sites (molal)	PHREEQC Sites (molal)	Total Exchangeable Lead (molal)		Percentage Agreement
						EPICS	PHREEQC	
1.0	5.0	0.08	0.047	2.34×10^{-7}	2.34×10^{-7}	4.84×10^{-6}	4.84×10^{-6}	100
	6.0	8.2	0.08	3.92×10^{-6}	3.91×10^{-6}	4.89×10^{-6}	4.84×10^{-6}	101
	7.0	9980	0.997	4.83×10^{-6}	4.82×10^{-6}	4.85×10^{-6}	4.84×10^{-6}	100
10.0	5.0	0.085	0.048	2.33×10^{-6}	2.33×10^{-6}	4.84×10^{-5}	4.84×10^{-5}	100
	6.0	7.29	0.79	3.84×10^{-5}	3.87×10^{-5}	4.81×10^{-5}	4.84×10^{-5}	99.3
	7.0	975	0.996	4.82×10^{-5}	4.82×10^{-5}	4.85×10^{-5}	4.84×10^{-5}	100
20.0	5.0	0.084	0.048	4.64×10^{-6}	4.64×10^{-6}	9.68×10^{-5}	9.68×10^{-5}	100
	6.0	6.4	0.77	7.46×10^{-5}	7.63×10^{-5}	9.51×10^{-5}	9.68×10^{-5}	98.2
	7.0	63	0.995	9.64×10^{-5}	9.63×10^{-5}	9.69×10^{-5}	9.68×10^{-5}	100
100	5.0	0.08	0.045	2.2×10^{-5}	2.3×10^{-5}	4.84×10^{-4}	4.84×10^{-4}	99.9
	6.0	2.0	0.518	2.5×10^{-4}	3.3×10^{-4}	4.08×10^{-4}	4.84×10^{-4}	84.4
	7.0	27.7	0.934	4.52×10^{-4}	4.74×10^{-4}	4.61×10^{-4}	4.84×10^{-4}	95.4
300	5.0	0.074	0.042	6.1×10^{-5}	6.33×10^{-5}	1.45×10^{-3}	1.45×10^{-3}	100
	6.0	0.26	0.108	1.57×10^{-4}	5.56×10^{-4}	1.05×10^{-3}	1.45×10^{-3}	72.6
	7.0	0.07	0.03	4.71×10^{-5}	7.2×10^{-4}	7.80×10^{-4}	1.45×10^{-3}	53.7

The increase in volume as the solutions are added together is included as part of the MIX keyword calculations. Therefore, the program is ideally suited to verifying the EPICS method.

[1] Dzombak and Morel (1990), reference 6.16, define two different types of surface sites in the diffuse layer model for hydrous ferric oxide. The two site types are needed to model cation adsorption only. The high affinity or strong sites typically enhance cation surface complexation at low pH. The strong sites are fewer in number than the low affinity or weak sites. Typically, the strong sites represent approximately 2.5 percent of the total sites. Because these simulations were designed to verify the calculational methods, a more detailed surface ionization and complexation model was not required.

Comparison of the calculated site concentrations and the model concentrations indicates that the two values are in close agreement. The data summarized in Table A1 demonstrate that the best agreement between calculated exchangeable lead and the model input amounts were at pH values of 5.0. The agreement between the EPICS calculated and PHREEQC model amounts of lead verifies that the calculation method is correct.

Increases in pH produce an increased value for K_d^{exch} and generally poorer agreement between the calculated and input lead values. The pH 7.0 data is particularly troubling with percentage agreement values as low as 53.7 percent. It is believed that changes in surface potential as the composition of the solution changes are responsible for the decrease in agreement. The SIC model calculations for lead suggest that the EPICS calculation method works best if the sorbed fraction is approximately 50 percent of the total lead in the system.

Calculations for Arsenic

Table A2 summarizes a series of PHREEQC model calculations using arsenic that were run at different initial Fe/As ratios and different final pH values. The model conditions have been previously described in the main portion of this report.

TABLE A2: Verification of EPICS Procedure-Arsenic Sorption Models

Arsenic Concentration (mg/L)	Fe/As Mole ratio	pH	Kd^{exch}	Fs	Calculated Sites (molal)	PHREEQC Sites (molal)	Total Exchangeable Arsenic (molal)		% Agreement
							EPICS	PHREEQC	
0.8	2.6	6.5	1.1×10^{1}	8.1×10^{-1}	9.0×10^{-6}	1.1×10^{-5}	9.25×10^{-6}	1.1×10^{-5}	83.5
12.4	2.6	7.0	9.0×10^{-2}	3.8×10^{-2}	6.3×10^{-6}	1.36×10^{-4}	3.57×10^{-5}	1.66×10^{-4}	21.5
193	2.6	7.5	9.0×10^{-3}	4.6×10^{-3}	1.18×10^{-5}	2.56×10^{-4}	2.33×10^{-3}	2.58×10^{-3}	90.5
167	2.6	8.0	1.2×10^{-2}	7.08×10^{-3}	1.58×10^{-5}	2.67×10^{-4}	1.98×10^{-3}	2.23×10^{-3}	88.7
157	2.6	9.0	1.6×10^{-2}	8.58×10^{-3}	1.79×10^{-5}	2.72×10^{-4}	1.84×10^{-3}	2.09×10^{-3}	87.9
160	2.6	10.0	1.4×10^{-2}	7.47×10^{-3}	1.60×10^{-5}	2.63×10^{-4}	1.89×10^{-3}	2.14×10^{-3}	88.4
12.1	5	7	6.0×10^{-1}	1.69×10^{-1}	2.72×10^{-5}	1.60×10^{-4}	2.82×10^{-5}	1.61×10^{-4}	17.5
166	5	8	-2.5×10^{-2}	-1.95×10^{-2}	-4.34×10^{-5}	8.65×10^{-5}	1.31×10^{-3}	2.22×10^{-3}	59.1
157	5	9	7.88×10^{-2}	3.97×10^{-2}	8.30×10^{-5}	9.66×10^{-4}	1.21×10^{-3}	2.09×10^{-3}	57.7

Table A3 Mineral Content of TOVP Aging Test Samples

Aging Time	Initial	Aged @ 4 °C				Aged @ 20 °C				Aged @ 50 °C			
		1M	2M	6M	10M	1M	2M	6M	10M	1M	2M	6M	10M
Mineral Content (wt. %):													54.16
Quartz	53.22	54.00	54.30	53.92	54.37	53.24	53.33	56.31	54.35	56.02	54.22	52.17	14.28
Illite-Sericitic	15.38	15.12	14.70	14.92	16.26	15.01	15.24	14.83	14.26	13.78	14.64	15.49	10.56
Kaolinite	10.55	12.26	12.66	10.87	7.10	12.28	12.66	7.50	10.06	10.18	12.45	10.83	5.55
Chlorite-Mg	5.21	5.42	5.43	5.33	5.27	5.34	5.51	5.14	5.65	5.60	5.38	5.25	0.44
Rutite	0.47	0.44	0.44	0.46	0.45	0.46	0.46	0.45	0.45	0.45	0.46	0.46	7.22
Gypsum	7.62	7.55	6.84	7.35	7.25	7.59	7.20	6.78	7.18	6.73	7.13	8.14	2.06
Geothite	2.49	2.14	1.95	2.30	2.42	2.43	2.29	2.40	2.06	1.96	2.06	2.69	2.48
Hydrobasaluminite	1.42			1.20	4.07			3.25	2.93	2.06		1.94	1.06
Annabergite	1.11	1.01	1.01	1.14	1.06	1.37	1.04	1.04	1.03	1.00	1.04	1.13	0.94
Scorodite	0.97	0.94	1.30	1.02	0.93	0.74	0.90	0.91	0.88	0.86	0.86	0.94	0.30
Stregthite	0.27	0.27	0.22	0.27	0.29	0.15	0.00	0.27	0.27	0.25	0.27	0.15	0.95
Jarosite	1.22	0.81	1.08	1.15	0.47	1.33	1.33	1.07	0.87	0.99	1.42	0.78	
Total	99.93	99.96	99.93	99.93	99.94	99.94	99.96	99.95	99.99	99.88	99.93	99.97	100.00

Table A4: Mineral Content of TOVP Aging Test Samples (Gypsum Removed)

Aging Time	Initial	Aged @ 4 °C				Aged @ 20 °C				Aged @ 50 °C			
		1M	2M	6M	10M	1M	2M	6M	10M	1M	2M	6M	10M
Mineral Content (wt. %):													
Quartz	59.42	59.39	57.53	56.78	57.49	56.66	57.31	54.69	57.77	57.52	57.44	57.49	55.59
Illite-Sericitic	15.54	17.34	16.08	16.84	17.23	16.11	15.68	17.10	17.04	16.84	17.20	17.88	15.57
Kaolinite	13.98	10.92	12.42	14.00	13.09	13.03	13.47	15.71	11.20	11.96	11.80	11.80	12.60
Chlorite-Mg	6.16	5.80	5.82	5.40	5.46	5.66	5.86	5.67	5.33	5.76	6.11	5.49	5.30
Rutite	0.47	0.48	0.46	0.67	0.51	0.49	0.47	0.52	0.47	0.48	0.48	0.49	0.47
Gypsum	0.18	0.18	0.20	0.15	0.23	0.17	0.18	0.26	0.29	0.30	0.29	0.29	0.35
Geothite	2.70	2.58	2.42	3.04	2.50	2.51	2.57	3.10	2.71	2.64	2.54	2.94	2.18
Hydrobasaluminite		0.67			0.02				1.19			1.16	
Annabergite	0.73	0.79	0.75	1.10	0.92	0.85	0.82	0.95	0.88	0.76	0.82	0.79	0.87
Scorodite	0.88	0.90	0.83	0.75	1.09	0.86	0.87	0.96	0.91	0.78	0.68	1.21	1.66
Stregthite	0.25	0.25	0.23	0.28	0.30	0.27	0.25	0.35	0.30	0.25	0.28	0.30	0.30
Jarosite	0.66	0.06	0.74	0.77	0.94	1.07	0.77	0.56	0.42	0.25	0.71		0.80
Sodium Chloride		0.48	2.24	0.13	0.21	2.09	1.58	0.07	1.29	0.18	1.48		3.78
Total	99.97	99.84	99.72	99.91	99.99	99.77	99.83	99.94	99.80	99.92	99.83	99.84	99.47

Table A.1
Chemical Analyses of Set 1 Solutions at Final pH Values

Analyte	Raffinate (mg/L)[1]	1-1		1-2		1-3		1-4		1-5	
		(mg/L)[1]	(% prec.)	(mg/L)[1]	(% prec.)	(mg/L)[1]	(% prec.)	(mg/L)[1]	(% prec.)	(mg/L)[1]	(% prec.)
pH	1.50	2.18	--	3.15	--	4.04	--	6.09	--	7.38	--
pe[2]	11.88	10.63	--	10.45	--	8.46	--	2.48	--	0.75	--
Al	420	410	2.4	460	(9.5)	290	31.0	0.50	99.9	0.50	99.9
As	732	150	79.5	6.70	99.1	0.54	99.9	0.08	100.0	0.06	100.0
Ca	760	760	--	680	--	620	--	610	--	650	--
Fe	2,400	1,600	33.3	730	69.6	570	76.3	340	85.8	2.2	99.9
K	210	200	5.0	210	0.0	200	5.0	200	5.0	200	5.0
Mg	260	270	(3.9)	290	(11.5)	280	(7.7)	270	(3.9)	240	7.7
Na	48	62	(29.2)	52	(8.3)	50	(4.2)	42	14.3	42	14.3
Ni	560	500	10.7	460	17.9	450	19.6	250	55.4	5.3	99.1
Si	260	280	(7.7)	270	(3.9)	140	46.2	17	93.5	3.2	98.8
Cl	14	13	7.1	17	(21.4)	11	21.4	16	(14.3)	18	(28.6)
SO4	14,100	10,200	27.7	7,400	47.5	6,100	56.7	3,800	73.1	2,800	80.1
Alkalinity[3]	<0.5	<0.5	--	<0.5	--	<0.5	--	<0.5	--	4.0	--

1. Except for pH and pe.
2. Values of pe determined through geochemical modelling.
3. Alkalinity below detection (<0.5mg/L) except for 1-5.

Table A.2
Chemical Analyses of Set 2 Solutions at Final pH Values

Analyte	Raffinate (mg/L)[1]	2-1		2-2		2-3		2-4		2-5		2-6		2-7	
		(mg/L)[1]	(% prec.)	(mg/L)[1]	(% prec.)	(mg/L)[1]	(% prec.)	(mg/L)[1]	(% prec.)	(% prec.)	(% prec.)	(mg/L)[1]	(% prec.)	(mg/L)[1]	(% prec.)
pH	1.50	2.01	--	3.03	--	4.06	--	6.37	--	6.37	--	7.08	--	8.01	--
pe[2]	11.88	10.71	--	10.48	--	8.55	--	1.92	--	1.92	--	0.81	--	0.67	--
Al	420	410	2.4	470	(11.9)	380	9.5	13	96.9	0.5	99.9	0.5	99.9	0.5	99.9
As	732	170	76.8	16	97.8	0.35	99.9	0.15	100.0	0.08	100.0	0.07	100.0	0.21	100.0
Ca	760	720	5.3	680	10.5	640	15.8	570	25.0	540	29.0	520	31.6	570	25.0
Fe	2,400	1,600	33.3	850	64.6	570	76.3	450	81.3	300	87.5	29	98.8	0.07	100.0
K	210	230	(8.7)	280	(33.3)	300	(42.9)	300	(42.9)	310	(47.6)	300	(42.9)	300	(42.9)
Mg	260	260	0.0	280	(7.7)	290	(11.5)	280	(7.7)	280	(7.7)	250	3.9	220	15.4
Na	48	1,700	--	3,300	--	4,300	--	5,400	--	6,300	--	6,800	--	7,100	--
Ni	560	500	10.7	500	10.7	470	16.1	430	23.2	280	50.0	48	91.4	2	99.6
Si	260	260	0.0	270	(3.9)	140	46.2	54	79.2	13	95.0	5.8	97.8	1.7	99.4
Cl	14	17	(21.4)	19	(35.7)	15	(7.1)	17	(21.4)	14	0.0	18	(28.6)	20	(42.9)
SO4	14,100	14,000	0.7	13,300	6.0	13,100	7.1	13,000	7.8	13,200	6.4	13,400	5.0	13,900	1.4
Alkalinity[3]	<0.5	<0.5	--	<0.5	--	<0.5	--	<0.5	--	<0.5	--	<0.5	--	17	--

1. Except for pH and pe.
2. Values of pe determined through geochemical modelling.
3. Alkalinity below detection (<0.5mg/L) except for 2-7.

Table A.3
Chemical Analyses of Set 3 Solutions at Final pH Values

Analyte	Raffinate (mg/L)[1]	3-1		3-2		3-3		3-4		3-5	
		(mg/L)[1]	(% prec.)	(mg/L)[1]	(% prec.)	(mg/L)[1]	(% prec.)	(mg/L)[1]	(% prec.)	(mg/L)[1]	(% prec.)
pH	1.50	2.33	--	3.11	--	4.15	--	6.03	--	7.05	--
Al	420	430	2.4	530	(26.2)	320	23.8	2	99.5	0.5	99.9
As	732	180	75.4	22.8	96.9	1.1	99.9	0.16	100.0	0.06	100.0
Ca	760	650	--	690	--	510	--	510	--	550	--
Fe	2,400	1,500	37.5	910	62.1	610	74.6	380	84.2	57	97.7
K	210	220	(4.8)	240	(14.3)	160	23.8	150	28.6	140	33.3
Mg	260	280	(7.7)	330	(26.9)	260	0.0	250	3.9	220	15.4
Na	48	78	(37.5)	61	(27.1)	46	4.2	35	27.1	37	22.9
Ni	560	470	16.1	480	14.3	440	21.4	320	42.9	56	90.0
Si	260	290	(11.5)	290	(11.5)	170	34.6	31	88.1	6.6	97.5
Cl	14	20	(42.9)	22	(57.1)	13	7.1	15	(7.1)	17	(21.4)
SO4	14,100	10,600	24.8	8,000	43.3	6,500	53.9	3,900	72.3	2,700	80.9
Alkalinity[2]	<0.5	<0.5	--	<0.5	--	<0.5	--	<0.5	--	<0.5	--

1. Except for pH.
2. Alkalinity below detection (<0.5mg/L).

Table A.4
Chemical Analyses of Set 4 Solutions at Final pH Values

Analyte	Raffinate (mg/L)[1]	4-1		4-2		4-3		4-4		4-5	
		(mg/L)[1]	(% prec.)	(mg/L)[1]	(% prec.)	(mg/L)[1]	(% prec.)	(mg/L)[1]	(% prec.)	(mg/L)[1]	(% prec.)
pH	1.50	2.08	--	3.06	--	4.10	--	5.89	--	7.29	--
Al	420	420	0.0	420	0.0	320	23.8	0.5	99.9	0.5	99.9
As	732	160	78.1	9.7	98.7	0.77	99.9	0.10	100.0	0.09	100.0
Ca	760	730	4.0	650	14.5	630	17.1	550	27.6	540	29.0
Fe	2,400	1,500	37.5	770	67.9	580	75.8	340	85.8	5.1	99.8
K	210	220	(4.8)	230	(9.5)	240	(14.3)	240	(14.3)	240	(14.3)
Mg	260	270	(3.9)	260	0.0	260	0.0	250	3.9	210	19.2
Na	48	1,600	--	2,800	--	3,600	--	5,200	--	6,200	--
Ni	560	490	12.5	460	17.9	460	17.9	360	35.7	14.8	97.4
Si	260	260	0.0	250	3.9	140	46.2	22	91.5	5.3	98.0
Cl	14	14	0.0	15	(7.1)	18	(28.6)	12	14.3	18	(28.6)
SO4	14,100	14,000	0.7	13,500	4.3	13,600	3.6	13,400	5.0	14,000	0.7
Alkalinity[2]	<0.5	<0.5	--	<0.5	--	<0.5	--	<0.5	--	10.0	--

3. Except for pH.
4. Alkalinity below detection (<0.5mg/L) except for 4-5.

Figure A.1: Set 1-2, Terminal pH 3.15, Electron Backscatter Image

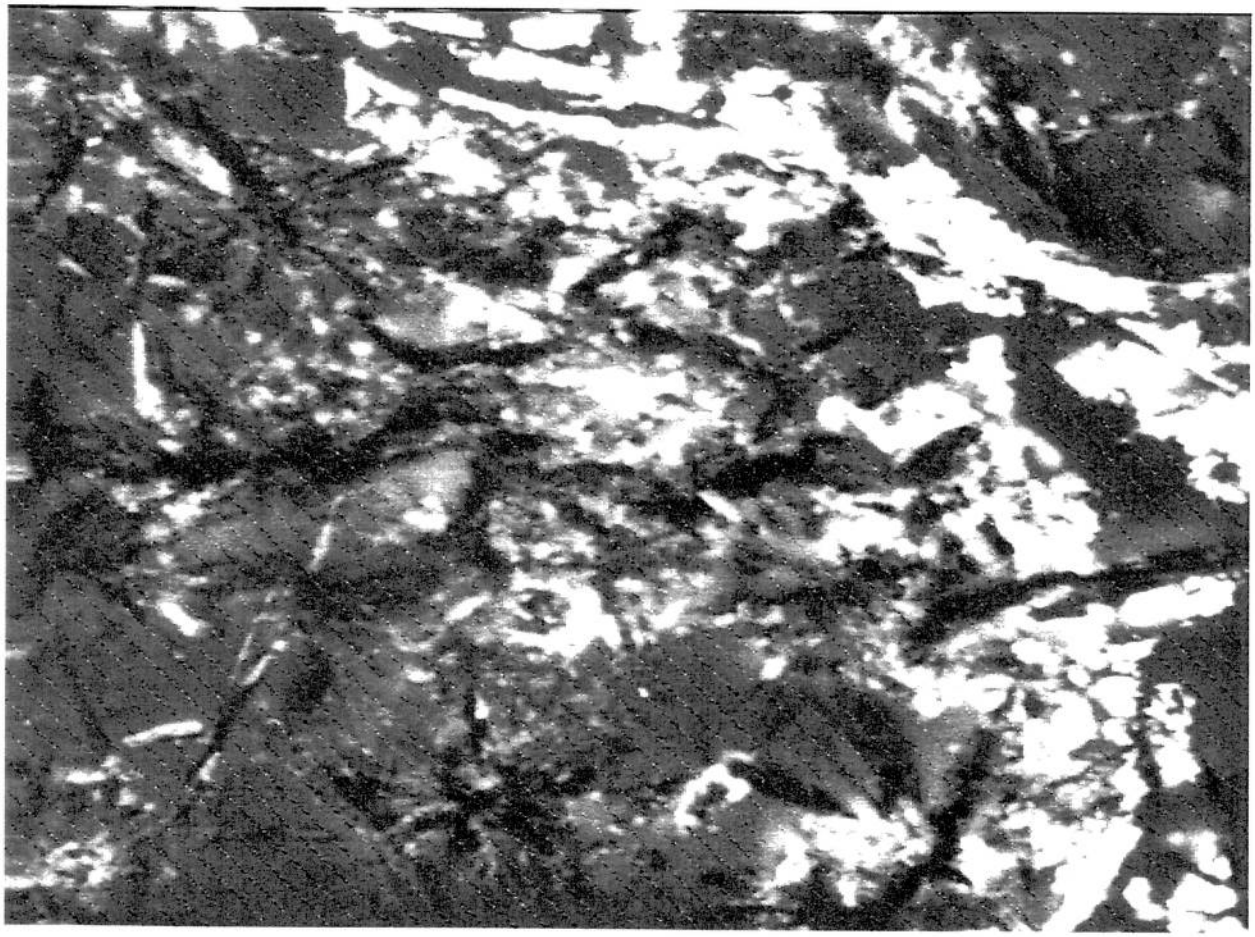

Figure A.1: Set 1-2, Terminal pH 3.15, Elemental Scan for Fe

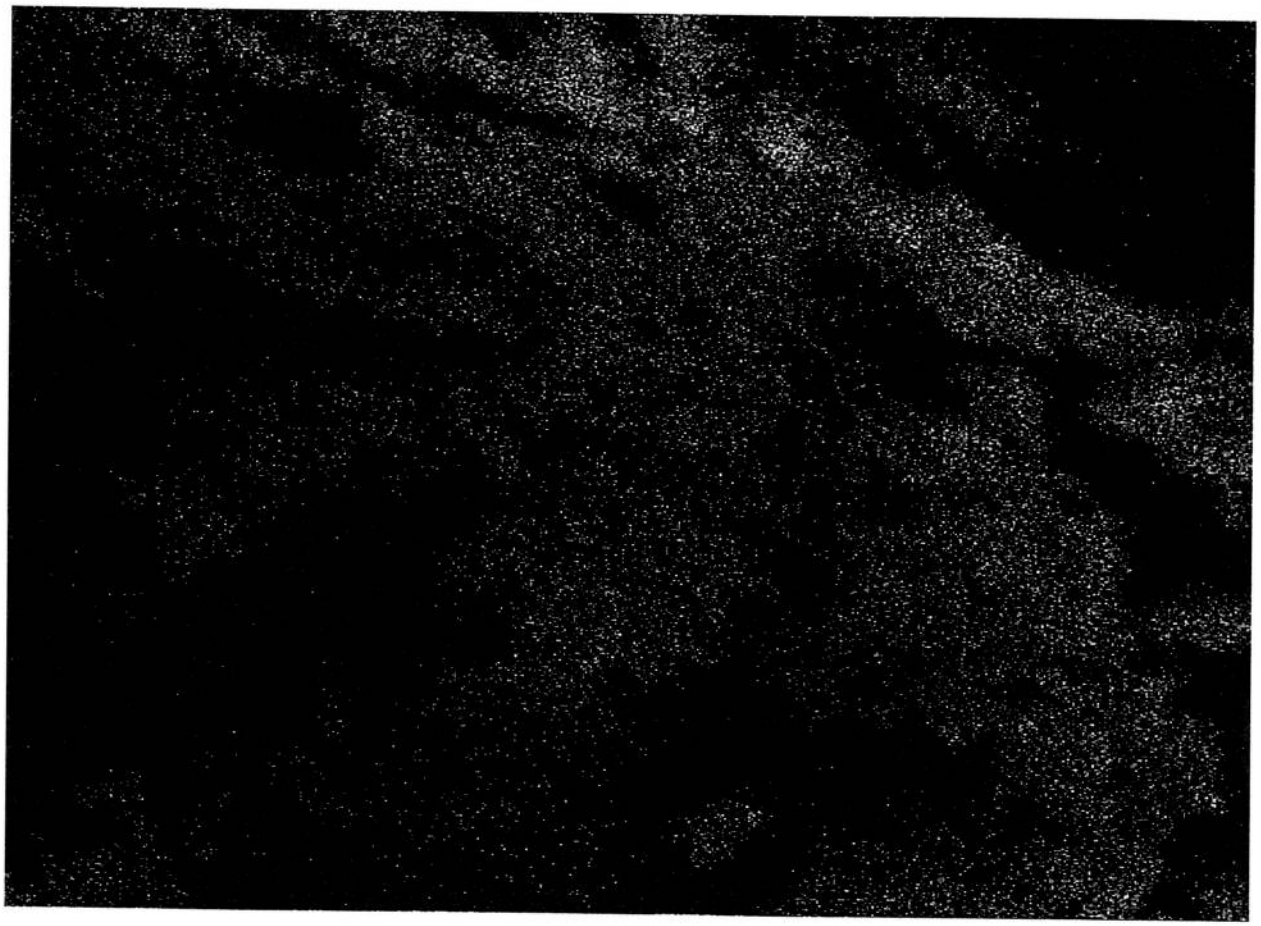

Figure A.1: Set 1-2, Terminal pH 3.15, Elemental Scan for As

Figure A.1: Set 1-2, Terminal pH 3.15, Elemental Scan for Ni

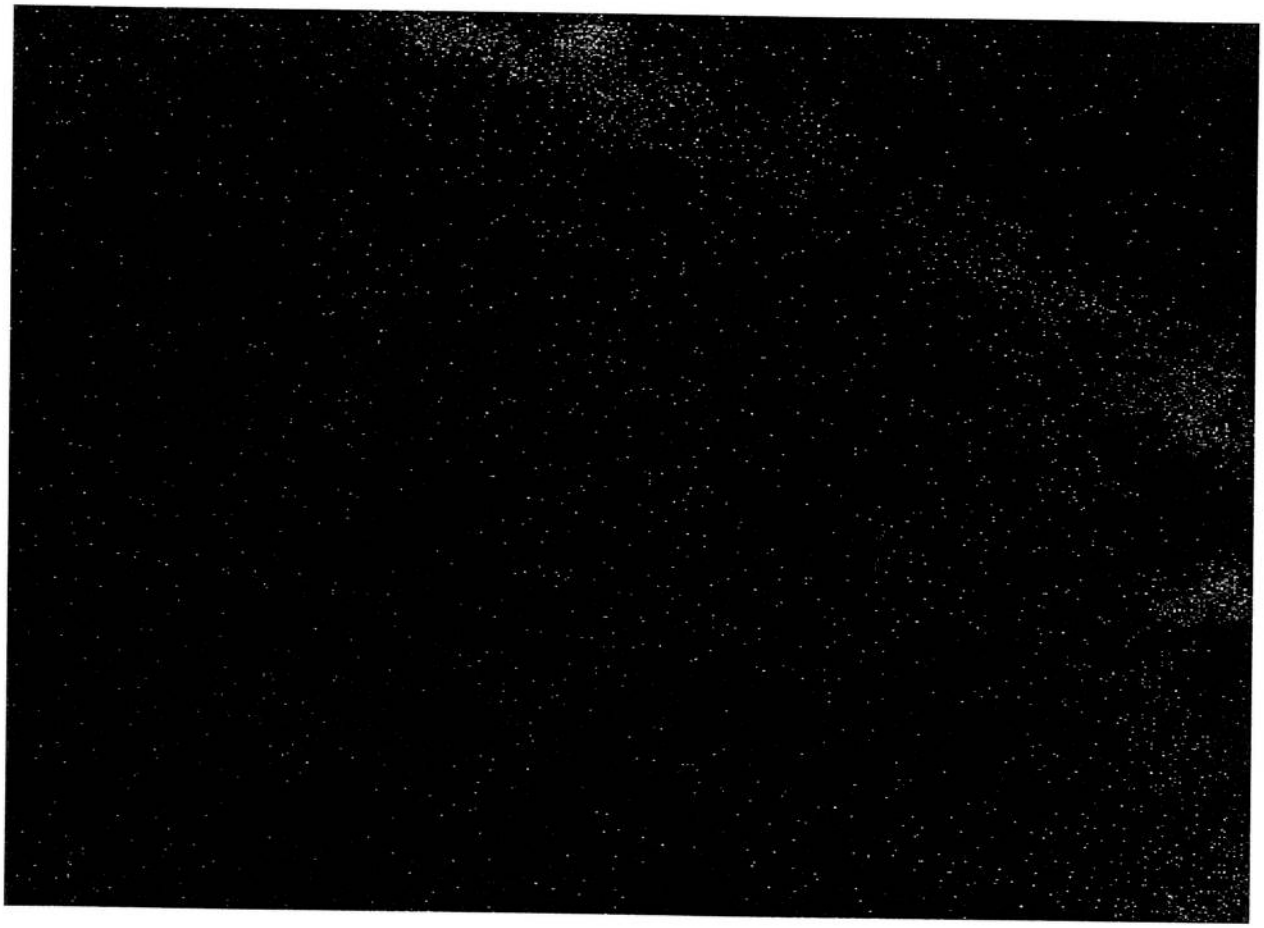

Figure A.1: Set 1-2, Terminal pH 3.15, Elemental Scan for Ca

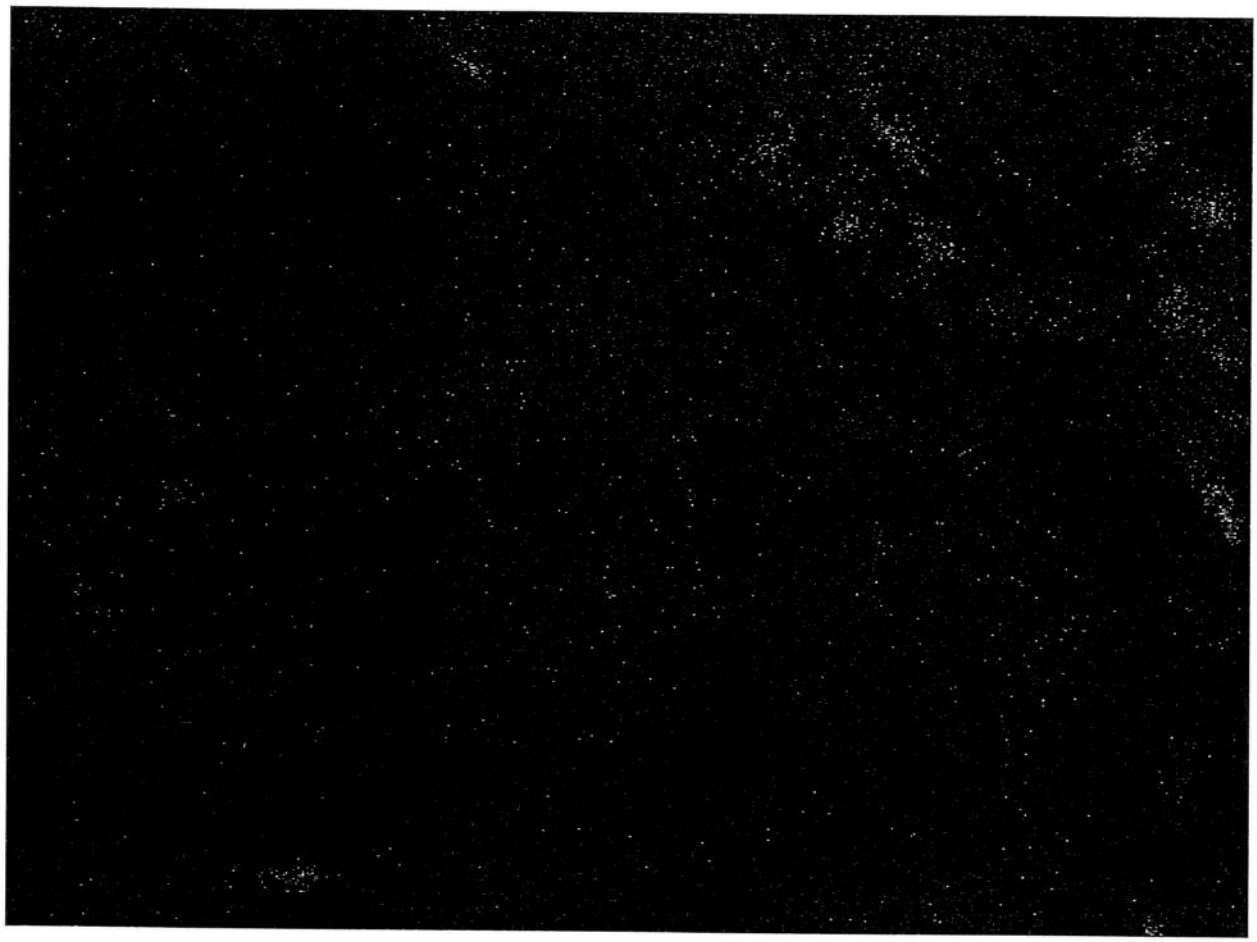

Figure A.1: Set 1-2, Terminal pH 3.15, Elemental Scan for S

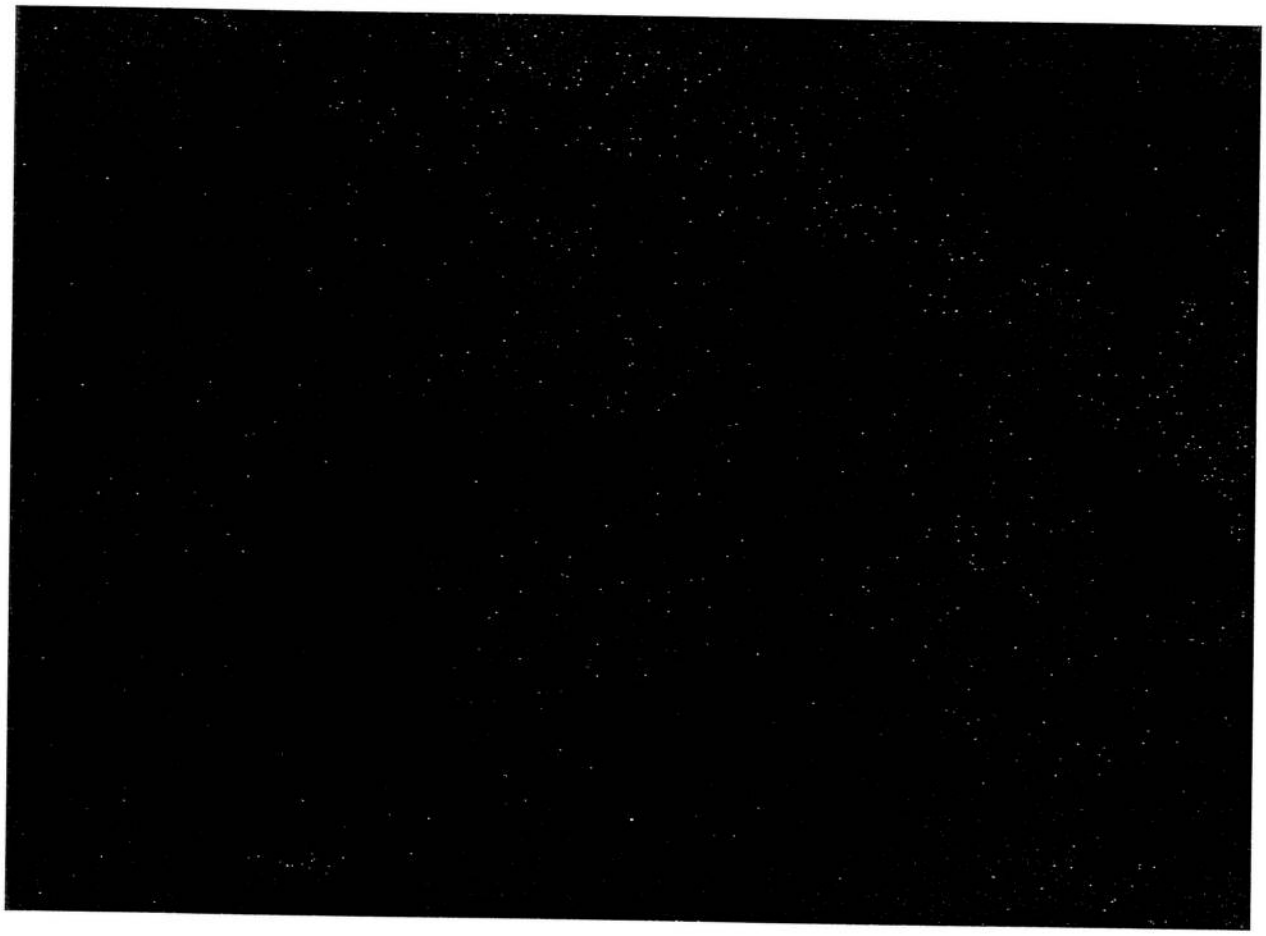

Figure A.1: Set 1-2, Terminal pH 3.15, Elemental Scan for Al

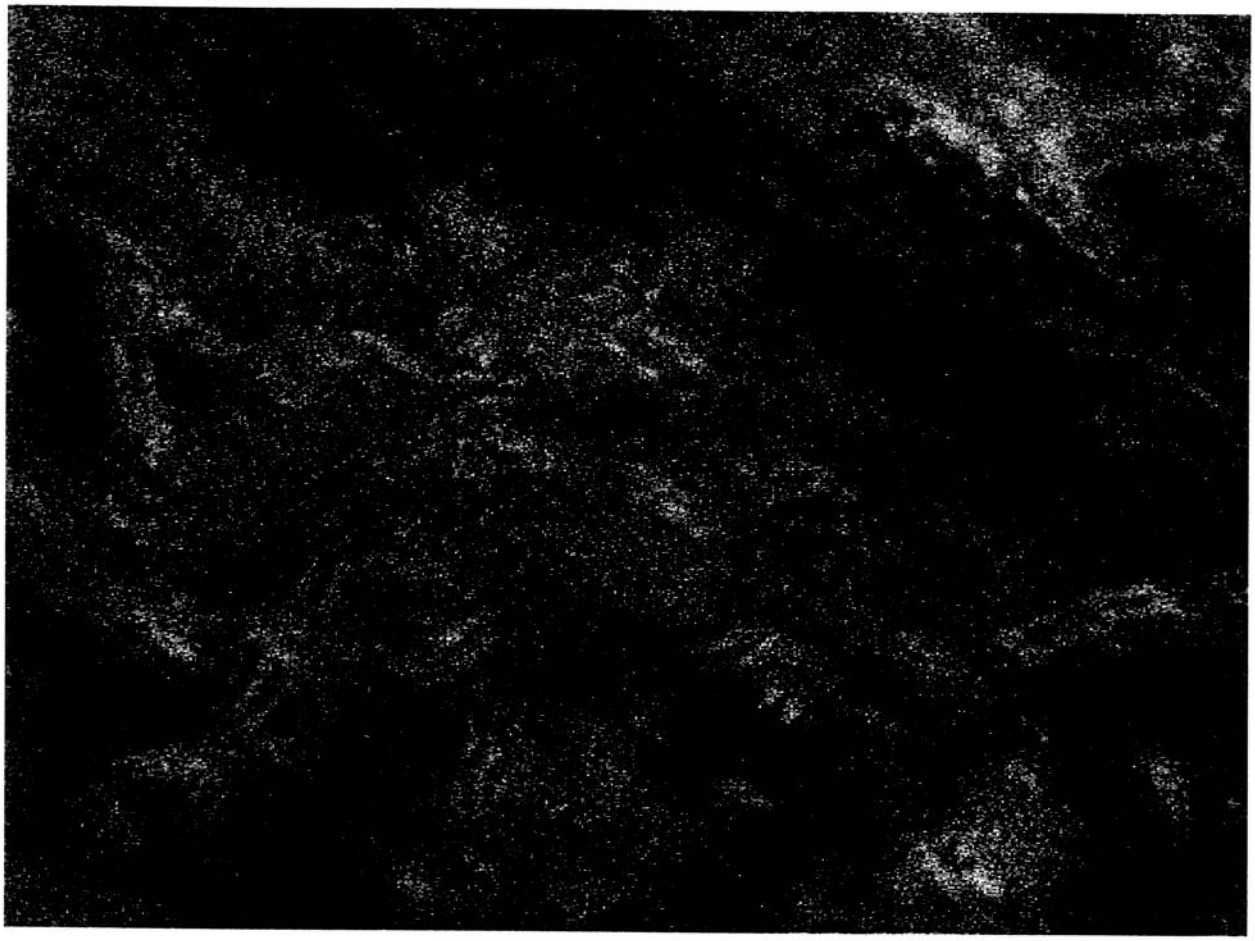

Figure A.2: Set 1-3, Terminal pH 4.04, Electron Backscatter Image

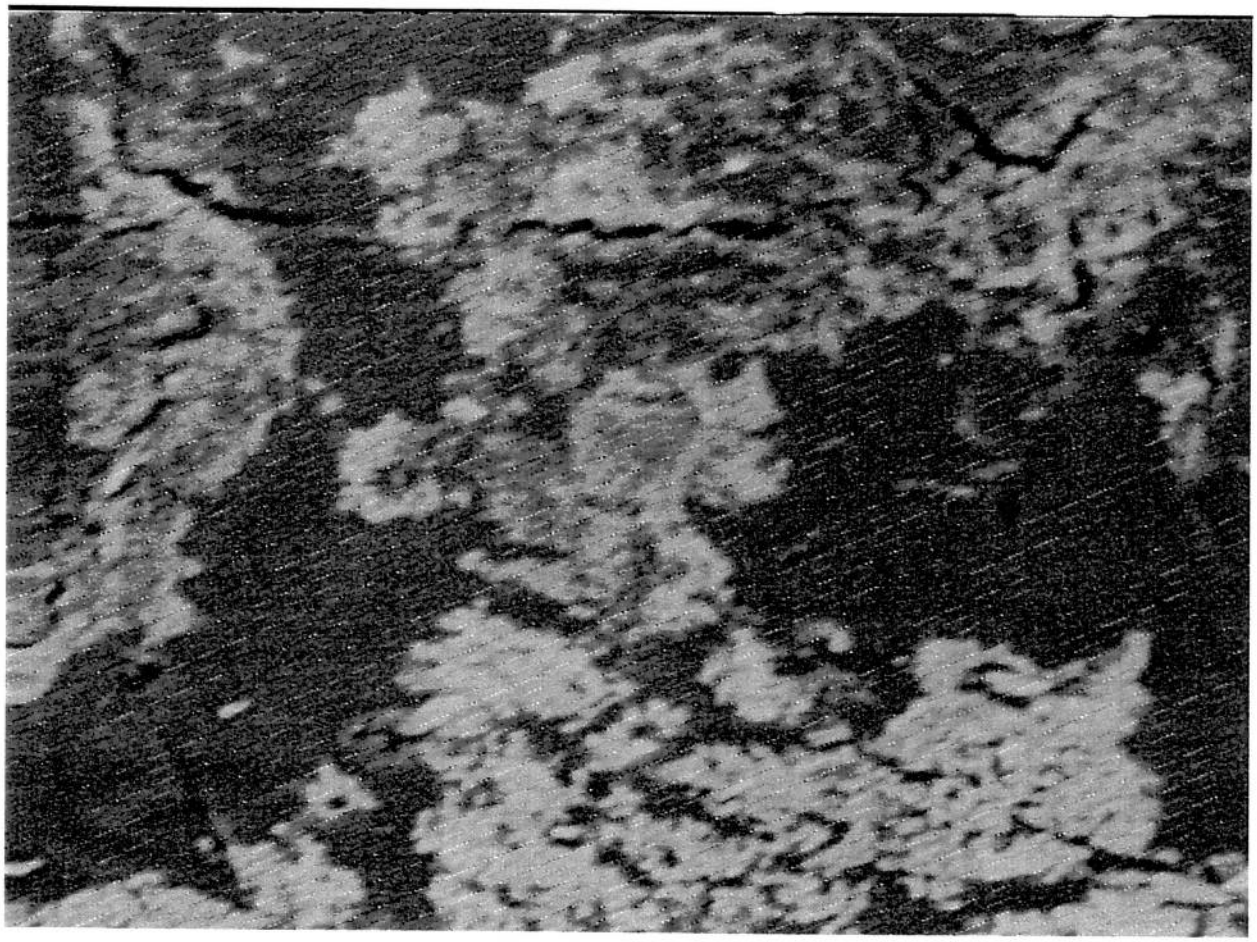

Figure A.2: Set 1-3, Terminal pH 4.04, Elemental Scan for Fe

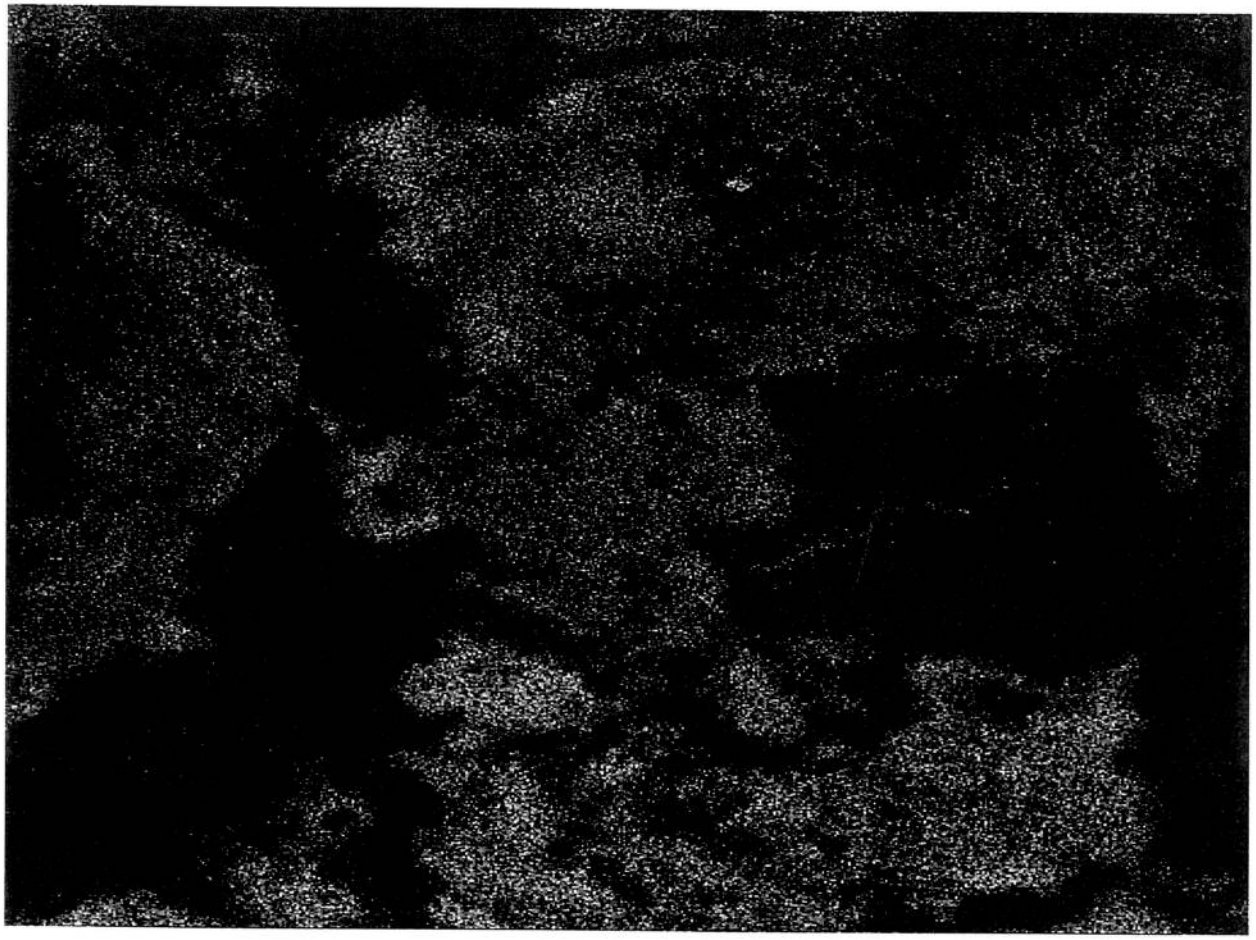

Figure A.2: Set 1-3, Terminal pH 4.04, Elemental Scan for As

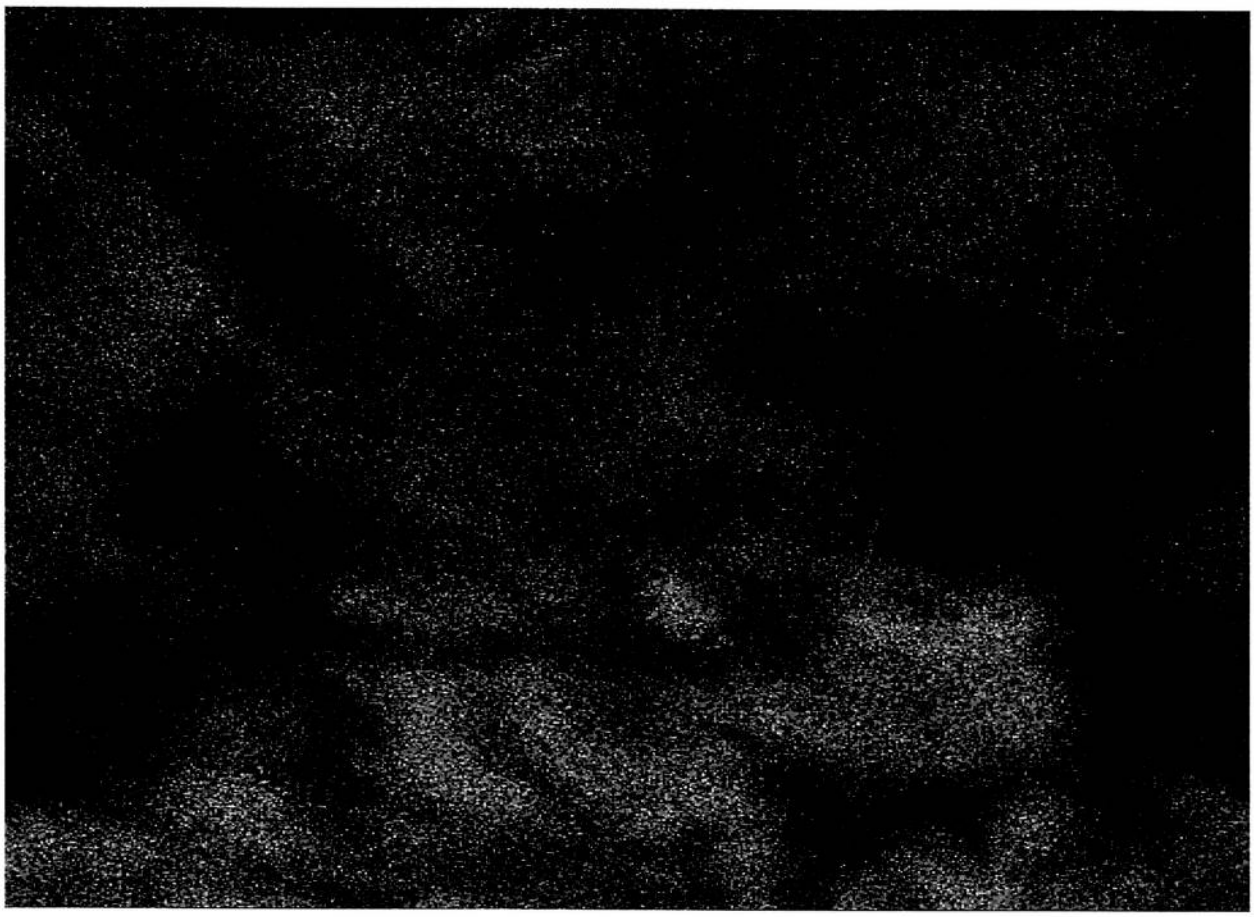

Figure A.2: Set 1-3, Terminal pH 4.04, Elemental Scan for Ni

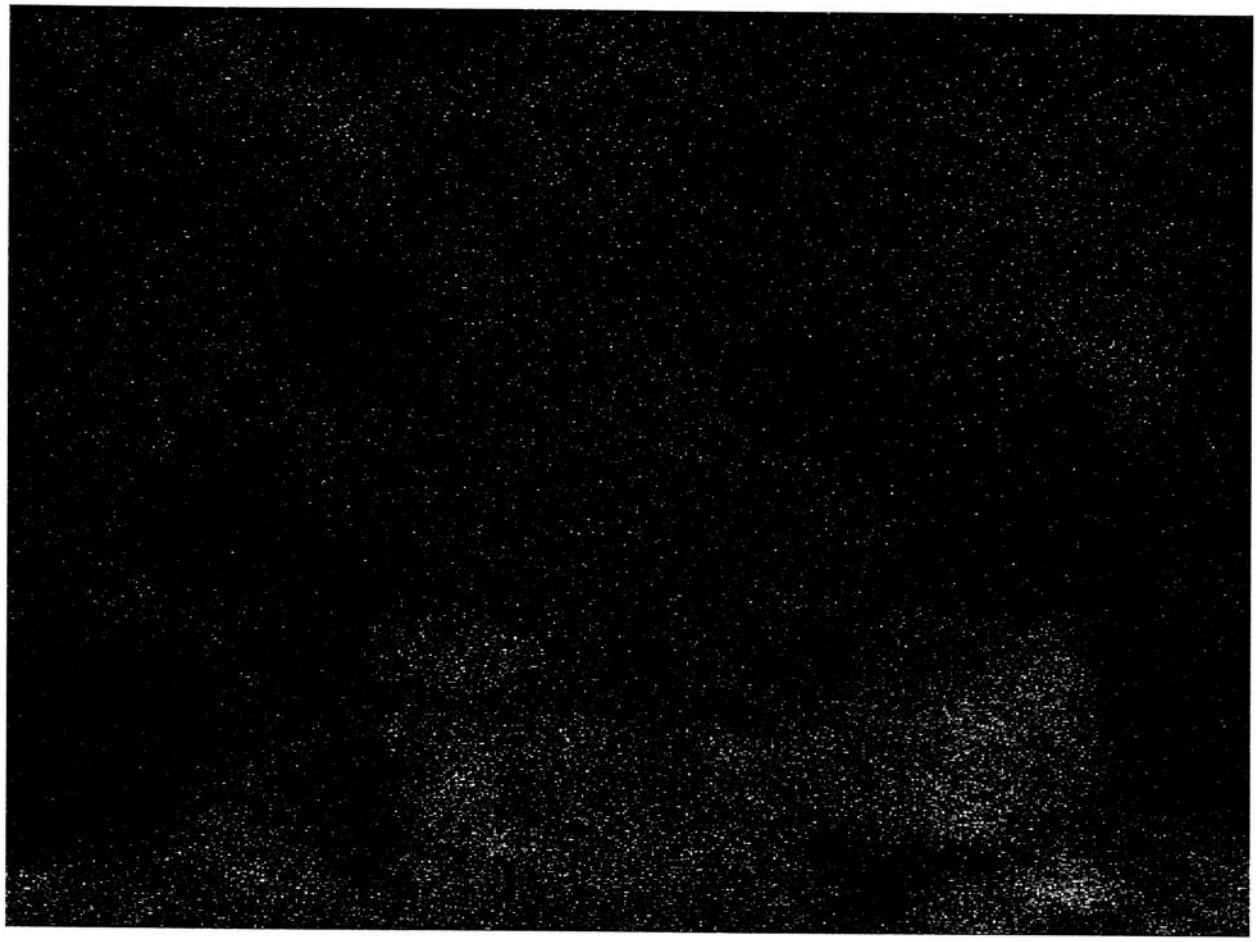

Figure A.2: Set 1-3, Terminal pH 4.04, Elemental Scan for Ca

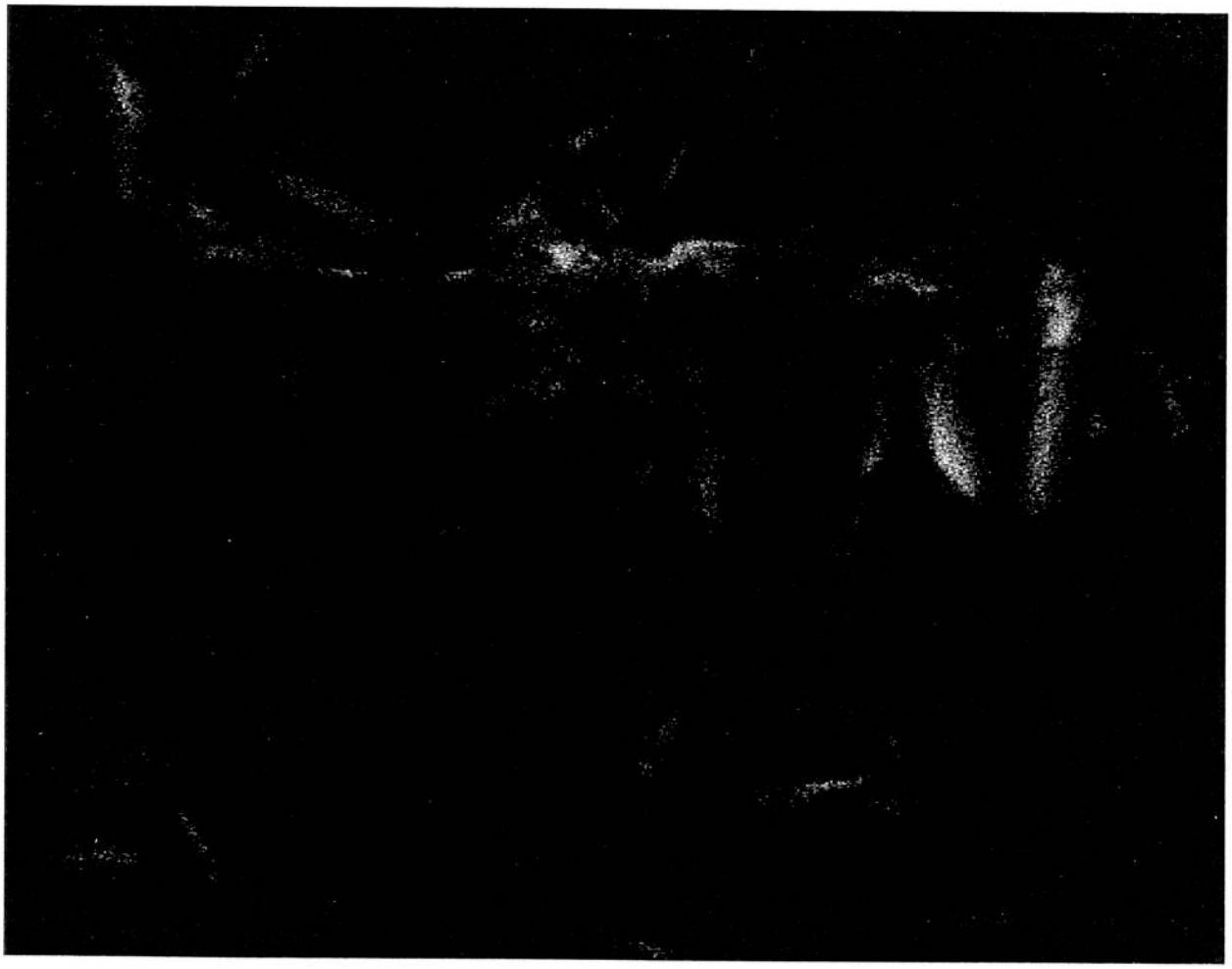

Figure A.2: Set 1-3, Terminal pH 4.04, Elemental Scan for S

Figure A.2: Set 1-3, Terminal pH 4.04, Elemental Scan for Al

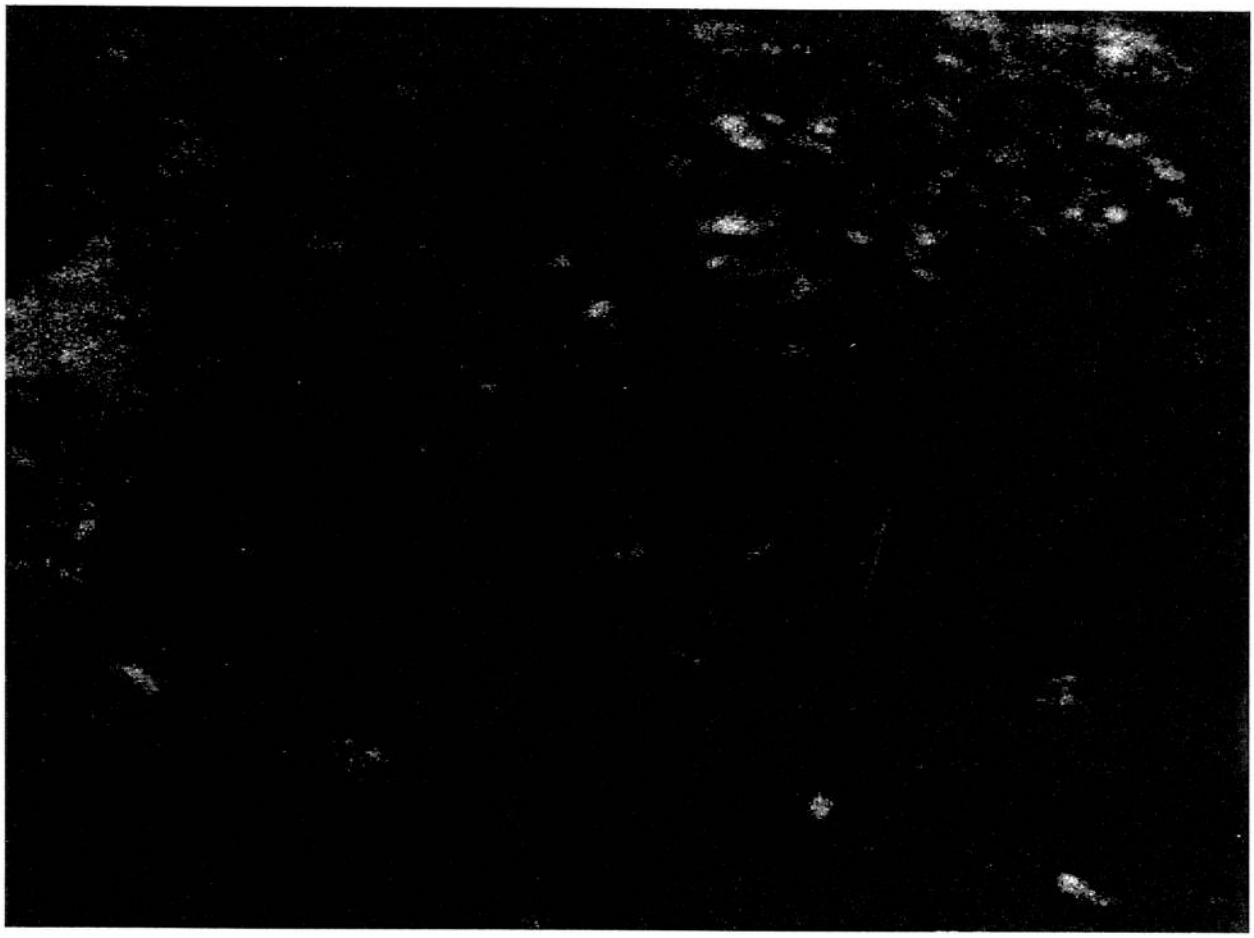

Figure A.2: Set 1-3, Terminal pH 4.04, Elemental Scan for Si

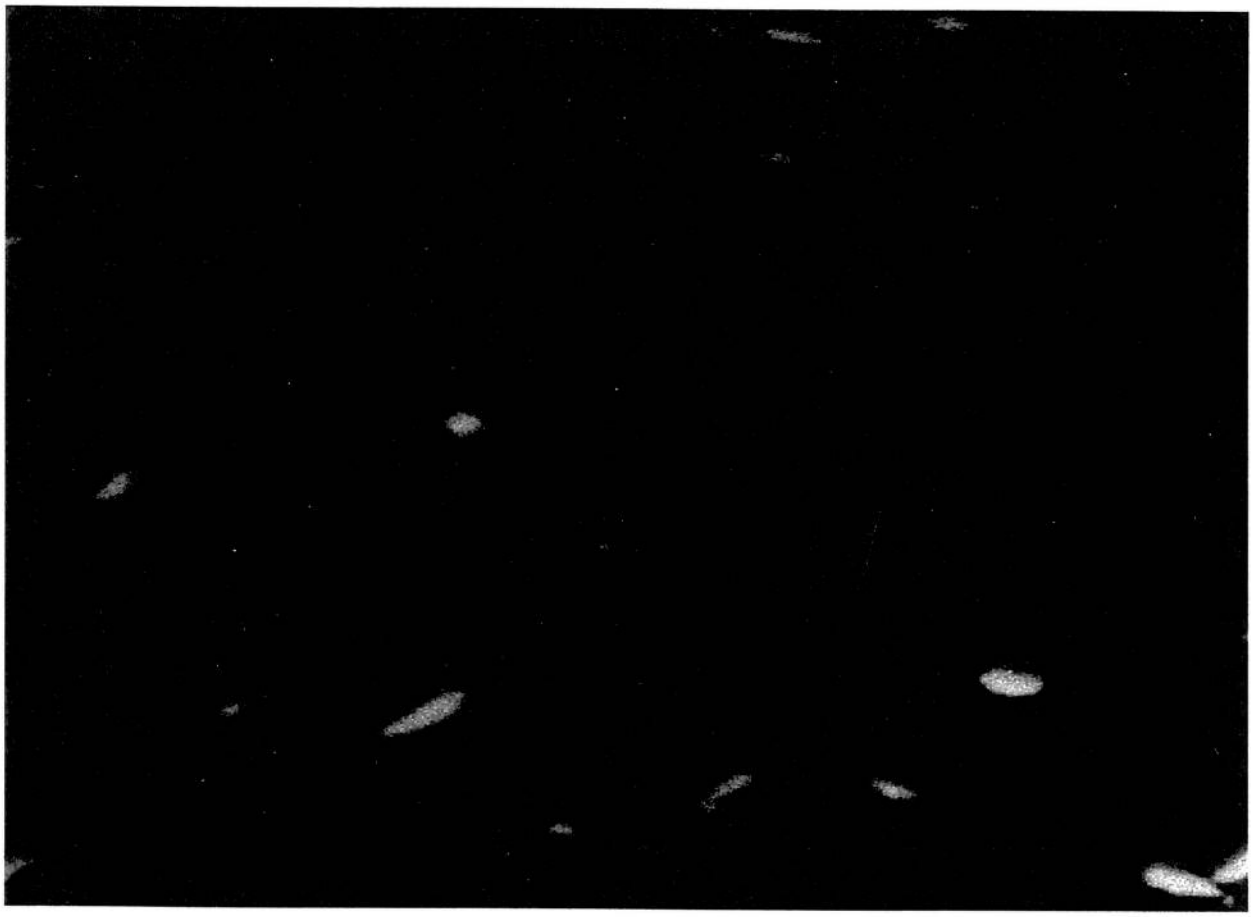

Figure A.3: Set 1-4, Terminal pH 6.09, Electron Backscatter Image

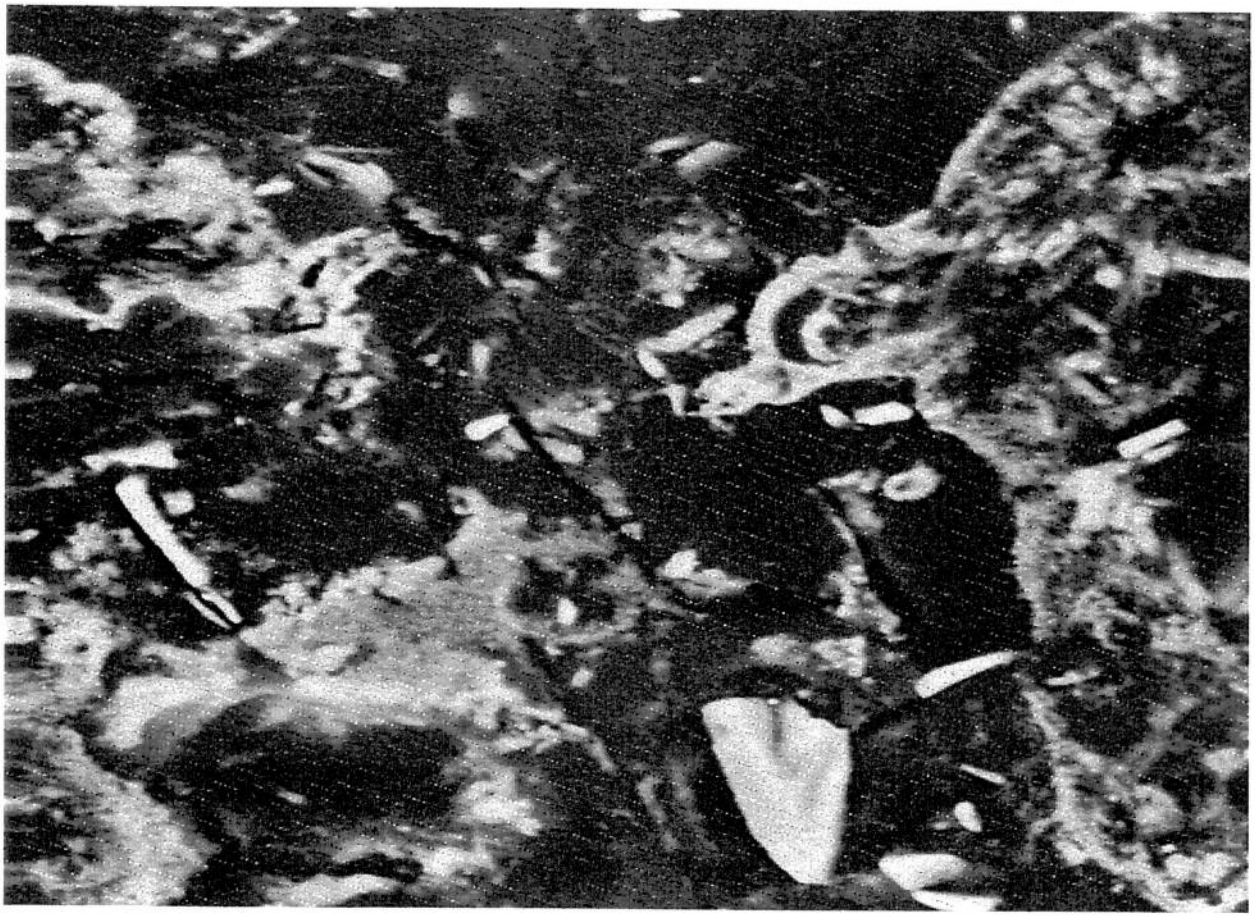

Figure A.3: Set 1-4, Terminal pH 6.09, Elemental Scan for Fe

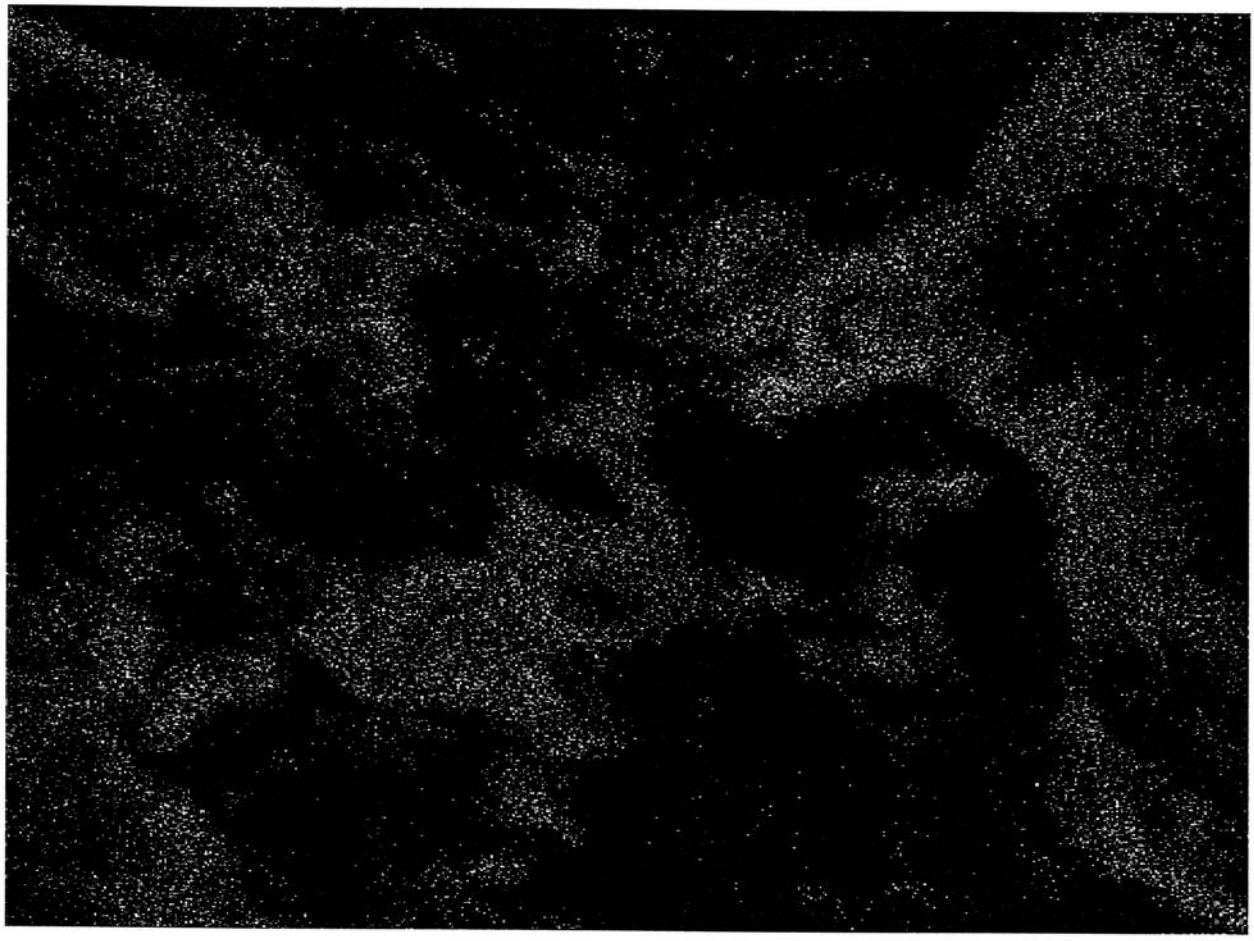

Figure A.3: Set 1-4, Terminal pH 6.09, Elemental Scan for As

Figure A.3: Set 1-4, Terminal pH 6.09, Elemental Scan for Ni

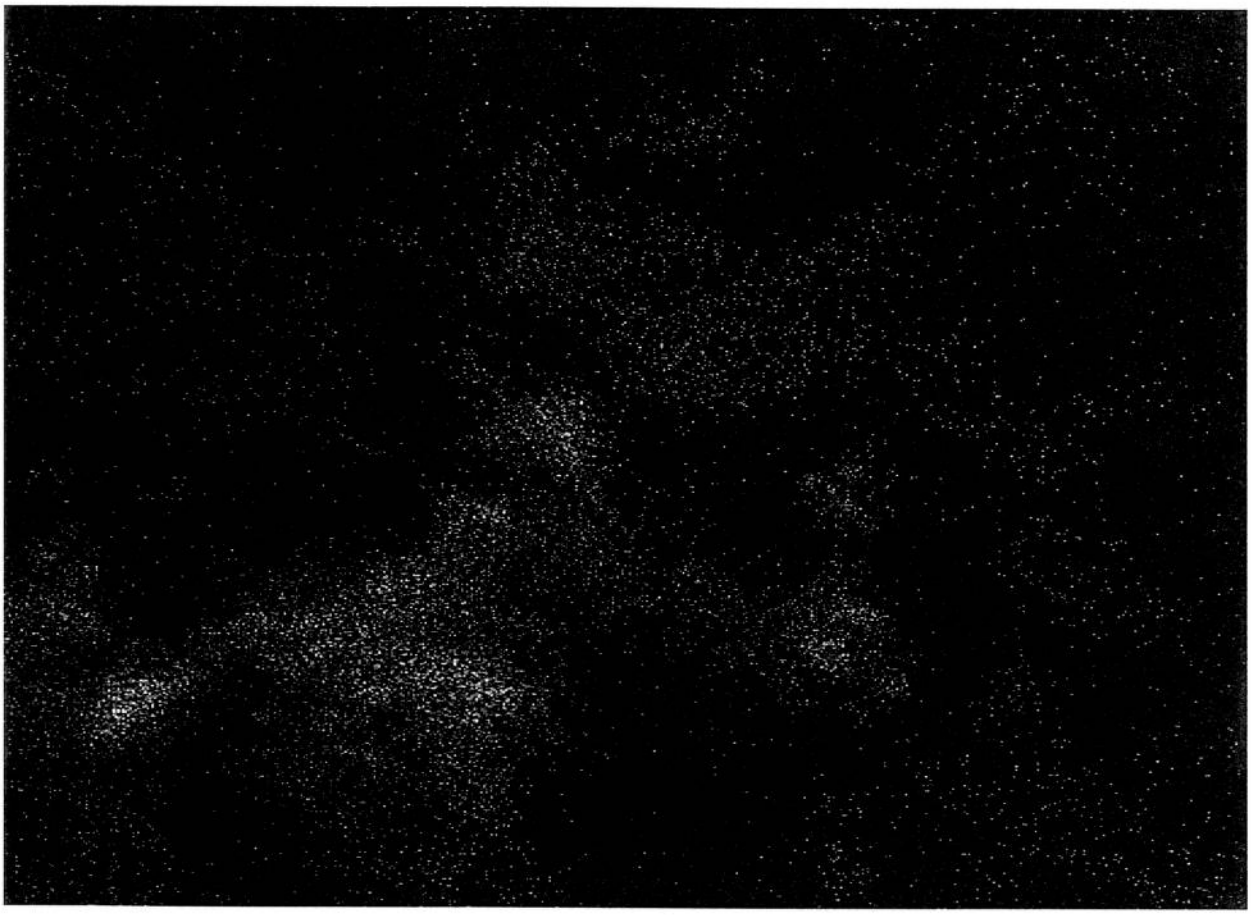

Figure A.3: Set 1-4, Terminal pH 6.09, Elemental Scan for Ca

Figure A.3: Set 1-4, Terminal pH 6.09, Elemental Scan for S

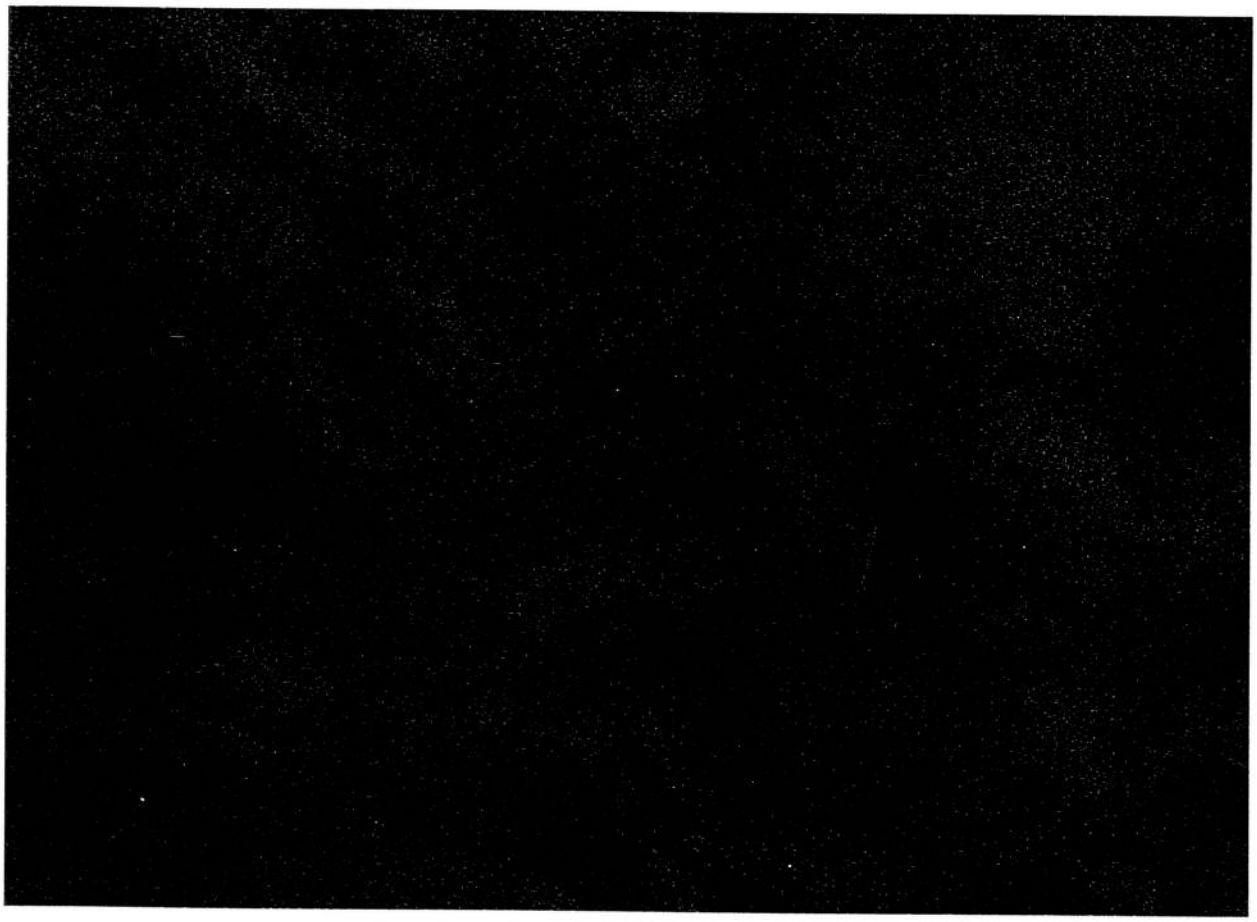

Figure A.3: Set 1-4, Terminal pH 6.09, Elemental Scan for Si

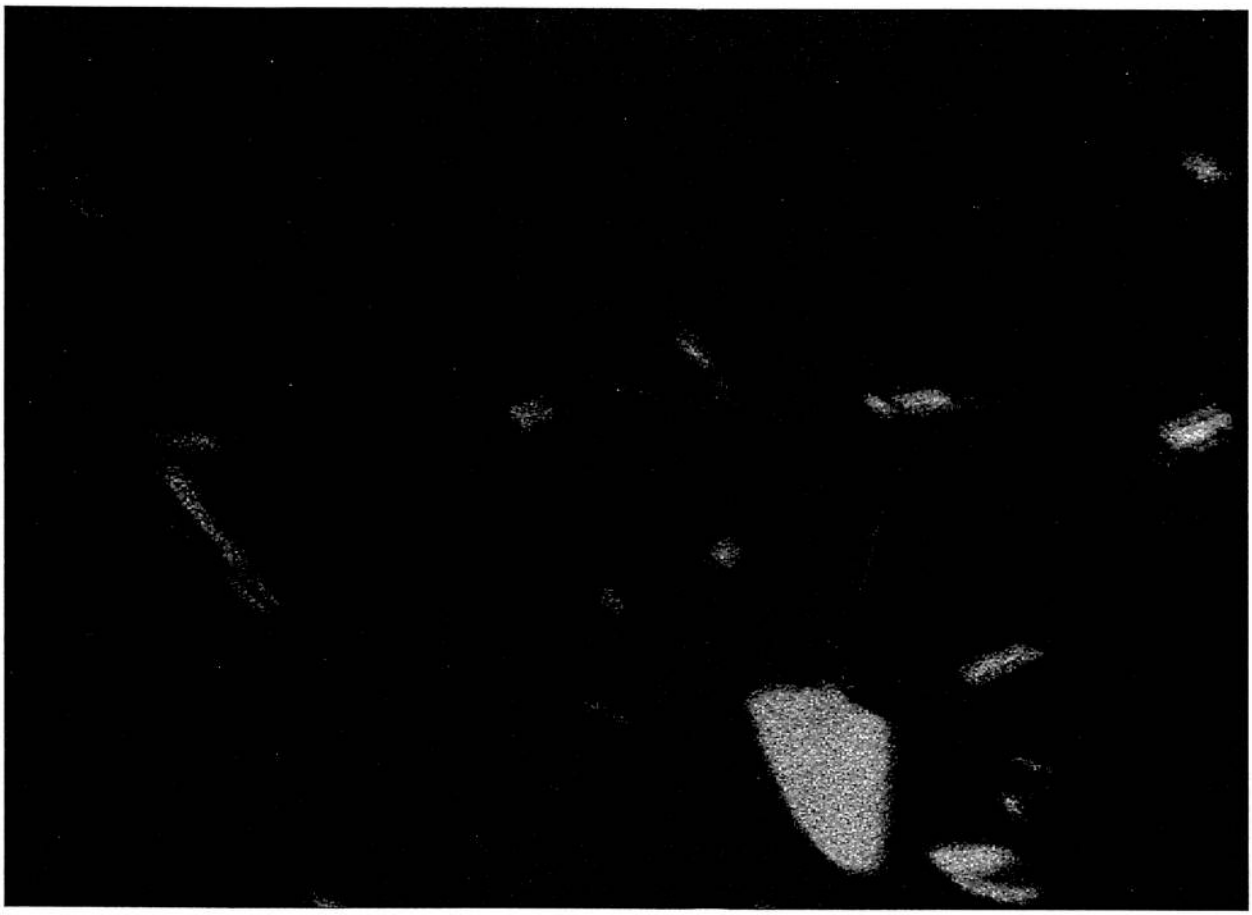

Figure A.3: Set 1-4, Terminal pH 6.09, Elemental Scan for Al

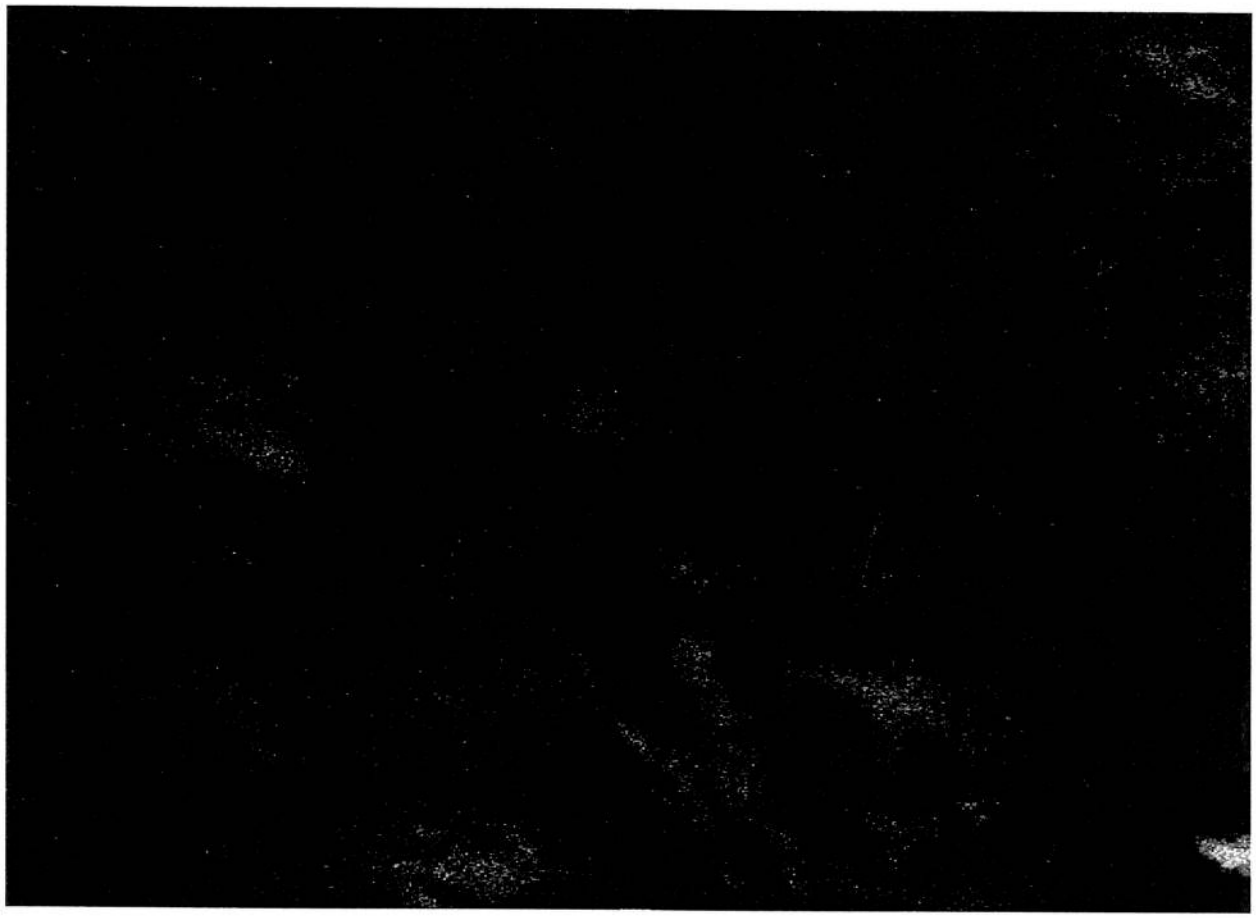

Figure A.4: Set 1-5, Terminal pH 7.38, Electron Backscatter Image

Figure A.4: Set 1-5, Terminal pH 7.38, Elemental Scan for Fe

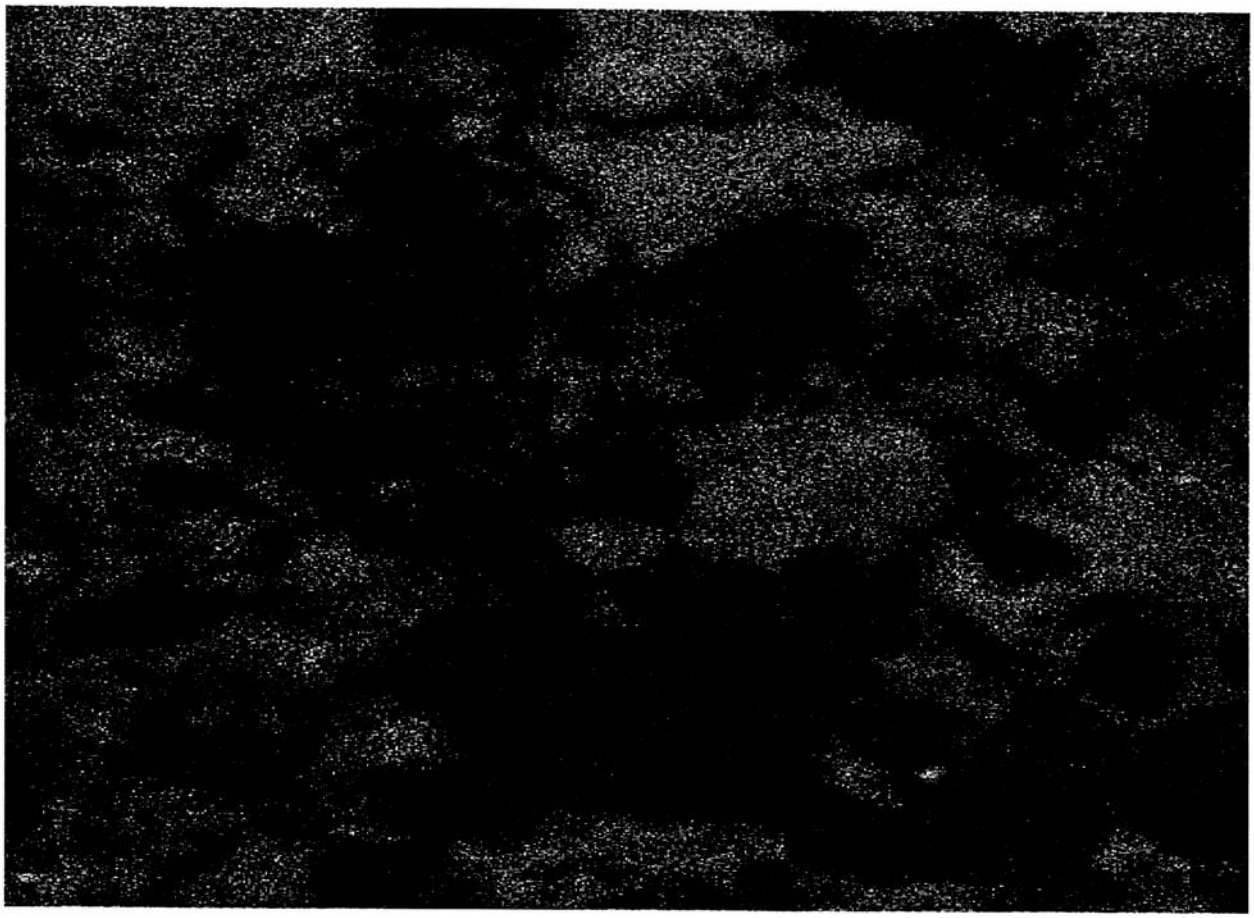

Figure A.4: Set 1-5, Terminal pH 7.38, Elemental Scan for As

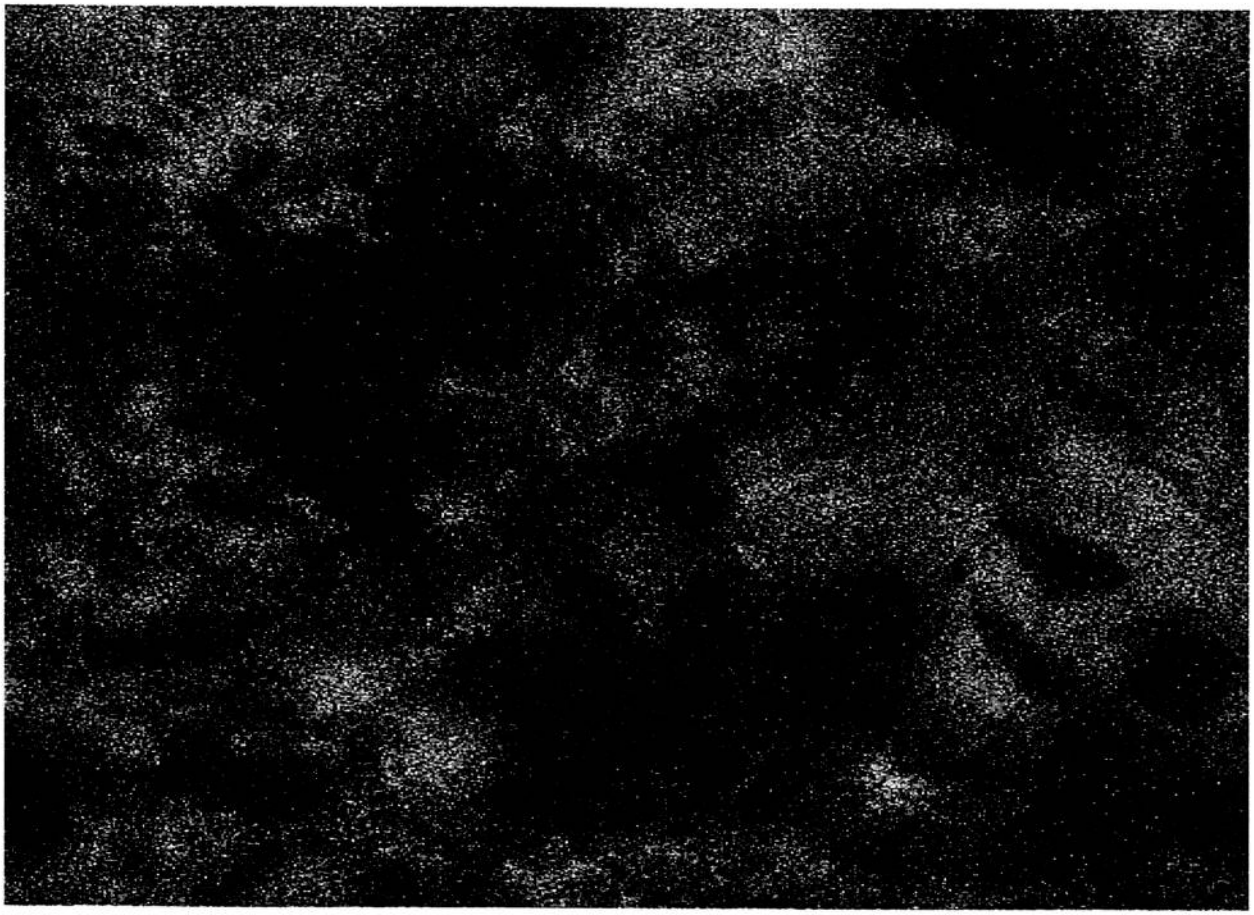

Figure A.4: Set 1-5, Terminal pH 7.38, Elemental Scan for Ni

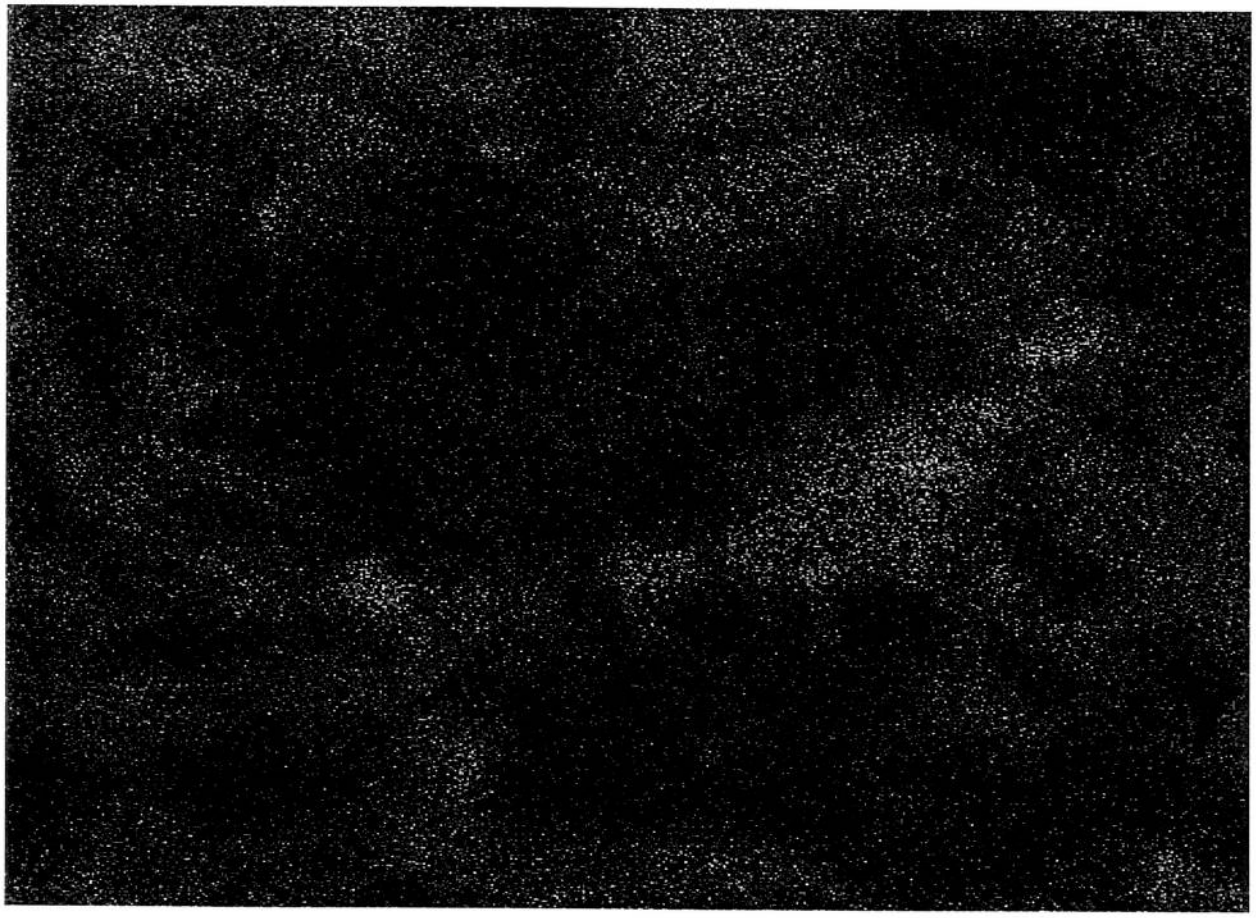

Figure A.4: Set 1-5, Terminal pH 7.38, Elemental Scan for Ca

Figure A.4: Set 1-5, Terminal pH 7.38, Elemental Scan for S

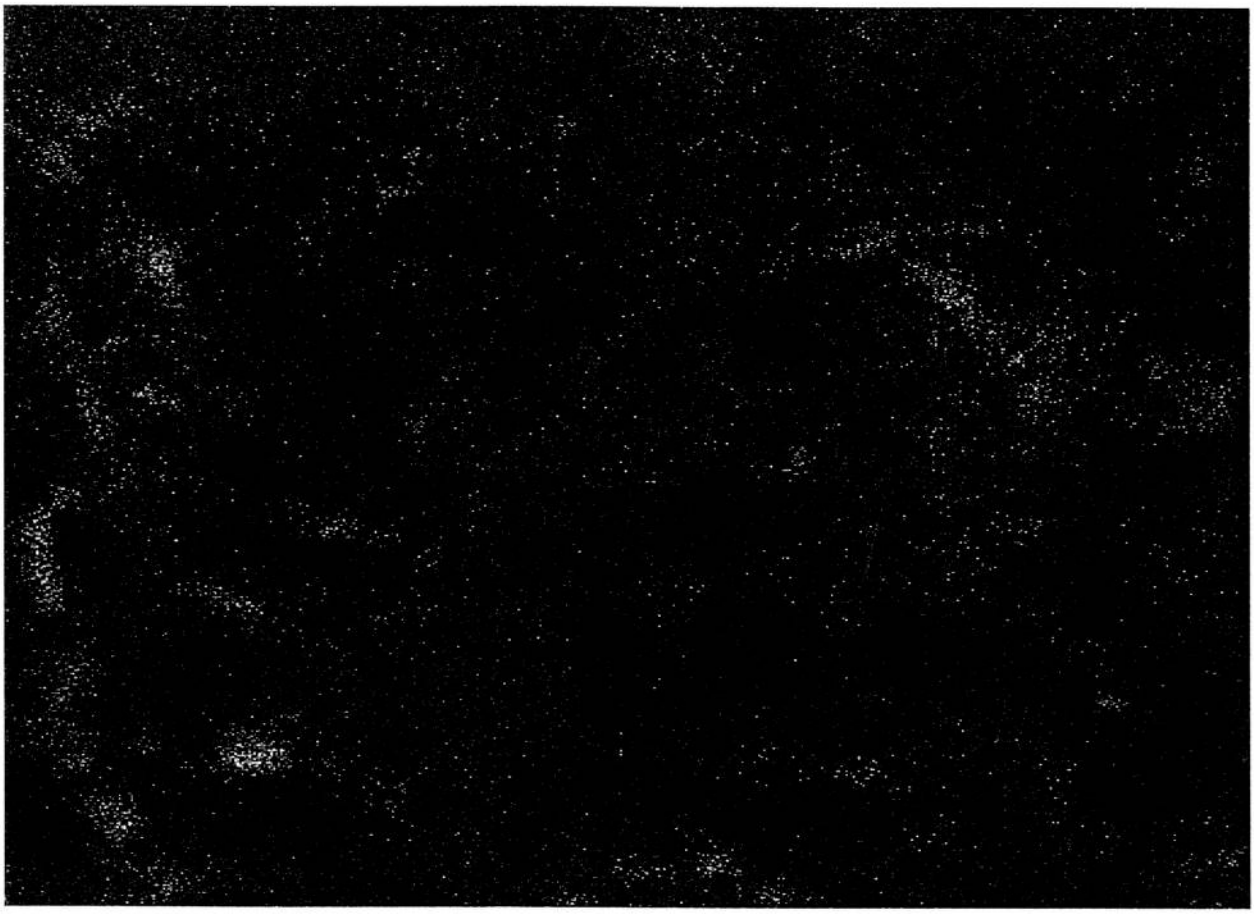

Figure A.4: Set 1-5, Terminal pH 7.38, Elemental Scan for Si

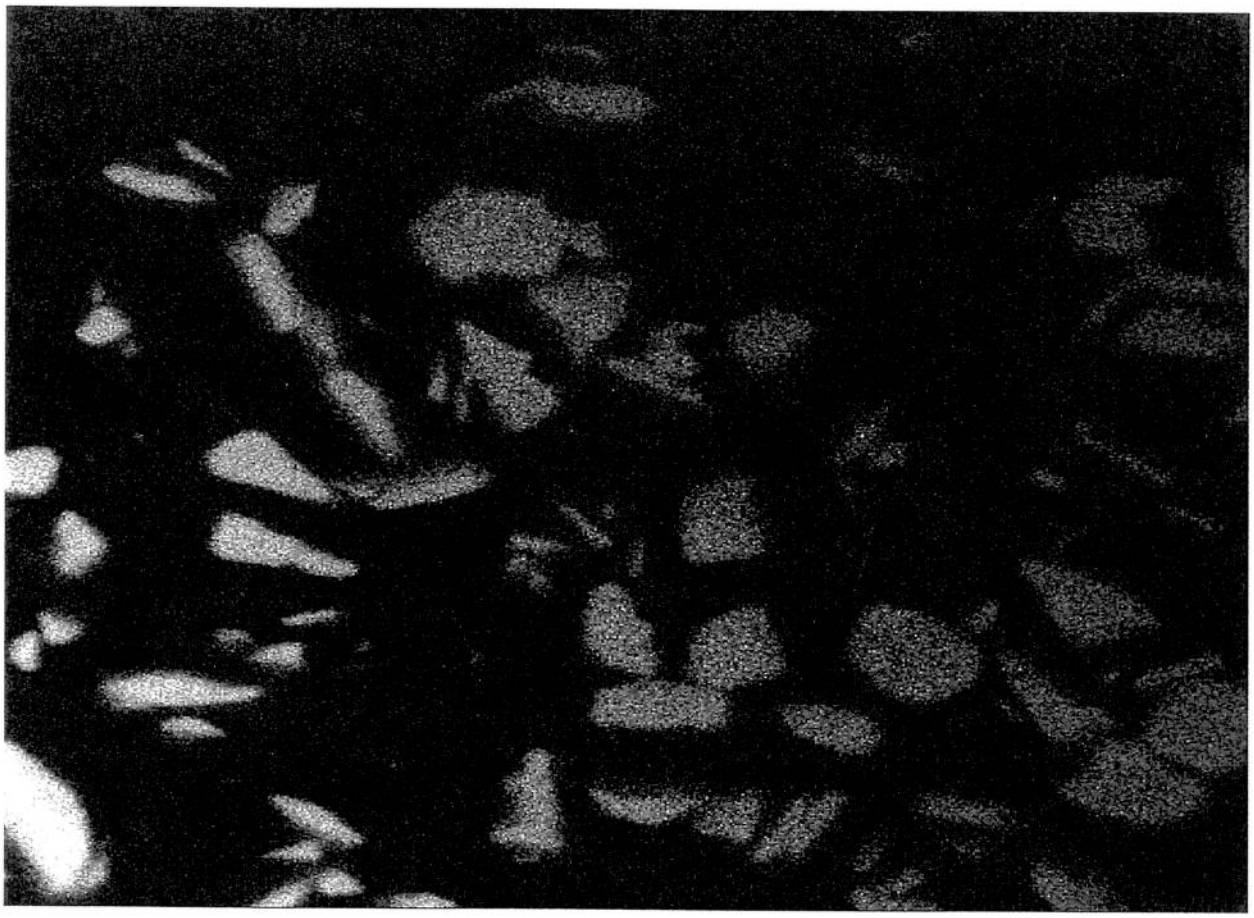

Figure A.4: Set 1-5, Terminal pH 7.38, Elemental Scan for Al

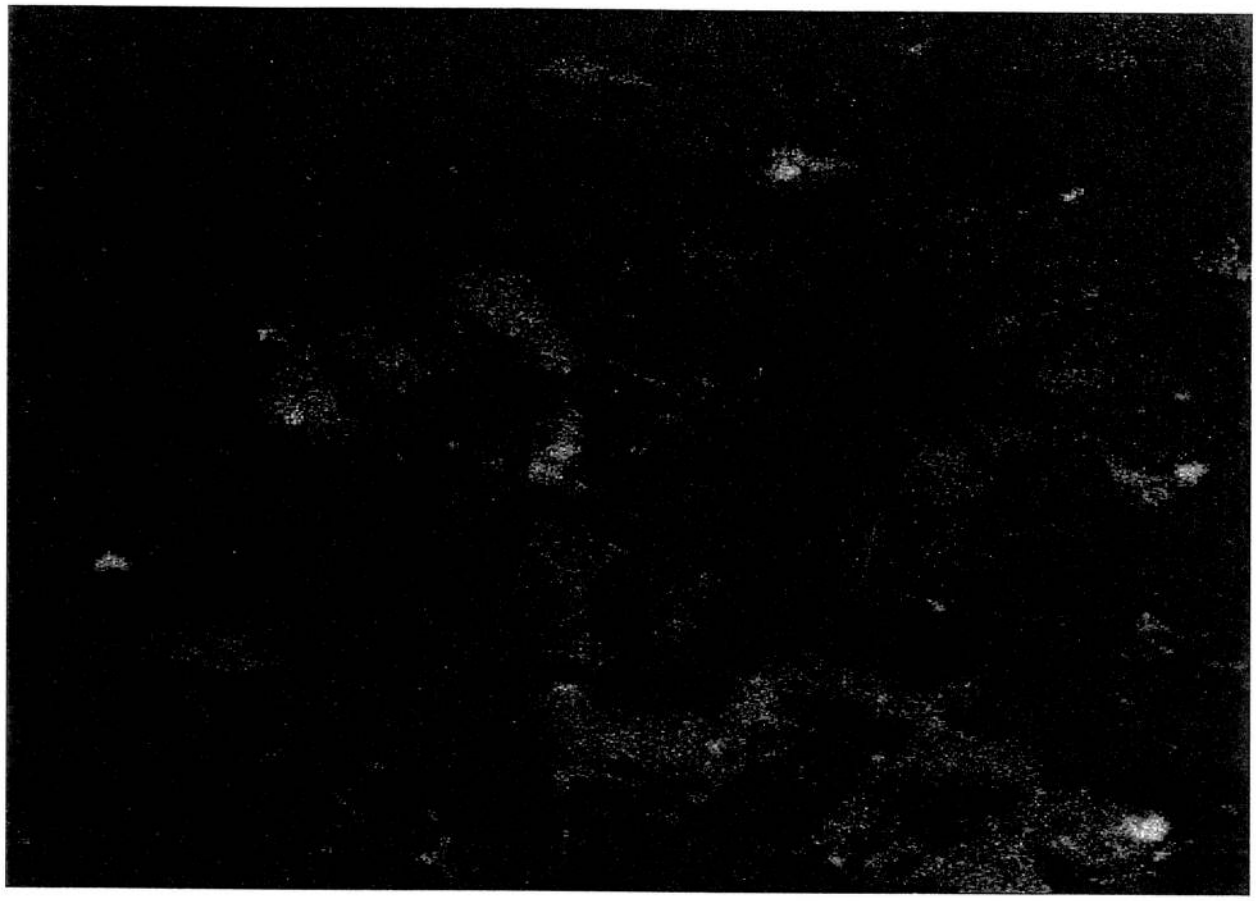

Figure A.4: Set 1-5, Terminal pH 7.38, Elemental Scan for Mg

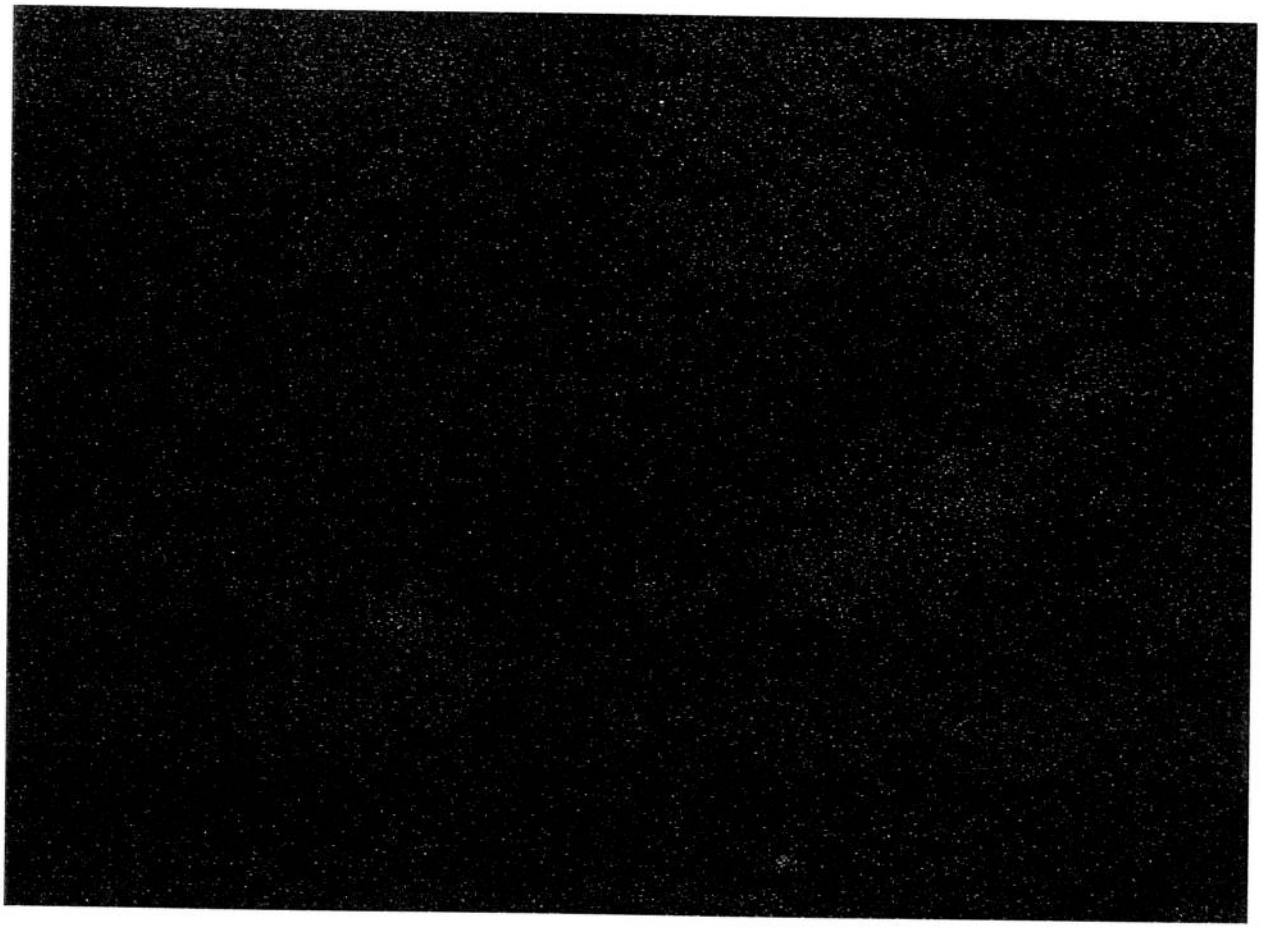

Table A.1: Neutralization Test Results for Sue E Ore Leached by Pressure Leaching (O_2) and Atmospheric Leaching (H_2O_2)

Pore Water Analyte	Units	Pressure Leaching		Atmospheric Leaching	
		Raffinate	Neutralized Tailings	Raffinate	Neutralized Tailings
pH		2.06	7.9	1.27	7.9
Eh	mV	547	388	619	399
Conductivity	mS/cm		7.72		8.03
Alkalinity	mg/L		<0.005		<0.005
Al	mg/L		<0.02		<0.02
As_{total}	mg/L	2,175	1.02	2,564	0.87
As(III)	mg/L	825	0.33	224	0.60
As(V)	mg/L	1,350	0.69	2,340	0.27
Ca	mg/L		436		423
Cl	mg/L		12.6		16.9
Fe	mg/L	105	<0.01	437	<0.01
K	mg/L		231		199
Mg	mg/L		29.4		29.9
Mo	mg/L	9.4	23.8	7.7	13.9
Ni	mg/L	2,040	0.23	1,880	0.27
P	mg/L		0.10		0.04
^{226}Ra	Bq/L		48.8		51.0
SO_4^{2-}	g/L		4.58		4.96
Si	mg/L		2.48		1.96
U	mg/L	4.5	0.05	12.2	0.07

Conditions

- Temperature 35°C
- Fe(III)/As_{total} molar ratio 3.6

Table A.2: SEPA Aging Test Results for Sue E Ore Leached by Pressure Leaching (O_2)

Pore Water Analyte	Units	Aging Time		
		0 hours	48 hours	120 hours
pH		7.23	7.00	7.56
Eh	mV	438	397	397
Conductivity	mS/cm	7.67	7.81	7.86
Alkalinity	mg/L			<0.005
Al	mg/L			<0.02
As_{total}	mg/L	1.19	1.49	1.49
As(III)	mg/L	0.80	0.27	0.59
As(V)	mg/L	0.39	1.22	0.90
Ca	mg/L			578
Cl	mg/L			8.04
Fe	mg/L			<0.02
K	mg/L			275
Mg	mg/L			37.4
Mo	mg/L	30.7	29.6	31.7
Ni	mg/L	0.29	0.33	0.31
P	mg/L			1.24
^{226}Ra	Bq/L			28.9
SO_4^{2-}	g/L			4.46
Si	mg/L			4.85
U	mg/L	6.9	9.9	5.8

Conditions

- Temperature 25°C

Table A.3: SEPA Aging Test Results for Sue E Ore Leached by Atmospheric Leaching (H_2O_2)

Pore Water Analyte	Units	Aging Time		
		0 hours	48 hours	120 hours
pH		7.32	7.62	7.58
Eh	mV	467	433	414
Conductivity	mS/cm	8.02	8.27	8.32
Alkalinity	mg/L			<0.005
Al	mg/L			<0.02
As_{total}	mg/L	1.03	1.26	1.24
As(III)	mg/L	0.22	0.21	0.24
As(V)	mg/L	0.81	1.05	1.00
Ca	mg/L			479
Cl	mg/L			15.3
Fe	mg/L			<0.02
K	mg/L			236
Mg	mg/L			39.7
Mo	mg/L	20.2	20.6	21.5
Ni	mg/L	0.39	0.40	0.42
P	mg/L			2.04
^{226}Ra	Bq/L			30.4
SO_4^{2-}	g/L			4.82
Si	mg/L			5.05
U	mg/L	0.13	0.16	0.29

Conditions:

- Temperature 25 °C

Tailings Optimization and Validation Status Report for 2004, July 2005 (TOVP, 2005a)

Table 4.2-8: Total Petroleum Hydrocarbon Analyses in Tailings Sediments

Analysis	Location and Elevation (masl)				
	TMF01-01-15A 364.4	TMF01-03-3A 376.4	TMF01-05-07 369.0	TMF01-06-6A 371.8	TMF01-04-4A 373.3
Sediments					
Extractable HC,C_{11}-C_{20} (ug/g)	610	590	<10	1100	32,000
Extractable HC,C_{21}-C_{36} (ug/g)	<10	<10	<10	<10	<10
Purgeable HC,C_6-C_{10} (ug/g)	<1	<1	<1	<1	<1
Total Petroleum HC (ug/g)	610	590	<10	1100	32,000
Benzene (ug/g)	<0.01	<0.01	<0.01	<0.01	<0.01
Ethylbenzene (ug/g)	<0.01	<0.01	<0.01	<0.01	<0.01
Toluene (ug/g)	<0.01	<0.01	<0.01	<0.01	<0.01
Xylene (ug/g)	2.2	<0.01	<0.01	2.6	n/a
Pore Water					
HCO_3^- 2001 (mg/L)	29	57	76	83	84
HCO_3^- 2002 (mg/L)	n/a	n/a	n/a	124	109
HCO_3^- 2003 (mg/L)	33	n/a	n/a	124	129
HCO_3^- 2004 (mg/L)	44	n/a	n/a	122	106

Table A.1: Chemical Analyses of Raffinate 2 Solutions at Final pH Values

Analyte	Raffinate	9-27-1	9-27-2	9-27-3	9-27-4	9-28-A	9-28-B
	(mg/L)[1]	(mg/L)[1]	(mg/L)[1]	(mg/L)[1]	(mg/L)[1]	(mg/L)[1]	(mg/L)[1]
pH	0.97	2.18	3.23	4.09	5.29	6.08	7.37
pe	11.32	10.88	9.932	7.831	4.661	2.9152	0.0169
Eh (mV)	668	642	586	462	275	172	1
Al	200	803	435	438	0.70	0.06	0.01
As^{3+}	447	100	6.70	1.42	0.645	0.471	0.204
As^{5+}	221	48.0	6.79	2.04	0.464	0.287	0.240
Ca	589	512	521	498	513	500	543
Cl	13	16	18	19	20	19	22
Cu	19	16	15	15	1.2	0.01	0.01
Fe^{2+}	685	540	460	462	392	315	20
Fe^{3+}	1169	881	353	233	207	91	4.5
K	357	394	638	745	568	164	213
Mg	229	1086	485	1011	518	340	310
Na	23	83	43	90	38	30	32
Ni	515	502	481	462	373	233	13
Si	190	582	329	238	62	19	4
SO_4^-	21430	10150	7840	6530	4750	3990	3070

1. Except for pH, pe and Eh

Table A.2: Chemical Analyses of Single Beaker Test Solutions at Final pH Values

Analyte	Raffinate	SB-2	SB-3	SB-4
	(mg/L)[1]	(mg/L)[1]	(mg/L)[1]	(mg/L)[1]
pH	0.97	3.92	5.66	7.34
pe	11.32	8.186	4.220	-3.389
Eh (mV)	668	483	249	-200
Al	200	448	1.05	0.06
As^{3+}	447	2.98	1.16	0.252
As^{5+}	221	2.91	0.922	0.103
Ca	589	661	903	1048
Cl	13	16	19	19
Cu	19	15	1.26	0.07
Fe^{2+}	685	450	440	280
Fe^{3+}	1169	450	440	280
K	357	202	256	240
Mg	229	338	438	644
Na	23	52	47	45
Ni	515	472	384	229
Si	190	52	47	45
SO_4^-	21430	6920	5740	4900

1. Except for pH, pe and Eh

Table A.3: Chemical Analyses of Synthetic Raffinate Neutralization Test Solutions at Final pH Values

Analyte	Raffinate	SR-1	SR-2	SR-3	SR-4	SR-5	SR-6
	(mg/L)[1]	(mg/L)[1]	(mg/L)[1]	(mg/L)[1]	(mg/L)[1]	(mg/L)[1]	(mg/L)[1]
pH	1.4	2.2	3.1	4.0	5.1	6.1	7.0
pe	11.29	11.22	10.92	8.42	8.28	8.15	9.29
Eh (mV)	668	664	646	498	490	482	550
Al	407	355	409	268	20	0.1	0.1
Ca	739	2.1	763	553	573	555	603
Cl	20	21	21	20	20	21	21
Fe^{2+}	785	573	340	464	149	64	0.14
Fe^{3+}	635	1012	1076	277	429	55	0.16
K	117	100	115	99	98	94	97
Mg	321	271	335	318	322	315	320
Na	60	58	61	62	62	62	64
Ni	568	511	565	485	433	266	46
Si	25	2.1	32	22	12	5	1.8
SO_4^-	24000	21000	18000	15000	20000	18000	12000

1. Except for pH, pe and Eh

APPENDIX A

DATA FILE ASSOCIATED WITH LABORATORY INVESTIGATIONS

Table A.1: Linear Combination Fitting of As XANES: Relative percentages of Arsenic oxidation states as determined from As K-edge XANES.

Sample		As^{-1} (relative %)	As^{3+} (relative %)	As^{5+} (relative %)
Borehole Samples				
Sample #	**masl**			
TMF08-01 SA01	419.9	50	5	45
TMF08-01 SA02	417.16	0	0	100
TMF08-01 SA03	414.11	0	0	100
TMF08-01 SA04	411.06	0	0	100
TMF08-01 SA05	408.01	0	0	100
TMF08-01 SA06	404.96	0	0	100
TMF08-01 SA07	401.97	0	0	100
TMF08-01 SA08	398.87	10	0	90
TMF08-01 SA09	398.26	12	0	88
TMF08-01 SA10	394.91	0	7	93
TMF08-01 SA11	391.25	15	20	65
TMF08-01 SA12	388.20	8	12	80
TMF08-01 SA13	386.07	15	15	70
TMF08-01 SA14	383.02	19	11	70
TMF08-01 SA15	379.06	36	0	64
TMF08-01 SA16	376.92	3	7	90
TMF08-01 SA17	373.88	40	0	60
TMF08-01 SA18	370.83	18	0	82
TMF08-01 SA19	366.86	0	12	88
TMF08-01 SA20	364.73	30	0	70
Mill Circuit Samples				
Ore		100	0	0
Raffinate		0	0	0
TN Flash Mix		41	0	59
TN thickener		0	0	100
CCD#6 U/F		33	0	67
TN#2		15	0	85
TN#1		35	0	65

Table A.2: Sue A Aging Test 2006-2009: High Iron Addition to Leaching

Jar#	Date	Age	As_{tot}	Ni	U	pH	ORP	Fe_{tot}
		(days)	(mg/L)	(mg/L)	(mg/L)		mV	(mg/L)
Jar#1	22-Jun-06	0	1.97	0.902	0.005	7.3		
Jar#2	22-Jul-06	30	2.72	0.659	0.018	6.8		
Jar#3	22-Aug-06	61	3.23	0.75	0.019	7.1	398	
Jar#4	22-Sep-06	92	2.81	0.91	0.011	7.1		
Jar#5	22-Oct-06	122	2.69	0.633	0.325			0.721
Jar#6	22-Nov-06	153	2.56	0.914	0.18			0.284
Jar#7	22-Feb-07	245	8.56	6.73	0.22	7.1	308	13.2
Jar#8	22-Apr-07	305	2.74	0.904	0.04	6.8	226	0.32
Jar#9	22-Jun-07	366	2.06	0.8		7.2		0.07
Jar#10	22-Aug-07	427	1.9	0.774	0.023			0.112
Jar#11	22-Oct-07	488	2.13	0.77	0.06	7.3	441	0.034
Jar#12	22-Dec-07	549	2.23	1.18	0.015	6.7	434	0.415
Jar#13	22-Jun-08	732	1.92	1.09	0.12	7.0	282	0.096
Jar#14	22-Dec-08	915	2.17	1.54	0.15	6.8	354	1.02
Jar#15	22-Jun-09	1098	1.66	1.45	0.183	7.4	265	1.13

Table A.3: TMF Sediment HC_{11-20} Analyses

Bore Hole	Sample	masl	HC_{11-20} (ug/g)	D.L.
TMF08-01	SA01	419.9	<10	10
	SA02	417.16	<10	10
	SA03	414.11	<10	10
	SA04	411.06	<10	10
	SA05	408.01	<10	10
	SA06	404.96	<10	10
	SA07	401.97	<10	10
	SA08	398.87	<10	10
	SA09	398.26	<10	10
	SA10	394.91	<10	10
	SA11	391.25	130	10
	SA12	388.20	<10	10
	SA13	383.02	<10	10
	SA15	379.06	<10	10
	SA16	376.92	<10	10
	SA17	373.88	<10	10
	SA18	370.83	<10	10
	SA19	366.86	46	10
	SA20	364.73	30	10
TMF08-03	SA01	413.80	<10	10
	SA02	411.98	<10	10
	SA03	410.76	<10	10
	SA04	409.23	190	10
	SA05	406.18	<10	10
	SA06	403.14	<10	10
	SA07	400.09	<10	10
	SA08	397.04	<10	10
	SA09	391.55	<10	10
	SA10	387.90	<10	10
	SA11	385.46	100	10
	SA12	382.10	<10	10
	SA13	378.75	95	10
	SA14	376.01	560	10
	SA15	372.96	90	10
	SA16	370.52	130	10

TMF HC Analyses 2013 Bore Holes TMF13-01 and TMF13-03

Bore Hole - Sample	Depth	Carbon, Inorganic	Carbon, Organic	Hydrocarbons, F2 (C10-C16)	Hydrocarbons, F3 (C16-C34)
	masl	%	%	mg/kg	mg/kg
TMF13-01					
TMF13-01_SA01_TM	**423.49**	0.03	0.29	3.5	5
TMF13-01_SA03_TM	**420.47**	0.11	0.35	3.5	5
TMF13-01_SA04_TM	**417.78**	0.07	0.24	3.5	5
TMF13-01_SA05_TM	**414.68**	0.03	0.25	3.5	5
TMF13-01_SA06_TM	**411.68**	0.03	0.18	3.5	5
TMF13-01_SA08_TM	**408.58**	0.03	0.2	3.5	5
TMF13-01_SA09_TM	**405.56**	0.05	0.49	3.5	5
TMF13-01_SA10_TM	**402.48**	0.02	0.53	3.5	5
TMF13-01_SA11_TM	**399.46**	0.01	0.6	3.5	5
TMF13-01_SA12_TM	**398.85**	0.04	2.09	3.5	5
TMF13-01_SA14_TM	**395.47**	0.03	0.41	3.5	5
TMF13-01_SA15_TM	**391.87**	0.41	1.33	3.5	5
TMF13-01_SA16_TM	**388.77**	0.01	0.77	3.5	5
TMF13-01_SA17_TM	**386.66**	0.02	0.66	3.5	5
TMF13-01_SA19_TM	**383.59**	0.11	0.38	3.5	5
TMF13-01_SA20_TM	**379.68**	0.08	0.36	3.5	5
TMF13-01_SA21_TM	**377.49**	0.1	0.22	3.5	5
TMF13-01_SA22_TM	**374.47**	0.06	0.41	3.5	5
TMF13-01_SA23_TM	**371.37**	0.23	1.32	3.5	5
TMF13-01_SA24_TM	**367.46**	0.03	0.55	3.5	5
TMF13-01_SA25_TM	**365.27**	0.06	0.29	3.5	5
TMF13-03					
TMF13-03_SA01_TM	**419.38**	0.12	0.29	3.5	5
TMF13-03_SA02_TM	**416.89**	0.13	0.28	3.5	5
TMF13-03_SA04_TM	**414.37**	0.02	0.32	3.5	5
TMF13-03_SA05_TM	**412.57**	0.05	0.3	3.5	5
TMF13-03_SA06_TM	**411.37**	0.04	0.68	3.5	5
TMF13-03_SA07_TM	**409.77**	0.04	0.68	3.5	5
TMF13-03_SA09_TM	**406.78**	0.04	0.24	3.5	5
TMF13-03_SA10_TM	**403.81**	0.04	0.53	3.5	5
TMF13-03_SA11_TM	**401.37**	0.02	0.44	3.5	5
TMF13-03_SA12_TM	**398.37**	0.33	0.66	3.5	5
TMF13-03_SA14_TM	**392.20**	0.02	0.59	3.5	5
TMF13-03_SA15_TM	**388.46**	0.03	1.22	3.5	5
TMF13-03_SA16_TM	**386.08**	0.06	3.13	3.5	5
TMF13-03_SA17_TM	**382.67**	0.06	0.73	3.5	5
TMF13-03_SA18_TM	**381.17**	0.02	0.63	3.5	5
TMF13-03_SA19_TM	**379.40**	0.05	0.66	3.5	5
TMF13-03_SA21_TM	**373.60**	0.01	0.32	3.5	5
TMF13-03_SA22_TM	**371.09**	0.01	0.64	3.5	5

Hydrocarbons, F4 (C34-C50)	Kerosene	HCO3-
mg/kg	µg/g	mg/L
5	240	121
5	10	52
5	10	41
5	86	146
5	10	45
5	10	76
5	10	46
5	10	260
5	10	41
5	11	212
5	10	251
5	24	145
5	10	188
5	10	204
5	10	143
5	10	155
5	10	202
5	10	250
5	10	234
5	10	157
5	490	102
5	63	48
5	52	41
5	92	49
5	22	150
5	10	54
5	15	76
5	10	82
5	10	143
5	10	221
5	22	376
5	10	421
5	10	209
5	10	388
5	790	590
5	100	351
5	280	245
5	130	237
5	180	179

Sample ID	Date	Time Collected	Time Received	Bottles	Total Fe (ppm)	Fe 2+ (ppm)	Fe 3+ (ppm)
TMF13-01_SA01_TP	4-Aug-13	7:43	7:50	2	0.883	0.82	0.06
TMF13-01_SA02_TP	4-Aug-13	9:45	9:50	0			0
TMF13-01_SA03_TP				2	0.356	0.43	-0.07
TMF13-01_SA04_TP	5-Aug-13	10:47	10:55	2	0.015	0.08	-0.07
TMF13-01_SA05_TP	13-Aug-13	13:29	13:30	2	0.143	0.30	-0.16
TMF13-01_SA06_TP	13-Aug-13	14:10	14:30	1	0.012	0.17	-0.16
TMF13-01_SA08_TP	13-Aug-13	14:56	15:10	1	0.014	0.11	-0.10
TMF13-01_SA09_TP	13-Aug-13	16:52	17:00	1	0.029	0.06	-0.03
TMF13-01_SA10_TP	14-Aug-13	6:46	6:45	1	3.83	4.1	-0.3
TMF13-01_SA11_TP	14-Aug-13	7:30	7:40	1	15.3	13	2
TMF13-01_SA12_TP	14-Aug-13	8:23	8:30	1	10.4	9.2	1.2
TMF13-01_SA14_TP	14-Aug-13	9:49	9:45	1	1.44	1.3	0.1
TMF13-01_SA15_TP	14-Aug-13	14:07	14:15	1	0.041	0.01	0.03
TMF13-01_SA16_TP	14-Aug-13	15:52	15:50	1	1.84	1.5	0.3
TMF13-01_SA17_TP	14-Aug-13	16:41	16:50	1	0.515	0.50	0.02
TMF13-01_SA19_TP	15-Aug-13	6:48	6:55	1	0.119	0.11	0.01
TMF13-01_SA20_TP	15-Aug-13	7:48	7:55	1	0.883	0.93	-0.05
TMF13-01_SA21_TP	15-Aug-13	9:47	10:00	1	2.10	1.8	0.3
TMF13-01_SA22_TP	15-Aug-13	10:47	10:50	2	1.30	1.0	0.3
TMF13-01_SA23_TP	15-Aug-13	13:21	13:30	1	0.674	0.64	0.03
TMF13-01_SA24_TP	15-Aug-13	14:24	14:30	1	8.20	6.8	1.4
TMF13-01_SA25_TP	15-Aug-13	15:14	15:15	1	0.126	0.10	0.03
TMF13-02_SA01_TP	7-Jul-13	14:51	14:55	1	0.337	0.36	-0.02
TMF13-02_SA02_TP	7-Jul-13	15:48	15:55	2	0.025	0.17	-0.14
TMF13-02_SA04_TP	8-Jul-13	7:05	7:15	1	0.018	n/a	
TMF13-02_SA05_TP	8-Jul-13	7:59	8:05	2	0.013	0.05	-0.04
TMF13-02_SA06_TP	8-Jul-13	9:23	9:30	2	0.067	0.01	0.06
TMF13-02_SA07_TP	8-Jul-13	13:53	14:00	2	0.194	0.19	0.00
TMF13-02_SA09_TP	8-Jul-13	15:11	15:15	2	0.043	0.03	0.01
TMF13-02_SA10_TP	8-Jul-13	16:50	16:57	2	2.50	2.0	0.5
TMF13-02_SA11_TP	16-Jul-13	13:57	14:00	2	0.066	0.04	0.03
TMF13-02_SA12_TP	16-Jul-13	15:37	16:00	2	1.34	0.89	0.45
TMF13-02_SA14_TP	16-Jul-13	16:47	17:00	2	1.14	1.1	0.0
TMF13-02_SA15_TP	17-Jul-13	6:53	7:00	2	0.249	0.21	0.04
TMF13-02_SA16_TP	17-Jul-13	8:06	8:15	2	2.42	2.3	0.2
TMF13-02_SA17_TP	17-Jul-13	9:34	9:45	1	3.79	3.1	0.7
TMF13-02_SA19_TP	18-Jul-13	6:52	7:00	1	0.720	0.78	-0.06
TMF13-02_SA20_TP	18-Jul-13	7:54	8:00	2	0.310	0.11	0.20
TMF13-02_SA21_TP	18-Jul-13	9:36	9:45	2	n/a	0.02	
TMF13-03_SA01_TP	1-Aug-13	13:15	13:15	2	0.157	0.20	-0.04
TMF13-03_SA02_TP	1-Aug-13	14:12	14:20	2	0.834	0.91	-0.08
TMF13-03_SA04_TP	1-Aug-13	15:55	16:00	2	1.24	1.2	0.1
TMF13-03_SA05_TP	1-Aug-13	16:46	17:00	2	1.74	2.1	-0.3
TMF13-03_SA06_TP	2-Aug-13	7:16	7:25	2	0.028	0.05	-0.02
TMF13-03_SA07_TP	2-Aug-13	8:35	8:40	2	0.022	0.02	0.00
TMF13-03_SA09_TP	2-Aug-13	10:04	10:15	2	0.015	0.05	-0.04
TMF13-03_SA10_TP	2-Aug-13	13:01	13:10	2	0.016	0.03	-0.01
TMF13-03_SA11_TP	2-Aug-13	13:52	14:00	2	1.29	1.0	0.3
TMF13-03_SA12_TP	2-Aug-13	16:00	16:00	2	0.938	0.35	0.59
TMF13-03_SA14_TP	2-Aug-13	16:43	16:50	2	1.21	0.76	0.45
TMF13-03_SA15_TP	3-Aug-13	9:39	9:45	2	0.053	0.07	-0.02
TMF13-03_SA16_TP	3-Aug-13	13:12	13:25	2	0.289	0.03	0.26
TMF13-03_SA17_TP	3-Aug-13	14:11	14:25	2	2.73	1.0	1.7
TMF13-03_SA18_TP	3-Aug-13	16:08	16:20	2	0.945	0.49	0.45
TMF13-03_SA19_TP	4-Aug-13	13:19	13:25	2	3.11	1.4	1.7
TMF13-03_SA21_TP	4-Aug-13	16:49	17:00	2	0.632	0.40	0.23
TMF13-03_SA22_TP	5-Aug-13	9:03	14:00	2	n/a	0.02	
TMF13-04_SA01_TP	2-Jul-13	16:12	7:00	2	0.242	0.29	-0.05
TMF13-04_SA02_TP	3-Jul-13	7:38	?	2	2.08	1.6	0.4
TMF13-04_SA03_TP	3-Jul-13	9:07	9:15	1	0.996	0.86	0.14

TMF13-04_SA04_TP	3-Jul-13	10:16	10:20	1	3.61	1.7	2.0
TMF13-04_SA05_TP	3-Jul-13	13:56	14:00	1	5.29	4.6	0.7
TMF13-04_SA06_TP	3-Jul-13	14:53	15:00	1	0.022	0.08	-0.06
TMF13-04_SA07_TP	3-Jul-13	15:50	16:00	1	0.173	0.17	0.00
TMF13-04_SA08_TP	3-Jul-13	16:34	16:45	1	0.256	0.33	-0.07
TMF13-04_SA09_TP	4-Jul-13	6:44	7:00	1	0.072	0.08	-0.01
TMF13-04_SA10_TP	4-Jul-13	7:42	7:45	1	0.124	0.13	-0.01
TMF13-04_SA11_TP	4-Jul-13	8:40	8:45	1	1.13	1.3	-0.1
TMF13-04_SA12_TP	4-Jul-13	10:32	10:40	2	0.022	0.07	-0.05
TMF13-04_SA13_TP	4-Jul-13	13:18	13:25	2	0.212	0.04	0.17
TMF13-04_SA14_TP	4-Jul-13	14:17	14:30	2	0.313	0.09	0.22
TMF13-04_SA15_TP	4-Jul-13	15:17	15:25	2	0.584	0.27	0.31
TMF13-04_SA16_TP	4-Jul-13	16:18	16:30	1	2.04	1.6	0.4
TMF13-04_SA17_TP	5-Jul-13	6:50	7:00	2	4.97	1.8	3.2
TMF13-04_SA18_TP	5-Jul-13	7:55	8:15	1	0.837	0.63	0.21
TMF13-04_SA19_TP	5-Jul-13	9:49	10:00	2	0.152	0.17	-0.02
TMF13-05_SA01_TP	30-Jul-13	13:56	14:00	2	0.220	0.01	0.21
TMF13-05_SA03_TP	30-Jul-13	14:44	14:45	2	0.593	0.77	-0.18
TMF13-05_SA05_TP	30-Jul-13	15:35	15:45	2	3.04	2.3	0.7
TMF13-05_SA06_TP	30-Jul-13	16:25	16:30	2	3.01	2.3	0.7
TMF13-05_SA07_TP	31-Jul-13	7:23	7:30	2	1.23	1.2	0.0
TMF13-05_SA09_TP	31-Jul-13	8:54	9:00	2	0.707	0.62	0.09
TMF13-05_SA11_TP	31-Jul-13	13:06	13:00	2	0.330	0.36	-0.03
TMF13-05_SA12_TP	31-Jul-13	14:04	14:10	2	9.67	1.4	8.3
TMF13-05_SA13_TP	31-Jul-13	15:32	15:45	2	2.08	0.63	1.45
TMF13-05_SA14_TP	1-Aug-13	7:15	7:25	2	0.381	0.18	0.20
TMF13-05_SA15_TP	1-Aug-13	8:55	9:05	2	1.88	1.2	0.7
TMF13-06_SA01_TP	5-Jul-13	13:36	13:45	2	1.32	0.43	0.89
TMF13-06_SA03_TP	5-Jul-13	14:40	14:45	1	3.53	0.87	2.66
TMF13-06_SA04_TP	6-Jul-13	6:56	7:00	2	1.21	0.44	0.77
TMF13-06_SA06_TP	6-Jul-13	7:44	7:50	2	3.52	0.90	2.62
TMF13-06_SA07_TP	6-Jul-13	8:35	8:40	2	1.98	1.1	0.8
TMF13-06_SA09_TP	6-Jul-13	10:30	10:35	2	0.078	0.13	-0.05
TMF13-06_SA11_TP	6-Jul-13	13:49	13:55	1	0.135	0.12	0.01
TMF13-06_SA12_TP	6-Jul-13	14:42	14:55	2	2.04	1.8	0.2
TMF13-06_SA13_TP	6-Jul-13	16:32	16:37	2	0.942	0.72	0.22
TMF13-06_SA14_TP	7-Jul-13	6:55	7:00	1	3.28	2.7	0.5
TMF13-06_SA15_TP	7-Jul-13	8:06	8:15	2	2.82	1.7	1.2
TMF13-06_SA16_TP	7-Jul-13	8:38	10:30	2	2.23	2.0	0.2
TMF13-07_SA01_TP	18-Jul-13	14:48	15:00	1	n/a	n/a	
TMF13-07_SA03_TP	20-Jul-13	6:57	7:07	2	0.249	0.27	-0.02
TMF13-07_SA04_TP	20-Jul-13	7:50	8:00	2	1.79	1.1	0.7
TMF13-07_SA06_TP	20-Jul-13	9:19	9:30	2	0.188	0.15	0.04
TMF13-07_SA07_TP	20-Jul-13	10:11	10:15	2	0.034	0.01	0.02
TMF13-07_SA09_TP	20-Jul-13	13:37	13:45	2	2.41	1.4	1.0
TMF13-07_SA10_TP	20-Jul-13	14:37	14:45	2	1.55	1.3	0.2
TMF13-07_SA12_TP	20-Jul-13	15:24	15:30	2	0.529	0.53	0.00

Total Iron was measured directly by ICP, with no chromatography prior to sample introduction.

Fe^{2+} measure by HACH.

Fe^{3+} calculated by difference.

All analyses performed by Greg Ehrmantraut at Areva McClean Lake Operation

Tailings Neutralization Process

Analyte	(mg/L)	(% prec.)
Al	420	0.0
As	732	0.0
Fe	2,400	0.0
Ni	560	0.0
Si	260	0.0

McCle

Solution pH 1.5

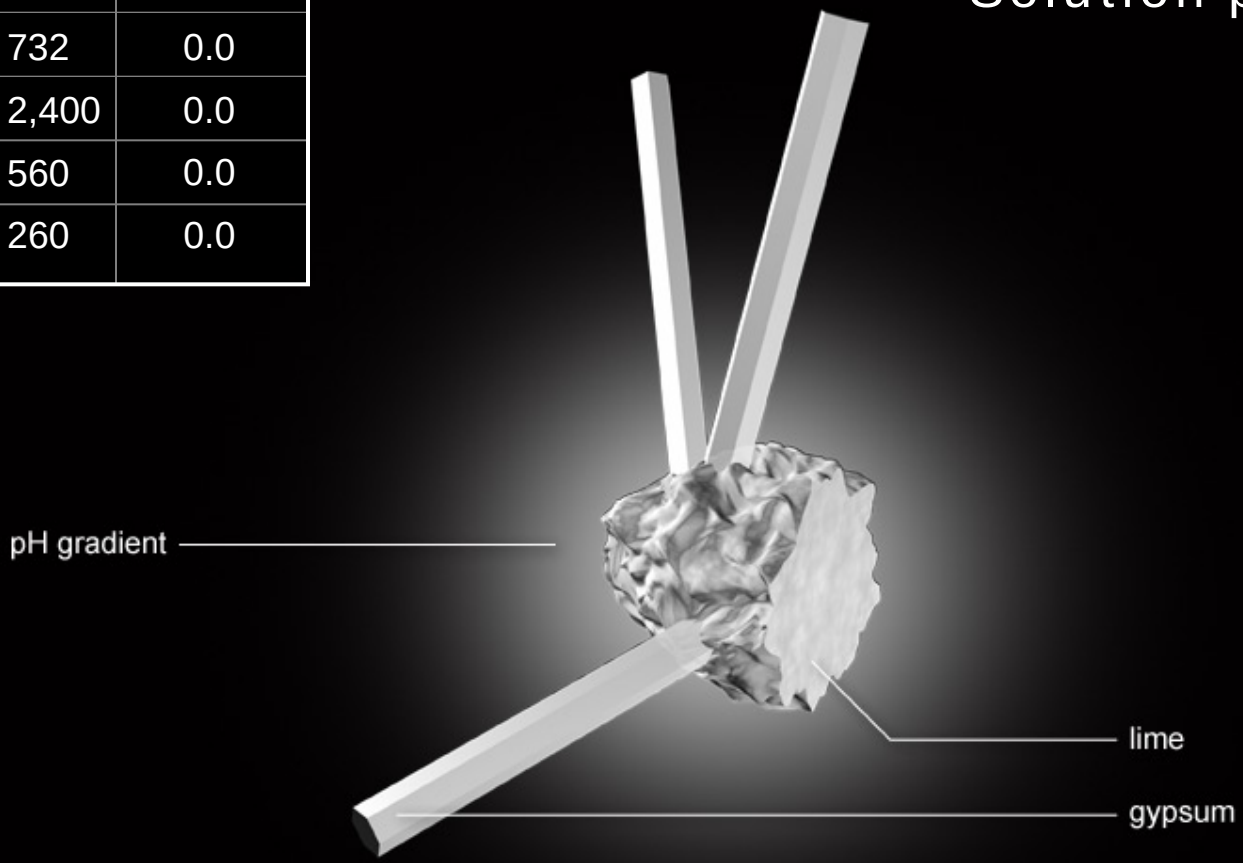

Tailings Neutralization Process

McClean Lake Operation

Analyte	(mg/L)	(% prec.)
Al	420	0.0
As	659	~10
Fe	2,328	~3
Ni	532	~5
Si	260	0.0

Solution pH 1.5

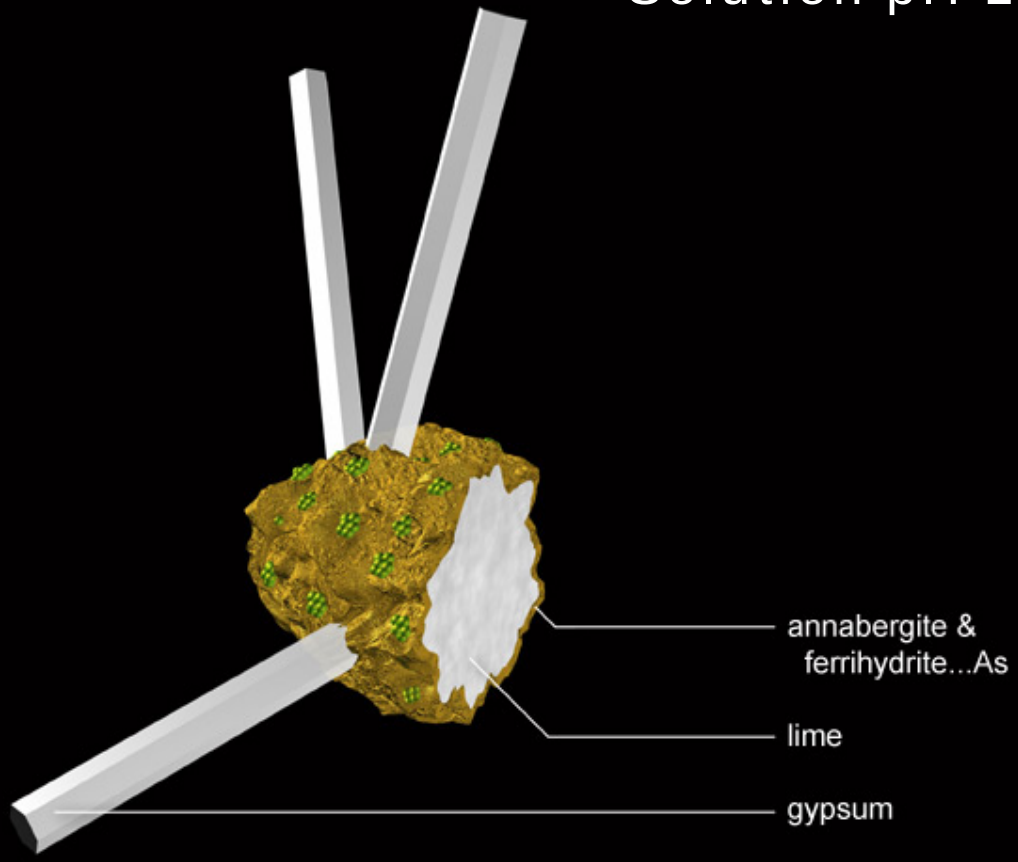

Tailings Neutralization Process

McClean Lake Operation

Analyte	(mg/L)	(% prec.)
Al	420	0.0
As	150	79.5
Fe	1,600	33.3
Ni	500	10.7
Si	260	0.0

Solution pH 2.2

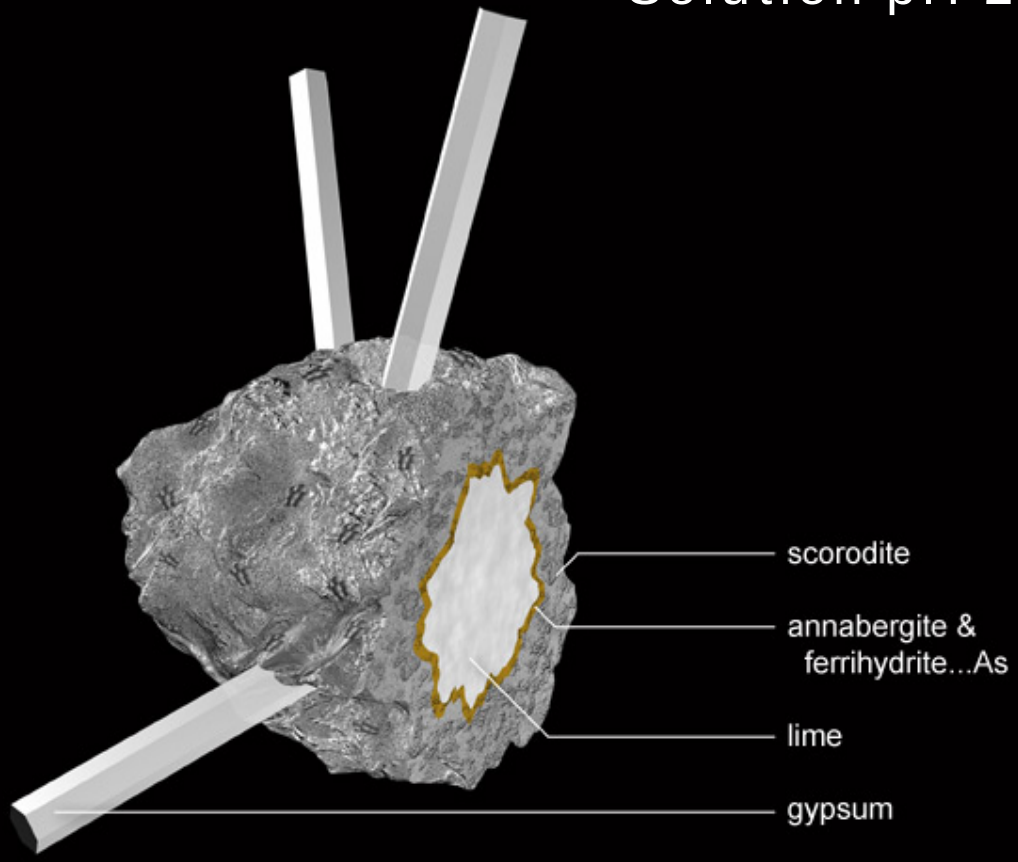

Tailings Neutralization Process

McClean Lake Operation

Analyte	(mg/L)	(% prec.)
Al	290	31.0
As	0.5	99.9
Fe	570	76.3
Ni	450	19.6
Si	140	46.2

Solution pH 4.0

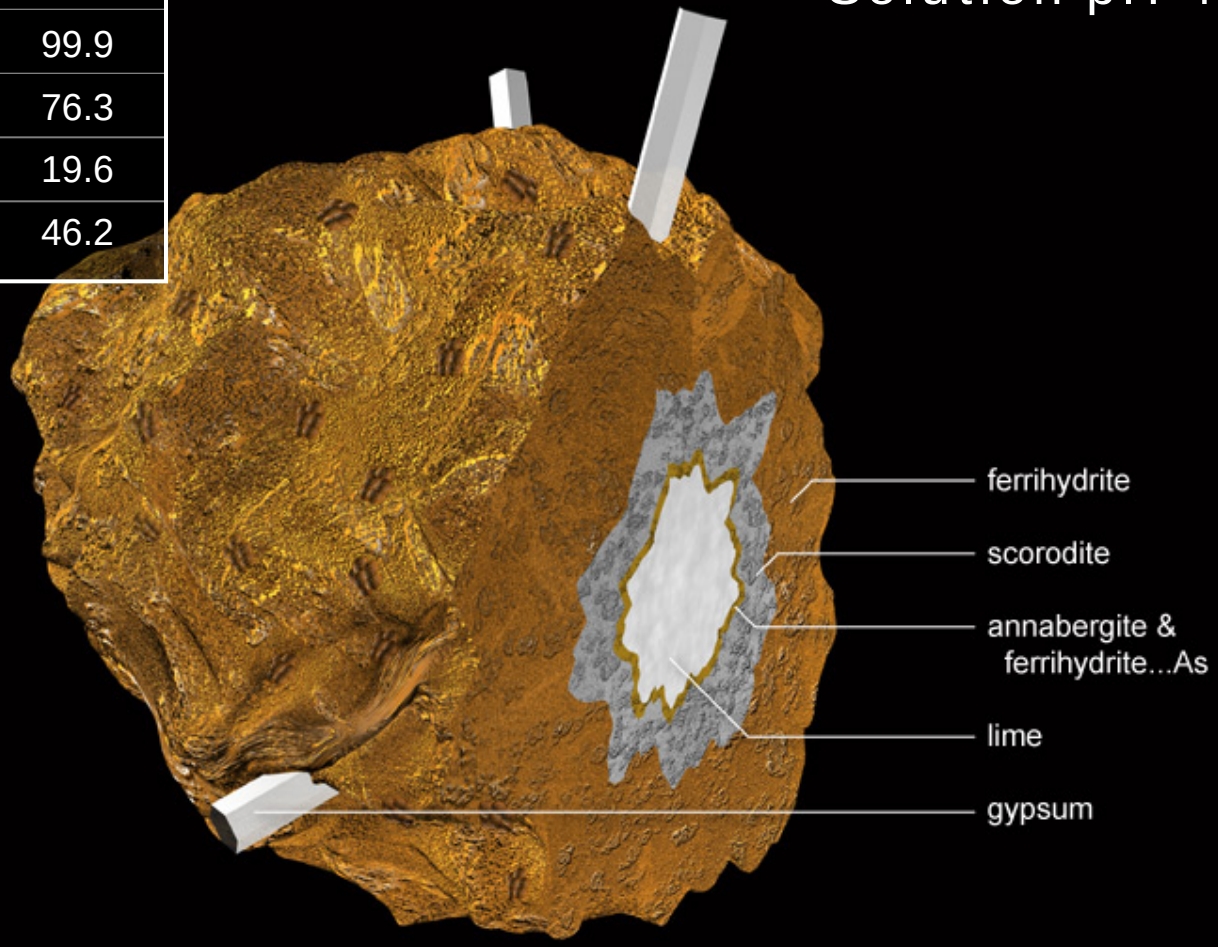

Tailings Neutralization Process

McClean Lake Operation

Analyte	(mg/L)	(% prec.)
Al	0.5	99.9
As	0.08	100.0
Fe	340	85.8
Ni	250	55.4
Si	17	93.5

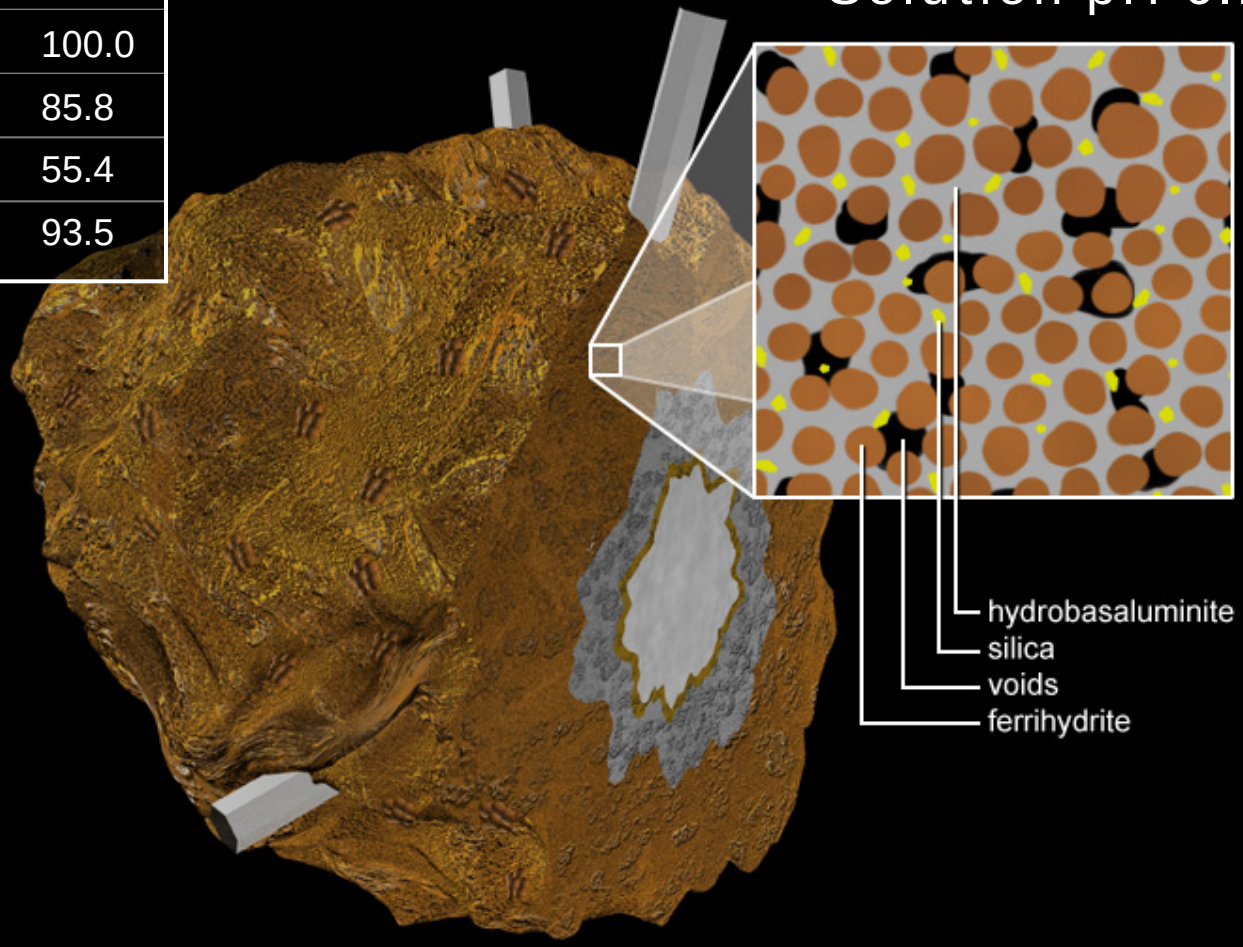

Tailings Neutralization Process

McClean Lake Operation

Analyte	(mg/L)	(% prec.)
Al	0.5	99.9
As	0.06	100.0
Fe	2.2	99.9
Ni	1.3	99.8
Si	3.2	98.8

Solution pH 7.4

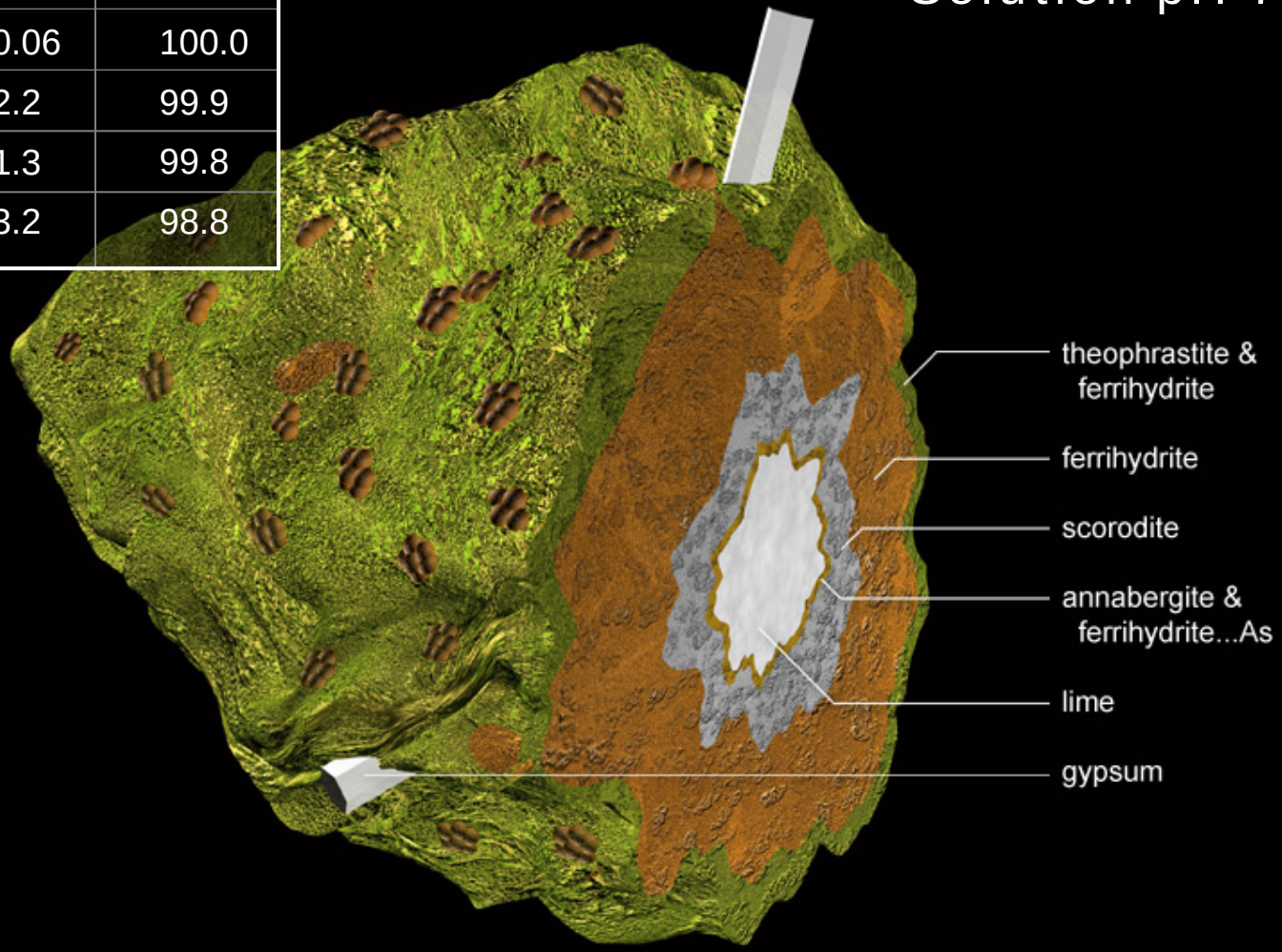

Tailings Neutralization Process

McClean Lake Operation

Analyte	(mg/L)	(% prec.)
Al	0.5	99.9
As	0.06	100.0
Fe	2.2	99.9
Ni	1.3	99.8
Si	3.2	98.8

Solution pH 7.4

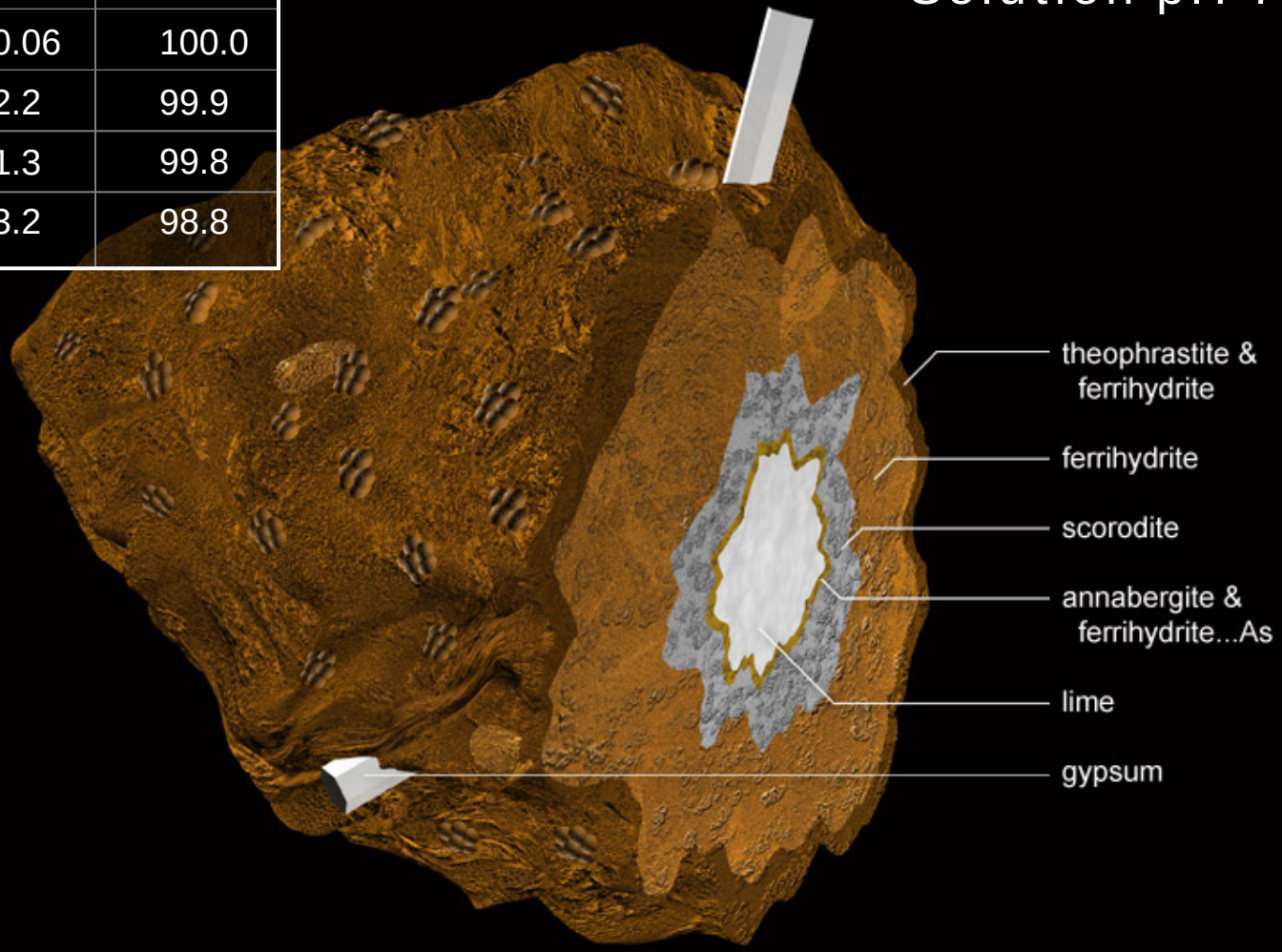

An update on the examination of calcium-containing minerals in the JEB Tailings Management Facility, McClean Lake, Saskatchewan: A soft X-ray absorption near-edge spectroscopy analysis

Peter E. R. Blanchard, Andrew P. Grosvenor*
Department of Chemistry, University of Saskatchewan, Saskatoon, SK, S7N 5C9

John Rowson, Kebbi Hughes, Caitlin Brown
AREVA Resources Canada, Saskatoon, SK, S7K 3X5

*Author to whom correspondence should be addressed
E-mail: andrew.grosvenor@usask.ca
Phone: (306) 966-4660
Fax: (306) 966-4730

1. Executive Summary

Soft X-ray XANES analysis was performed on a series of tailings samples collected from the JEB Tailings Management Facility (TMF) during the 2013 sampling campaign to determine if calcium carbonate (in the form of calcite or aragonite) forms in the TMF. Analysis of the Ca $L_{2,3}$-edge XANES spectra confirmed that gypsum was the major calcium-containing mineral species in the tailings samples. XANES analysis could not conclusively confirm the identity of minor calcium-containing mineral species. The C K-edge XANES analysis indicated that the solid carbon content in the tailings samples was organic. The characteristic features of calcium carbonate was not visible in the C K-edge XANES spectra of the tailings samples. Overall, the presence of calcium carbonate could not be confirmed from the Ca $L_{2,3}$-edge and C K-edge XANES analyses.

2. Experimental

C K-edge and Ca $L_{2,3}$-edge XANES spectra were collected on the high resolution spherical grating monochromator (SGM) undulator beamline (11ID-1) at the Canadian Light Source (Saskatoon, Canada).[1] Powder samples were either dusted on carbon tape (Ca $L_{2,3}$-edge) or drop-coated on a gold-plated silicon wafer (C K-edge). All samples were inserted into the vacuum chamber via a load lock chamber. The pressure inside the analysis chamber was maintained at better than ~10^{-9} mbar during the measurements. Ca $L_{2,3}$-edge spectra were collected from ~10 eV below to ~15 eV above the Ca L_3-edge absorption edge, with a step size of 0.1 eV. C K-edge spectra were collected in "Fast Scan" mode, which involves rapidly collecting multiple scans (60 scans, 30 s each) ranging from ~20 eV below to ~30 eV above the C K-edge absorption edge. The sample was moved between scans to reduce the effects of X-ray beam-induced damage. Spectra were collected using both total electron yield (TEY) and total

fluorescence yield (TFY) modes. TFY spectra were collected using a silicon drift detector. The Ca $L_{2,3}$-edge was calibrated against calcite, with the peak maximum of the L_3-edges set to 350.3 eV.[2] The C K-edge was calibrated against citric acid, with the maximum of the first derivative of the K-edge set to 288.6 eV.[3] All XANES spectra were analyzed using the Athena and CasaXPS software packages.[4,5] A quantitative analysis of the Ca $L_{2,3}$-edge XANES spectra was performed using principle component analysis (PCA) followed by a linear combination fitting (LCF) The energy range used for PCA and LCF analysis was -1 and +5 eV relative to the Ca L_3-edge absorption edge energy. Quantitative analysis was not performed on the C K-edge spectra because of the overlap of the C K-edge and K $L_{2,3}$-edges.

3. Results and Discussion

3.1. Ca L-edge XANES analysis

The Ca $L_{2,3}$-edge XANES spectra of the tailings samples and standards are shown in Figure 1. XANES spectra were collected from finely powdered and homogenized samples. Information on the major calcium-containing mineral species in the tailings samples can be obtained from the XANES spectra under these conditions. The Ca L-edge splits by spin-orbit coupling, resulting in two features corresponding to dipole-allowed $2p_{3/2} \rightarrow 3d$ (L_3-edge) and $2p_{1/2} \rightarrow 3d$ (L_2-edge) transitions. The L_3- and L_2-edge further splits into two major peaks; labelled A and B for the L_3-edge and A` and B` for the L_2-edge. This splitting is characteristic of Ca^{2+} and loosely corresponds to the crystal field splitting of the Ca 3d states.[6,7] The relative intensity and energy difference of features A (A`) and B (B`) will depend on the local coordination environment of the Ca^{2+} cation. Several low intensity features are observed below 349 eV and are attributed to core-hole effects.[8] As shown in Figure 2, the Ca L-edge of the tailings samples are similar to that of gypsum. This is consistent with the Ca K-edge XANES

analysis, which indicated that gypsum is the major calcium-containing mineral in the tailings. Note that feature B (B`) in the Ca $L_{2,3}$-edge spectra is more intense in the tailings samples than gypsum, likely indicating that other calcium-containing minerals may be present in the tailings samples.

Principal component analysis (PCA) was used to determine the number of calcium-containing mineral species present in the tailings. Assuming a XANES spectrum consists of a linear combination of spectra that make up the components of a mixture, a PCA calculation assumes that the minimum number of components that describe the variation in the data set is equivalent to the minimum number of chemical species.[9,10] The results of the PCA performed on the six tailings samples are shown in Figure 3a. Of the six components, the first component accounts for >99.99 % of the total variances. This indicates that there is very little variation in the tailings samples spectra. This was confirmed by calculating the IND values. The IND function is an empirical function developed by Malinowski to determine the minimum number of components required to describe a series of spectra.[11,12] It is generally accepted that the minimum number of components is given when the IND function is minimized.[11,12] As shown in Figure 3b, components 1 and 2 have similar minimum IND values, suggesting that each tailings sample may consist of one or two components.

A linear combination fitting (LCF) analysis was used to identify the calcium-containing mineral species in the TMF. Each normalized Ca $L_{2,3}$-edge spectrum was fitted by a linear combination of weighted standard spectra. The coefficients calculated in the LCF correspond to the concentration of each calcium species present. The number of components used in the fittings was restricted to two based on the results of the PCA. The standards used in the LCF are shown in Figure 1b. Results of the LCF are shown in Table 1 and the fitted Ca $L_{2,3}$-edge

XANES spectra are shown in Figure 4. Gypsum was the major calcium-containing mineral species in all fittings, accounting for ~90 at% of the calcium content in the tailings samples. It was not obvious from the LCF what minor calcium-containing minerals were present in the tailings samples. As shown in Figure 5, similar fittings were obtained when fitting the tailings sample spectra to gypsum and other calcium-containing mineral standards. It is possible that crystallinity may affect the lineshape of the Ca $L_{2,3}$-edge, which would affect the results of the LCF. The Ca $L_{2,3}$-edge lineshape may be different due to distortions of the Ca^{2+} coordination environment if gypsum in the tailings is of a lower crystallinity than the gypsum mineral standard. Although crystallinity did not appear to influence the lineshape of the Ca K-edge, the broader lineshape of the Ca K-edge compared to the L-edge may have masked these minor effects. The Ca $L_{2,3}$-edge XANES analysis confirms that gypsum is the major Ca-containing mineral species in the tailings samples.

3.2 C K-edge XANES analysis

The C K-edge XANES spectra of the tailings samples and standards are shown in Figure 6. The C K-edge corresponds to a dipole-allowed transition of a 1s electron in 2p states. Features corresponding to the K L_3-edge (~298 eV) and L_2-edge (~300.5 eV) are also observed in the spectra because potassium is found in several of the clay minerals (i.e., sericite, smectite) in the tailings.[13] As shown in Figure 7, there are two major features in the C K-edge. The first feature corresponds to a C 1s $\rightarrow \pi^*$ transition.[14,15] This feature is observed at higher energies in carbonate standards (i.e., calcite; 290.4 eV) compared to hydrocarbon standards (i.e., kerosene; 284.9 eV). The shift in energy is due to the larger electronegativity of oxygen compared to carbon.[16] The "charge" on the absorbing carbon atom increases and shifts the π^* transition to higher absorption energies as the electronegativity of the neighbouring atoms increases. The

second feature in the C K-edge corresponds to a C 1s → σ* transition. Multiple peaks are observed in this region of the C K-edge of carbonate species due to the interaction of carbon σ* states with next-nearest neighbour states (i.e. Ca 4p states). The σ* feature appears broader in kerosene. Broadening of this region of the C K-edge of kerosene may be due to multiple overlapping σ* transitions (i.e. C–C, C–H) because kerosene consists of a mixture of multiple hydrocarbon species.[17]

As shown in Figure 8, the C K-edge lineshape of the tailings samples is similar to that of kerosene, indicating that the major carbon species in the tailings are organic. The peak at 285 eV, characteristic of a C 1s → π*, suggests that these carbon species may be aromatics or olefins.[14] The feature at 292 eV in the spectra of the tailings samples was not observed in any of the carbon standards. This feature may correspond to a C 1s → σ* transition of an unidentified organic carbon species (i.e., amide, ketone, carboxylic acid) based on the energy of this feature.[14] The characteristic feature of carbonates (i.e., the C=O π* transition) was not observed in the tailings samples, indicating that carbonates are not a major carbon-containing species in the tailings.

4. Conclusions

Soft X-ray XANES was used to identify the calcium- and carbon-containing species in the tailings samples. The Ca L-edge XANES analysis identified gypsum as the major calcium-containing mineral in the tailings samples. However, LCF analysis could not conclusively identify the minor calcium-containing minerals species due to differences in the crystallinity of the mineral standards and the minerals found in the tailings. The C K-edge analysis also indicated that the major carbon species in the tailings were organic species. Overall, the soft X-ray analysis did not conclusively identify calcium carbonate in the tailings samples; however, it

cannot be concluded that calcium carbonate is not present as it may be present in concentrations below the detection limits of bulk XANES techniques. Ca K-edge μ-XANES spectra, which were collected using a smaller beamsize (i.e., μm), may identify minor calcium-containing species in the tailings that were not found using bulk-sensitive XANES. Analysis of the Ca K-edge μ-XANES spectra, collected on the Soft X-ray Microcharacterization Beamline (SXRMB) at the Canadian Light Source, is currently underway to identify the minor calcium-containing mineral species in the tailings samples.

5. References

1. Regier, T.; Krochak, J.; Sham, T. K.; Hu Y. F.; Thompson, J.; Blyth, R. I. R. Performance and capabilities of the Canadian Dragon: The SGM beamline at the Canadian Light Source. *Nucl. Instrum. Meth. A* **2007**, *582*, 93-95.

2. Fleet, M. E.; Liu X. Calcium $L_{2,3}$-edge XANES of carbonates, carbonate apatite, and oldhamite (CaS), *Am. Mineral*. **2009**, *94*, 1235-1241.

3. Solomon, D.; Lehmann, J.; Kinyangi, J.; Liang, B.; Heymann, K. Dathe, L.; Hanley, K.; Wirick, S.; Jacobsen, C. Carbon (1s) NEXAFS spectroscopy of biogeochemically relevant reference organic compounds. *Soil Sci. Soc. Am. J.* **2009**, *73*, 1817-1830.

4. Ravel, B.; Newville, M. ATHENA, ARTEMIS, HEPHAESTUS: data analysis for X-ray absorption spectroscopy using IFEFFIT. *J. Synchrotron Rad.* **2005**, *12*, 537-541.

5. Fairley, N. *CasaXPS*, version 2.3.17dev5.9n; Casa Software, Ltd.: Teignmouth, Devon, U.K., **2012** (www.casaxps.com).

6. Himpsel, F. J.; Karlsson, U. O.; McLean, A. B.; Terminello, L. J.; de Groot, F. M. F.; Abbate, M.; Fuggle, J. C.; Thole, B. T.; Sawatzky, G. A. Fine structure of the Ca 2p X-ray absorption edge for bulk compounds, surfaces, and interfaces. *Phys. Rev. B* **1991**, *43*, 6899-6907.

7. Politi, Y.; Metzler, R. .A.; Abrecht, M.; Gilbert, B.; Wilt, F. H.; Sagi, I.; Addadi, L.; Weiner, S.; Gilbert, P. Transformation mechanism of amorphous calcium carbonate into calcite in the sea urchin larval spicule. *Proc. Natl. Acad. Sci***. 2005**, *105*, 17362-17366.

8. De Groot, F. M. F.; Fuggle, J .C.; Thole, B. T.; Sawatzky, G. A. $L_{2,3}$ X-ray absorption edges of d^0 compounds: K^+, Ca^{2+}, Sc^{3+}, and Ti^{4+} in *Oh* (octahedral) symmetry. *Phys. Rev. B* **1990**, *41*, 928–937.

9. Fernández-Garcìa, M.; Márquez Alvarez, C.; Haller, G. L. XANES-TPR study of Cu – Pd bimetallic catalysts: application of factor analysis. *J. Phys. Chem.* **1995**, *99*, 12565–12569.

10. Beauchemin, S.; Hesterberg, D.; Beauchemin, M. Principal component analysis approach for modelling sulphur K-XANES spectra of humic acids. *Soil Sci. Soc. Am. J.* **2002**, *66*, 83-91.

11. Malinowski, E. R. Factor Analysis in Chemistry, 3rd ed., John Wiley & Sons, New York, 2002.

12. Malinowski, E. R. Theory of error in factor analysis. *Anal. Chem.* **1977**, *49*, 606-612.

13. Ahmed, A. A.; Kühn, O.; Leinweber, P. Controlled experimental soil organic matter modification for study of organic pollutant interactions in soil. *Sci. Total Environ.* **2012**, *441*, 151-158.

14. Cooney, R. R.; Urquhart, S. G. Chemical trends in the near-edge X-ray absorption fine structure of monosubstituted and para-bisubstituted benzenes. *J. Phys. Chem. B* **2004**, *108*, 18185-18191.

15. Yabuta, H.; Uesugi, M.; Naraoka, H.; Ito, M.; Kilcoyne, A. L. D. Sandford, S. A. Kitajima, F.; Mita, H.; Takano, Y.; Yada, T.; Karouji, Y.; Ishibashi, Y.; Okada, T.; Abe, M. X-ray absorption near edge structure spectroscopic study of Hayabusa category 3 carbonaceous particles. *Earth Planets Space* **2014**, *66*, 156.

16. Allred, A. L.; Rochow, E. G. A scale of electronegativity based on electrostatic forces. *J. Inorg. Nucl. Chem.* **1958**, *5*, 264-268.

17. Cody, G. D.; Botto, R. E.; Ade, H.; Behal, S.; Disko, M.; Wirick, S. Inner-shell spectroscopy and imaging of a subbituminous coal: In-situ analysis of organic and inorganic microstructure using C(1s)-,Ca(2p)-, and Cl(2s)-NEXAFS. *Energy Fuels* **1995**, *9*, 525-533.

Tables

Table 1. LCF results for the fitting of the Ca L-edge XANES spectra of the tailings samples.

Sample	Gypsum (at%)	Lime* (at%)	R-factor	χ^2
TMF13-01-SA12	91(2)	9(3)	0.00832	264
TMF13-01-SA19	93(2)	7(6)	0.00962	299
TMF13-01-SA22	93(2)	7(6)	0.00652	194
TMF13-03-SA12	89(3)	11(2)	0.00521	153
TMF13-03-SA15	87(2)	13(3)	0.00685	192
TMF13-03-SA19	87(2)	13(2)	0.00701	193

*Similar results were obtained when fitting the spectra of the tailings samples to calcite, aragonite, and powellite.

Figures

Figure 1

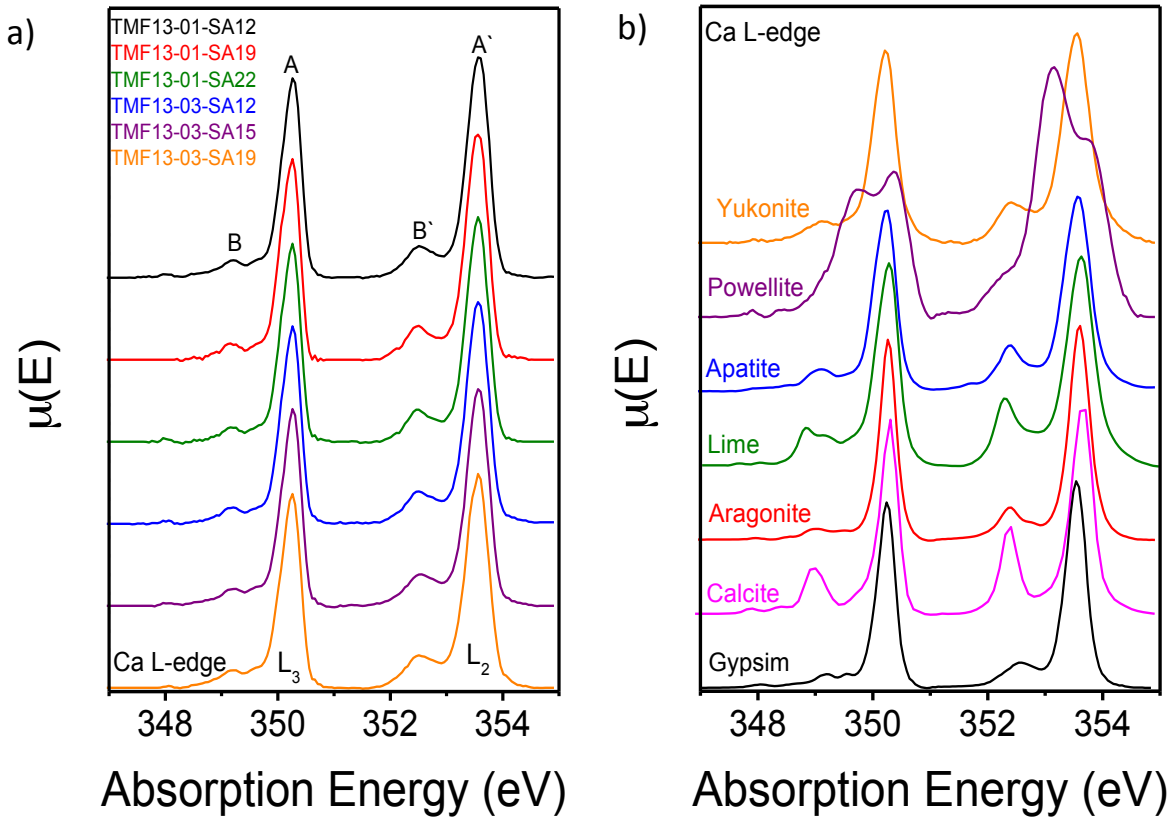

Figure 1. The Ca $L_{2,3}$-edge XANES spectra of a) the tailings samples and b) calcium-containing standards. Features A (A`) and B (B`) are discussed in the text.

Figure 2

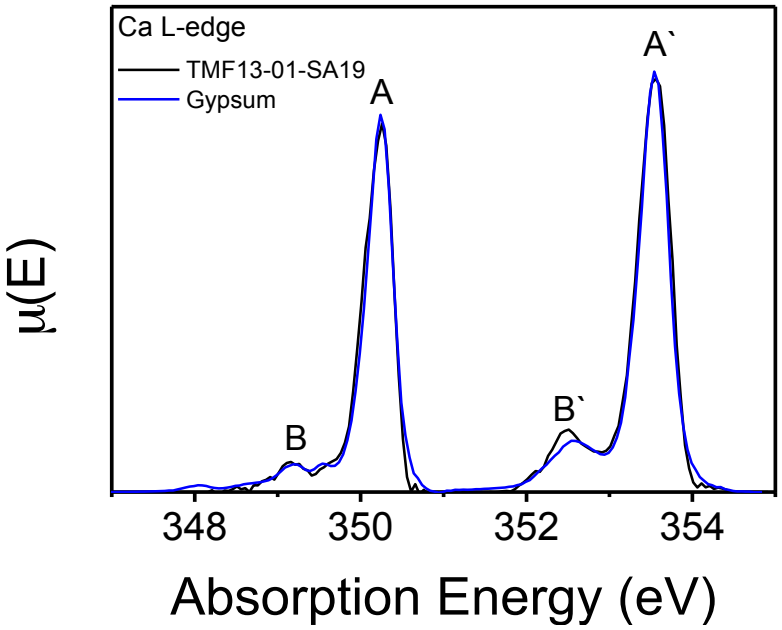

Figure 2. A comparison of the Ca L-edge XANES spectra of tailings sample TMF13-01-SA19 and gypsum. The lineshape of the tailings samples are generally similar to gypsum, suggesting that gypsum is the major calcium-bearing mineral in the tailings. Difference in the lineshape of the features B and B` suggests that other minor calcium phases are also present.

Figure 3

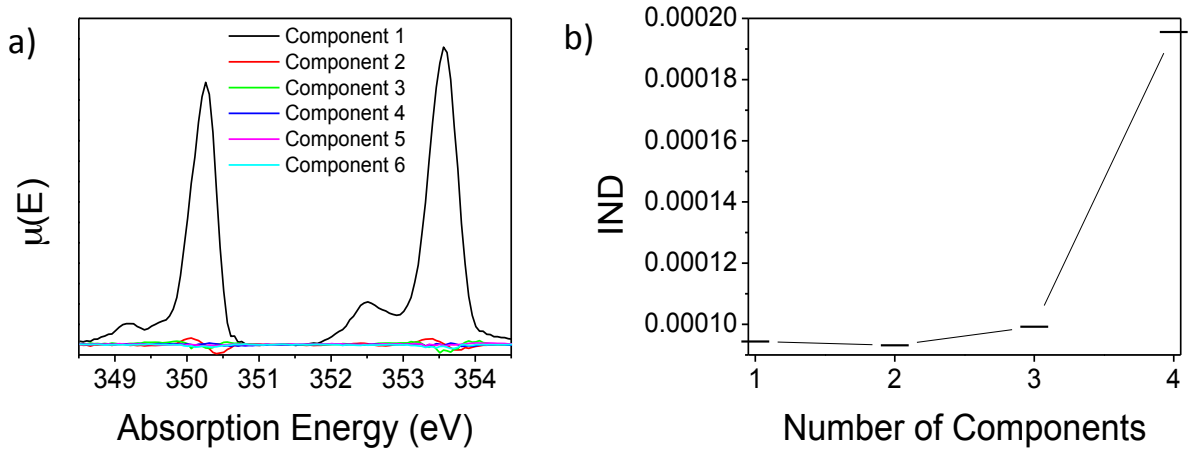

Figure 3. a) The principle components calculated from the PCA analysis of the six tailings samples are shown. Component 1 generally has the strongest intensity, accounting for >99.99 % of the variances. b) The IND function was calculated and plotted versus the number of components.

Figure 4

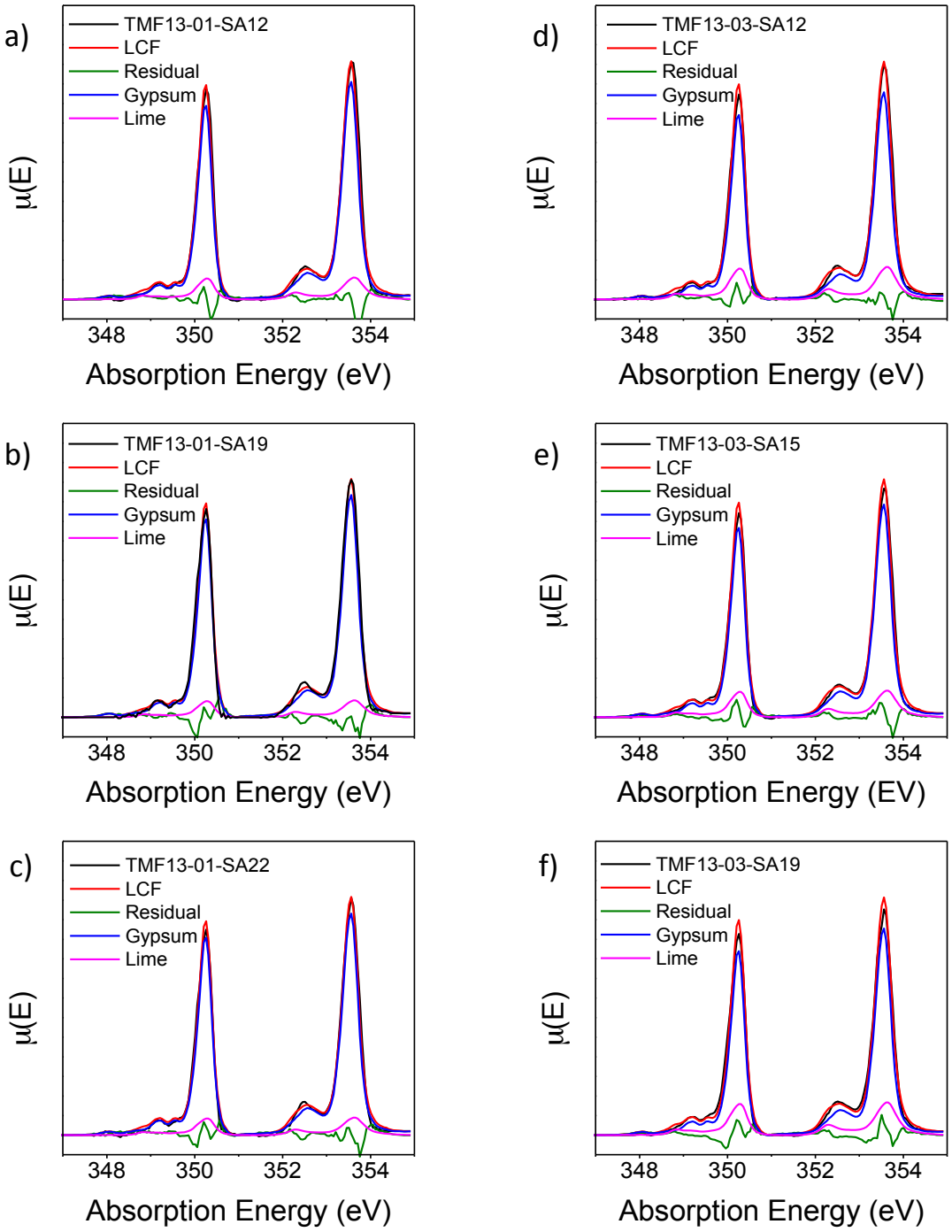

Figure 4. The fitted Ca $L_{2,3}$-edge XANES spectra of a) TMF13-01-SA12, b) TMF13-01-SA19, c) TMF13-01-SA22, d) TMF13-03-SA12, e) TMF13-03-SA15, and f) TMF13-03-SA19 are shown. The linear combination fitting of each spectrum shown in red and the residual is shown in green. The weighted spectra of the gypsum and lime are also shown.

Figure 5

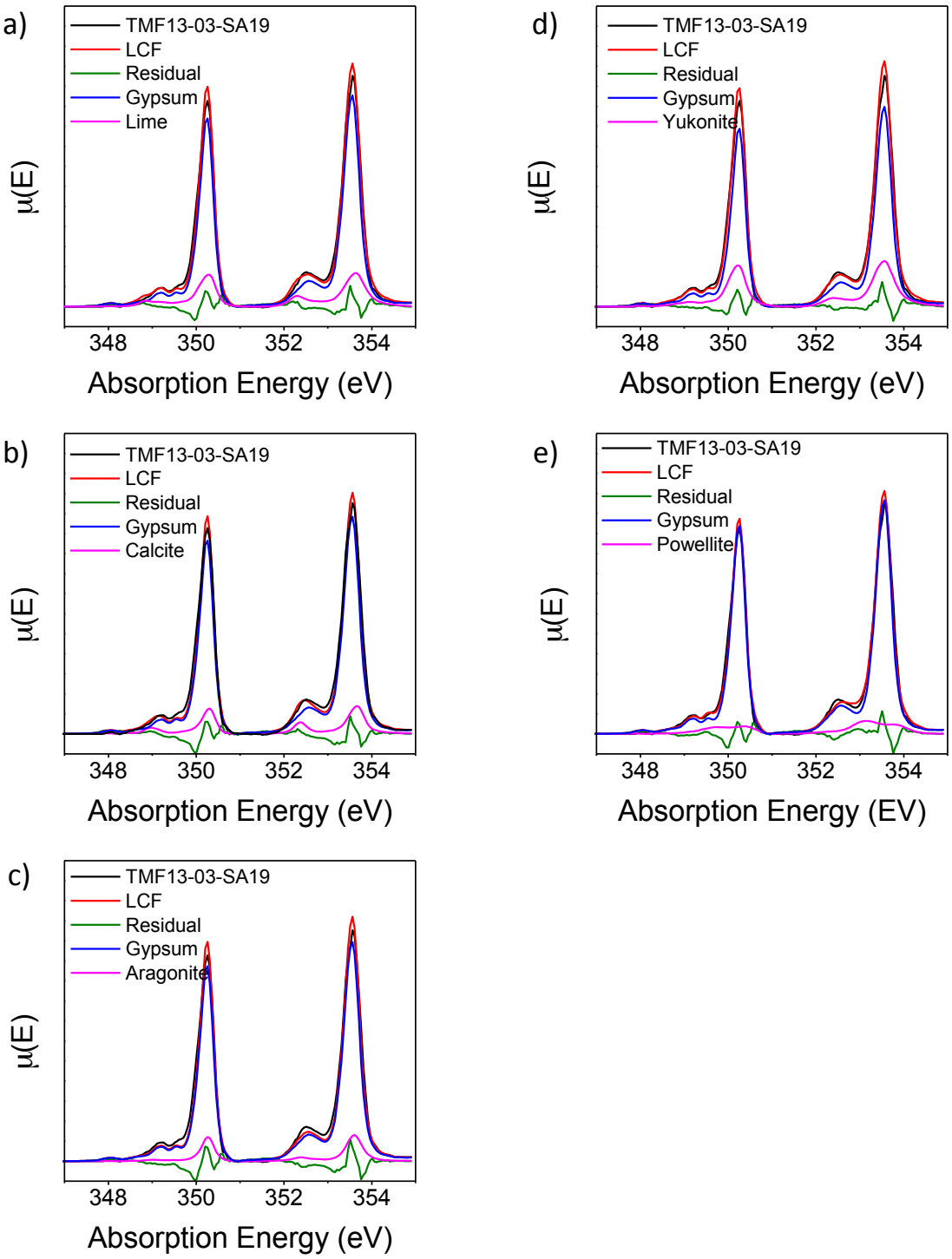

Figure 5. The Ca $L_{2,3}$-edge XANES spectrum of TMF13-03-SA19 fitted to gypsum and a) lime, b) calcite, c) aragonite, d) yukonite, and e) powellite. The concentration of gypsum is greater than 85 at% in all fittings.

Figure 6

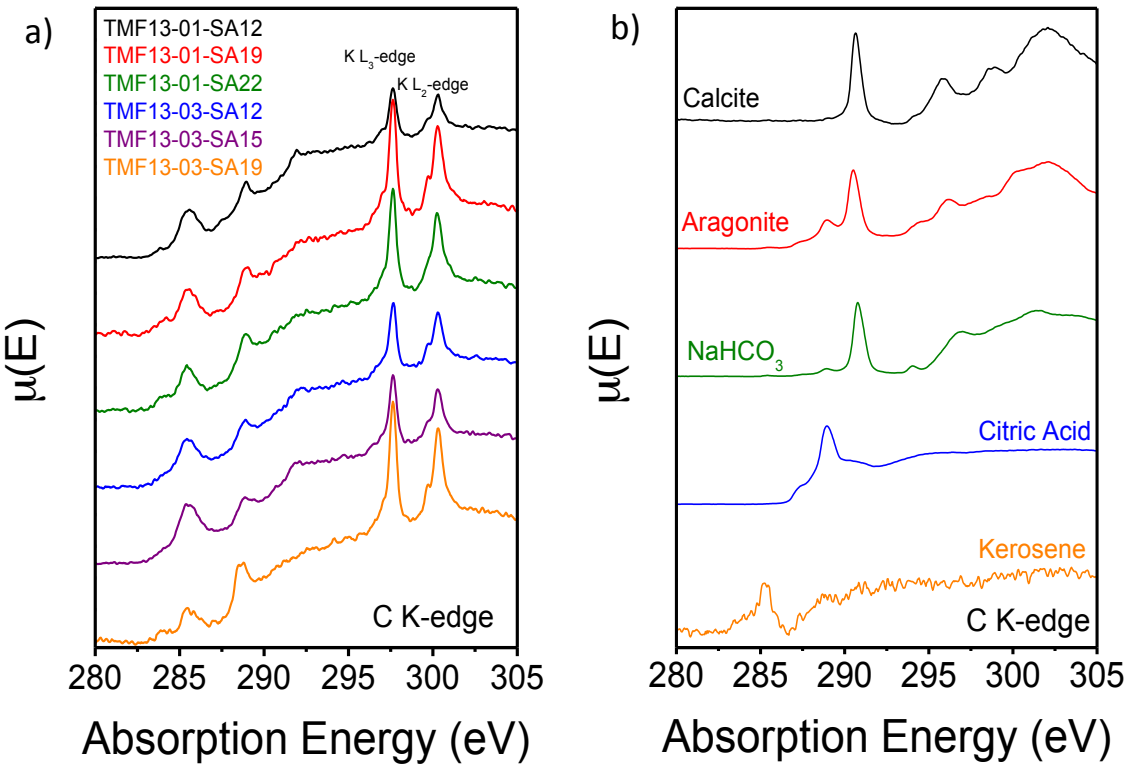

Figure 6. The C K-edge XANES spectra of a) the tailings samples and b) the carbon standards. Peaks corresponding to the K $L_{2,3}$-edge were observed in the tailings samples due to the presence of potassium-containing clay minerals in the tailings samples.

Figure 7

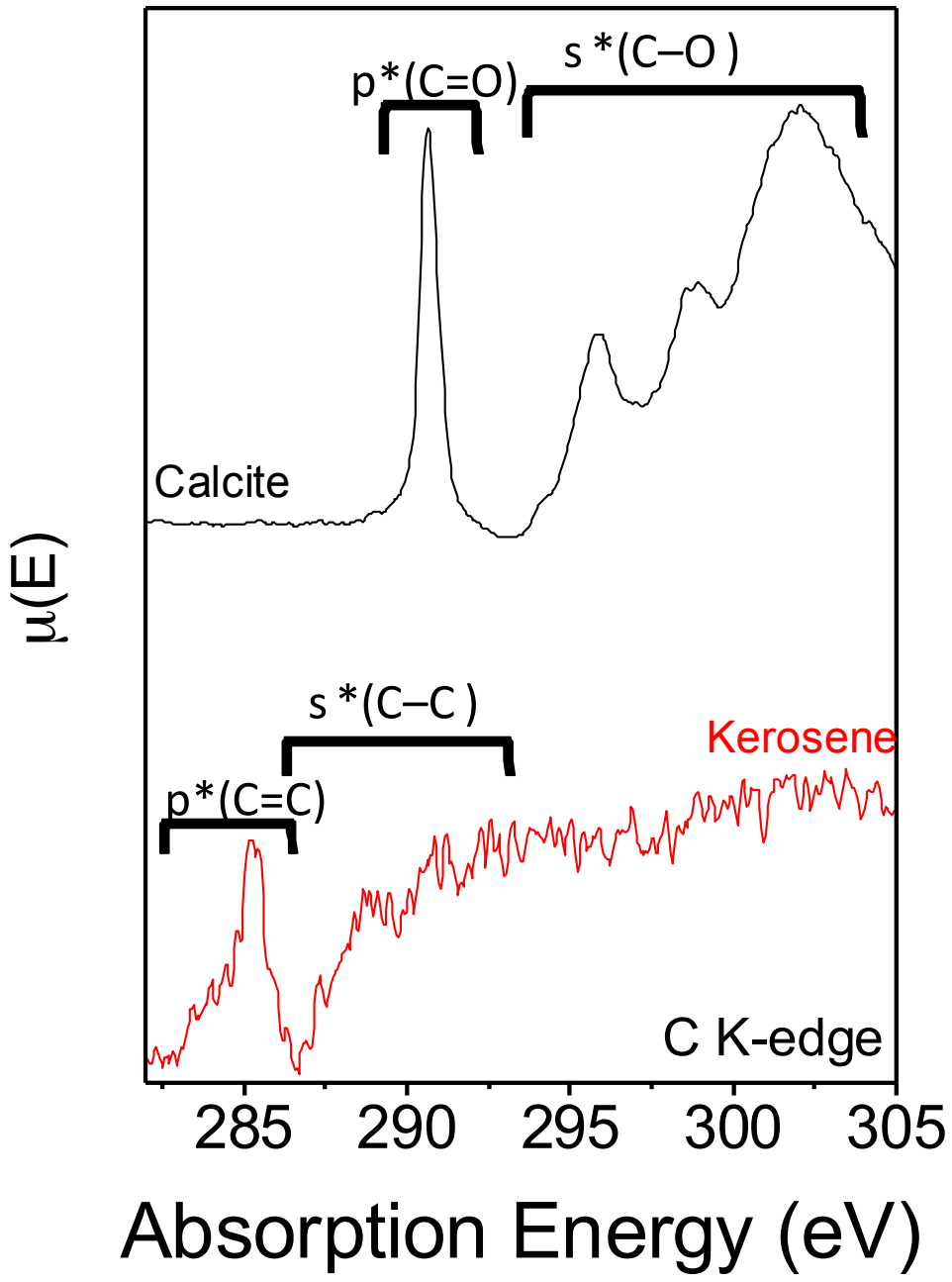

Figure 7. The C K-edge XANES spectra of calcite (top) and kerosene (bottom), highlighting features that correspond to the π* and σ* transitions. The π* transition of carbonates are found at higher energy compared to the π* transition of hydrocarbons.

Figure 8

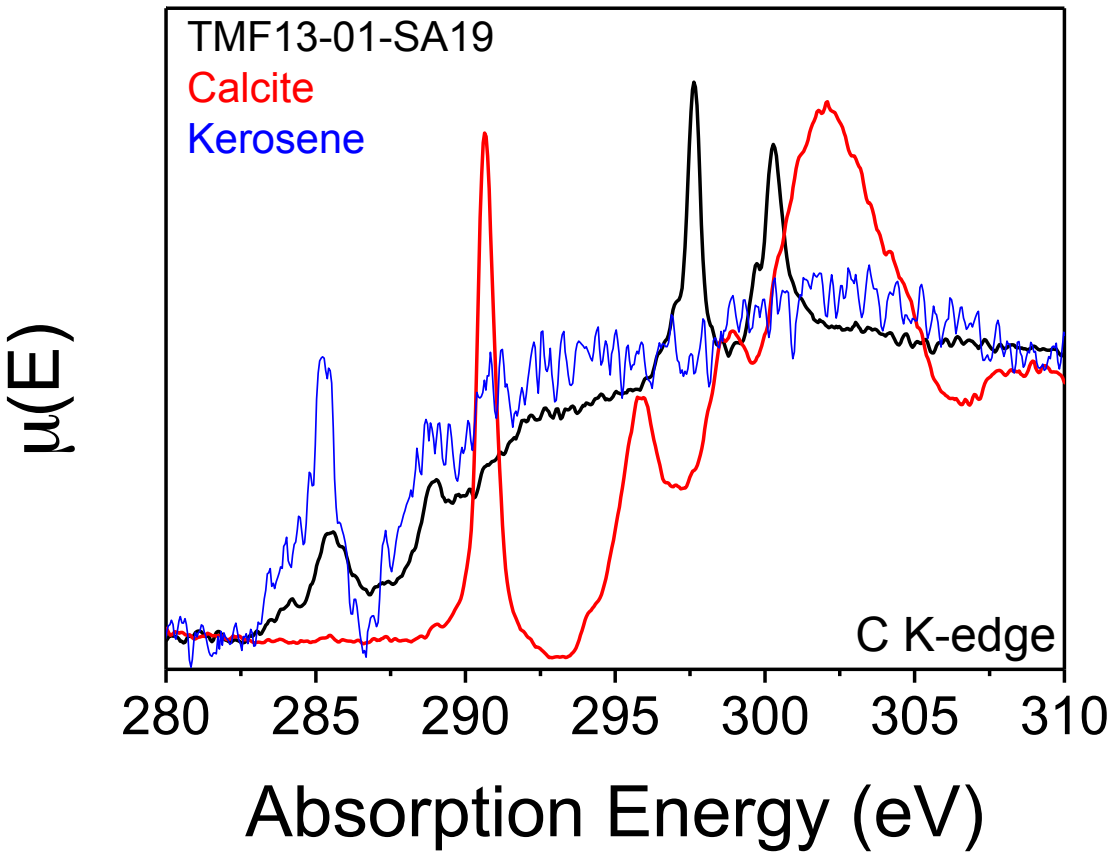

Figure 8. A comparison of the C K-edge XANES spectra of tailings sample TMF13-01-SA19 (black), carbonate (red), and kerosene (blue). Features in the C K-edge XANES spectra of the tailings sample are more similar to those observed in kerosene, suggesting that the major carbon species in the tailings samples are organic.

TOVP SUE A aging test FINAL DATA

#		Jar #1	Jar#2	Jar#3	Jar#4	Jar#5	Jar#6	Jar#7	Jar#8	Jar#9	Jar#10	Jar#11	Jar#12	Jar#13	Jar#14	Jar#15
DATE		22-Jun-06	22-Jul-06	22-Aug-06	22-Sep-06	22-Oct-06	22-Nov-06	22-Feb-07	22-Apr-07	22-Jun-07	22-Aug-07	22-Oct-07	22-Dec-07	22-Jun-08	22-Dec-08	22-Jun-09
Day		0	30	61	92	122	153	245	305	366	427	488	549	732	915	1098
AsT	mg/L	1.97	2.72	3.23	2.81	2.69	2.56	8.56	2.74	2.06	1.9	2.13	2.23	1.92	2.17	1.66
As(3+)	mg/L	0.67	0.093	0.45	0.08	0.07	0.099	0.112	0.116	0.14	0.06	0.42	0.088	0.094	0.086	0.14
As(5+)	mg/L	0.53	1.81	2.16	1.94	1.8	1.89	7.59	2.21	1.76	1.84	1.71	2.14	1.64	1.73	1.54
Ni	mg/L	0.902	0.659	0.75	0.91	0.633	0.914	6.73	0.904	0.8	0.774	0.77	1.18	1.09	1.54	1.45
U	mg/L	0.005	0.018	0.019	0.011	0.325	0.18	0.22	0.04		0.023	0.06	0.015	0.12	0.15	0.183
pH		7.3	6.8	7.1	7.1			7.1	6.8	7.2	n/a	7.3	6.7	7	6.8	7.4
ORP	mV			398				308	226	n/a	n/a	441	434	282	354	265
Fe total	mg/L					0.721	0.284	13.2	0.32	0.07	0.112	0.034	0.415	0.096	1.02	1.13
Fe2+	mg/L					0.03	0.01	0.15	0.07	0.02	0.09	0.03	0.03	0	0.03	0.11
Fe3+	mg/L					0.691	0.274	13.05	0.25	0.03	0.012	0.004	0.385	0.096	0.99	1.02
HCO3-	mg/L	0				132	66	54		56	59	59	57	59	59	61

Progress report on the X-ray diffraction and absorption spectroscopy study of the calcium speciation in the JEB Tailings Management Facility at McClean Lake, Saskatchewan

Peter E. R. Blanchard, Andrew P. Grosvenor*

Department of Chemistry, University of Saskatchewan, Saskatoon, SK, S7N 5C9

John Rowson, Kebbi Hughes, Caitlin Brown

AREVA Resources Canada, Saskatoon, SK, S7K 3X5

*Author to whom correspondence should be addressed
E-mail: andrew.grosvenor@usask.ca
Phone: (306) 966-4660
Fax: (306) 966-4730

Executive Summary

Dissolved bicarbonate (HCO_3^-) in the JEB Tailings Management Facility (TMF) can react with uranium to form water-soluble uranyl-carbonate complexes. Excess $Ca^{2+}_{(aq)}$ that forms under the conditions of the TMF is predicted to react with the bicarbonate to form calcium carbonate. The calcium speciation of a series of samples taken from the JEB Tailings Management Facility (TMF) during the 2013 sampling campaign were investigated by X-ray diffraction (XRD), X-ray absorption near-edge spectroscopy (XANES), and microprobe X-ray fluorescence (XRF) mapping to determine if calcium carbonate (in the form of calcite or aragonite) is present. Bulk XRD analysis indicated that the major crystalline phases present in the tailings were quartz (SiO_2) and gypsum ($CaSO_4*2H_2O$). Micro XRD (μ-XRD) also suggested that powellite ($CaMoO_4$) is present in the tailings. Preliminary XANES analysis suggested that the two major Ca-containing species were gypsum and powellite. No evidence of calcium carbonate was observed in the XRD and XANES results. This observation could indicate that calcium carbonate is not present in the TMF but it could also indicate that the concentration of calcium carbonate in the tailings is below the detection limits of the techniques used so far. Preliminary results suggest that X-ray microprobe techniques coupled with micro-XANES analysis may provide a better understanding of the minor Ca-containing species in the TMF. This research is ongoing.

1. Introduction

AREVA Resources Canada (AREVA) operates the JEB Tailings Management Facility (JEB TMF) to manage and dispose of pollutant elements generated in their uranium ore mining operations in Northern Saskatchewan. The JEB TMF is designed to reduce the migration of water-soluble elements that co-mineralize with U ore (i.e. As, Ni, Mo, and Se) by promoting the formation of water-insoluble mineral species, effectively "trapping" these elements of concern.[1] However, small amounts of hydrocarbons, primarily kerosene, used in the extraction process are gradually converted to water-soluble bicarbonate (HCO_3^-) due to the highly oxidized environment of the TMF. This dissolved bicarbonate may react with uranium oxides to form water-soluble uranyl-carbonate complexes.[2] Coincidentally, the TMF contains an abundance of calcium sulfate ($CaSO_4$) because of the addition of sulphuric acid (H_2SO_4) and lime (CaO) during the milling process. As the TMF is saturated with gypsum, dissolved Ca^{2+}(aq) present in the tailings can react with the dissolved bicarbonate to form calcium carbonate ($CaCO_3$), adopting either the calcite or aragonite structure. Gypsum is more soluble than calcium carbonate and this may promote the precipitation of calcium carbonate under the conditions of the tailings.[2] Production of calcium carbonate will lower the concentration of dissolved bicarbonate in the tailings pore water, limiting the formation of water-soluble uranyl-carbonate complexes.[2]

Knowledge of the precipitation of calcium carbonate would enhance models of how the TMF behaves over time. Although there is some indirect evidence of calcium carbonate precipitation from the decrease in concentration of $Ca^{2+}_{(aq)}$ in the pore water collected at deeper depths of the TMF,[2] calcium carbonate has not been directly observed. AREVA has been actively studying the mineralogy of the TMF for several years, particularly with respect to As-

and Fe-containing species.[3-5] These studies have recently expanded to include the study of the Mo mineralogy of the TMF using X-ray diffraction (XRD), X-ray absorption near-edge spectroscopy (XANES), and X-ray microprobe.[6] These techniques, particularly XANES and X-ray microprobe, have proven useful in identifying low concentration species in the TMF such as powellite ($CaMoO_4$).[6] As a continuation of our collaboration, these techniques are being utilized to gain a better understanding of the Ca-containing species in the TMF. Detailed XRD (bulk and micro) and preliminary XANES analyses have suggested that the main crystalline Ca-containing species in the tailings is gypsum. Analysis of the XANES spectra indicates that a small amount of powellite is also present in the tailings samples, which is consistent with our previous studies on the Mo speciation of the TMF.[6]

2. Experimental

2.1. Tailings sample description

The samples studied were collected during the 2013 sampling campaign of the JEB TMF. Samples were collected from two bore-hole locations in the TMF in approximately 3 m intervals. A total of six samples were provided for this study, with three samples being collected from the central bore-hole (TMF13-01-SA12, TMF13-01-SA19, TMF13-01-SA22) and three samples being collected from a periphery bore-hole (TMF13-03-SA15, TMF13-03-SA15, TMF13-03-SA19). All samples collected were vacuumed-sealed by engineers at the Safety, Health, Environmental, and Quality (SHEQ) department of AREVA Resource Canada prior to being transport to the University of Saskatchewan. Samples were received by the Grosvenor group and stored in a N_2-filled glove box prior to analysis

2.2 Bulk and micro powder XRD

Powder XRD patterns of the tailings samples were initially collected to determine which crystalline phase are present in the bulk material. Measurements were collected over an angular range of $10^{o} \leq 2\theta \leq 90^{o}$ using a PANalytical Empyrean X-ray diffractometer equipped with a Co $K\alpha_{1,2}$ X-ray source. Tailings samples were ground into a fine powder and mounted on glass slides using ethanol before being placed on a spinning stage to prevent preferred orientation effects.

Micro powder X-ray diffraction (μ-XRD) patterns were collected using the same diffractometer but equipped with a Cu $K\alpha_{1,2}$ X-ray source that was mounted in the "Point Focus" position. A mono-capillary attachment was used to reduce the X-ray spot size to a 200 μm diameter. Grains of the tailings samples were mounted onto a glass slide using ethanol. Samples were positioned in the diffractometer using an optical microscope to collect diffraction patterns from specific grains. Eight μ-XRD patterns were collected at various positions for each sample. All powder XRD patterns were analyzed using the PowderCell software package.[7]

2.3. Microprobe X-ray fluorescence mapping and Laue diffraction

Microprobe X-ray fluorescence (XRF) maps and Laue diffraction patterns were collected using the VerySensitive Elemental and Structural Probe Employing Radiation from a Synchrotron (VESPERS) 07B2-1 beamline at the Canadian Light Source (Saskatoon, Canada).[8] Samples were prepared by sealing a thin layer of grains of the tailings between two layers of Kapton tape. Samples were mounted perpendicular to the beamline and at an angle of 45^{o} from the horizontal direction. X-ray fluorescence emission spectra were collected using a single element Vortex silicon drift detector (SDD) and the diffraction patterns were imaged using a Pilatus CCD image plate located directly above the samples. All measurements were performed

using the "Pink Beam" mode, which includes all X-ray energies from 4 – 30 KeV (with a significant drop in flux occurring near 20 KeV). A 5 μm spot size was used for all measurements. Fluorescence maps were collected by rastering a 1000 μm x 1000 μm area using a 10 μm step size with a 1 s dwell time. Each Laue diffraction pattern was collected over 60 – 180 s. All fluorescence maps were created and analyzed using the SMAK software program.[9] Laue diffraction patterns were analyzed using the XMAS software program.[10]

2.4. Ca K-edge XANES

Ca K-edge XANES measurements were performed on the Soft X-ray Microcharacterization beamline (SXRMB; 06B1-1) at the Canadian Light Source (Saskatoon, Canada).[11] Finely powdered tailings samples were lightly dusted onto carbon tape mounted onto a multi-sample holder and covered in a single layer of Kapton foil. Powdered samples of the Ca-containing standards (gypsum, calcite, aragonite, lime, apatite, powellite, yukonite) were also mounted onto the same sample holder. A beam size of 1 mm x 1 mm was used to collect the spectra. Spectra were collected from -150 eV below the absorption edge energy to ~550 eV above the absorption edge energy with a step size of 0.15 eV near the edge. The energy range was selected using a silicon (111) crystal monochromator, which provided a monochromatic flux on the order of 10^{11} photons/sec with a resolution of 0.4 eV at 4 keV.[11] All spectra were measured in partial fluorescence yield (PFY) mode using a 4 element Ge detector. Spectra were calibrated against Ti metal, with the maximum of the first derivative of the Ti K-edge set to 4966 eV.[12] Multiple scans were collected for each spectrum.

All XANES spectra were analyzed using the Athena software program.[12] A quantitative analysis of the XANES spectra was performed using principle component analysis (PCA) followed by linear combination fitting (LCF) using the spectra of the standards The energy

range used for PCA and LCF analysis was -20 and +40 eV relative to the Ca K-edge absorption edge energy.

3. Results and discussion

3.1. Powder X-ray diffraction

The powder XRD patterns from the finely ground tailings samples collected using a relatively large X-ray beam spot size are shown in Figure 1. Powder XRD is a bulk sensitive technique that is capable of detecting the major crystalline phases in a powdered sample. The two most dominate crystalline phases observed in all patterns were quartz (SiO_2) and gypsum. Peaks representing small amounts of several clay species (sericite, smectite, kaolinite) were also observed. The diffraction peaks associated with gypsum are generally more intense in the peripheral bore-hole, particularly in the tailings sample collected from deeper depths of the TMF (i.e., TMF13-03-SA19). This suggests that the peripheral bore-hole contains a higher concentration of gypsum compared to the central bore-hole. The backgrounds of the diffraction patterns were also observed to be more intense in patterns from samples from the peripheral bore-hole, suggesting that the mineral species are of a lower crystallinity compared to those found in the central bore-hole. A similar observation was made during the powder XRD analysis of the 2008 tailings samples.[6] There was no evidence of either calcite or aragonite in the bulk powder XRD patterns. This observation is likely a result of the detection limits of XRD patterns collected from finely ground and homogenized samples using a large X-ray spot size, and is not an indication of the absence of calcium carbonate in the tailings.

Following the powder XRD analysis, the X-ray beam was focused down to 200 μm to perform μ-XRD experiments. Diffraction patterns were collected on several grains from each sample. (Note that the samples analyzed by μ-XRD were not powdered prior to analysis.) The

μ-XRD patterns collected from tailings sample TMF13-03-SA12 are shown in Figure 2. The patterns from the other tailings samples are shown in Appendix A (Figures A1 – A5). Analysis of the μ-XRD patterns collected from TMF13-03-SA12 (Figure 2) highlights the heterogeneous nature of the tailings samples. μ-XRD diffraction patterns only represent the composition of a few individual grains at most given the small spot size used during the μ-XRD experiments and the large grain size of the tailings. The width and intensity of the diffraction peaks were observed to vary from spot to spot, which is likely due to variations in crystallinity and preferred orientation effects, respectively. Diffraction peaks generally become broader with decreasing crystallite size. Variations in peak intensity are particularly evident in peaks associated with the quartz phase (cf. Scan 2 vs. Scan 6 in Figure 2), and are likely due to preferred orientation effects associated with variations in grain size and orientation.[6] The most common Ca-containing material identified in the μ-XRD patterns was gypsum (cf. Scans 1 and 3 in Figure 2). Several patterns provided support for the presence of powellite, which was also observed in the μ-XRD patterns of the 2008 tailings samples.[6] Diffraction peaks could also be indexed to rutile (TiO_2) (e.g., Scan 3 of sample TMF13-01-SA12 in Appending A)), which was not observed in the previous analysis.[6] Like our previous study,[6] a number of peaks are marked as "?" and remain unidentified. These peaks could not be indexed to either calcite or aragonite and may be an indication that the phase analysis of the tailings is incomplete.

3.2. Microprobe XRF mapping and Laue diffraction

XRF maps were collected from all tailings samples to determine the distribution of elements in these materials. The XRF maps from TMF13-01-SA12 are shown in Figure 3 while the other maps collected are presented in Appendix A (Figure A6 – Figure A10).

Relatively intense fluorescence signals were obtained for Ca, Ti, Fe, Ni, As, and U. Mo XRF maps of suitable quality could not be collected during this study. The Ca signal was generally weaker than that of the other elements because the Ca Kα emission is near the lower energy limit of the fluorescence detector used. Stronger Ca signals were generally found in tailings samples collected from deeper depths of the TMF (cf. Figures A7 and A10).

Laue diffraction patterns were collected from several different spots based on the results of the XRF analysis. The positions where Laue diffraction patterns were collected are marked on the Ti XRF map in Figure 3 (and Figures A6-A10). Two representative patterns from tailings sample TMF13-01-SA12 are shown in Figure 4. A number of variations in the Laue diffraction patterns were observed, which are likely due to variations in crystallite sizes. The Laue diffraction patterns from the tailings samples are currently being indexed to determine if any calcium carbonate species can be identified.

3.3. Ca K-edge XANES analysis

The Ca K-edge XANES spectra from all six tailings samples analyzed are shown in Figure 5a. The XANES spectra were collected from finely powdered and homogenized samples using a large X-ray spot size. Under these conditions, analysis of the Ca K-edge XANES spectra will provide information on the major Ca-containing species in the tailings. The Ca K-edge corresponds to a dipole-allowed transition of a 1s electron into unoccupied 4p states. The lineshape of the Ca K-edge XANES spectrum is heavily dependent on the local coordination environment and is often analyzed to identify specific Ca-containing species present in a mixture.[13-15] The Ca K-edge XANES spectra of the tailings samples have similar lineshapes, suggesting that they all consist of similar Ca-containing species. The spectra from the tailings samples were compared to spectra from several Ca-containing standards (see Figure 5b for

spectra from representative standards and Figure A11 in Appendix A for all standards studied). It was obvious by comparing these spectra that the spectra from the tailings are most similar to the spectrum from gypsum. The pre-edge feature observed in the Ca K-edge of the tailings samples is particularly indicative of gypsum. The spectra were analysed by principal component analysis followed by linear combination fitting in an attempt to determine if other Ca-containing species are present.

3.3.1. Principal Component Analysis (PCA)

Advanced analysis techniques are required to identify the different Ca-containing species present in the tailings samples. Principal component analysis (PCA) was used to determine the number of major Ca-containing species present in the tailings. Assuming a XANES spectrum consists of a linear combination of spectra that make up the components of a mixture, a PCA calculation decomposes a series of spectra into a set of components (eigenvectors) and weightings (eigenvalues) that describe the variation in the data set.[16,17] Although these components are mathematical constructs with no simple relationship to the chemical species that make up the spectra, it has been assumed here that the minimum number of components that describe the variation in the data set is equivalent to the minimum number of chemical species that make up a XANES spectrum.[16,17] An indicator function, known as an IND, was developed by Malinowski to determine the minimum number of components required to describe a series of spectra.[18,19] It is generally accepted that the minimum number of components is given when the IND function is minimized.[18,19] The number of components predicted by the IND function can be tested by reconstructing the set of spectra using the components calculated in the PCA.

PCA was performed on the six tailings samples, and the PCA results are shown in Figure 6a. A total of six components were calculated in the PCA calculation. The first component

calculated for each set of spectra accounts for >99 % of the total variances, which is common in PCA calculations of XANES spectra as the total variance in a set of spectra is usually small.[20] The second component is the only other component with an observable intensity, suggesting that there are only two components required to describe the variation in the set of spectra studied. This was confirmed by calculating the IND value (Figure 6b), which is at a minimum when the number of components equals two. Reconstructions of the spectra of tailings sample TMF13-03-SA12 (Figure 7) show no visible improvements when reproducing the spectra with two or three components, which tends to suggest that there are only two Ca-containing species in the Ca K-edge XANES spectra from the finely powdered tailings samples collected using a large X-ray spot size in this study.

3.3.2. Linear Combination Fitting (LCF) analysis

Linear combination fitting (LCF) analysis was used to identify the Ca-containing species in the TMF. Each normalized Ca K-edge spectrum was fitted by a linear combination of weighted standard spectra. The coefficients calculated in the LCF correspond to the concentration of each Ca species present. Based on the PCA calculations, the number of components used in the fittings was initially restricted to two. Best fits were determined by comparing the χ^2 value, which is an indicator of the goodness-of-fit. The smaller the χ^2 value, the better the fit.

Results of the best fits are tabulated in Table 1 and the fitted Ca K-edge XANES spectra are shown in Figure 8. The best fits were obtained when fitting the spectra with gypsum and powellite. The majority of Ca in the tailings samples was gypsum, with concentrations ranging from 80 – 86 at%, while the concentration of powellite ranged from 20 – 14 at%. Relatively good fits were also obtained when using lime in the fittings rather than powellite; however, the

concentration of lime determined by these fittings was small (~5 at%). To determine which of the three possible Ca-containing species were the major species in these samples, restrictions to the number of components used in the fittings were relaxed to allow for a third component. The concentration of lime was ~ 0 at% in all six fittings, suggesting that gypsum and powellite are the major Ca-containing species in the tailings. Relatively good fits to the high energy features of the spectra located between 4060 eV and 4070 eV were obtained. This region of a XANES spectrum is known to have contributions from multiple scattering resonances (MSR), a low-energy Extended X-ray Absorption Fine Structure (EXAFS) phenomenon that is highly dependent on the crystal structure and crystallinity.[21] The fittings in this region of the Ca K-edge of the tailings samples suggests that the Ca-containing species in the tailings may be highly crystalline because spectra from crystalline standards were used to fit the spectra from the tailings. This is consistent with the powder XRD patterns from these samples, as relatively narrow peaks representing crystalline gypsum were observed.

It is important to note that the fitting is generally poor for most spectra from the tailings in the energy region of ~4050 eV, particularly for samples collected from the peripheral bore-hole. Although this may suggest that there is another component in the tailings, fitting the spectra to three components was unsuccessful. As such, it is hypothesized that the misfit near 4050 eV is due to the gypsum standard used in this XANES study not being representative of gypsum in the TMF.

Attempts were made to fit the Ca K-edge XANES spectra with calcite and aragonite; however, these standards were rejected as components during the fittings. If calcium carbonate is present in the tailings, the concentration may be below the detection limits of the XANES spectra collected from finely powdered samples using a large X-ray spot size. As evident from

the μ-XRD study, a smaller X-ray beam size (i.e. μm-size) focused on specific regions of individual grains of the samples is likely required to detect the small concentration of calcium carbonate predicted to form in the tailings, if it is present at all.

4. Conclusions and Future Work

Structure and element specific techniques were used to identify the Ca-containing species in the TMF. Bulk and micro XRD analysis indicated that the major crystalline Ca-containing species in the tailings were gypsum and powellite. This conclusion was confirmed through PCA and LCF analysis of the Ca K-edge XANES spectra. Neither calcite nor aragonite was identified by the techniques described in the report.

Going forward, additional experiments will be conducted at the Canadian Light Source between January 2015 – June 2015 that may be more sensitive to low-concentration Ca species present in the tailings samples. First, C K-edge and Ca L-edge XANES spectra will be collected using the Spherical Grating Monochromator (SGM) beamline. The lineshape of these XANES spectra may exhibit a greater sensitivity to minor Ca-containing species, particularly calcium carbonate.[22] Second, microprobe XRF maps from grains of the tailings will be collected using the SXRMB beamline and a μm-sized X-ray beam. Ca K-edge XANES spectra using a μm-sized X-ray beam will be collected from the Ca-rich regions identified in the XRF maps, which may identify minor Ca-containing species in the tailings that were not observed when XANES spectra were collected using a larger X-ray spot size. The Laue diffraction patterns that were collected as part of the experiment already performed using the VESPERS beamline from regions that were identified by XRF mapping to contain high concentration of Ca will be indexed to further our understanding of the Ca species present in the tailings.

5. References

1. Rowson, J.; Schmid, B. Tailings Optimization and Validation Program; AREVA Resources Canada: Saskatoon, Saskatchewan, Canada, **2011**.

2. Rowson, J. Schmid, B. *Tailings Optimization and Validation Program*; AREVA Resources Canada, Saskatoon, Saskatchewan, **2011**.

3. Langmuir, D.; Mahoney, J.; Rowson, J. Solubility products of amorphous ferric arsenate and crystalline scorodite ($FeAsO_4 \cdot 2H_2O$) and their application to arsenic behaviour in buried mine tailings. *Geochim. Cosmochim. Acta* **2006**, *70*, 2942−2956.

4. Mahoney, J.; Slaughter, M.; Langmuir, D.; Rowson, J. Control of As and Ni releases from a uranium mill tailings neutralization circuit: Solution chemistry, mineralogy and geochemical modeling of laboratory study results. *Appl. Geochem.* **2007**, *22*, 2758−2776.

5. Chen, N.; Jiang, D. T.; Cutler, J.; Kotzer, T.; Jia, Y. F.; Demopoulos, G. P.; Rowson, J. W. Structural characterization of poorly-crystalline scorodite, iron(III)−arsenate co-precipitates and uranium mill neutralized raffinate solids using X-ray absorption fine structure spectroscopy. *Geochim. Cosmochim. Acta* **2009**, *73*, 3260−3276.

6. Hayes, J. R.; Grosvenor, A. P.; Rowson, J.; Hughes, K.; Frey, R. A.; Reid, J. Analysis of the Mo Speciation in the JEB Tailings Management Facility at McClean Lake, Saskatchewan. *Environ. Sci. Technol.* **2014**, *48* 4460-4467.

7. Kraus, W.; Nolze, G. POWDER CELL□A program for the representation and manipulation of crystal structures and calculation of the resulting X-ray powder patterns. *J. Appl. Crystallogr.* **1996**, *29*, 301−303.

8. Feng, R.; Gerson, A.; Ice, G.; Reininger, R.; Yates, B. McIntyre, S. VESPERS: a beamline for combined XRF and XRD measurements. *AIP Conf. Proc.* **2007**, *879*, 872-874.

9. Webb, S. M. The MicroAnalysis Toolkit: X-ray fluorescence image processing software. *AIP Conf. Proc.* **2011**, *196*, 196−199.

10 Tamura, N.; MacDowell, A. A.; Spolenak, R.; Valek, B. C.; Bravman, J. C.; Brown, W. L.; Celestre, R. S.; Padmore, H. A.; Batterman, B. W.; Patal, J. R. Scanning X-ray microdiffraction with submicrometer white beam for strain/stress and orientation mapping in thin films. *J. Synchrotron Radiat.* **2003**, *10*, 137−143.

11. Hu, Y. F.; Coulthard, I.; Chevrier, D.; Wright, G.; Igarashi, R.; Sitnikov, A.; Wates, B. W.; Hallin, E. L.; Sham, T. K.; Reininger, R. Perliminary commissioning and performance of the Soft X-ray Microcharacterization beamline at the Canadian Light Source. *AIP Conf. Proc.* **2010**, *1234*, 343-346.

12. Ravel, B.; Newville, M. ATHENA, ARTEMIS, HEPHAESTUS: data analysis for X-ray absorption spectroscopy using IFEFFIT. *J. Synchrotron Rad.* **2005**, *12*, 537-541.

13. Sowrey, F. E.; Skipper, L. J.; Pickip, D. M.; Drake, K. O.; Lin, Z.; Smith, M. E.; Newport, R. J. Systematic empirical analysis of calcium-oxygen coordination environment by calcium K-edge XANES. *Phys. Chem. Chem. Phys.* **2004**, *6*, 188-192.

14. Takahashi, Y.; Miyoshi, T.; Yabuki, S.; Inada, Y.; Shimizu, H. Observation of transformation of calcite to gypsum in mineral aerosols by Ca K-edge X-ray absorption near-edge structures (XANES). *Atmos. Environ.* **2008**, *42*, 6635-6541.

15. Liu, L. J.; Liu, H. J.; Cui, M. Q.; Hu, Y. F.; Zheng, L.; Zhao, Y. D.; Ma, C. Y.; Xi, S. B.; Yang, D. L.; Guo, Z. Y.; Wang, J. Determination of the calcium species in coal chars by Ca K-edge XANES analysis. *Chinese Phys. C* **2013**, *37*, 028003.

16. Fernández-Garcìa, M.; Márquez Alvarez, C.; Haller, G.L. XANES-TPR study of Cu – Pd bimetallic catalysts: application of factor analysis. *J. Phys. Chem.* **1995**, *99*, 12565–12569.

17. Beauchemin, S.; Hesterberg, D.; Beauchemin, M. Principal component analysis approach for modelling sulphur K-XANES spectra of humic acids. *Soil Sci. Soc. Am. J.* **2002**, *66*, 83-91.

18. E.R. Malinowski, Factor Analysis in Chemistry, 3rd ed., John Wiley & Sons, New York, 2002.

19. Malinowski, E.R. Theory of error in factor analysis. *Anal. Chem.* **1977**, *49*, 606-612.

20. Cassinelli, W. H.; Martins, L.; Passos, A. R.; Pulcinelli, S. H.; Santilli, C. V.; Rochet, A.; Briois, V. Multivariate curve resolution analysis applied to time-resolved synchrotron X-ray absorption spectroscopy monitoring of the activation of copper alumina catalyst. *Catal. Today* **2014**, *229*, 114-122.

21. Rehr, J. J. Theoretical approaches to X-ray absorption fine structure Re. Mod. Phys. **2000**, *72*, 621-654.

22. Naftel, S. J.; Sham, T. K.; Yiu, Y. M.; Yates, B. W. Calcium L-edge XANES study of some calcium compounds. *J. Synchrotron Rad.* **2001**, *8*, 255-257.

Table 1. Results of the LCF fitting of the Ca K-edge XANES spectra from the tailings samples. Calculated errors are in brackets

Sample	Gypsum (at%)	Powellite (at%)	R-factor	X^2
TMF13-01-SA12	82(3)	18(3)	0.0132	0.967
TMF13-01-SA19	86(2)	16(2)	0.00330	0.231
TMF13-01-SA22	80(2)	20(3)	0.00575	0.394
TMF13-01-SA12	86(2)	14(3)	0.00626	0.456
TMF13-01-SA15	85(3)	15(4)	0.00949	0.701
TMF13-01-SA19	85(3)	15(3)	0.00823	0.595

Figure 1.

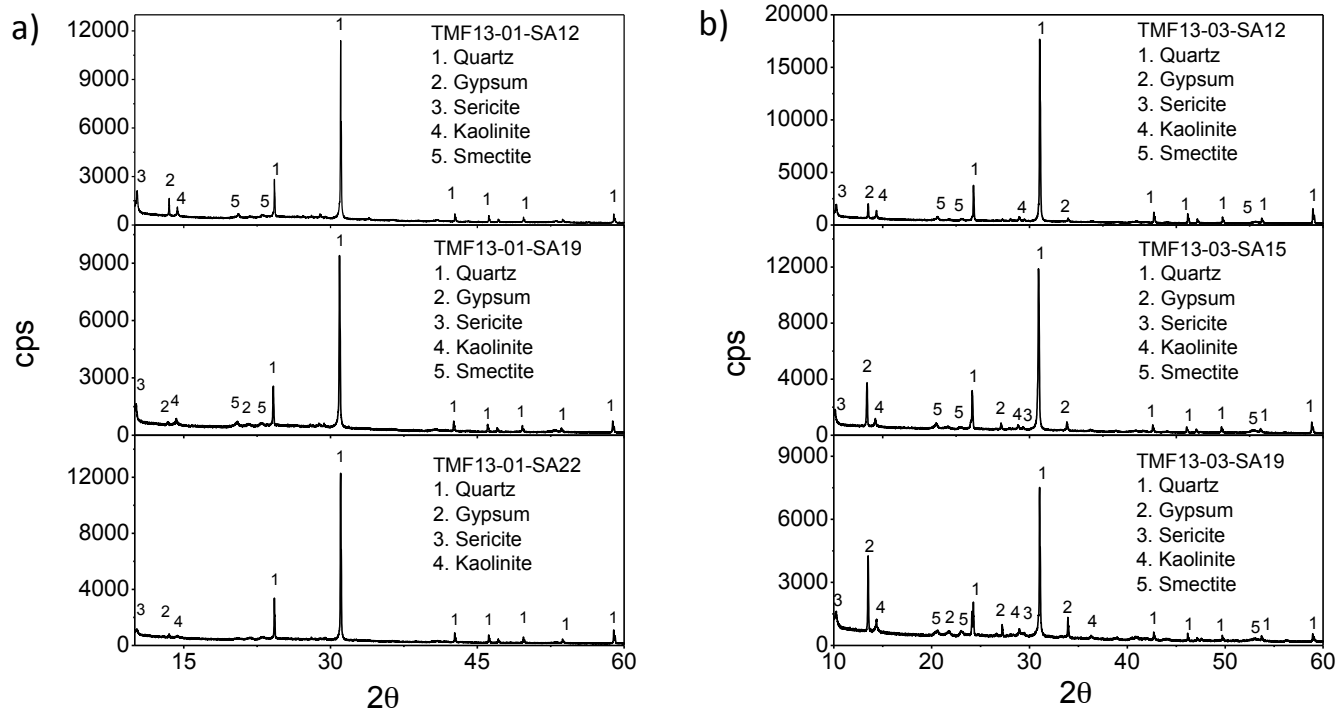

Figure 1. The bulk XRD patterns of tailings samples from the a) central and b) peripheral bore-holes. Major crystalline phases present in the tailings samples include quartz, gypsum, sericite, kaolinite, and smertite. No evidence of calcite or aragonite was observed. Note that the diffraction peaks are shifted compared to the μ-XRD patterns due to the different X-ray sources using to collect these diffraction patterns.

Figure 2.

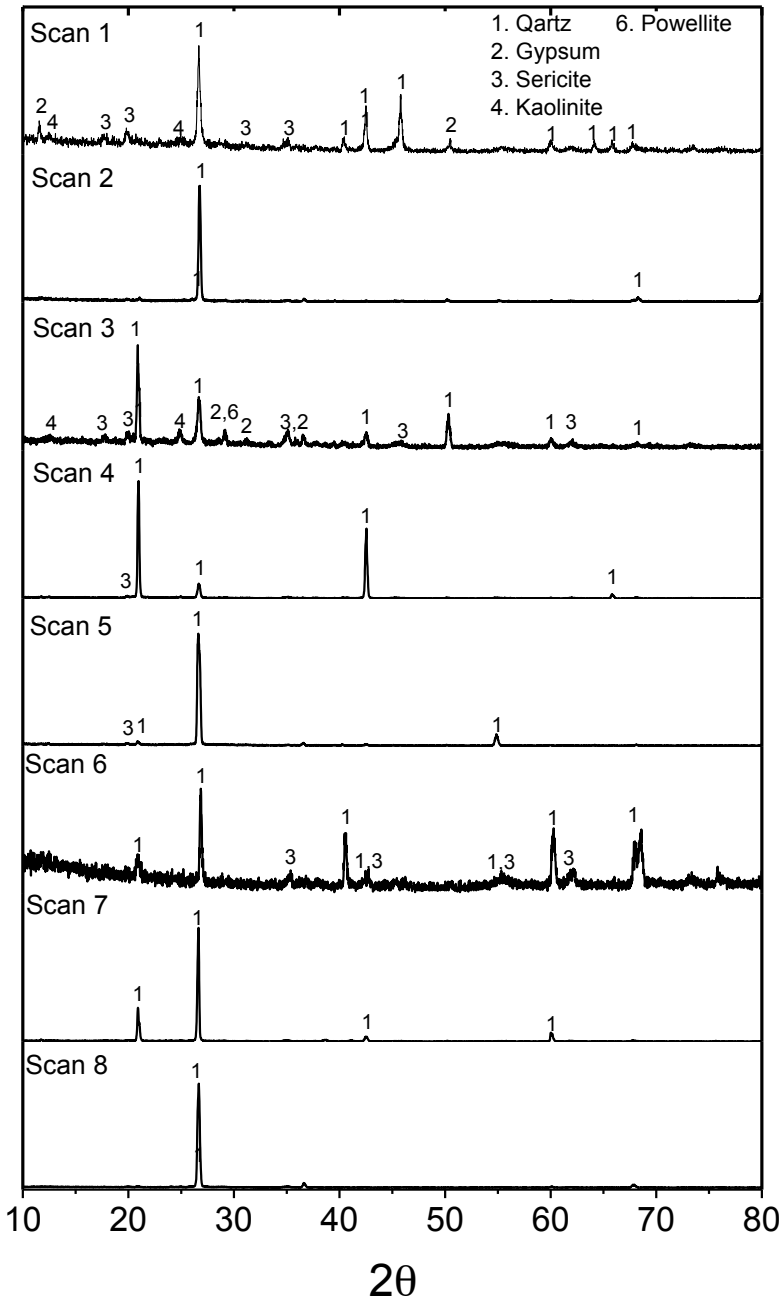

Figure 2. Micro-XRD patterns from the TMF13-03-SA12 tailings sample are shown. Possible evidence of gypsum and powellite are highlighted in scans 1 and 3, respectively. Note that the diffraction peaks are shifted compared to the bulk XRD patterns due to the different X-ray sources using to collect these diffraction patterns..

Figure 3

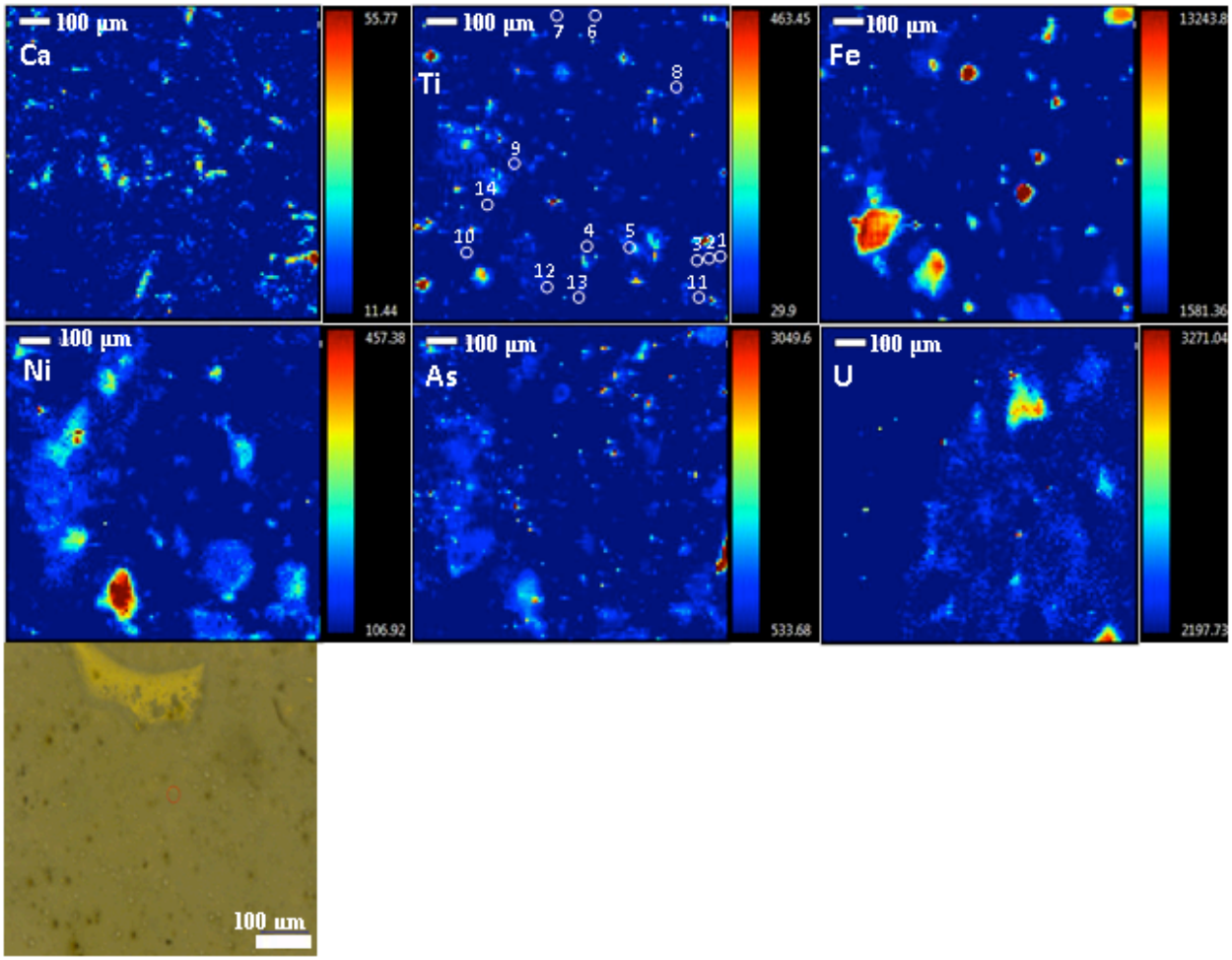

Figure 3. XRF maps for various elements found in tailings sample TMF13-01-SA12 are shown. Spots where Laue diffraction patterns were collected are labelled according to their scan number in the Ti map. An optical image of the mapped area is shown at the bottom of the figure.

Figure 4.

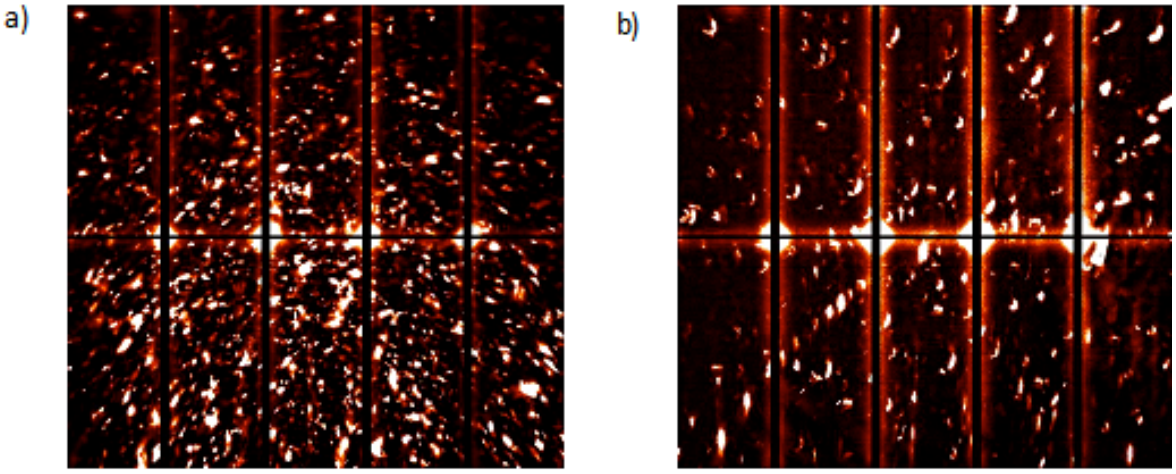

Figure 4. Laue diffraction patterns collected from a) spot 7 and b) spot 8 in the XRF map presented in Figure 3 from tailings sample TMF13-01-SA12.

Figure 5

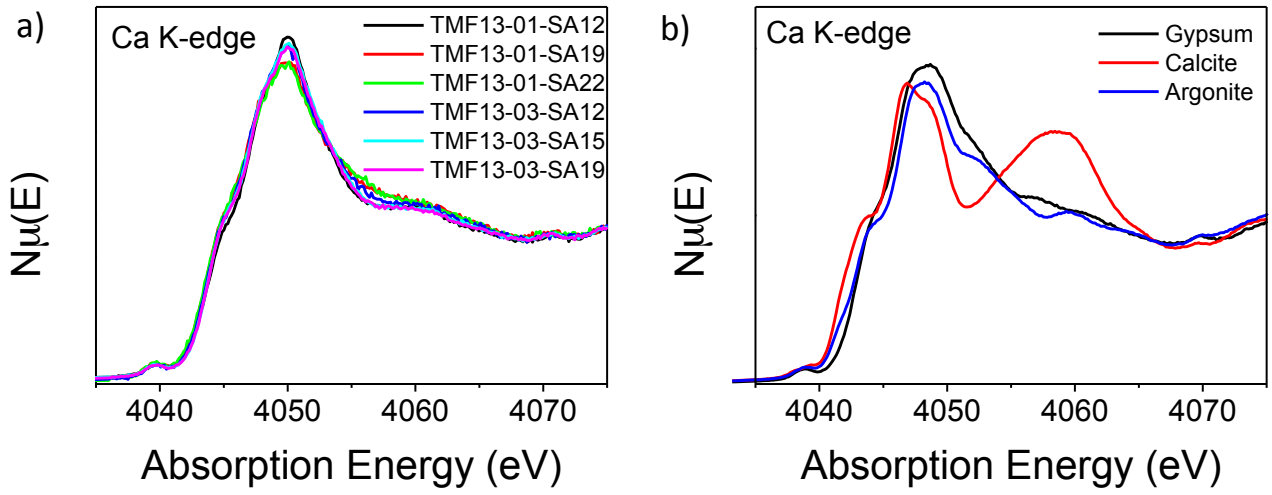

Figure 5. a) The Ca K-edge XANES spectra from the tailings samples analyzed are shown. All spectra had similar lineshapes. b) The Ca K-edge XANES spectra of gypsum, calcite, and aragonite are shown. Features in the spectra from the tailings samples were found to be similar to those of gypsum.

Figure 6

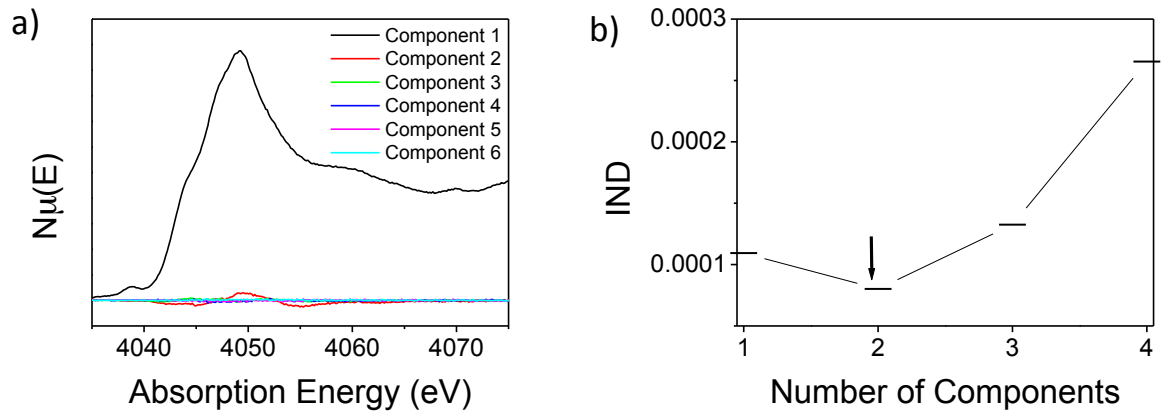

Figure 6. a) The principle components calculated from the PCA analysis of the six tailings samples are shown. Component 1 generally has the strongest intensity, accounting for >99 % of the variances. Components 3-6 appear to have no noticeable intensities. b) The IND function was calculated and plotted versus the number of components. The IND function approaches a minimum when the number of components is two, suggesting that the spectra consists of two Ca-containing species.

Figure 7

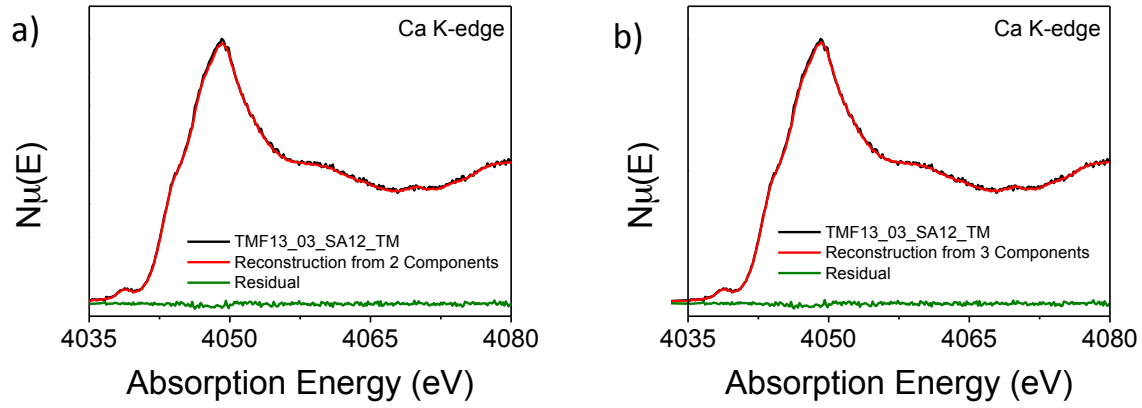

Figure 7. The reconstruction of the Ca K-edge XANES spectrum of tailings sample TMF13-01-SA12 using a) two components and b) three components. The use of three components did not result in a noticeable improvement in the reconstruction. This confirms the analysis of the IND function that indicated that the spectra from the tailings samples only contained two components.

Figure 8

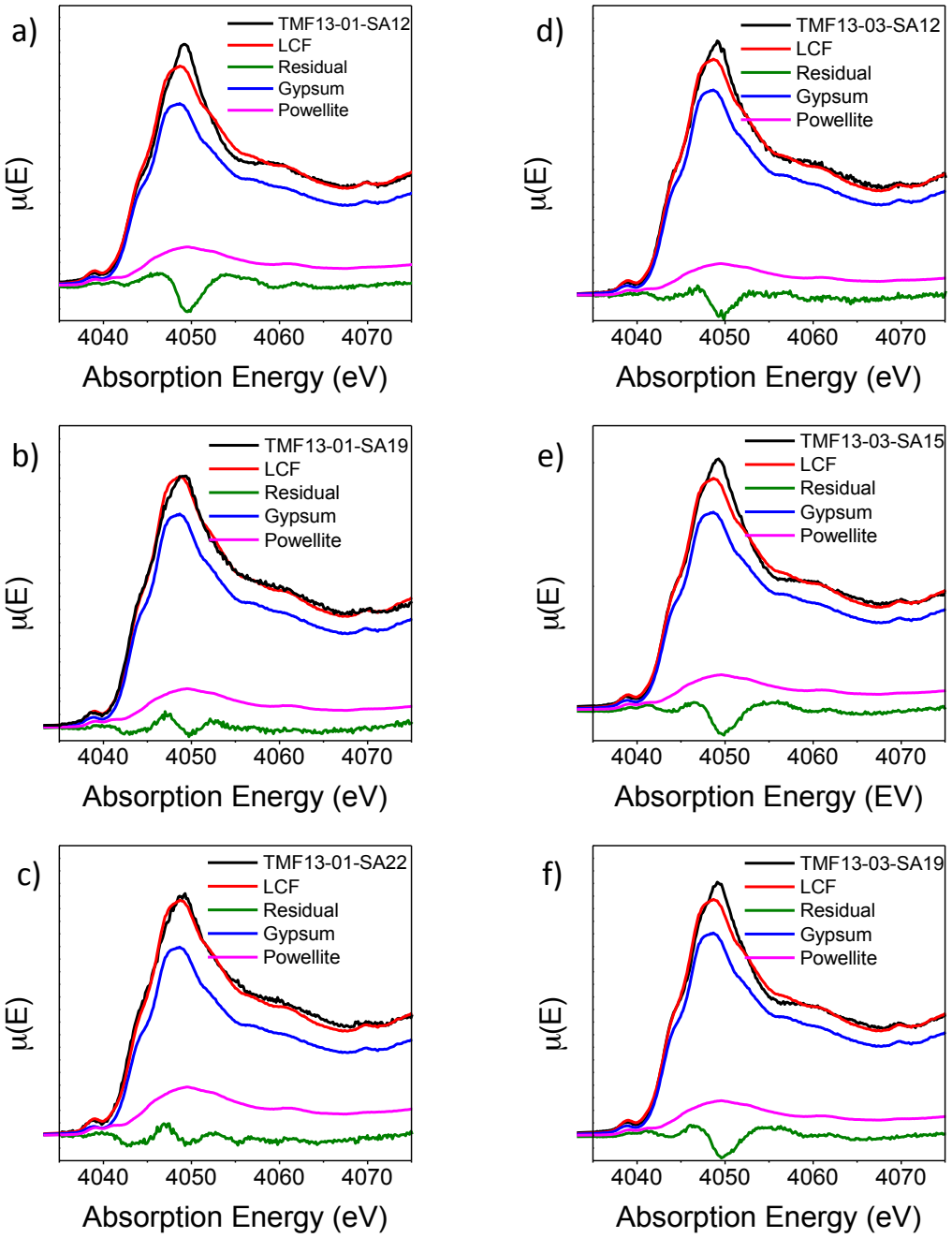

Figure 8. The fitted Ca K-edge XANES spectra of a) TMF13-01-SA12, b) TMF13-01-SA19, c)TMF13-01-SA22, d) TMF13-03-SA12, e) TMF13-03-SA15, and f) TMF13-03-SA19 are shown. The linear combination fitting of each spectrum is shown in red and the residual is shown in green. The weighted spectra of the standards used to the fit each spectrum are also shown.

Appendix A

Figure A1

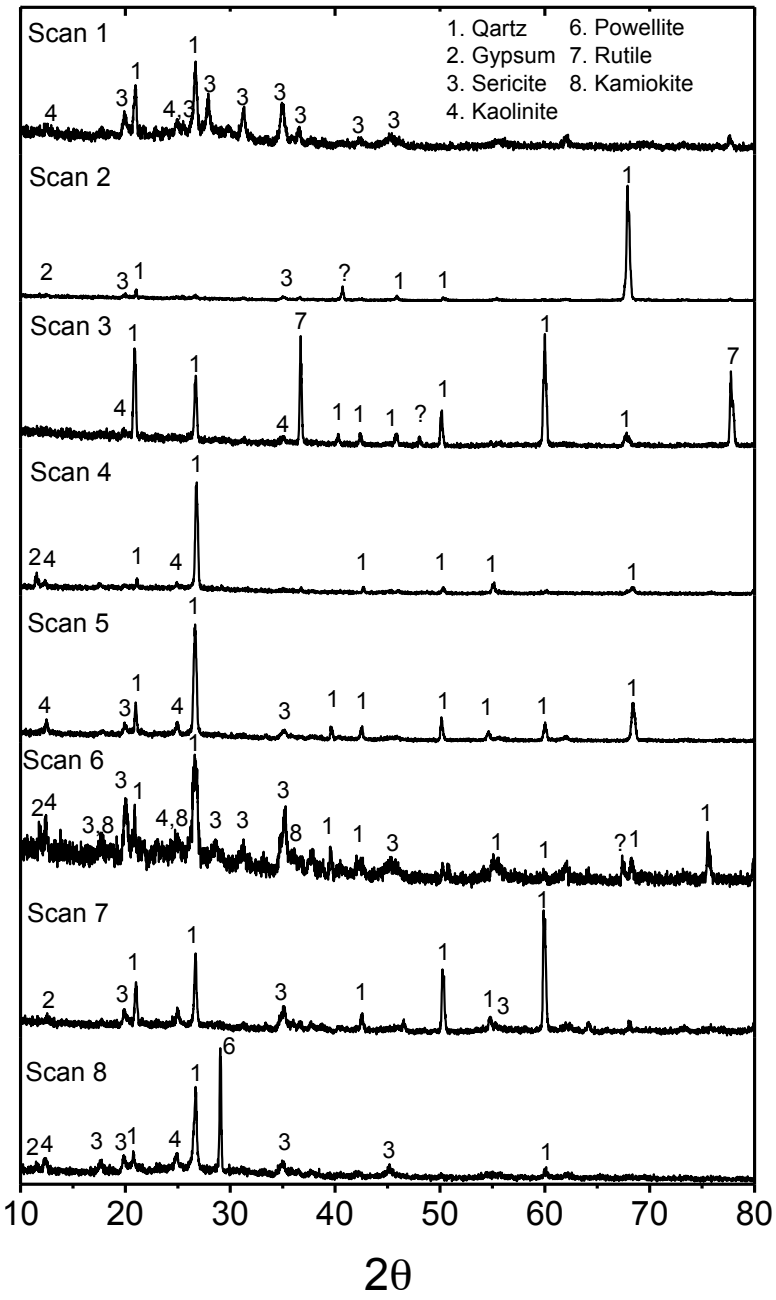

Figure A1. Micro-XRD patterns from the TMF13-01-SA12 sample are shown. Possible evidence of gypsum and powellite are highlighted in scans 4, 6, and 8. Note that the diffraction peaks are shifted compared to the bulk XRD patterns due to the different X-ray sources used to collect the diffraction patterns.

Figure A2

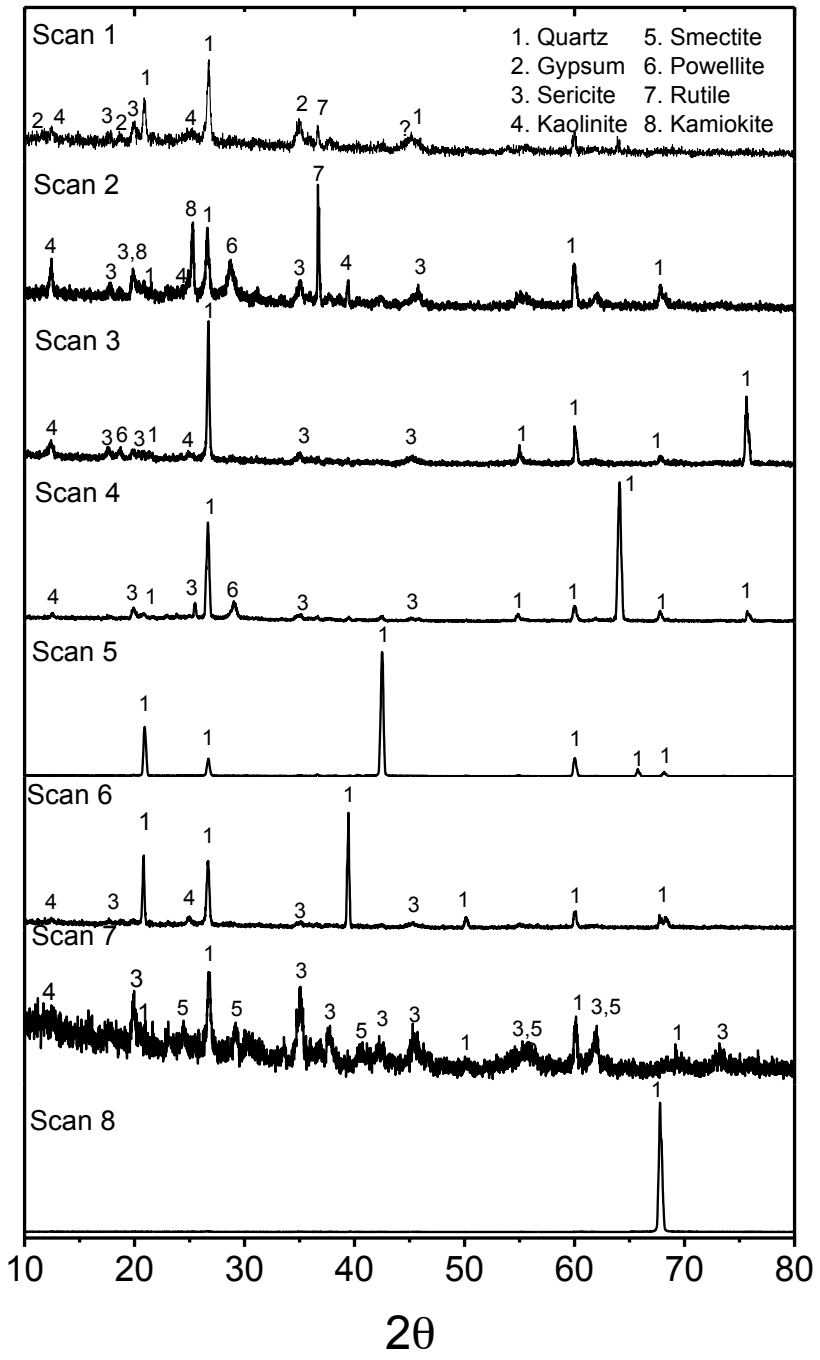

Figure A2. Micro-XRD patterns from the TMF13-01-SA19 sample are shown. Possible evidence of gypsum and powellite are highlighted in scans 1 and 4. Note that the diffraction peaks are shifted compared to the bulk XRD patterns due to the different X-ray sources used to collect the diffraction patterns.

Figure A3

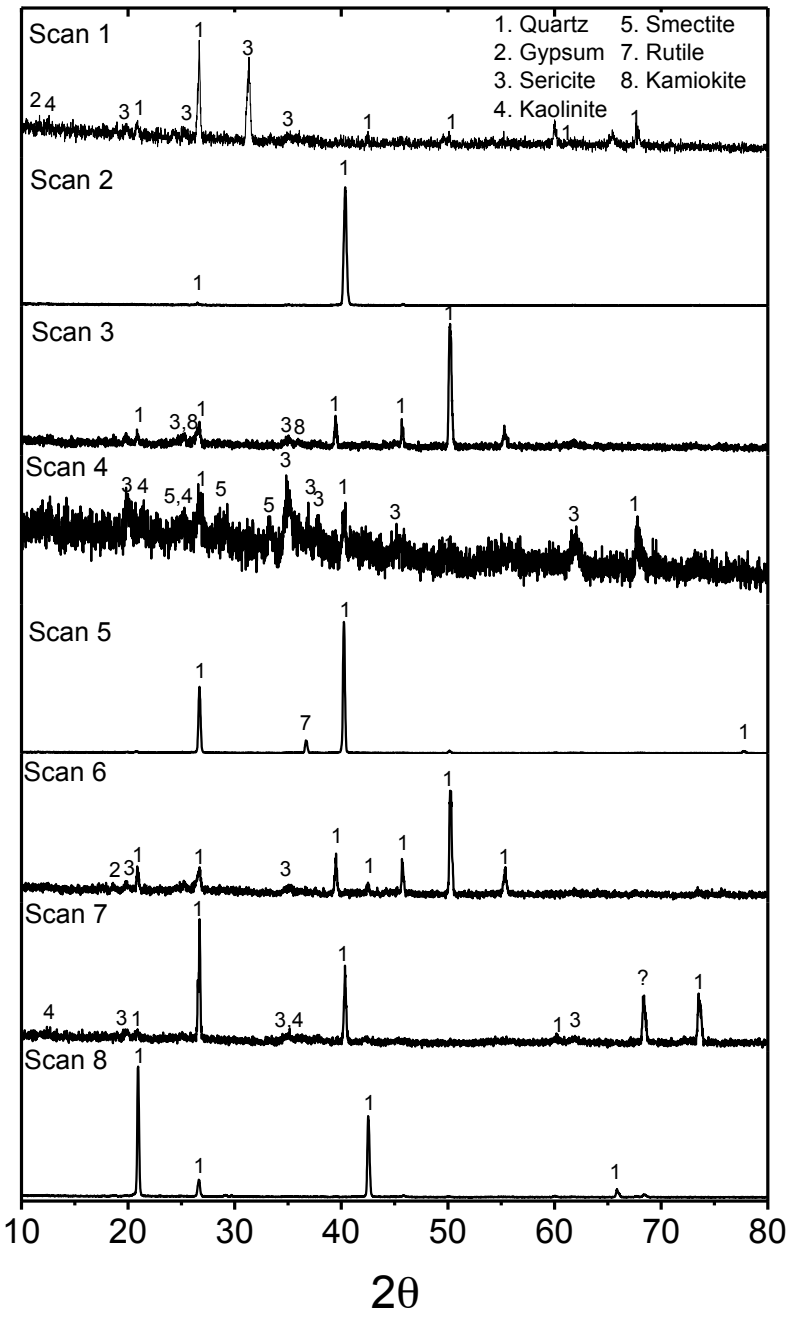

Figure A3. Micro-XRD patterns from the TMF13-01-SA22 sample are shown. Possible evidence of gypsum ais highlighted in scans 1 and 6. Note that the diffraction peaks are shifted compared to the bulk XRD patterns due to the different X-ray sources used to collect the diffraction patterns.

Figure A4

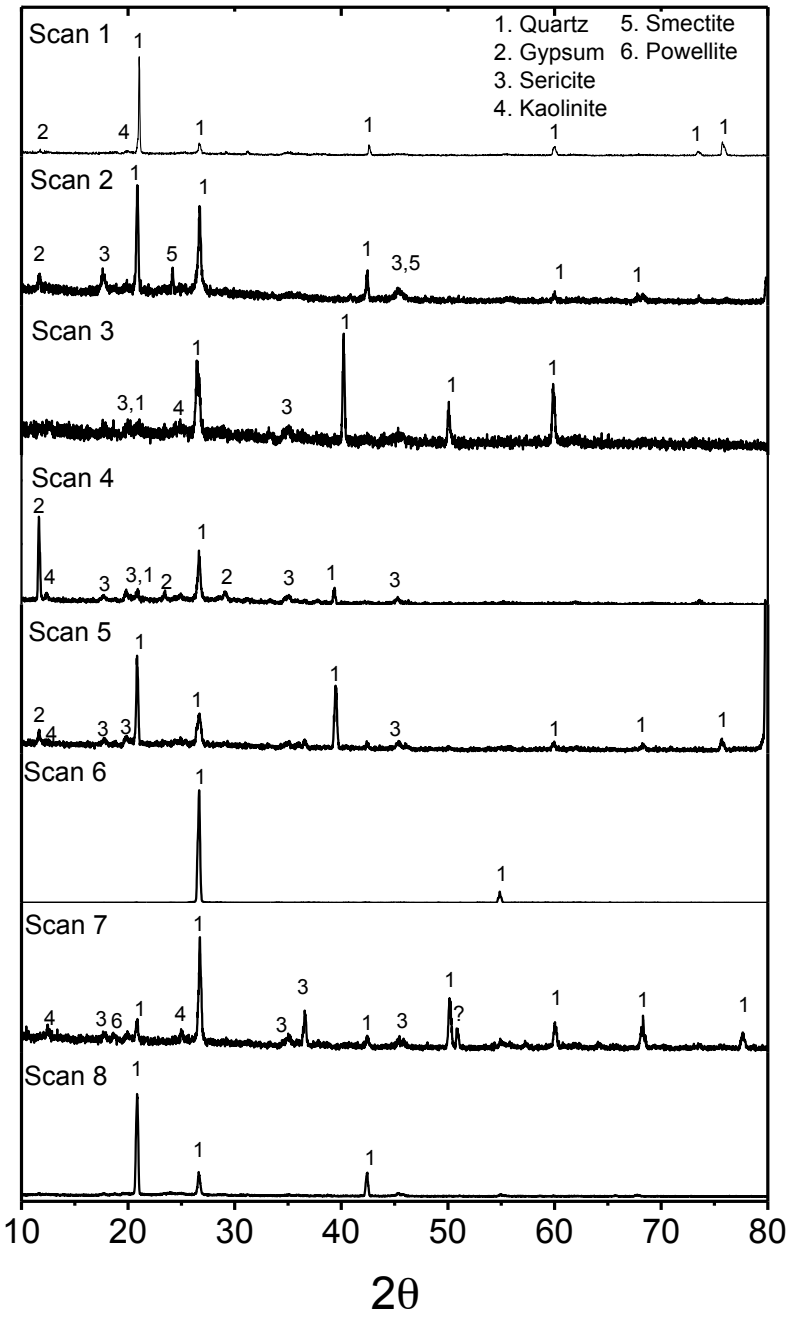

Figure A4. Micro-XRD patterns from the TMF13-03-SA15 sample are shown. Evidence of gypsum and powellite are highlighted in scans 1, 2, 4, 5, and 7. Note that the diffraction peaks are shifted compared to the bulk XRD patterns due to the different X-ray sources used to collect the diffraction patterns.

Figure A5

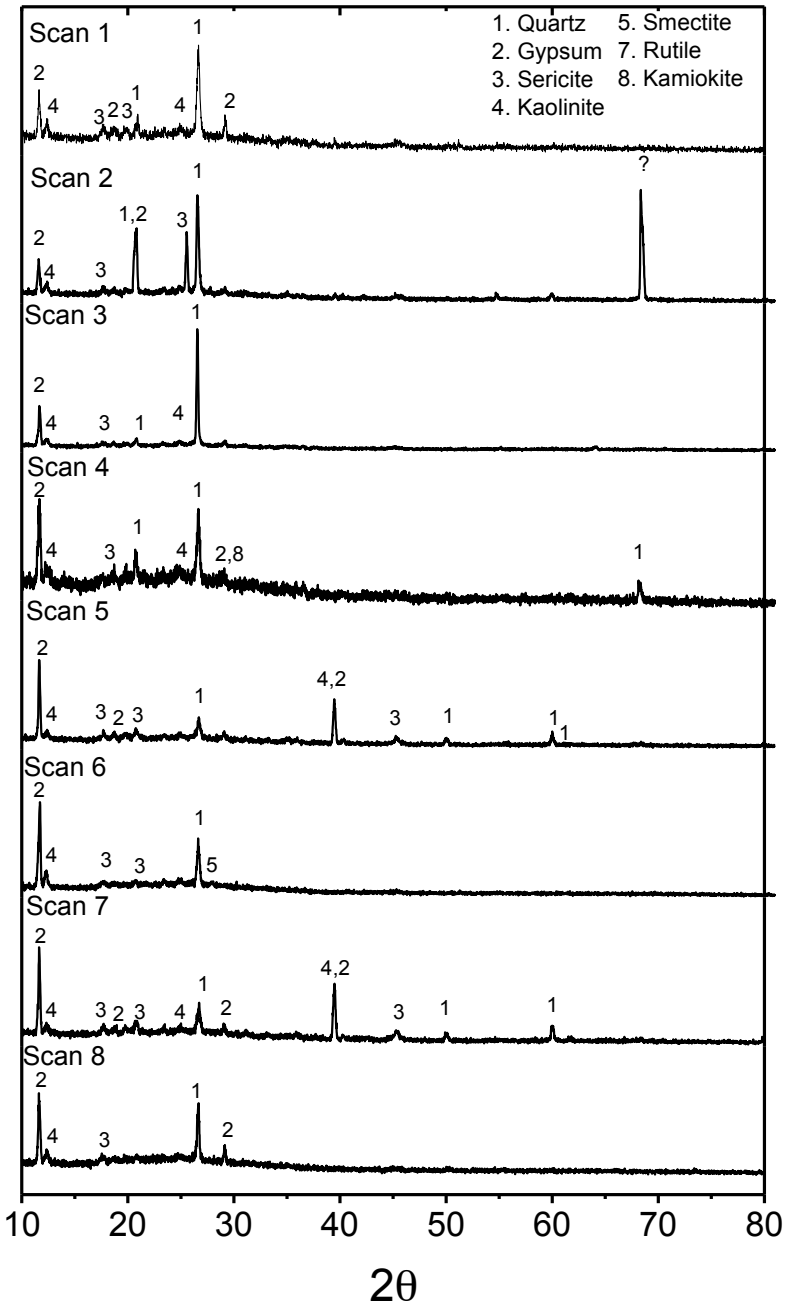

Figure A5. Micro-XRD patterns from the TMF13-03-SA19 sample are shown. Evidence of gypsum is observed in all scans. Note that the diffraction peaks are shifted compared to the bulk XRD patterns due to the different X-ray sources used to collect the diffraction patterns.

Figure A6

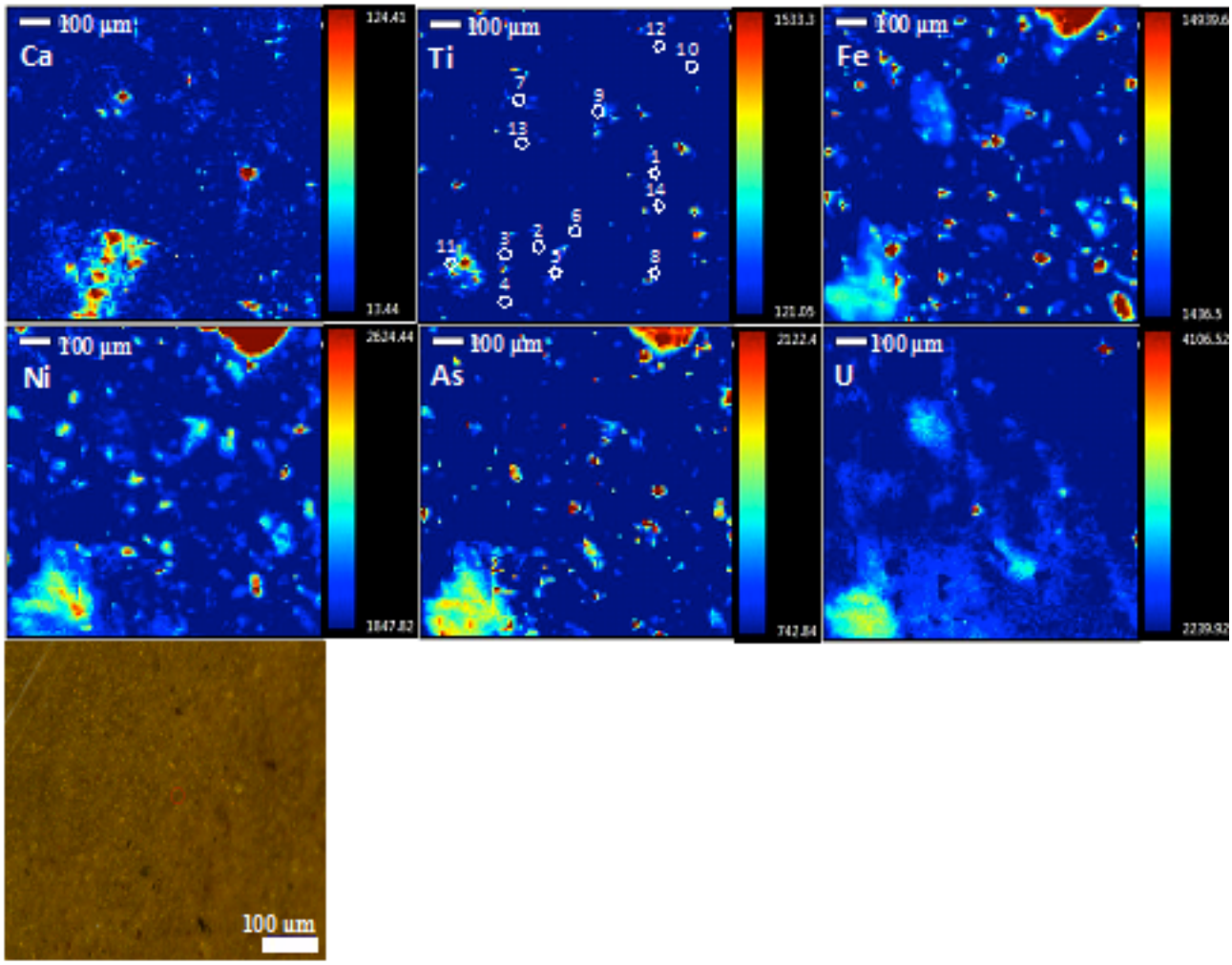

Figure A6. XRF maps for various elements found in tailings sample TMF13-01-SA19 are shown. Spots where Laue diffraction patterns were collected are labelled according to their scan number in the Ti map. An optical image of the mapped area is shown at the bottom of the figure.

Figure A7

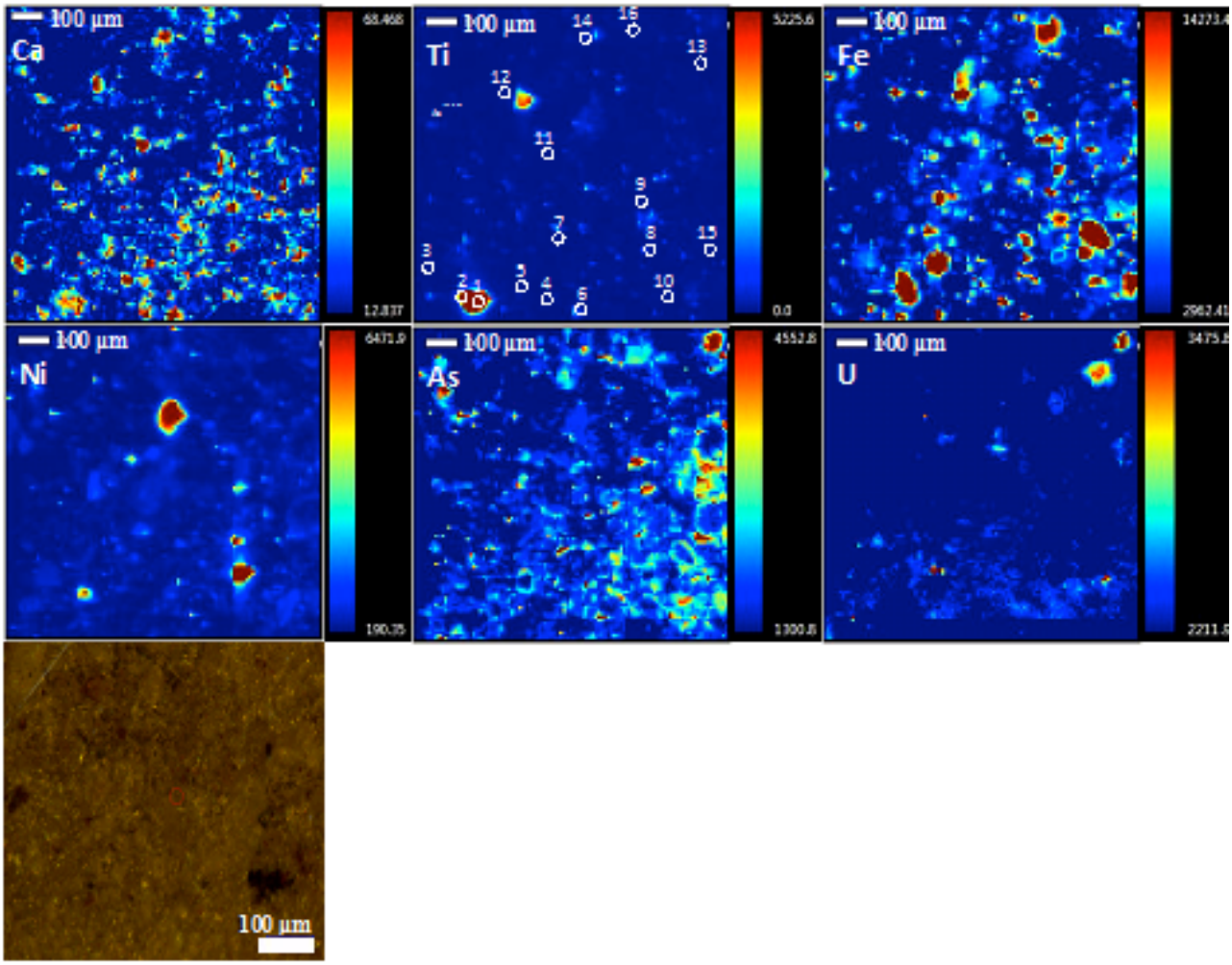

Figure A7. XRF maps for various elements found in tailings sample TMF13-01-SA22 are shown. Spots where Laue diffraction patterns were collected are labelled according to their scan number in the Ti map. An optical image of the mapped area is shown at the bottom of the figure.

Figure A8

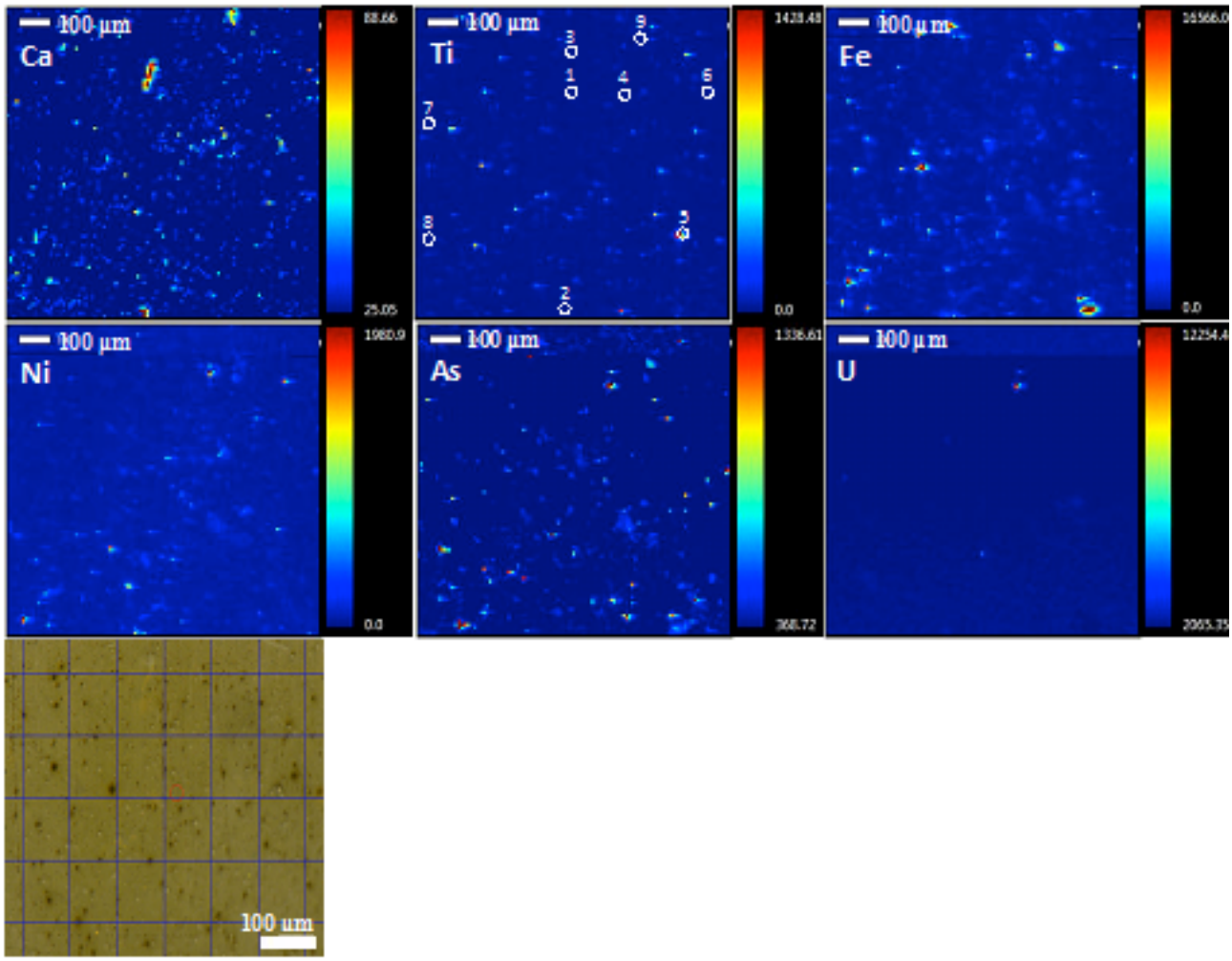

Figure A8. XRF maps for various elements found in tailings sample TMF13-03-SA12 are shown. Spots where Laue diffraction patterns were collected are labelled according to their scan number in the Ti map. An optical image of the mapped area is shown at the bottom of the figure.

Figure A9

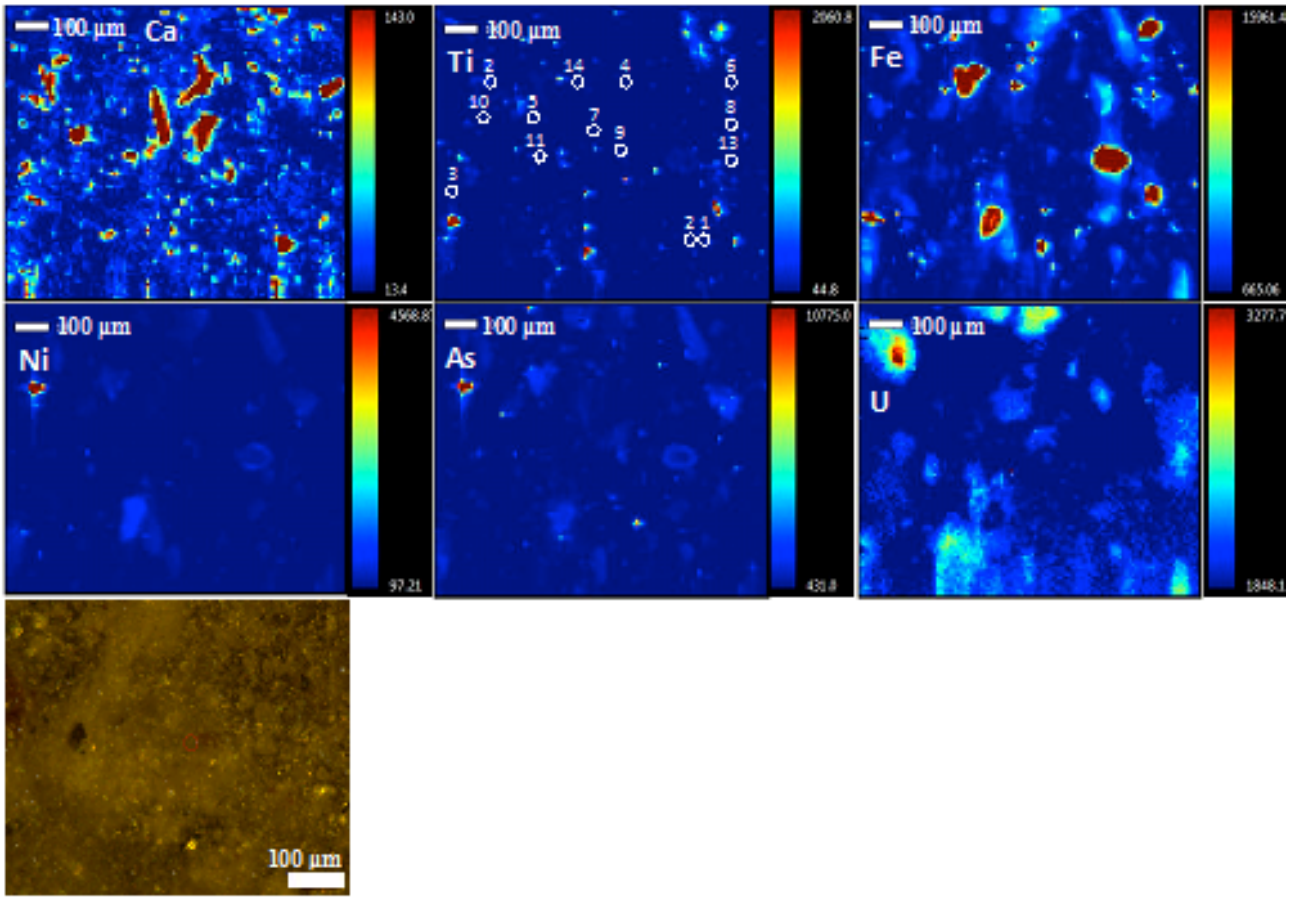

Figure A9. XRF maps for various elements found in tailings sample TMF13-03-SA15 are shown. Spots where Laue diffraction patterns were collected are labelled according to their scan number in the Ti map. An optical image of the mapped area is shown at the bottom of the figure.

Figure A10

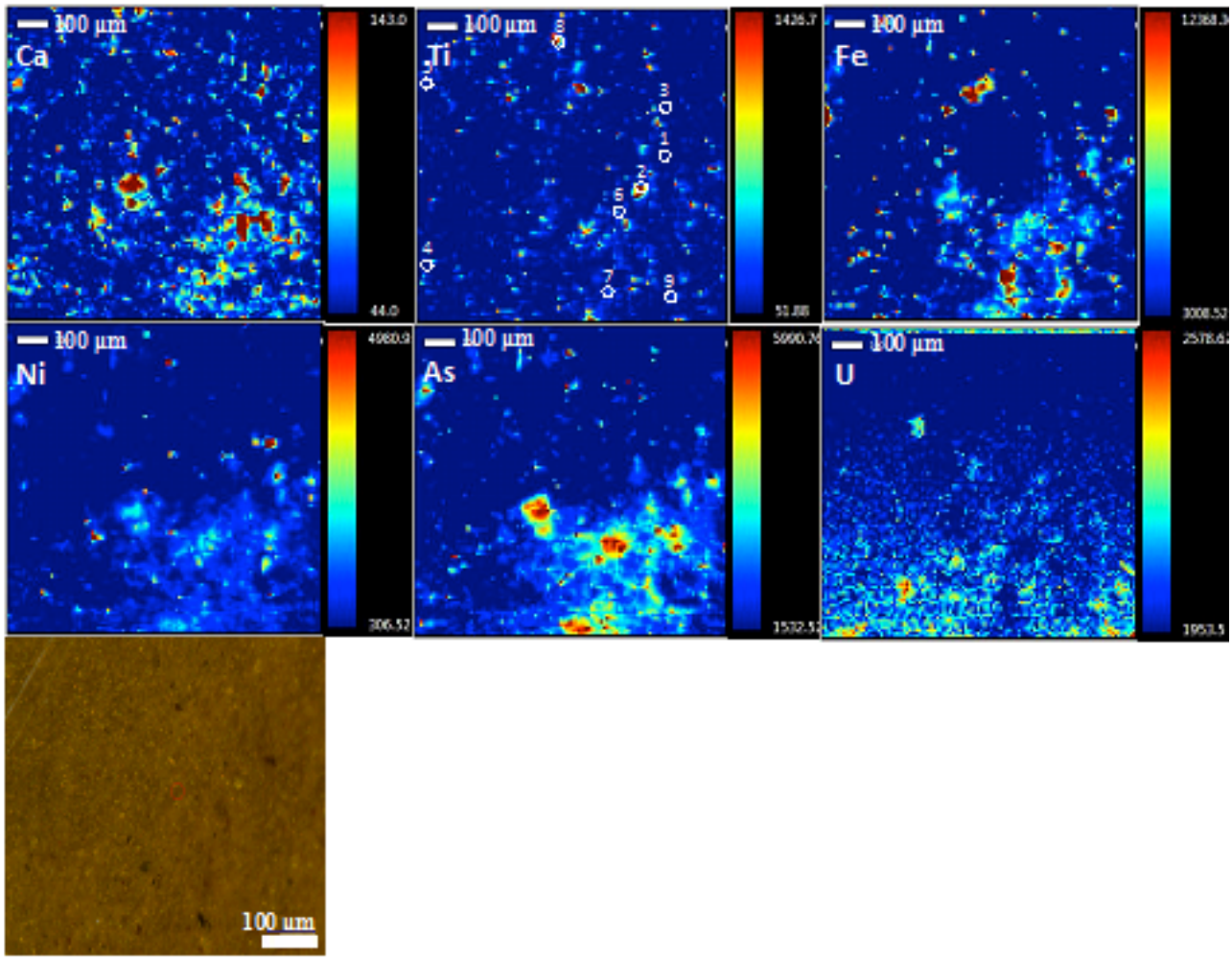

Figure A10. XRF maps for various elements found in tailings sample TMF13-03-SA19 are shown. Spots where Laue diffraction patterns were collected are labelled according to their scan number in the Ti map. An optical image of the mapped area is shown at the bottom of the figure.

Figure A11

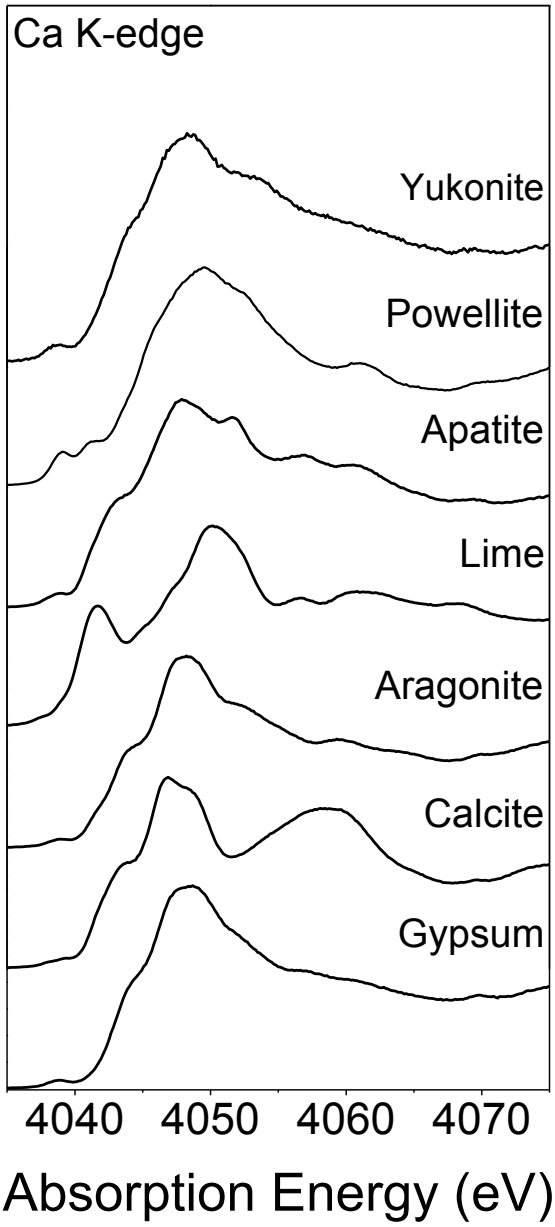

Figure A11. Ca K-edge XANES spectra from all of the standards used in the LCF analysis of the XANES spectra from the tailings samples are shown.

An update on the examination of the Ca-containing species in tailings samples from the JEB Tailings Management Facility, McClean Lake, Saskatchewan: Hard X-ray microprobe and Laue diffraction analysis

Peter E. R. Blanchard, Andrew P. Grosvenor*
Department of Chemistry, University of Saskatchewan, Saskatoon, SK, S7N 5C9

John Rowson, Kebbi Hughes, Caitlin Brown
AREVA Resources Canada, Saskatoon, SK, S7K 3X5

*Author to whom correspondence should be addressed
E-mail: andrew.grosvenor@usask.ca
Phone: (306) 966-4660
Fax: (306) 966-4730

Executive Summary:

X-ray fluorescence (XRF) microprobe mapping and Laue diffraction analysis was performed on a series of tailings samples collected from the JEB Tailings Management Facility (TMF) during the 2013 sampling campaign to determine if calcium carbonate (in the form of calcite or aragonite) forms in the TMF. A strong calcium signal was observed in all XRF maps. Several Laue diffraction patterns were collected from each sample and indexed against potential calcium-containing minerals that may be present in the TMF, as well as quartz. Although some of the more abundant crystalline phases (i.e. quartz and gypsum) could be identified, Laue diffraction analysis was hampered by the diffraction of multiple overlapping crystallites. The presence of calcium carbonate in the tailings samples could not be confirmed from the Laue diffraction analysis.

Experimental:

Microprobe X-ray fluorescence (XRF) maps and Laue diffraction patterns were collected using the VerySensitive Elemental and Structural Probe Employing Radiation from a Synchrotron (VESPERS) 07B2-1 beamline at the Canadian Light Source (Saskatoon, Canada).[1] Samples were prepared by sealing a thin layer of grains of the tailings between two layers of Kapton tape. Samples were mounted perpendicular to the beamline and at an angle of 45^{o} from the horizontal direction. X-ray fluorescence emission spectra were collected using a single element Vortex silicon drift detector (SDD) and the diffraction patterns were imaged using a Pilatus CCD image plate located directly above the samples. All measurements were performed using the "Pink Beam" mode, which includes all X-ray energies from 4–30 KV (with a significant drop in flux occurring near 20 KV). A 5 μm x 5 μm spot size was used for all measurements. Fluorescence maps were collected by rastering a 1000 μm x 1000 μm area using a 10 μm step size with a 1 s dwell time. Each Laue diffraction pattern was collected over 60–180 s. All fluorescence maps were created and analyzed using the SMAK software program.[2] Laue diffraction patterns were analyzed using the XMAS software program.[3]

Results and Discussion:

XRF maps were collected from all tailings samples to determine the distribution of elements in these materials. The XRF maps are shown in Figures 1–6. Relatively intense fluorescence signals were obtained for Ca, Ti, Fe, Ni, As, and U. Mo XRF maps of suitable quality could not be collected during this study. The Ca signal was generally weaker than that of the other elements because the Ca Kα emission is near the lower energy limit of the fluorescence detector used. Stronger Ca signals were generally found in tailings samples collected from deeper depths of the TMF (cf. Figures 2 and 6).

Laue diffraction patterns were collected from several different spots based on the results of the XRF analysis. The positions where Laue diffraction patterns were collected are marked on the Ti XRF maps in Figures 1–6. Representative Laue diffraction patterns collected from TMF13-01-SA19 tailings sample are shown in Figure 7. A X-ray pink beam spot size of 5 x 5 μm was used to collect each diffraction pattern. Ideally, the spot size should be on the order of the size of the crystallites and the resulting diffraction pattern should resemble a single-crystal X-ray diffraction pattern. However, most Laue diffraction patterns, such as the patterns shown in Figures 7a and 7b, contained non-circular diffraction spots of various sizes. Although this may be due to lattice deformities or multiple grain sizes,[4,5] it is most likely due to diffraction from multiple crystallites. The X-ray beam used in this analysis has a large penetrating depth and can be diffracted by overlapping crystallites. Therefore, the Laue diffraction patterns reported here may contain contributions from two or more phases.

The Laue diffraction patterns were indexed to the crystal structure of known standards, including the most likely calcium-containing minerals that could be present in the JEB TMF (i.e. gypsum, powellite, lime, calcite, and aragonite). Patterns were also indexed to quartz, as it was the most abundant crystalline mineral in the JEB TMF (as determined by XRD). Results of the

Laue diffraction fittings are tabulated in Table 1. Representative indexed Laue diffraction patterns are shown in Figure 8. Ideally, the number of indexed diffraction spots should be close to the number of observed diffraction spots.[6] However, due to diffraction from multiple crystallites, the resulting indexed patterns were not definitive fits. In most patterns, the low symmetry phases (i.e. calcite and aragonite) produced the largest numbers of indexed diffraction spots. This was most likely due to the indexing of diffraction spots from multiple crystallites. Note that the highest symmetry phase (lime) produced the smallest number of indexed peaks. Some diffraction patterns, such as the one shown in Figure 8a, could be confidently indexed if the diffraction patterns contained well-defined circular spots of similar size, an indication that most of the diffraction was occurring from a single crystallite. In most cases, these well-defined diffraction patterns were indexed to gypsum or quartz. The pattern collected from spot 9 of tailings sample TMF13-01-SA19 (Figure 8b) could be indexed to calcite; however, this was not a definitive fit.

Conclusion:

Synchrotron microprobe analysis was used to investigate the calcium-containing minerals in the JEB TMF. Calcium-rich regions were observed in the XRF maps of all tailings samples. Several Laue diffraction patterns were collected from each sample. In general, the Laue diffraction patterns consisted of several non-circular spots of varies sizes, an indication of diffraction from multiple overlapping crystallites. This can lead to the false identification of crystalline phases. For example, the highest number of indexed peaks were obtained when indexing the diffraction patterns to low symmetry crystalline phases (i.e. aragonite and calcite). Quartz and gypsum could be identified from Laue diffraction patterns consisting of circular diffraction spots of similar sizes, indicating that diffraction was occurring from a single crystallite. Analysis of the tailings samples by Laue diffraction was not able to conclusively determine if calcium carbonate (i.e., calcite or aragonite) was present in the tailings samples. XRF microprobe analysis is a powerful technique, as it can identify the location of specific elements in heterogeneous samples. Work has already begun to collect XRF microprobe maps from the tailings samples followed by the collection of Ca K-edge micro-XANES (X-ray absorption near edge spectroscopy) spectra using a beam size on the order of μm and the SXRMB beamline located at the CLS. The smaller X-ray spot size used in the collection of micro-XANES spectra may allow for the identification of minor calcium-containing minerals present in the tailings that could not be identified by collection of XANES spectra using a larger beam size (e.g., mm beam size).

References

1. Feng, R.; Gerson, A.; Ice, G.; Reininger, R.; Yates, B. McIntyre, S. VESPERS: a beamline for combined XRF and XRD measurements. *AIP Conf. Proc.* **2007**, *879*, 872-874.
2. Webb, S. M. The MicroAnalysis Toolkit: X-ray fluorescence image processing software. *AIP Conf. Proc.* **2011**, *196*, 196−199.
3. Tamura, N.; MacDowell, A. A.; Spolenak, R.; Valek, B. C.; Bravman, J. C.; Brown, W. L.; Celestre, R. S.; Padmore, H. A.; Batterman, B. W.; Patal, J. R. Scanning X-ray microdiffraction with submicrometer white beam for strain/stress and orientation mapping in thin films. *J. Synchrotron Radiat.* **2003**, *10*, 137−143.
4. Hofmann, F.; Song, X.; Abbey, B.; Jun, T. S.; Korsunsky, A. M. High-energy transmission Laue micro-beam X-ray diffraction: a probe for intra-granular lattice orientation and elastic strain in thicker samples. *J. Synchrotron Radiat.* **2012**, *19*, 307-318.
5. Hofmann, F.; Song, X.; Dolbnya, I.; Abbey, B.; Korsunsky, A. M. Probing intra-granular deformation by micro-beam Laue diffraction. *Procedia Eng.* **2009**, *1*, 193-196.
6. Rindby, A.; Engström, P.; Janssens, K. The use of a scanning X-ray microprobe for simultaneous XRF/XRD studies of fly-ash particles. *J. Synchrotron Radiat.* **1997**, *4*, 228−235.

T**ables**

Table 1. A summary of the Laue diffraction results of the tailings samples. Associated space groups, and space group numbers, for each phase are also listed.

Sample	Spot	# of indexed peaks					
		Quartz *$P3_221$* (#154)	Gypsum *C2/c* (#15)	Powellite *$I4_1/a$* (#88)	Lime *$Fm\bar{3}m$* (#225)	Calcite *$R\bar{3}c$* (#167)	Aragonite *C2/m* (#12)
TMF13-01-SA12	1	53	103	72	22	83	81
	2	53	103	73	29	81	84
	3	81	146	96	23	110	134
	4	69	147	87	31	60	100
	5	56	99	71	43	94	82
	6	131	205	142	36	172	203
	7	82	127	84	26	99	103
	8	67	109	76	37	92	101
TMF13-01-SA19	1	171	171	131	32	139	195
	2	126	142	82	30	133	132
	3	112	225	157	40	166	196
	4	130	226	170	27	176	221
	5	109	224	157	42	163	204
	6	25	32	24	14	21	26
	7	25	24	28	17	34	37
	8	29	38	28	15	36	36
	9	26	31	23	19	40	39
TMF13-01-SA22	1	47	78	58	27	75	101
	2	60	102	64	25	64	91
	3	88	124	88	28	133	105
	4	109	77	47	20	68	78
	5	23	32	21	15	23	28
	6	35	28	26	12	26	32
	7	22	57	31	20	45	42
	8	35	63	52	17	41	46
	9	130	232	134	35	154	184
	10	125	216	154	35	209	205
	11	83	196	127	32	173	162
	12	55	69	43	17	53	52
	13	131	257	158	40	234	252
TMF13-03-SA12	1	56	78	61	26	59	63
	2	75	121	98	20	100	133
	3	50	69	50	18	61	91
	4	45	33	35	20	45	39

	5	43	57	48	20	48	46
	6	47	47	38	18	44	42
	7	72	84	44	16	64	72
TMF13-03-SA15	1	72	121	86	27	90	134
	2	74	96	72	24	68	92
	3	55	98	73	25	76	80
	4	89	155	79	26	115	149
	5	110	207	130	31	145	179
	6	56	111	70	21	65	98
	7	132	185	129	35	145	187
	8	38	98	66	22	69	89
	9	76	114	84	22	100	101
	10	115	128	86	30	97	152
	11	126	252	196	47	196	235
TMF13-03-SA19	1	123	233	198	43	195	227
	2	101	110	91	32	98	99
	3	121	212	147	29	167	199
	4	138	220	149	34	192	212
	5	103	213	138	27	145	192
	6	84	136	106	23	72	144
	7	95	165	103	27	145	168
	8	78	105	70	31	78	80
	9	37	69	41	19	77	75
	10	61	68	55	23	51	65
	11	122	216	162	35	122	205
	12	137	235	139	33	135	247
	13	129	120	80	23	68	110
	14	97	120	67	25	78	95

Figures

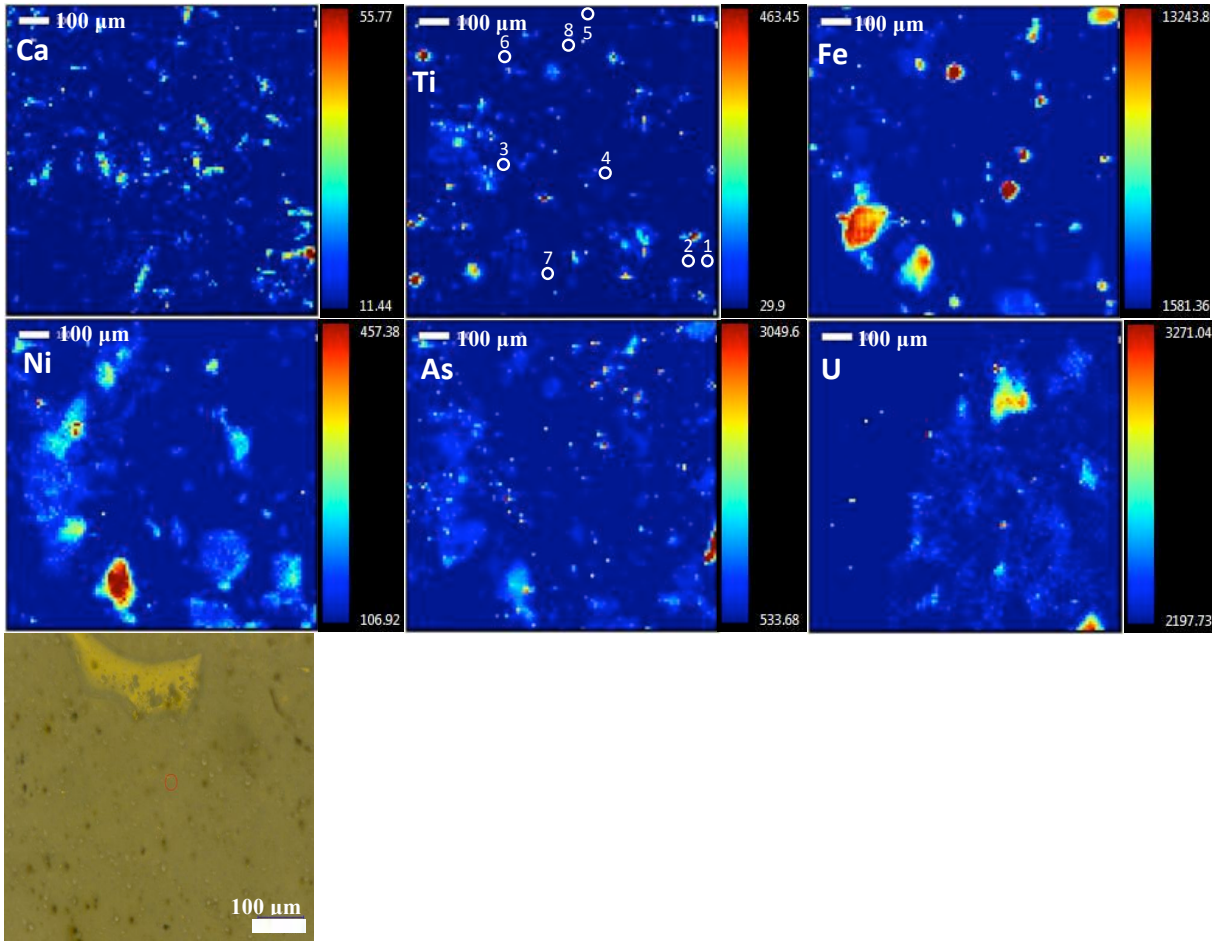

Figure 1. XRF maps of various elements found in tailings sample TMF13-01-SA12 are shown. Spots where Laue diffraction patterns were collected are labelled according to their scan number in the Ti map. An optical image of the mapped area is shown at the bottom of the figure.

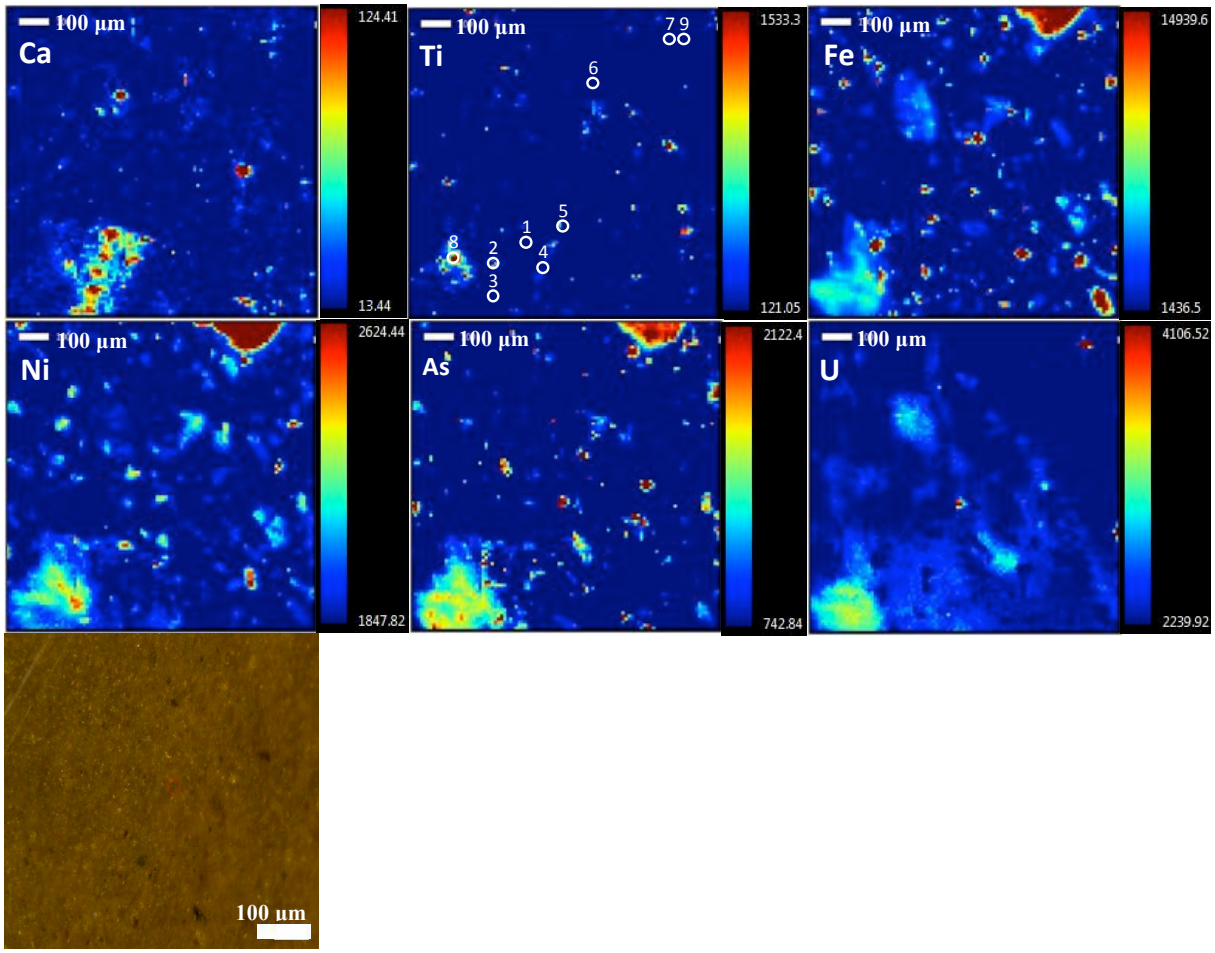

Figure 2. XRF maps of various elements found in tailings sample TMF13-01-SA19 are shown. Spots where Laue diffraction patterns were collected are labelled according to their scan number in the Ti map. An optical image of the mapped area is shown at the bottom of the figure.

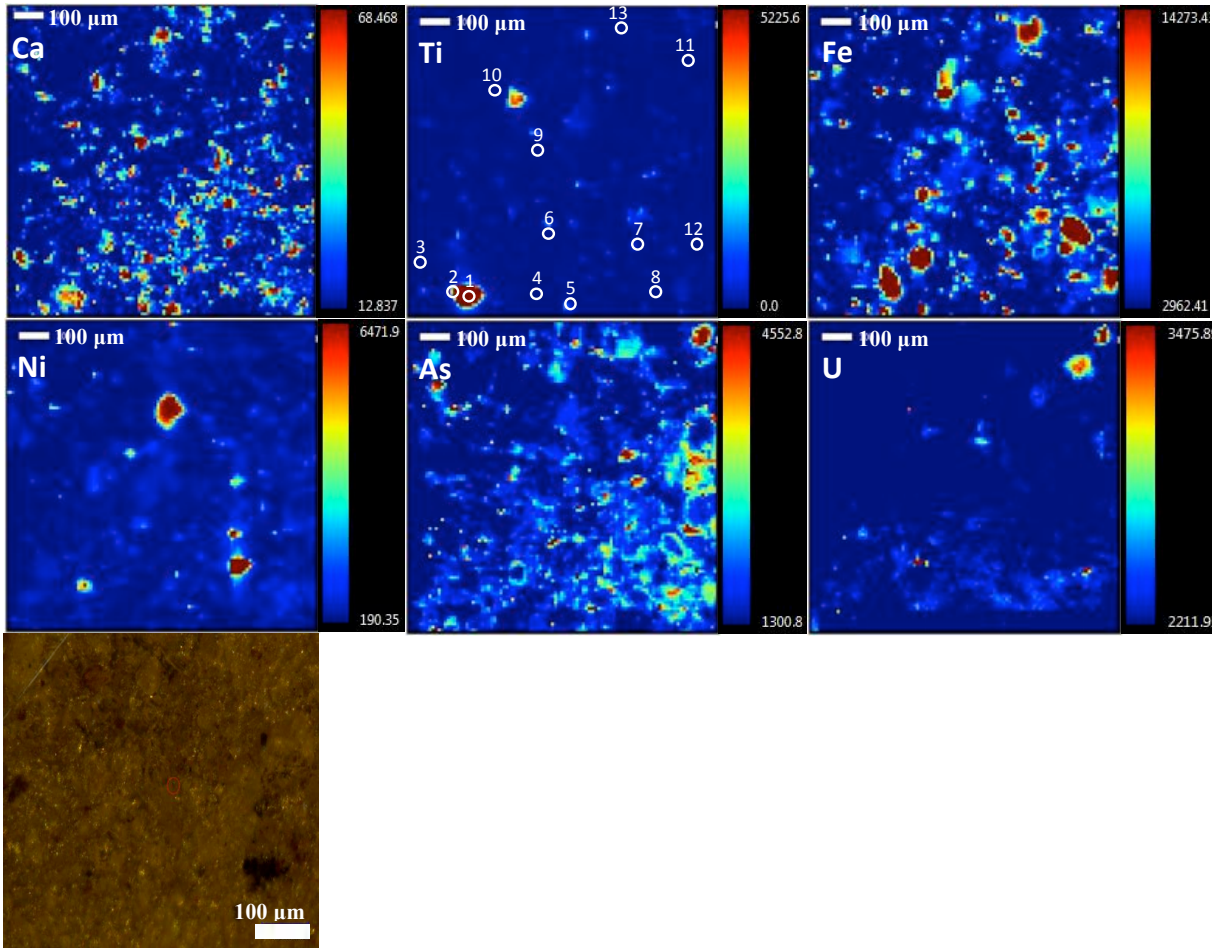

Figure 3. XRF maps of various elements found in tailings sample TMF13-01-SA22 are shown. Spots where Laue diffraction patterns were collected are labelled according to their scan number in the Ti map. An optical image of the mapped area is shown at the bottom of the figure.

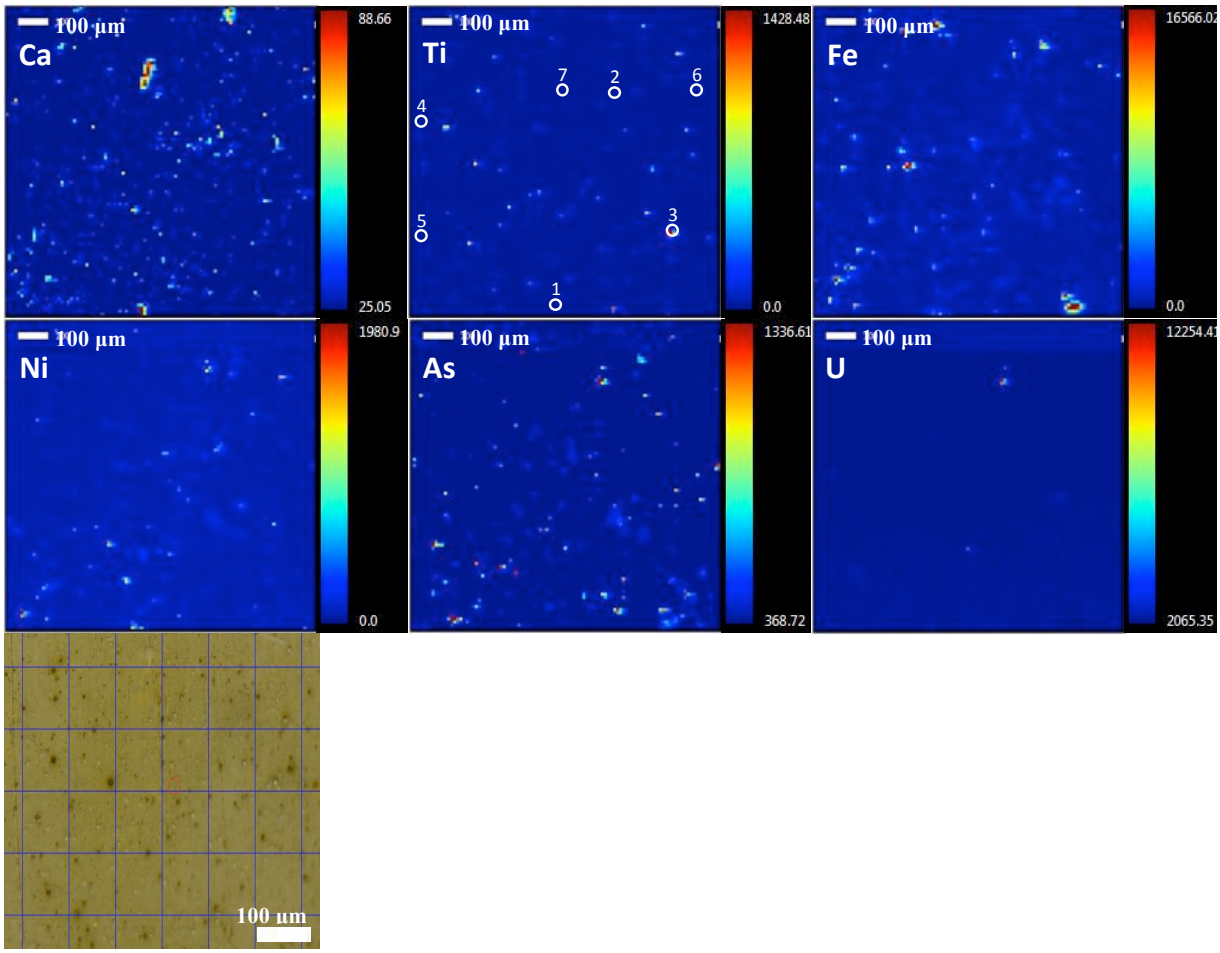

Figure 4. XRF maps of various elements found in tailings sample TMF13-03-SA12 are shown. Spots where Laue diffraction patterns were collected are labelled according to their scan number in the Ti map. An optical image of the mapped area is shown at the bottom of the figure.

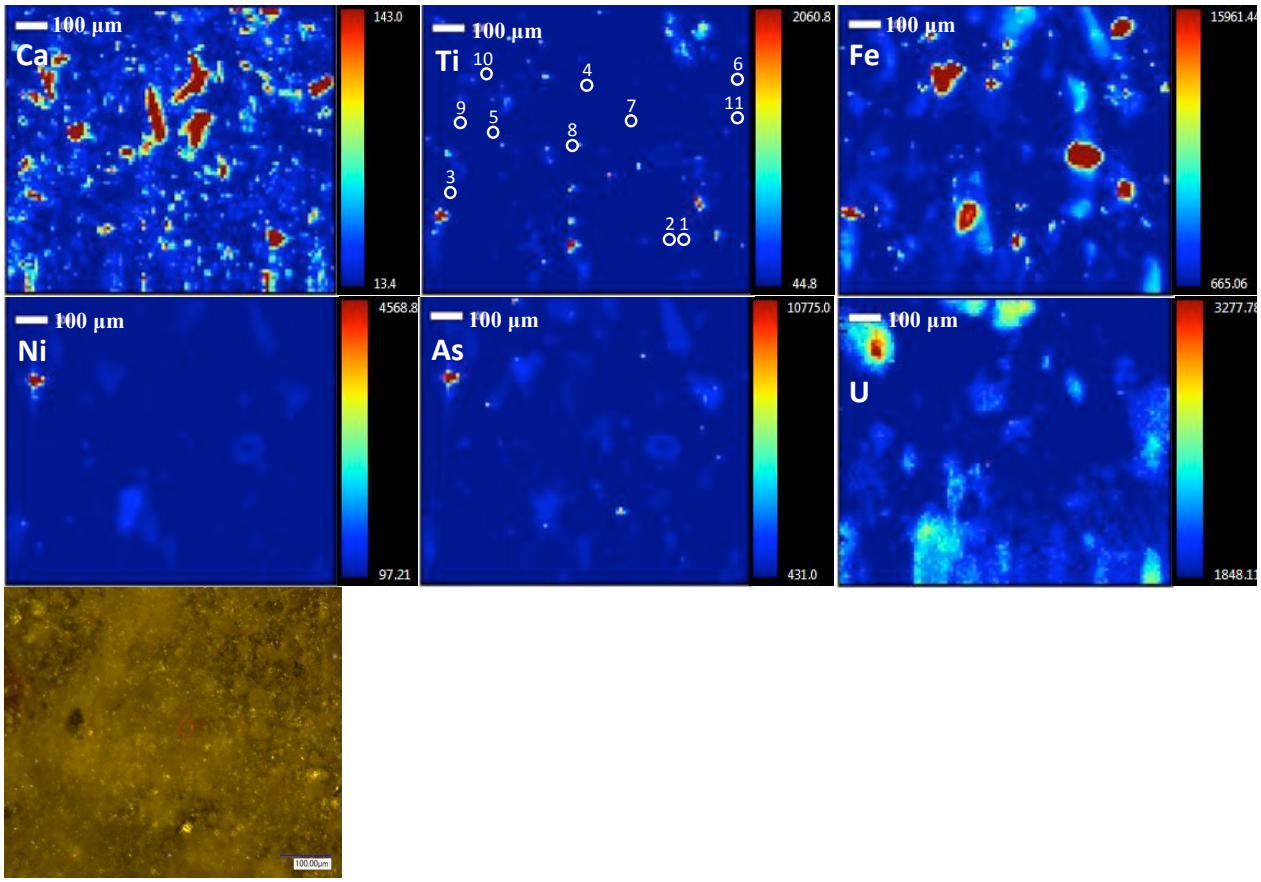

Figure 5. XRF maps of various elements found in tailings sample TMF13-03-SA15 are shown. Spots where Laue diffraction patterns were collected are labelled according to their scan number in the Ti map. An optical image of the mapped area is shown at the bottom of the figure.

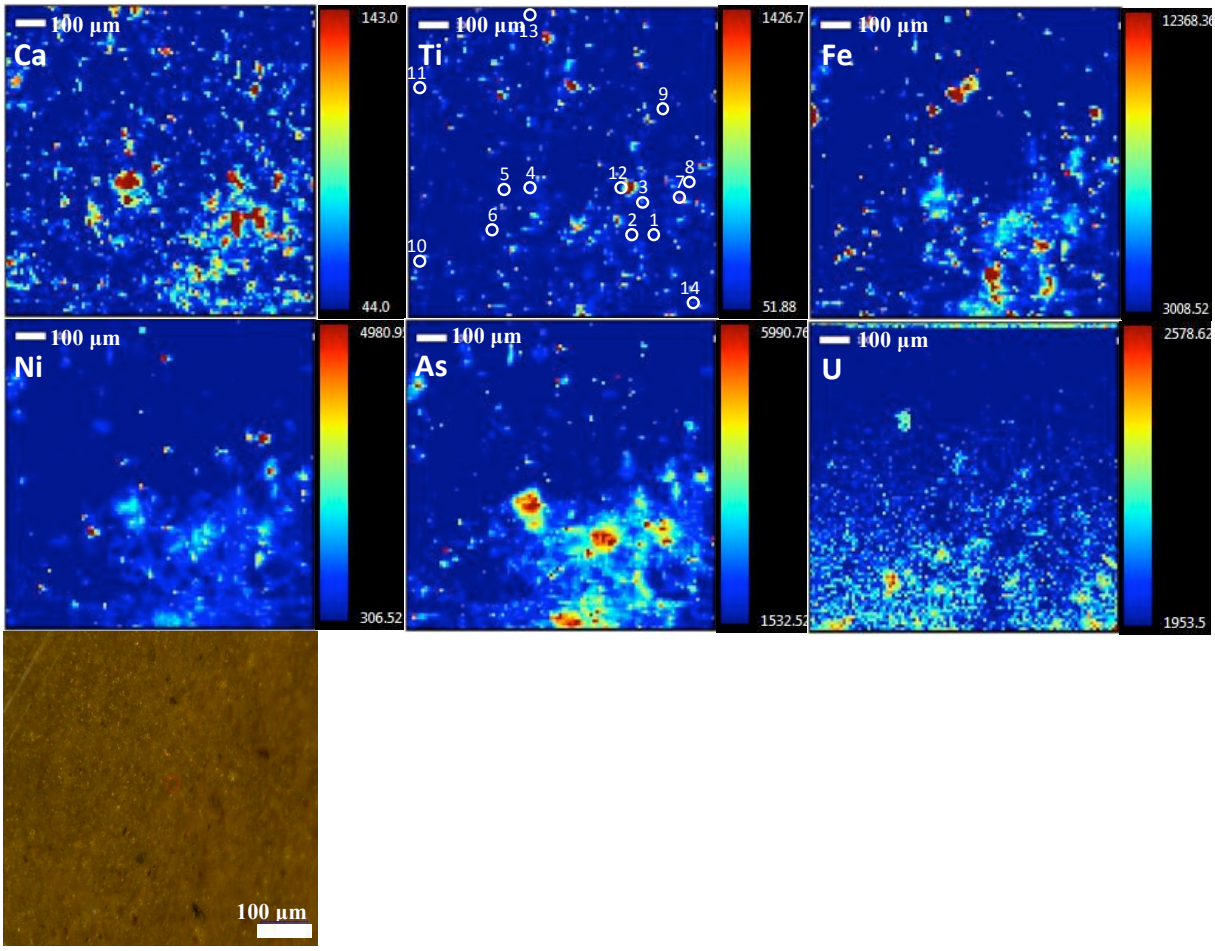

Figure 6. XRF maps of various elements found in tailings sample TMF13-03-SA19 are shown. Spots where Laue diffraction patterns were collected are labelled according to their scan number in the Ti map. An optical image of the mapped area is shown at the bottom of the figure.

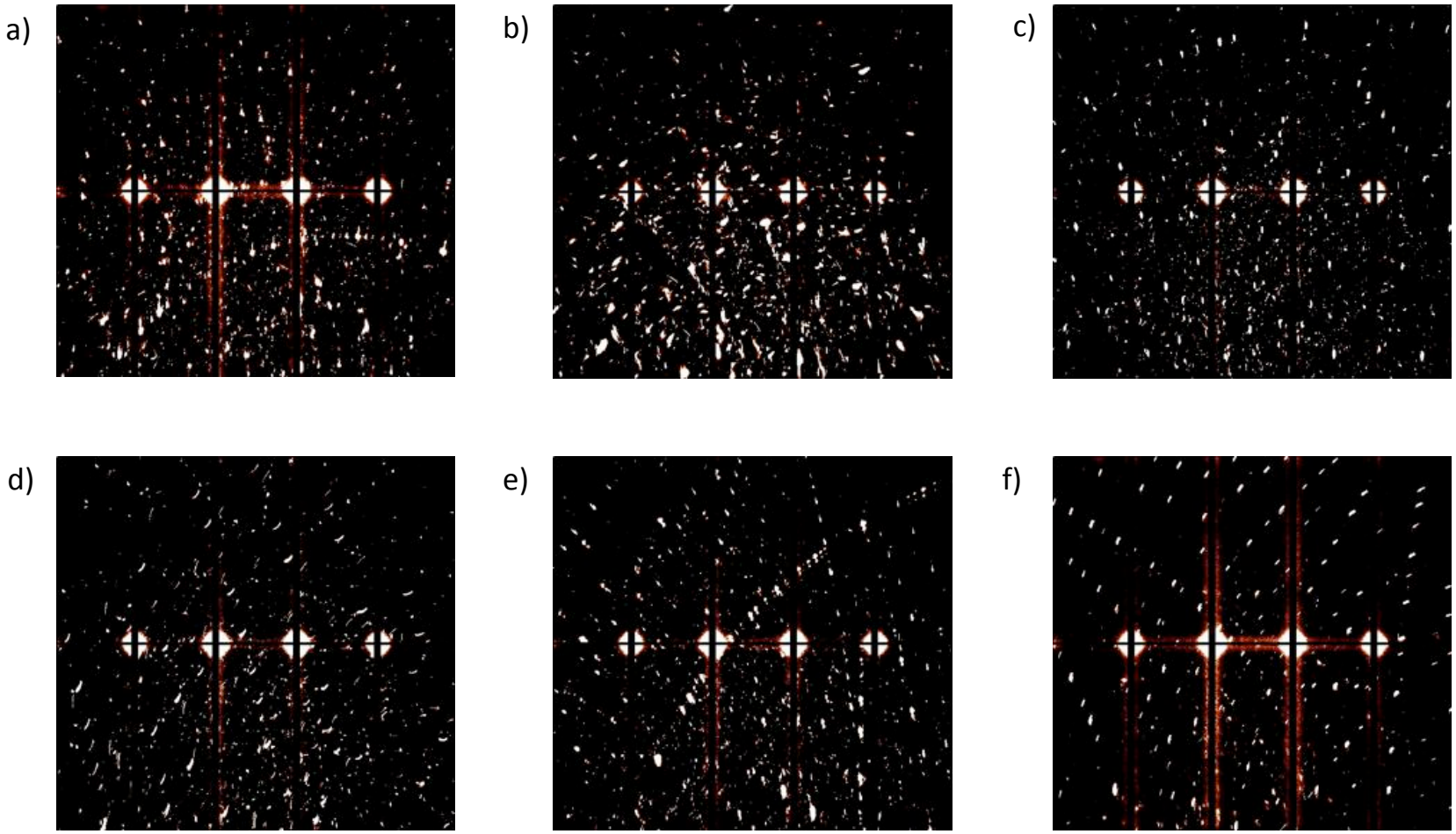

Figure 7. Laue Diffraction patterns collected using a 5 x 5 μm size beam from tailings sample TMF13-03-SA19 at the following positions marked in the XRF map shown in Figure 6: a) spot 1, b) spot 3, c) spot 5, d) spot 10, e) spot 11, and f) spot 12. The diffraction patterns collected from spot 3, spot 5, and spot 10 have different diffraction spot sizes, indicating that diffraction may be occurring from multiple grains. The diffraction pattern from spot 11 was indexed best to gypsum while the diffraction pattern from spot 12 was indexed best to quartz.

a) b)

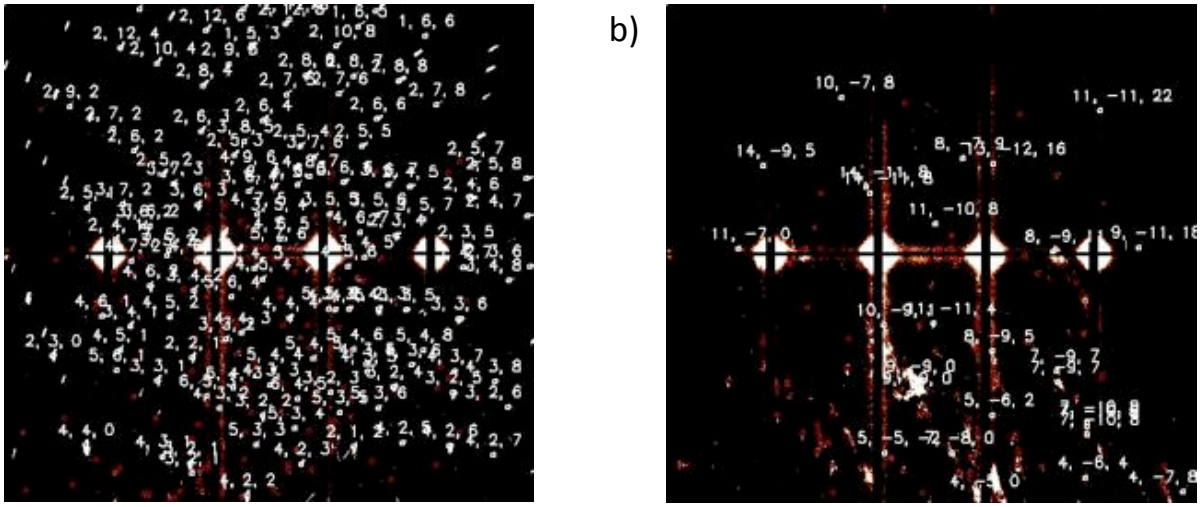

Figure 8. a) The Laue diffraction pattern collected from spot 12 from tailings sample TMF13-03-SA19 indexed to quartz. b) The Laue diffraction pattern collected from spot 9 from tailings sample TMF13-01-SA19 indexed to calcite.

CONFIDENTIAL REPORT

QEMSCAN Analysis

Prepared for Orano

By Steven Creighton, PhD
Saskatchewan Research Council
Mining and Minerals

SRC Publication No. 13478-5C19

March 2019

CONFIDENTIAL REPORT

QEMSCAN Analysis

Prepared for Orano

By Steven Creighton, PhD
Saskatchewan Research Council
Mining and Minerals

SRC Publication No. 13478-5C19

March 2019

Advanced Microanalysis Centre™
Saskatchewan Research Council
125 – 15 Innovation Blvd.
Saskatoon, SK S7N 2X8
Tel: 306-385-4066

Table of Contents

Executive Summary iii
Sample receiving and preparation 1
QEMSCAN operation 1
Analytical Statistics 1
Modal Mineralogy 2
Primary vs. Secondary Minerals 10
Grain size histograms 15
Grain Images 19
TMF18-01-01 20
TMF18-01-02 21
TMF18-01-03 22
TMF18-01-06 23
TMF18-01-10 24
TMF18-01-11 25
TMF18-01-13 26
TMF18-01-15 27
TMF18-01-17 28
TMF18-01-20 29
TMF18-01-26 30
TMF18-02-03 31
TMF18-03-01 32
TMF18-03-02 33
TMF18-03-05 34
TMF18-03-07 35
TMF18-03-09 36
TMF18-03-12 37
TMF18-03-14 38
TMF18-03-18 39
TMF18-03-19 40
TMF18-03-21 41
Primary Mineral Grain Images 42
TMF18-01-01 42
TMF18-01-02 42

TMF18-01-03 42
TMF18-01-06 43
TMF18-01-10 43
TMF18-01-11 43
TMF18-01-13 43
TMF18-01-15 44
TMF18-01-17 44
TMF18-01-20 44
TMF18-01-26 44
TMF18-02-03 45
TMF18-03-01 45
TMF18-03-02 45
TMF18-03-05 46
TMF18-03-07 46
TMF18-03-09 46
TMF18-03-12 46
TMF18-03-14 47
TMF18-03-18 47
TMF18-03-19 47
TMF18-03-21 47

Table of Figures

Figure 1: Complex modal mineralogy of all the samples 3
Figure 2: Complex modal mineralogy of samples from Cigar Lake tailings 8
Figure 3: Complex modal mineralogy of samples not from Cigar Lake 9
Figure 4: Abundance (weight percent) of Primary and Secondary minerals in the samples 10
Figure 5: Modal mineralogy of grains containing >10% "primary" minerals in Cigar Lake samples (normalized to 100%; weight percent) 12
Figure 6: Modal mineralogy of grains containing >10% "Primary" minerals in samples not from Cigar Lake (normalized to 100%; weight percent) 13

Table of Tables

Table 1: QEMSCAN operational statistics 1
Table 2: Complex mineralogy of the samples (weight percent abundance) 4
Table 3: Modal mineralogy divided into Primary and Secondary minerals (weight percent) 11
Table 4: Modal mineralogy of grains containing “Primary” minerals 14

Executive Summary

- Quartz and clays are the predominant minerals in all samples comprising at least 80% of the samples (weight percent) combined
- The relative abundance of quartz and clay minerals is highly variable with some samples being dominated by quartz (e.g. TMF18-01-10 – 81%) and others having considerably less quartz (e.g. TMF18-03-05 – 17%)
- "Primary" minerals comprise only a minor amount of the total samples – all samples are less than 5% and most are less than 1%
- The Cigar Lake samples have the highest abundance of primary minerals
- Mineralogy of primary minerals are predominantly iron-(Cu)- sulphides in most samples
- Gersdorffite is a significant component in the primary mineralogy of TMF18-01-03, -01-15, -01-26, -03-05, -03-07, -03-14 and -03-19
- Uraninite is significant in samples TMF18-01-20, -01-26, 03-14 and 03-19
- The size of grains containing primary minerals is typically <25µm and all distributions are positively skewed

Sample receiving and preparation

A 5g portion of each sample was mixed with 15ml of premixed two-component epoxy and poured into 30mm diameter polypropylene molds and allowed to harden overnight. The hardened samples were demolded and the analytical surface was prepared to a final polish using 1µm diamond polishing compound. Each sample was coated with a 15nm thick layer of amorphous carbon to ensure electrical conductivity of the sample surface.

QEMSCAN operation

The QEMSCAN in the SRC Advanced Microanalysis Centre is built on an FEI Quanta 650 scanning electron microscope fitted with a field emission gun (10nm resolution) and dual Bruker XFlash 5030 energy dispersive spectrometers with a maximum throughput of 1.5Mcps.

QEMSCAN analyses are a collection of back-scattered electron images and semi-quantitative point chemical analyses. The grain images and EDS data are combined using image analysis to calculate various parameters such as particle size distribution, mineral associations and liberation, modal abundances, etc.

Operating conditions were set to 25kV and 10nA beam current, measured in a Faraday cup at the sample surface. Data were collected in Particle Mineral Analysis (PMA) mode with a point spacing of 5µm. Raw X-ray energy spectra were compared to a mineral composition database customized for this project.

Analytical Statistics

Statistics from the QEMSCAN analyses are tabulated below (Table 1).

Table 1: QEMSCAN operational statistics

Sample ID	**TMF18-01-01**	**TMF18-01-02**	**TMF18-01-03**	**TMF18-01-10**
Size Fraction	-1000/+20	-1000/+20	-1000/+20	-1000/+20
Mass Percent	100	100	100	100
Pixel Spacing (µm)	4.76	4.76	4.76	4.76
Particles Analyzed	50,131	42,023	43,551	35,468
X-Ray data points	1,751,862	1,660,848	1,149,662	945,076
Sample ID	**TMF18-01-11**	**TMF18-01-13**	**TMF18-01-15**	**TMF18-01-17**
Size Fraction	-1000/+20	-1000/+20	-1000/+20	-1000/+20
Mass Percent	100	100	100	100
Pixel Spacing (µm)	4.76	4.76	4.76	4.76
Particles Analyzed	47,767	28,375	40,528	35,526
X-Ray data points	1,296,260	633,002	763,737	791,356
Sample ID	**TMF18-01-20**	**TMF18-01-26**	**TMF18-02-03**	**TMF18-03-01**

Size Fraction	-1000/+20	-1000/+20	-1000/+20	-1000/+20
Mass Percent	100	100	100	100
Pixel Spacing (µm)	4.76	4.76	4.76	4.76
Particles Analyzed	43,880	43,609	42,086	36,394
X-Ray data points	1,078,172	1,077,973	1,180,985	964,752
Sample ID	**TMF18-03-02**	**TMF18-03-05**	**TMF18-03-07**	**TMF18-03-09**
Size Fraction	-1000/+20	-1000/+20	-1000/+20	-1000/+20
Mass Percent	100	100	100	100
Pixel Spacing (µm)	4.76	4.76	4.76	4.76
Particles Analyzed	36,430	37,489	38,894	35,423
X-Ray data points	1,552,835	1,422,977	867,925	944,158
Sample ID	**TMF18-03-12**	**TMF18-03-14**	**TMF18-03-18**	**TMF18-03-19**
Size Fraction	-1000/+20	-1000/+20	-1000/+20	-1000/+20
Mass Percent	100	100	100	100
Pixel Spacing (µm)	4.76	4.76	4.76	4.76
Particles Analyzed	33,255	37,931	41,454	34,090
X-Ray data points	802,043	1,038,106	1,057,577	869,961
Sample ID	**TMF18-03-21**			
Size Fraction	-1000/+20			
Mass Percent	100			
Pixel Spacing (µm)	4.76			
Particles Analyzed	41,510			
X-Ray data points	1,082,362			

Modal Mineralogy

Modal mineralogy is calculated from the combined analysis of the BSE images and the mineral identification from the EDS data. The volumetric abundance of the minerals is converted to mass percent from density data for typical mineral compositions. The modal mineralogy data following is compiled in several different groupings to highlight various features.

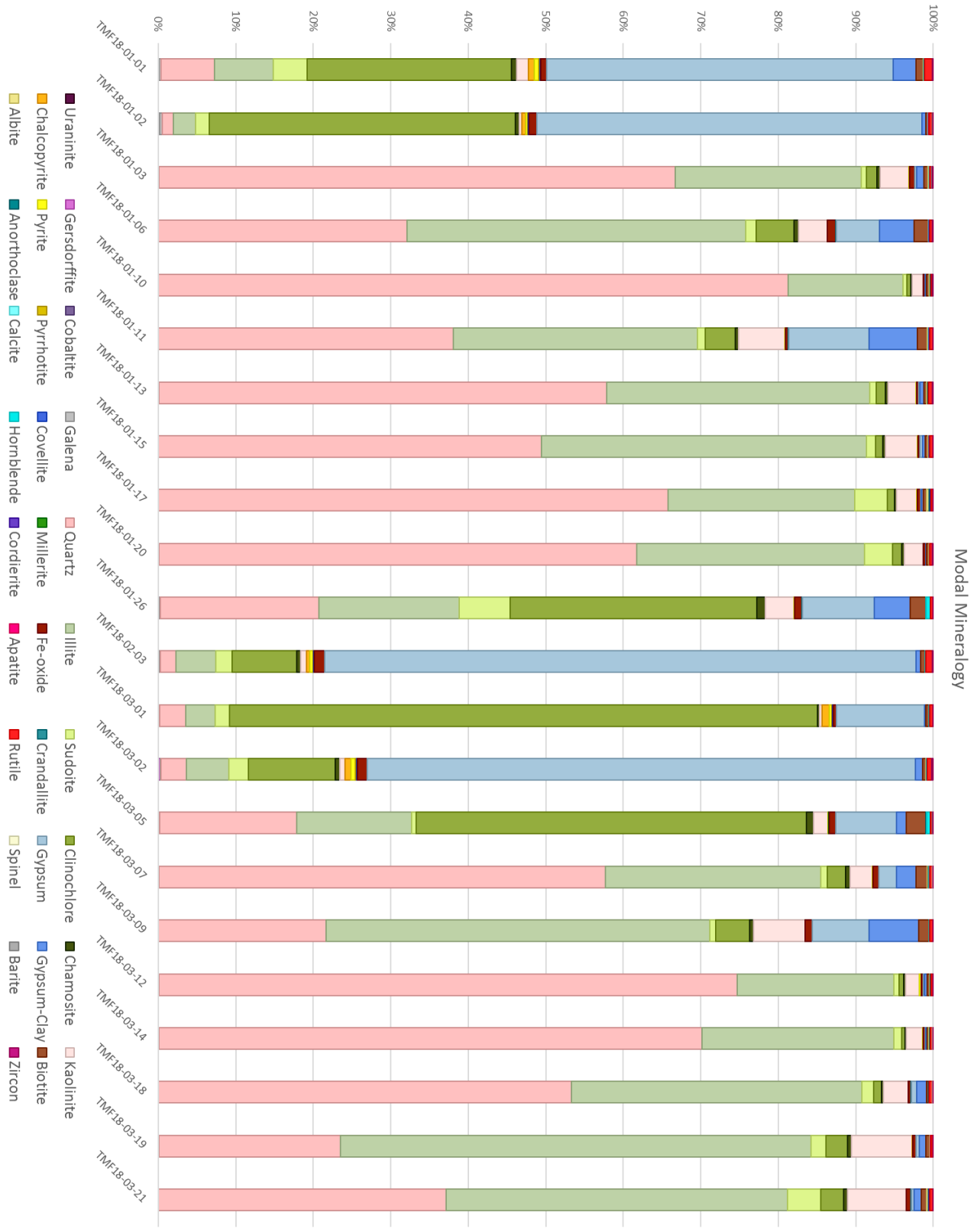

Figure 1: Complex modal mineralogy of all the samples

Table 2: Complex mineralogy of the samples (weight percent abundance)

	TMF18-01-01	TMF18-01-02	TMF18-01-03	TMF18-01-06	TMF18-01-10	TMF18-01-11
Uraninite	0.02	0.01	0.00	0.00	0.00	0.00
Gersdorffite	0.06	0.12	0.12	0.01	0.01	0.02
Cobaltite	0.02	0.02	0.00	0.00	0.00	0.00
Galena	0.23	0.36	0.01	0.01	0.00	0.03
Quartz	6.97	1.47	66.52	32.10	81.27	38.07
Illite	7.58	2.82	24.04	43.68	14.79	31.45
Sudoite	4.32	1.79	0.64	1.36	0.51	0.98
Clinochlore	26.41	39.53	1.39	4.84	0.47	3.92
Chamosite	0.65	0.44	0.42	0.59	0.23	0.45
Kaolinite	1.54	0.36	3.73	3.73	1.40	5.92
Chalcopyrite	0.74	0.52	0.00	0.00	0.00	0.00
Pyrite	0.57	0.28	0.06	0.02	0.02	0.06
Pyrrhotite	0.15	0.08	0.02	0.00	0.00	0.00
Covellite	0.07	0.08	0.00	0.00	0.00	0.00
Millerite	0.00	0.00	0.01	0.00	0.00	0.01
Fe-oxide	0.76	1.00	0.63	1.10	0.21	0.40
Crandallite	0.02	0.00	0.03	0.03	0.01	0.03
Gypsum	44.68	49.61	0.25	5.54	0.04	10.40
Gypsum-Clay	2.97	0.56	0.91	4.51	0.17	6.18
Biotite	0.99	0.23	0.55	1.85	0.30	1.33
Albite	0.01	0.03	0.12	0.01	0.17	0.11
Anorthoclase	0.01	0.01	0.05	0.00	0.06	0.04
Calcite	0.03	0.01	0.00	0.05	0.00	0.03
Hornblende	0.08	0.07	0.02	0.04	0.01	0.07
Cordierite	0.01	0.00	0.01	0.01	0.01	0.01
Apatite	0.02	0.01	0.00	0.00	0.00	0.00
Rutile	0.96	0.49	0.29	0.39	0.18	0.42
Spinel	0.00	0.00	0.01	0.00	0.02	0.01
Barite	0.01	0.02	0.01	0.00	0.00	0.01
Zircon	0.14	0.07	0.16	0.10	0.12	0.06

	TMF18-01-13	TMF18-01-15	TMF18-01-17	TMF18-01-20	TMF18-01-26	TMF18-02-03
Uraninite	0.00	0.00	0.00	0.02	0.11	0.05
Gersdorffite	0.03	0.02	0.00	0.02	0.09	0.07
Cobaltite	0.00	0.00	0.00	0.00	0.00	0.01
Galena	0.04	0.01	0.01	0.02	0.07	0.14
Quartz	57.79	49.38	65.72	61.64	20.47	2.01
Illite	33.97	41.93	24.15	29.45	18.12	5.12

	TMF18-01-13	TMF18-01-15	TMF18-01-17	TMF18-01-20	TMF18-01-26	TMF18-02-03
Sudoite	0.83	1.21	4.18	3.58	6.54	2.10
Clinochlore	1.17	0.94	0.92	1.17	31.84	8.38
Chamosite	0.32	0.29	0.29	0.36	1.04	0.49
Kaolinite	3.59	4.16	2.58	2.42	3.76	0.78
Chalcopyrite	0.00	0.00	0.01	0.00	0.01	0.42
Pyrite	0.08	0.05	0.04	0.02	0.06	0.39
Pyrrhotite	0.00	0.00	0.00	0.00	0.01	0.07
Covellite	0.00	0.00	0.00	0.00	0.00	0.08
Millerite	0.00	0.00	0.00	0.00	0.01	0.00
Fe-oxide	0.25	0.29	0.45	0.29	0.93	1.36
Crandallite	0.01	0.01	0.01	0.03	0.03	0.01
Gypsum	0.20	0.34	0.07	0.02	9.24	76.32
Gypsum-Clay	0.48	0.35	0.25	0.09	4.63	0.55
Biotite	0.33	0.28	0.42	0.31	2.02	0.58
Albite	0.17	0.15	0.36	0.06	0.03	0.01
Anorthoclase	0.07	0.07	0.16	0.02	0.01	0.00
Calcite	0.00	0.00	0.00	0.01	0.00	0.04
Hornblende	0.06	0.00	0.01	0.00	0.54	0.02
Cordierite	0.01	0.01	0.04	0.03	0.03	0.01
Apatite	0.00	0.00	0.00	0.01	0.01	0.01
Rutile	0.44	0.42	0.25	0.32	0.31	0.85
Spinel	0.01	0.00	0.01	0.01	0.00	0.00
Barite	0.00	0.00	0.00	0.00	0.01	0.04
Zircon	0.14	0.07	0.05	0.09	0.04	0.09

	TMF18-03-01	TMF18-03-02	TMF18-03-05	TMF18-03-07	TMF18-03-09	TMF18-03-12
Uraninite	0.01	0.05	0.00	0.01	0.00	0.03
Gersdorffite	0.03	0.18	0.15	0.03	0.00	0.03
Cobaltite	0.01	0.02	0.00	0.00	0.00	0.01
Galena	0.11	0.12	0.01	0.04	0.03	0.06
Quartz	3.37	3.23	17.71	57.66	21.61	74.54
Illite	3.84	5.51	14.81	27.76	49.55	20.25
Sudoite	1.79	2.48	0.56	0.79	0.73	0.66
Clinochlore	75.87	11.27	50.37	2.37	4.37	0.59
Chamosite	0.32	0.54	0.91	0.61	0.53	0.24
Kaolinite	0.26	0.71	1.89	2.88	6.64	1.82
Chalcopyrite	1.00	0.77	0.00	0.00	0.00	0.00
Pyrite	0.32	0.59	0.09	0.03	0.01	0.20
Pyrrhotite	0.07	0.09	0.01	0.00	0.01	0.01
Covellite	0.09	0.13	0.00	0.00	0.00	0.00

	TMF18-03-01	TMF18-03-02	TMF18-03-05	TMF18-03-07	TMF18-03-09	TMF18-03-12
Millerite	0.00	0.00	0.03	0.00	0.00	0.00
Fe-oxide	0.38	1.26	0.84	0.76	0.91	0.23
Crandallite	0.01	0.00	0.03	0.03	0.03	0.01
Gypsum	11.37	70.75	7.86	2.28	7.29	0.16
Gypsum-Clay	0.21	0.93	1.23	2.50	6.40	0.39
Biotite	0.36	0.42	2.49	1.43	1.38	0.29
Albite	0.01	0.03	0.06	0.21	0.01	0.10
Anorthoclase	0.00	0.01	0.03	0.06	0.00	0.05
Calcite	0.00	0.01	0.00	0.05	0.01	0.01
Hornblende	0.07	0.04	0.48	0.05	0.02	0.01
Cordierite	0.00	0.00	0.00	0.01	0.01	0.01
Apatite	0.01	0.01	0.01	0.00	0.01	0.00
Rutile	0.42	0.60	0.31	0.36	0.41	0.23
Spinel	0.00	0.00	0.00	0.03	0.00	0.01
Barite	0.01	0.01	0.05	0.00	0.00	0.01
Zircon	0.06	0.21	0.04	0.05	0.06	0.05

	TMF18-03-14	TMF18-03-18	TMF18-03-19	TMF18-03-21
Uraninite	0.05	0.00	0.08	0.00
Gersdorffite	0.01	0.00	0.01	0.02
Cobaltite	0.00	0.00	0.00	0.00
Galena	0.01	0.04	0.03	0.04
Quartz	70.07	53.29	23.38	37.10
Illite	24.80	37.44	60.76	44.07
Sudoite	0.98	1.55	1.86	4.27
Clinochlore	0.44	0.95	2.85	2.95
Chamosite	0.16	0.25	0.47	0.54
Kaolinite	2.09	3.21	7.87	7.50
Chalcopyrite	0.00	0.00	0.01	0.01
Pyrite	0.08	0.04	0.06	0.06
Pyrrhotite	0.00	0.00	0.01	0.00
Covellite	0.00	0.00	0.01	0.00
Millerite	0.00	0.00	0.00	0.00
Fe-oxide	0.26	0.35	0.36	0.57
Crandallite	0.02	0.01	0.02	0.03
Gypsum	0.06	0.74	0.42	0.36
Gypsum-Clay	0.16	1.21	0.86	0.91
Biotite	0.22	0.27	0.45	0.67
Albite	0.14	0.04	0.10	0.25
Anorthoclase	0.06	0.03	0.04	0.10

	TMF18-03-14	TMF18-03-18	TMF18-03-19	TMF18-03-21
Calcite	0.00	0.00	0.00	0.01
Hornblende	0.01	0.01	0.01	0.02
Cordierite	0.01	0.02	0.02	0.04
Apatite	0.01	0.00	0.00	0.00
Rutile	0.27	0.45	0.29	0.43
Spinel	0.02	0.01	0.00	0.01
Barite	0.00	0.00	0.00	0.00
Zircon	0.07	0.08	0.04	0.05

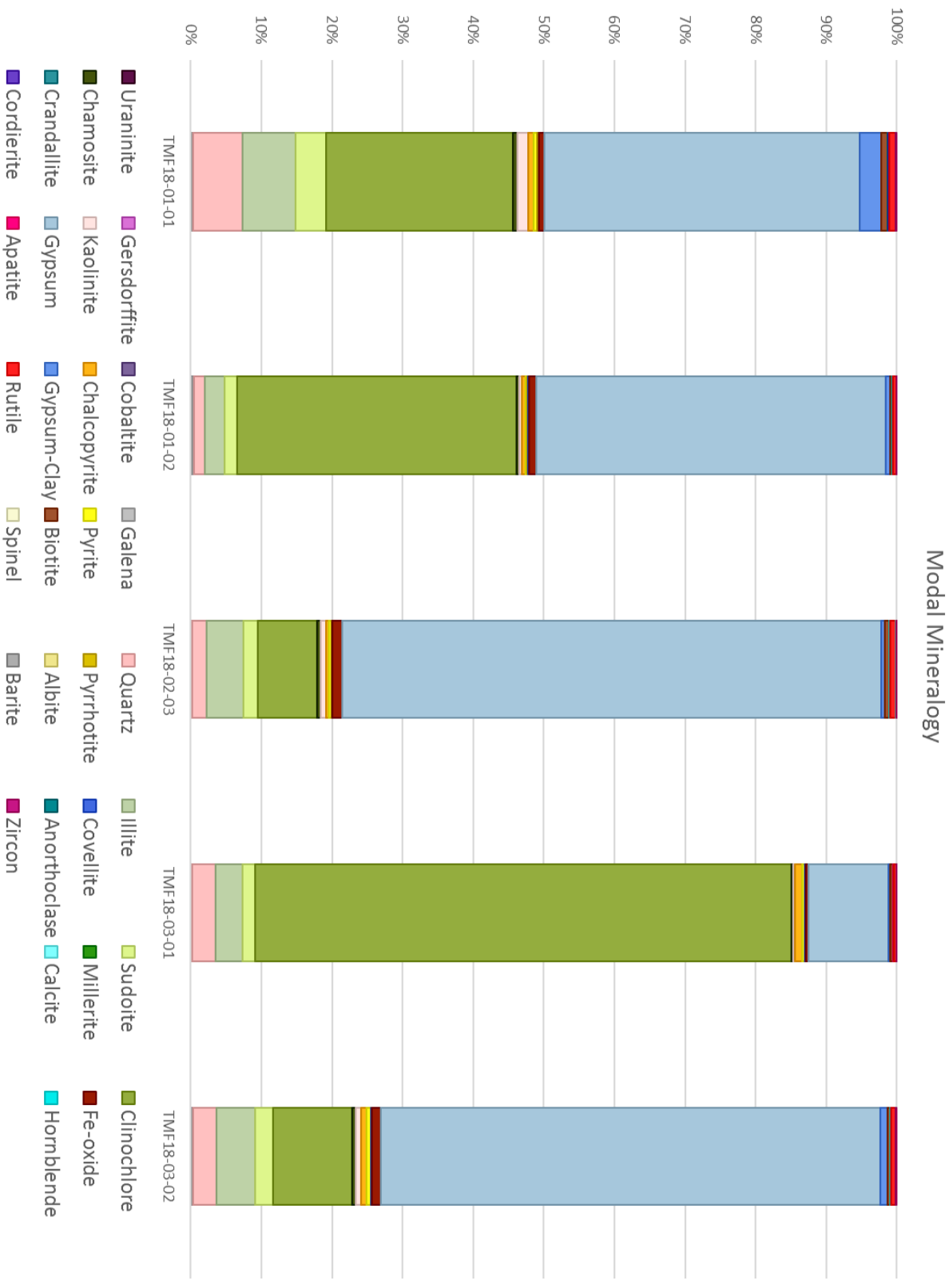

Figure 2: Complex modal mineralogy of samples from Cigar Lake tailings

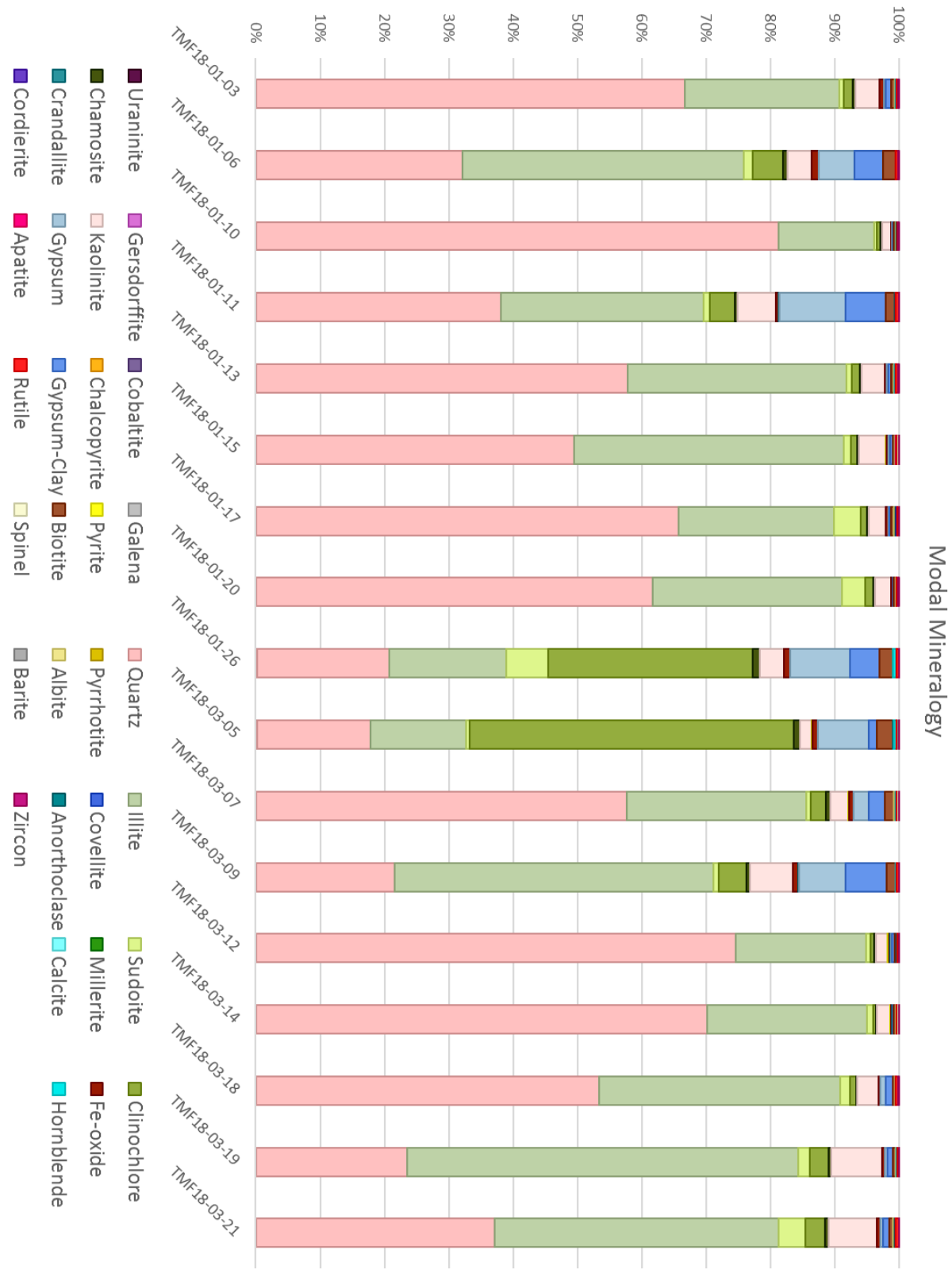

Figure 3: Complex modal mineralogy of samples not from Cigar Lake

Primary vs. Secondary Minerals

The following plots and tables outline the breakdown of the observed mineralogy into two broad categories – Primary and Secondary. Primary minerals are considered to be derived from the original mineralogy of the samples and have passed through the extraction processes more or less intact. The Primary minerals include: uraninite, gersdorffite, cobaltite, arsenopyrite, ilmenite, galena, chalcopyrite, pyrite, pyrrhotite, sphalerite, iron oxides and zircon. Quartz is likely a primary mineral but is included in the Secondary list because it is not of environmental or toxicological significance. The other Secondary minerals include residual feldspars, clays, gypsum, calcite and apatite.

Particles of primary minerals commonly occur in grains composed of a mixture of primary and secondary minerals. The modal mineralogy of grains with >10% primary minerals is shown below.

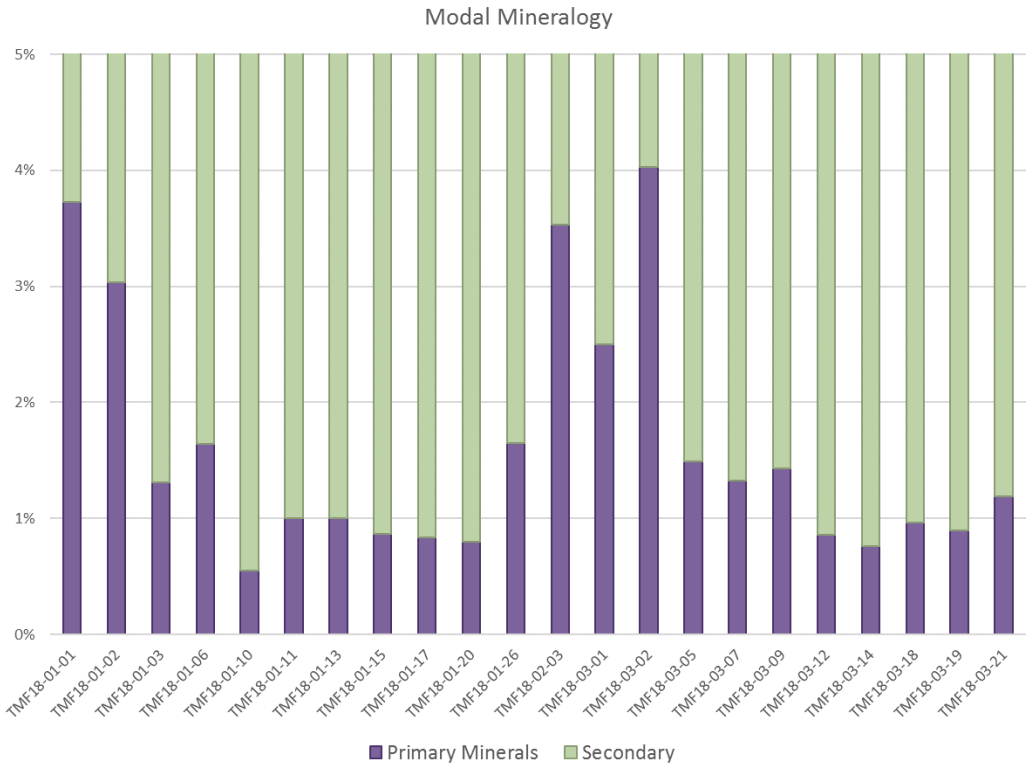

Figure 4: Abundance (weight percent) of Primary and Secondary minerals in the samples

Table 3: Modal mineralogy divided into Primary and Secondary minerals (weight percent)

	TMF18-01-01	TMF18-01-02	TMF18-01-03	TMF18-01-06	TMF18-01-10	TMF18-01-11
Primary	3.73	3.03	1.31	1.64	0.55	1.00
Secondary	96.27	96.97	98.69	98.36	99.45	99.00

	TMF18-01-13	TMF18-01-15	TMF18-01-17	TMF18-01-20	TMF18-01-26	TMF18-02-03
Primary	1.00	0.86	0.83	0.80	1.65	3.53
Secondary	99.00	99.14	99.16	99.20	98.35	96.47

	TMF18-03-01	TMF18-03-02	TMF18-03-05	TMF18-03-07	TMF18-03-09	TMF18-03-12
Primary	2.50	4.03	1.49	1.32	1.43	0.85
Secondary	97.50	95.97	98.51	98.68	98.57	99.15

	TMF18-03-14	TMF18-03-18	TMF18-03-19	TMF18-03-21
Primary	0.76	0.96	0.90	1.19
Secondary	99.24	99.04	99.10	98.81

Figure 5: Modal mineralogy of grains containing >10% "primary" minerals in Cigar Lake samples (normalized to 100%; weight percent)

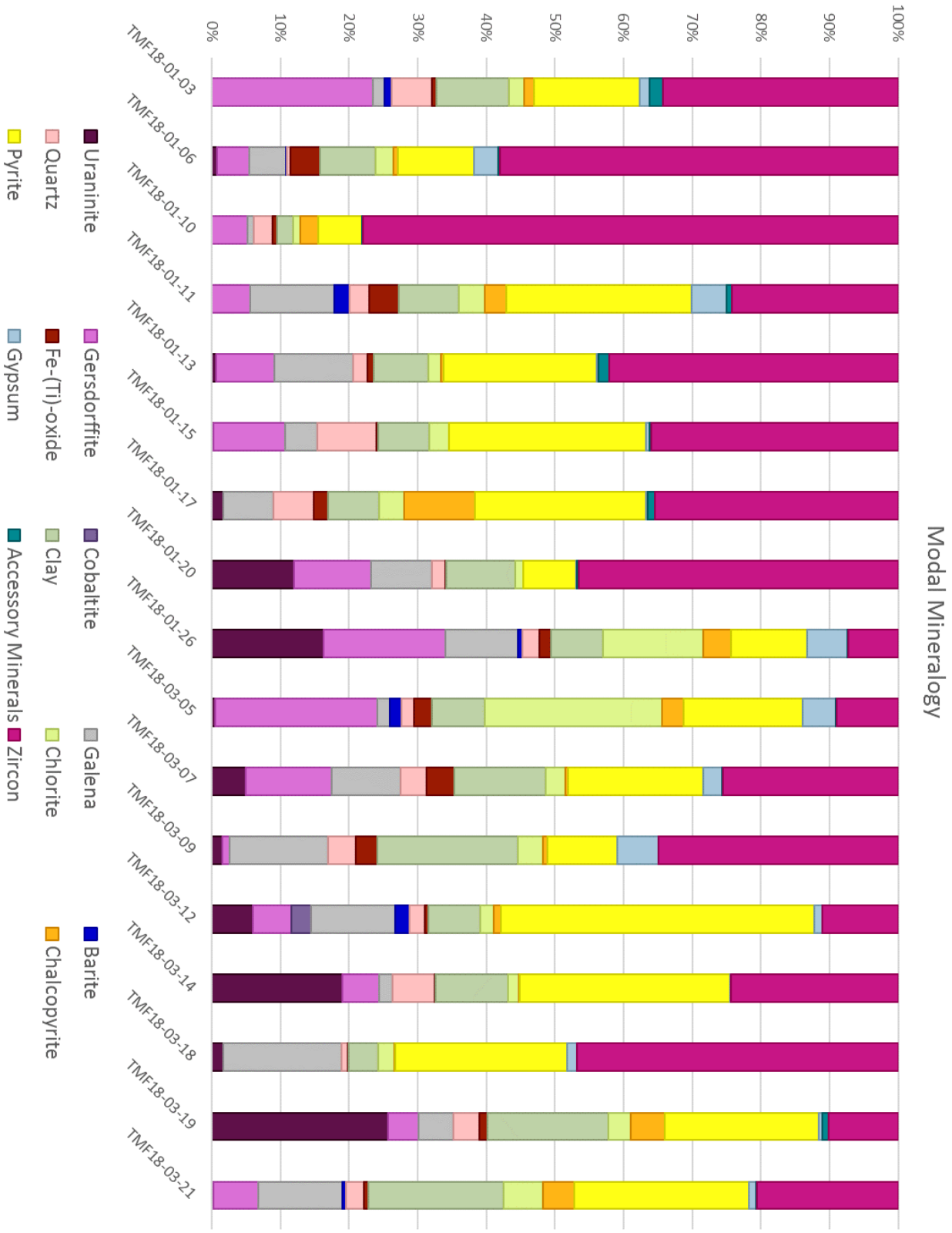

Figure 6: Modal mineralogy of grains containing >10% "Primary" minerals in samples not from Cigar Lake (normalized to 100%; weight percent)

Table 4: Modal mineralogy of grains containing "Primary" minerals (weight percent normalized to 100%)

	TMF18-01-01	TMF18-01-02	TMF18-02-03	TMF18-03-01	TMF18-03-02
Uraninite	0.790	1.039	2.762	1.066	1.878
Gersdorffite	2.786	6.331	3.982	1.058	5.471
Cobaltite	0.585	0.700	0.372	0.371	0.483
Galena	5.932	5.413	6.366	3.168	3.044
Barite	0.119	0.127	0.162	0.011	0.116
Quartz	1.394	0.313	0.475	0.568	0.100
Fe-(Ti)-oxide	1.115	1.042	2.451	0.623	1.025
Clay	1.757	1.186	1.229	2.592	1.087
Chlorite	14.253	23.400	6.424	39.591	8.945
Chalcopyrite	23.303	19.457	23.675	29.826	22.146
Pyrite	26.161	15.759	28.255	12.148	22.630
Gypsum	15.112	19.409	16.370	6.123	24.050
Accessory Minerals	0.691	0.403	0.307	0.262	0.314
Zircon	6.004	5.421	7.170	2.592	8.711

	TMF18-01-03	TMF18-01-06	TMF18-01-10	TMF18-01-11	TMF18-01-13	TMF18-01-15
Uraninite	0.000	0.791	0.000	0.000	0.595	0.261
Gersdorffite	23.425	4.622	5.158	5.598	8.448	10.439
Cobaltite	0.048	0.000	0.000	0.000	0.000	0.000
Galena	1.673	5.370	0.960	12.245	11.486	4.654
Barite	1.056	0.135	0.000	2.208	0.076	0.000
Quartz	5.886	0.476	2.782	2.865	2.104	8.569
Fe-(Ti)-oxide	0.617	4.333	0.594	4.331	0.920	0.317
Clay	10.591	8.174	2.380	8.692	7.887	7.465
Chlorite	2.252	2.523	1.003	3.839	1.881	2.906
Chalcopyrite	1.415	0.635	2.606	3.098	0.413	0.000
Pyrite	15.451	11.090	6.394	27.081	22.281	28.713
Gypsum	1.311	3.616	0.050	5.102	0.275	0.413
Accessory Minerals	2.064	0.172	0.123	0.711	1.520	0.335
Zircon	34.212	58.063	77.950	24.230	42.114	35.929

	TMF18-01-17	TMF18-01-20	TMF18-01-26	TMF18-03-05	TMF18-03-07	TMF18-03-09
Uraninite	1.712	11.974	16.319	0.435	4.895	1.536
Gersdorffite	0.000	11.269	17.721	23.682	12.529	1.077
Cobaltite	0.000	0.000	0.000	0.000	0.000	0.000
Galena	7.258	8.850	10.509	1.845	10.108	14.332
Barite	0.000	0.000	0.672	1.713	0.000	0.000
Quartz	5.885	1.904	2.485	1.789	3.778	4.067
Fe-(Ti)-oxide	2.093	0.104	1.760	2.583	3.967	3.120

	TMF18-01-17	TMF18-01-20	TMF18-01-26	TMF18-03-05	TMF18-03-07	TMF18-03-09
Clay	7.400	10.134	7.578	7.763	13.415	20.484
Chlorite	3.617	1.095	14.629	25.797	2.889	3.669
Chalcopyrite	10.308	0.000	4.034	3.134	0.362	0.659
Pyrite	24.937	7.728	11.010	17.420	19.653	10.103
Gypsum	0.322	0.135	5.948	4.779	2.805	6.074
Accessory Minerals	1.022	0.223	0.139	0.173	0.078	0.000
Zircon	35.446	46.584	7.194	8.888	25.520	34.878

	TMF18-03-12	TMF18-03-14	TMF18-03-18	TMF18-03-19	TMF18-03-21
Uraninite	6.020	19.070	1.647	25.620	0.191
Gersdorffite	5.589	5.257	0.000	4.512	6.542
Cobaltite	2.893	0.000	0.000	0.000	0.000
Galena	12.201	2.049	17.224	5.023	12.279
Barite	2.128	0.000	0.000	0.066	0.587
Quartz	2.235	6.043	0.991	3.835	2.522
Fe-(Ti)-oxide	0.470	0.154	0.134	1.066	0.639
Clay	7.570	10.622	4.227	17.644	19.797
Chlorite	1.941	1.558	2.315	3.227	5.711
Chalcopyrite	1.101	0.061	0.147	4.951	4.493
Pyrite	45.670	30.659	25.139	22.478	25.562
Gypsum	1.113	0.134	1.375	0.611	1.004
Accessory Minerals	0.029	0.000	0.000	0.883	0.062
Zircon	11.042	24.392	46.803	10.086	20.610

Grain size histograms

The size-frequency distribution of grains containing >10% primary minerals are shown below. The data is binned from 6 to 100µm in 2µm steps. The vertical axis on all plots is grain count per bin.

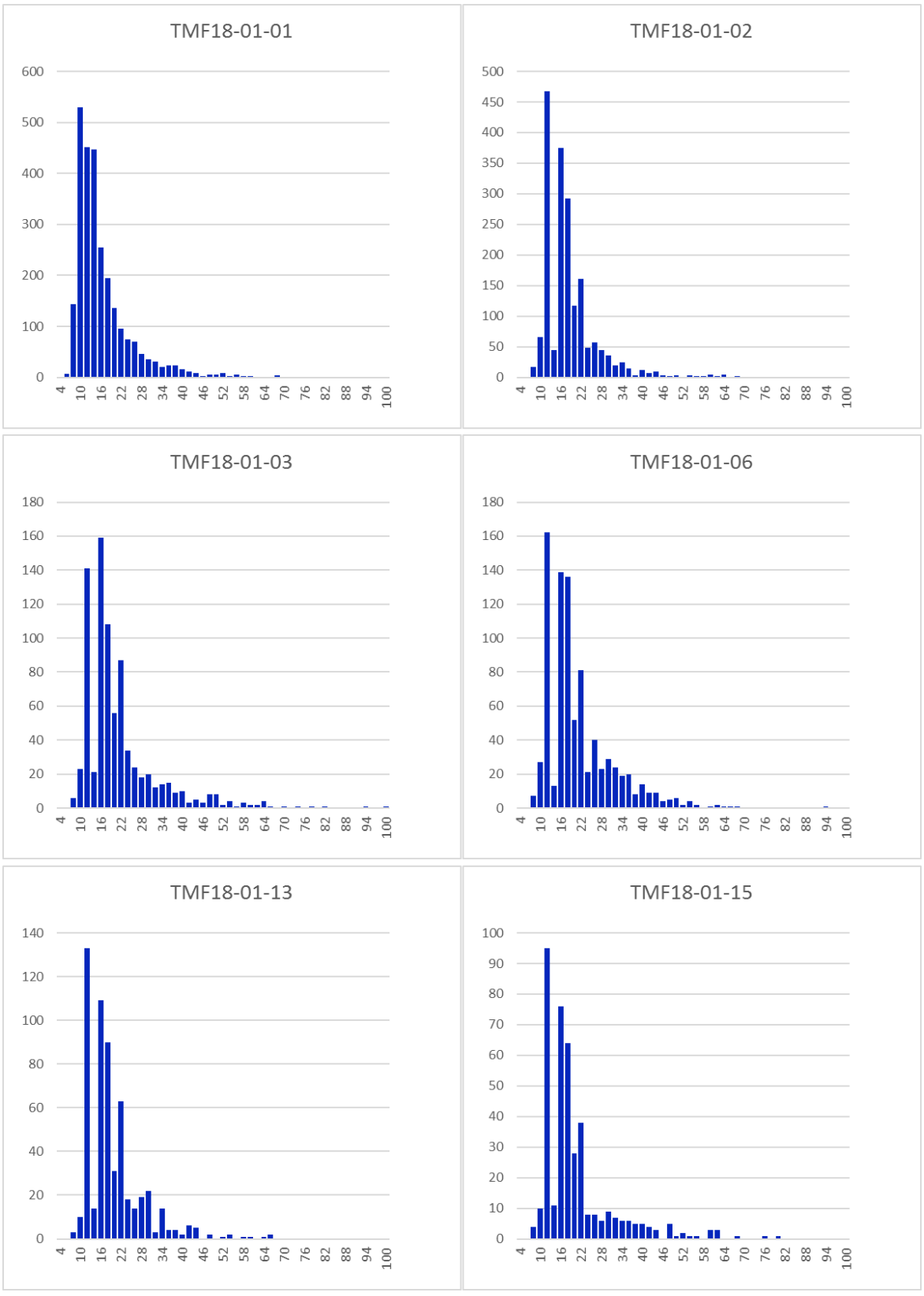
TMF18-01-01
TMF18-01-02
TMF18-01-03
TMF18-01-06
TMF18-01-13
TMF18-01-15

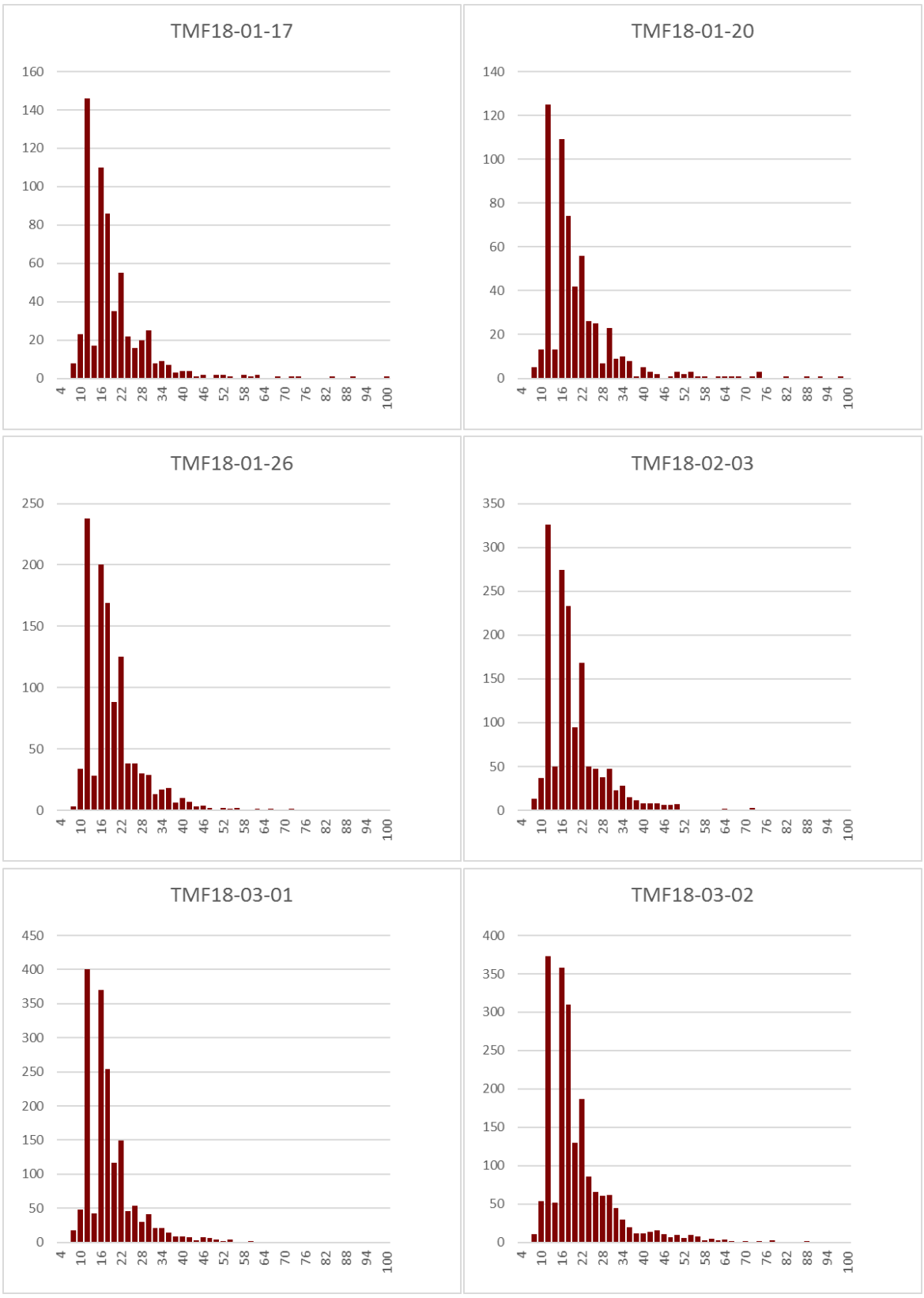
TMF18-01-17
TMF18-01-20
TMF18-01-26
TMF18-02-03
TMF18-03-01
TMF18-03-02

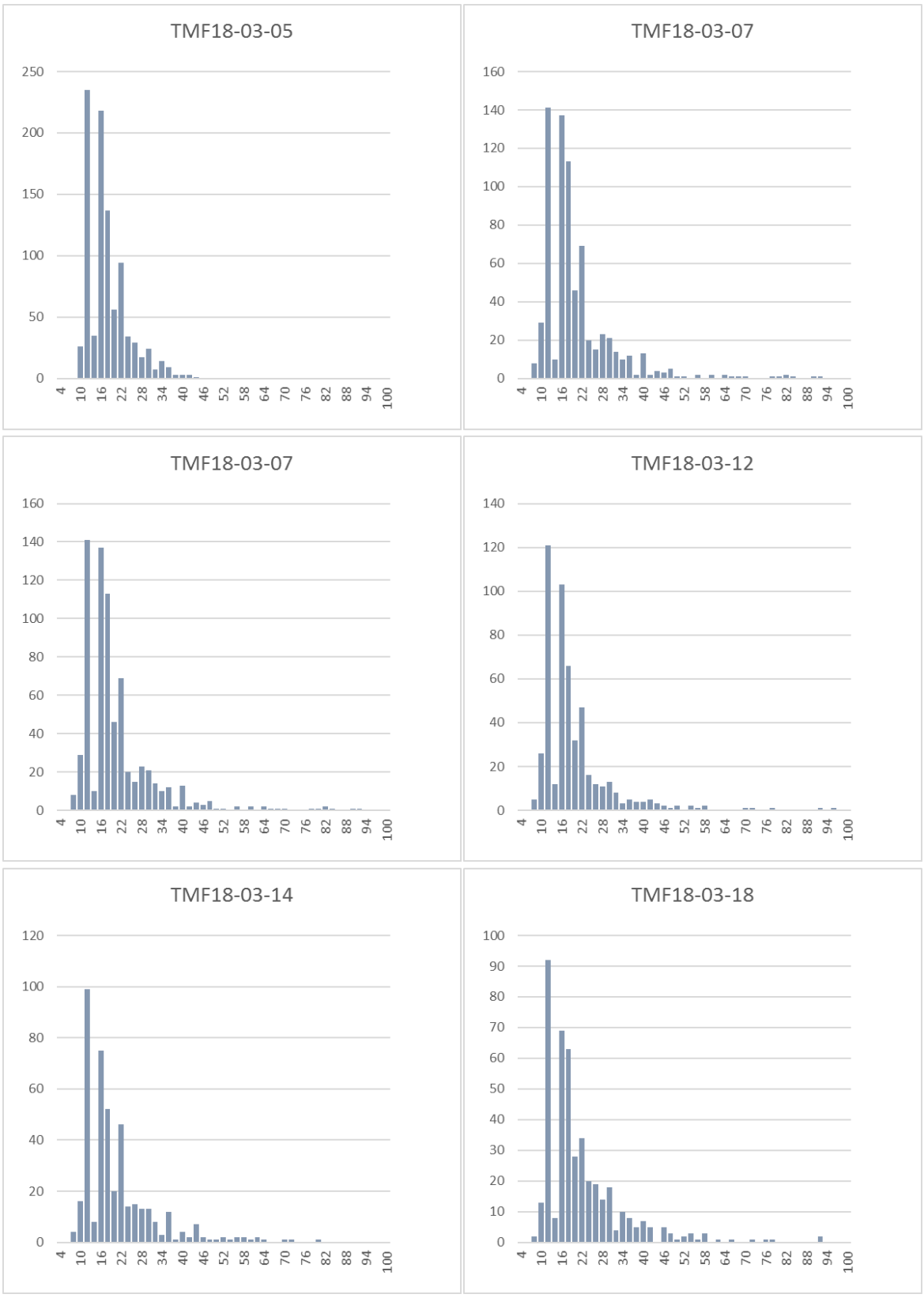
TMF18-03-05
TMF18-03-07
TMF18-03-07
TMF18-03-12
TMF18-03-14
TMF18-03-18

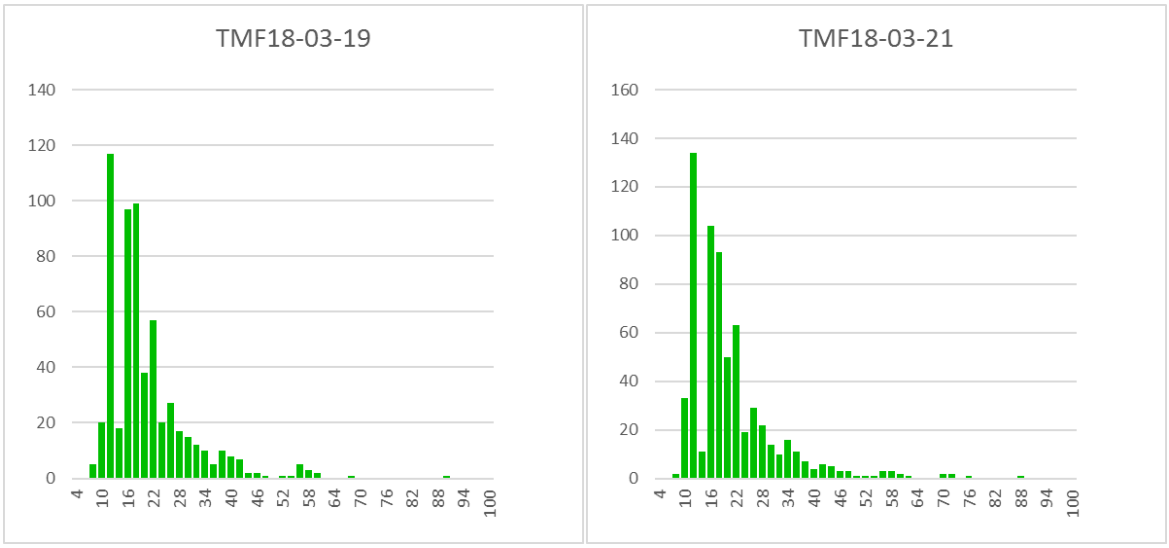

Grain Images

The following pages contain grain images from each of the samples. The first set of images are representative of the whole complex mineralogy. The second set is images representative of grains containing primary minerals (>10% by area).

TMF18-01-01

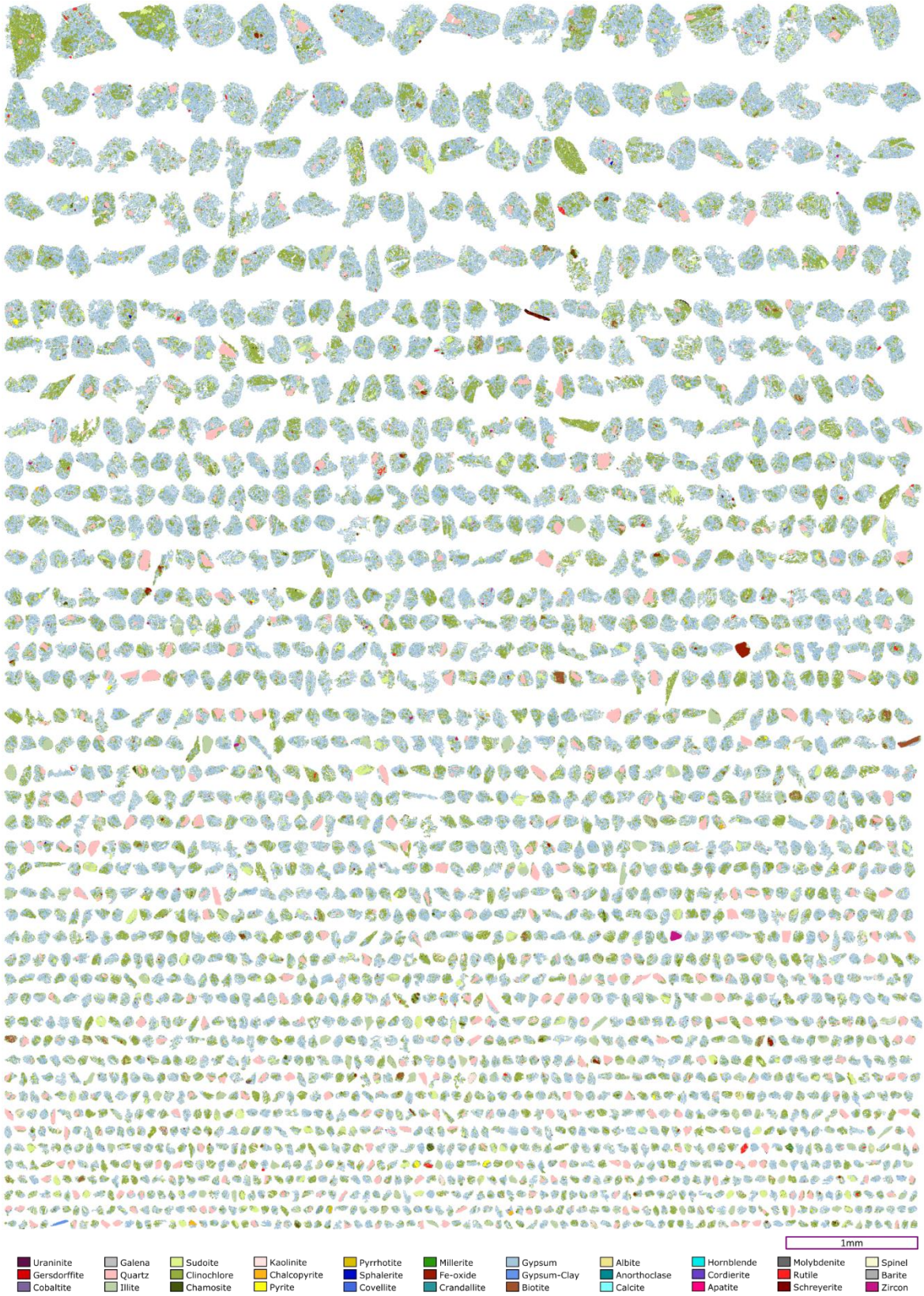
1mm
Uraninite
Gersdorffite
Cobaltite
Galena
Quartz
Illite
Sudoite
Clinochlore
Chamosite
Kaolinite
Chalcopyrite
Pyrite
Pyrrhotite
Sphalerite
Covellite
Millerite
Fe-oxide
Crandallite
Gypsum
Gypsum-Clay
Biotite
Albite
Anorthoclase
Calcite
Hornblende
Cordierite
Apatite
Molybdenite
Rutile
Schreyerite
Spinel
Barite
Zircon

TMF18-01-02

1mm
Uraninite
Gersdorffite
Cobaltite
Galena
Quartz
Illite
Sudoite
Clinochlore
Chamosite
Kaolinite
Chalcopyrite
Pyrite
Pyrrhotite
Sphalerite
Covellite
Millerite
Fe-oxide
Crandallite
Gypsum
Gypsum-Clay
Biotite
Albite
Anorthoclase
Calcite
Hornblende
Cordierite
Apatite
Molybdenite
Rutile
Schreyerite
Spinel
Barite
Zircon

TMF18-01-03

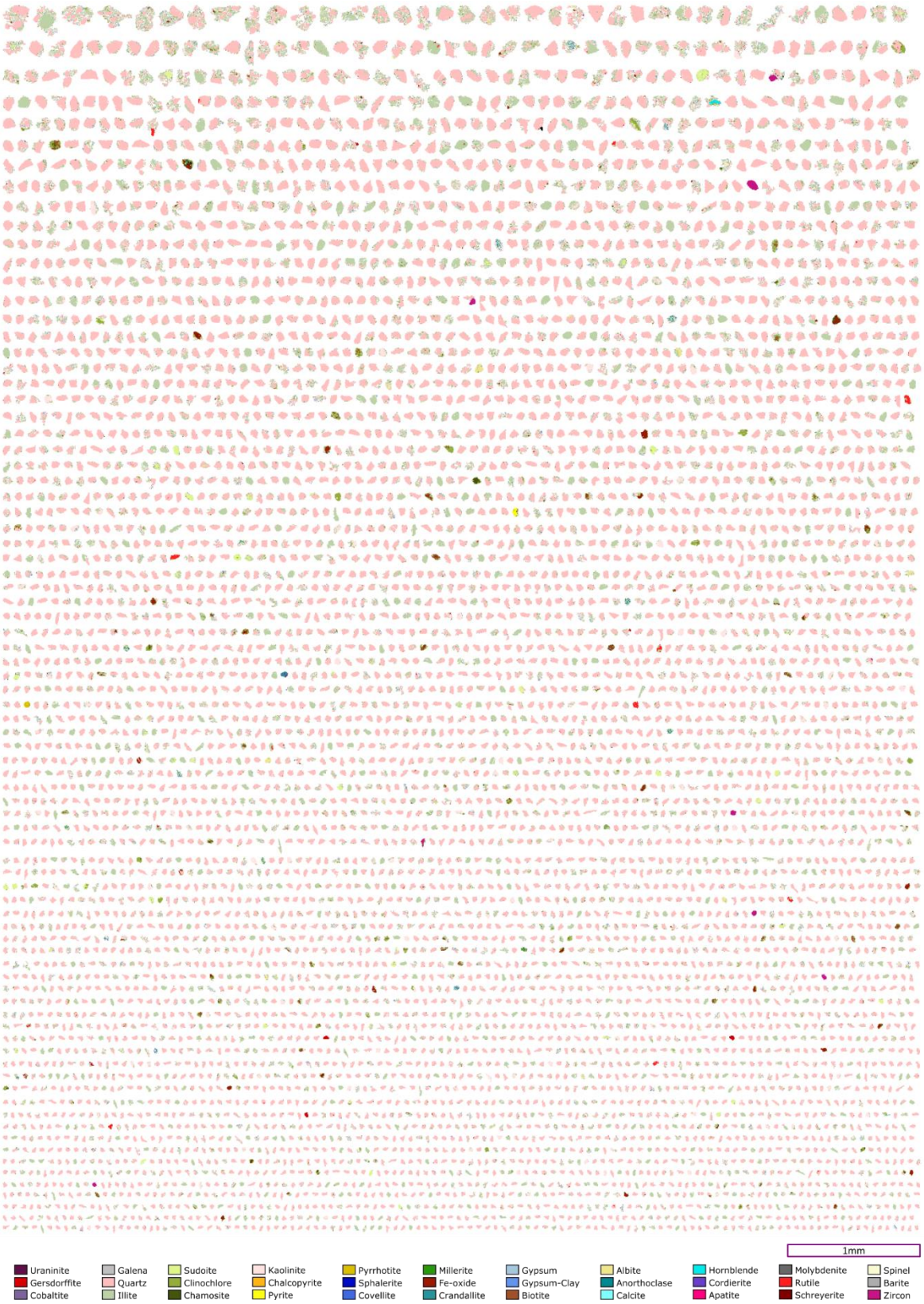
1mm
Uraninite
Gersdorffite
Cobaltite
Galena
Quartz
Illite
Sudoite
Clinochlore
Chamosite
Kaolinite
Chalcopyrite
Pyrite
Pyrrhotite
Sphalerite
Covellite
Millerite
Fe-oxide
Crandallite
Gypsum
Gypsum-Clay
Biotite
Albite
Anorthoclase
Calcite
Hornblende
Cordierite
Apatite
Molybdenite
Rutile
Schreyerite
Spinel
Barite
Zircon

TMF18-01-06

1mm
Uraninite
Gersdorffite
Cobaltite
Galena
Quartz
Illite
Sudoite
Clinochlore
Chamosite
Kaolinite
Chalcopyrite
Pyrite
Pyrrhotite
Sphalerite
Covellite
Millerite
Fe-oxide
Crandallite
Gypsum
Gypsum-Clay
Biotite
Albite
Anorthoclase
Calcite
Hornblende
Cordierite
Apatite
Molybdenite
Rutile
Schreyerite
Spinel
Barite
Zircon

TMF18-01-10

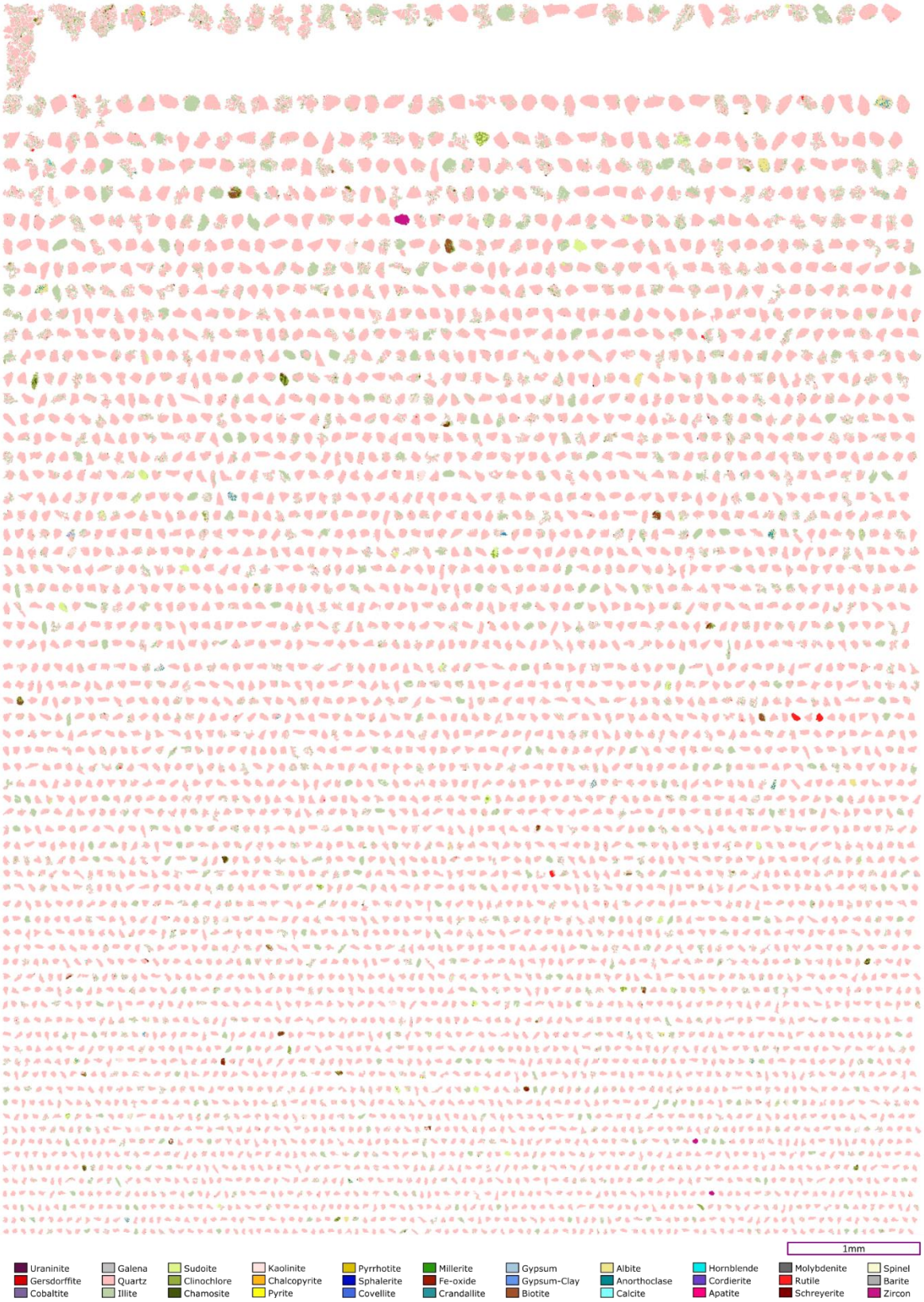
1mm
Uraninite
Gersdorffite
Cobaltite
Galena
Quartz
Illite
Sudoite
Clinochlore
Chamosite
Kaolinite
Chalcopyrite
Pyrite
Pyrrhotite
Sphalerite
Covellite
Millerite
Fe-oxide
Crandallite
Gypsum
Gypsum-Clay
Biotite
Albite
Anorthoclase
Calcite
Hornblende
Cordierite
Apatite
Molybdenite
Rutile
Schreyerite
Spinel
Barite
Zircon

TMF18-01-11

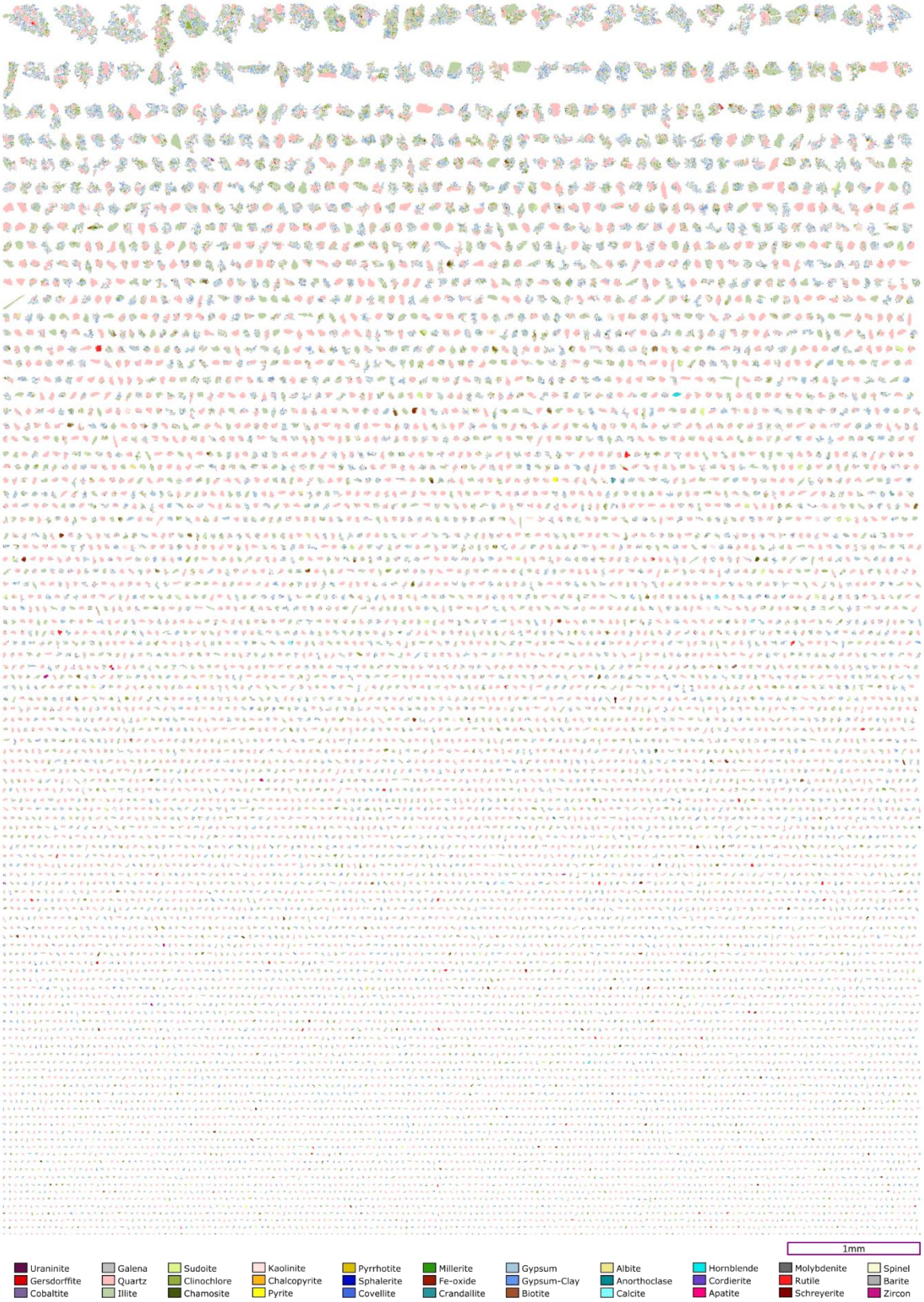
1mm
Uraninite
Gersdorffite
Cobaltite
Galena
Quartz
Illite
Sudoite
Clinochlore
Chamosite
Kaolinite
Chalcopyrite
Pyrite
Pyrrhotite
Sphalerite
Covellite
Millerite
Fe-oxide
Crandallite
Gypsum
Gypsum-Clay
Biotite
Albite
Anorthoclase
Calcite
Hornblende
Cordierite
Apatite
Molybdenite
Rutile
Schreyerite
Spinel
Barite
Zircon

TMF18-01-13

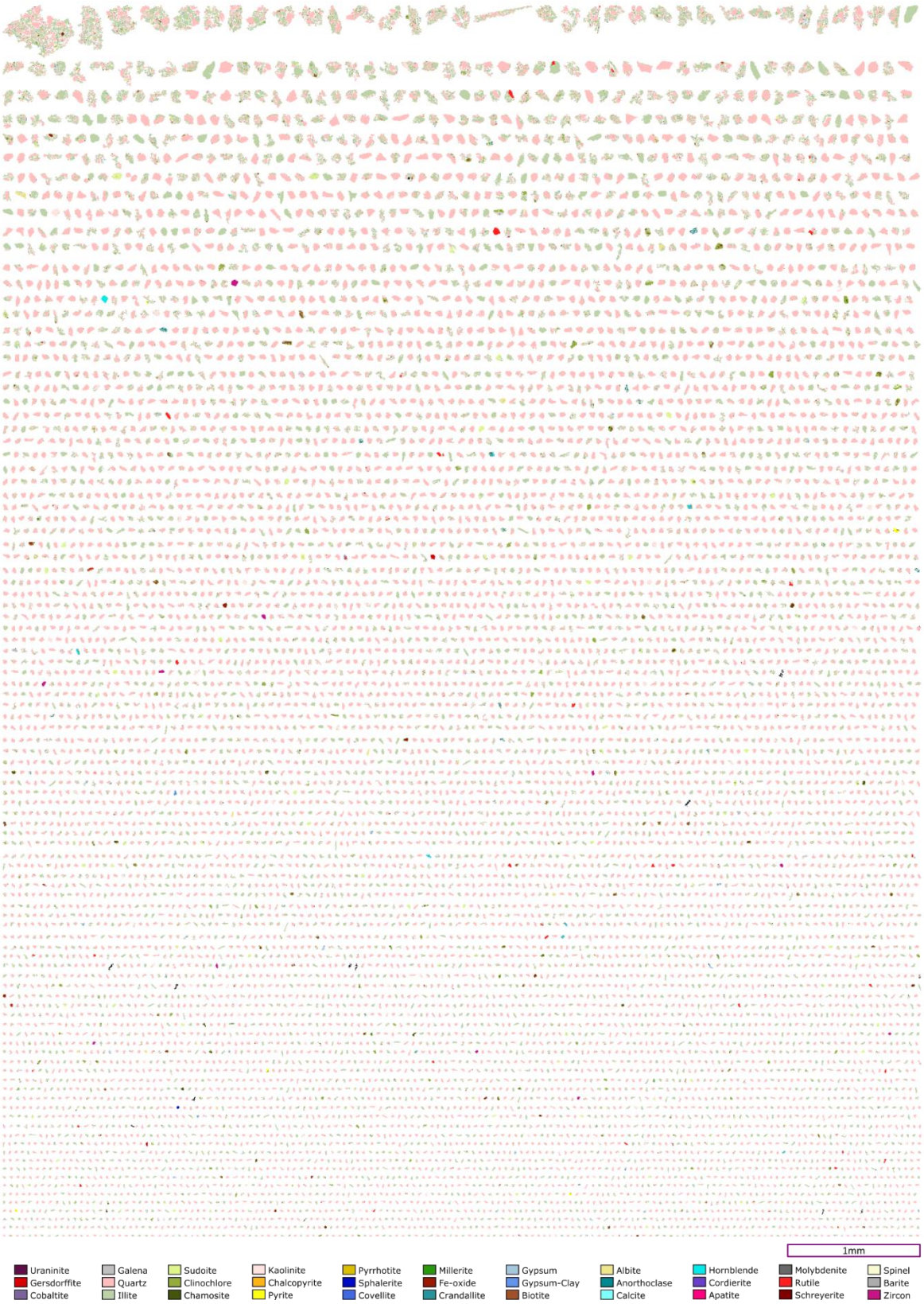
1mm
Uraninite
Gersdorffite
Cobaltite
Galena
Quartz
Illite
Sudoite
Clinochlore
Chamosite
Kaolinite
Chalcopyrite
Pyrite
Pyrrhotite
Sphalerite
Covellite
Millerite
Fe-oxide
Crandallite
Gypsum
Gypsum-Clay
Biotite
Albite
Anorthoclase
Calcite
Hornblende
Cordierite
Apatite
Molybdenite
Rutile
Schreyerite
Spinel
Barite
Zircon

TMF18-01-15

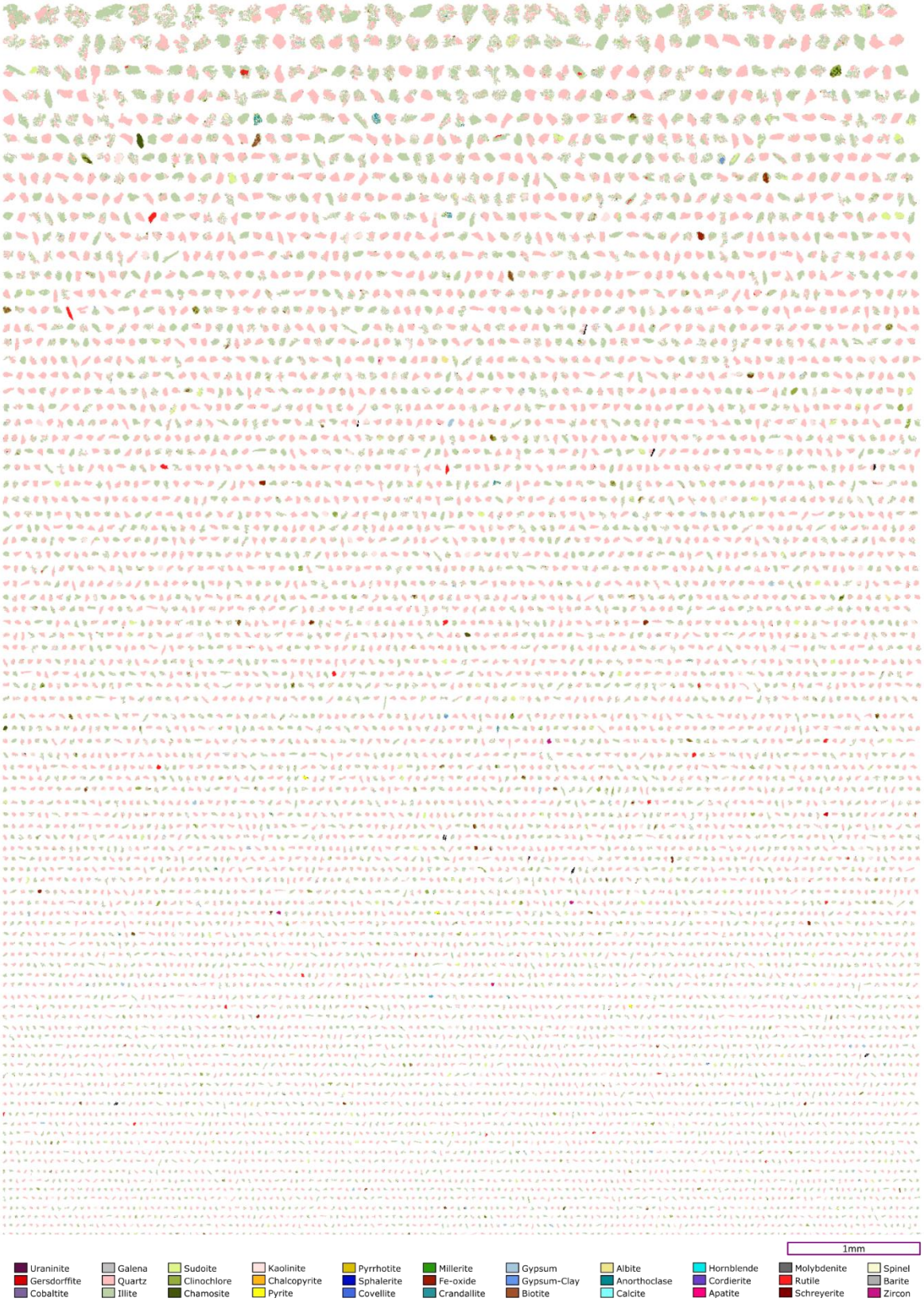
1mm
Uraninite
Gersdorffite
Cobaltite
Galena
Quartz
Illite
Sudoite
Clinochlore
Chamosite
Kaolinite
Chalcopyrite
Pyrite
Pyrrhotite
Sphalerite
Covellite
Millerite
Fe-oxide
Crandallite
Gypsum
Gypsum-Clay
Biotite
Albite
Anorthoclase
Calcite
Hornblende
Cordierite
Apatite
Molybdenite
Rutile
Schreyerite
Spinel
Barite
Zircon

TMF18-01-17

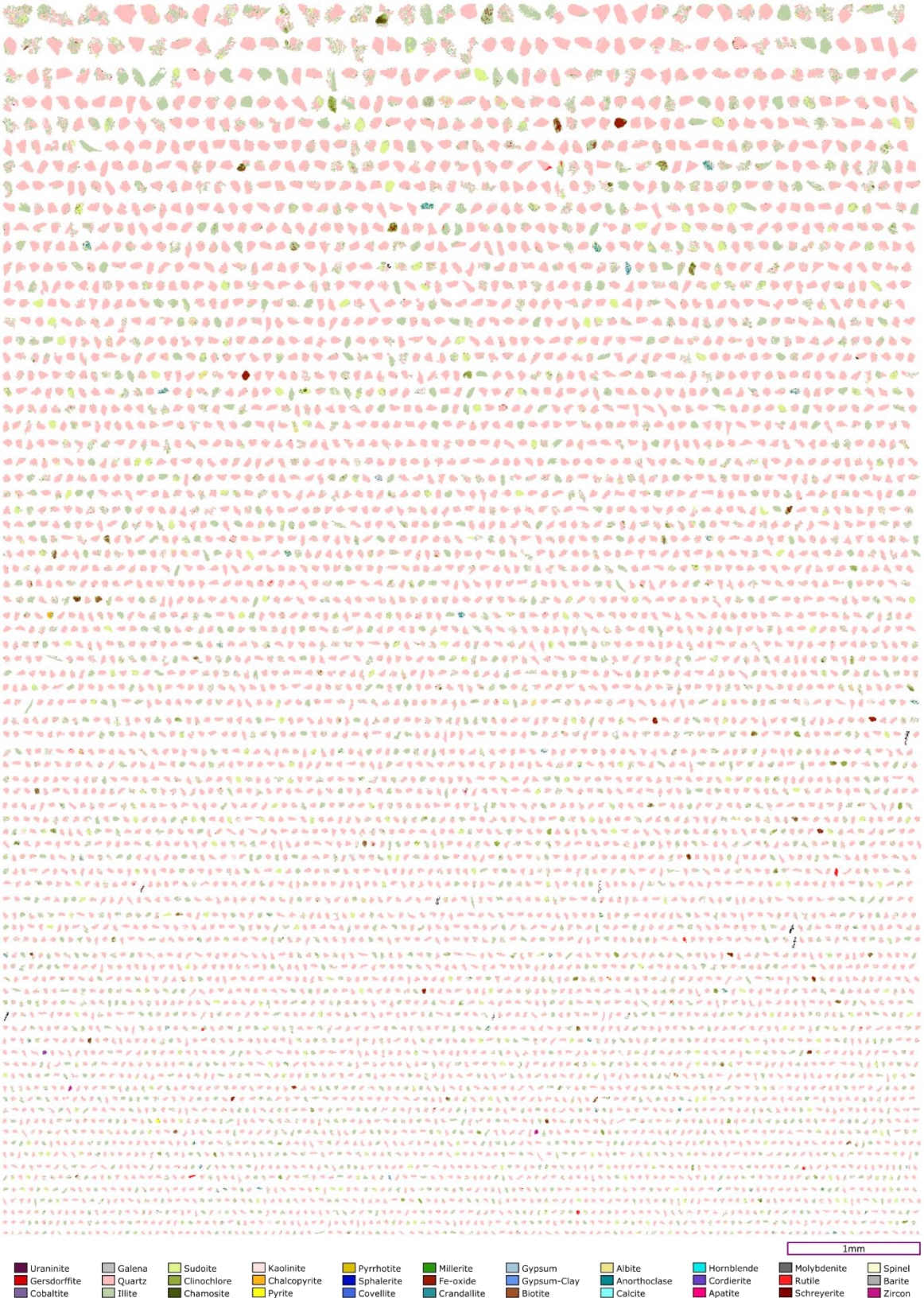
1mm
Uraninite
Gersdorffite
Cobaltite
Galena
Quartz
Illite
Sudoite
Clinochlore
Chamosite
Kaolinite
Chalcopyrite
Pyrite
Pyrrhotite
Sphalerite
Covellite
Millerite
Fe-oxide
Crandallite
Gypsum
Gypsum-Clay
Biotite
Albite
Anorthoclase
Calcite
Hornblende
Cordierite
Apatite
Molybdenite
Rutile
Schreyerite
Spinel
Barite
Zircon

TMF18-01-20

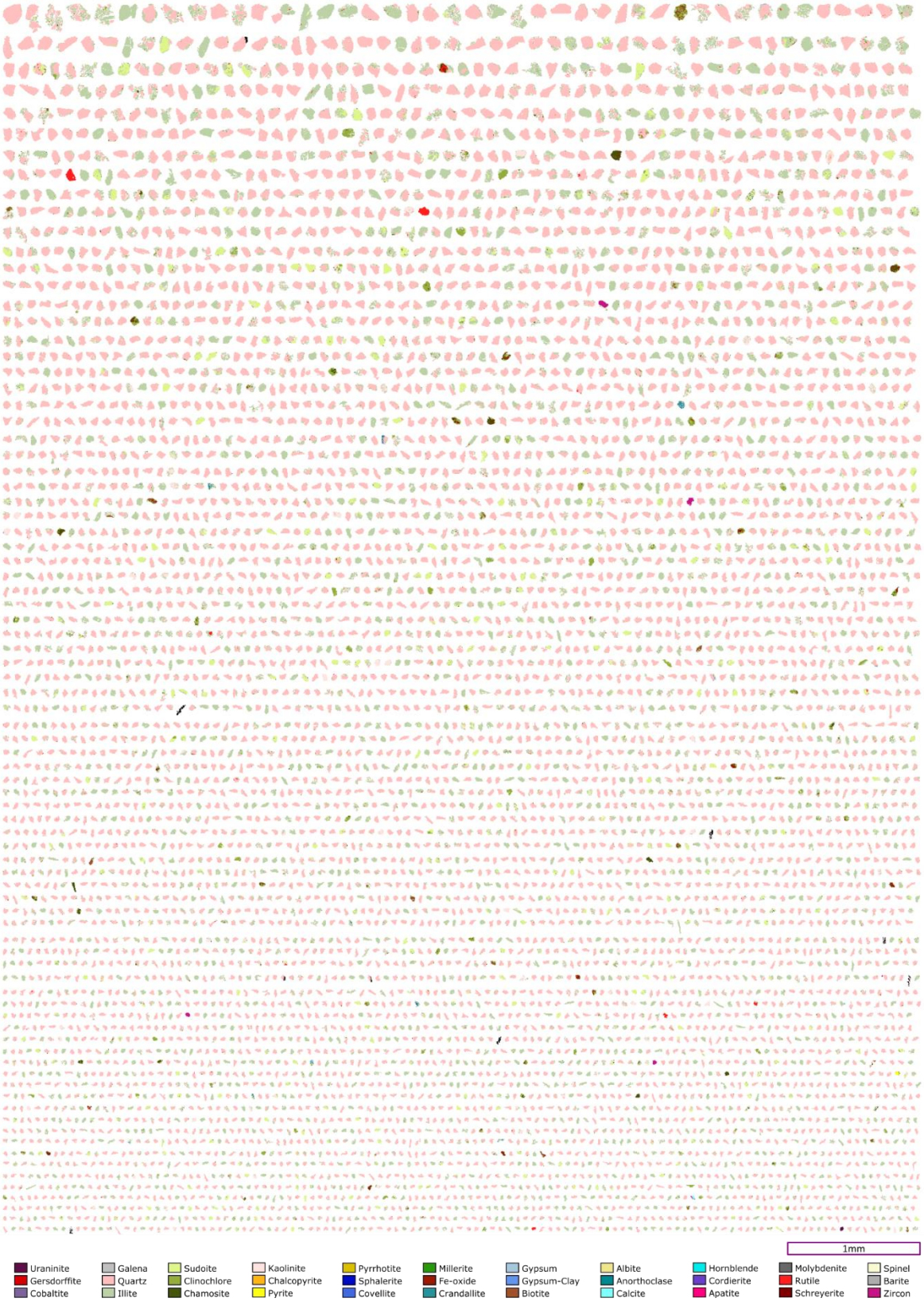
1mm
Uraninite
Gersdorffite
Cobaltite
Galena
Quartz
Illite
Sudoite
Clinochlore
Chamosite
Kaolinite
Chalcopyrite
Pyrite
Pyrrhotite
Sphalerite
Covellite
Millerite
Fe-oxide
Crandallite
Gypsum
Gypsum-Clay
Biotite
Albite
Anorthoclase
Calcite
Hornblende
Cordierite
Apatite
Molybdenite
Rutile
Schreyerite
Spinel
Barite
Zircon

TMF18-01-26

1mm
Uraninite
Gersdorffite
Cobaltite
Galena
Quartz
Illite
Sudoite
Clinochlore
Chamosite
Kaolinite
Chalcopyrite
Pyrite
Pyrrhotite
Sphalerite
Covellite
Millerite
Fe-oxide
Crandallite
Gypsum
Gypsum-Clay
Biotite
Albite
Anorthoclase
Calcite
Hornblende
Cordierite
Apatite
Molybdenite
Rutile
Schreyerite
Spinel
Barite
Zircon

TMF18-02-03

1mm
Uraninite
Gersdorffite
Cobaltite
Galena
Quartz
Illite
Sudoite
Clinochlore
Chamosite
Kaolinite
Chalcopyrite
Pyrite
Pyrrhotite
Sphalerite
Covellite
Millerite
Fe-oxide
Crandallite
Gypsum
Gypsum-Clay
Biotite
Albite
Anorthoclase
Calcite
Hornblende
Cordierite
Apatite
Molybdenite
Rutile
Schreyerite
Spinel
Barite
Zircon

TMF18-03-01

1mm
Uraninite
Gersdorffite
Cobaltite
Galena
Quartz
Illite
Sudoite
Clinochlore
Chamosite
Kaolinite
Chalcopyrite
Pyrite
Pyrrhotite
Sphalerite
Covellite
Millerite
Fe-oxide
Crandallite
Gypsum
Gypsum-Clay
Biotite
Albite
Anorthoclase
Calcite
Hornblende
Cordierite
Apatite
Molybdenite
Rutile
Schreyerite
Spinel
Barite
Zircon

TMF18-03-02

1mm
Uraninite
Gersdorffite
Cobaltite
Galena
Quartz
Illite
Sudoite
Clinochlore
Chamosite
Kaolinite
Chalcopyrite
Pyrite
Pyrrhotite
Sphalerite
Covellite
Millerite
Fe-oxide
Crandallite
Gypsum
Gypsum-Clay
Biotite
Albite
Anorthoclase
Calcite
Hornblende
Cordierite
Apatite
Molybdenite
Rutile
Schreyerite
Spinel
Barite
Zircon

TMF18-03-05

1mm
Uraninite
Gersdorffite
Cobaltite
Galena
Quartz
Illite
Sudoite
Clinochlore
Chamosite
Kaolinite
Chalcopyrite
Pyrite
Pyrrhotite
Sphalerite
Covellite
Millerite
Fe-oxide
Crandallite
Gypsum
Gypsum-Clay
Biotite
Albite
Anorthoclase
Calcite
Hornblende
Cordierite
Apatite
Molybdenite
Rutile
Schreyerite
Spinel
Barite
Zircon

TMF18-03-07

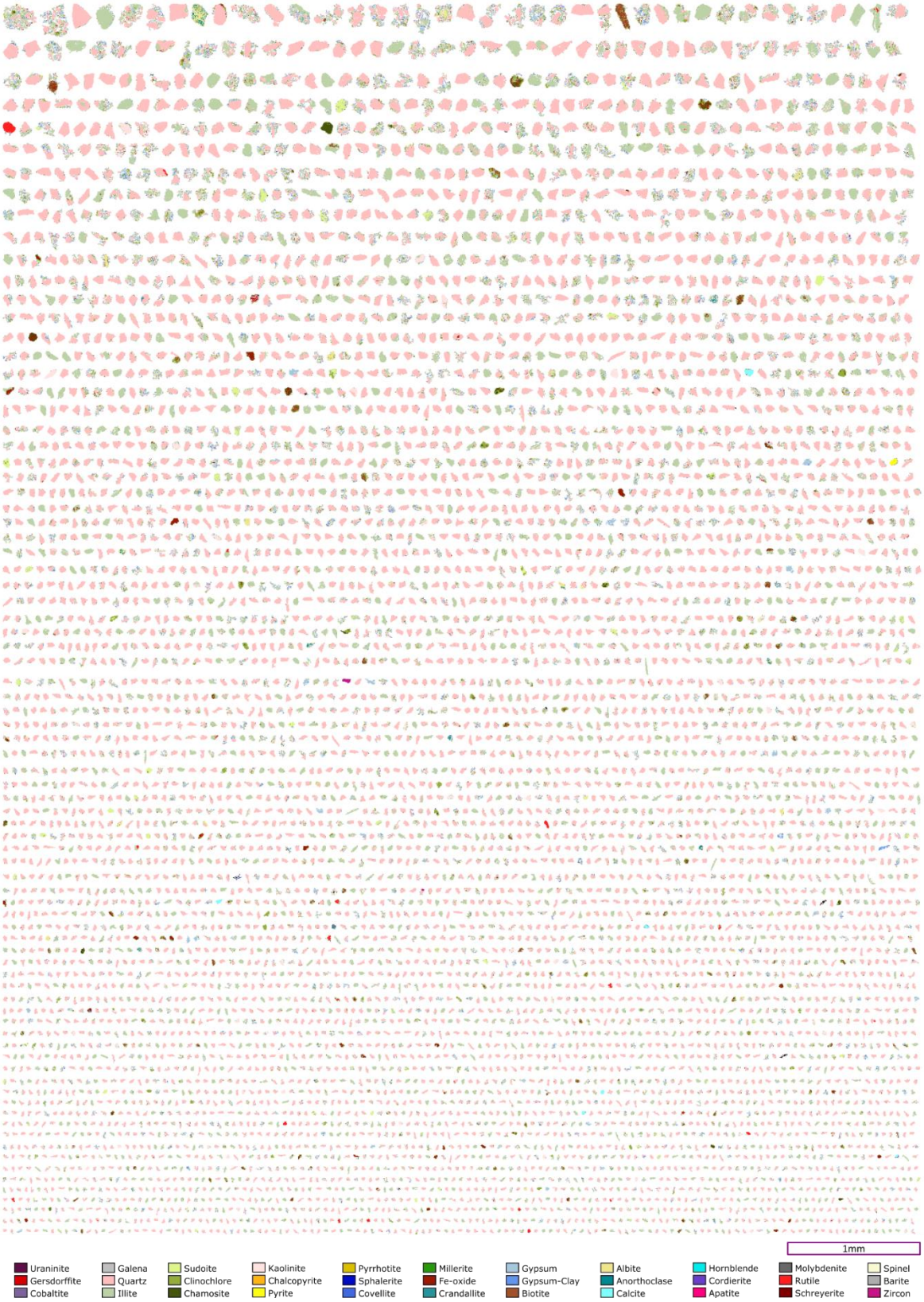
1mm
Uraninite
Gersdorffite
Cobaltite
Galena
Quartz
Illite
Sudoite
Clinochlore
Chamosite
Kaolinite
Chalcopyrite
Pyrite
Pyrrhotite
Sphalerite
Covellite
Millerite
Fe-oxide
Crandallite
Gypsum
Gypsum-Clay
Biotite
Albite
Anorthoclase
Calcite
Hornblende
Cordierite
Apatite
Molybdenite
Rutile
Schreyerite
Spinel
Barite
Zircon

TMF18-03-09

1mm
Uraninite
Gersdorffite
Cobaltite
Galena
Quartz
Illite
Sudoite
Clinochlore
Chamosite
Kaolinite
Chalcopyrite
Pyrite
Pyrrhotite
Sphalerite
Covellite
Millerite
Fe-oxide
Crandallite
Gypsum
Gypsum-Clay
Biotite
Albite
Anorthoclase
Calcite
Hornblende
Cordierite
Apatite
Molybdenite
Rutile
Schreyerite
Spinel
Barite
Zircon

TMF18-03-12

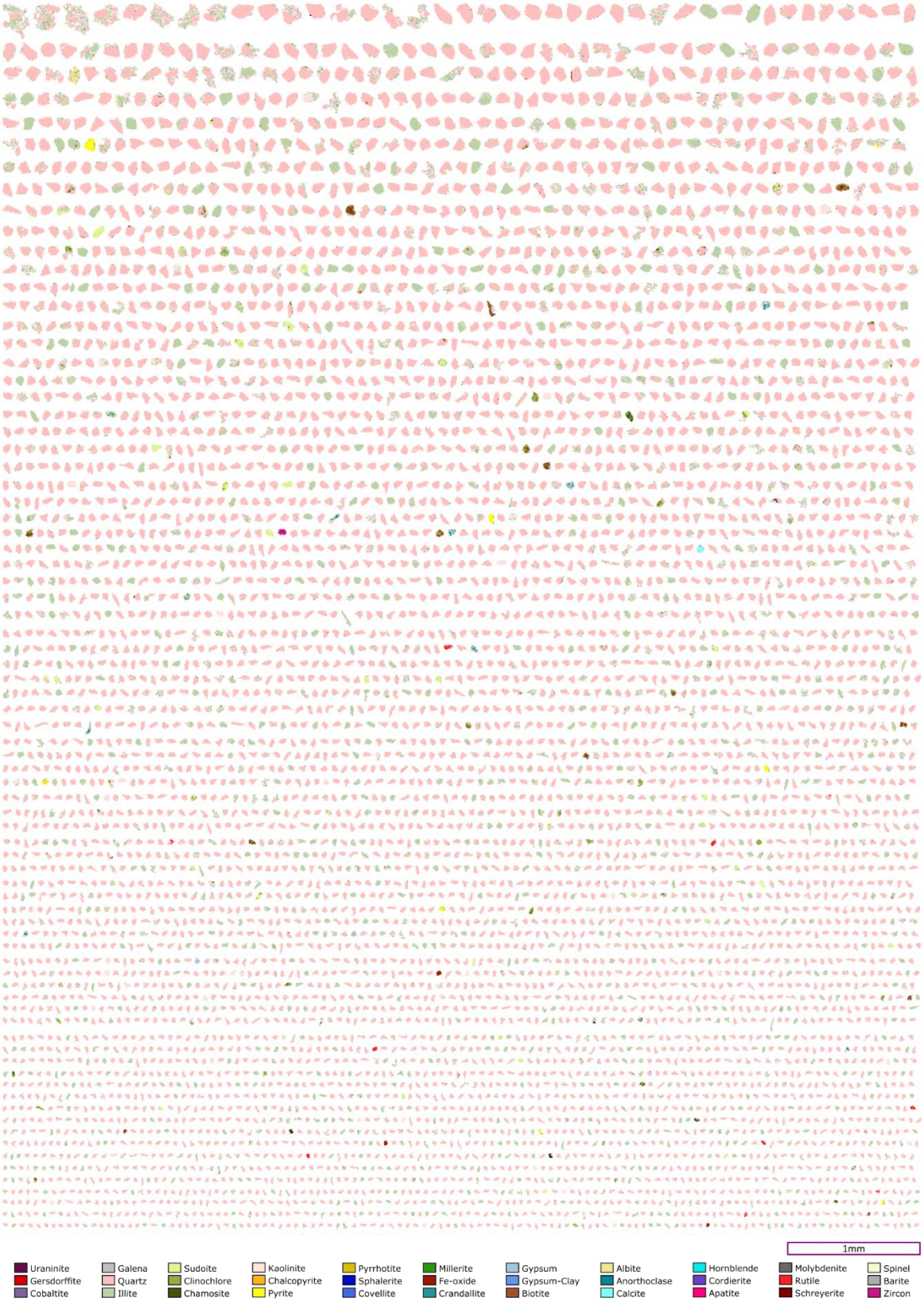
1mm
Uraninite
Gersdorffite
Cobaltite
Galena
Quartz
Illite
Sudoite
Clinochlore
Chamosite
Kaolinite
Chalcopyrite
Pyrite
Pyrrhotite
Sphalerite
Covellite
Millerite
Fe-oxide
Crandallite
Gypsum
Gypsum-Clay
Biotite
Albite
Anorthoclase
Calcite
Hornblende
Cordierite
Apatite
Molybdenite
Rutile
Schreyerite
Spinel
Barite
Zircon

TMF18-03-14

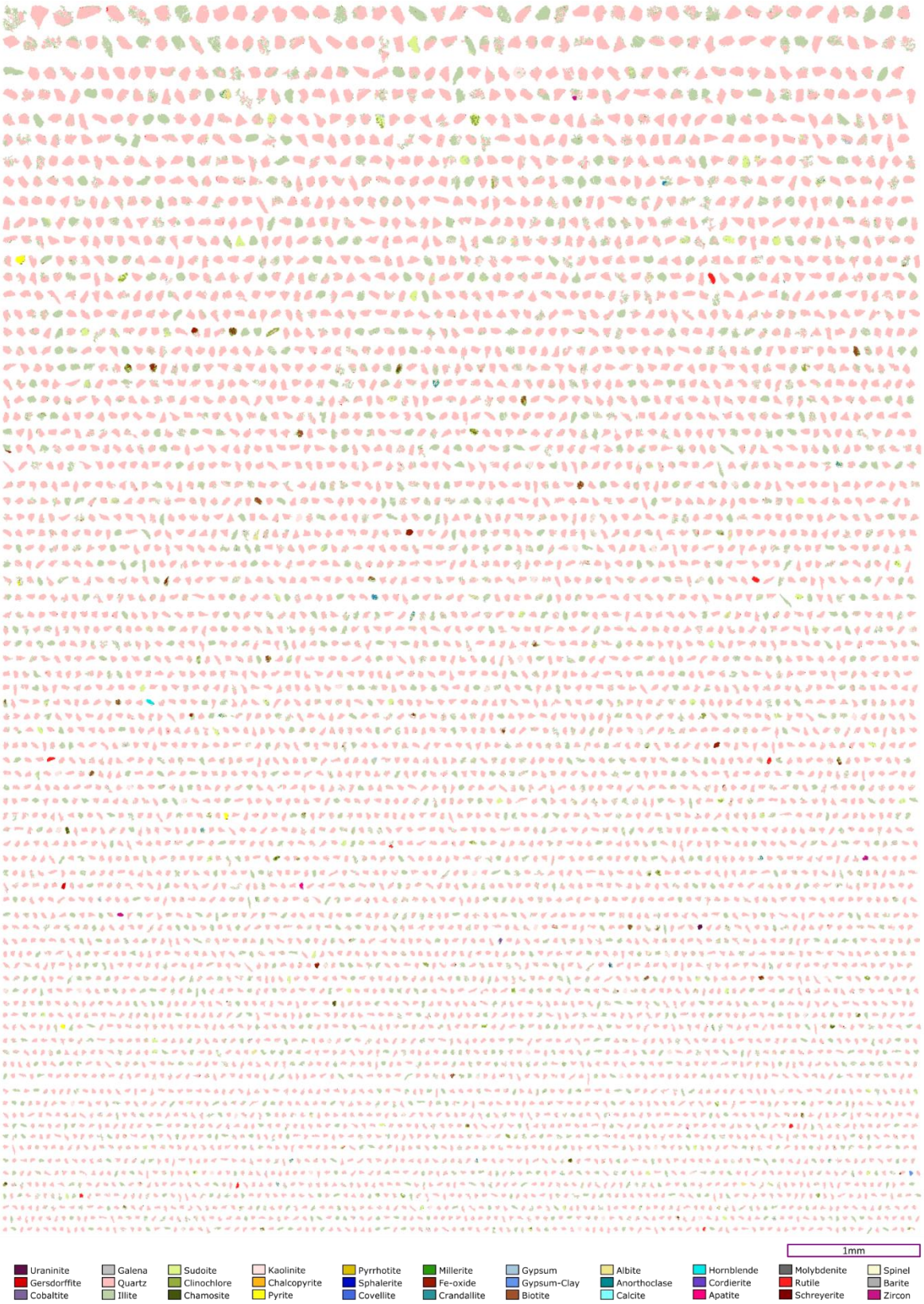
1mm
Uraninite
Gersdorffite
Cobaltite
Galena
Quartz
Illite
Sudoite
Clinochlore
Chamosite
Kaolinite
Chalcopyrite
Pyrite
Pyrrhotite
Sphalerite
Covellite
Millerite
Fe-oxide
Crandallite
Gypsum
Gypsum-Clay
Biotite
Albite
Anorthoclase
Calcite
Hornblende
Cordierite
Apatite
Molybdenite
Rutile
Schreyerite
Spinel
Barite
Zircon

TMF18-03-18

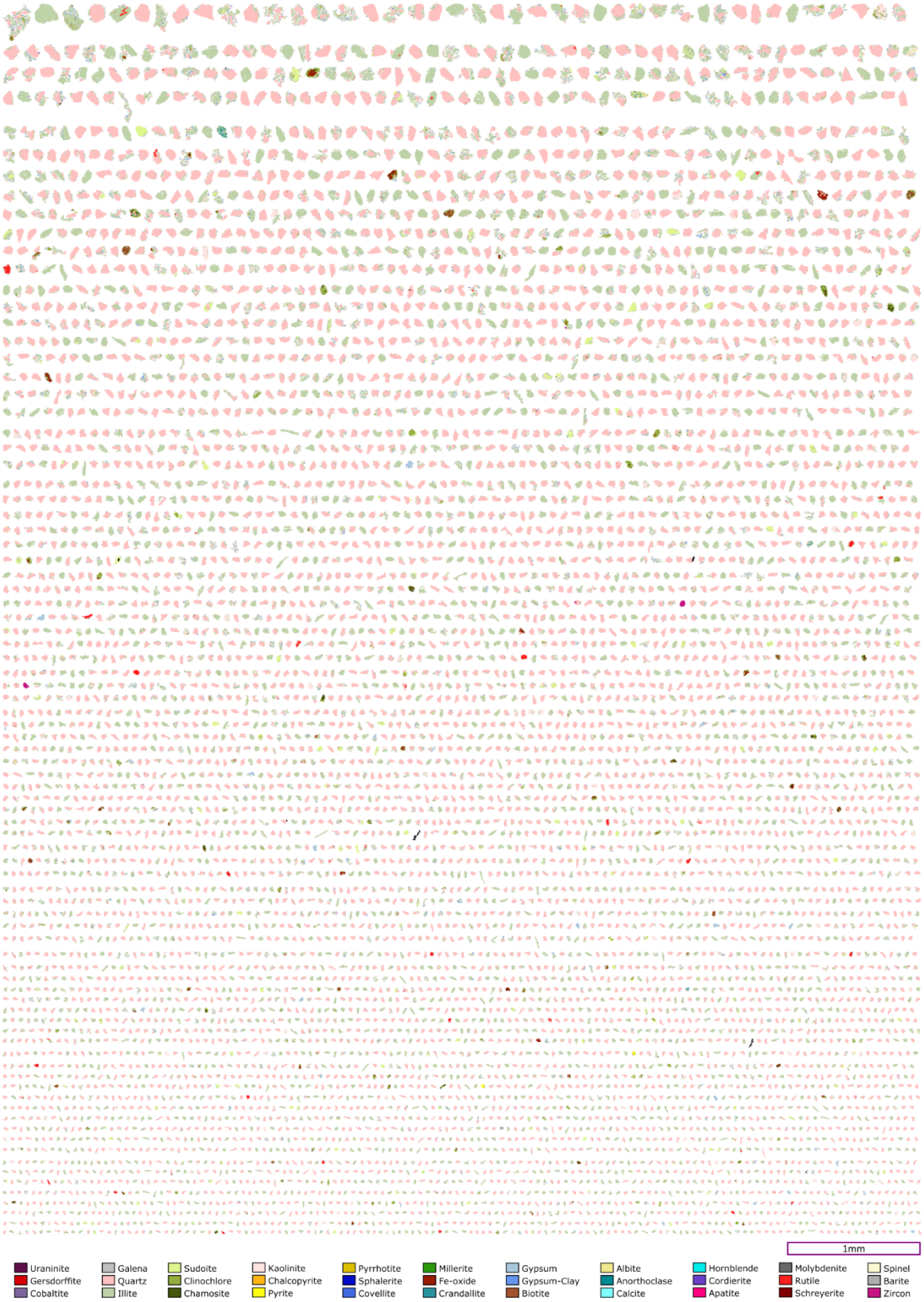
1mm
Uraninite
Gersdorffite
Cobaltite
Galena
Quartz
Illite
Sudoite
Clinochlore
Chamosite
Kaolinite
Chalcopyrite
Pyrite
Pyrrhotite
Sphalerite
Covellite
Millerite
Fe-oxide
Crandallite
Gypsum
Gypsum-Clay
Biotite
Albite
Anorthoclase
Calcite
Hornblende
Cordierite
Apatite
Molybdenite
Rutile
Schreyerite
Spinel
Barite
Zircon

TMF18-03-19

1mm
Uraninite
Gersdorffite
Cobaltite
Galena
Quartz
Illite
Sudoite
Clinochlore
Chamosite
Kaolinite
Chalcopyrite
Pyrite
Pyrrhotite
Sphalerite
Covellite
Millerite
Fe-oxide
Crandallite
Gypsum
Gypsum-Clay
Biotite
Albite
Anorthoclase
Calcite
Hornblende
Cordierite
Apatite
Molybdenite
Rutile
Schreyerite
Spinel
Barite
Zircon

TMF18-03-21

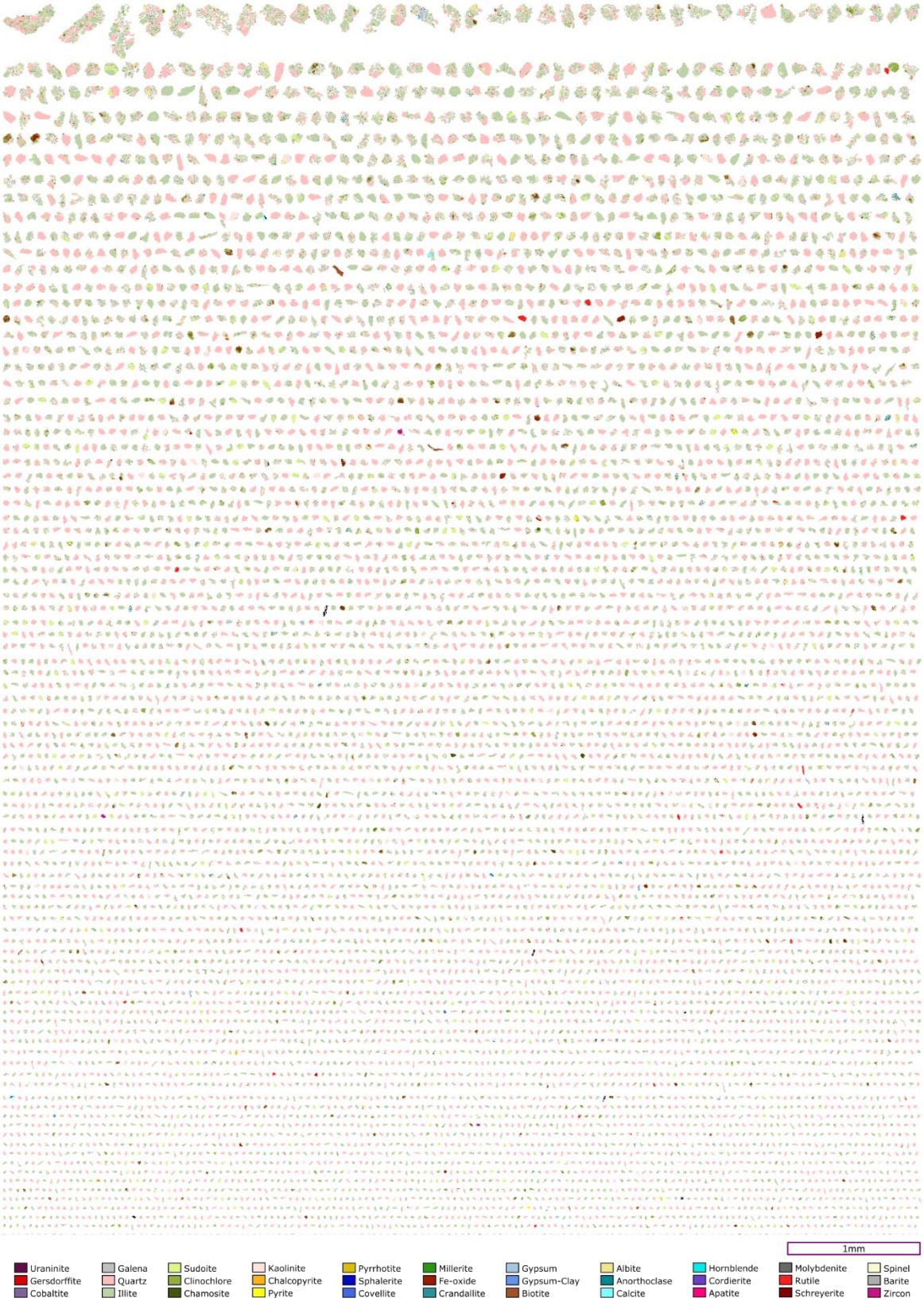
1mm
Uraninite
Gersdorffite
Cobaltite
Galena
Quartz
Illite
Sudoite
Clinochlore
Chamosite
Kaolinite
Chalcopyrite
Pyrite
Pyrrhotite
Sphalerite
Covellite
Millerite
Fe-oxide
Crandallite
Gypsum
Gypsum-Clay
Biotite
Albite
Anorthoclase
Calcite
Hornblende
Cordierite
Apatite
Molybdenite
Rutile
Schreyerite
Spinel
Barite
Zircon

Primary Mineral Grain Images

TMF18-01-01

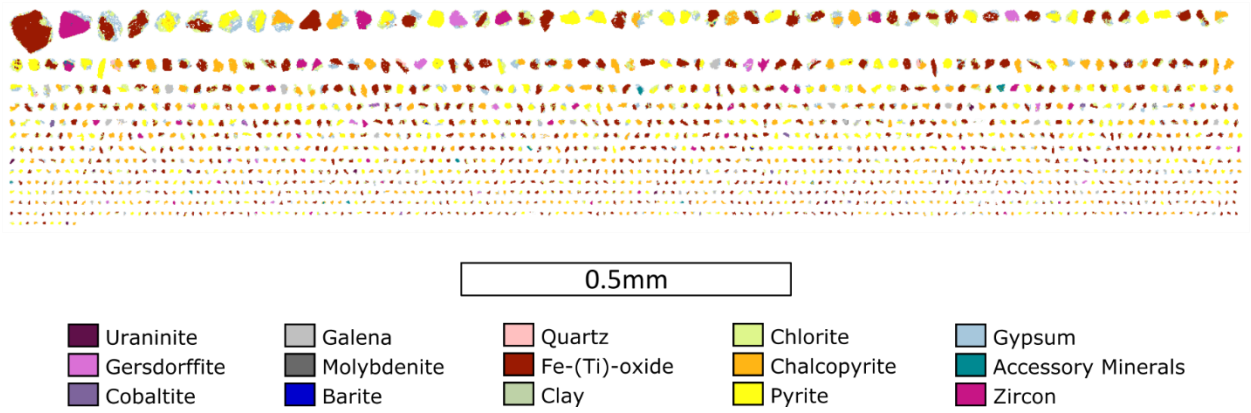

TMF18-01-02

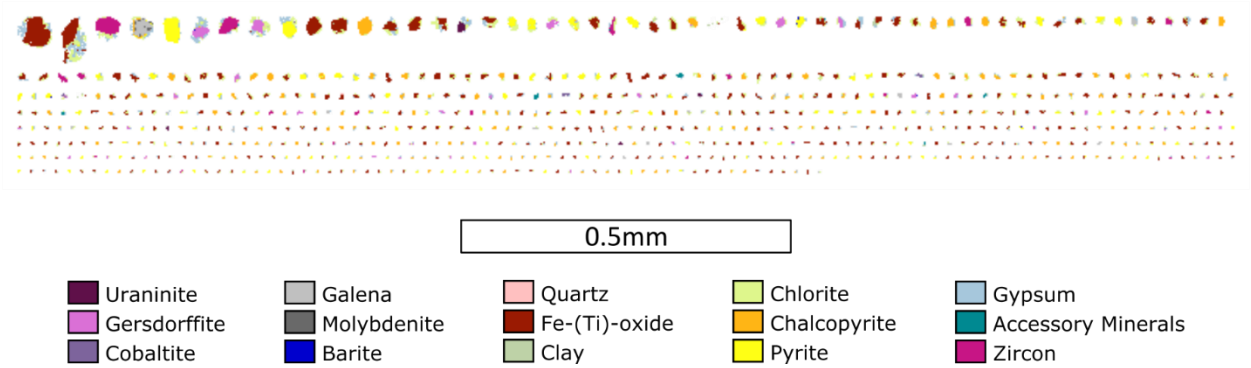

TMF18-01-03

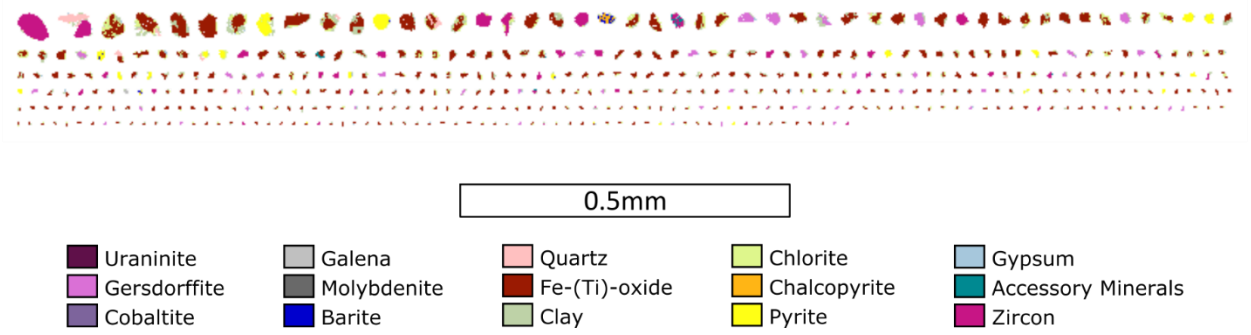

TMF18-01-06

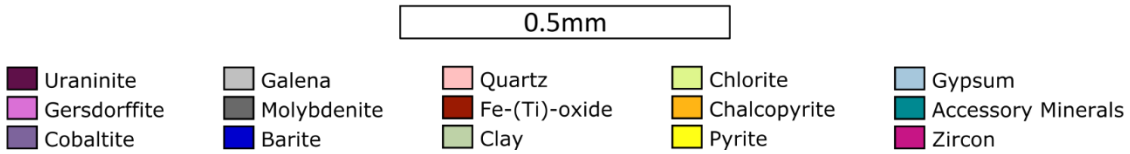

TMF18-01-10

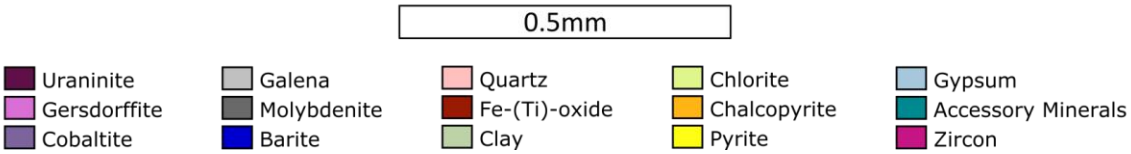

TMF18-01-11

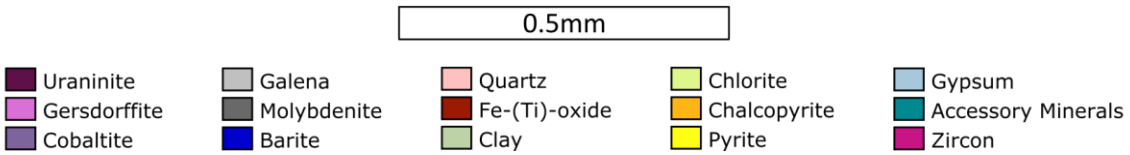

TMF18-01-13

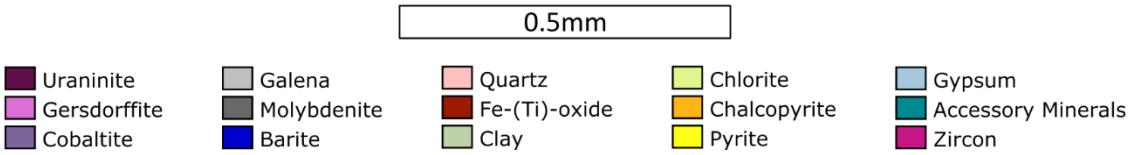

TMF18-01-15

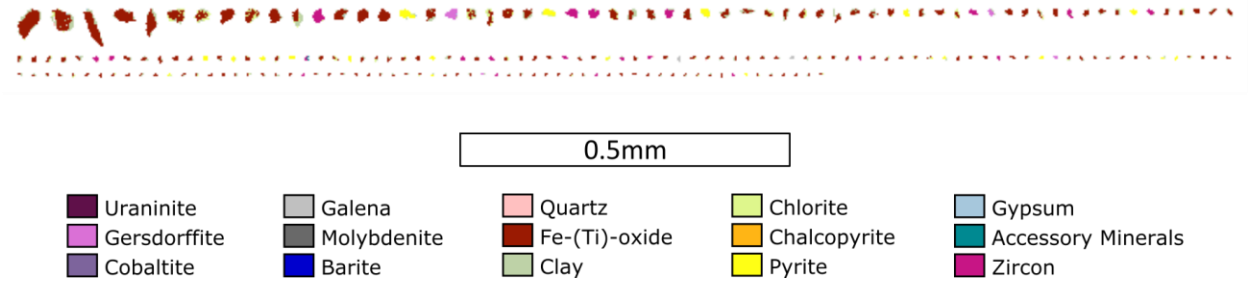

TMF18-01-17

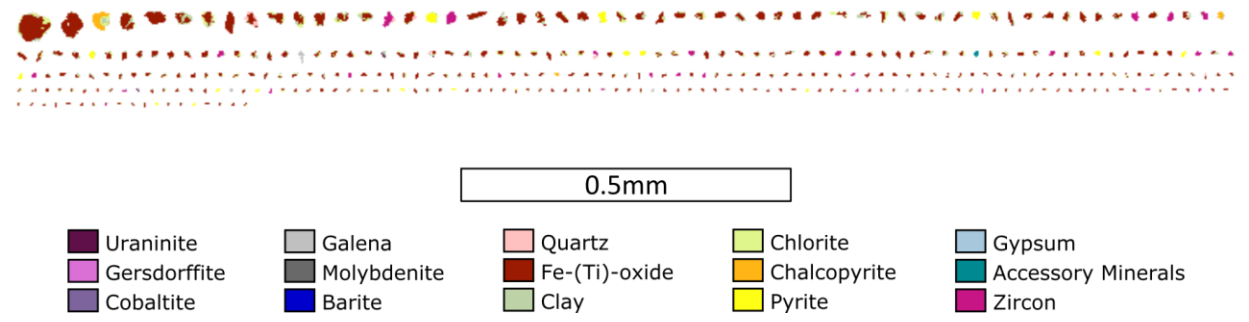

TMF18-01-20

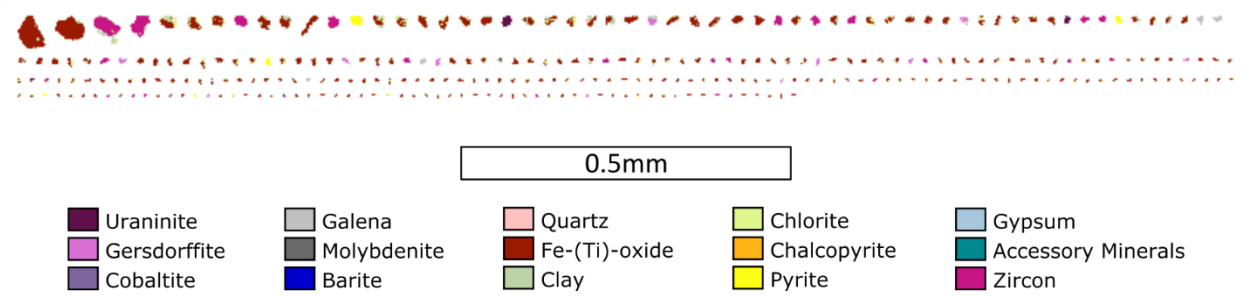

TMF18-01-26

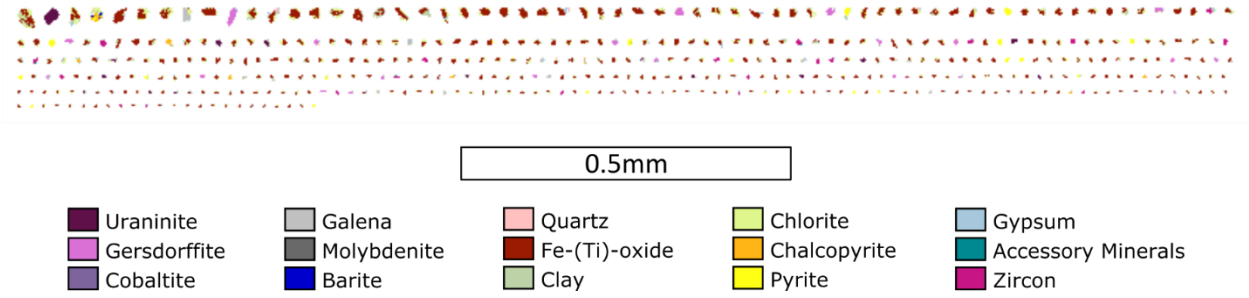

TMF18-02-03

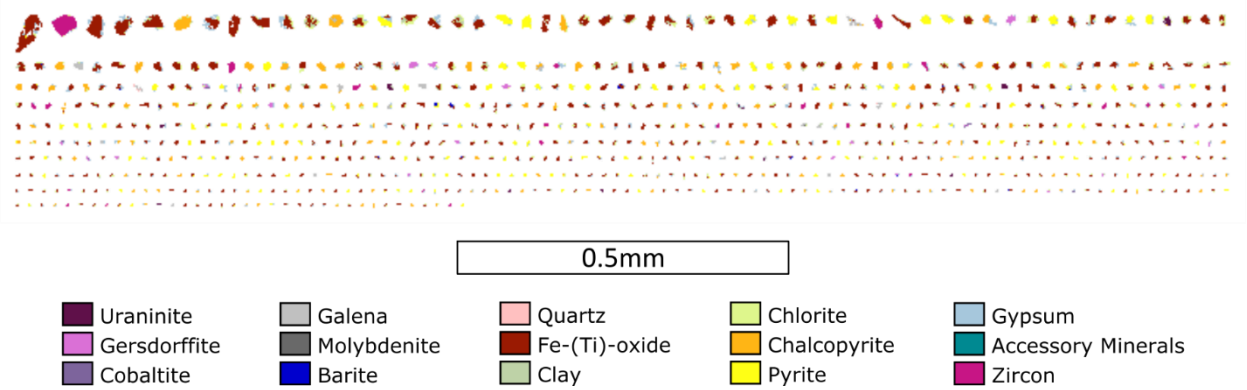

TMF18-03-01

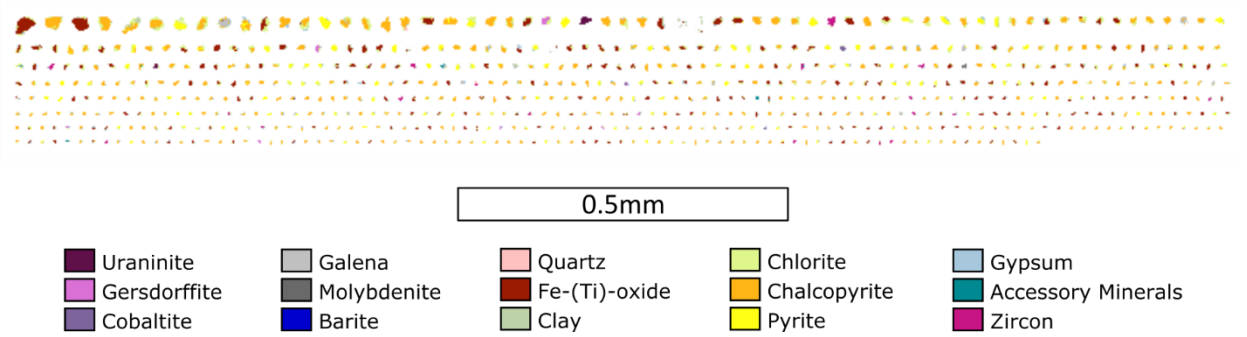

TMF18-03-02

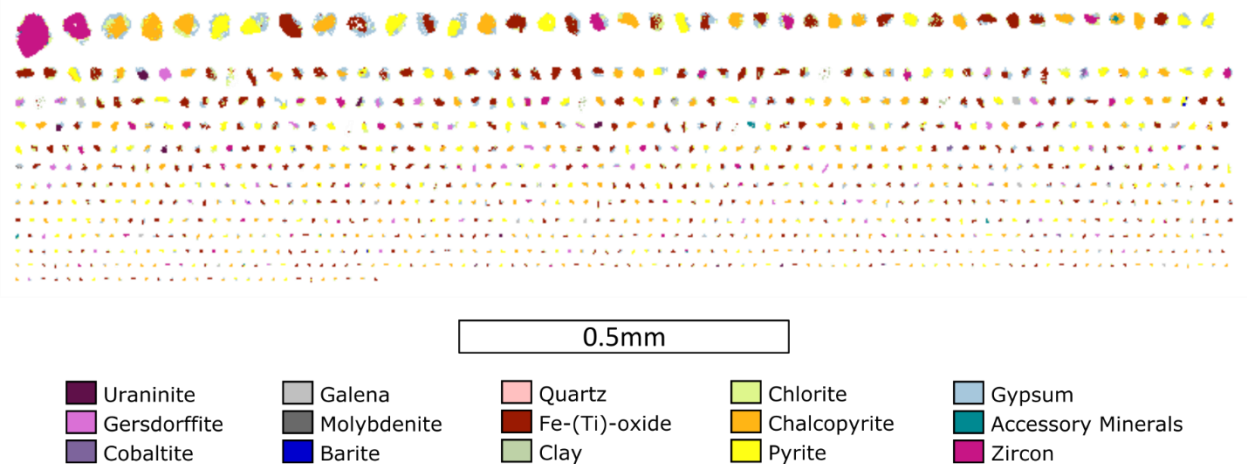

TMF18-03-05

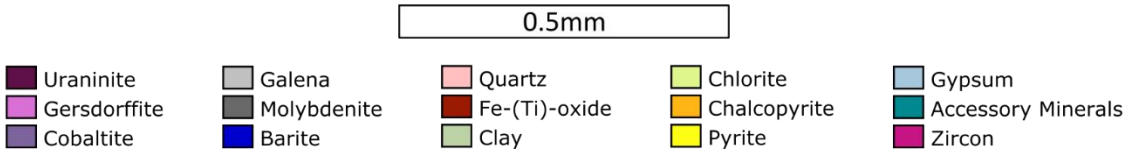

TMF18-03-07

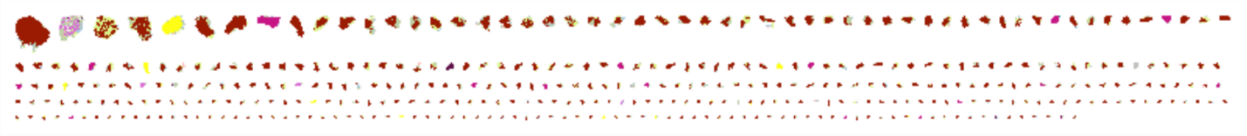

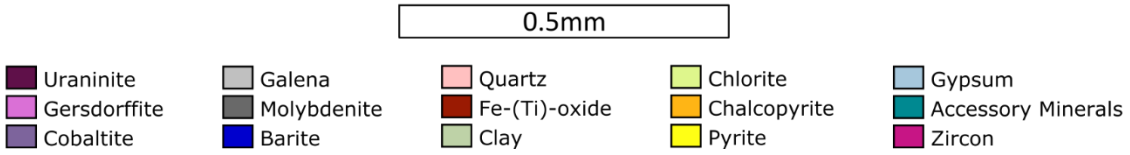

TMF18-03-09

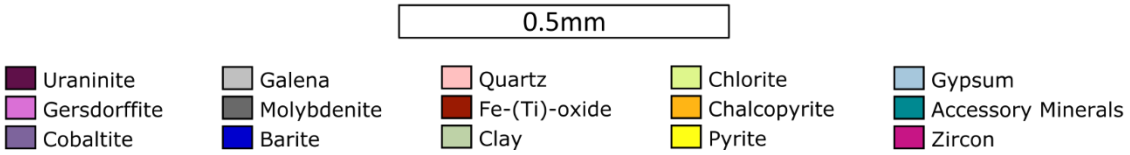

TMF18-03-12

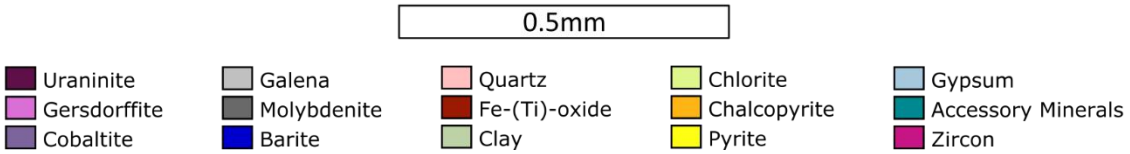

TMF18-03-14

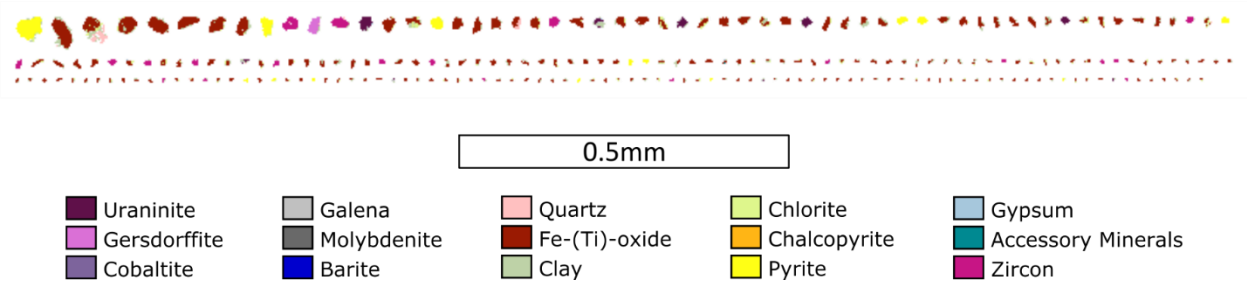

TMF18-03-18

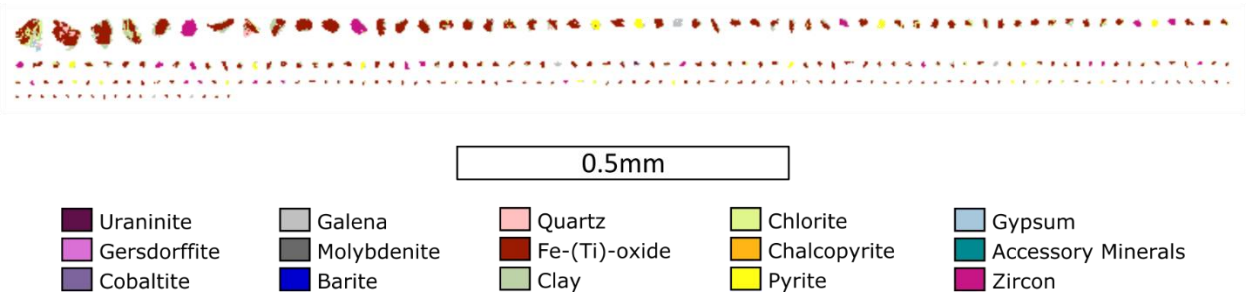

TMF18-03-19

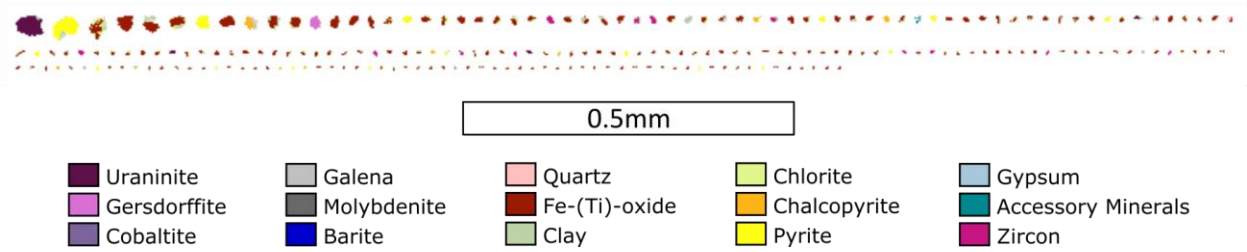

TMF18-03-21

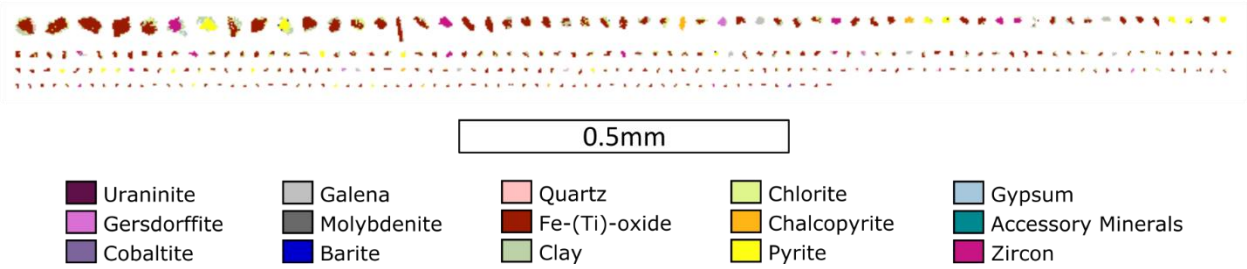

MEMORANDUM

Issued for Use

To:	Joseph, ESSILFIE-DUGHAN	**Date:**	April 21, 2025
c:		**Memo No.:**	002
From:	Seth Xeflide	**File:**	P-02-2025
Subject:	JEB Tailings Management Facility Water Balance Model Update		

1.0 INTRODUCTION

Orano Canada Inc. (Orano) retained DS Evex Group Limited (Evex) to update the JEB Tailings Management Facility (TMF) water balance model (Orano 2019[1]). Evex understands that the model report will be used to inform operational decisions and included in the tailings Technical Information document which will be presented to regulators.

The purpose of this memorandum is to provide current results of the JEB TMF water balance model. The objective of the model is to improve operation efficiency and for forecasting purposes. This model incorporates meteorological, hydrogeological, tailings, and JEB TMF Pond water level data current as of October 31, 2024. The calibration period for the updated model spans from September 1, 2014, to October 27, 2024. A prediction period from October 21, 2024 to March 31, 2025 was simulated to estimate the total anticipated water balance volumes up to March 31, 2025.

The JEB TMF water balance model is developed in GoldSim[2] software (version 14.0 R4) to gain understanding of how the water and tailings inflow, meteorological (temperature, precipitation, and evaporation) and water outflow components affect the water level in the JEB TMF pit. The schematic for the various water balance components for the model is presented in Figure 1-1.

[1] Orano 2019. JEB TMF Water Balance Model Update. December 11, 2019
[2] GoldSim Technology Group LLC. (2024). GoldSim Version 14.0 R4 #471 October 2024

DS Evex Group Limited
738 Skyview Ranch Grove NE
Calgary, AB T2N 0R9 CANADA
Tel 587 525 8496

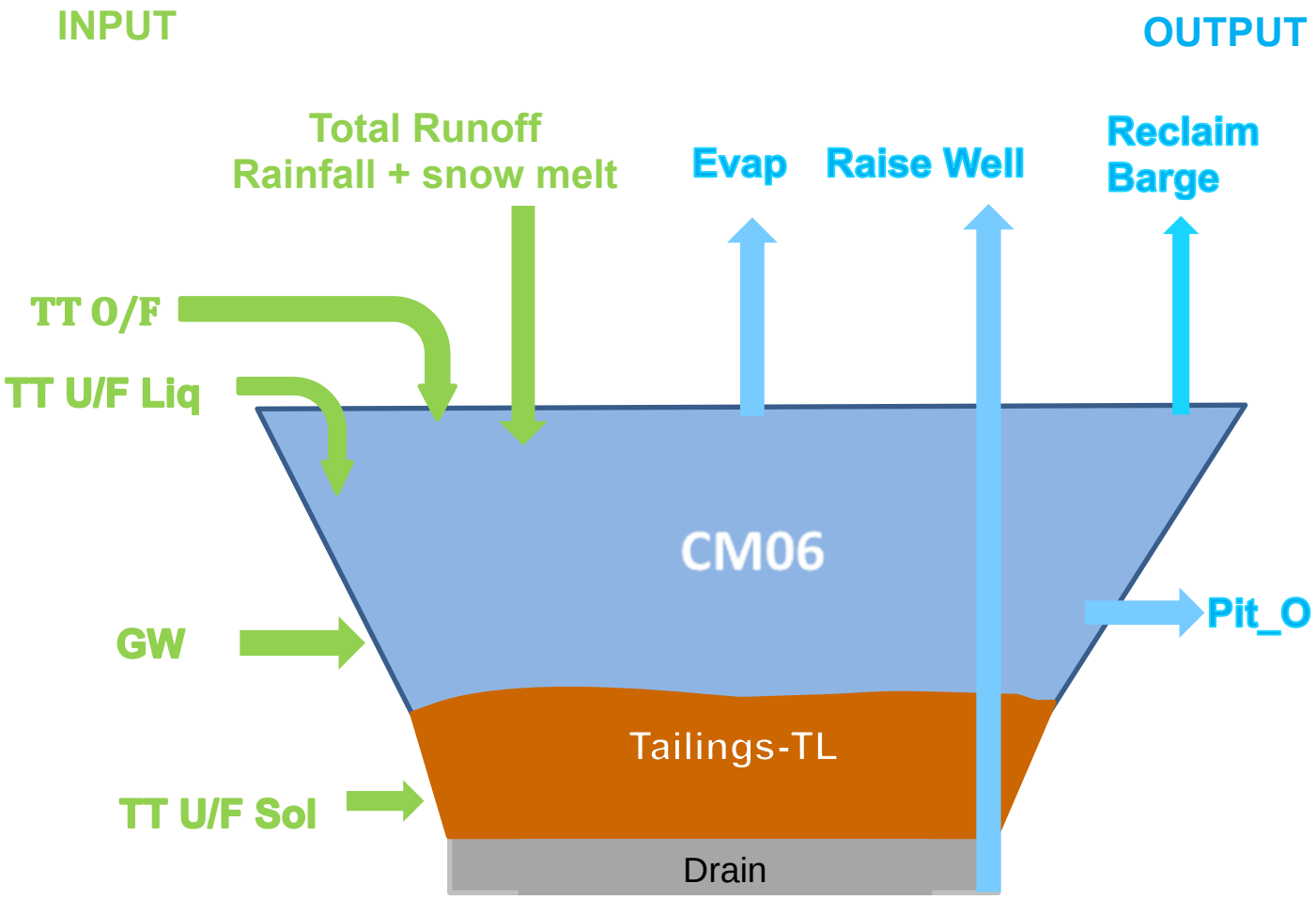

Figure 1-1: General water balance schematic for JEB TMF pit.

Where:
TT O/F is the total tailings thickener overflow volume.
TT U/F Liq is the total tailings thickener underflow liquid volume.
TT U/F Sol is the total tailings thickener underflow solid volume.
Total Runoff Rainfall +Snowmelt is the total volume from snow and rainfall (direct precipitation and runoff).
GW is the groundwater inflow.
Pit_O is the pit water outflow to the surrounding GW.
Evap is the direct evaporation from the pit.
Raise Well is the pumping volume from the raise well.
Reclaim Barge is the total volume pumped from TMF pond to the JEB water treatment plant.

DS Evex Group Limited
738 Skyview Ranch Grove NE
Calgary, AB T2N 0R9 CANADA
Tel 587.225.3699

2.0 METHODS AND DATA

This section presents the input data and methods used for the updated JEB TMF pit water balance model.

2.1 Input Data

2.1.1 Meteorological, Pit Water Level, Groundwater Level, Tailings Data

This section describes the input data sources used in the model, including meteorological parameters (temperature, precipitation, and evaporation), tailings-related inflow and outflow parameters, pit water levels, and groundwater levels and flow conditions. A summary of these data sources is provided in Table 2-1.

Meteorological data for the model was sourced from the McClean Lake JEB meteorological station (Table 2-1). For periods where this data is missing, data from Environment Canada & Climate Change (ECCC) climate station at Collins Bay were utilized. A review of precipitation data from the JEB meteorological station revealed errors in the 2024 dataset. For instance, the data indicated continuous precipitation between February 11 and April 29, except for February 13 and April 27. As a result, precipitation data (January 1 to December 31st, 2024) from the Environment Canada & Climate Change (ECCC) climate station at Collins Bay Cameco were used instead.

The JEB TMF pit water level (CMO6) and all tailings data including daily raise water pumping volume, daily reclaim barge volume, daily tailings overflow liquid volume, tailings underflow liquid volume, tailings underflow solid volume, tailings percent solids, and tailings dry mass were sourced from the McClean Lake mill operational insight database. Groundwater inflow to the JEB TMF pit and the pit water outflow into the surrounding groundwater system were estimated using analytical solutions described in Section 2.1.5.

Table 2-1: JEB TMF model input and output data sources.

Component	Data Source	Comments
Total Runoff	Precipitation data from JEB meterological station and Environment Canada Station at Collins Bay.	Runoff calculated using daily precipitation and pit area. Contributing area for the JEB TMF based on values reported by Golder 2018. The direct precipitation and runoff to the pit is determined from daily precipitation data based on the contributing area and runoff coefficients. During the winter/spring months, the runoff due to snow melt is calculated with a temperature-based snow accounting routine on a daily basis. When the mean daily temperature is lower than 1°C, no runoff is assumed to occur, and all the winter precipitation is stored as a snow stock which is melted when temperature becomes positive.
Tailings Overflow- (TT O/F)	Operational insight	Daily total volume.
Tailings thickner underflow-Liquid (TT U/F Liq)	Operational insight	Daily total volume.
Tailings thickner underflow solid-U/F Sol	Calculated	Calculated based on dry mass of tails and placed dry density. The placed density is based on the 2018 Tailings Optimization and Verification Program (TOVP).
Groundwater -(GW) flow	Calculated	Groundwater inflow calculated using the Dupuit Approximation and Darcy equation.
Groundwater level	Operational insight	Used to calculate pit water outflow to surrounding groundwater system.
JEB water level (CMO6)	Operational insight	The model was calibrated against monitored water level in the JEB TMF pit.
Evaporation-(Evap)	Environment and Climate Change Canada	Evaporation was assumed for the JEB TMF pit and the pit catchment area. Evaporation is based on evapotranspiration values obtained from Environment Canada Brochet Lake Station, Manitoba measured from over the period of 1949 to 1976.
Raise Well	Operational insight	The daily total volume of pond outflow resulting from raise well pumping was estimated as a calibration parameter.
Reclaim Barge	Operational insight	Daily total volume.

DS Evex Group Limited
738 Skyview Ranch Grove NE
Calgary, AB T2N 0R9 CANADA
Tel 587.225.3699

A map showing the locations of groundwater monitoring wells near the JEB TMF pit is provided in Figure 2-1. Figures 2-2 to 2-5 compare the JEB TMF pond elevation with groundwater elevations from near-field monitoring wells (surrounding the pit) completed in the overburden, upper sandstone, lower sandstone, and basement aquifers, respectively. These figures indicate that between October 2023 to April 2024, pit water elevation increased sharply resulting in the pit water elevation being higher than the surrounding groundwater elevation with the potential of outflow of the pit water into the surrounding groundwater system. This period coincides with no pumping of reclaim pond water due to shut down of the JEB water treatment plant (WTP) for maintenance.

The hydrographs (Figures 2-2 to 2-5) indicate that, during the referenced period, the potentiometric surface in portions of the groundwater system—particularly in the northeastern (associated with the 95-1 series wells) and southeastern (associated with the 95-2 series wells) areas—was higher than the pond water level. This hydraulic gradient suggests the potential for localized groundwater inflow into specific sections of the pit. Visual inspection of the hydrograph shows that since April 2024, the JEB pit elevation has begun to decline coinciding with the resumption of pumping reclaim pond water to the JEB WTP.

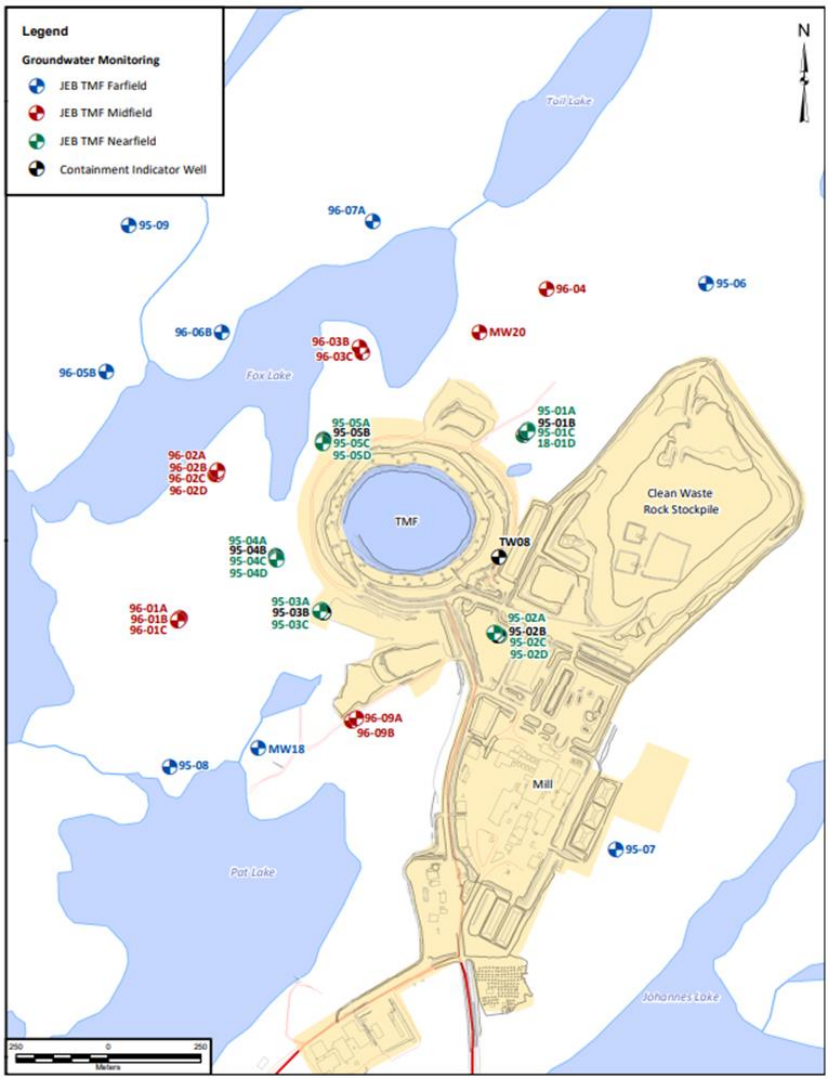

Figure 2-1: JEB TMF pit showing location of groundwater monitoring wells.

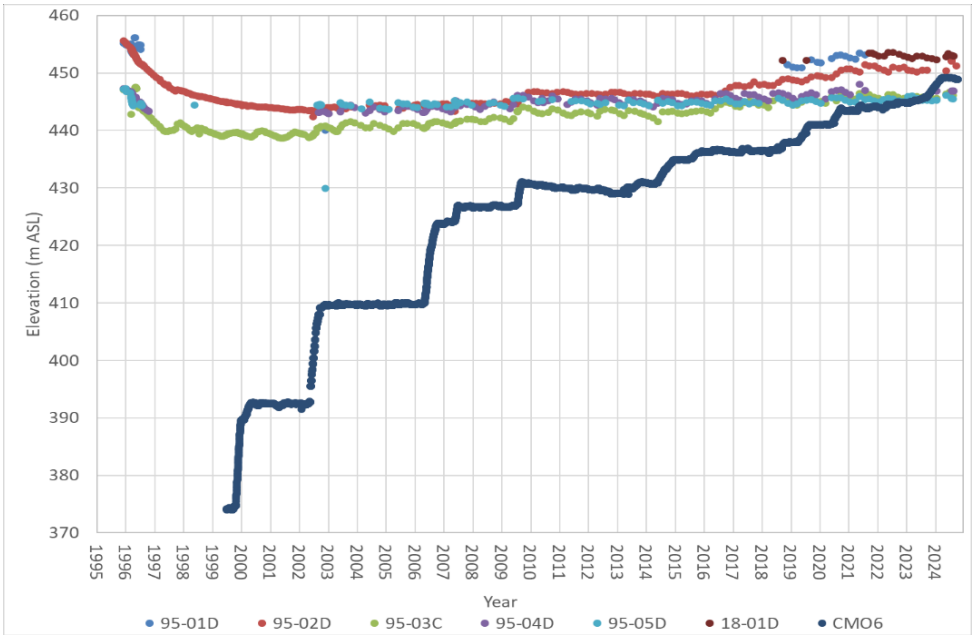

Figure 2-2: Comparison of JEB TMF Pond elevation and hydraulic head of nearfield overburden wells.

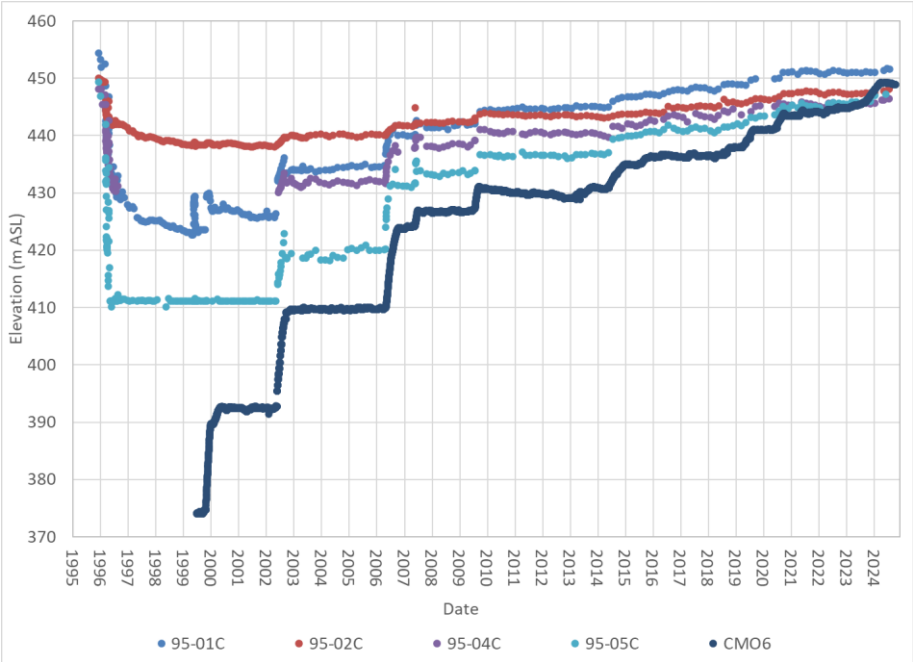

Figure 2-3: Comparison of JEB TMF Pond elevation and hydraulic head of nearfield upper sandstone wells.

DS Evex Group Limited
738 Skyview Ranch Grove NE
Calgary, AB T2N 0R9 CANADA
Tel 587.225.3699

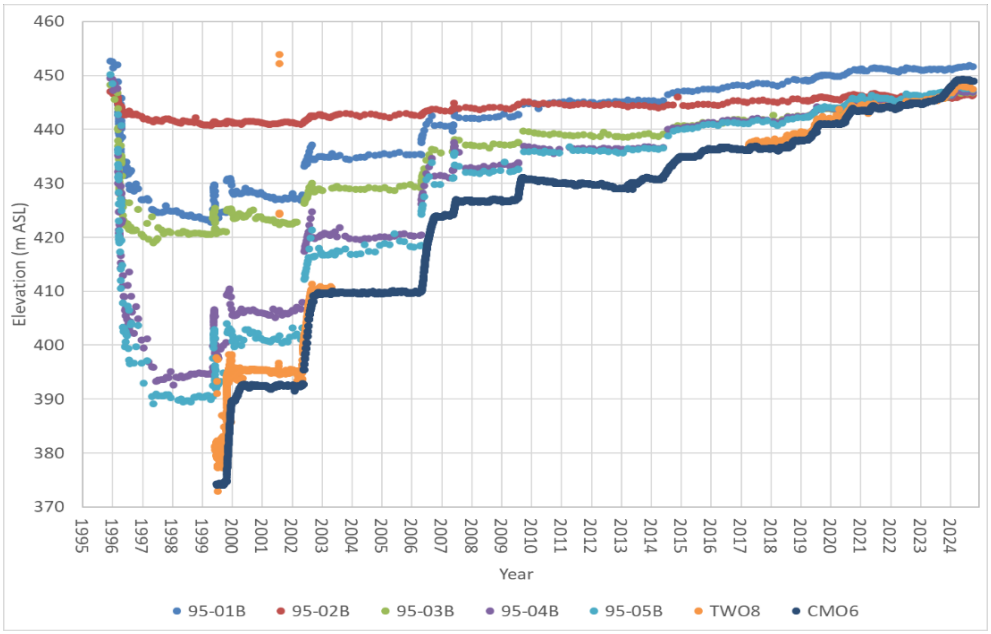

Figure 2-4: Comparison of JEB TMF Pond elevation and hydraulic head of nearfield lower sandstone wells.

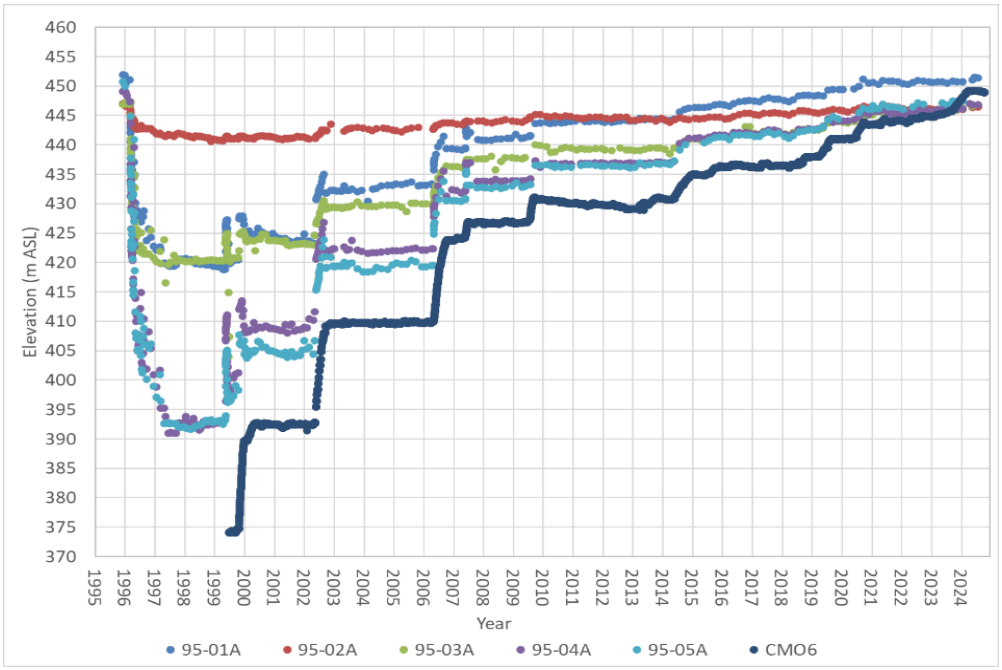

Figure 2-5: Comparison of JEB TMF Pond elevation and hydraulic head of nearfield basement wells.

2.1.2 Catchment Area

The JEB TMF pit area, measuring 216,000 m³ (Golder, 2018[3]), was used to calculate runoff, including snowmelt and rain runoff. The runoff area within the pit was defined so that the available runoff area was calculated as the difference between the JEB TMF pit area and the pond surface. The contributing catchment area was determined based on the mill terrace area of 181,850 m³ (Golder, 2018). Figure 2-6 shows the JEB site layout showing the mill terrace area.

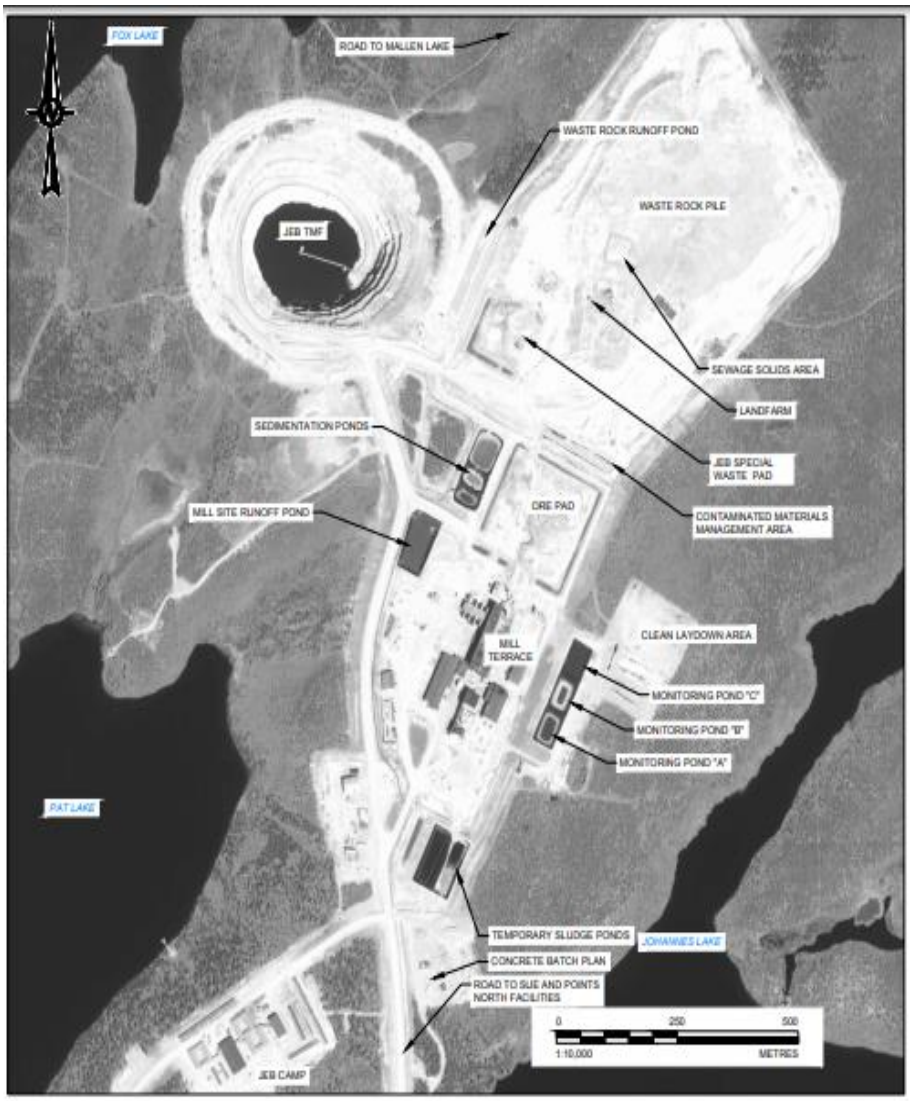

Figure 2-6: Site layout plan showing the mill terrace area.

[3] Golder Associates Ltd. 2018. JEB Tailings Management Facility Optimization Stage 2 and Expansion Stage 1 Design Report.

DS Evex Group Limited
738 Skyview Ranch Grove NE
Calgary, AB T2N 0R9 CANADA
Tel 587.225.3699

2.1.3 JEB TMF Pit and Catchment Evapotranspiration

Monthly evapotranspiration observed at the Brochet Lake, MB station, in the northern Manitoba (Environment Canada) was used for this model. The monthly values were disaggregated into daily values. These values were assumed to be accurate enough at the McClean site (Plagnes et al., 2017)[4]. In the model, evaporation comprises evapotranspiration over the catchment area and the direct evaporation over the tailings pond.

2.1.4 Runoff and Direct Precipitation

The direct precipitation and runoff into the JEB Pit were calculated using daily precipitation data, accounting for the catchment area and runoff coefficients. During the winter and spring months, snowmelt runoff was estimated daily using a temperature-based snow accounting model. When the mean daily temperature falls below 1°C, no runoff is assumed, and all winter precipitation is stored as a snow stock (Eq. 1). This snow stock melts and contributes to runoff once the temperature rises above 0°C.

Snow Stock = Snow Stock (day-1) + Precipitation day *Eq.1*

Runoff of winter precipitation (Snow melt) is assumed to occur when the mean daily temperature becomes higher than 0°C. Then, a fraction of the snow stock melts according to the Degree-day melt factor K and the difference between the mean daily temperature and the melt temperature (Eq. 2). This fraction is affected by a snow melt runoff coefficient, which is a calibration factor.

$$\text{Snow melt} = K * (T_{daily} - T_{melt}) \quad \textit{Eq.2}$$

During this period, total runoff is calculated as the sum of daily rainfall runoff and snowmelt runoff, continuing until the snow stock is completely depleted. The calibration factor (K) is adjusted to ensure that the snow stock fully melts before the end of May each year, in line with field observations. For the McClean Lake site, previous models (Valérie et al., 2017) have established a calibrated K value of 4. During the open water season, total runoff (rainfall runoff) is determined based on the runoff volume generated by each precipitation event.

The snow accumulation and snow melt runoff were applied to the JEB TMF pit catchment which includes the mill terrace catchment area and the in-pit contributing drainage area (i.e., pit walls). Evex understands that the runoff from the mill terrace is stored in the mill site runoff pond and then pumped into the JEB TMF. However, neither the pumping schedule nor the pumping volume/rate is known, as the pumping is not metered. Consequently, during model implementation, runoff from the mill terrace is assumed to report directly to the JEB TMF. Direct snow onto JEB TMF pit was applied using a similar formulation for the snow melt runoff, but with a coefficient of 1 (i.e. all the snow that fell onto the pit melts into the pit).

4 Plagnes,V., Schmid,B., Mitchell, B., and Judd-Henrey, I. 2017. Water balance modelling of a uranium mill effluent management system. Journal of Hydrology. http://dx.doi.org/10.1016/j.jhydrol.2017.03.051

The total precipitation to JEB TMF pit is the sum of any direct precipitation (direct rain and snow melt into pit) to the pit lake on a given day, and the total runoff volume (from snow melt runoff and rainfall runoff) for that day.

2.1.5 Groundwater Inflow

Groundwater inflow was taken from a flow rate versus water elevation correlation, developed based on the Dupuit analytical solution for unconfined radial flow into a circular excavation (Bear 1962[5]). This approach simplifies groundwater flow equations by assuming nearly horizontal flow and ignoring vertical gradients. This method assumes:

- Steady-state flow conditions.
- A circular pit with vertical sidewalls.
- Horizontal flow toward the pit.
- The water table remains nearly horizontal away from the pit.

The groundwater inflow was estimated using the following equation (eq. 3):

$$Q = 2\pi K \frac{(h_0^2 - h^2)}{ln\left(\frac{r}{r_w}\right)} \qquad Eq.3$$

Where:
Q is the groundwater inflow into the pit (m^3/s);
K is the hydraulic conductivity, (m/s);
h_0 is pre-mining groundwater elevation, (m);
h is the pit elevation, (m);
r is the radius of the pit at the given elevation, (m); and
r_w reference radius (assumed 0.1 m for calculations).

If the pit elevation was below the water table ($h > h_0$) groundwater inflow was calculated; otherwise, inflow was set to zero (i.e., $h < h_0$).

Table 2-3 presents the hydraulic parameters—hydraulic conductivity, pre-mining groundwater elevation, and thickness—for different geological units (overburden, upper sandstone, lower sandstone, and basement), which were used as input for the analytical groundwater inflow solution. The groundwater inflow to the pit was modeled using the Python programming language, and the corresponding script is provided in Appendix A. The total inflow is obtained by summing contributions from all geological layers: overburden, upper sandstone, lower sandstone and basement. Figure 2-7 illustrates the calculated groundwater inflow rate to the JEB TMF pit as a function of pit height,

[5] Bear, J (1972). Dynamics of Fluids in Porous Media. Elsevier.

DS Evex Group Limited
738 Skyview Ranch Grove NE
Calgary, AB T2N 0R9 CANADA
Tel 587.225.3699

along with the dewatering rates from the pit during mining. The dewatering rates shown in Figure 2-7 are based on the total pumping rates from 30 dewatering wells installed around the pit. These rates are based on data from 2001 to 2013 (Figure 2-8).

Table 2-2: Input Used to Calculate Groundwater Inflow to JEB TMF.

Parameter	Symbol	Value	Unit	Comments
Hydraulic Conductivity (Overburden)	K	7.32×10^{-7}	m/s	Geometric mean hydraulic conductivity for overburden wells in the JEB area
Hydraulic Conductivity (Upper Sandstone)	K	1.99×10^{-7}	m/s	Geometric mean hydraulic conductivity for upper sandstone wells in the JEB area
Hydraulic Conductivity (Lower Sandstone)	K	5.30×10^{-7}	m/s	Geometric mean hydraulic conductivity for lower sandstone wells in the JEB area
Hydraulic Conductivity (Basement)	K	4.47×10^{-7}	m/s	Geometric mean hydraulic conductivity for basement wells in the JEB area
Pre-mining water level (overburden)	ho	455.663	m	Maximum groundwater elevation in overburden observation wells at the JEB area
Pre-mining water level (upper sandstone)	ho	454.394	m	Maximum groundwater elevation in upper sandstone observation wells at the JEB area
Pre-mining water level (lower sandstone)	ho	452.705	m	Maximum groundwater elevation in lower sandstone observation wells at the JEB area
Pre-mining water level (basement)	ho	451.937	m	Maximum groundwater elevation in lower sandstone observation wells at the JEB area
Pit radius	r	7.54 to 258.255	m	Based on diameter of as-built TMF Pit. Radii correspond to pit elevation of 343 m to 457 m, respectively

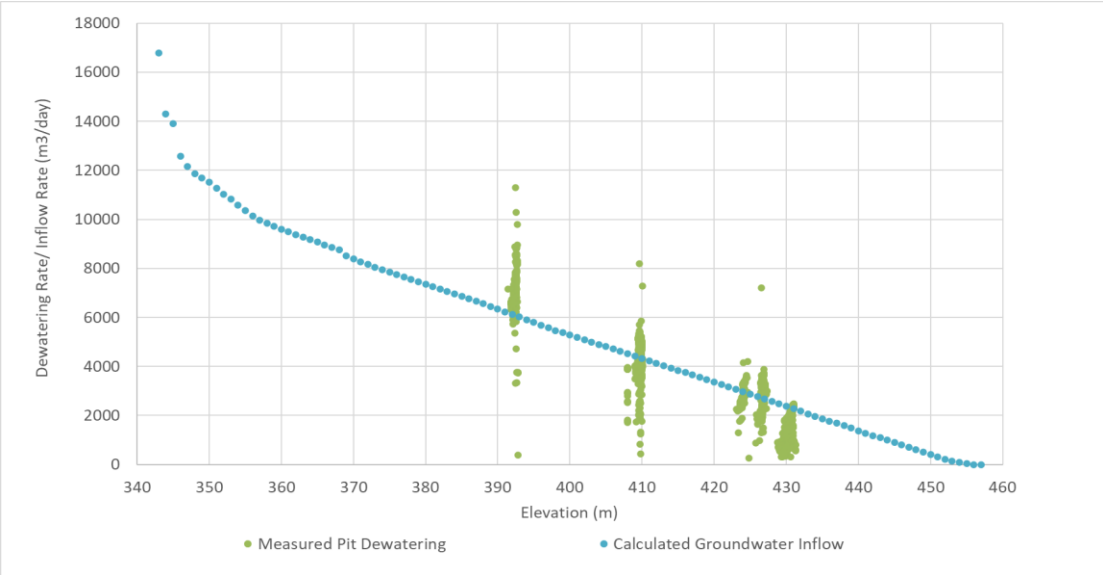

Figure 2-7: Calculated groundwater inflow to JEB TMF pit.

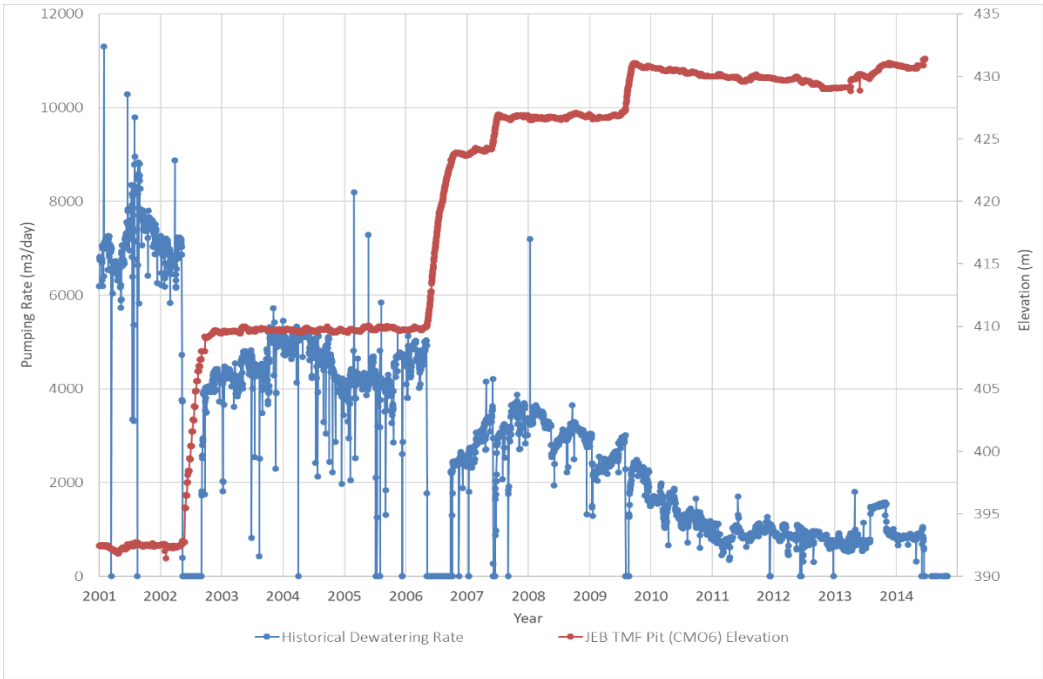

Figure 2-8: Comparison of JEB pit elevation and historical dewatering rate.

DS Evex Group Limited
738 Skyview Ranch Grove NE
Calgary, AB T2N 0R9 CANADA
Tel 587.225.3699

Groundwater Inflow/Outflow-from October 2023 to October 2024.

As discussed in Section 2.1.1 and illustrated in Figures 2-2 to 2-5, the relative elevation of the pond compared to the surrounding groundwater levels suggests that pit water began discharging into the surrounding groundwater system in October 2023. While this indicates net outflow from the pond, groundwater level data also suggest localized inflow into the pond—particularly from the northeastern and southeastern portions of the pit—during the same period.

To estimate this inflow and outflow for the period from October 2023 to October 2024, Darcy's Law is applied. This is done using groundwater elevation data from the near-field groundwater observation wells (Figure 2-1) and the pond elevation. The input parameters for groundwater inflow and outflow are provided in Appendix B, while the hydraulic conductivity values for the overburden, upper sandstone, lower sandstone, and basement layers are listed in Table 2-2. The Darcy equation is presented in Equation 4 below.

$$Q = KA\frac{(h_{gw} - h_p)}{L} \qquad Eq.4$$

Where:
Q is the groundwater inflow to or outflow from the pit (m^3/s).
K is the hydraulic conductivity, (m/s);
A is the cross-sectional area (m^2);
h_{gw} is groundwater elevation, (m);
h_p is the pond elevation, (m); and
L is the horizontal distance from observation well to the pit (m).

If the groundwater elevation in each observation well is greater than the pond elevation ($h_{gw} > h_p$) groundwater will flow into the pit; otherwise, the pit water discharges into the surrounding groundwater (i.e., $h_{gw} < h_p$). During implementation of the Darcy equation a model domain of 500 m by 500 m was assumed. The resulting groundwater inflow and outflow is presented in Figure 2-9. The python implementation of the Darcy flow is presented in Appendix C.

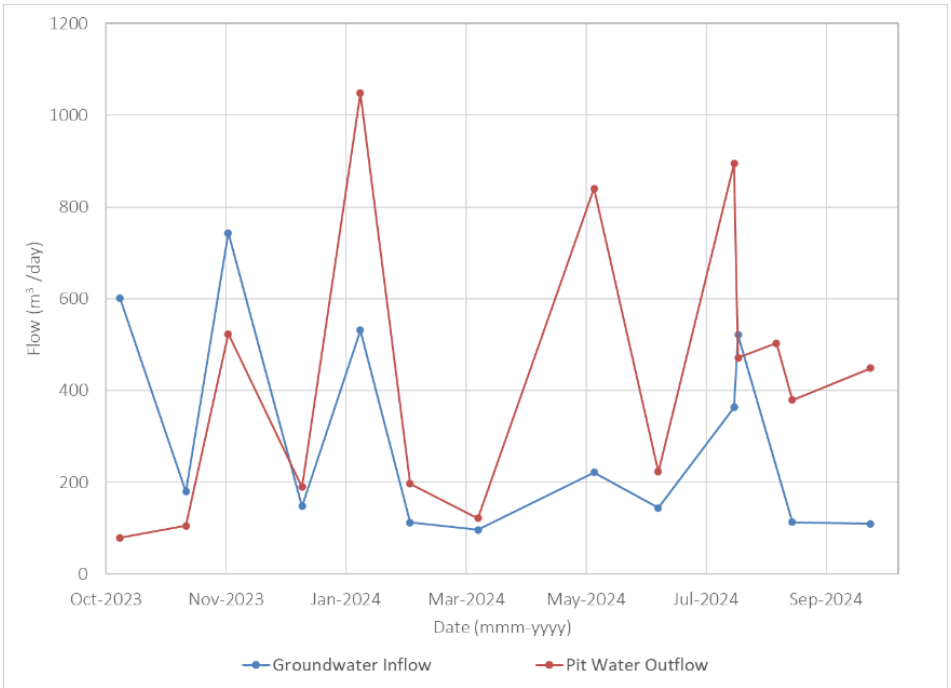

Figure 2-9: Calculated groundwater inflow to the JEB TMF pit and pond water discharge to surrounding groundwater.

2.1.6 Tailings data

Tailings Solids Underflow Volume

The tailings underflow volume was estimated using the measured tailings dry mass (tonnes) and the measured dry bulk density. The dry density for the JEB/Sue tailings was designated as a calibration parameter, ranging from 770 to 1,100 kg/m³. The dry tailings density for Cigar Lake ore (i.e., after October 1, 2016) was estimated to range from 490 to 830 kg/m³ (Orano, 2020[6]). These values were specified as calibration parameters during the simulation. In this model it was assumed that tailings deposition started on June 27, 1999.

Tailings Thickener Overflow and Tailings Thickener Underflow Liquid Volume

Tailings thickener overflow and tailings thickener underflow liquid volumes are available for the period September 1, 2014 (model start date) to October 31, 2024.

Reclaim Water

Reclaim water pumping from the reclaim barge is available for the period September 1, 2014, to October 31, 2024.

6 Orano 2020. McClean Lake Operation – Tailings Management Technical Information Document (TID)

DS Evex Group Limited
738 Skyview Ranch Grove NE
Calgary, AB T2N 0R9 CANADA
Tel 587.225.3699

Raise Well Pumping

Raise well pumping rate data are available for the period from September 1, 2014, to October 31, 2024. Since a portion of the raise well water originates from the surrounding groundwater (i.e., not all water is drawn from the TMF pond), its composition reflects mixed sources. Figure 2-10 presents the average annual sulphate concentrations in the JEB TMF Pond and the raise well from 2014 to 2024. The consistently lower sulphate concentrations in the raise well compared to the pond suggest that a portion of the raise well water is derived from the surrounding groundwater. This inference informed the model simulation.

Figure 2-10: Comparison of average annual sulfate concentrations in JEB TMF Pond water and raise well water.

2.1.7 Calibration

The model was calibrated to the monitored JEB TMF pit water levels from September 1, 2014, to October 20, 2024, based on available JEB meteorological data. The model was calibrated by varying four main parameters (i.e. calibration parameters); runoff factor for rain (Rain Factor), snow melt runoff (Snow Factor) for snow melt raise well fraction (fraction of raise water from the pond), and dry density of Cigar Lake tails. An optimization procedure was implemented in GoldSim for the studied periods, with these four parameters as optimization variables during the calibration. This procedure consists of minimizing the root mean square error (RMSE) given by equation 5.

$$RMSE = \sqrt{\frac{(Calculated\ JEB\ Pond\ Level_i - Observed\ JEB\ Pond\ Level_i)^2}{N}} \qquad Eq.5$$

Where:

$\text{Calculated JEB TMF Level}_i$ is i[th] value of the calculated water level in JEB TMF Pond.

$\text{Observed JEB TMF Level}$ is the i[th] value of the observed water level in JEB TMF Pond; and

N is the number of observations in the JEB TMF water level time series.

The RMSE allows obtaining the parameters combination that minimizes the difference between calculated water levels and the observed water level in the JEB TMF Pond. The RMSE is a measure of the spread of the measured JEB TMF Pond level about the calculated water level.

3.0 RESULTS

3.1 Calibrated JEB Model Results

A plot of the calculated and the measured JEB TMF Pond levels is presented in Figure 3-1. Key calibration statistics is presented on Table 3-1 and the calibrated values are presented on Table 3-2. The root mean square error (RMSE) of the calibration is 0.27 m with a normalized root mean square error of 1.65%. The mean error (ME) and mean absolute error (MAE) of the calibration were also estimated to be -0.003 m and 0.20 m respectively. The marginal negative value of the ME indicates that on average the model calculated water levels are slightly lower (-0.003 m on average) than the measured water levels in the JEB TMF pit.

A normalized root-mean square error of 1.65% indicates that the calibration is satisfactory for purposes of being used for predicting future water level in the pit. The calibrated model was used to predict water balance component (input and output) to the end of . The water balance elements are presented in Section 3.2.

DS Evex Group Limited
738 Skyview Ranch Grove NE
Calgary, AB T2N 0R9 CANADA
Tel 587.225.3699

Table 3-1: Calibration statistics of JEB TMF.

Statistics	Value	Unit	Interpretation
Number of Water Level Records (N)	3568	-	-
Root Mean Square Error (RMSE)	0.265	m	On average, the model's predicted water levels deviate from the measured values by ~26.5 cm. For a tailings pond, this is a relatively small absolute error, especially if operational thresholds span several metres.
Normalized Root Mean Square Error (NRMSE)	1.65	%	The RMSE is only 1.65% of the full range of observed water levels. This suggests the model captures the natural variation in pond levels very well.
Mean Error (ME)	-0.003	m	The model has a slight negative bias (~3 mm), meaning it slightly underestimates water levels overall, but this is negligible.
Mean Absolute Error (MAE)	0.198	m	On average, absolute deviation is ~20 cm, which reinforces the model's overall accuracy.

Table 3-2: Calibration parameters.

Parameter	Unit	Value	Comment
Rain Factor	-	0.52	These values are affected by mill terrace runoff. Runoff from the mill terrace is assumed to report directly to the JEB TMF Pond but in practice the runoff was stored first in the mill site pond before pumping to the TMF.
Runoff Factor	-	0.58	
Dry Density of JEB/Sue Tailings	kg/m^3	951.8	Values correspond to September 1, 2014, to October 1, 2016.
Dry Density of Cigar Lake Tailings	kg/m^3	649.8 & 679.6	The values correspond to the periods from October 2, 2016, to December 31, 2019, and from January 1, 2020, onward
Raise Well Fraction	-	0.18-0.87	The lowest calibrated fraction (0.18) corresponds to the periods 2020 and 2021 and the highest fraction (0.87) corresponds to 2014.

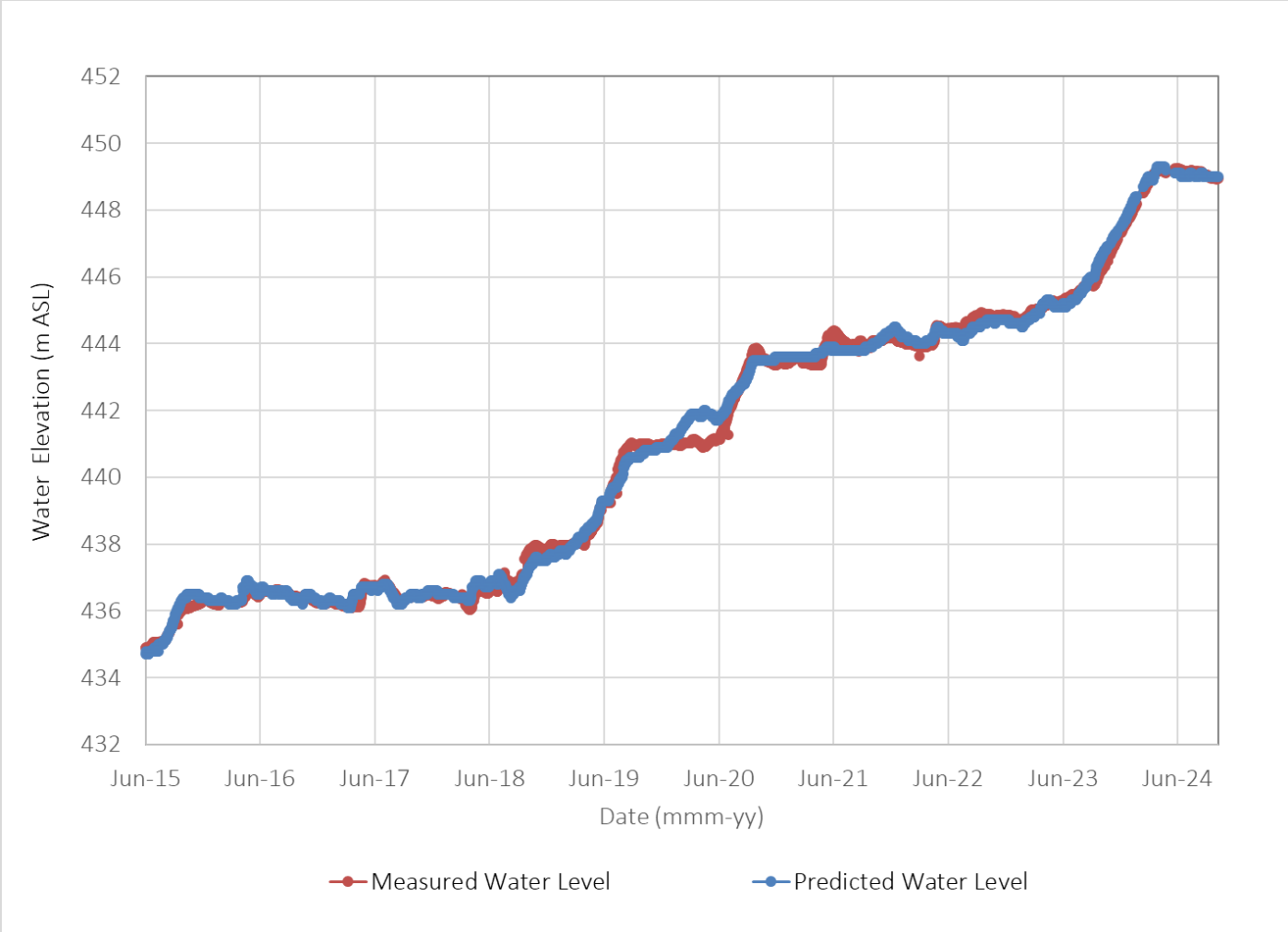

Figure 3-1: Calibrated JEB TMF Pond water level.

Figure 3-2 compares the calibrated raise well cumulative volume with the measured raise well cumulative volume. The plot shows that generally, the calibrated volume progressively deviates from the actual measured volume over time. This observation is expected, as tailings deposition and consolidation over time restrict flow through the tailings. The calibrated raise well fraction ranged from 0.18 to 0.87 (Table 3-2). The lowest raise well fraction (0.18) from the TMF pit occurred between 2020 and 2021 whilst the highest fraction (0.87) occurred in 2014.

DS Evex Group Limited
738 Skyview Ranch Grove NE
Calgary, AB T2N 0R9 CANADA
Tel 587.225.3699

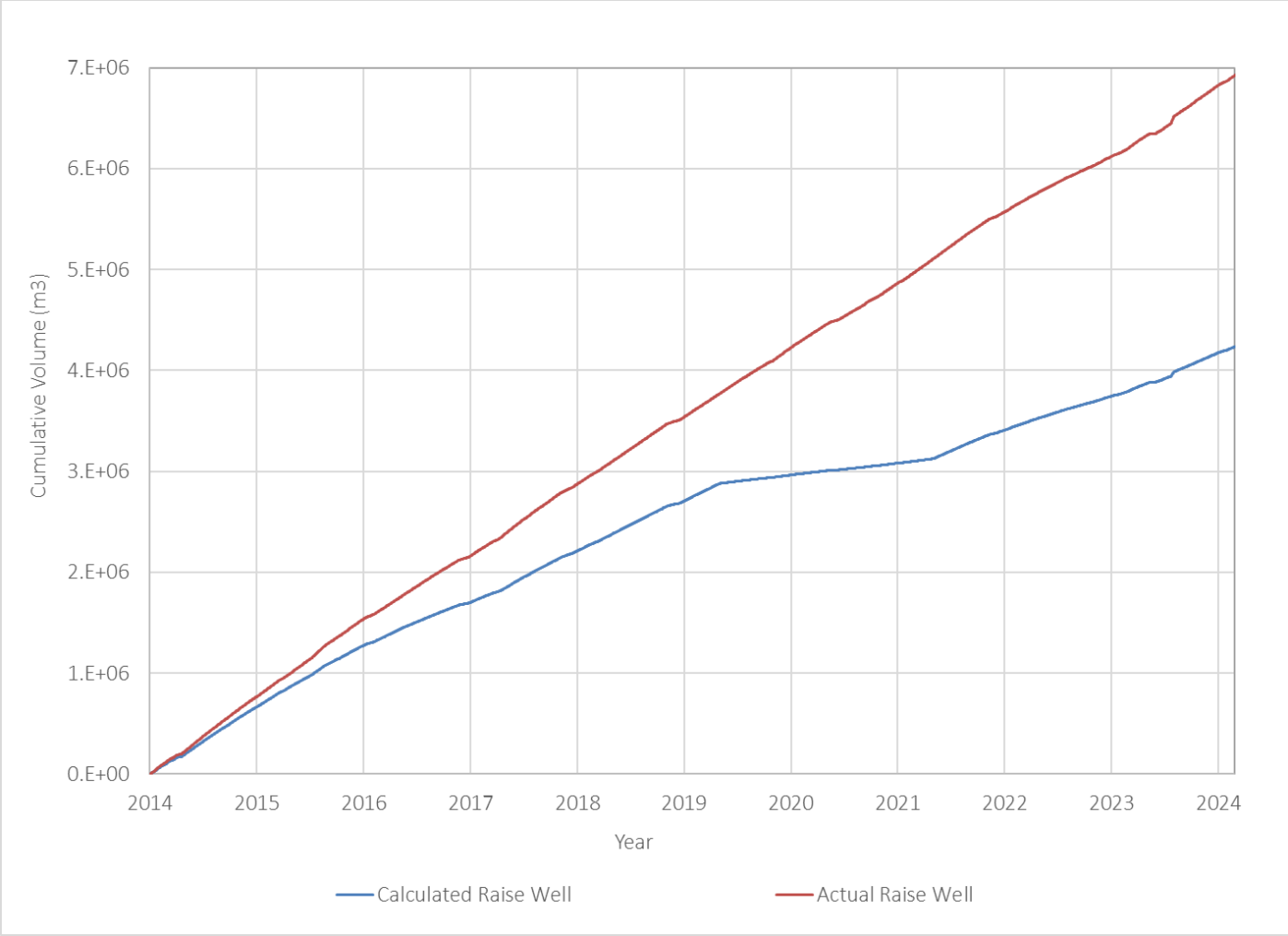

Figure 3-2: Calculated cumulative raise well volume compared to measured cumulative raise well volume.

3.2 JEB TMF Pit Water Balance Component

- The raise well daily pumping rate from November 1, 2024, to March 31, 2025, was assigned a constant value of 2, 000 m^3/day (the average volume from October 31, 2024, to January 1, 2023, was estimated to be 1,728 m^3/day). During simulation this volume was multiplied by a raise well fraction of 0.61 to estimate the volume of water (i.e., 1,220 m^3/day) removed from the JEB TMF pit. This fraction represents the calibrated value for 2022 to 2024.

- The reclaim barge daily pumping rate from November 1, 2024, to March 31, 2024, was assigned a constant value of 1,330 m3/day, based on the average pumping rate from October 31,2024 to January 1, 2023.

- The daily tailings thickener underflow liquid (TTUF) volume from November 1 to March 31, 2024, was assigned a constant value of 1019 m^3/day, based on the average values from October 31,2024 to January 1, 2023.

- The daily tailings thickener total overflow (TTOF) volume from November 1 to March 31, 2024, was assigned a constant value of 1,522 m^3/day, based on the average values from October 31,2024 to January 1, 2023.

- The tailings dry mass and percent solids from November 1 to March 31, 2024, was assigned a constant value of 247.6 tonnes and 20.5 respectively, based on the average values from October 31 to January 1, 2023.

The annual total predicted volume (inflow and outflow) from September 1, 2014, to March 31, 2025 as shown in Figure 1-1, is presented in Figure 3-3. Also shown on Figure 3-3 is the inflow and outflow volumes excluding solid tailings. Table 3-3 provides the corresponding annual total inflow and outflow volumes. The 2014 and 2025 volumes in Figure 3-3, and Table 3-3 represent totals for the periods September to December 2014 and January to March 2025.

Key observations from Table 3-3 and Figure 3-3:

- Inflow volumes generally exceed outflow volumes throughout the given period, except in 2016, 2017 & 2022, when solid tailings were excluded from the inflow volumes. In this case, the outflow marginally exceeded inflow by approximately 67,000 m^3, 49,000 m^3, and 74,000 m^3, respectively. The difference in total inflow volume between the two scenarios (with and without solid tailings) is approximately 900,000 m^3 (i.e., 917,000 m^3)
- The average annual inflow and outflow volumes (2015–2024) are approximately 1,500,000 m^3 and 1,300,000 m^3, respectively, for all water balance components. When solid tailings are excluded, the average annual inflow volume is approximately 1,400,000 m^3.
- The lowest total inflow and outflow occurred in 2020 .

DS Evex Group Limited
738 Skyview Ranch Grove NE
Calgary, AB T2N 0R9 CANADA
Tel 587.225.3699

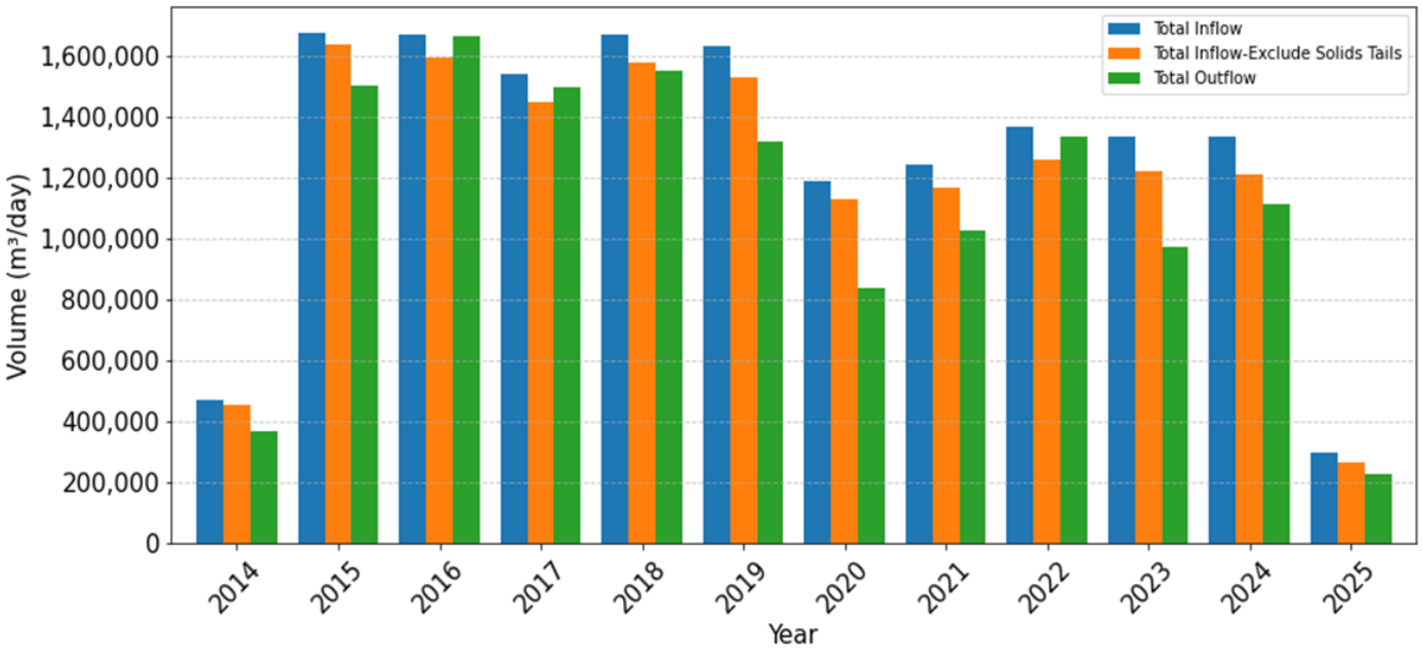

Figure 3-3: Total annual inflow and outflow volumes. (The 2014 & 2025 volumes represent totals over the periods September to December & January to March, respectively).

Table 3-3: Annual total inflow and outflow volumes.

Year	Total Inflow-Include Solids Tails (m^3)	Total Inflow-Exclude Solids Tails (m^3)	Total Outflow (m^3)
2014*	4.74E+05	4.58E+05	3.67E+05
2015	1.68E+06	1.64E+06	1.50E+06
2016	1.67E+06	1.60E+06	1.66E+06
2017	1.54E+06	1.45E+06	1.50E+06
2018	1.67E+06	1.58E+06	1.55E+06
2019	1.63E+06	1.53E+06	1.32E+06
2020	1.19E+06	1.13E+06	8.39E+05
2021	1.24E+06	1.17E+06	1.03E+06
2022	1.37E+06	1.26E+06	1.34E+06
2023	1.34E+06	1.22E+06	9.72E+05
2024	1.34E+06	1.21E+06	1.12E+06
2025*	2.97E+05	2.67E+05	2.30E+05

***Note:** The 2014 volumes represent totals over the period September to December 2014 and January to March 2025.

The predicted cumulative volumes of all water balance components are shown in Figure 3-4. Figure 3-5 illustrates the predicted total tailings solid volume available in the JEB TMF from September 1, 2014 (~1,877,000 m^3) to March 31,

2025 (~2,800,000 m³). During this period, approximately one million cubic metres (917, 000 m³) of tailings solids were deposited.

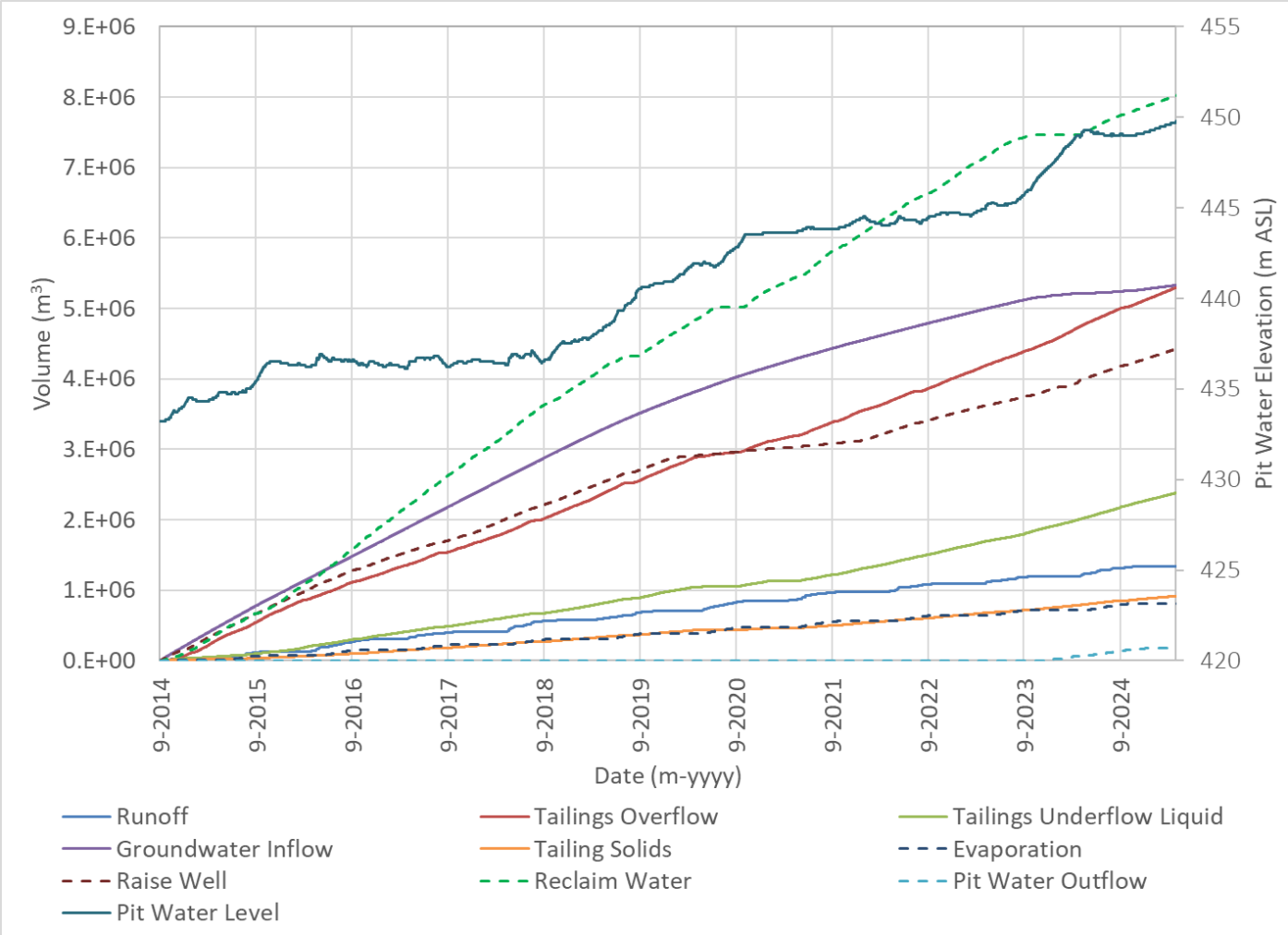

Figure 3-4: Predicted cumulative volume of water balance components into and out of JEB TMF pit from September 1, 2014 to March 31, 2025. Also shown is the predicted JEB TMF pit water level.

DS Evex Group Limited
738 Skyview Ranch Grove NE
Calgary, AB T2N 0R9 CANADA
Tel 587.225.3699

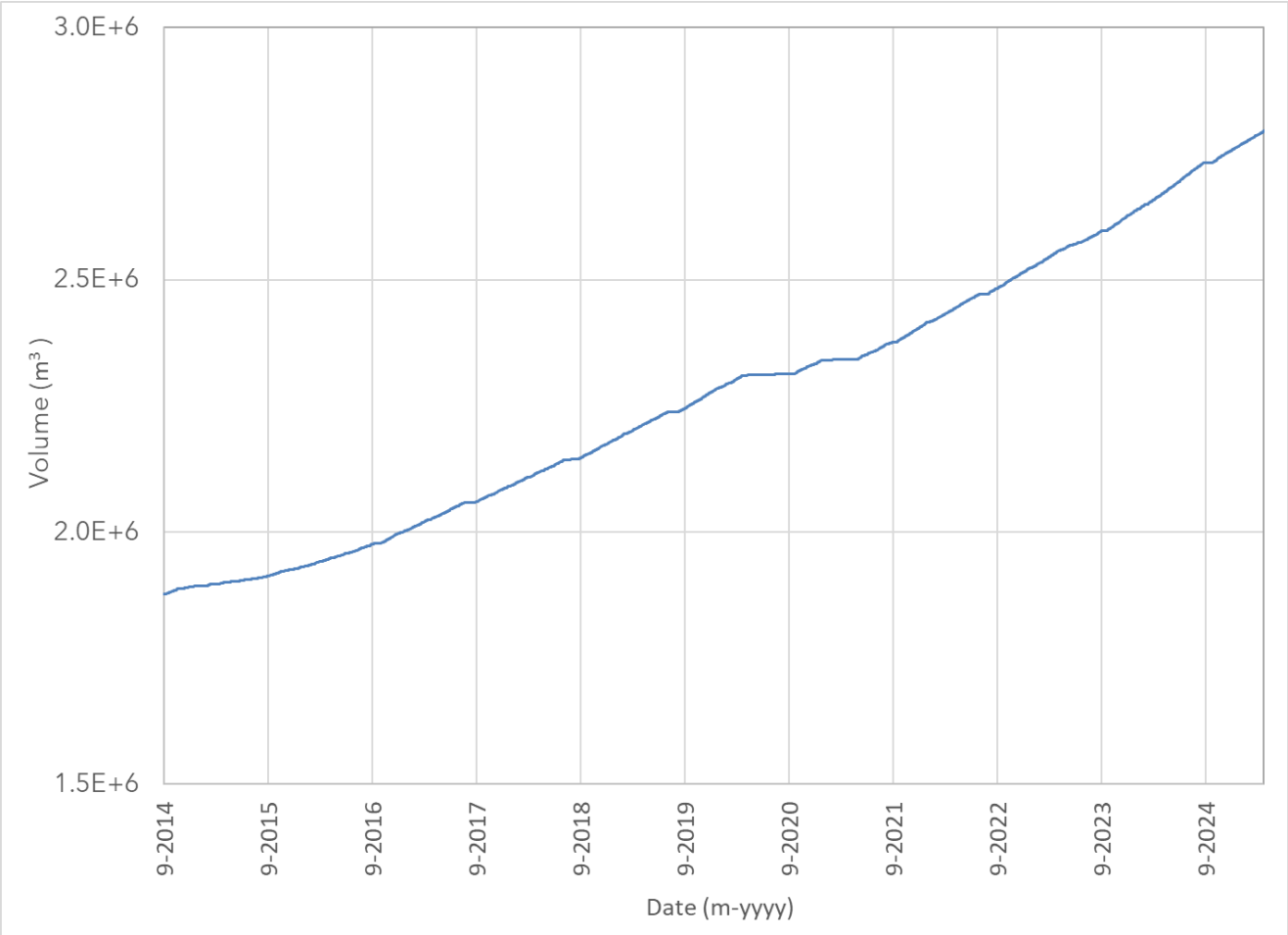

Figure 3-5: Predicted cumulative available tailings solids volume in JEB TMF pit from September 1, 2014, to March 31, 2025.

The predicted annual water balance components (inflow and outflow elements) from September 2014 to the end of 2024 are summarized in Table 3-4. Table 3-5 presents the percentage contribution of each inflow water balance component. It is important to note that the water balance components in Tables 3-4 and 3-5 include the volume of water stored (i.e., net groundwater inflow, runoff, tailings underflow & overflow liquid) at the beginning of each year, except for 2014, which reflects the model's start date of September 2014. Consequently, the percentage contributions in Table 3-5 account for the storage volume in JEB TMF pit at the start of each year. The predicted inflow and outflow components are based on average[7] precipitation values.

The storage values represent the estimated net water volume in the JEB TMF pit at the end of each year, calculated as net inflow minus outflow. Based on the model's predictions (summarized in Tables 3-4 & 3-5):

[7] Average year precipitation is based on (July) 2006 precipitation data obtained from Collins Bay.

- **End-of-Year Storage**: The net water storage in JEB TMF pit at the end of 2024 is approximately 1.6 million m³ (as shown in Table 3-4) and increasing to approximately 1.63 million m³ by the end of March 2025. On average, the water storage at the end of each year (full year; 2015 to 2024) is about 1.1 million m³.

- **Primary Inflow Sources:** Majority of natural inflow to the pit originates from groundwater, which accounts for approximately 13.6% (~500,800 m³) of all water balance components on average annually.

- **Runoff Contribution**: Annual runoff (rainfall & snowmelt) on average account for approximately 4% (~149,000 m^3) of the total water balance components (sum of inflow and outflow; Table 3-4), while evaporation contributes about 2.2%. This implies that the net average annual runoff into JEB TMF pit is approximately 1.8% (equivalent to ~68,000 m³).

- **Pit Water Outflow**: Predicted total pit water discharge from the pit into the surrounding groundwater from 2023 and 2024 was estimated to be 175,000 m^3. The annual average pit discharge for the two years is approximately 87,000 m^3, accounting for approximately 0.5% of the total water balance component.

- **Change in Storage**: The volume of water in the JEB TMF pit has increased by approximately 1.1 million m^3 from September 2014 to March 31, 2025 (Table 3-4; change in storage).

Figure 3-6 presents a time series plot of water and solid tailings in the JEB TMF pit from September 1, 2014, to March 31, 2025. It also depicts the combined volume of tailings and water present in the JEB TMF during this period. The figure indicates that by March 31, 2025, the total volume of solid tailings and water in the JEB TMF is approximately 4.4 million m³, consisting of approximately 1.6 million m³ of water and 2.8 million m³ of tailings.

DS Evex Group Limited
738 Skyview Ranch Grove NE
Calgary, AB T2N 0R9 CANADA
Tel 587.225.3699

Table 3-4: Calculated volume of water inflow and outflow for JEB TMF pit.

Year	Start of Year Water Volume (m^3)	INFLOW				Total Inflow (m^3)	OUTFLOW				Total Outflow (m^3)	Change In storage (m^3)	End of Year Water Volume (m^3)
		GW Inflow (m^3)	Runoff (m^3)	Tailings Underflow Liquid (m^3)	Tailings Overflow Liquid (m^3)		Evaporation (m^3)	Pit Water Outflow (m^3)	Reclaim Water (m3)	Raise Well (m^3)			
2014*	7.11E+05	2.69E+05	3.96E+04	3.70E+04	1.13E+05	**4.58E+05**	7.80E+03	0.00E+00	1.57E+05	201,952	**3.67E+05**	9.12E+04	8.02E+05
2015	7.91E+05	7.46E+05	1.33E+05	1.11E+05	6.51E+05	**1.64E+06**	6.65E+04	0.00E+00	7.59E+05	677,414	**1.50E+06**	1.38E+05	9.28E+05
2016	9.00E+05	7.02E+05	1.95E+05	2.16E+05	4.85E+05	**1.60E+06**	8.37E+04	0.00E+00	1.02E+06	555,149	**1.66E+06**	-6.66E+04	8.34E+05
2017	8.18E+05	6.99E+05	1.19E+05	1.91E+05	4.41E+05	**1.45E+06**	7.45E+04	0.00E+00	1.01E+06	414,786	**1.50E+06**	-4.86E+04	7.69E+05
2018	7.56E+05	6.86E+05	1.95E+05	1.88E+05	5.12E+05	**1.58E+06**	7.68E+04	0.00E+00	9.39E+05	533,722	**1.55E+06**	3.16E+04	7.88E+05
2019	7.53E+05	5.93E+05	1.36E+05	2.48E+05	5.52E+05	**1.53E+06**	8.00E+04	0.00E+00	7.45E+05	496,736	**1.32E+06**	2.06E+05	9.59E+05
2020	9.48E+05	4.72E+05	1.66E+05	1.38E+05	3.57E+05	**1.13E+06**	9.03E+04	0.00E+00	6.23E+05	126,538	**8.39E+05**	2.94E+05	1.24E+06
2021	1.22E+06	3.87E+05	1.52E+05	1.85E+05	4.47E+05	**1.17E+06**	8.55E+04	0.00E+00	8.23E+05	119,414	**1.03E+06**	1.43E+05	1.37E+06
2022	1.35E+06	3.50E+05	1.26E+05	2.98E+05	4.87E+05	**1.26E+06**	8.36E+04	0.00E+00	8.45E+05	406,746	**1.34E+06**	-7.44E+04	1.27E+06
2023	1.26E+06	2.85E+05	1.10E+05	3.09E+05	5.20E+05	**1.22E+06**	7.47E+04	2.14E+04	5.35E+05	340,140	**9.72E+05**	2.52E+05	1.51E+06
2024	1.51E+06	9.85E+04	1.44E+05	3.74E+05	5.93E+05	**1.21E+06**	8.41E+04	1.54E+05	4.37E+05	441,447	**1.12E+06**	9.28E+04	1.60E+06
2025*	1.59E+06	4.13E+04	4.60E+03	8.40E+04	1.37E+05	**2.67E+05**	0.00E+00	0.00E+00	1.20E+05	109,980	**2.30E+05**	3.73E+04	1.63E+06
Average (m^3)	**1.0E+06**	**5.0E+05**	**1.5E+05**	**2.3E+05**	**5.0E+05**	1.4E+06	**8.0E+04**	**1.7E+04**	**7.7E+05**	**4.1E+05**	1.3E+06	**9.7E+04**	**1.1E+06**

Note: * Volumes represent totals over the periods: September to December 2014, and January to March 2025.
Average values represent full-year data for the period 2015–2024.

Table 3-5: Percent contributions of water inflow and outflow for JEB TMF pit.

Year	Start of Year Water Volume (%)	GW Inflow (%)	Runoff (%)	Tailings Underflow Liquid (%)	Tailings Overflow Liquid (%)	Evaporation (%)	Pit Water Outflow (%)	Reclaim Water (%)	Raise Well Water (%)
2015*	46.3	17.5	2.6	2.4	7.4	0.5	0.0	10.2	13.2
2015	20.1	19.0	3.4	2.8	16.5	1.7	0.0	19.3	17.2
2016	21.6	16.9	4.7	5.2	11.7	2.0	0.0	24.6	13.3
2017	21.7	18.5	3.2	5.1	11.7	2.0	0.0	26.8	11.0
2018	19.5	17.6	5.0	4.8	13.2	2.0	0.0	24.2	13.7
2019	20.9	16.5	3.8	6.9	15.3	2.2	0.0	20.7	13.8
2020	32.5	16.2	5.7	4.7	12.2	3.1	0.0	21.3	4.3
2021	35.7	11.3	4.4	5.4	13.1	2.5	0.0	24.1	3.5
2022	34.2	8.9	3.2	7.6	12.3	2.1	0.0	21.4	10.3
2023	36.4	8.2	3.2	8.9	15.0	2.2	0.6	15.5	9.8
2024	39.3	2.6	3.8	9.8	15.5	2.2	4.0	11.4	11.5
2025*	76.2	2.0	0.2	4.0	6.6	0.0	0.0	5.7	5.3
Average (%)	**28.2**	**13.6**	**4.0**	**6.1**	**13.7**	**2.2**	0.5	**20.9**	**10.9**

DS Evex Group Limited
738 Skyview Ranch Grove NE
Calgary, AB T2N 0R9 CANADA
Tel 587.225.3699

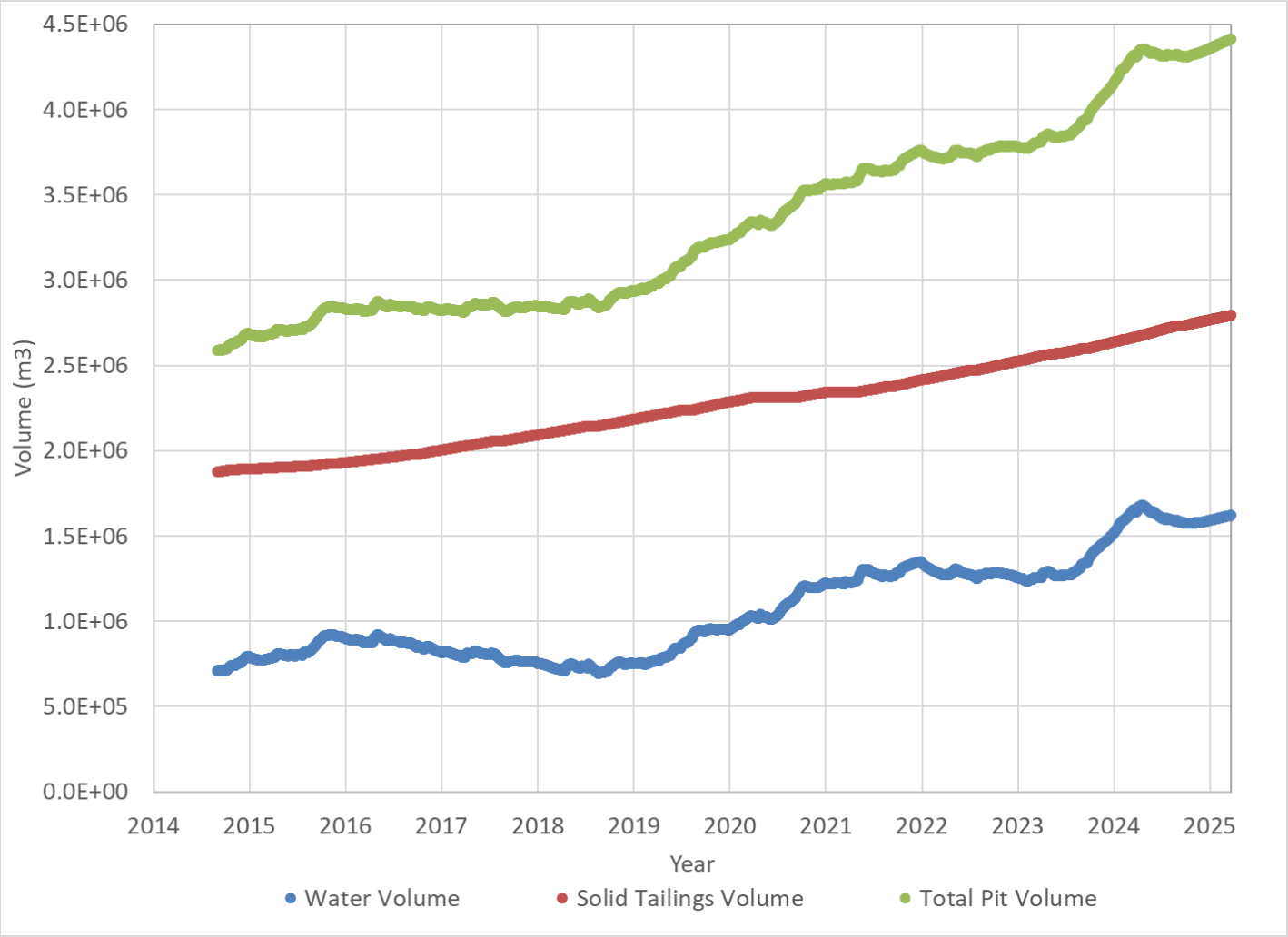

Figure 3-6: Time series plot of predicted available tailings and water in the JEB TMF from September 1, 2014, to March 31, 2025.

4.0 SUMMARY AND CONCLUSIONS

This memo presents the results of the JEB TMF water balance model using historic JEB TMF pit water level data. The model has been calibrated against measured water levels for the JEB TMF pit from September 1, 2014, to October 27, 2024. The calibrated JEB TMF pit model was used to predict water balance components (inflow and outflow) from September 1, 2014, to March 31, 2025.

The model predicts that the volume of water stored in the JEB TMF will be approximately 1.6 million cubic metres by the end of 2024. This volume is expected to increase by about 300,000 cubic metres by the end of March 2025, with the majority of natural inflow coming from groundwater. The combined volume of water and solid tailings in the JEB TMF pit increased from approximately 2.6 million cubic metres in September 1, 2014 to approximately 4.4 million cubic metres at the end of March 2025.

5.0 MODEL LIMITATIONS

A water balance model approximates a complex hydrological and hydrogeological system. The modeling process requires many assumptions to simplify the complex system. Because the model used is an approximation, the predictions made by it have uncertainties associated with them. The level of uncertainty associated with the model can be reduced by including as much valid field information (input data) as possible.

Further, the model's predictive accuracy is limited by the assumption of constant daily rates for key inflow and outflow components—including raise well pumping, reclaim barge withdrawal, tailings thickener flows, and tailings solids content—during the November 1, 2024, to March 31, 2025, period, which may not capture temporal variability or operational fluctuations.

In this study, the 2024 JEB precipitation data was identified as erroneous; therefore, precipitation data from Collins Bay, provided by ECCC, was used. The evapotranspiration values applied in the JEB TMF model were based on monthly evapotranspiration observed at the Brochet Lake, MB station, in the northern Manitoba, which may differ from actual site-specific values. Groundwater inflow to the JEB TMF pit was estimated using an analytical technique based on simplifying assumptions.

It was assumed that water from the JEB TMF pit outflows into the surrounding groundwater system whenever the pond elevation exceeds the groundwater elevations in nearfield wells completed in overburden, sandstone, and basement units near the pit. The outflow calculation is based on groundwater elevation data available from October 2023 to October 2024. During model implementation it was assumed that the calculated pit water outflow continued until December 2024 which is an uncertainty in the model.

DS Evex Group Limited
738 Skyview Ranch Grove NE
Calgary, AB T2N 0R9 CANADA
Tel 587 525 8496

6.0 LIMITATIONS OF REPORT

This report and its contents are intended for the sole use of Orano Canada Inc. (Orano) and their agents. DS Evex Group Limited does not accept any responsibility for the accuracy of any of the data, the analysis, or the conclusions contained or referenced in the report when the report is used or relied upon by any Party other than Orano, or for any Project other than the subject site. Any such unauthorized use of this report is at the sole risk of the user.

Appendix

Appendix A-Python Script for Implementing the Dupuit Approximation for Groundwater Inflow into JEB TMF Pit

```python
"""
*****************************************************************************************
* Title: Groundwater Inflow into JEB TMF Pit using Dupuit Aprroximation                 *
* Author: Seth Xeflide                                                                  *
* Company: DS Evex Group Limited                                                        *
* Date:February 7, 2025                                                                 *
* Python Version: 3.11.4
*****************************************************************************************
"""
import numpy as np
import pandas as pd
import matplotlib.pyplot as plt
import ace_tools_open as tools

# Given data
elevations = np.arange(343, 458)  # Elevations from 343 m to 457 m
diameters = np.array([
    15.08, 30.75, 34.00, 56.31, 65.38, 71.89, 74.68, 77.40, 84.02, 91.09,
    96.81, 104.94, 114.73, 122.92, 130.25, 133.93, 136.71, 138.80, 140.57,
    142.17, 143.70, 145.20, 146.67, 148.16, 149.71, 152.26, 169.78, 174.32,
    181.04, 183.13, 184.97, 186.80, 188.70, 190.91, 193.19, 194.93, 196.42,
    197.79, 199.12, 200.44, 201.78, 203.16, 204.65, 206.55, 210.03, 212.76,
    214.83, 219.86, 224.14, 228.65, 234.18, 239.72, 244.85, 250.14, 256.78,
    261.52, 263.59, 265.02, 266.30, 267.51, 268.66, 269.81, 270.96, 272.13,
    273.35, 274.69, 276.28, 278.63, 281.98, 283.78, 285.19, 286.46, 287.63,
    288.78, 289.93, 291.13, 292.40, 293.79, 296.97, 302.20, 304.68, 307.88,
    310.66, 313.77, 320.11, 324.14, 327.15, 330.21, 332.93, 342.52, 357.03,
    363.82, 365.79, 367.66, 369.74, 372.48, 378.86, 399.31, 404.40, 409.42,
    415.90, 422.02, 427.74, 434.82, 442.95, 447.24, 462.20, 470.71, 472.61,
    475.02, 491.77, 497.70, 503.85, 511.04, 516.51
])

# Convert diameters to radii
radii = diameters / 2
```


DS Evex Group Limited
738 Skyview Ranch Grove NE
Calgary, AB T2N 0R9 CANADA
Tel 587.225.3699

```
35
36 # Define the revised geologic parameters
37 geologic_units = {
38     "Overburden": {"thickness": 13.36, "K": 7.32E-07, "h0": 455.663},
39     "Upper Sandstone": {"thickness": 22.50, "K": 1.98866E-07, "h0": 454.394},
40     "Lower Sandstone": {"thickness": 66.96, "K": 5.29968E-07, "h0": 452.705},
41     "Basement": {"thickness": 100, "K": 4.47003E-08, "h0": 451.937}
42
43
44 }
45
46 # Define analytical solution for groundwater inflow into a circular pit
47 def groundwater_inflow(r, h, K, h0):
48     """Estimate groundwater inflow into a pit using Dupuit's assumptions."""
49     if h < h0:  # Only inflow if the pit is below the initial water table
50         return (2 * np.pi * K * (h0**2 - h**2)) / np.log(r / 0.1)  # using reference well at r=0.1m
51     return 0
52
53 # Compute inflow for each depth
54 inflow_rates = []
55 for i, h in enumerate(elevations):
56     total_inflow = 0
57     for unit in geologic_units.values():
58         K = unit["K"]
59         h0 = unit["h0"]
60         inflow = groundwater_inflow(radii[i], h, K, h0)
61         total_inflow += inflow
62     inflow_rates.append(total_inflow)
63
64 # Convert inflow to m³/day
65 inflow_rates = np.array(inflow_rates) * 86400  # Convert m³/s to m³/day
66
67 # Create DataFrame for results
68 df_results = pd.DataFrame({
69     "Elevation (m)": elevations,
70     "Pit Radius (m)": radii,
71     "Groundwater Inflow (m³/day)": inflow_rates
72 })
73
74 # Display results
75 tools.display_dataframe_to_user(name="Updated Groundwater Inflow Estimates", dataframe=df_results)
76
77 # Plot the results
78 plt.figure(figsize=(10, 5))
79 plt.plot(df_results["Elevation (m)"], df_results["Groundwater Inflow (m³/day)"], marker="o", linestyle="-")
80 plt.xlabel("Elevation (m)")
81 plt.ylabel("Groundwater Inflow (m³/day)")
82 plt.title("Groundwater Inflow with Revised Hydraulic Parameters")
83 plt.grid()
84 plt.show()
```

Appendix

Appendix B-Groundwater and JEB TMF Pit Elevations and Distance Information for Darcy Flow Calculation

Table B-1: Groundwater Elevation and Pit Elevation used to Calculate Groundwater Flow

Well ID	Date	Hydraulic Head (masl)	Geologic Unit	Tailing Pond Elevation (masl)
95-05D	2023-10-08	445.290	Overburden	445.913
95-03C	2023-10-08	445.739	Overburden	445.913
95-02D	2023-10-08	450.519	Overburden	445.913
18-01D	2023-10-08	452.607	Overburden	445.913
TW08	2023-11-10	445.777	Lower Standstone	446.486
95-01B	2023-11-10	450.985	Lower Standstone	446.486
95-02B	2023-11-10	445.857	Lower Standstone	446.486
95-03B	2023-11-10	445.737	Lower Standstone	446.486
95-04B	2023-11-10	445.903	Lower Standstone	446.486
95-05B	2023-11-10	446.377	Lower Standstone	446.486
95-05D	2023-12-01	445.183	Overburden	446.923
95-03C	2023-12-01	445.613	Overburden	446.923
95-02D	2023-12-01	450.519	Overburden	446.923
18-01D	2023-12-01	452.607	Overburden	446.923
95-04C	2023-12-01	445.545	Upper Sandstone	446.923
95-05C	2023-12-01	445.955	Upper Sandstone	446.923
95-01C	2023-12-01	450.972	Upper Sandstone	446.923
95-02C	2023-12-01	447.398	Upper Sandstone	446.923
TW08	2023-12-01	446.206	Lower Standstone	446.923
95-01B	2023-12-01	451.057	Lower Standstone	446.923
95-02B	2023-12-01	445.868	Lower Standstone	446.923
95-03B	2023-12-01	445.893	Lower Standstone	446.923
95-04B	2023-12-01	446.063	Lower Standstone	446.923
95-05B	2023-12-01	446.556	Lower Standstone	446.923
95-01A	2023-12-01	450.687	Basement	446.923
95-02A	2023-12-01	445.739	Basement	446.923
95-03A	2023-12-01	445.935	Basement	446.923
95-04A	2023-12-01	445.998	Basement	446.923
95-05A	2023-12-01	447.325	Basement	446.923
TW08	2024-01-07	446.873	Lower Standstone	447.598
95-02B	2024-01-07	445.897	Lower Standstone	447.598
95-03B	2024-01-07	446.338	Lower Standstone	447.598
95-04B	2024-01-07	446.604	Lower Standstone	447.598
95-01B	2024-01-07	451.265	Lower Standstone	447.598
95-05D	2024-02-05	445.298	Overburden	448.100
95-03C	2024-02-05	445.553	Overburden	448.100
95-04D	2024-02-05	446.857	Overburden	448.100
95-02D	2024-02-05	450.429	Overburden	448.100
18-01D	2024-02-05	452.298	Overburden	448.100
95-04C	2024-02-05	445.599	Upper Sandstone	448.100
95-05C	2024-02-05	446.997	Upper Sandstone	448.100
95-02C	2024-02-05	447.424	Upper Sandstone	448.100
95-01C	2024-02-05	450.972	Upper Sandstone	448.100
TW08	2024-02-05	446.805	Lower Standstone	448.082
95-02B	2024-02-05	451.101	Lower Standstone	448.082
95-03B	2024-02-05	446.245	Lower Standstone	448.082
95-04B	2024-02-05	446.285	Lower Standstone	448.082
95-05B	2024-02-05	447.414	Lower Standstone	448.082
95-01B	2024-02-05	445.827	Lower Standstone	448.082
95-01A	2024-02-05	450.749	Basement	448.100
95-02A	2024-02-05	446.010	Basement	448.100
95-03A	2024-02-05	446.206	Basement	448.100
95-04A	2024-02-05	446.197	Basement	448.100
95-05A	2024-02-05	447.433	Basement	448.100
18-01D	2024-02-05	452.298	Basement	448.100
TW08	2024-03-01	447.226	Lower Standstone	448.505
95-02B	2024-03-01	445.896	Lower Standstone	448.505
95-04B	2024-03-01	446.641	Lower Standstone	448.505
95-01B	2024-03-01	451.276	Lower Standstone	448.505
TW08	2024-04-04	447.994	Lower Standstone	449.067
95-02B	2024-04-04	445.898	Lower Standstone	449.067
95-01B	2024-04-04	451.431	Lower Standstone	449.067
95-03C	2024-06-01	446.320	Overburden	449.234
95-02D	2024-06-01	450.339	Overburden	449.234
18-01D	2024-06-01	452.790	Overburden	449.234
95-05D	2024-06-01	446.120	Overburden	449.234
95-02C	2024-06-01	447.806	Upper Sandstone	449.234
95-01C	2024-06-01	451.375	Upper Sandstone	449.234
95-04C	2024-06-01	446.223	Upper Sandstone	449.234
95-02C	2024-06-01	447.806	Upper Sandstone	449.234
TW08	2024-07-03	447.935	Lower Standstone	448.082
95-02B	2024-07-03	446.388	Lower Standstone	448.082
95-03B	2024-07-03	446.980	Lower Standstone	448.082
95-04B	2024-07-03	446.930	Lower Standstone	448.082
95-05B	2024-07-03	447.618	Lower Standstone	448.082
95-01B	2024-07-03	451.658	Lower Standstone	448.082
95-02D	2024-08-10	452.048	Overburden	449.162
95-03C	2024-08-10	446.296	Overburden	449.162
95-04D	2024-08-10	446.832	Overburden	449.162
95-05D	2024-08-10	445.592	Overburden	449.162
95-02C	2024-08-10	448.086	Upper Sandstone	449.170
95-01C	2024-08-10	451.624	Upper Sandstone	449.170
95-04C	2024-08-10	446.446	Upper Sandstone	449.170
95-02C	2024-08-10	448.086	Upper Sandstone	449.170
95-01A	2024-08-10	450.564	Basement	449.162
95-02A	2024-08-10	446.521	Basement	449.162
95-03A	2024-08-10	446.815	Basement	449.162
95-04A	2024-08-10	446.850	Basement	449.162
95-02D	2024-08-10	452.048	Overburden	449.143
18-01D	2024-08-12	453.081	Overburden	449.162
TW08	2024-08-12	447.850	Lower Standstone	449.162
95-02B	2024-08-12	446.482	Lower Standstone	449.162
95-03B	2024-08-12	446.852	Lower Standstone	449.162
95-04B	2024-08-12	446.931	Lower Standstone	449.162
95-05B	2024-08-12	447.615	Lower Standstone	449.162
95-01B	2024-08-12	451.680	Lower Standstone	449.162
18-01D	2024-08-12	453.081	Overburden	449.143
95-03C	2024-08-31	446.296	Overburden	449.143
95-04D	2024-08-31	446.832	Overburden	449.143
95-05D	2024-08-31	445.455	Overburden	449.143
TW08	2024-09-08	448.390	Lower Standstone	449.109
95-02B	2024-09-08	446.480	Lower Standstone	449.109
95-03B	2024-09-08	447.052	Lower Standstone	449.109
95-04B	2024-09-08	447.406	Lower Standstone	449.109
95-05B	2024-09-08	448.188	Lower Standstone	449.109
95-01B	2024-09-08	451.883	Lower Standstone	449.109
TW08	2024-10-17	448.390	Lower Standstone	448.935
95-02B	2024-10-17	446.300	Lower Standstone	448.935
95-03B	2024-10-17	446.828	Lower Standstone	448.935
95-04B	2024-10-17	446.892	Lower Standstone	448.935
95-05B	2024-10-17	447.366	Lower Standstone	448.935
95-01B	2024-10-17	451.636	Lower Standstone	448.935

DS Evex Group Limited
738 Skyview Ranch Grove NE
Calgary, AB T2N 0R9 CANADA
Tel 587.225.3699

Table B-2: Distance Between Nearfield Wells and JEB TMF Pit

Well ID	Distance (m)
95-01A	192.98
95-01B	201.8
95-01C	206.8
18-01D	212.12
95-02A	221.28
95-02B	213.61
95-02C	208.21
95-02D	203.5
95-03A	131.97
95-03B	139.35
95-03C	140.17
95-04A	157.86
95-04B	156.67
95-04C	156.72
95-04D	156.89
95-05A	115.36
95-05B	109.57
95-05C	108.9
95-05D	106.55
TW08	50

Appendix C-Python Script for Implementing the Darcy Approximation for Groundwater Inflow into JEB TMF Pit

```python
"""
*****************************************************************************************
* Title: Groundwater Inflow into JEB TMF Pit using Darcy Law                            *
* Author: Seth Xeflide                                                                   *
* Company: DS Evex Group Limited                                                         *
* Date:February 7, 2025                                                                  *
* Python Version: 3.11.4                                                                 *
*****************************************************************************************
"""

import pandas as pd
import numpy as np
import matplotlib.pyplot as plt
from scipy.interpolate import interp1d
import ace_tools_open as tools

# Load the dataset
file_path = "E:\\JEB_PIT_INFLOW\Book7.xlsx"
xls = pd.ExcelFile(file_path)
df = pd.read_excel(xls, sheet_name='Sheet1 (2)')

# Clean column names
df.columns = df.columns.str.strip()

# Define well distances
well_distances = {
    "95-01A": 192.98, "95-01B": 201.8, "95-01C": 206.8, "18-01D": 212.12,
    "95-02A": 221.28, "95-02B": 213.61, "95-02C": 208.21, "95-02D": 203.5,
    "95-03A": 131.97, "95-03B": 139.35, "95-03C": 140.17, "95-04A": 157.86,
    "95-04B": 156.67, "95-04C": 156.72, "95-04D": 156.89, "95-05A": 115.36,
    "95-05B": 109.57, "95-05C": 108.9, "95-05D": 106.55, "TW08": 50
}

```


DS Evex Group Limited
738 Skyview Ranch Grove NE
Calgary, AB T2N 0R9 CANADA
Tel 587.225.3699

```
# Define hydraulic conductivity values
geologic_units = {
    "Overburden": 7.32E-07,
    "Upper Sandstone": 1.98866E-07,
    "Lower Sandstone": 5.29968E-07,
    "Basement": 4.47003E-08
}

# Map distances and hydraulic conductivities
df["Distance (m)"] = df["Well ID"].map(well_distances)
df["Hydraulic Conductivity (m/s)"] = df["Geologic Unit"].map(geologic_units)

df = df.dropna(subset=["Distance (m)", "Hydraulic Conductivity (m/s)"])

# Define pit elevation and diameter
diameters = [
    (343, 15.08), (344, 30.75), (345, 34.00), (346, 56.31), (347, 65.38), (348, 71.89),
    (349, 74.68), (350, 77.40), (351, 84.02), (352, 91.09), (353, 96.81), (354, 104.94),
    (355, 114.73), (356, 122.92), (357, 130.25), (358, 133.93), (359, 136.71), (360, 138.80),
    (361, 140.57), (362, 142.17), (363, 143.70), (364, 145.20), (365, 146.67), (366, 148.16)
]

pit_df = pd.DataFrame(diameters, columns=["Elevation (masl)", "Diameter (m)"])
interp_func = interp1d(pit_df["Elevation (masl)"], pit_df["Diameter (m)"], kind="linear", fill_value="extrapolate")
df["Interpolated Diameter (m)"] = interp_func(df["Tailing Pond Elevation (masl)"])
df["Pit Radius (m)"] = df["Interpolated Diameter (m)"] / 2

# Define model domain
model_domain_size = 500  # 0.5 km by 0.5 km

df["Cross-Sectional Area (m²)"] = model_domain_size * df["Interpolated Diameter (m)"]
df["Hydraulic Gradient"] = (df["Groundwater Elevation (masl)"] - df["Tailing Pond Elevation (masl)"]) / df["Distance (m)"]

# Apply Darcy's Law for linear flow
df["Q (m³/s)"] = df["Hydraulic Conductivity (m/s)"] * df["Cross-Sectional Area (m²)"] * df["Hydraulic Gradient"]
df["Q (m³/day)"] = df["Q (m³/s)"] * 86400

# Consolidate inflow/outflow
total_flow = df.groupby("Date")["Q (m³/day)"].sum().reset_index()

# Display results
tools.display_dataframe_to_user(name="Groundwater Inflow/Outflow (Linear Flow Assumption)", dataframe=total_flow)

# Plot results
plt.figure(figsize=(10, 5))
plt.plot(total_flow["Date"], total_flow["Q (m³/day)"], marker='o', linestyle='-', label="Groundwater Flow")
plt.xlabel("Date")
plt.ylabel("Groundwater Flow (m³/day)")
plt.title("Groundwater Inflow/Outflow Over Time")
plt.axhline(0, color='black', linestyle='--', linewidth=1)
plt.xticks(rotation=45)
plt.legend()
plt.grid(True)
plt.show()
```

REPORT

Groundwater Flow and Solute Transport Modelling Update - 2025

JEB TMF Expansion Project

Submitted to:

Orano Canada Inc.

817 - 45th Street West
Saskatoon, SK S7K 3X5

Submitted by:

WSP Canada Inc.

CA0051344.8282-001-R-RevA-GW Model Update

June 9, 2025

Distribution List

1 Electronic Copy - Orano Canada Inc.

1 Electronic Copy - WSP

Table of Contents

1 INTRODUCTION 5

2 BACKGROUND 5

2.1 JEB Pit 5

2.2 Hydrostratigraphic Units 8

2.3 Groundwater Flow Directions 9

3 NUMERICAL MODEL 14

3.1 Selection of Model Code 14

3.2 Finite Element Mesh 14

3.3 Hydrostratigraphy and Model Parameters 14

3.4 Boundary Conditions 15

3.5 Model Calibration Check 23

3.5.1 Calibration Scenarios and Model Setup 23

3.5.2 Calibration Check - Operational Pumping Scenarios 23

3.5.3 Calibration Check – Pumping Test Trial 28

4 OPERATIONAL AND POST CLOSURE PREDICTIONS 30

4.1 Full Build Capacity 30

4.2 Post Closure 31

4.2.1 Post Closure Scenarios 31

4.2.2 Results 31

5 SOLUTE TRANSPORT PREDICTIONS 35

5.1 Methods 35

5.2 Source Characterization 35

5.3 Solute Transport 36

5.3.1 Source Term Model 37

5.3.1.1 Input Parameters 40

5.3.2 Solute Transport Solution 41

5.3.2.1 Input Parameters 42

5.4 Results....44

6 SUMMARY AND CONCLUSIONS....1

APPENDIX A
Predicted Seepage Migration Pathways (Particle Tracking Analysis)

APPENDIX A
Predicted Seepage Migration Pathways (Particle Tracking Analysis)

APPENDIX A
Predicted Seepage Migration Pathways (Particle Tracking Analysis)

APPENDIX A
Predicted Seepage Migration Pathways (Particle Tracking Analysis)

APPENDIX A
Predicted Seepage Migration Pathways (Particle Tracking Analysis)

TABLES

Table 1: Summary of Groundwater Inflow to Operation Sump and Dewatering Wells....8

Table 2: Summary of Hydraulic Conductivity Test Results (based on Tremblay 2006) 9

Table 3: Summary of Calibrated Hydraulic Conductivity Values 15

Table 4: Predicted versus Measured Inflows to Operation Sump and Dewatering Wells 24

Table 5: Predicted versus Measured Hydraulic Head 27

Table 6: Field Trial Pumping Test Summary....28

Table 7: Comparison of Modelled Flow Rates to Field Trial Pumping Test Observation 29

Table 8: Predicted Long-Term Solute Concentrations in Tailings Pore Water....36

Table 9: Source Term Model Input Parameters 40

Table 10: Solute Transport Calculation Input Parameters 44

Table 11: Solute Transport Sensitivity Analysis Inputs....44

Table 12: Expanded JEB TMF Predicted Peak Mass Flux 46

Table 13: Expanded JEB TMF Predicted Receptor Surface Water Quality....47

Table 14: Expanded JEB TMF Upper Bound Receptor Surface Water Quality....48

FIGURES

Figure 1: Site Location and Topography 6
Figure 2: JEB Pit Contour Plan and Location of Dewatering Wells 7
Figure 3: JEB TMF Monitoring Well Location Plan 11
Figure 4: Measured Pre-mining Head Contours in Overburden 12
Figure 5: Measured Pre-mining Head Contours in Sandstone 13
Figure 6: Finite Element Mesh 17
Figure 7: Boundary Conditions 18
Figure 8: Inferred Regional Faults 19
Figure 9: Hydraulic Conductivity - Overburden 20
Figure 10: Hydraulic Conductivity – Upper Sandstone 21
Figure 11: Hydraulic Conductivity – Lower Sandstone 22
Figure 12: Measured vs Predicted Hydraulic Heads - Pre-Mining and Full Dewatered Conditions 25
Figure 13: Measured vs Predicted Hydraulic Heads – 426.75 m Pond Elevation Level 26
Figure 14: Predicted Advective Contaminant Transport Pathways from the Tailings Management Facility – Post Closure 33
Figure 15: Water Balance Components of the JEB TMF 34
Figure 16: Conceptual Source Term Model 39
Figure 17: Sensitivity Analysis Results for Uranium 49
Figure 18: Predicted and Bounding Case Long Term Effects to Fox Lake 50
Figure 19: Mass Flux to Receptors vs Time 51

APPENDICES

APPENDIX A
Predicted Seepage Migration Pathways (Particle Tracking Analysis)

1 INTRODUCTION

This report presents the results of an updated hydrogeologic assessment of the JEB Tailings Management Facility (TMF) (Figure 1) on behalf of Orano Canada Inc. (Orano). The objectives of the work were to estimate groundwater inflow to the TMF that may occur during operation of the TMF, to assess if seepage through the TMF during operations would discharge to the TMF drain at the base of the tailings, and to assess the solute transport pathways from the TMF under post closure conditions.

The assessment presented in this report expands on work previously conducted in support of the JEB TMF (Areva 2016, Golder 2019, Golder 2021). The work utilizes an existing groundwater model that was developed and calibrated to measured site operational data. As part of this assessment, the model was updated to reflect a revised interpretation of regional faults and updated tailings source concentrations, both of which were provided to WSP by Orano. As the changes in the regional faults do not affect the local geology near the JEB TMF, incorporation of these revised regional faults had negligible influence on model predictions.

2 BACKGROUND

The conceptual hydrogeological model for the TMF has been developed as part of previous hydrogeological assessments (COGEMA 2004; Golder 2009: Golder 2019). This understanding of site conditions was used in the creation of local and regional scale numerical models that have been used to assess groundwater conditions around several tailings pits, including the JEB TMF (AREVA 2011b, Golder 2019). A summary of the key features in the conceptual model is provided below.

2.1 JEB Pit

The mining of the JEB pit began in October 1995 with overburden stripping, and it continued through to the completion of ore mining in July 1997. The JEB pit is approximately 120 m deep from the lowest point at the bottom of the pit (342 m ASL) to natural ground surface near the raise pump house (462 m ASL). The dimensions of the top of the pit are approximately 350 m in the north-south direction and 460 m in the east-west direction.

During mining operations, pit dewatering was accomplished using a combination of perimeter dewatering wells and an operation sump at the base of the pit (in-pit sump dewatering). Figure 2 shows the JEB pit contour plan and former locations of dewatering wells. The purpose of the dewatering system was to intercept clean groundwater before it enters the pit and to control water levels within the TMF. Any water that seeps past the dewatering ring was collected by the operation sump and pumped to treatment. Pumping rates varied significantly among the dewatering wells, from 0 cubic metres per day (m^3/day) up to 956 m^3/day.

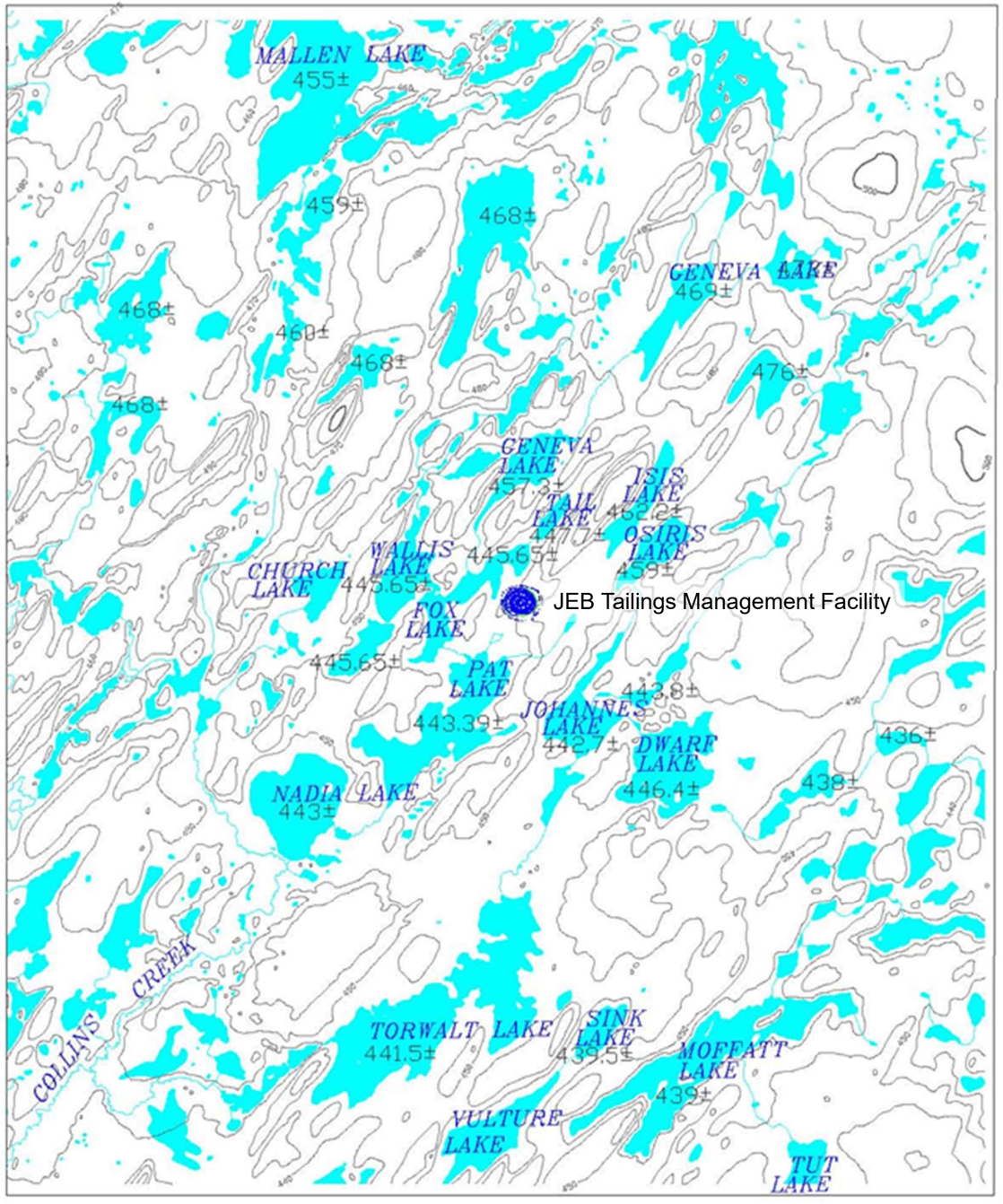

CLIENT orano

CONSULTANT wsp

YYYY-MM-DD	2025-05-01
PREPARED	KJ
DESIGNED	KJ
REVIEWED	
APPROVED	

PROJECT
JEB TMF
GROUNDWATER FLOW AND SOLUTE TRANSPORT

TITLE
SITE LOCATION AND TOPOGRAPHY

PROJECT NO.	PHASE	REV.	FIGURE
CA0051344.8282	4000	A	**1**

IF THIS MEASUREMENT DOES NOT MATCH WHAT IS SHOWN, THE SHEET SIZE HAS BEEN MODIFIED FROM: ANSI B

0 25mm

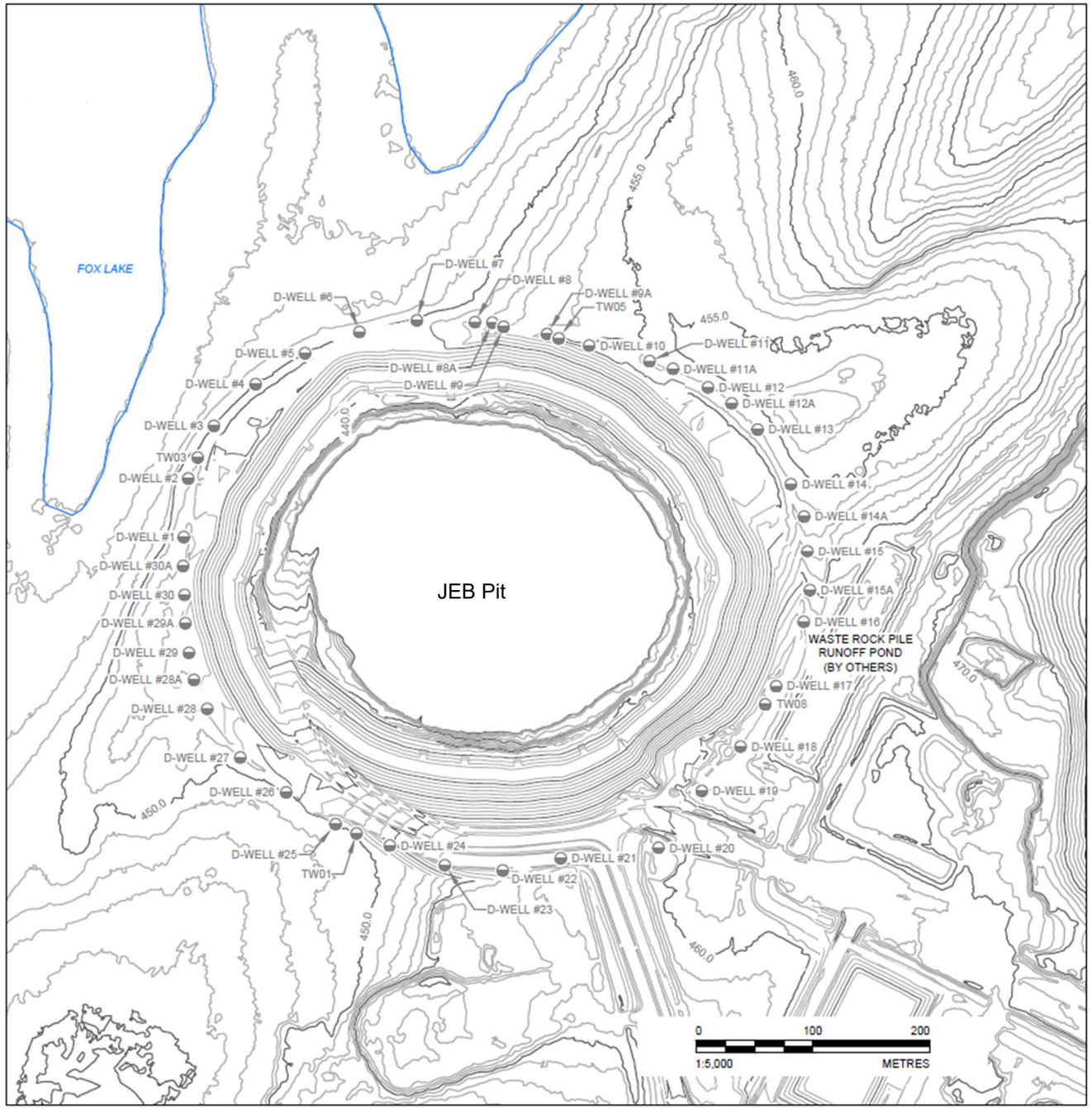

CLIENT

orano

CONSULTANT

wsp

YYYY-MM-DD	2025-05-01
PREPARED	KJ
DESIGNED	KJ
REVIEWED	
APPROVED	

PROJECT

JEB TMF
GROUNDWATER FLOW AND SOLUTE TRANSPORT

TITLE

JEB PIT CONTOUR PLAN AND LOCATION OF DEWATERING WELLS

PROJECT NO.	PHASE	REV.	FIGURE
CA0051344.8282	4000	A	**2**

IF THIS MEASUREMENT DOES NOT MATCH WHAT IS SHOWN, THE SHEET SIZE HAS BEEN MODIFIED FROM: ANSI B

25 mm

0

During operations, the TMF pond water level was maintained at a given working level for extended periods of time and adjusted periodically as required to provide additional volume for tailings placement. The hydraulic head in the drain at the bottom of the pit was maintained at or slightly below the TMF pond water level by pumping water from the dewatering drift via the raise wells.

Daily dewatering rates were collected since the beginning of mining operations in March 1996 and throughout TMF operations to the present. Groundwater inflow into the pit was estimated by performing a water balance for the facility based on monitored inflows and outflows, estimated precipitation runoff, evaporation from the TMF pond, and the change in storage within the TMF (COGEMA 2005). The groundwater inflow to the TMF, calculated from the water balance, varied in a narrow range, from 2,300 m^3/day (fully dewatered) to 1,200 m^3/day (pond elevation of 426.75 m ASL). Table 1 presents a summary of groundwater collected by the dewatering wells as well as that reporting to the TMF. Total groundwater inflow to the dewatering wells and TMF varied from 10,700 m^3/day (fully dewatered) to 4,000 m^3/day (pond elevation of 426.75 m).

Table 1: Summary of Groundwater Inflow to Operation Sump and Dewatering Wells

Operational Conditions	Period		Dewatering Rates (m^3/day)		
	From	To	Inflow to Dewatering Wells	Inflow to TMF Operation Sump	Total Groundwater Inflow
Fully Dewatered	1 May 1998	1 May 1999	8,400	2,300	10,700
Pond 374.0 m	30 June 1999	10 September 1999	7,300	2,600	9,900
Pond 392.5 m	13 August 2000	30 April 2002	6,300	2,300	8,600
Pond 410.0 m	15 October 2002	6 May 2006	4,300	2,600	6,900
Pond 426.75 m	1 July 2007	30 June 2009	2,800	1,200	4,000

m^3/day = cubic metres per day.

2.2 Hydrostratigraphic Units

The general hydrostratigraphy encountered at the JEB TMF area, in descending order of elevation, includes the following units:

- Overburden;
- Upper Sandstone;
- Lower Sandstone;
- Basement Regolith; and
- Intact Basement.

The overburden, approximately 5 to 20 m thick, is heterogeneous with hydraulic conductivity varying by several orders of magnitude from one location to another depending on the clay content and the abundance of boulders and large cobbles.

The sandstone unit, approximately 60 to 200 m thick, has a relatively low permeability matrix, but is fractured on both the local and regional scales. At the scale of a few meters, the sandstone unit likely behaves as a fractured media for flow with hydraulic contrasts governed by the properties of a few fractures. For larger scales (10s to 100s of meters), the fracture density and the connection between fractures appear to be high enough that the

sandstone behaves as equivalent porous media (Tremblay 2006). On this larger scale, there appears to be a contrast in bulk hydraulic conductivity between the upper and lower part of the sandstone. At locations where it is less permeable due to a finer matrix and less open fractures, the upper sandstone can act as an aquitard or semi-confining layer separating the more permeable overburden aquifer and the underlying more permeable lower sandstone. In contrast, at locations where it is more permeable, the upper sandstone can act as an aquifer bounded vertically by the less permeable overburden and the underlying less permeable lower sandstone. Both the upper and lower units of the sandstone are affected by major faults that influence the distribution of hydraulic heads.

The basement rock includes a variety of crystalline rocks. Overlying the more competent basement rock is a layer of paleo-weathered basement rock (regolith). The thickness of the regolith varies from a few metres to approximately 50 m. In general, the regolith has permeability much lower than the sandstone, either equal or slightly greater than the permeability of the basement.

Several testing programs have been undertaken since 1989 to characterize the hydraulic properties of the various hydrostratigraphic units in the JEB TMF area. Laboratory and field tests conducted include laboratory falling head testing, single borehole packer tests, single borehole response tests, and pumping tests. Table 2 presents a summary of hydraulic conductivity testing for the JEB area.

Table 2: Summary of Hydraulic Conductivity Test Results (based on Tremblay 2006)

Description	Hydraulic Conductivity (m/s) Pumping Test	Hydraulic Conductivity (m/s) Single Well Response Tests	
		Range[£]	Average[¥]
Overburden	1×10^{-7}	10^{-7} to 10^{-4}	2×10^{-6}
Upper Sandstone	1×10^{-5}	10^{-8} to 10^{-5}	4×10^{-7}
Lower Sandstone		10^{-8} to 10^{-4}	2×10^{-6}
Basement Regolith	-	10^{-9} to 10^{-5}	2×10^{-7}
Basement	-		$<10^{-8}$

[£] based on Packer and Slug Test Results.

[¥] geometric mean.

m/s = metres per second.

2.3 Groundwater Flow Directions

The topography of the JEB area was formed by tectonics, glacial depositions of tills, sands and gravels, and differential weathering. The relief of the area is defined by muskeg-covered, poorly drained terrain. Near the JEB pit, the muskeg layer is generally 1.0 to 1.5 m thick (AREVA 2011b). The lowest elevation corresponds to Pat Lake at approximately 443.5 m ASL, while the highest elevation corresponds to two drumlins at approximately 470 m ASL, located directly to the northeast and southeast of the JEB pit.

Near the JEB TMF, ground elevation varies from 450 to 460 m ASL. The JEB area includes a series of lakes, including Fox, Pat, Isis, Osiris, and Johannes lakes, which influence both surface water and groundwater flow.

Figure 3 shows locations of the piezometers and monitoring wells installed in the overburden and bedrock surrounding the JEB TMF. In general, hydraulic head data were collected monthly across a network of piezometers and/or monitoring wells surrounding the JEB TMF.

The interpreted pre-mining hydraulic head distributions within the overburden and lower sandstone units are presented in Figure 4 and Figure 5, respectively. Local topographic features are the main control for the flow of shallow groundwater within the overburden units. In general, the direction of shallow groundwater flow in the JEB area is inferred to be east to west, with recharge in highlands and discharging to low lying bogs and lakes such as Fox Lake and Pat Lake. Deep groundwater flow is influenced to a greater degree by regional topographic and stratigraphic features. The topography is poorly drained and slopes gently to the south from the JEB area to Collins Creek. The surface of the basement rock confining unit slopes significantly to the south from the JEB TMF. Head contours shown in Figure 5 indicate the southerly flow of deep groundwater from the JEB TMF toward Collins Creek, indicating strong influence of the structural base of the sandstone on deep groundwater flow (Tremblay 2006).

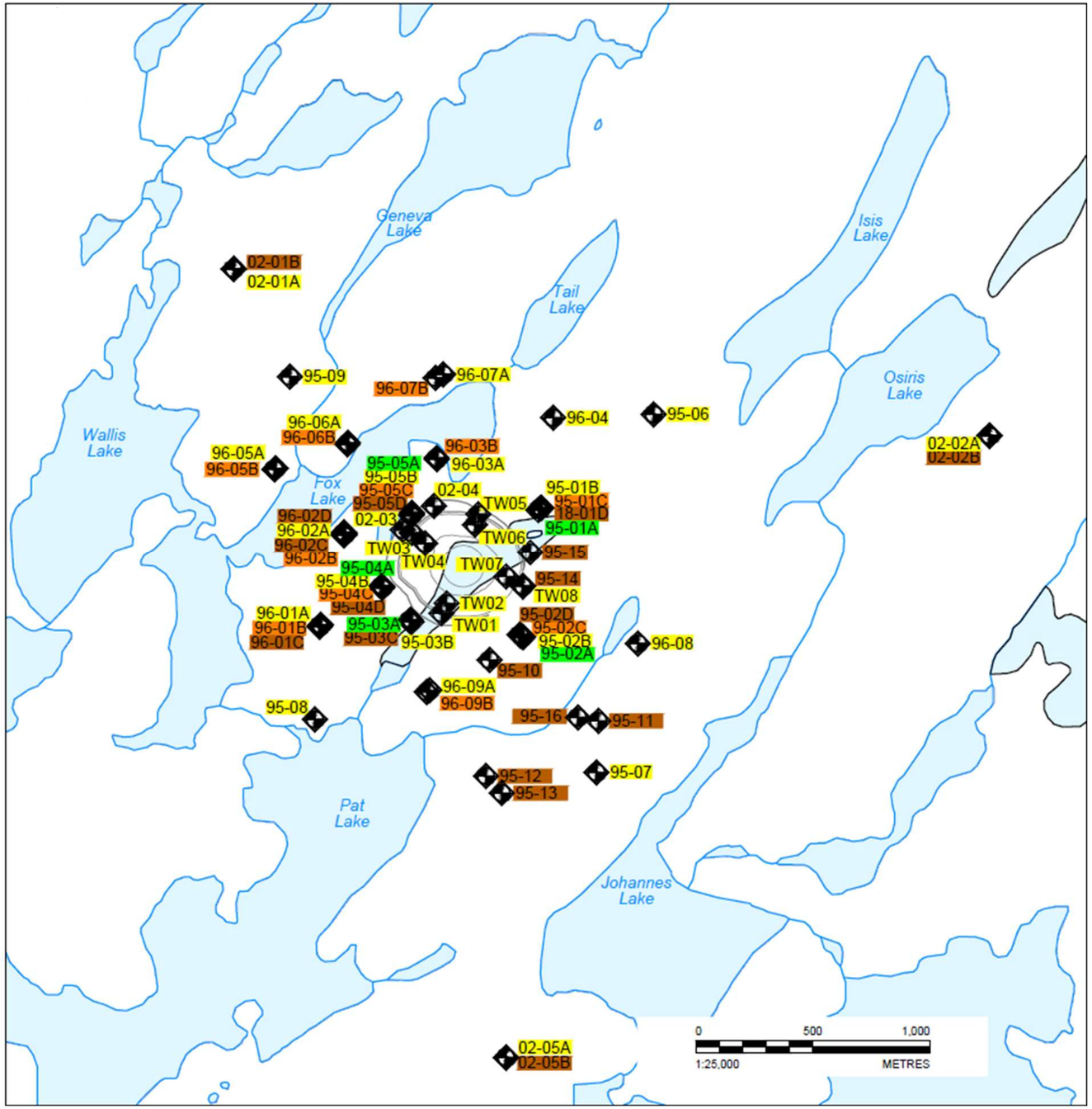

LEGEND

- MONITORING WELL
- HYDROSTRATIGRAPHIC UNIT - OVERBURDEN
- HYDROSTRATIGRAPHIC UNIT - UPPER SANDSTONE
- HYDROSTRATIGRAPHIC UNIT - LOWER SANDSTONE
- HYDROSTRATIGRAPHIC UNIT - BASEMENT

CLIENT: orano

CONSULTANT: wsp

YYYY-MM-DD	2025-05-01
PREPARED	KJ
DESIGNED	KJ
REVIEWED	
APPROVED	

PROJECT
JEB TMF
GROUNDWATER FLOW AND SOLUTE TRANSPORT

TITLE
JEB TMF MONITORING WELL LOCATION PLAN

PROJECT NO.	PHASE	REV.	FIGURE
CA0051344.8282	4000	A	**3**

IF THIS MEASUREMENT DOES NOT MATCH WHAT IS SHOWN, THE SHEET SIZE HAS BEEN MODIFIED FROM: ANSI B

0 25 mm

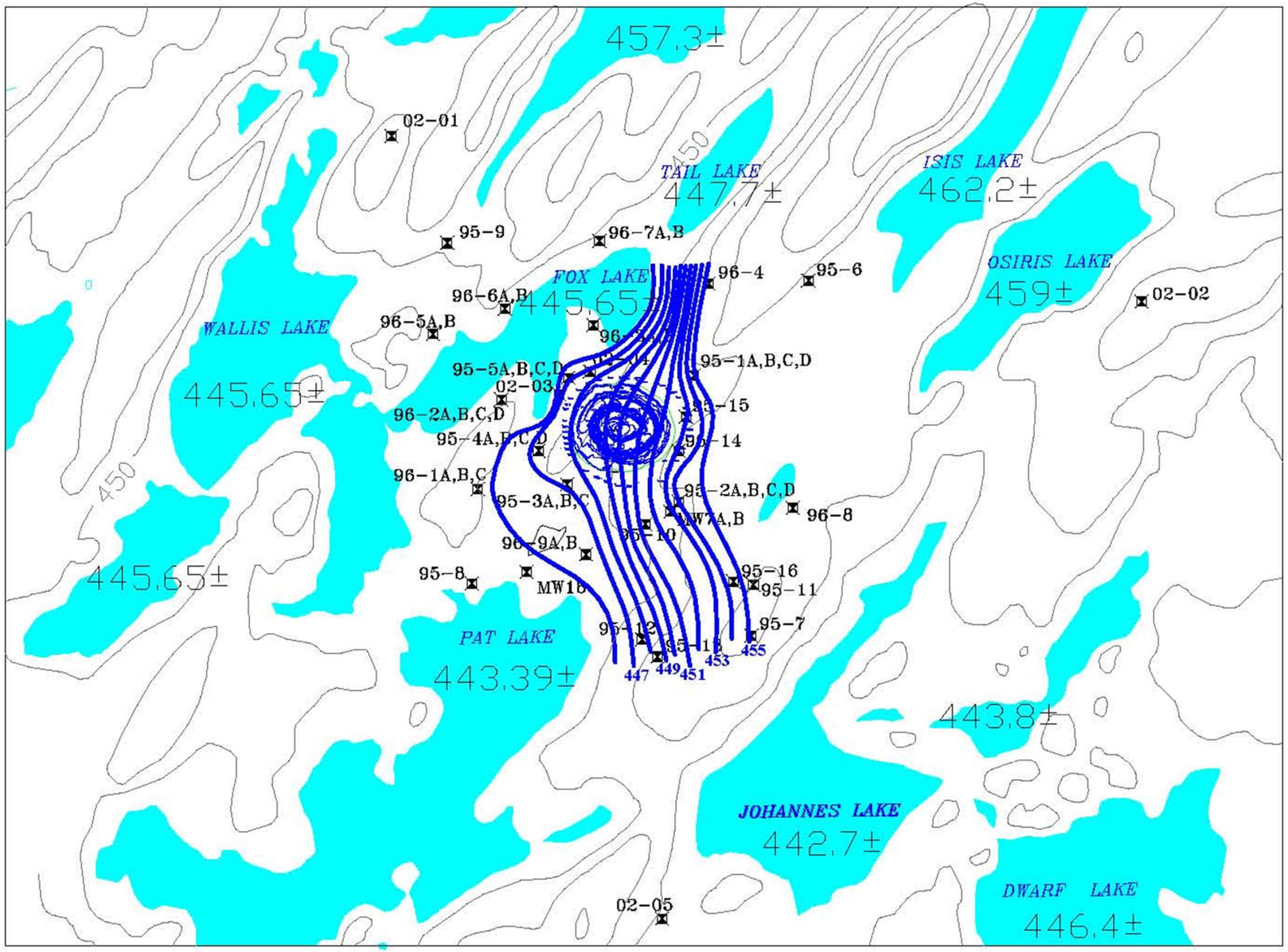

CLIENT: orano

CONSULTANT: wsp

YYYY-MM-DD	2025-05-01
PREPARED	KJ
DESIGNED	KJ
REVIEWED	
APPROVED	

PROJECT
JEB TMF
GROUNDWATER FLOW AND SOLUTE TRANSPORT

TITLE
MEASURED PRE-MINING HEAD CONTOURS IN OVERBURDEN

PROJECT NO.	PHASE	REV.	FIGURE
CA0051344.8282	4000	A	**4**

IF THIS MEASUREMENT DOES NOT MATCH WHAT IS SHOWN, THE SHEET SIZE HAS BEEN MODIFIED FROM: ANSI B
0 25 mm

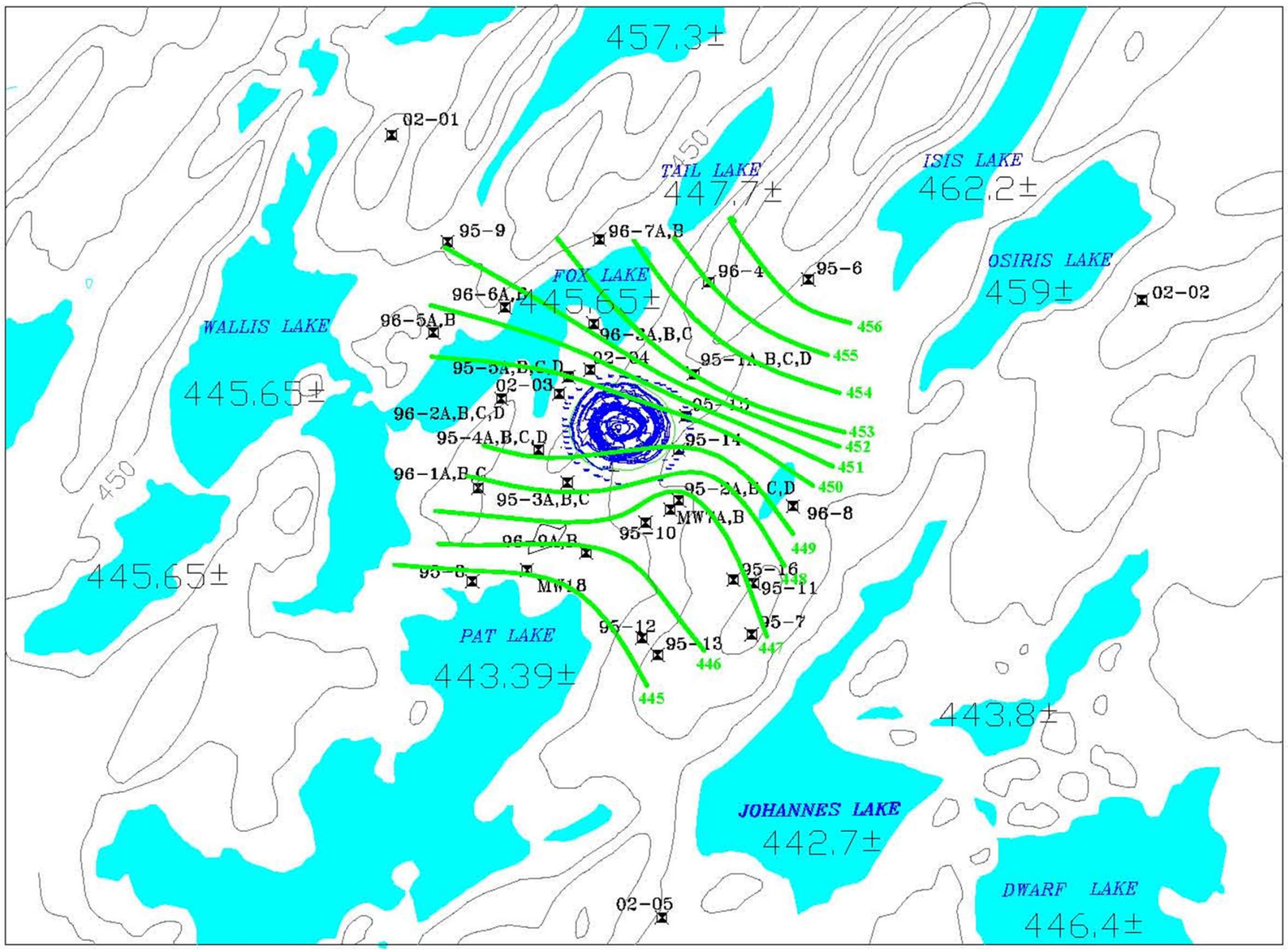

CLIENT

orano

CONSULTANT

wsp

YYYY-MM-DD	2025-05-01
PREPARED	KJ
DESIGNED	KJ
REVIEWED	
APPROVED	

PROJECT

JEB TMF
GROUNDWATER FLOW AND SOLUTE TRANSPORT

TITLE

MEASURED PRE-MINING HEAD CONTOURS IN LOWER SANDSTONE

PROJECT NO.	PHASE	REV.	FIGURE
CA0051344.8282	4000	A	**5**

IF THIS MEASUREMENT DOES NOT MATCH WHAT IS SHOWN, THE SHEET SIZE HAS BEEN MODIFIED FROM: ANSI B
0 25 mm

3 NUMERICAL MODEL

This assessment utilized an existing groundwater model (WSP 2019, WSP 2021) that was updated to incorporate revised regional faults. The following section describes the model construction and checks on the quality of the model calibration following incorporation of the revised regional fault network to existing groundwater model.

3.1 Selection of Model Code

The groundwater model is developed in FEFLOW (v8). This code was selected for its ability to represent the key components of the conceptual hydrogeologic model, including large contrasts in hydraulic conductivity (e.g., the drain filter material vs. underlying bedrock), complex pit geometry, and unsaturated conditions that exist in the overburden and bedrock near the TMF during operation.

3.2 Finite Element Mesh

The finite element mesh used in the model is presented in Figure 6. The lateral model boundaries are set sufficiently far from the TMF to allow adequate representation of pre-mining, operational and closure conditions.

Horizontally the model is approximately centred on the TMF area and extends up to 15 km in the east-west direction and 14 km in the north-south direction. The planar area of the model domain was about 130 square kilometres.

The mesh consisted of approximately 828,000 triangular elements with a spacing of approximately 5 to 10 m near the TMF. Element size was expanded to approximately 100 m along the model perimeter. Overall, the horizontal mesh spacing is considered to be of appropriate detail for simulation of the groundwater conditions at the TMF.

Vertically, the model was discretised into 14 layers of variable thickness. Relative to the previous model, an additional layer was added to refine the representation of the liner (set to two layers thick everywhere in the model). The top of layer one was set to ground surface elevation, which ranged from 410 to 500 m. The bottom of layer 14 was set to a constant elevation of 200 m. This elevation is approximately 150 m below the base of the TMF.

3.3 Hydrostratigraphy and Model Parameters

The groundwater model incorporates the updated regional faults (Figure 8) and five hydrostratigraphic units, as follows:

- Overburden (Model Layers 1 through 6)
- Upper Sandstone (Model Layers 7 and 8)
- Lower Sandstone (Model Layers 9 through 11)
- Basement Regolith (Model Layer 12)
- Intact Basement (Model Layers 13 and 14)

The JEB TMF was subdivided into the following units:

- Cover and berms (model layer 1)
- Tailings (Model Layers 2 through 8)
- Sand filter material (Model Layer 8)

- Gravel and rock drain material (Model Layers 9)

Hydraulic conductivity values assigned to the model are based on the previously calibrated model (Golder 2019), and are summarized on Table 3 and presented on Figure 9 through Figure 11.

Table 3: Summary of Calibrated Hydraulic Conductivity Values

Hydrostratigraphic Unit	Calibrated Hydraulic Conductivity (m/s)	
	Horizontal	Vertical
Overburden	8×10^{-8} to 8×10^{-7}	1.5×10^{-8} to 8×10^{-7}
Upper Sandstone	1×10^{-6} to 8×10^{-6}	1×10^{-6} to 8×10^{-6}
Lower Sandstone	4×10^{-6} to 5×10^{-5}	4×10^{-6} to 5×10^{-5}
Basement Regolith	1.5×10^{-7}	1.5×10^{-7}
Basement	5×10^{-8}	5×10^{-9}
Local and Regional Faults	1×10^{-8} to 2×10^{-5}	1×10^{-8} to 2×10^{-5}
Tailings	1×10^{-8}	1×10^{-8}
Sand Filter	5×10^{-4}	5×10^{-4}
Gravel and Rock Filter	5×10^{-3}	5×10^{-3}

m/s = metres per second

In updating the model, an error was identified in the previous groundwater model for the assigned anisotropy of the local fault to the east of the TMF. This was corrected in this model update.

3.4 Boundary Conditions

The boundary conditions were kept consistent with Golder (2019). Four types of boundary conditions were used in the model: head dependent, specified head, specified flux, and no-flow. The location of these boundaries is illustrated in Figure 7 and described below.

Head dependent boundaries were assigned to nodes in layer 1 to layer 6 to represent all watercourses and surface water bodies within the model domain. The boundaries were set equal to the reported average water level elevation (AREVA 2011b) or to ground surface elevation if the water level elevation was unknown. Groundwater flow through these boundaries was inferred to be impeded by lower permeability sediments at the base of the lakes and creeks, with the conductance set through previous model calibration (Golder 2019).

Specified head boundaries were assigned to the bottom of the base drain and to the top of the tailings to simulate the tailings pond. The heads were varied according to the simulated pond elevation for the calibration and predictive stages.

Specified flux boundaries were assigned to the top of layer one to represent recharge from precipitation. The assigned recharge is 58 mm/yr, which is based on previous model calibration (Golder 2019).

Specified flux boundaries were used to simulate the dewatering wells. The rates assigned to the dewatering wells was varied for each calibration stage according to the production rates measured during operation.

No-flow boundaries were used to represent inferred groundwater flow divides at the lateral extents of the model. A no-flow boundary was assigned along the bottom of the model at 200 m elevation. Groundwater flow below 200 m elevation was expected to have negligible effect on model predictions due to the inferred low permeability of the

intact bedrock, and the decrease in permeability with depth typically observed in fractured bedrock (Stober and Bucher 2007).

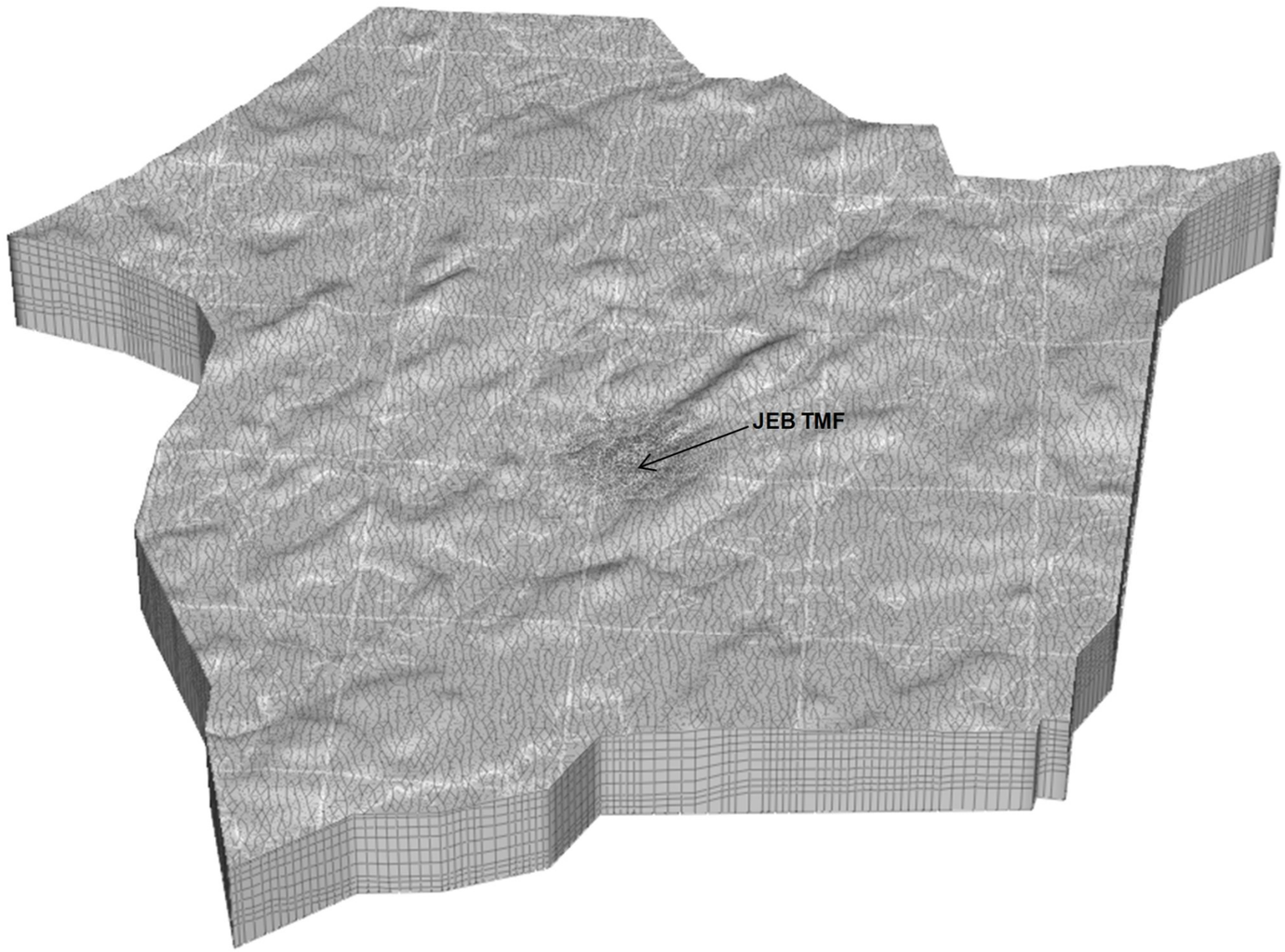

2.5 km
(5x vertical exaggeration)

CLIENT orano

CONSULTANT wsp

YYYY-MM-DD	2025-05-01
PREPARED	KJ
DESIGNED	KJ
REVIEWED	
APPROVED	

PROJECT
JEB TMF
GROUNDWATER FLOW AND SOLUTE TRANSPORT

TITLE
FINITE ELEMENT MESH

PROJECT NO.	PHASE	REV.	FIGURE
CA0051344.8282	4000	A	**6**

IF THIS MEASUREMENT DOES NOT MATCH WHAT IS SHOWN, THE SHEET SIZE HAS BEEN MODIFIED FROM: ANSI B
0 25mm

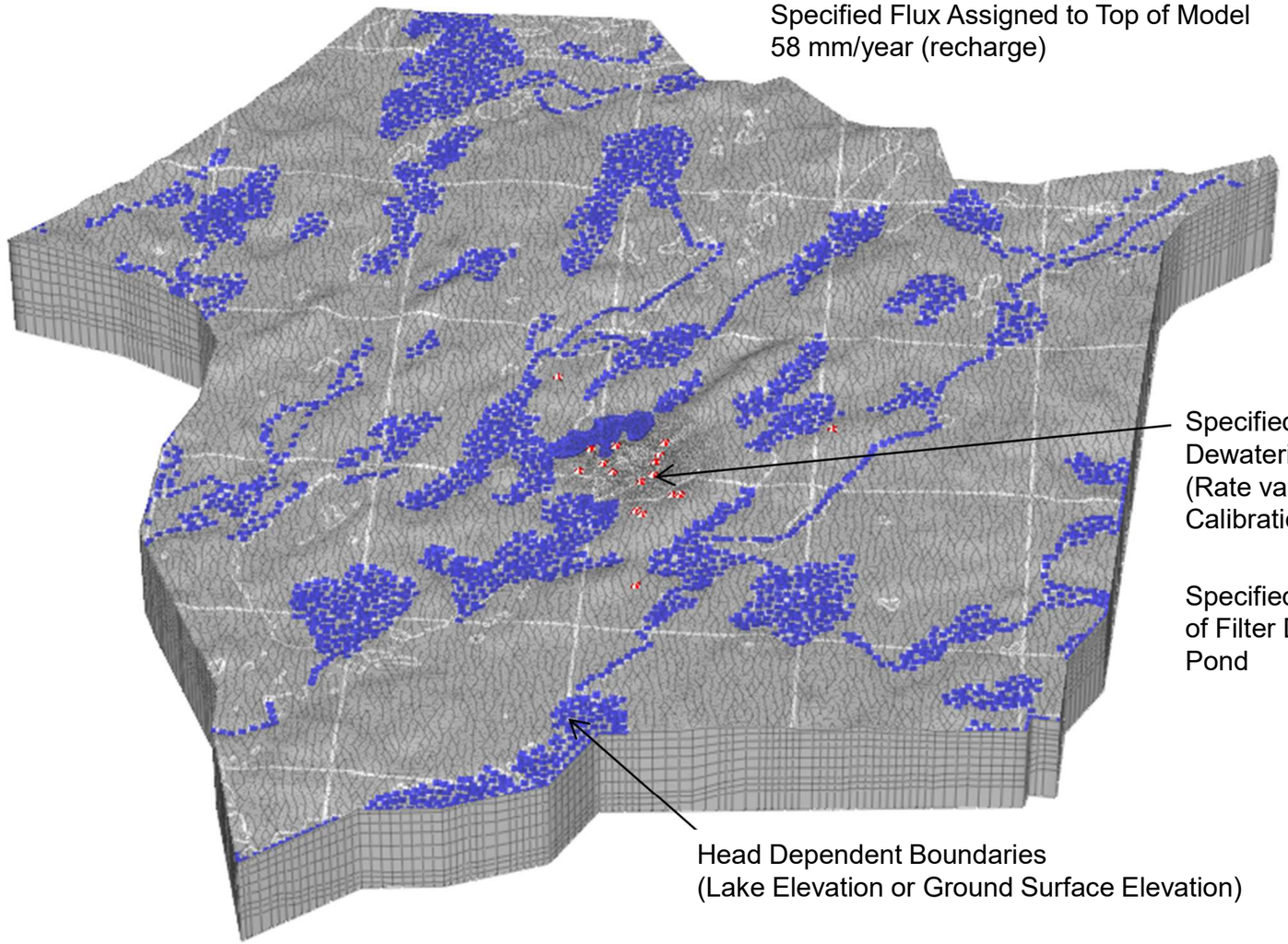

Specified Flux Assigned to Top of Model
58 mm/year (recharge)

Specified Flux
Dewatering Wells
(Rate varied according to
Calibration Stage)

Specified Head to Base
of Filter Drain and Top of
Pond

Head Dependent Boundaries
(Lake Elevation or Ground Surface Elevation)

Specified Flux of Zero to Base and Sides of Model Domain

2.5 km
(5x vertical exaggeration)

CLIENT orano

CONSULTANT wsp

YYYY-MM-DD	2025-05-01
PREPARED	KJ
DESIGNED	KJ
REVIEWED	
APPROVED	

PROJECT
JEB TMF
GROUNDWATER FLOW AND SOLUTE TRANSPORT

TITLE
BOUNDARY CONDITIONS

PROJECT NO.	PHASE	REV.	FIGURE
CA0051344.8282	4000	A	**7**

IF THIS MEASUREMENT DOES NOT MATCH WHAT IS SHOWN, THE SHEET SIZE HAS BEEN MODIFIED FROM ANSI B
25 mm
0

Legend

- Deposits and Showings - Athabasca Basin
- Regional Fault
- Possible Fault
- Probable Fault
- Study Area
- Lake
- River

N

Huskie
J Zone
Roughrider
Midwest A
Midwest
Dawn Lake
Jeb
Tent Seal Zone
Eagle Point
Collins Bay A
Collins Bay B
Tamarack
McClean North Pods
Caribou
Sue
McClean South Pods
McClean South Area
Q10
Rabbit Lake
Natona Bay
Shamus
Horseshoe
Raven

5 0 5
Kilometers

CLIENT: orano

CONSULTANT: wsp

YYYY-MM-DD	2025-05-01
PREPARED	KJ
DESIGNED	KJ
REVIEWED	
APPROVED	

PROJECT
JEB TMF
GROUNDWATER FLOW AND SOLUTE TRANSPORT

TITLE
INFERRED REGIONAL FAULTS (PROVIDED BY ORANO)

PROJECT NO.	PHASE	REV.	FIGURE
CA0051344.8282	4000	A	**8**

IF THIS MEASUREMENT DOES NOT MATCH WHAT IS SHOWN, THE SHEET SIZE HAS BEEN MODIFIED FROM: ANSI B

0 25 mm

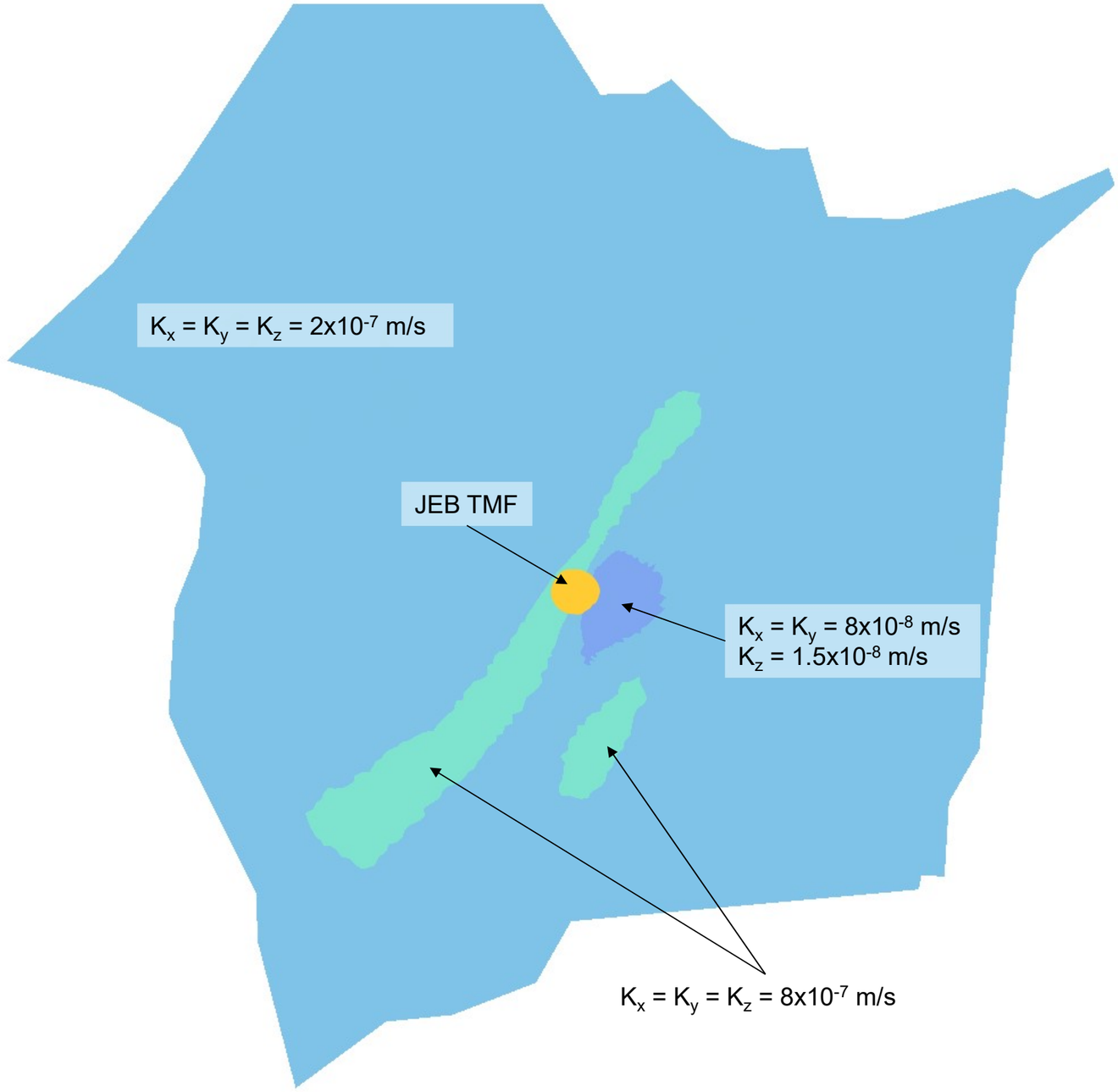

N

0 5001000

[m]

IF THIS MEASUREMENT DOES NOT MATCH WHAT IS SHOWN, THE SHEET SIZE HAS BEEN MODIFIED FROM: ANSI B

0 25 mm

CLIENT: orano

CONSULTANT: wsp

YYYY-MM-DD	2025-05-01
PREPARED	KJ
DESIGNED	KJ
REVIEWED	
APPROVED	

PROJECT
JEB TMF
GROUNDWATER FLOW AND SOLUTE TRANSPORT

TITLE
HYDRAULIC CONDUCTIVITY - OVERBURDEN

PROJECT NO.	PHASE	REV.	FIGURE
CA0051344.8282	4000	A	**9**

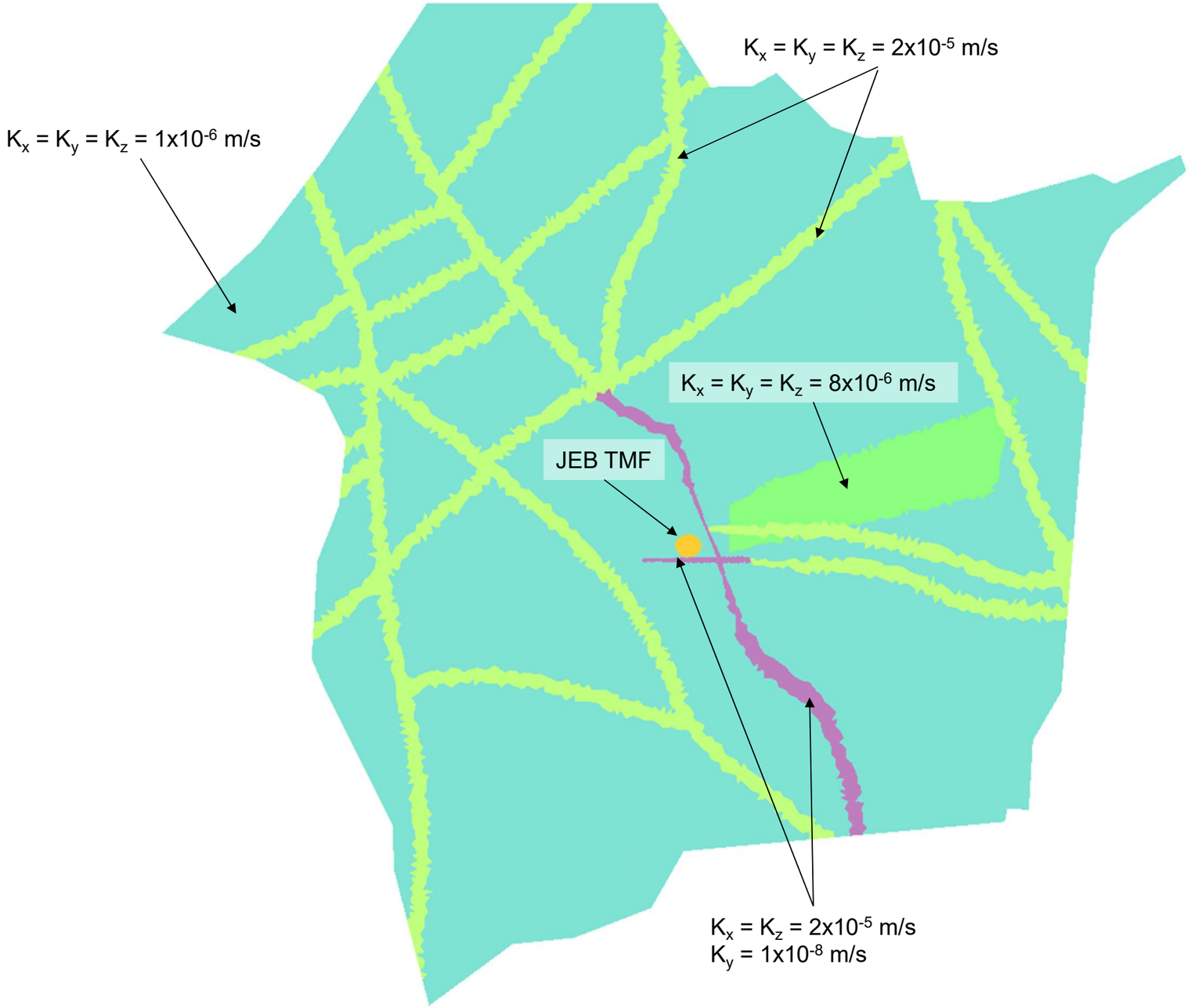

N

0 5001000

[m]

CLIENT

orano

CONSULTANT

wsp

YYYY-MM-DD	2025-05-01
PREPARED	KJ
DESIGNED	KJ
REVIEWED	
APPROVED	

PROJECT

JEB TMF
GROUNDWATER FLOW AND SOLUTE TRANSPORT

TITLE

HYDRAULIC CONDUCTIVITY – UPPER SANDSTONE

PROJECT NO.	PHASE	REV.	FIGURE
CA0051344.8282	4000	A	**10**

IF THIS MEASUREMENT DOES NOT MATCH WHAT IS SHOWN, THE SHEET SIZE HAS BEEN MODIFIED FROM: ANSI B

0 25 mm

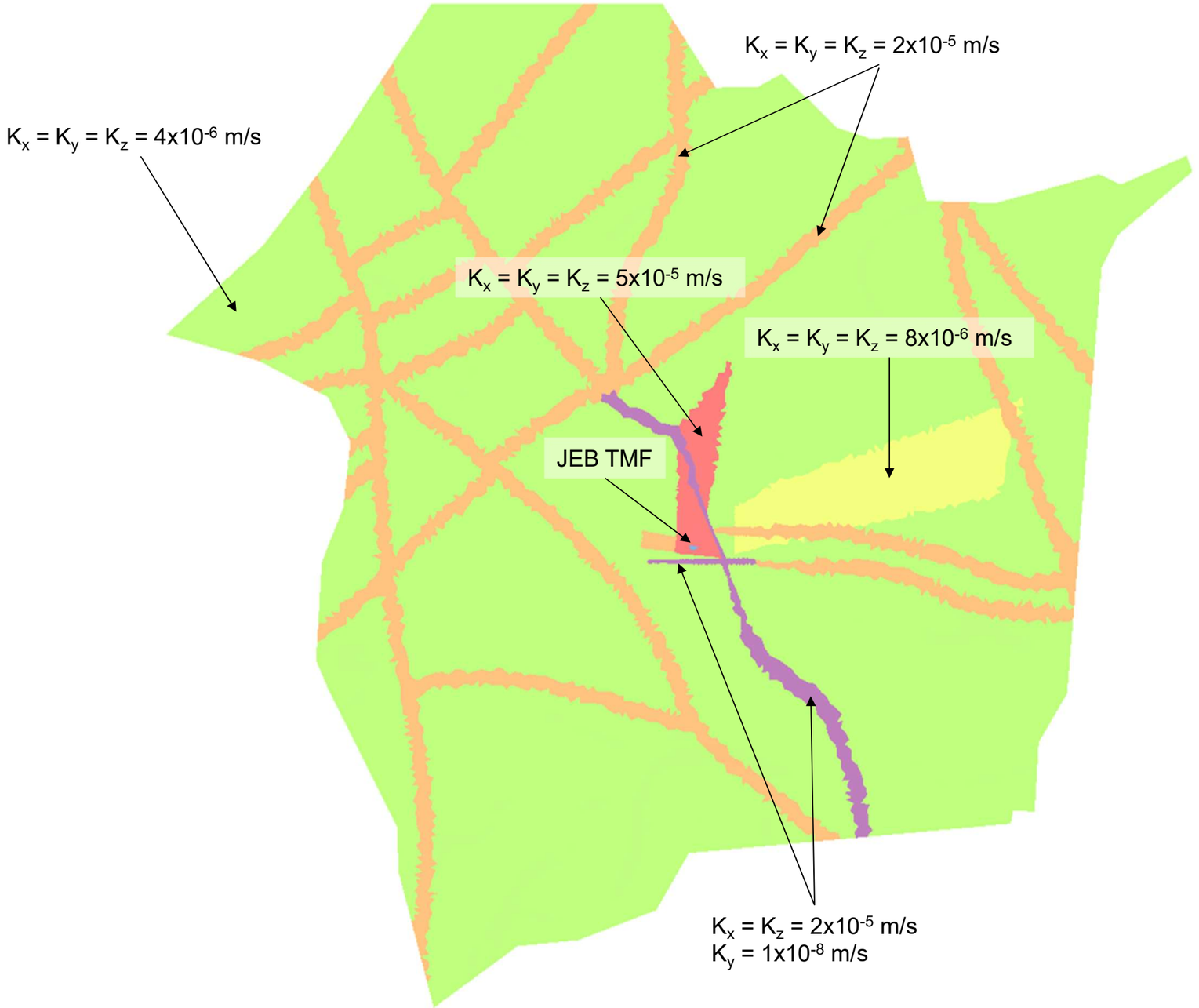

N

0 5001000

[m]

CLIENT orano

CONSULTANT wsp

YYYY-MM-DD	2025-05-01
PREPARED	KJ
DESIGNED	KJ
REVIEWED	
APPROVED	

PROJECT
JEB TMF
GROUNDWATER FLOW AND SOLUTE TRANSPORT

TITLE
HYDRAULIC CONDUCTIVITY – LOWER SANDSTONE

PROJECT NO.	PHASE	REV.	FIGURE
CA0051344.8282	4000	A	**11**

IF THIS MEASUREMENT DOES NOT MATCH WHAT IS SHOWN, THE SHEET SIZE HAS BEEN MODIFIED FROM: ANSI B

0 25 mm

3.5 Model Calibration Check

3.5.1 Calibration Scenarios and Model Setup

With incorporated changes in the model, the ability of the model to reproduce previous calibration stages from the past modelling was checked. The check was completed for 4 calibration scenarios:

- Pre-mining conditions (December 1995)
- Fully dewatered conditions (May 1999)
- TMF water level at 426.75 m ASL (June 2009)
- Field pumping trials (inflows for stage 3 and 4, January 2021)

The data used in the calibration check consisted of hydraulic heads measured in piezometers installed in the sandstone, regolith and/or basement, and measured groundwater inflows to the TMF operation sump (except for the field pumping trials). Water levels recorded in the overburden were generally reviewed but not used in the model calibration as perched groundwater conditions and partial dewatering is inferred to have occurred in the overburden, which could not be accurately reproduced by the numerical model. In addition, the screen lengths in the overburden wells were relatively long, which makes it difficult to assess what elevation the hydraulic head measurement is representative of. This is especially important during operational conditions when vertical gradients likely developed in overburden.

Each of the simulations were completed as steady-state runs. This is considered reasonable for the field pumping trials, given the observed near-instantaneous response of the base drain elevation with respect to changes in the drain pumping rate (Golder 2021). Field trail simulations were completed a JEB TMF pond elevation at 443.4 m ASL.

3.5.2 Calibration Check - Operational Pumping Scenarios

Table 4 presents a summary of the model predicted and measured inflow rates from the TMF and dewatering wells for applicable calibration stages. Consistent with previous modelling and with the model updates a reasonable match was obtained to the measured data. In general, predicted inflow was within 10 % of measured inflow.

Figure 12 and Figure 13 present a summary of the model predicted and measured hydraulic head for each of the calibration stages. Predicted and measured hydraulic head values are also presented in Table 5. Overall, the calibration quality is still reasonable and the calibrated model is considered to be capable of predicting future inflows to the TMF within the level of accuracy required for this assessment. Overall, the normalized root-mean-square error in the calibration stages ranged from 8% to 11%. These values are consistent with error ranges in the previous model and near the upper end of the range normally used in hydrogeological studies. Given the complexity of the geology and enhanced permeability features near the pit, and the reasonable calibration match to measured inflows, these results were considered acceptable.

Table 4: Predicted versus Measured Inflows to Operation Sump and Dewatering Wells

Operating Condition	Inflows (m^3/day)	
	Measured	Predicted
Pre-mining conditions (December 1995)	-	-
Fully dewatered conditions (May 1999)	10,700	10,900
TMF water level at 426.75 m ASL (June 2009)	4,000	4,350

m^3/day = cubic metres per day

A. Pre-ming Conditions

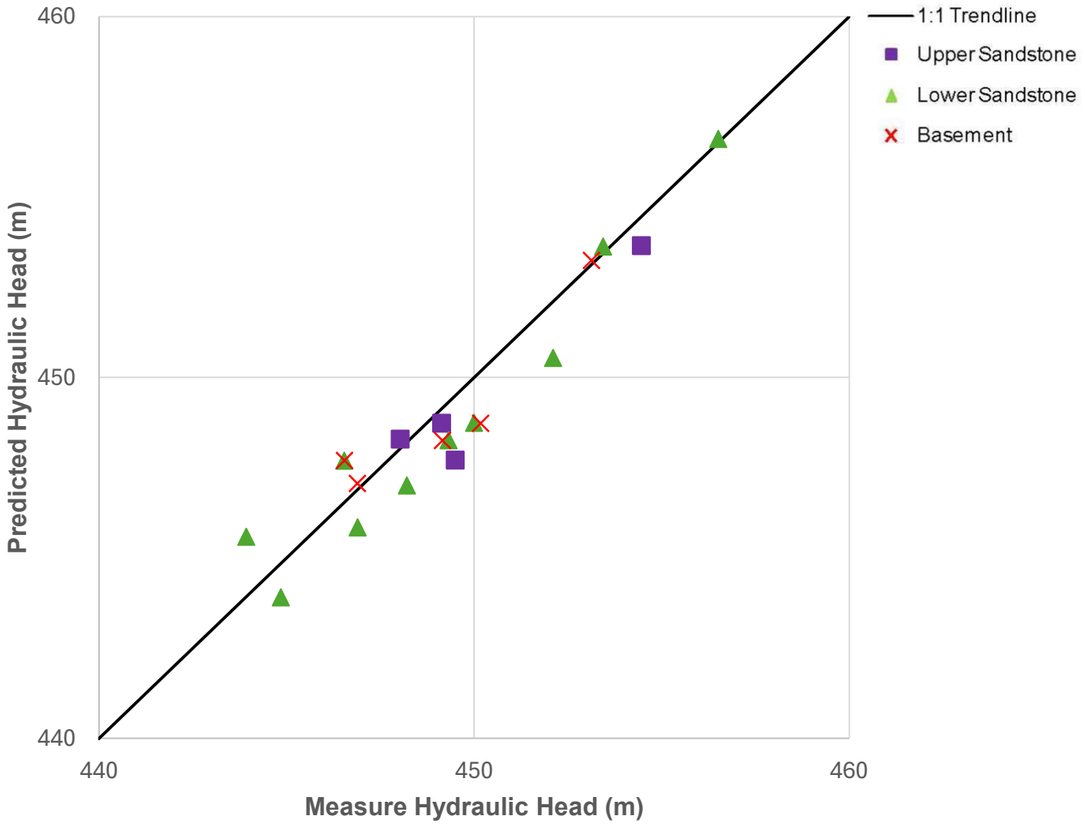

Mean Absolute Error (m)	0.90
Normalized Mean Absolute Error (m)	7.18%
Root Mean Square Error (m)	1.05
Normalized Root Mean Square Error	8.32%
Mean Error (m)	-0.39

B. Fully Dewatered Conditions

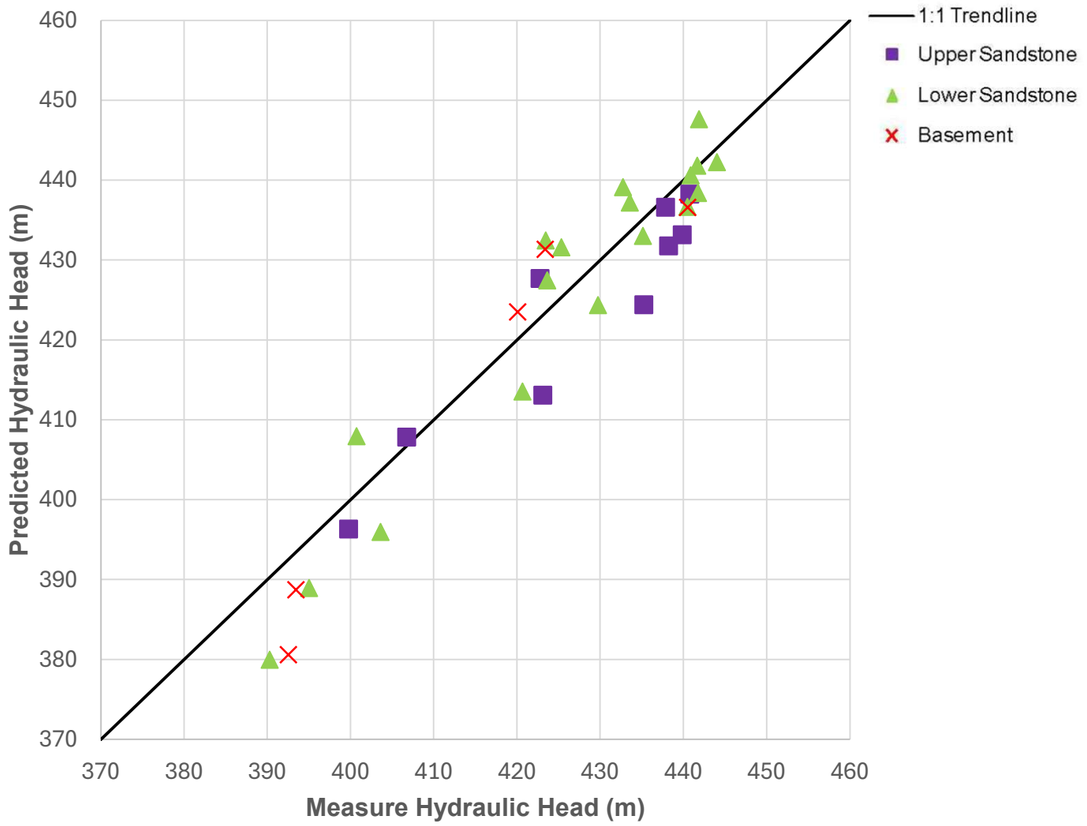

Mean Absolute Error (m)	5.28
Normalized Mean Absolute Error (m)	9.83%
Root Mean Square Error (m)	6.10
Normalized Root Mean Square Error	11.35%
Mean Error (m)	-1.54

CLIENT orano

CONSULTANT wsp

YYYY-MM-DD	2025-05-01
PREPARED	KJ
DESIGNED	KJ
REVIEWED	
APPROVED	

PROJECT
JEB TMF
GROUNDWATER FLOW AND SOLUTE TRANSPORT

TITLE
MEASURED VERSUS PREDICTED HYDRAULIC HEAD
PRE-MINING AND FULLY DEWATERED CONDITIONS

PROJECT NO.	PHASE	REV.	FIGURE
CA0051344.8282	4000	A	12

IF THIS MEASUREMENT DOES NOT MATCH WHAT IS SHOWN, THE SHEET SIZE HAS BEEN MODIFIED FROM: ANSI B
0 25 mm

C. Pond Elevation of 426.75 m

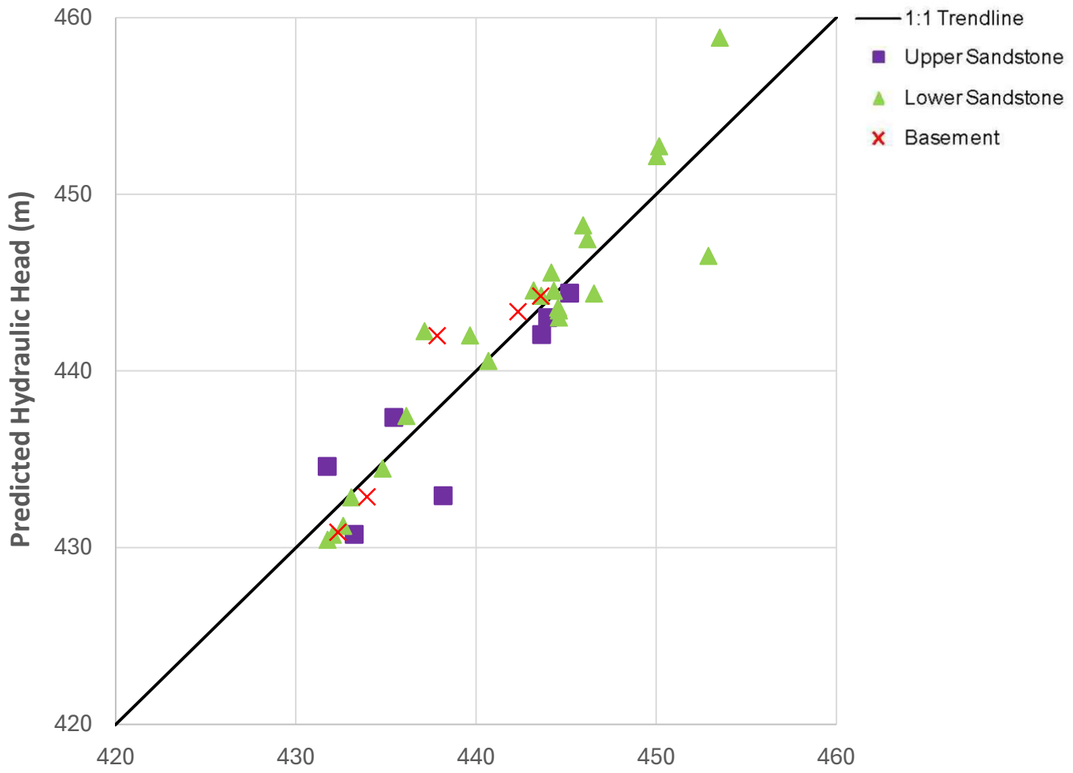

Mean Absolute Error (m)	1.92
Normalized Mean Absolute Error (m)	8.80%
Root Mean Square Error (m)	2.46
Normalized Root Mean Square Error	11.27%
Mean Error (m)	0.17

CLIENT orano

CONSULTANT wsp

YYYY-MM-DD	2025-05-01
PREPARED	KJ
DESIGNED	KJ
REVIEWED	
APPROVED	

PROJECT
JEB TMF
GROUNDWATER FLOW AND SOLUTE TRANSPORT

TITLE
MEASURED VERSUS PREDICTED HYDRAULIC HEAD – 426.75 METRE POND ELEVATION LEVEL

PROJECT NO.	PHASE	REV.	FIGURE
CA0051344.8282	4000	A	13

IF THIS MEASUREMENT DOES NOT MATCH WHAT IS SHOWN, THE SHEET SIZE HAS BEEN MODIFIED FROM: ANSI B
0 25 mm

Table 5: Predicted versus Measured Hydraulic Head

Station	Unit	Pre-mining		Fully Dewatered		Pond 426.75 m ASL	
		Measured (m)	Predicted (m)	Measured (m)	Predicted (m)	Measured (m)	Predicted (m)
02-05B	Overburden	445.44	445.64	-	-	-	-
95-01D	Overburden	455.20	454.61	-	-	-	-
95-02D	Overburden	454.28	448.34	-	-	-	-
95-03C	Overburden	447.04	447.10	-	-	-	-
95-04D	Overburden	447.16	448.32	-	-	-	-
95-05D	Overburden	446.92	448.72	-	-	-	-
95-10	Overburden	451.57	447.87	-	-	-	-
95-11	Overburden	452.16	447.88	-	-	-	-
95-12	Overburden	447.50	445.90	-	-	-	-
95-13	Overburden	448.34	445.68	-	-	-	-
95-14	Overburden	453.22	450.39	-	-	-	-
95-15	Overburden	452.70	449.59	-	-	-	-
95-16	Overburden	454.36	448.89	-	-	-	-
95-01C	Upper sandstone	454.45	453.66	422.73	427.71	-	-
95-02C	Upper sandstone	449.49	447.72	437.81	436.60	-	-
95-04C	Upper sandstone	448.02	448.30	-	-	438.17	432.95
95-05C	Upper sandstone	449.12	448.74	-	-	433.23	430.75
96-01B	Upper sandstone	-	-	438.17	431.78	443.64	442.06
96-02B	Upper sandstone	-	-	406.70	407.84	435.44	437.38
96-03B	Upper sandstone	-	-	399.72	396.34	431.73	434.60
96-05B	Upper sandstone	-	-	439.81	433.16	445.20	444.40
96-06B	Upper sandstone	-	-	435.22	424.41	443.97	443.03
96-07B	Upper sandstone	-	-	423.08	413.10	-	-
96-09B	Upper sandstone	-	-	440.74	438.27	-	-
02-01A	Lower sandstone	-	-	-	-	450.04	452.16
02-02A	Lower sandstone	-	-	-	-	453.53	458.87
02-03	Lower sandstone	-	-	-	-	432.63	431.23
02-04	Lower sandstone	-	-	-	-	431.76	430.44
02-05A	Lower sandstone	443.92	445.59	-	-	444.19	445.57
95-01B	Lower sandstone	453.43	453.63	423.60	427.45	443.20	444.56
95-02B	Lower sandstone	446.53	447.70	440.45	436.64	443.62	444.25
95-03B	Lower sandstone	448.20	447.01	423.44	432.45	437.14	442.24
95-04B	Lower sandstone	449.31	448.27	394.99	388.95	433.08	432.85
95-05B	Lower sandstone	449.99	448.75	390.25	379.96	432.06	430.73
95-06	Lower sandstone	456.50	456.61	441.86	447.63	450.17	452.71
95-07	Lower sandstone	446.89	445.85	441.65	441.80	444.33	444.53
95-08	Lower sandstone	444.84	443.91	444.00	442.24	444.60	443.42
95-09	Lower sandstone	452.10	450.55	433.53	437.19	446.19	447.46

Table 5: Predicted versus Measured Hydraulic Head

Station	Unit	Pre-mining		Fully Dewatered		Pond 426.75 m ASL	
		Measured (m)	Predicted (m)	Measured (m)	Predicted (m)	Measured (m)	Predicted (m)
96-01A	Lower sandstone	-	-	425.30	431.57	439.67	442.01
96-02A	Lower sandstone	-	-	400.70	407.94	436.14	437.44
96-03A	Lower sandstone	-	-	403.60	395.95	434.82	434.47
96-04	Lower sandstone	-	-	432.73	439.13	445.95	448.24
96-05A	Lower sandstone	-	-	435.10	433.01	446.55	444.38
96-06A	Lower sandstone	-	-	429.71	424.34	444.60	443.02
96-07A	Lower sandstone	-	-	420.63	413.54	440.69	440.57
96-08	Lower sandstone	-	-	440.84	440.61	452.90	446.51
96-09A	Lower sandstone	-	-	441.74	438.38	444.56	443.57
TW01	Lower sandstone	-	-	-	-	-	-
TW02	Lower sandstone	-	-	-	-	-	-
TW03	Lower sandstone	-	-	-	-	-	-
TW04	Lower sandstone	-	-	-	-	-	-
TW05	Lower sandstone	-	-	-	-	-	-
TW06	Lower sandstone	-	-	-	-	-	-
TW07	Lower sandstone	-	-	-	-	-	-
TW08	Lower sandstone	-	-	-	-	-	-
95-01A	Basement	453.12	453.25	420.06	423.51	442.33	443.35
95-02A	Basement	446.54	447.71	440.50	436.59	443.60	444.24
95-03A	Basement	446.88	447.07	423.36	431.34	437.84	441.99
95-04A	Basement	449.15	448.26	393.41	388.71	433.95	432.87
95-05A	Basement	450.17	448.74	392.51	380.60	432.34	430.87

m = metres; m ASL = metres above sea level

3.5.3 Calibration Check – Pumping Test Trial

A field trial pumping test was conducted at the TMF between December 1, 2020, and February 6, 2021 to evaluate hydraulic response and TMF pumping rates (Golder 2021). During the field trial pumping test, the pumping rates were varied between 1,809 m^3/day and 776 m^3/day. Table 6 summarizes the average pumping rates and base drain water elevation for the field trial pumping test at Stage 3 and Stage 4.

Table 6: Field Trial Pumping Test Summary

Stage	Start	End	Measured Average Pumping Rate (m^3/d)	Base Drain Water Elevation (m ASL)	TMF Water Elevation (m ASL)	Fox Lake Water Elevation (m ASL)	Pond Head Differential (Pond – Drain) (m)	Fox Lake Head Differential (Pond – Fox) (m)
3	31-Dec-2020	15-Jan-2021	1,502	440.9	443.4	445.7	2.5	4.8
4	16-Jan-2021	26-Jan-2021	934	442.5	443.4	445.7	0.9	3.2

m^3/d = cubic metres per day; m ASL = meters above sea level; m = metres

Consistent with previous modelling in 2021, the groundwater model was configured to evaluate two states of the field pumping trial, including

- Stage 3, where the groundwater elevation in the base drain was at elevation 440.0 m ASL. At this stage in the field pumping trials, the base drain pumping rate was approximately 1,500 m3/day.
- Stage 4, where the groundwater elevation in the base drain was at elevation 442.5 m ASL. At this stage in the field pumping trials, the base drain pumping rate was approximately 930 m3/day.

Results of the simulations were compared to the base drain pumping rates observed during the field pumping trial (Table 7). For Stage 3 of the pumping trials, the simulated groundwater inflow to the drain was approximately 1,550 m^3/d, which compares well to the average measured value of 1,502 m^3/d. For Stage 4, the simulated groundwater inflow to the drain was 1,200 m^3/d, which compares well to the average measured value of 934 m^3/d. The updated model therefore still reasonably reproduces measured data.

Table 7: Comparison of Modelled Flow Rates to Field Trial Pumping Test Observation

Stage	Measured Average Drain Pumping Rate (m^3/d)	Base Drain Water Elevation (m ASL)	TMF Water Elevation (m ASL)	Predicted Inflow to Drain (m^3/d)
3	1,502	440.9	443.4	1,550
4	934	442.5	443.4	1,200

m^3/d = cubic metres per day; m ASL = meters above sea level; m = metres

4 OPERATIONAL AND POST CLOSURE PREDICTIONS

Groundwater flow and solute transport models were previously developed in earlier evaluations of the JEB TMF (Golder 2019; Golder 2021). With the updates to the groundwater model, the updated predictions are provided for the full build capacity with a tailing's elevation of 465.5 m ALS to evaluate if there are any changes to the operating base drain elevation required to maintain groundwater capture.

The flow model was also used to simulate seepage conditions from the TMF after decommissioning with a consolidated tailing elevation of 465.5 m ASL. Seepage pathways and flow rates from this simulation are inputs to a groundwater solute model (as described in Section 5).

4.1 Full Build Capacity

The groundwater flow model was used to evaluate the operating base drain elevation required to maintain groundwater capture with the JEB TMF operating at full build capacity after the 468 Expansion. The model was configured to include tailings to an elevation of 465.5 m ASL, a pond elevation of 467 m ASL and a berm crest elevation of 468 m ASL.

The following steps were taken to evaluate the groundwater capture:

- The model was run using a base drain elevation with a head differential relative to the surface water elevation of Fox Lake (445.65 m ASL). The simulation was run to steady-state conditions.
- The degree of groundwater capture was evaluated by completing a particle tracking analysis, where groundwater flow particles were released from the TMF pond and tailings and forward tracked through the groundwater flow system to their ultimate point of discharge.
- If the groundwater particle tracking analysis indicated that containment was not achieved (i.e., groundwater particles discharged from the model anywhere except the base drain) then the model was re-run using a lower base drain elevation and the particle tracking analysis was repeated.

Results of the predictive simulations indicate that containment is achieved when the base drain elevation is specified at an elevation of 439.7 m ASL (i.e., 6 m lower than Fox Lake) or lower. Figures A1 and A2 in APPENDIX A illustrate the groundwater particle traces drain elevations of 439.7 m ASL and 438.7 m ASL, respectively. As shown in the figures, the particle traces generally follow a path directly towards the drain. A small portion of particles travel towards the west along by the east-west trending conductive feature in the sandstone that intersects the south side of the JEB TMF before returning to the drain.

In addition to the base case scenario above (scenario using the calibrated model parameters), four additional simulations were completed to evaluate the potential sensitivity of model outcomes with the base drain elevation set at 7 m below the Fox Lake water elevation:

- The hydraulic conductivity was increased in the overburden by a factor of 10.
- The anisotropy (vertical permeability) was reduced in the sandstone by a factor of 10.
- The hydraulic conductivity of the liner was increased by a factor of 10 (i.e., from $1x10^{-9}$ m/s to $1x10^{-8}$ m/s).

Hydraulic containment was maintained for each sensitivity scenario except when the liner hydraulic conductivity was increased by a factor of 10. The same scenarios were run with the base drain elevation set at 8 m below the Fox Lake water elevation and hydraulic containment was maintained for all scenarios. Sensitivity runs for both base drain elevations are illustrated in Figures A2 to A9.

Groundwater inflows to the base drain for the base case scenarios were 2,050 m^3/d when the drain elevation was 438.7 m ASL (7 m head differential) and 2,250 m^3/d when the drain elevation was 437.7 m ASL (8m head differential).

4.2 Post Closure

4.2.1 Post Closure Scenarios

The updated model was used to assess the transport pathway of groundwater discharging from the TMF following decommissioning of the TMF with a consolidated tailings elevation of 465.5 m ASL, which conservatively represents the post decommissioning scenario as it does not account for the reduction of the tailings surface area accompanying consolidation of the tailings during the decommissioning period. The assessment in the groundwater model considers advective transport only and does not include other mechanisms that could affect contaminant transport (e.g., dispersion, biochemical degradation).

For the post closure scenarios, pumping from the base drain was considered to remain inactive following mine closure, and it was considered that the top of the TMF is covered by a low permeability barrier. The infiltration (i.e., net percolation) through the low permeability barrier was assessed as part of the soil cover design report (Golder 2011) and was estimated to be 10 mm/yr. The soil cover design in this report is conceptual and intended to demonstrate the feasibility of the construction of a cover to limit net percolation to these values, as required to ensure the overall performance of the decommissioned TMF. The cover design requirements will be refined prior to closure through the detailed design process considering the results of the proposed test cover program and continued sampling of the tailings and the analysis of overall TMF performance through the TOVP. The selected cover to be implemented at the time of decommissioning will limit net percolation rates to values that are suitably protective of the receiving environment.

Two post closure scenarios were simulated. In the first scenario, the expected infiltration of 10 mm/yr was assigned to layer 1 in the area of the expanded TMF to represent net percolation of precipitation through the soil cover. In the second scenario the infiltration was increased to 20 mm/yr. In addition to the two post closure scenarios varying the net percolation rate, two sensitivity simulations were completed to support the solute transport assessment (Section 5) where the hydraulic conductivity of the tailings was adjusted by an order of magnitude above and below the base case value (i.e., from $1x10^{-9}$ m/s for the low hydraulic conductivity scenario to $1x10^{-7}$ m/s for the high hydraulic conductivity scenario).

4.2.2 Results

Figure 14 presents the predicted advective transport pathway for the base case net percolation rate of 10 mm/yr. Seepage pathways for the higher net percolation rate are not shown, but are similar to the 10 mm/yr scenario. Discharge from the TMF is predicted to migrate south-west towards Fox Lake and Pat Lake. Approximately 68% of the predicted flow discharges to Fox Lake Basin and 32% of the flow discharges to Pat Lake. The corresponding average specific discharge along the pathway to Fox Lake is 0.0066 metres per day (m/day) and to Pat Lake is 0.0006 m/d. Specific discharge was estimated based on the particle paths to the receptors, considering the groundwater velocity along each pathway and an effective porosity of 11% for sandstone. The average travel distance is estimated to be approximately 280 m and 790 m, respectively.

The model results indicated that, in general, the discharge from the TMF originates from the net percolation of precipitation through the soil cover (5.8 to 11.6 m^3/day) (Figure 15). Precipitation that infiltrates through the cover is predicted to migrate through the tailings and discharge to the sandstone and to the base drain. A small portion (approximately 2%) of the simulated groundwater flow through the tailings originates from the surrounding environment and liner, typically in the upper portions of the Cigar Lake tailings.

Sensitivity runs were conducted to examine the effect of varying the tailings hydraulic conductivity on the post-decommissioning TMF water balance (Figure 15). The results indicate that negligible changes to the total outflow from the tailings occurred for the case where the hydraulic conductivity of the tailings was reduced by an order of magnitude, and that a greater portion of the flow occurred through the Cigar Lake tailings. For the case where the tailings hydraulic conductivity was increased by an order of magnitude, the total flow out of the tailings mass increased by approximately 5%. An additional sensitivity simulation was completed to evaluate the influence of removing the liner from the TMF. Results of this simulation indicate that removal of the liner resulted in an approximate 5% increase in the groundwater flow through the Cigar Lake tailings, which originated as lateral flow from the surrounding environment.

To assist in mass loading calculations, the specific discharge through the sandstone surrounding the TMF and through the base drain was estimated based on sections situated perpendicular to the direction of groundwater flow along the pathway. The specific discharge through the sandstone near the TMF was estimated to be generally between 2.5×10^{-5} m/day and 2.0×10^{-2} m/day. The specific discharge in the lower sandstone is predicted to be higher than the upper sandstone, which is considered reasonable given the greater hydraulic conductivity in lower sandstone. The specific discharge in the upper sandstone is predicted to be between 2.5×10^{-5} and 2×10^{-4} m/day, whereas the discharge in the lower sandstone is predicted to be between 1.6×10^{-3} and 2.0×10^{-2} m/day. The average specific discharge through the sand filter is estimated to be approximately 0.04 m/day.

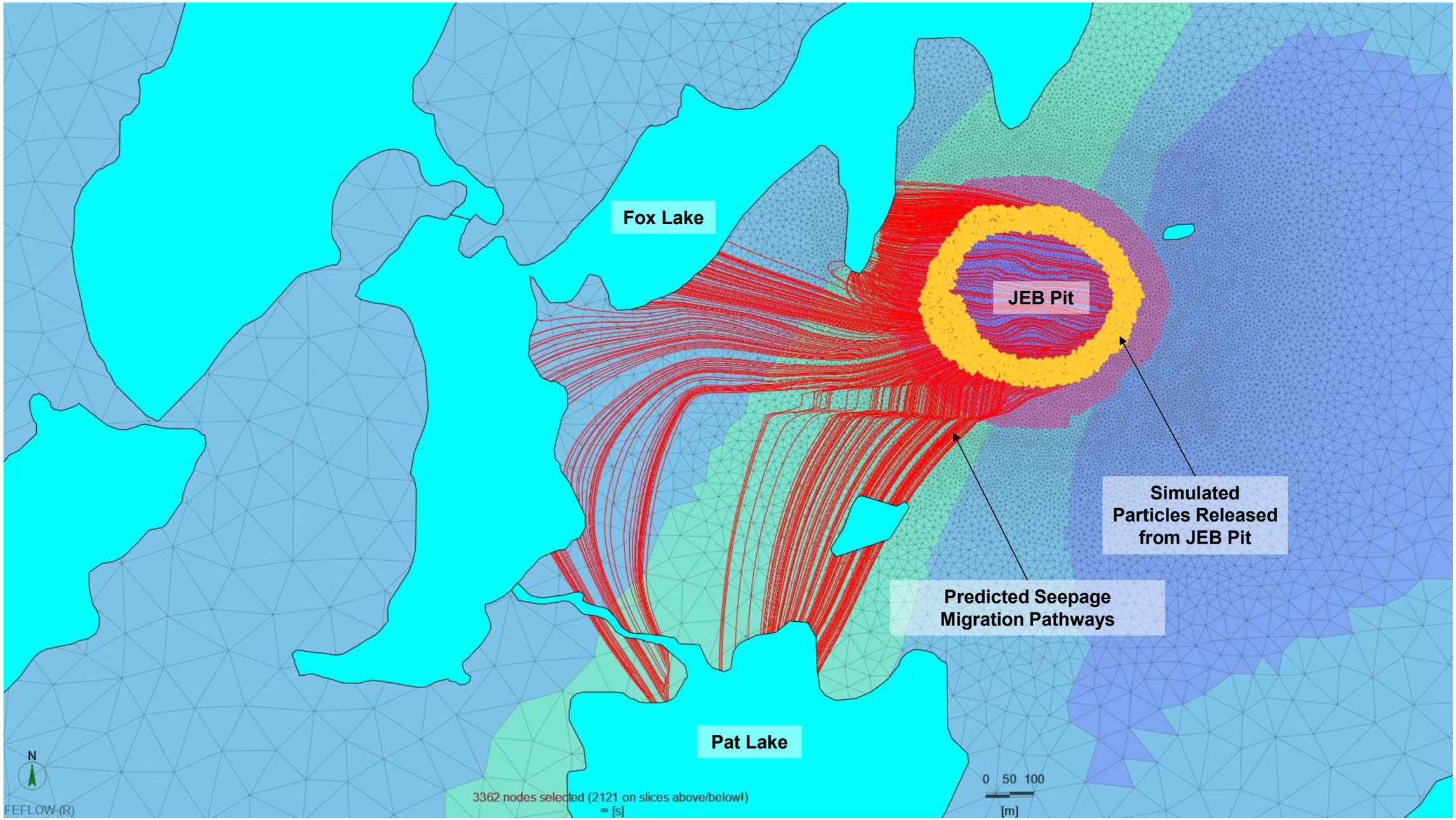

CLIENT orano

CONSULTANT wsp

YYYY-MM-DD	2025-05-01
PREPARED	KJ
DESIGNED	KJ
REVIEWED	
APPROVED	

PROJECT
JEB TMF
GROUNDWATER FLOW AND SOLUTE TRANSPORT

TITLE
PREDICTED ADVECTIVE CONTAMINANT TRANSPORT PATHWAYS FROM THE TAILINGS MANAGEMENT FACILITY – POST CLOSURE

PROJECT NO.	PHASE	REV.	FIGURE
CA0051344.8282	4000	A	**14**

IF THIS MEASUREMENT DOES NOT MATCH WHAT IS SHOWN, THE SHEET SIZE HAS BEEN MODIFIED FROM: ANSI B
0 25 mm

SENSITIVITY ANALYSIS: HYDRAULIC CONDUCTIVITY OF TAILINGS

LOW-K TAILINGS

TAILINGS K = 1X10^{-9} m/s , RECHARGE = 10 mm/a

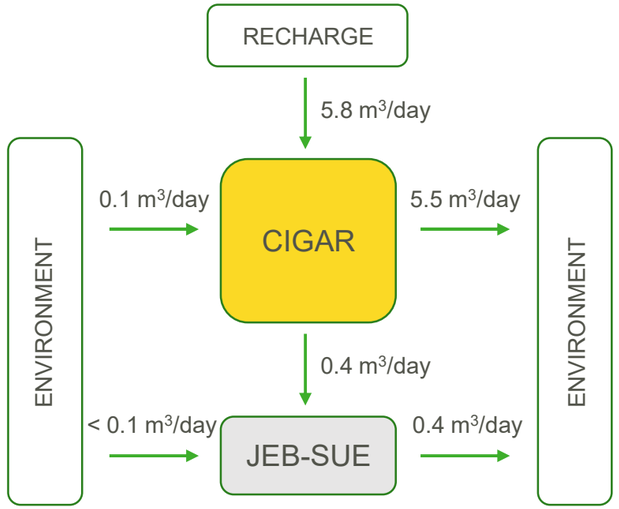

BASE CASE

TAILINGS K = 1X10^{-8} m/s, RECHARGE = 10 mm/a

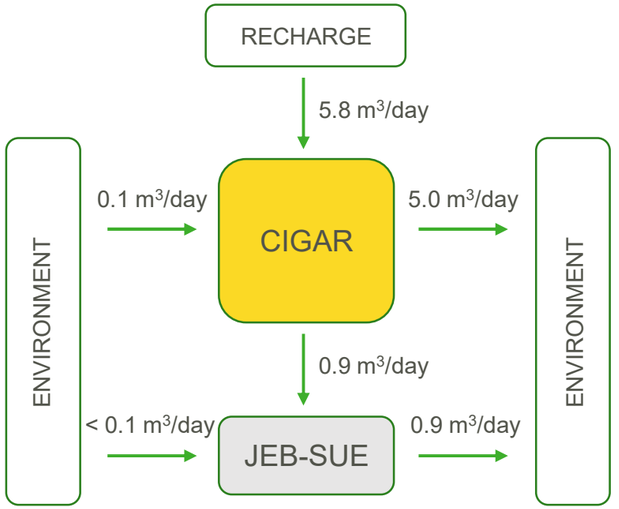

HIGH-K TAILINGS

TAILINGS K = 1X10^{-7} m/s , RECHARGE = 10 mm/a

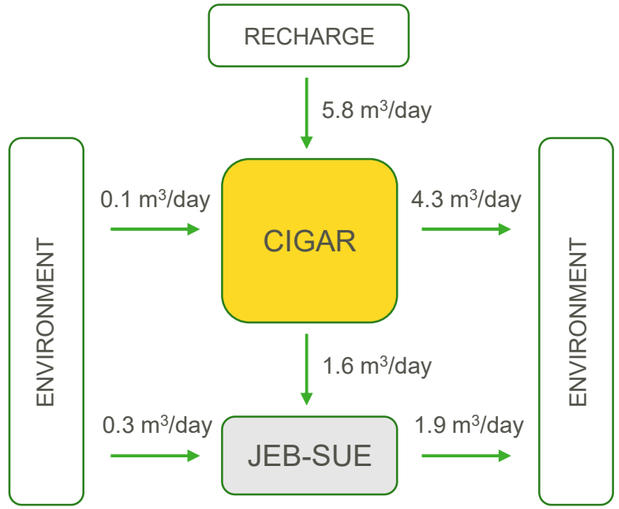

SENSITIVITY ANALYSIS: RECHARGE

LOW RECHARGE

TAILINGS K = 1X10^{-8} m/s, RECHARGE = 5 mm/a

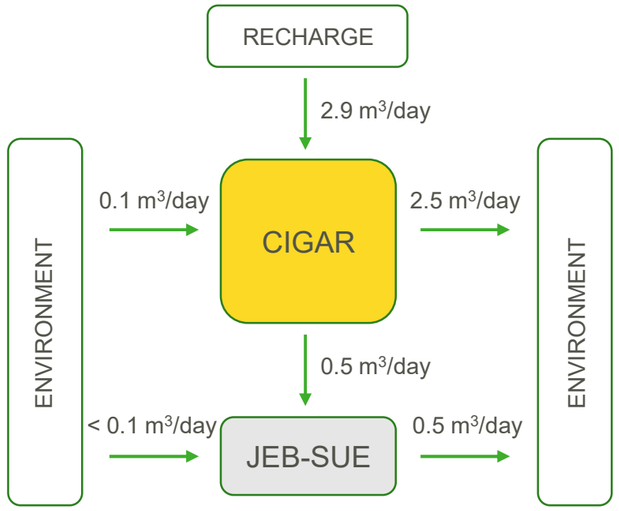

HIGH RECHARGE AND UPPER BOUND

TAILINGS K = 1X10^{-8} m/s, RECHARGE = 20 mm/a

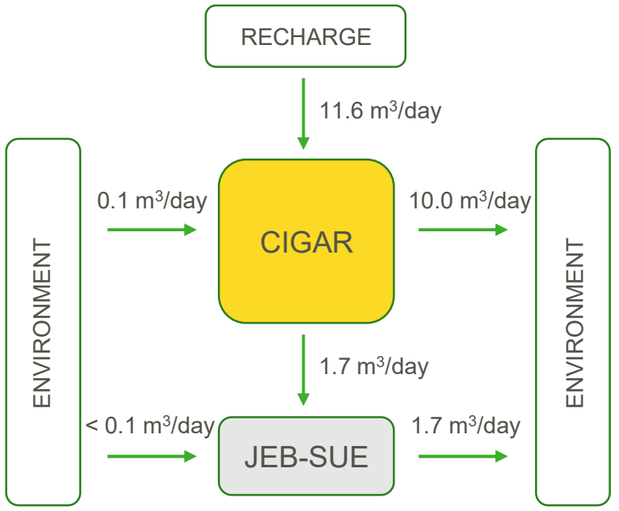

SENSITIVITY ANALYSIS: LINER REMOVAL

BASE CASE WITHOUT LINER

TAILINGS K = 1X10^{-8} m/s, RECHARGE = 10 mm/a

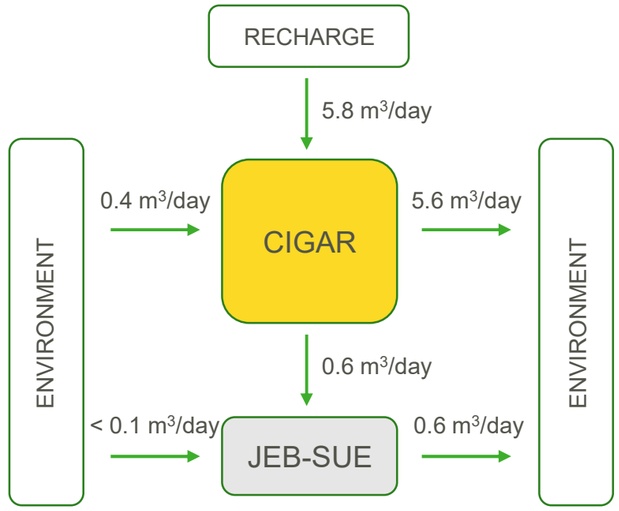

CLIENT orano

CONSULTANT wsp

YYYY-MM-DD	2025-05-01
PREPARED	KJ
DESIGNED	KJ
REVIEWED	
APPROVED	

PROJECT
JEB TMF
GROUNDWATER FLOW AND SOLUTE TRANSPORT

TITLE
WATER BALANCE COMPONENTS OF THE JEB TMF

PROJECT NO.	PHASE	REV.	FIGURE
CA0051344.8282	4000	A	**15**

IF THIS MEASUREMENT DOES NOT MATCH WHAT IS SHOWN, THE SHEET SIZE HAS BEEN MODIFIED FROM ANSI B
0 25mm

5 SOLUTE TRANSPORT PREDICTIONS

Potential post-decommissioning effects associated with the JEB TMF derive from the release of soluble constituents from the tailings mass to the groundwater system, which acts as a pathway for subsequent transport to surface water receptors. The release and transport of solutes are influenced by the chemical and physical properties of the tailings within the decommissioning facility and the groundwater flow regime in the area of the TMF. In consideration of the geochemical characteristics of the tailings source, peak long-term effects have been shown to correspond to steady-state transport conditions (AREVA 2009) in which the mass flux released from the source equals that arriving at receptors for all but radioactive species.

The solute transport analysis used to calculate solute loadings to receptors from the JEB TMF couples one-dimensional solute transport solutions with the particle tracking method. A local-scale finite element groundwater flow model was developed in FEFLOW and used to simulate flow in and around the decommissioned JEB TMF (Section 4.2). Particles were placed within the TMF and tracked down-gradient to receptors. Representative groundwater velocities and travel distances were applied to solute transport calculations for pathways to each receptor in GoldSim® (GTG 2025). A model was developed using GoldSim® to predict the mass flux of solutes released from the facility to the groundwater flow system and subsequently determine the initial solute concentrations in groundwater for each flow path. Solute mass loadings to receptors were estimated based on mass flux predictions from the GoldSim® model for the most sensitive solute species and groundwater flow simulation results, which provide partitioning of groundwater flows between individual surface water receptors.

5.1 Methods

The groundwater flow system acts as a pathway for potential interactions between constituents of the tailings within the JEB TMF and the receiving environment. As a result, the assessment of long-term effects of tailings disposal focuses on the post-decommissioning groundwater flow regime in the JEB area, the geotechnical and geochemical properties of the tailings mass, the mechanisms for solute release from the decommissioned facility, and transport to the receiving environment.

5.2 Source Characterization

The physical and chemical characteristics of the tailings within the JEB TMF are required to define both the source concentrations of soluble tailings constituents and the predicted post-decommissioning groundwater flow conditions.

The hydraulic conductivity of the consolidated tailings mass is of primary interest for predicting groundwater flow conditions in and around the decommissioned JEB TMF. Orano has undertaken testing of laboratory produced tailings from the various ores to be processed through the McClean Lake mill and of production tailings collected from the tailings preparation circuit and from the TMF. Testing included conventional consolidation tests, triaxial permeability tests, and falling head permeability tests. These test results have been used to define tailings hydraulic conductivity as a function of void ratio, or density. A hydraulic conductivity value of 1×10^{-8} m/s has been found to be achievable at the tailings densities expected to be achieved within decommissioned JEB TMF (AREVA 2015). This value has been applied to cells representing tailings within the flow model (Section 3).

Soluble concentrations of tailings constituents within tailings pore water have a controlling effect on the mass flux out of the decommissioned facility. Orano has undertaken numerous geochemical studies for the purpose of predicting long-term solute concentrations within the tailings pore water. A standard methodology has been developed to determine tailings pore water source terms for comparison over eight tailings sampling campaigns,

presented in the McClean Lake Tailings Technical Information Document (TID) (AREVA 2015). Source concentrations in tailings pore water used in this assessment were provided by Orano which are based on 2023 in situ sampling. Table 8 presents solute concentrations in tailings pore water for selected constituents for both the JEB-Sue and Cigar Lake tailings types.

Table 8: Predicted Long-Term Solute Concentrations in Tailings Pore Water

Constituent	Unit	Cigar Lake Tailings		JEB-Sue Tailings	
		Prediction	Upper Bound	Prediction	Upper Bound
Chloride	mg/L	118.12	145.15	43.86	82.7
Sulfate	mg/L	3292.61	4325	2205.84	2578
Ammonia	mg/L	13.29	35.55	11.69	24.4
Arsenic	mg/L	0.76	1.78	1.27	2.98
Cadmium	mg/L	0.00041	0.0011	0.0009	0.0022
Cobalt	mg/L	0.047	0.27	0.15	0.47
Copper	mg/L	0.004	0.017	0.0019	0.0046
Lead	mg/L	0.0009	0.007	0.0021	0.0142
Molybdenum	mg/L	5.34	13.68	8	14.09
Nickel	mg/L	0.168	0.63	2.37	8.11
Selenium	mg/L	0.007	0.032	0.0095	0.052
Vanadium	mg/L	0.0043	0.0077	0.021	0.18
Zinc	mg/L	0.008	0.032	0.026	0.7
Polonium-210	Bq/L	0.51	0.62	0.75	3.55
Lead-210	Bq/L	2.29	6.25	2.2	4
Radium-226	Bq/L	4.11	7.7	4.63	16
Thorium-230	Bq/L	1	1.1	1.11	1.55
Uranium	mg/L	3.08	7.59	9.37	53.36

EIS = environmental impact statement; mg/L = milligrams per litre; Bq/L = Becquerel per litre

5.3 Solute Transport

For the case of steady-state transport from a source to a receptor with no decay in transit, the mass flux from the source also defines the peak rate of solute loading to the receptor. Therefore, in this case, the mass flux from the source determines the ultimate long-term concentration at the receptor.

Solute release may be due to advection, which is a function of groundwater movement, and/or molecular diffusion, which is a function of chemical gradients. As such, factors that may influence solute mass flux out of the source include the groundwater flow in and around the source, the development of chemical gradients and the chemical properties of the solute.

WSP has examined the potential to complete full scale 3D coupled groundwater flow and solute transport for the JEB TMF. It was found that very fine scale meshing (millimetre scale discretization adjacent to the tailings mass) is required to provide consistent results between the analytical and numerical solutions with respect to the estimate of mass release at the tailings/host rock interface. At coarser scale discretization, it was found that the numerical models tended to over predict the amount of mass released from the tailings source. Upscaling the

model size and associated numerical discretization from the local to regional scale would not prove practical; run times would be excessive and not feasible. The general findings of this work were presented at GeoRegina 2014 (Tremblay et al. 2014,); and these findings remain applicable given current computing resources.

For this reason, “state-of-practice” in the analysis of these kinds of evaluations remains one of application of 3D numerical models to resolve the groundwater flow distribution combined with analytical solutions to solve the solute transport equations. This has been the approach WSP has adopted to support technical evaluations (and licensing) of Cameco’s in-pit tailings disposal facilities at Key Lake and Rabbit Lake, as well as completed work for Canadian Nuclear Laboratories environmental assessments at Chalk River and Whiteshell and the Teck Frontier Project environmental assessment.

With respect to assessing the long-term performance of the expanded JEB TMF, the GoldSim® software package (Version 14.0 R2) was used to simulate the transport of solutes from the tailings through the groundwater flow system to down gradient surface water receptors (i.e., Fox Lake and Pat Lake). GoldSim® is a commercially available, highly graphical, flexible, object-oriented computer program that is designed to provide the user with an understanding of the factors which control the performance of an engineered or natural system (as defined by a user specified mathematical model) and to predict the future behaviour (performance) of the defined system. GoldSim® was originally developed by Golder in the 1990’s as a comprehensive modelling program for assessing the performance of high-level radioactive waste repositories. More recently, GoldSim® has been used for addressing a wider range of non-nuclear environmental issues including site decommissioning and environmental risk assessment.

In January 2004, the GoldSim® Technology Group (an independent software and consulting company) was formed and the GoldSim® modelling software is now maintained and distributed by this company. A detailed description of the GoldSim® software, including example applications and manuals, is provided on their company website at www.GoldSim.com**.** The GoldSim® program is fully documented in the Main Users Guide (GTG 2025) and the Contaminant Transport Module Users Guide (GTG 2025). Version 14.0 R2 was used for the predictive calculations completed in this report.

5.3.1 Source Term Model

The conceptual model considers low-permeability tailings in direct contact with a high-permeability host rock for the portion of the tailings from the base of the pit to (approximately) elevation 436 m ASL. Tailings above elevation 436 m ASL (including only Cigar Lake-type tailings) are separated from the host rock and overburden by a low permeability liner system. As groundwater flows past the tailings mass, diffusive flux of solutes occurs across the tailings/host rock interface and tailings/liner interface (where applicable) into the active flow zone, in which chemical gradients develop until equilibrium is reached between the mass flux out of the tailings and the rate of removal by groundwater flow. In addition, groundwater originating as infiltration to the tailings mass flows through the tailings, resulting in some component of advective flux out of the tailings mass. Figure 16 provides a graphical representation of the conceptual model.

Within GoldSim®, the advective and diffusive components of mass flux are calculated separately. Advective flux is calculated as:

$J_A = Q_T C_0$ (Equation 1)

where:

Q_T = flow out of the tailings mass (L^3/T); and

C_0 = tailings source concentration (M/L^3).

Diffusive flux out of the tailings mass and through the groundwater flow zone normal to the direction of flow is calculated by applying Fick's Second Law:

$$\partial C/\partial t = D^* \frac{\partial^2 C}{\partial x^2} \qquad \text{(Equation 2)}$$

where:

C = solute concentration (M/L^3);

t = time (T);

D^* = effective diffusion coefficient (L^2/T); and

x = position (L).

The source concentrations within tailings pore water were considered to remain constant over time (i.e., no decay of the source at the tailings/host rock interface).

The concentration profiles adjacent to the tailings mass were calculated by dividing the zones into arrays of "mixing" cells within GoldSim® for a ten-metre wide active flow zone within the sandstone host rock and the constructed liner within the glacial drift. Diffusive mass flux was calculated between each of the cells and groundwater flow within the sandstone, normal to the direction of diffusion, was imposed across each cell based on predictions obtained from the three-dimensional flow model. For calculation of diffusion across the constructed liner, the flow through the liner parallel to the tailings interface was considered to be negligible and the concentration at the outside of the liner was assumed to be zero, which conservatively maximizes the calculated concentration gradient. Figure 16 shows the discretization applied to the flow zone adjacent to the tailings mass within GoldSim®.

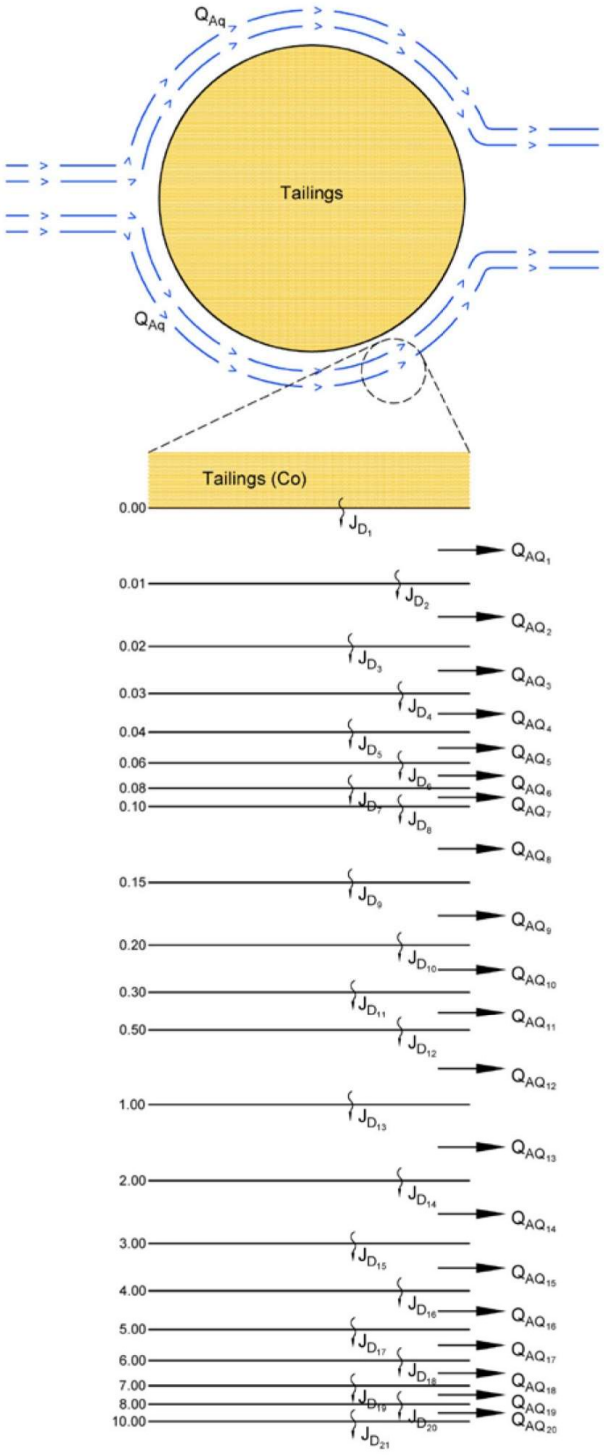

Goldsim

CLIENT orano

CONSULTANT wsp

YYYY-MM-DD	2025-05-21
PREPARED	KJ
DESIGN	JDS/KRC
REVIEW	
APPROVED	

PROJECT
JEB TMF
GROUNDWATER FLOW AND SOLUTE TRANSPORT

TITLE
CONCEPTUAL SOURCE TERM MODEL

PROJECT No.	PHASE	Rev.	FIGURE
CA0051344.8282	4000	A	**16**

5.3.1.1 Input Parameters

Input parameters for mass flux calculations are summarized in Table 9 and are discussed below.

The effective porosity (n_e) of sandstone samples collected from the JEB site was determined by laboratory testing (COGEMA 1997). Values were found to typically range from 6% to 16%. An average value of 11% was applied to mass flux calculations.

The effective diffusion coefficient (D^*) of a solute within a geologic media is calculated as the product of the aqueous diffusion coefficient (D_d) and a tortuosity factor (ω) (Fetter 1999). The tortuosity factor takes into account the effects of the geologic medium on the rate of diffusion. An effective diffusion coefficient of 3.0×10^{-11} m^2/s was applied to the mass flux calculation. This value represents effective diffusion coefficients determined for arsenic and radium with a tortuosity factor of 0.07, from radial diffusion tests conducted on sandstone core from the JEB site (COGEMA 1997).

The surface area of the tailings mass within the JEB TMF was determined based on as-built survey data for the facility and the design of expansion (468 Expansion) earthworks. Surface areas of the sides and top of the tailings within the facility were determined with computer-aided design software as a function of the height of tailings within the facility. The surface area of tailings in contact with the pit walls and drain is 123,000 square metres (m^2) (including 41,300 m^2 contact area with Cigar Lake tailings and 82,100 m^2 contact area with JEB-Sue tailings); that in contact with the liner is 127,600 m^2, and that of the top surface is 211,500 m^2.

The net percolation of precipitation through the low permeability barrier was assessed as part of the soil cover design report (Golder 2011) and was estimated to be 10 mm/yr, with an upper bound of 20 mm/yr.

The specific discharge through the sandstone adjacent to the tailings mass applied to the solute transport calculation was conservatively selected as the greatest value (i.e., 0.04 m/day through sand filter) predicted by the flow model (Section 4.2.2).

Table 9: Source Term Model Input Parameters

Parameter	TMF Expansion
Elevation Tailings Surface (JEB-Sue)	~422 m ASL
Elevation Tailings Surface (Cigar Lake)	~422 m ASL to 465.5 m ASL
Sandstone effective porosity (n_e)	11%
Effective Diffusion Coefficient (D^*)	$3x10^{-11}$ m^2/s
Tailings Lateral Surface Area (Cigar Lake, lined portion)	127,600 m^2
Tailings Lateral Surface Area (Cigar Lake, unlined portion)	41,300 m^2
Tailings Lateral Surface Area (JEB-Sue)	82,100 m^2
Tailings Lateral Surface Area (Total; A_L)	251,000 m^2
Tailings Top Surface Area (A_T; *applies to Cigar Lake Tailings*)	211,500 m^2
Cover Infiltration Rate (q_i)	10 mm/year to 20 mm/year
Specific Discharge Sandstone (q_{SS})	0.04 m/day

TMF = Tailings Management Facility; m ASL = metres above sea level; m^2/s = square metres per second; mm/day = millimetres per day.

5.3.2 Solute Transport Solution

Solute transport analyses describe the migration of solute in groundwater between a source and receptor, considering advective and diffusive transport mechanisms, and attenuation due to sorption behaviour and decay in transit.

The solute transport analysis performed for the decommissioned JEB TMF couples a one-dimensional solution to the advection-dispersion equation with particle tracking analysis conducted within the flow model. This method was used to calculate the mass of solute transported from the decommissioned JEB TMF to surface water receptors as a function of time. Particle tracking was performed in FEFLOW. The hydraulic head distribution calculated by FEFLOW was used to calculate the flow path followed by each particle assigned by the user. Representative travel distance and velocity of the first ten particles discharging to each receptor were applied to solute transport calculations.

The source term model described in the preceding section was applied to calculate the initial concentrations of solutes for each pathway. The one-dimensional advection-dispersion equation was solved for each aquifer pathway within GoldSim® using concentrations calculated by the source term model as a boundary condition and the corresponding travel distance and velocity distributions for each pathway. Within GoldSim®, computations are performed for each aquifer pathway by creating a temporary set of linked cell elements during the simulation, which are subsequently removed at the end of the simulation. Because the cells are linked together via advective and diffusive mechanisms, the behaviour of the cell network is mathematically described using a coupled system of differential equations. In effect, the network of cells created within an aquifer pathway is mathematically equivalent to a finite difference network. GoldSim® numerically solves the coupled system of equations to compute the solute mass present in the pathway and the mass fluxes leaving the pathway as a function of time.

The geometry of the pathways was defined by specifying the length and cross-sectional area of the aquifer, based on the results of particle tracking analyses and hydrostratigraphy. The specified aquifer infill medium and fluid saturation are used to determine the quantities of media in each cell. Advective and diffusive flux links are automatically created by GoldSim® to appropriately model advection, dispersion, and diffusion through the linked cells.

Mass enters at one end of the aquifer pathway, advects along (and disperses and diffuses within) the pathway, and then exits at the other end. Aquifer pathways (and hence the cells that are internally created to represent them) contain a fluid medium and a solid medium which can impact transport (e.g., by modifying the porosity of the pathway and/or acting to sorb and hence retard species). Radioactive decay and ingrowth are also considered for transport calculations performed for each pathway.

The governing equation for one-dimensional transport of a solute can be written as:

$$R\frac{\partial c}{\partial t} = D_x\frac{\partial^2 c}{\partial x^2} - u\frac{\partial c}{\partial x} - \lambda Rc \quad \text{(Equation 3)}$$

$$u = \frac{V_D}{n_e} \quad \text{(Equation 4)}$$

$$R = 1 + \frac{K_D}{n_e} \quad \text{(Equation 5)}$$

where:

V_D = Darcy velocity (L/T)

u= pore water velocity (L/T)

R = retardation factor

ρ_D = bulk dry density (M/L^3)

K_D =distribution coefficient (L^3/M)

n_e = effective porosity (-)

D_x = dispersion coefficient in the direction of flow (L^2/T)

t = time (T)

x = position in the direction of flow (L)

c = solute concentration (M/L^3)

λ = first order decay rate (T^{-1})

To simulate transport of solutes involved in sequential first-order decay reactions, Equation 3 is applied to the first species in the decay chain and coupled with the following, which represents transport of the remaining species:

$$R_i \frac{\partial c_i}{\partial t} = D_x \frac{\partial^2 c_i}{\partial x^2} - u \frac{\partial c_i}{\partial x} - \lambda_i R_i c_i + \lambda_{i+1} R_{i+1} c_{i+1} \qquad \text{(Equation 6)}$$

for i = 1…n

5.3.2.1 Input Parameters

Input parameters applied to solute transport calculations are summarized in Table 10. The following provides a discussion of the selection of the input parameters:

Travel Distance

The average travel distance (x) was estimated from the particle paths to be approximately 280 m to Fox Lake North Basin and approximately 790 m to Pat Lake.

Groundwater Velocity

Groundwater velocity (v) was estimated based on the particle paths to the receptors (first ten particles), considering the simulated specific discharge along each pathway, an effective porosity of 11% for sandstone. The calculated groundwater velocities were approximately to 0.06 m/d to Fox Lake and approximately 0.005 m/day to Pat Lake.

Longitudinal Dispersivity

Longitudinal dispersivity (α) is a scale-dependent parameter that accounts for mechanical mixing during transport of solute through an aquifer. Dispersivity is generally recognized to increase with flow path distance. Based on a literature review, it may be noted that typically longitudinal dispersivity is observed to be approximately ten percent of the flow path distance (Gelhar et al. 1992). As such, for transport calculations the longitudinal dispersivity was taken to be ten percent of the travel distance.

Distribution Coefficient

Partitioning of solute between liquid and solid phases along the pathway may be described in terms of a distribution coefficient (k_d). The distribution coefficient is the slope of a linear sorption isotherm and represents the ratio for the amount of solute adsorbed to solid phase to the concentration of dissolved solute for an instantaneous and fully reversible sorption process. Sorption behaviour acts to reduce the rate of solute migration with respect to the rate of groundwater movement during transient transport conditions, in which concentrations at a point along the pathway change with time. Therefore, sorption behaviour simply delays the breakthrough time of solute at a receptor but does not affect the steady-state concentration or mass flux where decay does not occur along the pathway. In the case of decay of the solute along the pathway, greater sorption will result in reduced mass flux to the receptor since more mass is lost due to decay over longer transport times.

Reversible sorption behaviour along the groundwater flow path was accounted for through the application of distribution coefficients for selected constituents. These include arsenic, nickel, thorium-230, radium-226, lead-210, and polonium-210. The remaining constituents were assigned distribution coefficients of zero (i.e., no sorption).

Distribution coefficients determined for arsenic partitioned to sandstone and sand on the Cigar Lake, Key Lake, and Midwest sites ranged from 1 to 100 litres per kilogram (L/kg) (COGEMA and CLMC 2001). A value of 1 L/kg was also found to be consistent with the lowest default value recommended for arsenic for environmental assessment (Thibault et al. 1990). Based on the above information, a conservative value of 1 L/kg was used to simulate sorption of arsenic during transport. Given the effective porosity of 11% and a bulk dry density of 2,400 kilograms per cubic metre (typical of sandstone in the area), a k_d of 1 L/kg translates to a retardation factor of approximately 20, which is to say that arsenic would move at a rate approximately 20 times slower than groundwater.

Sorption tests were conducted on sandstone samples collected from the JEB site. Results indicate a distribution coefficient of 50 L/kg describes sorption of radium-226 to sandstone. Radium-226 distribution coefficient values ranged from 3.8 to 128 L/kg for sandstone units within the Athabasca basin (COGEMA 1997). Measured values fall within the range reported for the region; therefore, they are considered suitable for application to solute transport calculations. Conservative values of 1 L/kg were applied to the remaining radionuclides.

Site specific nickel sorption test data are not available. A distribution coefficient of 2 L/kg was selected to simulate sorption of nickel based on values previously reported by Cameco (1994).

Radioactive Decay

Radioactive decay (λ) was incorporated into the transport simulations for uranium, thorium-230, radium-226, lead-210, and polonium-210. First order decay constants were calculated for each radioisotope based on each representative half-life.

Table 10: Solute Transport Calculation Input Parameters

Parameter	Model Input
Travel Distance (x)	Fox Lake Pathway: 280 m; Pat Lake Pathway 790 m
Groundwater Velocity (v)	Fox Lake Pathway: 0.06m/day; Pat Lake Pathway 0.005 m/d
Specific Discharge (q)[(a)]	Fox Lake Pathway: 0.0066 m/d; Pat Lake Pathway: 0.00056 m/d
Seepage Pathway Width	Fox Lake Pathway: 100 m; Pat Lake Pathway: 500 m
Units Thickness	Overburden: 20 m; Sandstone: 80 m
Dispersivity (α)	0.1x
Distribution Coefficient (k_d)	^{230} Th, ^{210} Pb, ^{210} Po, As: 1 L/kg Ni: 2 L/kg ^{226} Ra: 50 L/kg
First order decay constant (λ)	U: 1.55 E-10 1/year ($T_{1/2}$ = 4.5E9 year; A = 1.24 E4 Bq/g) ^{230} Th: 8.7 E-6 1/year ($T_{1/2}$ = 8000 year; A = 7.19 E8 Bq/g) ^{226} Ra: 4.3 E-4 1/year ($T_{1/2}$ = 1620 year; A = 3.62 E10 Bq/g) ^{210} Pb: 3.1 E-2 1/year ($T_{1/2}$ = 22.3 year; A = 2.83 W12 Bq/g) ^{210} Po: 1.83 1/year ($T_{1/2}$ = 0.378 year; A = 1.67 E14 Bq/g)

[(a)] Specific discharge is calculated using the porosity of sandstone, which is 0.11
TMF = Tailings Management Facility; m = metre; m/day = metres per day; L/kg = litres per kilogram; Bq/g = Becquerel per gram

5.4 Results

A parametric sensitivity analysis was conducted to identify those input parameters exerting the greatest influence on calculated mass loading rates from the decommissioned TMF. Table 11 presents the ranges of values of input parameters applied to the sensitivity analysis. Value ranges were selected to represent reasonable variation of each parameter. Mass flux calculations were performed while varying each input parameter individually over the selected range. Figure 17 presents the results of the sensitivity analysis for uranium. It is apparent based on the results that the cover infiltration rate and tailings pore water source concentrations exert the greatest control over the predicted mass flux from the decommissioned TMF. Based on the results of the sensitivity analysis, prediction and upper bound scenarios were developed for calculation of peak mass flux to receptors. The prediction case considered expected input parameter values and the upper bound case considered the compounding effects of increasing the cover infiltration from the predicted rate of 10 mm/year to the maximum rate of 20 mm/year and applying the probable maximum constituent source concentrations in tailings pore water.

Table 11: Solute Transport Sensitivity Analysis Inputs

Parameter	Minimum Value	Central Value	Maximum Value
Source Concentration (mg/L)	0.5*Predicted Long-Term Value	Predicted Long-Term Value	2* Predicted Long-Term Value
Sandstone effective porosity (n_e)	1%	11%	20%
Effective Diffusion Coefficient (D^*)	6 x 10^{-12} m^2/s	3 x 10^{-11} m^2/s	1.5 x 10^{-10} m^2/s
Cover Infiltration Rate (q_i)	5 mm/yr	10 mm/yr	20 mm/yr
Specific Discharge Sandstone (q_{SS})	0.004 m/day	0.04 m/day	0.4 m/day
Tailings Hydraulic Conductivity ($K_{tailings}$)	1x10^{-9} m/s	1x10^{-8} m/s	1x10^{-7} m/s
Removal of Liner	N/A	Liner K = 1x10^{-9} m/s	Liner removed

mg/L = milligrams per litre; m^2/s = square metres per second; mm/yr = milligrams per year; m/day = metres per day; m/s = metres per second

Predicted and upper bound mass flux from the expanded JEB TMF were calculated with the GoldSim® model based on the results of the groundwater flow model for the expanded TMF (Section 4.2) and updated source concentrations (Table 9). Predicted values were calculated using best estimates of net percolation through the soil cover into the tailings and source concentrations and upper bound values were based on maximum probable values of net percolation and source concentrations. Calculated predicted and upper bound case steady state mass fluxes of pore water constituents are presented in Table 12. The calculated mass fluxes from the expanded TMF were taken as 70% discharging via groundwater to the north basin of Fox Lake and 30% to Pat Lake. The total mass loadings out of the TMF were applied to Pat Lake since that which reports to Fox Lake would report to Pat Lake by overland flow. The incremental concentrations for each receptor were calculated based on the calculated mass loadings and the average annual flows through the north basin of Fox Lake (5,763 m^3/day), Fox Lake (14,743 m^3/day) and Pat Lake (18,465 m^3/day) (AREVA 2011b).

Table 13 and Table 14 respectively present predicted and upper bound incremental constituent concentrations for Fox Lake and Pat Lake. Predicted constituent concentrations for most species in all receiving waters are typically indistinguishable from to marginally above baseline concentrations and less than Saskatchewan Environmental Quality Guidelines (SEQG) for protection of aquatic life. Calculated cadmium, cobalt and lead concentrations exceed SEQG criteria, however this is an artefact of the guideline being less than the baseline concentrations for these constituents. For all three constituents, the incremental concentration is negligible in relation to the baseline concentration.

Figure 18 graphically presents predicted long-term water quality in Fox Lake North Basin for selected constituents. Resulting concentrations of solutes are compared to baseline concentrations (AREVA 2009) and to SEQG for protection of aquatic life. Predicted long-term water quality is within water quality guidelines for all constituents except uranium for the upper bound simulation. Arsenic and uranium appear to be the most sensitive constituents with predictions approaching 28% of objective values and upper bound values approaching 72% of the surface water arsenic guideline and exceeding the surface water uranium guideline.

Solute transport calculations were performed for the predicted rates of constituent loading from the TMF to the active groundwater flow zone, as derived by the source term model. The results of the solute transport analysis are presented in terms of mass flux to surface water receptors as a function of time and are plotted for arsenic, nickel, uranium and radium-226 in Figure 19 for Fox Lake and Pat Lake. Predicted and upper bound steady state mass fluxes to receptors for all constituents are presented in Table 13 and Table 14.

Table 12: Expanded JEB TMF Predicted Peak Mass Flux

Constituent	Cigar Lake Tailings Pore Water Concentration		JEB-Sue Tailings Pore Water Concentration		Mass Flux Out of Tailings		Mass Flux To Fox Lake		Mass Flux To Pat Lake	
	(mg/L or Bq/L)		(mg/L or Bq/L)		(kg/a or MBq/a)		(kg/a or MBq/a)		(kg/a or MBq/a)	
	Prediction	Upper Bound	Prediction	Upper Bound	Prediction	Upper Bound	Prediction	Upper Bound	Prediction	Upper Bound
Chloride	118.12	145.15	43.86	82.7	259	622	181	435	259	622
Sulphate	3292.61	4325	2205.84	2578	7706	18612	5394	13029	7706	18612
Ammonia	13.29	35.55	11.69	24.4	33	156	23	109	33	156
Arsenic	0.76	1.78	1.27	2.98	2.16	9.19	1.52	6.44	2.16	9.19
Cadmium	0.00041	0.0011	0.0009	0.0022	0.00128	0.00597	0.00089	0.00418	0.00128	0.00597
Cobalt	0.047	0.27	0.15	0.47	0.17	1.41	0.12	0.99	0.17	1.41
Copper	0.004	0.017	0.0019	0.0046	0.01	0.07	0.01	0.05	0.01	0.07
Lead	0.0009	0.007	0.0021	0.0142	0.003	0.038	0.002	0.027	0.003	0.038
Molybdenum	5.34	13.68	8	14.09	14.7	63.6	10.3	44.5	14.7	63.6
Nickel	0.168	0.63	2.37	8.11	1.54	8.89	1.08	6.23	1.54	8.89
Selenium	0.007	0.032	0.0095	0.052	0.02	0.16	0.01	0.11	0.02	0.16
Vanadium	0.0043	0.0077	0.021	0.18	0.019	0.173	0.01	0.12	0.019	0.173
Zinc	0.008	0.032	0.026	0.7	0.03	0.68	0.02	0.48	0.03	0.68
Polonium-210[(a)]	0.51	0.62	0.75	3.55	15.6	46.4	13	48	13	49
Lead-210[(a)]	2.29	6.25	2.2	4	20	69	13	48	13	49
Radium-226[(a)]	4.11	7.7	4.63	16	10.2	41.2	0.13	0.47	0.15	0.50
Thorium-230[(a)]	1	1.1	1.11	1.55	2.56	5.45	1.79	3.80	2.5	5.3
Uranium	3.08	7.59	9.37	53.36	11	72	8	50	11	72

[(a)]Polonium-210, Lead-210, Radium-226 and thorium-230 are expressed as Bq/L or Bq/a.
mg/L = milligrams per litre; Bq/L = Becquerel per litre; kg/a = kilograms per year; MBq/a = Megabecquerel per year.

Table 13: Expanded JEB TMF Predicted Receptor Surface Water Quality

Constituent	Units	Baseline Concentration			Incremental Concentration			Resulting Concentration			Water Quality Criteria
		Fox Lake North Basin	Fox Lake	Pat Lake	Fox Lake North Basin	Fox Lake	Pat Lake	Fox Lake North Basin	Fox Lake	Pat Lake	SEQG- Fresh Water Aquatic Life
Chloride	mg/L	0.133	0.133	0.12	8.60E-02	3.36E-02	3.83E-02	0.22	0.17	0.16	120 [b,e]
Sulfate	mg/L	0.633	0.633	0.71	2.56E+00	1.00E+00	1.14E+00	3.20	1.64	1.85	128-429[c]
Ammonia	mg/L	0.021	0.021	0.014	1.08E-02	4.23E-03	4.82E-03	0.032	0.025	0.019	1.54[a,e,f]
Arsenic	mg/L	0.00052	0.00052	0.00074	7.20E-04	2.81E-04	3.19E-04	0.00124	0.00080	0.00106	0.005[a,b,e]
Cadmium	mg/L	0.001	0.001	0.001	4.25E-07	1.66E-07	1.89E-07	**0.0010**	**0.0010**	**0.0010**	0.00004 – 0.00037[b,e]
Cobalt	mg/L	0.001	0.001	0.001	5.66E-05	2.21E-05	2.52E-05	**0.0011**	0.0010	0.0010	0.001[d]
Copper	mg/L	0.002	0.002	0.002	2.98E-06	1.17E-06	1.33E-06	0.0020	0.0020	0.0020	0.002 – 0.004[a]
Lead	mg/L	0.005	0.005	0.006	9.53E-07	3.73E-07	4.25E-07	**0.0050**	**0.0050**	**0.0060**	0.001[a]
Molybdenum	mg/L	0.005	0.005	0.005	4.90E-03	1.92E-03	2.19E-03	0.0099	0.0069	0.0072	0.073- 31[a,b,e]
Nickel	mg/L	0.003	0.003	0.003	5.12E-04	2.00E-04	2.03E-04	0.0035	0.0032	0.0032	0.025-0.15[a]
Selenium	mg/L	0.001	0.001	0.001	6.26E-06	2.45E-06	2.79E-06	0.0010	0.0010	0.0010	0.001[a]
Vanadium	mg/L	0.01	0.01	0.01	6.40E-06	2.50E-06	2.86E-06	0.010	0.010	0.010	-
Zinc	mg/L	0.006	0.006	0.006	9.71E-06	3.80E-06	4.33E-06	0.0060	0.0060	0.0060	0.030[a]
Polonium-210	Bq/L	0.008	0.008	0.006	6.07E-03	2.37E-03	1.98E-03	0.014	0.010	0.008	-
Lead-210	Bq/L	0.022	0.022	0.02	6.01E-03	2.35E-03	1.95E-03	0.028	0.024	0.022	-
Radium-226	Bq/L	0.005	0.005	0.006	6.37E-05	2.49E-05	2.20E-05	0.0051	0.0050	0.0060	0.11[b]
Thorium-230	Bq/L	0.012	0.012	0.013	8.50E-04	3.32E-04	3.68E-04	0.013	0.012	0.013	-
Uranium	mg/L	0.0006	0.0006	0.0006	3.63E-03	1.42E-03	1.62E-03	0.0042	0.0020	0.0022	0.015[a,b,e]

[a] SSWQO – Saskatchewan Surface Water Quality Objective for the Protection of Aquatic Life (Water Security Agency 2015)
[b] SEQG – Saskatchewan Environmental Quality Guidelines (GS: as reported on April 24, 2025)
[c] BC – British Columbia Water Quality Guideline (BCMOE 2025)
[d] FEQG – Federal Environmental Quality Guideline (EC 2017)
[e] CWQG – Canadian Water Quality Guidelines (CCME: as reported on April 24, 2025)
[f] Ammonia guildelines are temperature and pH dependent. Value shown for pH = 7.5 and temperature = 20oC
Bold indicates an exceedance of SEQG
mg/L = milligrams per litre; Bq/L = Becquerel per litre; CCME = Canadian Council of Ministers of the Environment; SEQG = Saskatchewan Environmental Quality Guidelines

Table 14: Expanded JEB TMF Upper Bound Receptor Surface Water Quality

Constituent	Units	Baseline Concentration			Incremental Concentration			Resulting Concentration			Water Quality Criteria
		Fox Lake North Basin	Fox Lake	Pat Lake	Fox Lake North Basin	Fox Lake	Pat Lake	Fox Lake North Basin	Fox Lake	Pat Lake	SEQG- Fresh Water Aquatic Life
Chloride	mg/L	0.133	0.133	0.12	2.07E-01	8.08E-02	9.22E-02	0.34	0.21	0.21	120 [b,e]
Sulfate	mg/L	0.633	0.633	0.71	6.19E+00	2.42E+00	2.76E+00	6.82	3.05	3.47	128-429[c]
Ammonia	mg/L	0.021	0.021	0.014	5.17E-02	2.02E-02	2.31E-02	0.073	0.041	0.037	1.54[a,e,f]
Arsenic	mg/L	0.00052	0.00052	0.00074	3.06E-03	1.20E-03	1.35E-03	0.00358	0.00172	0.00209	0.005[a,b,e]
Cadmium	mg/L	0.001	0.001	0.001	1.99E-06	7.76E-07	8.85E-07	**0.0010**	**0.0010**	**0.0010**	0.00004 – 0.00037[b,e]
Cobalt	mg/L	0.001	0.001	0.001	4.69E-04	1.83E-04	2.09E-04	**0.0015**	**0.0012**	**0.0012**	0.001[d]
Copper	mg/L	0.002	0.002	0.002	2.29E-05	8.94E-06	1.02E-05	0.0020	0.0020	0.0020	0.002 – 0.004[a]
Lead	mg/L	0.005	0.005	0.006	1.27E-05	4.96E-06	5.66E-06	**0.0050**	**0.0050**	**0.0060**	0.001[a]
Molybdenum	mg/L	0.005	0.005	0.005	2.12E-02	8.27E-03	9.43E-03	0.0262	0.0133	0.0144	0.073- 31[a,b,e]
Nickel	mg/L	0.003	0.003	0.003	2.96E-03	1.16E-03	1.17E-03	0.0060	0.0042	0.0042	0.025-0.15[a]
Selenium	mg/L	0.001	0.001	0.001	5.46E-05	2.13E-05	2.43E-05	**0.0011**	0.0010	0.0010	0.001[a]
Vanadium	mg/L	0.01	0.01	0.01	5.77E-05	2.25E-05	2.57E-05	0.010	0.010	0.010	-
Zinc	mg/L	0.006	0.006	0.006	2.27E-04	8.87E-05	1.01E-04	0.0062	0.0061	0.0061	0.030[a]
Polonium-210	Bq/L	0.008	0.008	0.006	2.29E-02	8.94E-03	7.29E-03	0.031	0.017	0.013	-
Lead-210	Bq/L	0.022	0.022	0.02	2.27E-02	8.86E-03	7.21E-03	0.045	0.031	0.027	-
Radium-226	Bq/L	0.005	0.005	0.006	2.24E-04	8.74E-05	7.42E-05	0.0052	0.0051	0.0061	0.11[b]
Thorium-230	Bq/L	0.012	0.012	0.013	1.81E-03	7.07E-04	7.82E-04	0.014	0.013	0.014	-
Uranium	mg/L	0.0006	0.0006	0.0006	2.38E-02	9.32E-03	1.06E-02	**0.0244**	0.0099	0.0112	0.015[a,b,e]

[a] SSWQO – Saskatchewan Surface Water Quality Objective for the Protection of Aquatic Life (Water Security Agency 2015)
[b] SEQG – Saskatchewan Environmental Quality Guidelines (GS: as reported on April 24, 2025)
[c] BC – British Columbia Water Quality Guideline (BCMOE 2025)
[d] FEQG – Federal Environmental Quality Guideline (EC 2017)
[e] CWQG – Canadian Water Quality Guidelines (CCME: as reported on April 24, 2025)
[f] Ammonia guildelines are temperature and pH dependent. Value shown for pH = 7.5 and temperature = 20oC
Bold indicates an exceedance of SEQG
mg/L = milligrams per litre; Bq/L = Becquerel per litre; CCME = Canadian Council of Ministers of the Environment; SEQG = Saskatchewan Environmental Quality Guidelines

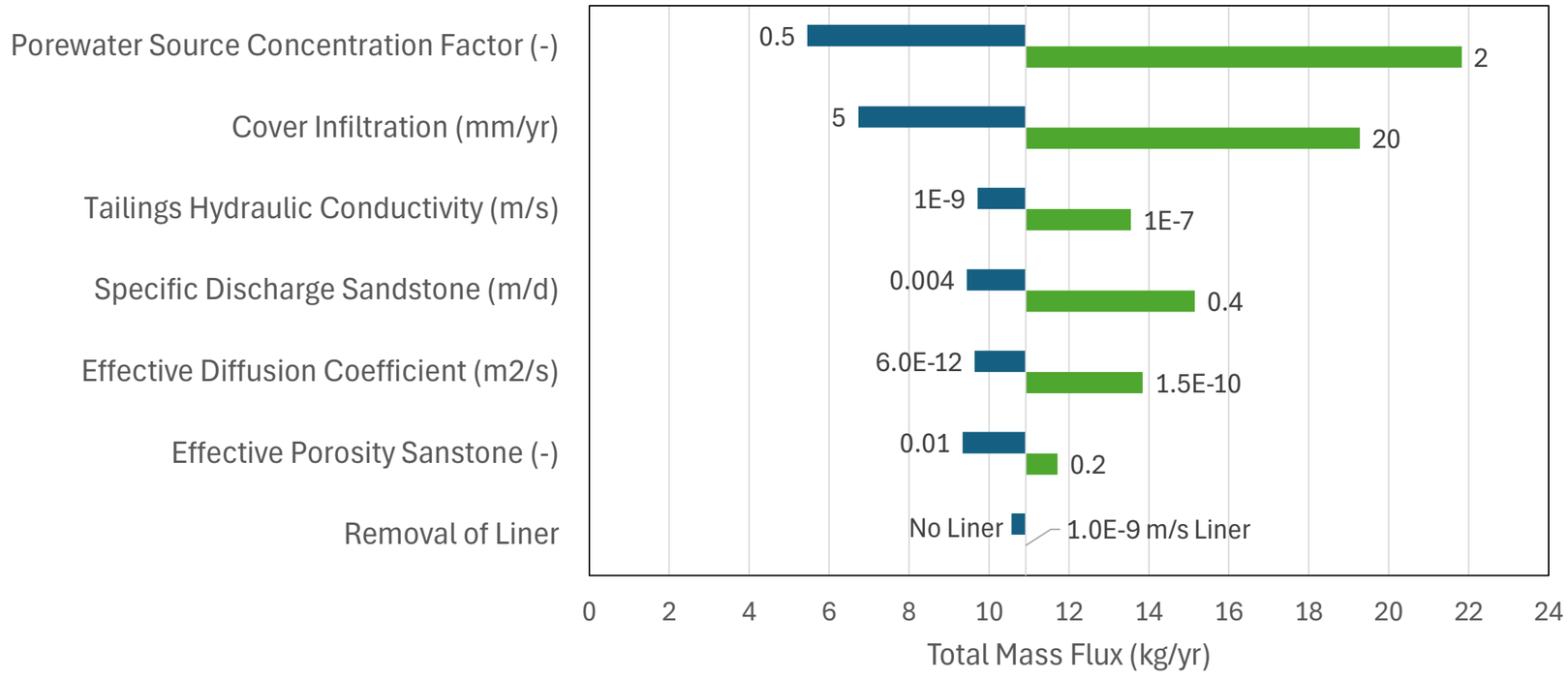

CLIENT orano

CONSULTANT wsp

YYYY-MM-DD	2025-05-01
PREPARED	KJ
DESIGNED	KJ
REVIEWED	
APPROVED	

PROJECT
JEB TMF
GROUNDWATER FLOW AND SOLUTE TRANSPORT

TITLE
SENSITIVITY ANALYSIS RESULTS FOR URANIUM

PROJECT NO.	PHASE	REV.	FIGURE
CA0051344.8282	4000	A	**17**

IF THIS MEASUREMENT DOES NOT MATCH WHAT IS SHOWN, THE SHEET SIZE HAS BEEN MODIFIED FROM: ANSI B
25mm
0

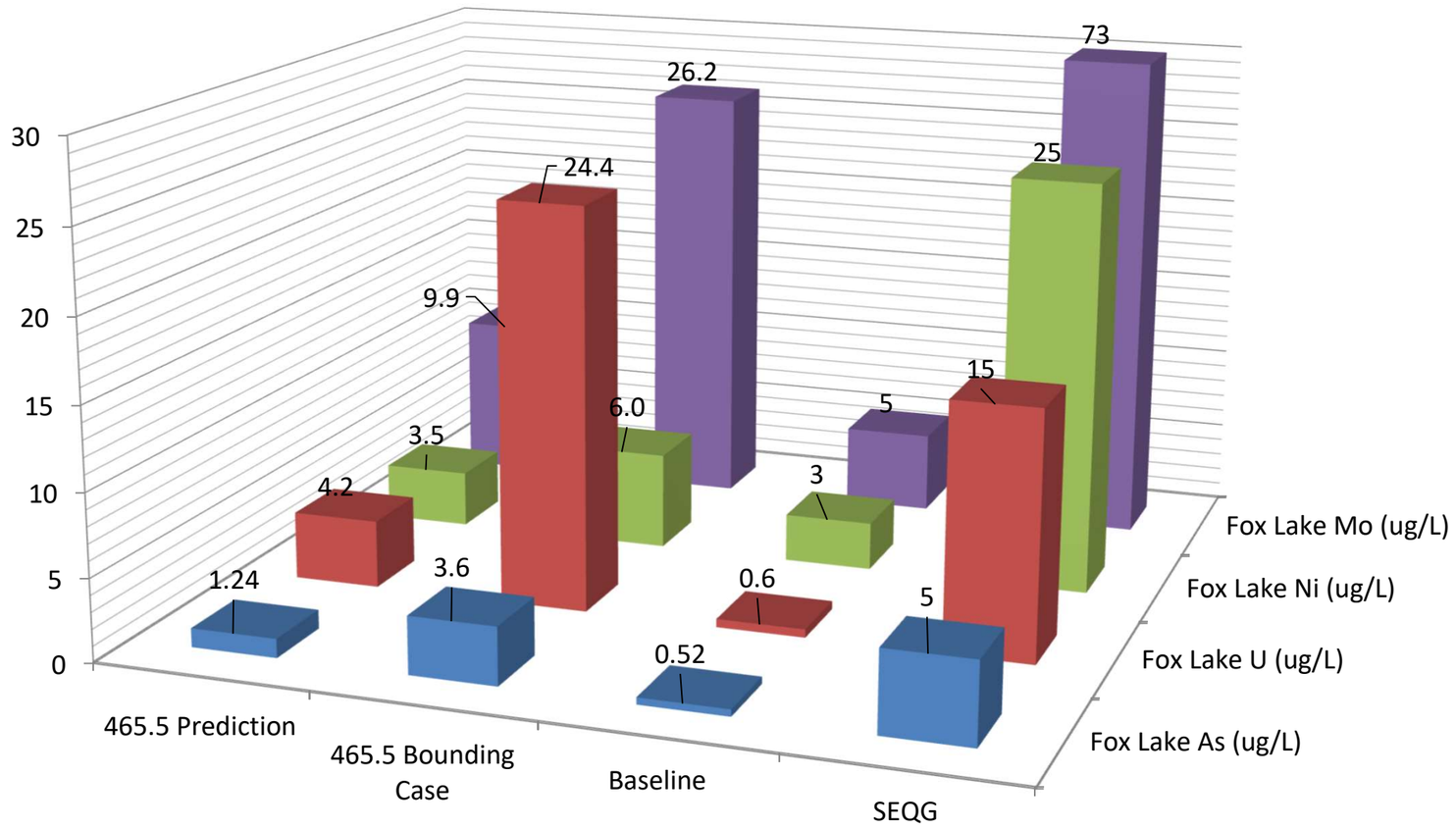

	465.5 Prediction	465.5 Bounding Case	Baseline	SEQG
Fox Lake As (ug/L)	1.24	3.6	0.52	5
Fox Lake U (ug/L)	4.2	24.4	0.6	15
Fox Lake Ni (ug/L)	3.5	6.0	3	25
Fox Lake Mo (ug/L)	9.9	26.2	5	73

CLIENT orano

CONSULTANT wsp

YYYY-MM-DD 2025-05-01
PREPARED KJ
DESIGNED KJ
REVIEWED
APPROVED

PROJECT
JEB TMF
GROUNDWATER FLOW AND SOLUTE TRANSPORT

TITLE
PREDICTED AND BOUNDING CASE LONG TERM EFFECTS TO FOX LAKE

PROJECT NO. CA0051344.8282 | PHASE 4000 | REV. A | FIGURE **18**

IF THIS MEASUREMENT DOES NOT MATCH WHAT IS SHOWN, THE SHEET SIZE HAS BEEN MODIFIED FROM: ANSI B
25 mm
0

Fox Lake

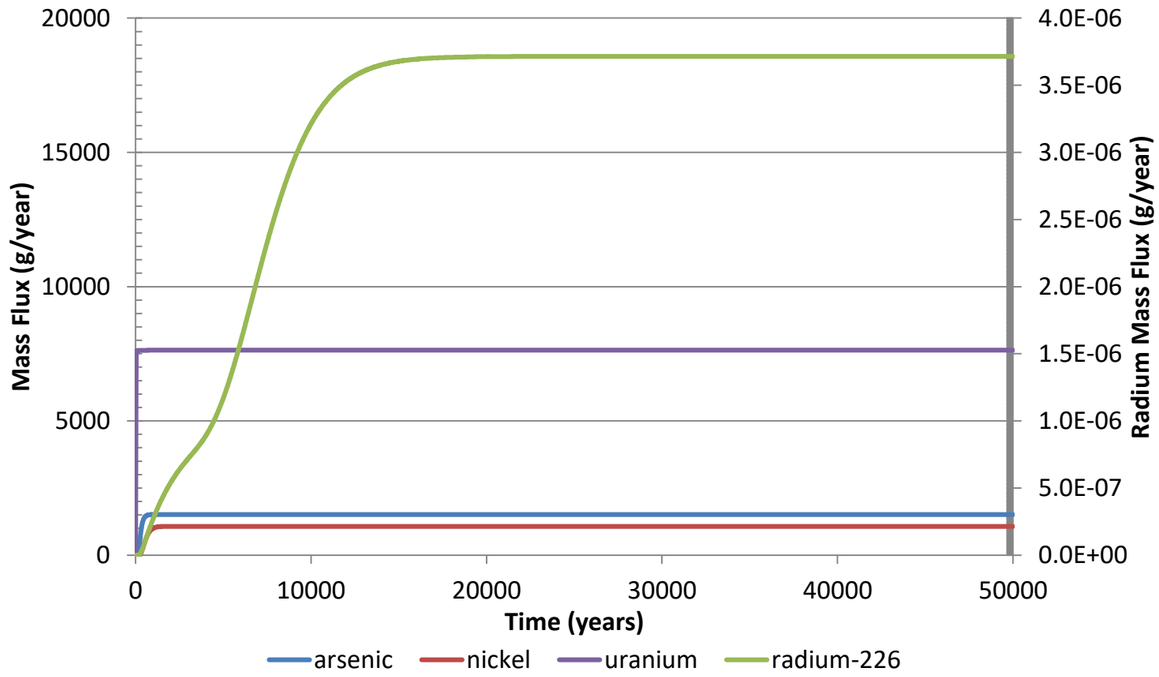

Pat Lake

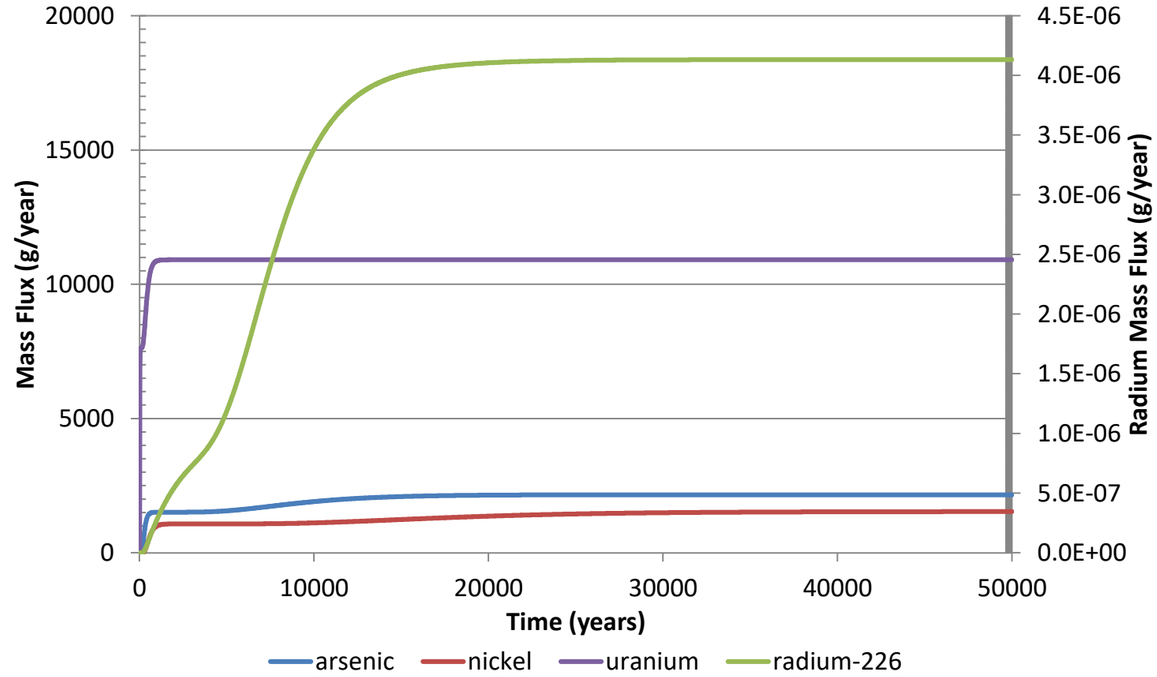

CLIENT orano

CONSULTANT wsp

YYYY-MM-DD	2025-05-01
PREPARED	KJ
DESIGNED	KJ
REVIEWED	
APPROVED	

PROJECT
JEB TMF
GROUNDWATER FLOW AND SOLUTE TRANSPORT

TITLE
MASS FLUX TO RECEPTORS VS TIME

PROJECT NO.	PHASE	REV.	FIGURE
CA0051344.8282	4000	A	**19**

IF THIS MEASUREMENT DOES NOT MATCH WHAT IS SHOWN, THE SHEET SIZE HAS BEEN MODIFIED FROM: ANSI B
25 mm
0

The peak mass flux to the receptors coincides with the condition of steady-state transport, at which time no change in solute concentrations occurs with time at any given point along the pathway. Under this condition, the mass flux to the receptor equals that leaving the source, where no decay occurs in transit. These conditions are predicted because of the application of a non-depleting source. For the case of radionuclide such as radium-226, the mass flux to the receptor is lower than that leaving the source due to attenuation along the pathway owing to sorption, which allows time for radioactive decay to occur.

The average arrival time of a solute plume at a given point along the pathway may be defined as the time at which the solute concentration reaches half of the ultimate steady-state value. The arrival time will vary from one solute to another depending on the degree of attenuation. For unattenuated species, the average arrival time to Fox Lake is approximately 20 years. Moderately attenuated species such as arsenic and nickel show breakthrough at receptors in 280 to 540 years. Arrival time for radium-226 is expected to occur in approximately 6,520 years with peak radium-226 loadings occurring after approximately 20,800 years.

6 SUMMARY AND CONCLUSIONS

WSP updated the previously developed groundwater model to include revised regional faults provided by Orano. Following this update, WSP confirmed that the updated model reasonable reproduces measured data from tested operational stages and a field pumping trial.

The updated model was used to complete predictive simulations of the 468 Expansion and to predict solute transport pathways from the TMF following mine closure. For full build 468 Expansion (tailings elevation of 465.5 m ASL and ≤467 m ASL TMF pond elevation), hydraulic containment was maintained in each sensitivity scenarios if the base drain elevation is maintained 8 m or more below the Fox Lake elevation. Base drain pumping rates are expected to be approximately 2,250 m^3/d for a head differential of 8 m between the TMF pond and base drain.

The key monitoring data that support hydraulic containment continue to be water elevation data used for head differential determination; therefore, the JEB TMF pond, Fox Lake and drift monitoring well water elevations must continue to be monitored regularly.

Discharge from the TMF following mine closure is predicted to migrate east and south towards Fox and Pat Lake. In general, the volume of discharge from the TMF is mainly derived from the net percolation of precipitation through the low permeability cover with a small component from groundwater inflow. Approximately 68% of the TMF flow discharges to Fox Lake and 32% discharges to Pat Lake.

Arsenic and uranium appear to be the most sensitive constituents with predictions approaching 28% of objective values and upper bound values approaching 72% of the surface water arsenic guideline and exceeding the surface water uranium guideline. Predicted long-term cadmium, cobalt and lead concentrations exceed surface water quality guidelines because they reflect baseline concentration values and are not due to mass loading from the TMF.

Signature Page

WSP Canada Inc.

Kartik Jain, M.A.Sc.
Mine Water Group

Jennifer Levenick, M.Sc.
Mine Water Group

Mike Tremblay, M.Sc., P.Eng.
Geotechnical Engineering, Prairies and North

KJ/JL/MT

https://wsponlinecan.sharepoint.com/sites/ca-ca0051344.8282/shared documents/05. technical/4000_reporting/ca0051344.8282-001-r-reva-gw model update_9jun_2025.docx

REFERENCES

AREVA (AREVA Resources Canada Inc.). 2009. Caribou Project Environmental Impact Statement, February, Saskatoon, Saskatchewan.

AREVA. 2011a. McClean Lake Operation – Tailings Optimization and Validation Program Validation of Long Term Tailings Performance Report (2009), April, Saskatoon, Saskatchewan

AREVA). 2011b. McClean Lake Operation – Technical Information Document. Hydrogeology and Groundwater Modelling of the Collins Creek Basin, December, Saskatoon, Saskatchewan

AREVA. 2015. McClean Lake Operation Tailings Management Technical Information Document. Version 2, Revision 0. May 2015

AREVA. 2016. McClean Lake Operation – Notification to Expand the JEB Tailings Management Facility. June 2016.

Cameco (Cameco Corporation). 1994. The McArthur River Project Environmental Impact Statement, Saskatoon, Saskatchewan.

Cameco and AREVA. 2008. Rabbit Lake Solution Processing Project Environmental Impact Statement, January, Saskatoon, Saskatchewan.

COGEMA (COGEMA Resources Inc.). 1997. McClean lake Project JEB Tailings Management Facility. December. Saskatoon. Saskatchewan.

COGEMA. 2004. McClean Lake Operation, Tailing Management, Technical Information Document, February 2004 – Version 1.

COGEMA and Cigar Lake Mining Corporation (CLMC). 2001. Disposal of Cigar Lake Waste Rock environmental Impact Statement, August, Saskatoon, Saskatchewan.

Diersch, H.G. 2010. FEFLOW Finite Element Subsurface Flow and Transport Simulation System. WASY Institute for Water Resources Planning and System Research Ltd., Berlin, Germany.

Fetter, C. W. 1999. Contaminant Hydrogeology. Prentice Hall Inc. Upper Saddle River, Jew Jersey.

Gelhar, L.W., C. Welty, and K.R. Rehfeldt. 1992. A critical review of data on field-scale dispersion in aquifers. Water Resources, V.28, N.7, p. 1955-1974

Golder (Golder Associates Ltd.). 2009. Draft Report on Hydrogeological Assessment of Mining Options, McClean Lake, Saskatchewan. April 2009.

Golder. 2011. JEB TMF Expansion Stage 1 Project Soil Cover Design.

Golder. (2019). *Groundwater Flow and Solute Transport Report - JEB TMF Expansion Stage 2 Project.* Saskatoon.

Golder. (2020). *Drift Monitoring Well Decommissioning Plan for JEB TMF Expansion Stage 2 Embankment.* Technical Memorandum.

Golder. (2021). *Assessment of JEB TMF Hydraulic Containment and Monitoring.* Technical Memorandum.

GTG (GoldSim® Technology Group). 2025. GoldSim® User's Guide. Version 15, January 2025.

GTG (GoldSim® Technology Group). 2025. GoldSim® Contaminant Transport Module User's Guide. Version 15, January 2025.

Harbaugh, A.W. 2005. MODFLOW-2005, the U.S. Geological Survey Modular Ground-Water Model—The Ground-Water Flow Process. U.S. Geological Survey Techniques and Methods 6-A16.

Stober I., K. Bucher. 2007 Hydraulic Properties of the Crystalline Basement. Hydrogeology Journal. Vol.15, Issue 2, pp 213-224.

Thibault, D.H., M.I. Sheppard, P.A. Smith, 1990, A Critical Compilation and Review of Default Solid/Liquid Partition Coefficients, Kd, for use in Environmental Assessments. Atomic Energy of Canada Limited.

Tremblay M., B. Schmid, G. Misfeldt, R McLaren, 2014, An Approach to Solute Transport Prediction for an In-Pit Uranium Tailings Management Facility. In proceeding of the 67th Canadian Geotechnical Conference, Regina, Saskatchewan.

LIMITATIONS

USE OF THE REPORT AND ITS CONTENT

This report has been prepared for the exclusive use of Orano. The factual information, descriptions, interpretations, comments, recommendations, and electronic files contained herein are specific to the project described in this report and do not apply to any other project or site. Under no circumstances may this information be used for any other purposes than those specified in the scope of work unless explicitly stipulated in the text of this report or formally authorized by WSP. This report must be read in its entirety as some sections could be falsely interpreted when taken individually or out-of-context. As well, the final version of this report and its content supersedes any other text, opinion or preliminary version produced by WSP.

WSP shall not be held responsible for damages resulting from unpredictable or unknown underground conditions, from erroneous information provided by and/or obtained from sources other than WSP, and from ulterior changes in the site conditions unless WSP has been notified by Orano of any occurrence, activity, information or discovery, past or future, susceptible of modifying the underground conditions described herein, and have had the opportunity of revising its interpretations, comments and recommendations. Furthermore, WSP shall not be held responsible for damages resulting from any future modification to the applicable regulations, standards and criteria, for any use of this report and its content by a third party, and/or for its use for purposes other than those intended. WSP shall not be held responsible for any decrease, real or perceived, of a property's value or any failure to complete a transaction, as a consequence of this report.

References to acts and regulations that may be contained in this report are informally provided on a technical basis. Since acts and regulations are subject to interpretation, WSP recommends Orano to consult with legal counsel to obtain suitable advice.

GROUNDWATER MODELLING GENERAL LIMITATIONS

The professional groundwater modelling services performed as described in this report were conducted in a manner consistent with that level of care and skill normally exercised by other members of the engineering and science professions currently practising under similar conditions, subject to the quality and quantity of available data, the time limits, and financial and physical constraints applicable to the services. Unless otherwise specified, the results of previous or simultaneous work provided by sources other than WSP and quoted and/or used herein are considered as having been obtained according to recognised and accepted professional rules and practices and therefore deemed valid. This model provides a predictive scientific tool to evaluate the impacts on a real groundwater system of specified hydrological stresses and/or to compare various scenarios in a decision-making process. However, despite the professional care taken during the construction of the model and in conducting the simulations, its accuracy is bound to the normal uncertainty associated to groundwater modelling and no warranty, expressed or implied, is made.

APPENDIX A

Predicted Seepage Migration Pathways (Particle Tracking Analysis)

Plan View

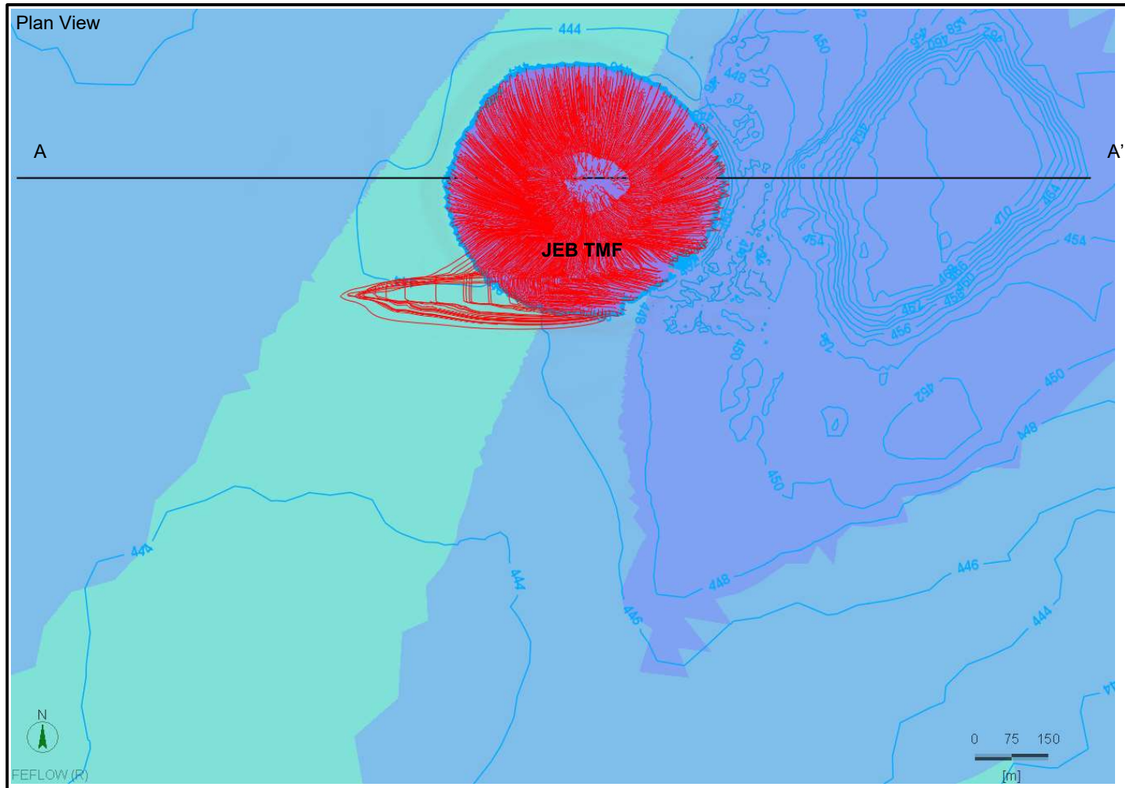

SCENARIO 1 : BASE DRAIN ELEVATION 439.7 M ASL

BASE DRAIN WATER ELEVATION (MASL)	FOX LAKE ELEVATION (MASL)	PAT LAKE ELEVATION (MASL)	HEAD DIFFERENTIAL, $DH_{FOX\ LAKE}$ (M)	GROUNDWATER INFLOW TO DRAIN (M^3/D)
439.7	445.7	443.4	6	1855

A

A'

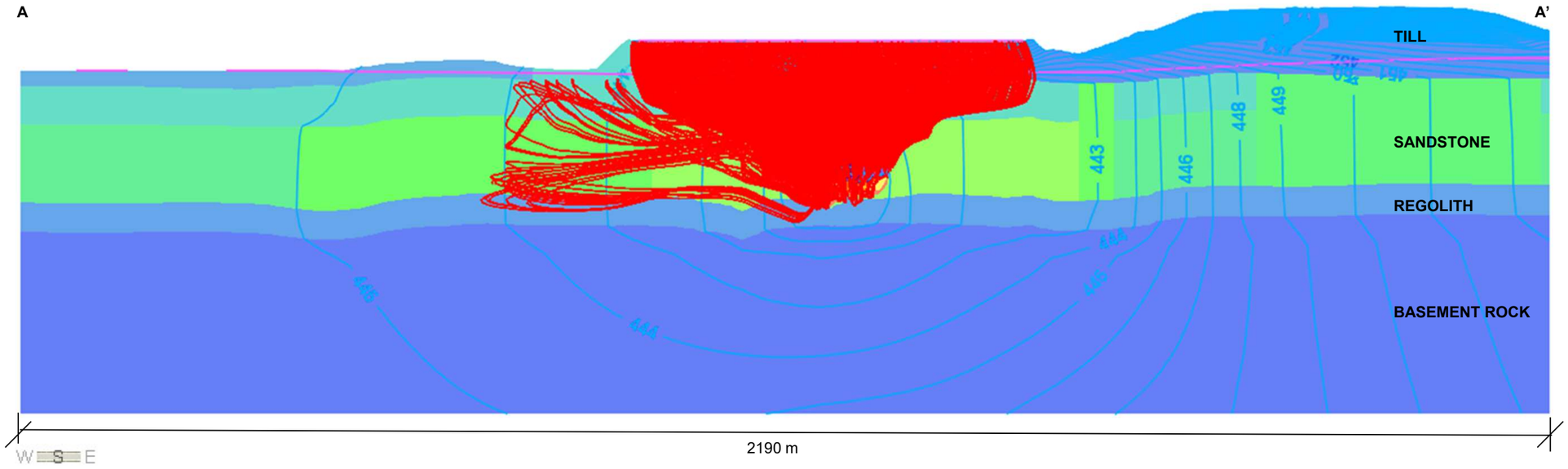

HYDRAULIC CONDUCTIVITY, K (M/S)

- 0.01
- 0.001
- 0.0001
- 1e-05
- 1e-06
- 1e-07
- 1e-08
- 1e-09

LEGEND

- CROSS-SECTION LINE
- WATER TABLE
- HYDRAULIC HEAD (M)
- PARTICLE PATH LINE

NOTE(S)

VERTICAL EXAGGERATION FOR CROOSS-SECTION 1:2
M = METER
M/S = METERS PER SECOND
M^3/DAY = CUBIC METRES PER DAY
MASL = METERS ABOVE SEA LEVEL

CLIENT: orano

CONSULTANT: wsp

YYYY-MM-DD	2025-05-01
PREPARED	KJ
DESIGNED	KJ
REVIEWED	
APPROVED	

PROJECT
JEB TMF
GROUNDWATER FLOW AND SOLUTE TRANSPORT

TITLE
GROUNDWATER PARTICLE TRACKING ANALYSIS
SCENARIO 1
BASE DRAIN ELEVATION 439.7 M ASL

PROJECT NO.	PHASE	REV.	FIGURE
CA0051344.8282	4000	A	**A1**

IF THIS MEASUREMENT DOESN'T MATCH WHAT IS SHOWN, THE SHEET SIZE HAS BEEN MODIFIED FROM ANSI B

25mm

0

Prediction_FullBuild_468_high K cigar -6m dh low K cigar_2025_linerDp_BC_fig.dac

Plan View

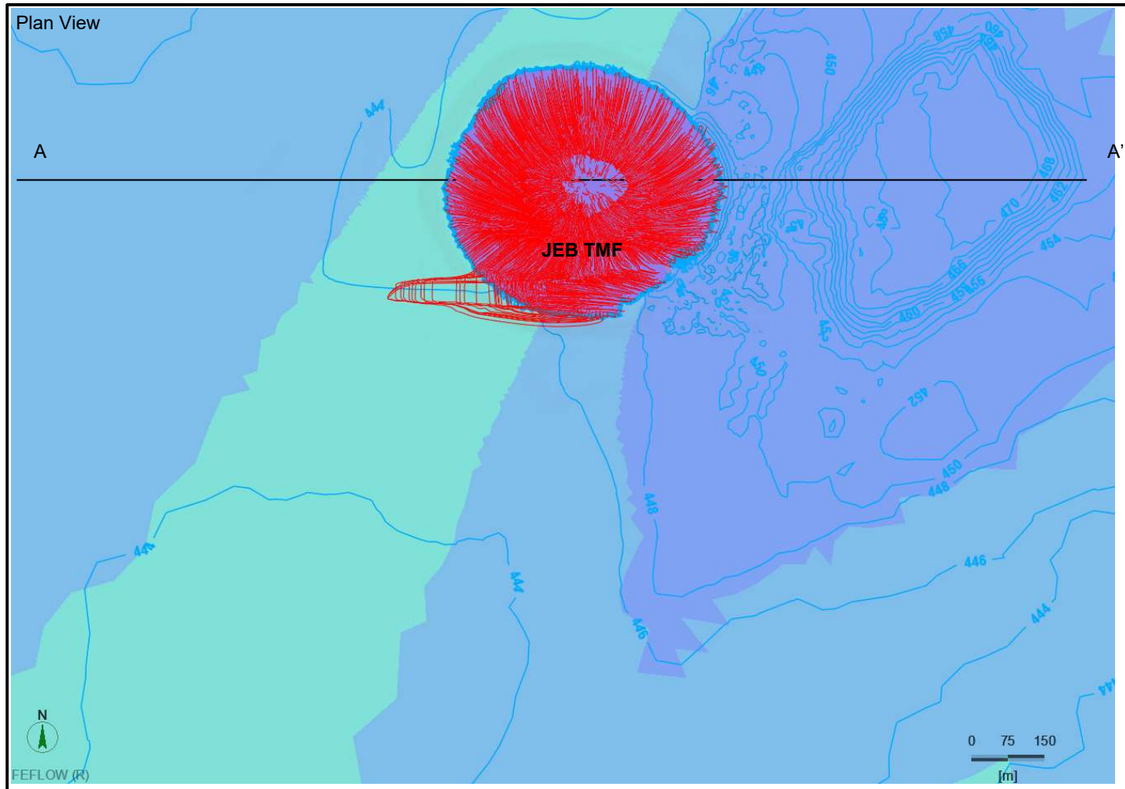

SCENARIO 2 : BASE DRAIN ELEVATION 438.7 M ASL

BASE DRAIN WATER ELEVATION (MASL)	FOX LAKE ELEVATION (MASL)	PAT LAKE ELEVATION (MASL)	HEAD DIFFERENTIAL, $DH_{FOX\ LAKE}$ (M)	GROUNDWATER INFLOW TO DRAIN (M^3/D)
438.7	445.7	443.4	7	2,050

A

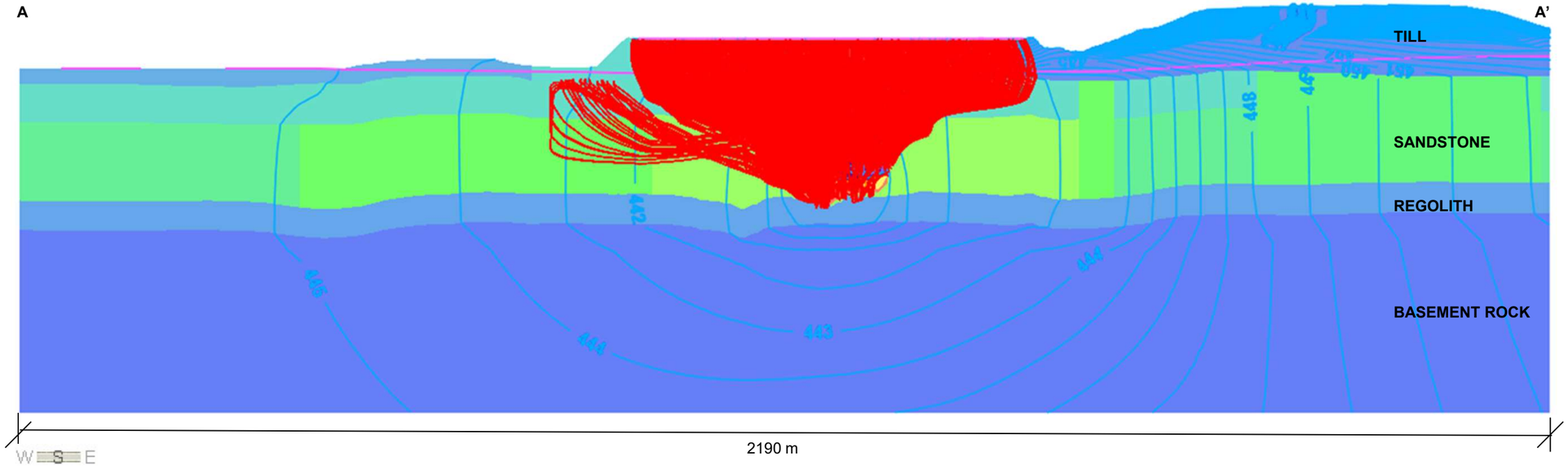

HYDRAULIC CONDUCTIVITY, K (M/S)

- 0.01
- 0.001
- 0.0001
- 1e-05
- 1e-06
- 1e-07
- 1e-08
- 1e-09

LEGEND

- CROSS-SECTION LINE
- WATER TABLE
- HYDRAULIC HEAD (M)
- PARTICLE PATH LINE

NOTE(S)

VERTICAL EXAGGERATION FOR CROOSS-SECTION 1:2
M = METER
M/S = METERS PER SECOND
M^3/DAY = CUBIC METRES PER DAY
MASL = METERS ABOVE SEA LEVEL

CLIENT: orano

CONSULTANT: wsp

YYYY-MM-DD	2025-05-01
PREPARED	KJ
DESIGNED	KJ
REVIEWED	
APPROVED	

PROJECT
JEB TMF
GROUNDWATER FLOW AND SOLUTE TRANSPORT

TITLE
GROUNDWATER PARTICLE TRACKING ANALYSIS
SCENARIO 2
BASE DRAIN ELEVATION 438.7 M ASL

PROJECT NO.	PHASE	REV.	FIGURE
CA0051344.8282	4000	A	**A2**

IF THIS MEASUREMENT DOES NOT MATCH WHAT IS SHOWN, THE SHEET SIZE HAS BEEN MODIFIED FROM: ANSI B
25 mm
0
Prediction_FullBuild_468 high K-cigar -7m dh low K-cigar_2025_linear3b_BC_fig.dac

SCENARIO 2 – SENSITIVITY 1: BASE DRAIN ELEVATION 438.7 M ASL

DESCRIPTION	BASE DRAIN WATER ELEVATION (MASL)	FOX LAKE ELEVATION (MASL)	PAT LAKE ELEVATION (MASL)	HEAD DIFFERENTIAL, $DH_{FOX\ LAKE}$ (M)	GROUNDWATER INFLOW TO DRAIN (M^3/D)
HYDRAULIC CONDUCTIVITY INCREASED BY A FACTOR OF 10 IN THE OVERBURDEN.	438.7	445.7	443.4	7	2,200

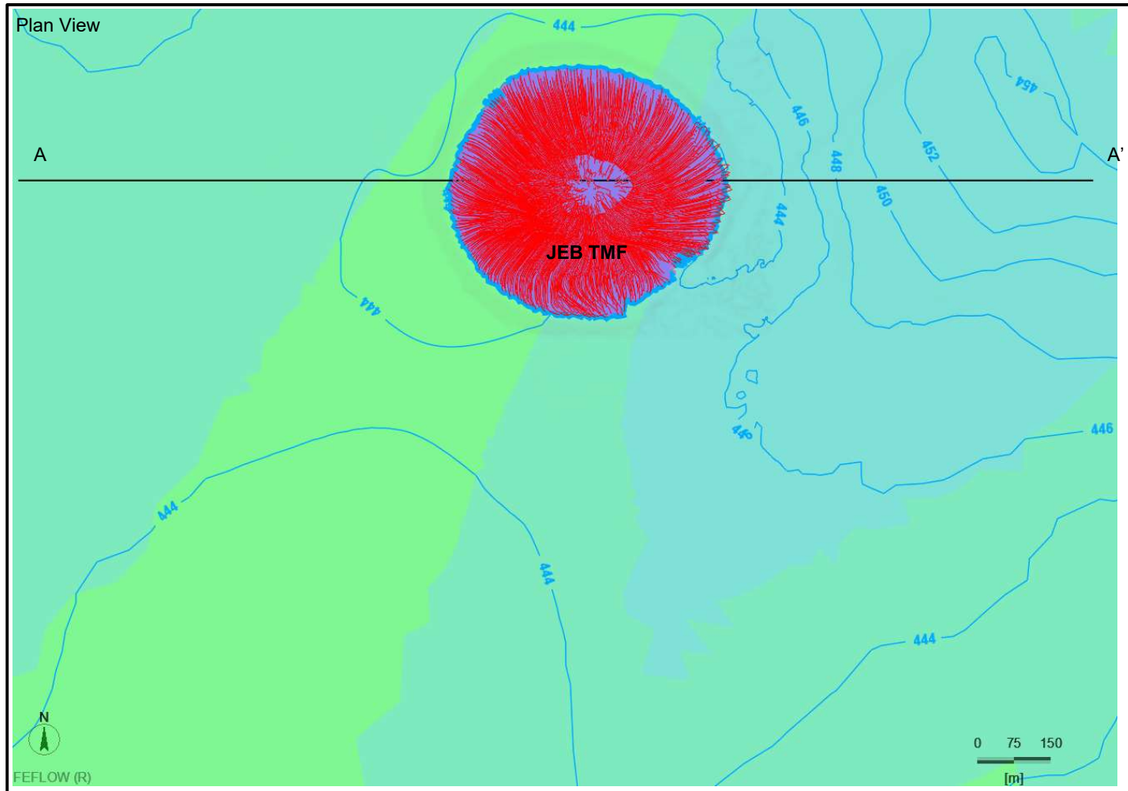

A

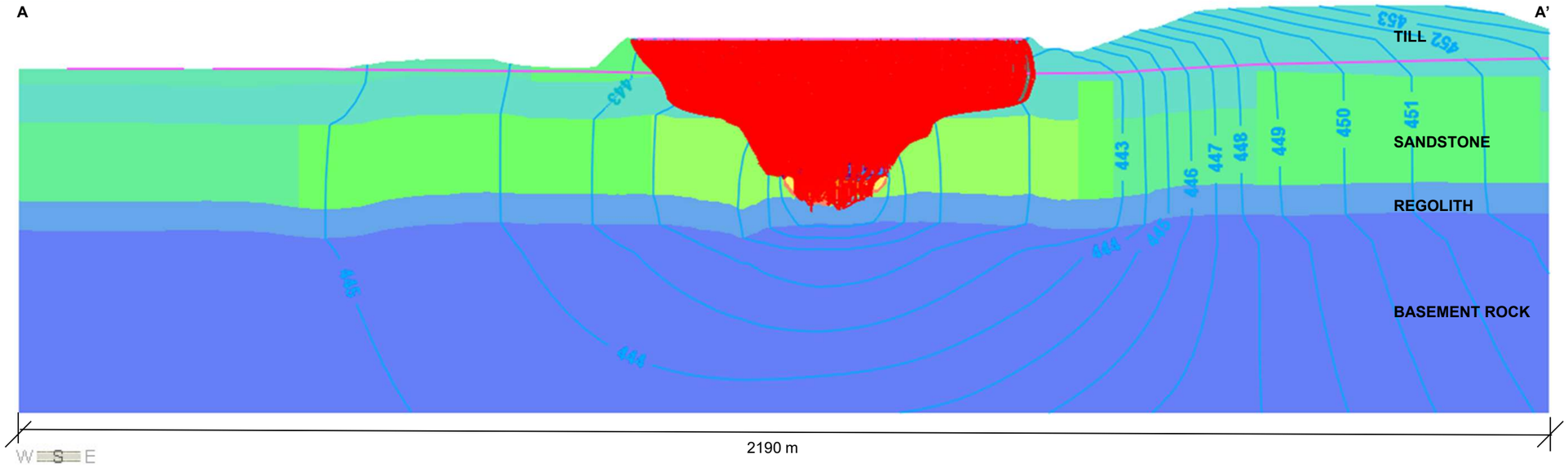

HYDRAULIC CONDUCTIVITY, K (M/S)

- 0.01
- 0.001
- 0.0001
- 1e-05
- 1e-06
- 1e-07
- 1e-08
- 1e-09

LEGEND

- CROSS-SECTION LINE
- WATER TABLE
- HYDRAULIC HEAD (M)
- PARTICLE PATH LINE

NOTE(S)

VERTICAL EXAGGERATION FOR CROOSS-SECTION 1:2
M = METER
M/S = METERS PER SECOND
M^3/DAY = CUBIC METRES PER DAY
MASL = METERS ABOVE SEA LEVEL

CLIENT: orano

CONSULTANT: wsp

YYYY-MM-DD	2025-05-01
PREPARED	KJ
DESIGNED	KJ
REVIEWED	
APPROVED	

PROJECT
JEB TMF
GROUNDWATER FLOW AND SOLUTE TRANSPORT

TITLE
GROUNDWATER PARTICLE TRACKING ANALYSIS
SCENARIO 2 - SENSITIVITY 1
BASE DRAIN ELEVATION 438.7 M ASL

PROJECT NO.	PHASE	REV.	FIGURE
CA0051344.8282	4000	A	**A3**

Prediction_FullBuild_468_high K cigar_-7m dh low K cigar_2025_lines3b_BC_dlv_fig.dac

IF THIS MEASUREMENT DOES NOT MATCH WHAT IS SHOWN, THE SHEET SIZE HAS BEEN MODIFIED FROM: ANSI B

0 25 mm

SCENARIO 2 - SENSITIVITY 2: BASE DRAIN ELEVATION 438.7 M ASL

DESCRIPTION	BASE DRAIN WATER ELEVATION (MASL)	FOX LAKE ELEVATION (MASL)	PAT LAKE ELEVATION (MASL)	HEAD DIFFERENTIAL, $DH_{FOX\ LAKE}$ (M)	GROUNDWATER INFLOW TO DRAIN (M^3/D)
ANISOTROPY (VERTICAL PERMEABILITY [KV]) WAS REDUCED IN THE SANDSTONE BY A FACTOR OF 10.	438.7	445.7	443.4	7	2,020

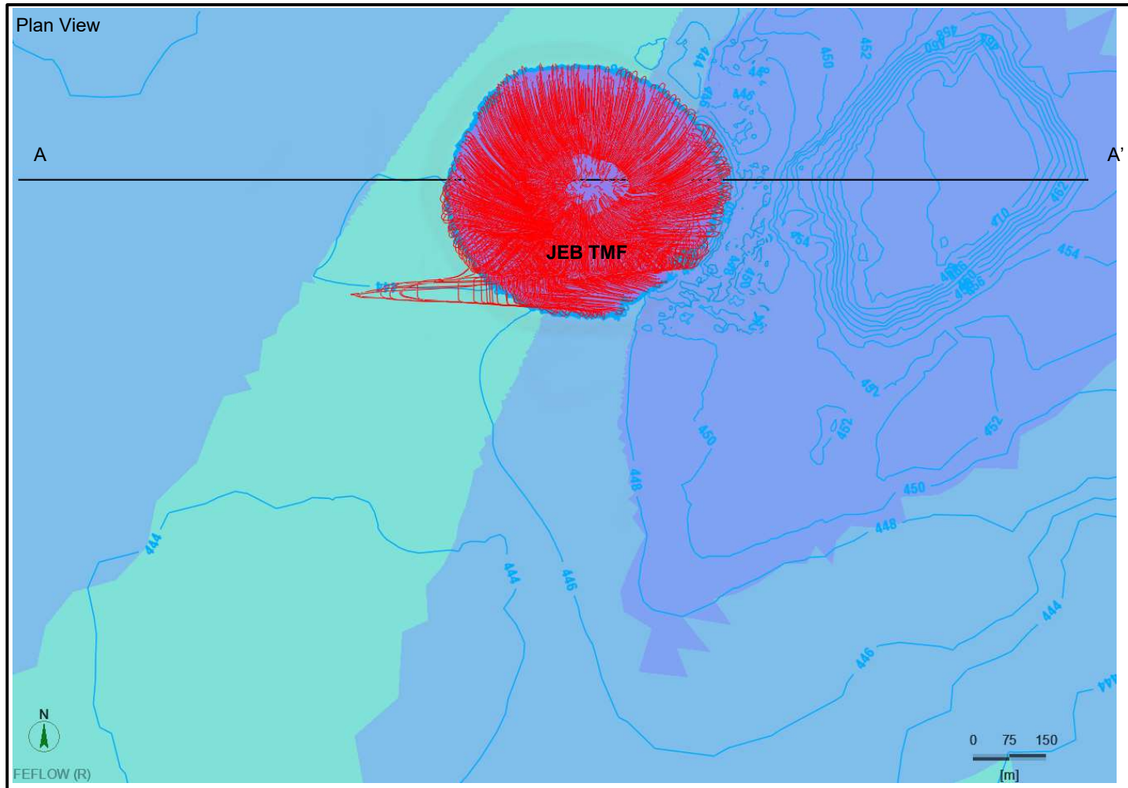

A

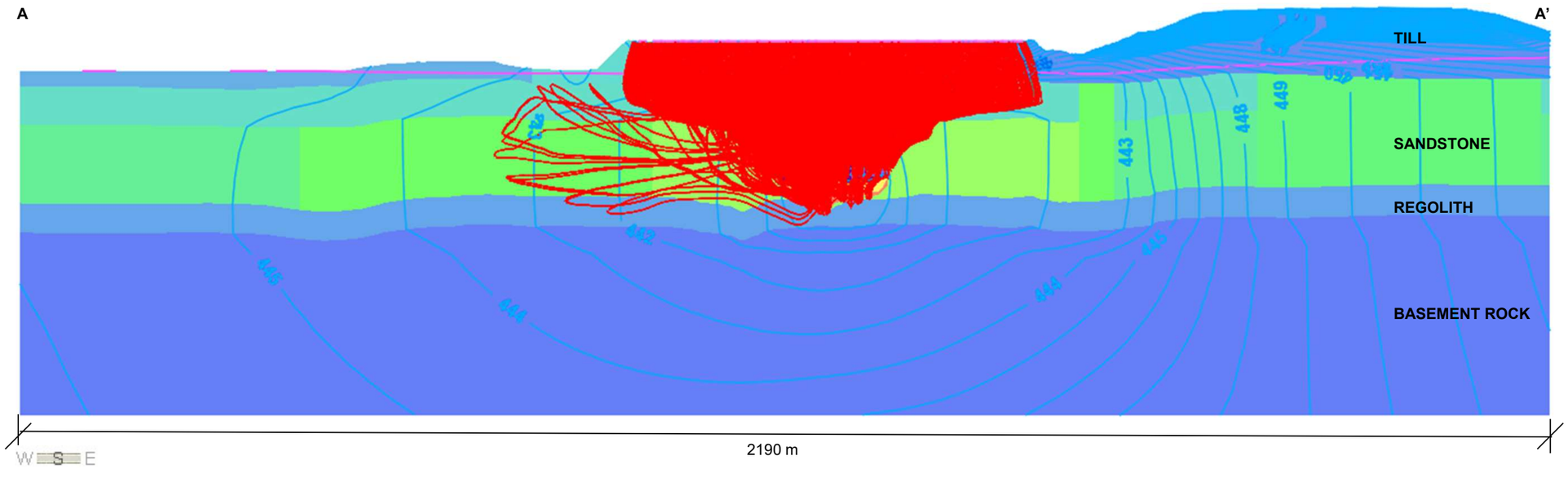

HYDRAULIC CONDUCTIVITY, K (M/S)

- 0.01
- 0.001
- 0.0001
- 1e-05
- 1e-06
- 1e-07
- 1e-08
- 1e-09

LEGEND

- CROSS-SECTION LINE
- WATER TABLE
- HYDRAULIC HEAD (M)
- PARTICLE PATH LINE

NOTE(S)

VERTICAL EXAGGERATION FOR CROOSS-SECTION 1:2
M = METER
M/S = METERS PER SECOND
M^3/DAY = CUBIC METRES PER DAY
MASL = METERS ABOVE SEA LEVEL

CLIENT: orano

CONSULTANT: wsp

YYYY-MM-DD	2025-05-01
PREPARED	KJ
DESIGNED	KJ
REVIEWED	
APPROVED	

PROJECT
JEB TMF
GROUNDWATER FLOW AND SOLUTE TRANSPORT

TITLE
GROUNDWATER PARTICLE TRACKING ANALYSIS
SCENARIO 2 - SENSITIVITY 2
BASE DRAIN ELEVATION 438.7 M ASL

PROJECT NO.	PHASE	REV.	FIGURE
CA0051344.8282	4000	A	**A4**

Prediction_FullBuild_468_high K cigar - 7m dh low K cigar_2025_lowr3b_BC_SST_fig.dac

IF THIS MEASUREMENT DOES NOT MATCH WHAT IS SHOWN, THE SHEET SIZE HAS BEEN MODIFIED FROM: ANSI B

25 mm

SCENARIO 2 - SENSITIVITY 3: BASE DRAIN ELEVATION 438.7 M ASL

DESCRIPTION	BASE DRAIN WATER ELEVATION (MASL)	FOX LAKE ELEVATION (MASL)	PAT LAKE ELEVATION (MASL)	HEAD DIFFERENTIAL, $DH_{FOX\ LAKE}$ (M)	GROUNDWATER INFLOW TO DRAIN (M^3/D)
HYDRAULIC CONDUCTIVITY OF THE LINER WAS INCREASED BY A FACTOR OF 10 (I.E., FROM $1X10^{-9}$ M/S TO $1X10^{-8}$ M/S).	438.7	445.7	443.4	7	2,100

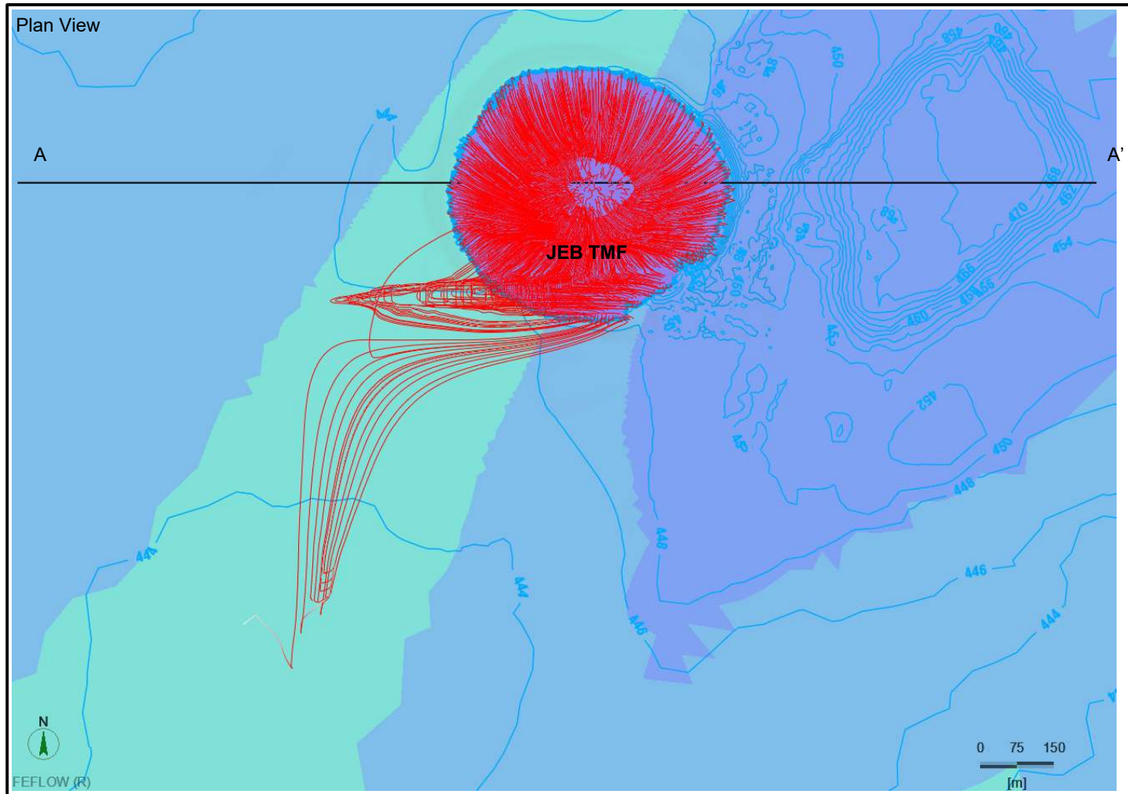

A

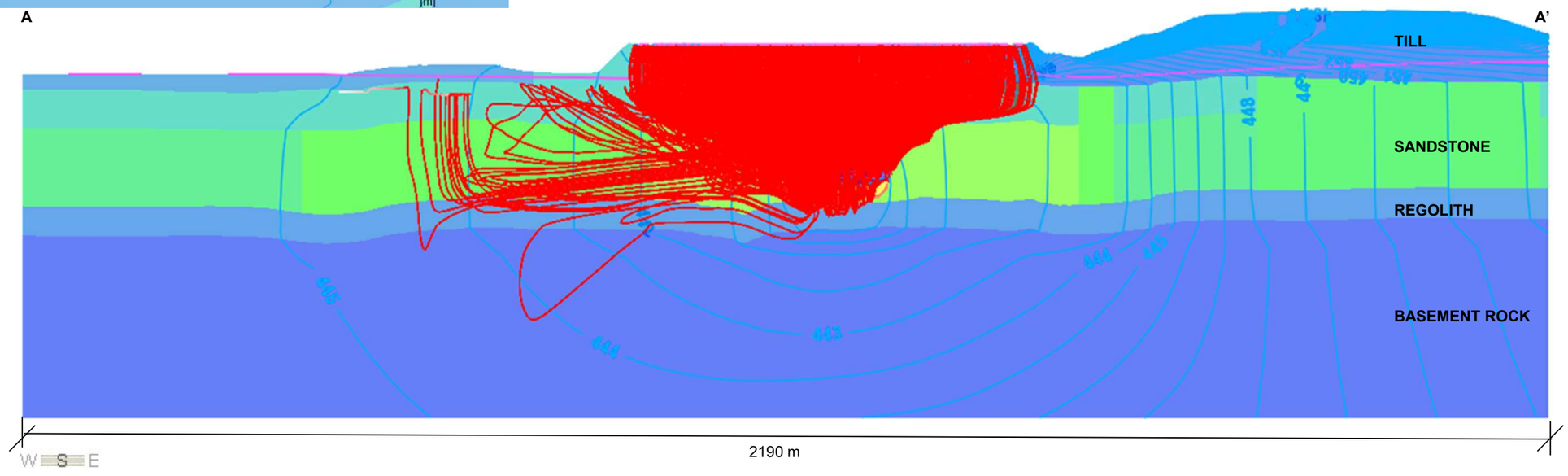

HYDRAULIC CONDUCTIVITY, K (M/S)

- 0.01
- 0.001
- 0.0001
- 1e-05
- 1e-06
- 1e-07
- 1e-08
- 1e-09

LEGEND

- CROSS-SECTION LINE
- WATER TABLE
- HYDRAULIC HEAD (M)
- PARTICLE PATH LINE

NOTE(S)

VERTICAL EXAGGERATION FOR CROOSS-SECTION 1:2
M = METER
M/S = METERS PER SECOND
M^3/DAY = CUBIC METRES PER DAY
MASL = METERS ABOVE SEA LEVEL

CLIENT: orano

CONSULTANT: wsp

YYYY-MM-DD	2025-05-01
PREPARED	KJ
DESIGNED	KJ
REVIEWED	
APPROVED	

PROJECT
JEB TMF
GROUNDWATER FLOW AND SOLUTE TRANSPORT

TITLE
GROUNDWATER PARTICLE TRACKING ANALYSIS
SCENARIO 2 - SENSITIVITY 3
BASE DRAIN ELEVATION 438.7 M ASL

PROJECT NO.	PHASE	REV.	FIGURE
CA0051344.8282	4000	A	**A5**

IF THIS MEASUREMENT DOES NOT MATCH WHAT IS SHOWN, THE SHEET SIZE HAS BEEN MODIFIED FROM: ANSI B
25 mm
0
Prediction_FullBuild_468 high K cxgar -7m dh low K cxgar_2025_liner3b_BC_liner_fig.dac

SCENARIO 3: BASE DRAIN ELEVATION 437.7 M ASL

BASE DRAIN WATER ELEVATION (MASL)	FOX LAKE ELEVATION (MASL)	PAT LAKE ELEVATION (MASL)	HEAD DIFFERENTIAL, $DH_{FOX\ LAKE}$ (M)	GROUNDWATER INFLOW TO DRAIN (M^3/D)
437.7	445.7	443.4	8	2,250

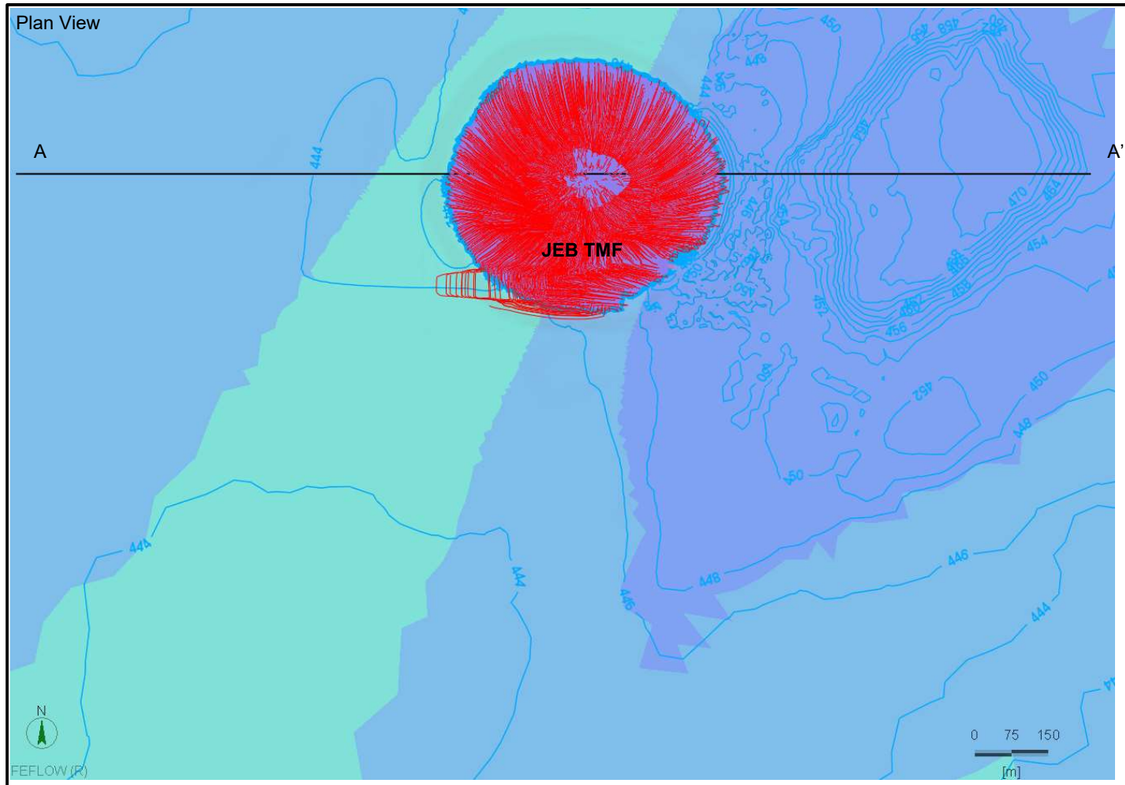

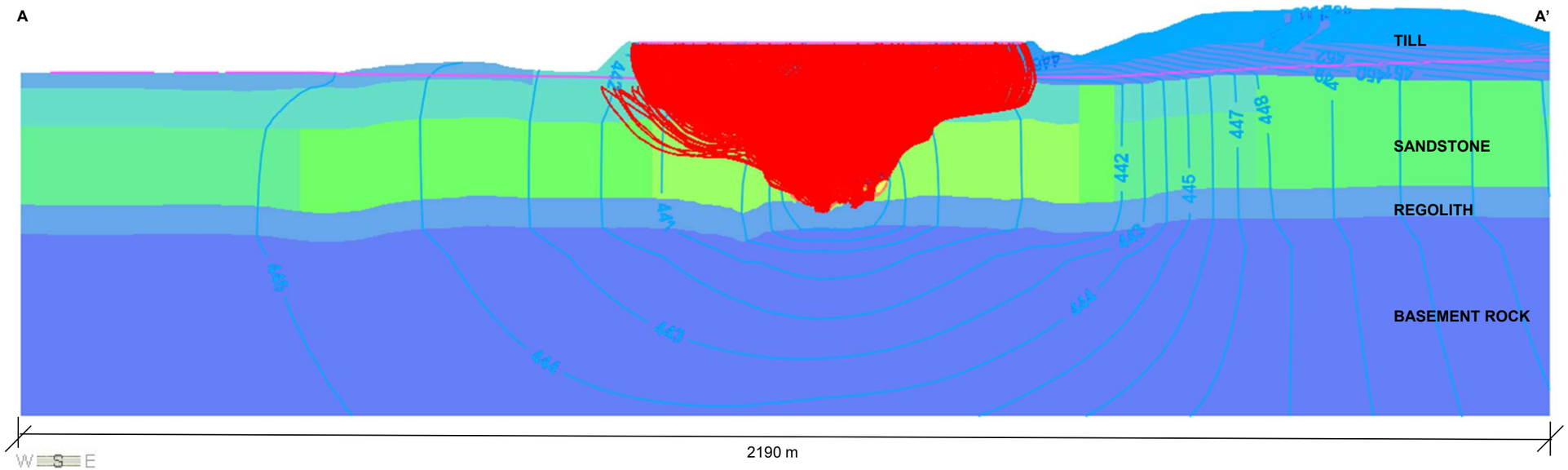

HYDRAULIC CONDUCTIVITY, K (M/S)

- 0.01
- 0.001
- 0.0001
- 1e-05
- 1e-06
- 1e-07
- 1e-08
- 1e-09

LEGEND

- CROSS-SECTION LINE
- WATER TABLE
- HYDRAULIC HEAD (M)
- PARTICLE PATH LINE

NOTE(S)

VERTICAL EXAGGERATION FOR CROOSS-SECTION 1:2
M = METER
M/S = METERS PER SECOND
M^3/DAY = CUBIC METRES PER DAY
MASL = METERS ABOVE SEA LEVEL

CLIENT: orano

CONSULTANT: wsp

YYYY-MM-DD	2025-05-01
PREPARED	KJ
DESIGNED	KJ
REVIEWED	
APPROVED	

PROJECT
JEB TMF
GROUNDWATER FLOW AND SOLUTE TRANSPORT

TITLE
GROUNDWATER PARTICLE TRACKING ANALYSIS
SCENARIO 3
BASE DRAIN ELEVATION 437.7 M ASL

PROJECT NO.	PHASE	REV.	FIGURE
CA0051344.8282	4000	A	**A6**

IF THIS MEASUREMENT DOES NOT MATCH WHAT IS SHOWN, THE SHEET SIZE HAS BEEN MODIFIED FROM: ANSI B
0 25 mm
Prediction_FullBuild_468 high K.cgsr -8m dh low K.cgsr_2025_line2b_BC_fig.dac

SCENARIO 3 – SENSITIVITY 1: BASE DRAIN ELEVATION 437.7 M ASL

DESCRIPTION	BASE DRAIN WATER ELEVATION (MASL)	FOX LAKE ELEVATION (MASL)	PAT LAKE ELEVATION (MASL)	HEAD DIFFERENTIAL, $DH_{FOX\ LAKE}$ (M)	GROUNDWATER INFLOW TO DRAIN (M^3/D)
HYDRAULIC CONDUCTIVITY INCREASED BY A FACTOR OF 10 IN THE OVERBURDEN.	437.7	445.7	443.4	8	2,431

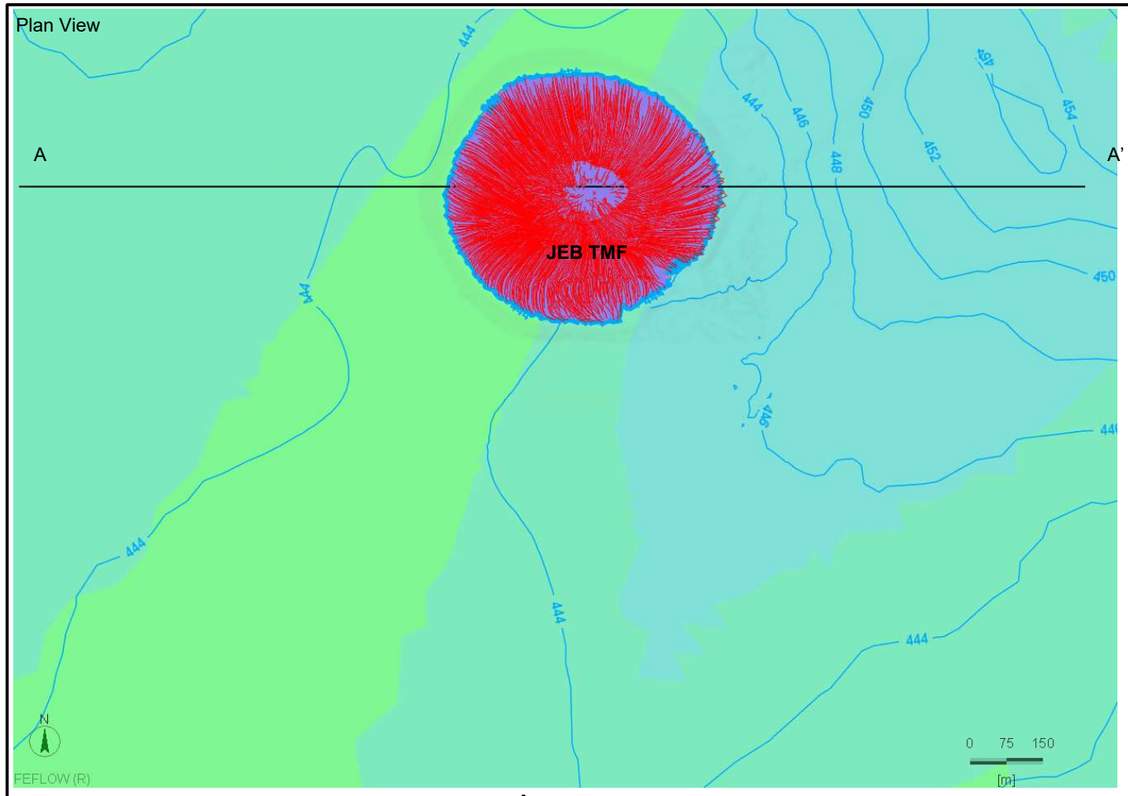

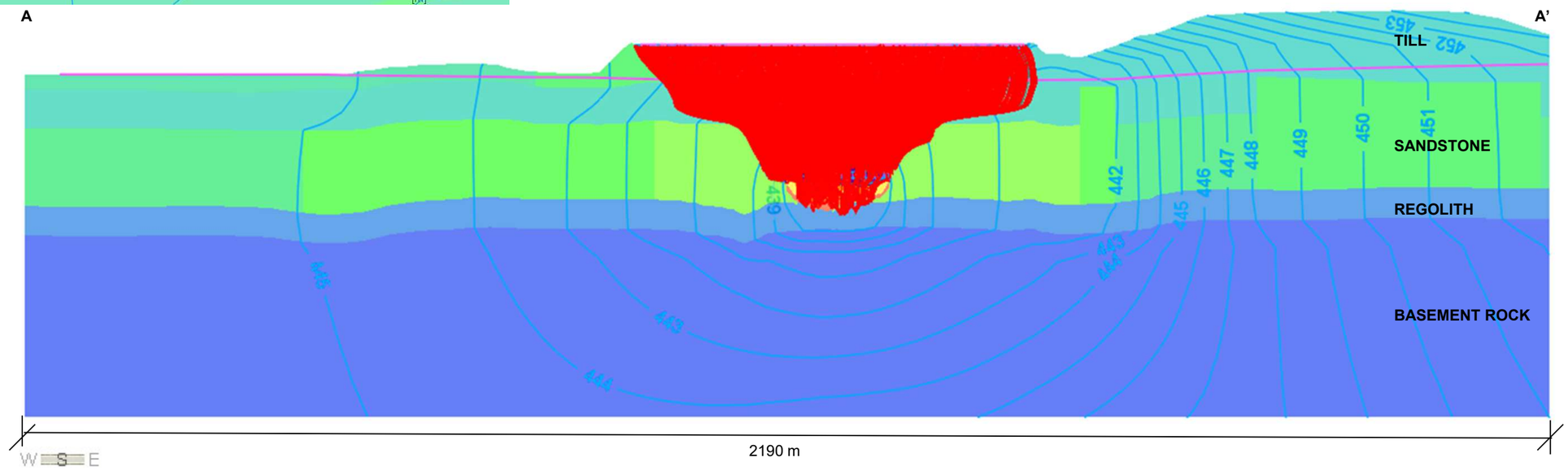

HYDRAULIC CONDUCTIVITY, K (M/S)

- 0.01
- 0.001
- 0.0001
- 1e-05
- 1e-06
- 1e-07
- 1e-08
- 1e-09

LEGEND

- CROSS-SECTION LINE
- WATER TABLE
- HYDRAULIC HEAD (M)
- PARTICLE PATH LINE

NOTE(S)

VERTICAL EXAGGERATION FOR CROOSS-SECTION 1:2
M = METER
M/S = METERS PER SECOND
M^3/DAY = CUBIC METRES PER DAY
MASL = METERS ABOVE SEA LEVEL

CLIENT: orano

CONSULTANT: wsp

YYYY-MM-DD	2025-05-01
PREPARED	KJ
DESIGNED	KJ
REVIEWED	
APPROVED	

PROJECT
JEB TMF
GROUNDWATER FLOW AND SOLUTE TRANSPORT

TITLE
GROUNDWATER PARTICLE TRACKING ANALYSIS
SCENARIO 3 - SENSITIVITY 1
BASE DRAIN ELEVATION 437.7 M ASL

PROJECT NO.	PHASE	REV.	FIGURE
CA0051344.8282	4000	A	**A7**

IF THIS MEASUREMENT DOES NOT MATCH WHAT IS SHOWN, THE SHEET SIZE HAS BEEN MODIFIED FROM ANSI B
25 mm
0
Prediction_FullBuild_468_high K cigar -9m dh low K cigar_2025_linerDb_BC_dtv_fig.dac

SCENARIO 3 - SENSITIVITY 2: BASE DRAIN ELEVATION 437.7 M ASL

DESCRIPTION	BASE DRAIN WATER ELEVATION (MASL)	FOX LAKE ELEVATION (MASL)	PAT LAKE ELEVATION (MASL)	HEAD DIFFERENTIAL, $DH_{FOX\ LAKE}$ (M)	GROUNDWATER INFLOW TO DRAIN (M^3/D)
ANISOTROPY (VERTICAL PERMEABILITY [KV]) WAS REDUCED IN THE SANDSTONE BY A FACTOR OF 10.	437.7	445.7	443.4	8	2,181

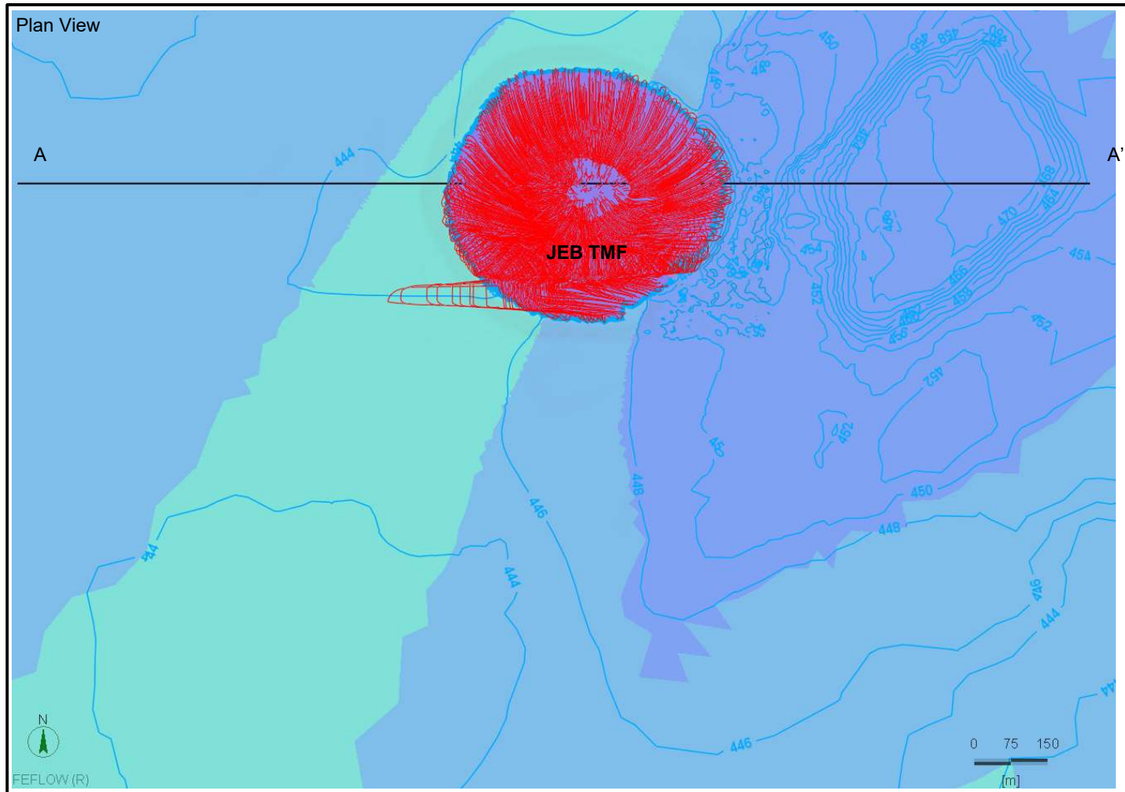

A

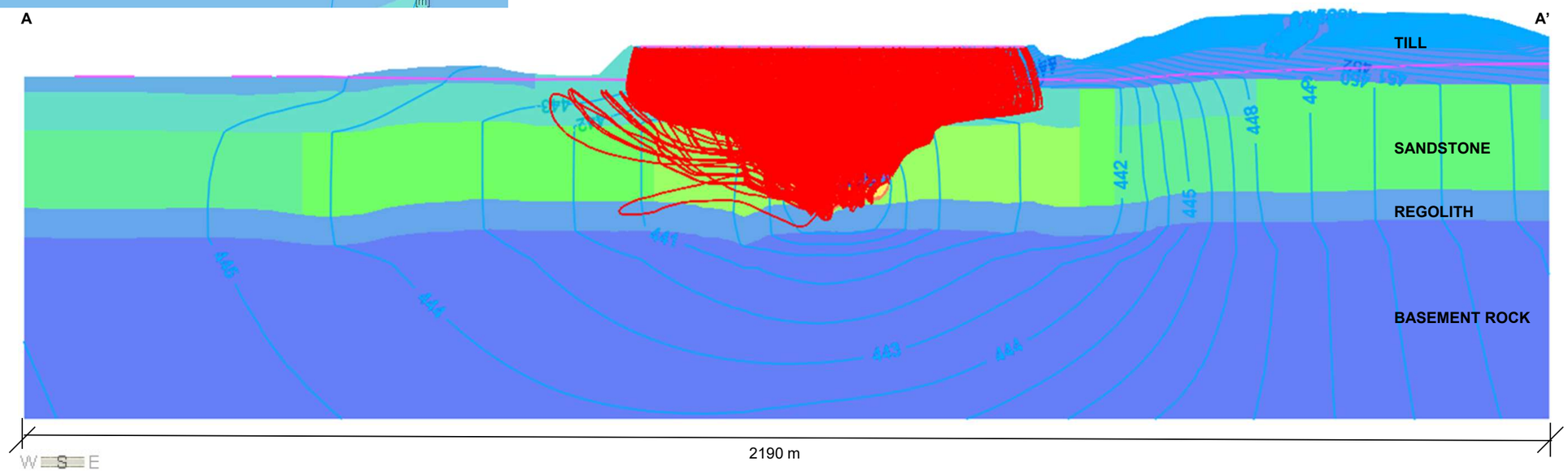

LEGEND
- CROSS-SECTION LINE
- WATER TABLE
- HYDRAULIC HEAD (M)
- PARTICLE PATH LINE

NOTE(S)
VERTICAL EXAGGERATION FOR CROOSS-SECTION 1:2
M = METER
M/S = METERS PER SECOND
M^3/DAY = CUBIC METRES PER DAY
MASL = METERS ABOVE SEA LEVEL

CLIENT: orano

CONSULTANT: wsp

YYYY-MM-DD	2025-05-01
PREPARED	KJ
DESIGNED	KJ
REVIEWED	
APPROVED	

PROJECT
JEB TMF
GROUNDWATER FLOW AND SOLUTE TRANSPORT

TITLE
GROUNDWATER PARTICLE TRACKING ANALYSIS
SCENARIO 3 - SENSITIVITY 2
BASE DRAIN ELEVATION 437.7 M ASL

PROJECT NO.	PHASE	REV.	FIGURE
CA0051344.8282	4000	A	**A8**

IF THIS MEASUREMENT DOES NOT MATCH WHAT IS SHOWN, THE SHEET SIZE HAS BEEN MODIFIED FROM: ANSI B
25 mm
0

Prediction_FullBuild_468 hygh K-cigar -9m dh low K-cigar_2025_linear3b_BC_SST_fig.dac

SCENARIO 3 – SENSITIVITY 3: BASE DRAIN ELEVATION 437.7 M ASL

DESCRIPTION	BASE DRAIN WATER ELEVATION (MASL)	FOX LAKE ELEVATION (MASL)	PAT LAKE ELEVATION (MASL)	HEAD DIFFERENTIAL, $DH_{FOX\ LAKE}$ (M)	GROUNDWATER INFLOW TO DRAIN (M^3/D)
HYDRAULIC CONDUCTIVITY OF THE LINER WAS INCREASED BY A FACTOR OF 10 (I.E., FROM $1X10^{-9}$ M/S TO $1X10^{-8}$ M/S).	437.7	445.7	443.4	8	2,300

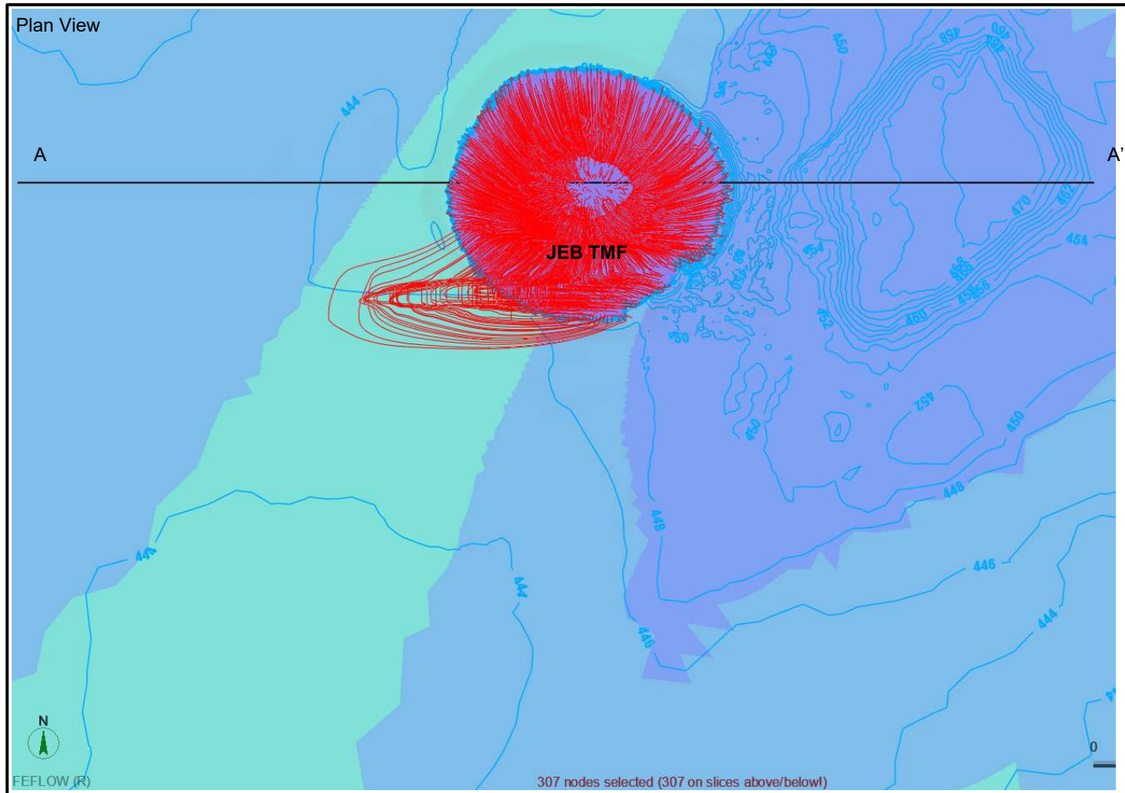

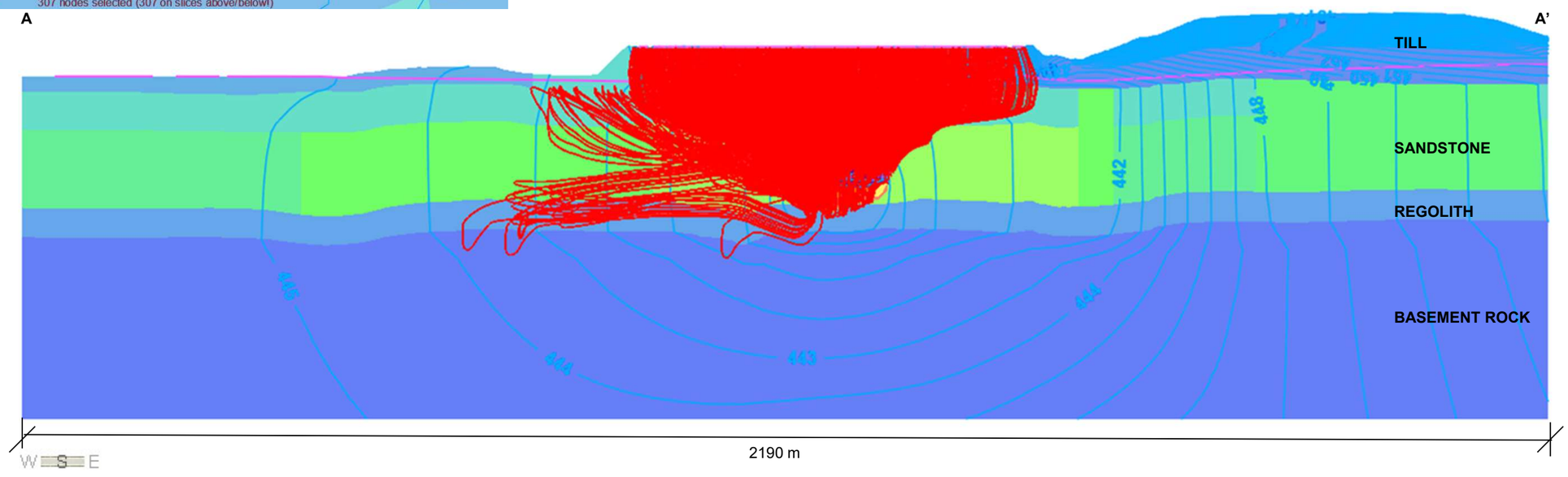

HYDRAULIC CONDUCTIVITY, K (M/S)

- 0.01
- 0.001
- 0.0001
- 1e-05
- 1e-06
- 1e-07
- 1e-08
- 1e-09

LEGEND

- CROSS-SECTION LINE
- WATER TABLE
- HYDRAULIC HEAD (M)
- PARTICLE PATH LINE

NOTE(S)

VERTICAL EXAGGERATION FOR CROOSS-SECTION 1:2
M = METER
M/S = METERS PER SECOND
M^3/DAY = CUBIC METRES PER DAY
MASL = METERS ABOVE SEA LEVEL

CLIENT: orano

CONSULTANT: wsp

YYYY-MM-DD	2025-05-01
PREPARED	KJ
DESIGNED	KJ
REVIEWED	
APPROVED	

PROJECT
JEB TMF
GROUNDWATER FLOW AND SOLUTE TRANSPORT

TITLE
GROUNDWATER PARTICLE TRACKING ANALYSIS
SCENARIO 3 – SENSITIVITY 3
BASE DRAIN ELEVATION 437.7 M ASL

PROJECT NO.	PHASE	REV.	FIGURE
CA0051344.8282	4000	A	**A9**

IF THIS MEASUREMENT DOES NOT MATCH WHAT IS SHOWN, THE SHEET SIZE HAS BEEN MODIFIED FROM ANSI B
25 mm
0

Prediction_FullBuild_468 high K-cigar -9m dh low K-cigar_2025_Inver3b_BC_Inver_fig.dac

wsp.com